Engineering Characterization of Ground Motion

Task I: Effects of Characteristics of Free-Field Motion on Structural Response

Prepared by R. P. Kennedy, S. A. Short, K. L. Merz, F. J. Tokarz/SMAI
I. M. Idriss, M. S. Power, K. Sadigh/WCC

Structural Mechanics Associates, Inc.

Woodward-Clyde Consultants

**DO NOT MICROFILM
COVER**

MASTER

NOTICE

NOTICE

Availability of Reference Materials Cited in NRC Publications

Most documents cited in NRC publications will be available from one of the following sources:

1. The NRC Public Document Room, 1717 H Street, N.W.
   Washington, DC 20555

2. The NRC/GPO Sales Program, U.S. Nuclear Regulatory Commission,
   Washington, DC 20555

3. The National Technical Information Service, Springfield, VA 22161

Although the listing that follows represents the majority of documents cited in NRC publications, it is not intended to be exhaustive.

Referenced documents available for inspection and copying for a fee from the NRC Public Document Room include NRC correspondence and internal NRC memoranda; NRC Office of Inspection and Enforcement bulletins, circulars, information notices, inspection and investigation notices; Licensee Event Reports; vendor reports and correspondence; Commission papers; and applicant and licensee documents and correspondence.

The following documents in the NUREG series are available for purchase from the NRC/GPO Sales Program: formal NRC staff and contractor reports, NRC-sponsored conference proceedings, and NRC booklets and brochures. Also available are Regulatory Guides, NRC regulations in the *Code of Federal Regulations,* and *Nuclear Regulatory Commission Issuances.*

Documents available from the National Technical Information Service include NUREG series reports and technical reports prepared by other federal agencies and reports prepared by the Atomic Energy Commission, forerunner agency to the Nuclear Regulatory Commission.

Documents available from public and special technical libraries include all open literature items, such as books, journal and periodical articles, and transactions. *Federal Register* notices, federal and state legislation, and congressional reports can usually be obtained from these libraries.

Documents such as theses, dissertations, foreign reports and translations, and non-NRC conference proceedings are available for purchase from the organization sponsoring the publication cited.

Single copies of NRC draft reports are available free, to the extent of supply, upon written request to the Division of Technical Information and Document Control, U.S. Nuclear Regulatory Commission, Washington, DC 20555.

Copies of industry codes and standards used in a substantive manner in the NRC regulatory process are maintained at the NRC Library, 7920 Norfolk Avenue, Bethesda, Maryland, and are available there for reference use by the public. Codes and standards are usually copyrighted and may be purchased from the originating organization or, if they are American National Standards, from the American National Standards Institute, 1430 Broadway, New York, NY 10018.

GPO Printed copy price: $8.50

DISCLAIMER

DISCLAIMER

Portions of this document may be illegible in electronic image products. Images are produced from the best available original document.

Engineering Characterization of Ground Motion

Task I: Effects of Characteristics of Free-Field Motion on Structural Response

Prepared by
R. P. Kennedy, S. A. Short, K. L. Merz, F. J. Tokarz, Structural Mechanics Associates, Inc.
I. M. Idriss, M. S. Power, K. Sadigh, Woodward-Clyde Consultants

Structural Mechanics Associates, Inc.
Newport Beach, CA 92660

Under Contract to:
Woodward-Clyde Consultants
Walnut Creek, CA 94596

DISCLAIMER

FOREWORD

This report presents the results of the first task of a two-task study on the engineering characterization of earthquake ground motion for nuclear power plant design. The overall objective of this study is to develop recommendations for methods for selecting design response spectra or acceleration time histories to be used to characterize motion at the foundation level of nuclear power plants.

Task I of the study, presented herein, develops a basis for selecting design response spectra, taking into account the characteristics of free-field ground motion found to be significant in causing structural damage. Task II of the study, to be completed later in 1984, will provide recommendations for methods for selecting response spectra and time histories incorporating wave passage and soil-structure interaction effects and Task I results.

This study is being conducted under Contract No. NRC 04-80-192 with the U.S. Nuclear Regulatory Commission (USNRC). Woodward-Clyde Consultants (WCC) is the prime contractor for the project. Task I has been carried out primarily by Structural Mechanics Associates, Inc. (SMA), as a subcontractor to WCC.

In addition to the listed authors of this report, several individuals made important contributions to the study. These individuals included T. R. Kipp and H. Banon of SMA; and C.-Y. Chang and R. R. Youngs of WCC. Project consultants, W. J. Hall of the University of Illinois, Champaign; J. E. Luco of the University of California, San Diego; J. M. Roesset of the University of Texas, Austin; H. B. Seed of the University of California, Berkeley; and N. C. Tsai of NCT Engineering, Inc., Lafayette, California, provided a detailed review of draft versions of the report and made many useful comments. J. F. Costello provided overall technical guidance and review in his role as technical representative of the USNRC for this research project.

TABLE OF CONTENTS

TABLE OF CONTENTS (Continued)

1. INTRODUCTION

This report provides a summary of the results obtained during the first phase of an ongoing project with the objective of providing guidance and the development of procedures for the characterization of earthquake ground motion used for design of nuclear power plant structures. The overall study effort is divided into two separate tasks:

I: The development of a basis for selecting design response spectra based on free-field motion.

II: The development of recommendations for methods for selecting design response spectra and time histories to be used as input motions at the foundation level.

This report is concerned with the Task I effort only. The work performed consists of (1) the development of a procedure for estimating reduction factors that provide equal-damage effective response spectra, (2) the comparison of ground motions on the basis of equal structural damage potential and (3) a review of the design basis and observed behavior of actual structures due to past damaging earthquakes.

1.1 BACKGROUND (LITERATURE REVIEW)

The ground motion input for the seismic evaluation and design of nuclear power plants is generally defined in terms of a design response spectrum for which the structure is expected to remain elastic. The design response spectrum is generally a broadbanded spectrum with broad frequency content. It expresses the peak linear response of a whole series of single-degree-of-freedom oscillators at a specified damping level. Either site-independent or site-dependent response spectra are specified. A site-independent sprectrum uses a broad standard spectrum shape which is considered applicable to a wide range of local geologic and seismological conditions, while a site-dependent spectrum tends to be less broadbanded as it depends at least in part on particular local site conditions. Figure 1-1 presents a representative site-independent

response spectrum which has been commonly used for nuclear power plants in the United States [USNRC (1973a)]. This spectrum (as well as most other site-independent spectra) is anchored to a design ground acceleration with the entire spectrum normally being defined in terms of this one ground motion parameter. Newmark (1973) states that in the frequency region of interest (approximately 1.8 to 10 Hz) for stiff nuclear power plant structures, the design spectra are most appropriately anchored to the design ground acceleration. Thus, as a minimum the ground motion parameter which must be defined is the design ground acceleration.

Seismologists have tended to concentrate on defining ground motion in terms of an instrumental peak acceleration, which represents the absolute peak acceleration recorded during the entire earthquake motion by a reliable strong-motion instrument situated at the free ground surface (i.e., not significantly influenced by soil-structure interaction or local topographic conditions). This parameter represents a relatively easily determined quantitative value not strongly influenced by subjective judgments. Unfortunately, as illustrated by many studies (e.g., see Hoffman, 1974; Page and others, 1972; Housner, 1975, 1979; Housner and Jennings, 1977; Newmark, 1975; Blume, 1979; Nuttli, 1979, Kennedy, 1980), the instrumental peak acceleration is, by itself, a poor measure of the damaging potential of earthquake ground motions. It has been noted, particularly in connection with near-source motions due to low-to-moderate-magnitude earthquakes, that structures have performed much better during earthquakes than would be predicted considering the instrumental peak acceleration to which the structures were subjected. Examples of this behavior may be seen from the 1966 Parkfield earthquake, the 1971 Pacoima Dam earthquake record, the 1972 Ancona earthquakes, and the 1972 Melendy Ranch Barn earthquake record. These earthquake records had instrumental peak accelerations of between 0.5 and 1.2g and yet, only minor damage occurred in the vicinity of the recording sites. In these cases and others, the differences in measured ground motion, design levels, and observed behavior is so great that it cannot be reconciled with typical safety factors associated with elastic seismic analyses used for design. This subject is discussed in more detail in Newmark and Hall, 1982.

The problem with instrumental peak acceleration is twofold. First, a limited number of high frequency spikes of high acceleration but very short duration have little effect on the elastic response spectra within the region of primary interest (1.8 to 10 Hz). This problem can be corrected through the use of a design ground acceleration value that is often called "effective peak acceleration" and is defined herein as that acceleration at which the design response spectrum is anchored at zero-period (or very high frequency). The design ground acceleration can be defined by the methods reviewed by Kennedy (1980, 1981) if the purpose is to anchor an elastic response spectrum for computing peak elastic structural response. However, the second problem is that an elastic response spectrum anchored to any of these design ground acceleration values or to the instrumental peak acceleration does not provide a good measure of damage to structures. Elastic response spectra describe elastic response while structure damage is related to structures being strained into the inelastic range in which the duration of motion or the number of cycles of straining as well as the nature of such cycles substantially influence the damage. The elastic spectrum ignores the effect of duration and underestimates the effect of the number of cycles of near-peak excursions on damage.

1.1.1 Effective Ground Acceleration for Anchoring Elastic Spectra

Much research has been conducted for the purpose of defining "effective" design ground accelerations to use as anchor accelerations for elastic design spectra. In general, the elastic response spectrum used in design should have a broad frequency content and should be smooth (i.e., not contain large differences in spectral amplitude for minor shifts in natural frequency). This is required because the specific frequency content of a future earthquake ground motion cannot be accurately specified and two different ground motions recorded at the same site may have different frequency content. However, recorded instrumental ground motions often lead to elastic response spectra with narrower frequency content than smooth design spectra and with many peaks and valleys (i.e., substantial differences in the spectral response for minor shifts in natural frequency). The narrow frequency content of the spectra and

the differences in amplitudes between peaks and valleys increases as the effective duration of the motion decreases. Thus, real spectra derived from actual short duration earthquake records differ more from the broad idealized design spectra than do spectra derived from the recorded long duration records. Yet normally, it may not be prudent in design to take advantage of the narrow frequency content and large differences between the amplitudes of peaks and valleys associated with these short duration spectra because their frequency content could vary over a wide range for different earthquakes. One often proposed solution to this problem is to anchor the broad design spectrum to a reduced "effective" ground acceleration such that "on the average" the broad frequency, smooth design spectrum will predict about the same elastic response as would be predicted by the actual spectra.

Even within the higher frequency range (1.8 to 10 Hz) the elastic response spectrum values are primarily influenced by the energy contained within a number of cycles of ground motion and are little influenced by a few spikes of very high acceleration. Blume (1979) has shown that clipping the highest 30% off the measured acceleration time history (using only 70% of the record, in an absolute sense, closest to the zero line) produced only about a 5% reduction in the elastic response spectrum. Similar results have been shown by Schnabel and Seed (1973) and Ploessel and Slosson (1974). Newmark (1976) has shown that the elastic response spectrum from the 1.25g Pacoima Dam record can be conservatively enveloped within the frequency range of interest by a broadbanded design spectrum anchored to a design ground acceleration of 0.75g. These findings have led to a number of recommendations for defining an effective design acceleration, A_D, including the use of sustained or repeatable peak acceleration (Nuttli, 1979), the use of an equivalent cyclic motion (Whitman, 1978), and the use of filtered time histories in which high frequency spikes are removed by passing the measured time history through an 8 to 9 Hz cutoff frequency filter (Page and others, 1972; Ploessel and Slosson, 1974). Based upon a review of these recommendations, Kennedy (1980) has suggested that the effective design acceleration, A_D for elastic response might be defined by:

$$A_D = 1.25 * A_{3F} \qquad (1\text{-}1)$$

where A_{3F} is the third highest peak acceleration from the filtered time history record. The filter chosen by Page (1972) which is centered at 8.5 Hz with a value of 1.0 at 8.0 Hz and 0.0 at 9.0 Hz appears to be a reasonable filter approach. This definition is illustrated using the 1.25g Pacoima Dam record. Figure 1-2 presents the unfiltered and filtered Pacoima Dam record. The third highest peak, A_{3F}, from the filtered record is 0.62g as opposed to an unfiltered peak acceleration of approximately 1.2g. The A_D from Equation 1-1 is 0.78g which agrees with Newmark's (1976) recommendations for this record. On the other hand, for the 1940 north-south El Centro record in which there were several lower frequency near-peak excursions the design ground acceleration, A_D, would be essentially equal to the instrumental peak acceleration of 0.35g by this definition.

Another approach to defining an effective "elastic" design ground motion is in terms of the energy content of the earthquake. Arias (1970) and Housner (1975) have suggested that E(T) given by:

$$E(T) = \int_{t_o}^{t_o + T_D} a^2(t)dt \qquad (1\text{-}2)$$

can serve as a measure of the total energy between time t_o and time $t_o + T_D$. The Arias Intensity is proportional to E(T). In Equation 1-2, a(t) represents the instrumental acceleration at time t, and T_D is the duration of strong motion. The average rate of energy input (earthquake power) is then given by:

$$P = E(T)/T_D \qquad (1\text{-}3)$$

Alternately, Mortgat (1979), and McCann and Shah (1979) have suggested the root-mean-square acceleration, rms, as the ground motion parameter of interest. This rms acceleration is given by:

$$\text{rms} = \sqrt{P} \qquad\qquad\qquad (1\text{-}4)$$

Both the power, P, and rms acceleration are heavily influenced by the procedure used to select the duration of strong motion, T_D. Often the duration of strong motion has been selected as the time between the first and last excursion of the absolute acceleration above a selected percentage of the peak acceleration (such as 10 or 20 percent) or the time between the first and last crossing of a particular acceleration level (such as 0.05g). Such definitions give anomalous results for duration, power, and rms acceleration for a record such as the 1940 El Centro record which appears to consist of three distinct zones of strong motion during the time history. Kennedy, (1980) has suggested that the cumulative time the ground motion exceeds a selected percentage (such as 10 percent) of the peak acceleration provides a more consistent estimate of the strong motion duration, power, and rms acceleration for a number of records. Duration defined in this manner is referred to as T_D'' in this report.

In the analytical studies reported in later chapters of this report, the strong duration, T_D' is defined by:

$$T_D' = T_M - T_{0.05} \quad \text{where} \quad T_M = \max \left\{ \begin{matrix} T_{0.75} \\ T_{pa} \end{matrix} \right\} \qquad (1\text{-}5)$$

where $T_{0.75}$ and $T_{0.05}$ represent the time at which 75% and 5%, respectively, of the total energy as measured by $\int a^2 \, dt$ has been reached. If the time of maximum positive or negative ground acceleration occurs after $T_{0.75}$, then the time T_{pa} of the first zero crossing after the time of peak acceleration is used in lieu of $T_{0.75}$. The reasons for the use of this definition of duration are described in Chapter 2. Strong durations by this definition are shown in Table 2-3. For the San Fernando records with peak ground accelerations in excess of 0.2g, the strong durations T_D' were generally 5 to 6 seconds while T_D'' was generally 9 to 10 seconds. Thus, these records might be said to have 5 to 6 seconds of strong duration, or 9 to 10 seconds depending upon the strong duration definition. By some other definitions, these records would have strong durations of about 12 seconds. The reported strong duration can differ by more than a factor of 2 depending on the definition.

Use of the rms acceleration as the basis for the design acceleration, A_D, has many attractions. It is an easily computed quantity once a definition for T_D is accepted. As shown by Mortgat (1979), it enables a design acceleration to be selected at any desired probability of exceedance. A design acceleration defined in this fashion can be used to define the elastic response spectrum with a given probability of exceedance. The design acceleration is related to the rms acceleration by:

$$A_D = K_p * rms \qquad (1-6)$$

where K_p is a function of the acceptable exceedance probability for each individual peak of the time history. Considering the design acceleration as a median estimate of the maximum acceleration over the duration of strong motion for a stationary random Gaussian motion, Vanmarcke and Lai (1980) have determined K_p to be:

$$K_p = \sqrt{2 \ln (2.8 \ T_D/T_o)} \qquad (1-7)$$

except K_p is not less than $\sqrt{2}$, where T_o is the predominant period of the ground motion which can be taken to be between 0.2 and 0.4 seconds for most records. Kennedy (1980) has reported that Equations 1-6 and 1-7 appear to work well for defining a design acceleration to which elastic response spectra can be anchored.

The usage of Equations 1-2 through 1-7 can be illustrated using the 0.7g 1972 Melendy Ranch recording (Figure 1-3) and the 0.18g 1952 Taft recording (Figure 1-4). Both records contain relatively similar total energy content despite the nearly fourfold greater instrumental peak acceleration for the Melendy Ranch record. The Melendy Ranch record has a much shorter strong motion duration (T_D'') of about 1.5 seconds versus about 16 seconds for the Taft record. With these durations, the design accelerations given by Equations 1-6 and 1-7 are 0.34g for the Melendy Ranch record and 0.14g for the Taft record. The design acceleration ranges from less than 50 percent of the instrumental peak acceleration for Melendy Ranch to 70 percent for Taft which illustrates the expected effect of the short duration for Melendy Ranch.

For several earthquake records, Table 1-1 compares instrumental peak accelerations, and design accelerations given by Equations 1-1 or 1-6 and 1-7 ($T_0 = 0.3$ seconds) based on a duration, T_D''. Also presented is the strong motion duration, T_D''. In each case, the design acceleration from Equations 1-1 or 1-6 and 1-7 is judged to be a consistent basis for anchoring the design response spectrum for the purpose of computing elastic response in the 1.8 to 10 Hz frequency range. One can note the influence of duration on the ratio of A_D to A_{IP} (instrumental peak acceleration) for elastic response.

Either the approach of Equation 1-1 or Equations 1-6 and 1-7 have been reported by Kennedy (1980) to provide reasonable estimates of "effective" design accelerations to be used to anchor elastic design response spectra for elastic analyses. However, it was already mentioned that comparisons of elastic response do not provide a good description of relative damage from two different ground motions. Therefore, neither method of defining a design acceleration provides an adequate characterization of the damage capability of earthquake ground motion in every case.

1.1.2   Effect of Duration on Damage Capability

There are energy absorbing mechanisms that occur during seismic response of structures that limit the resisting force levels such that a limited number of cycles of very high acceleration input ground motion might result in only minor damage and not affect the primary function of the structural system. Such energy absorbing mechanisms include concrete cracking, minor bond slip of reinforcement bars, friction at bolted connections and other locations, and other mechanisms. These energy absorbing mechanisms cause nonlinear behavior of sufficient amount to considerably reduce required design force levels from those calculated assuming totally elastic behavior. For each cycle of earthquake motion, energy absorption has a small deteriorating or degrading effect on the structure; for sufficient numbers of cycles these degrading effects would eventually accumulate to produce noticeable structural damage. For example, when a reinforced concrete shear wall is subjected to sufficient transverse shear forces during an earthquake, the concrete will crack

even though the steel continues to behave elastically. This would constitute acceptable behavior even for a critical facility such as a nuclear power plant. Such a member in shear would exhibit softer unloading stiffness and degrading stiffness during reloading because the concrete cracks do not heal during unloading and the concrete begins to deteriorate. For a limited number of cycles of seismic response such that the energy of the seismic excitation was less than the energy absorption capacity of the structure, such a structure as that described would shake down to pseudo-elastic behavior possibly at a reduced stiffness and possibly with some permanent set but the structure would be stable and safe and would not have experienced significant damage (Figure 1-5). On the other hand, for a strong earthquake in which the number of cycles of seismic response is such that the energy of the seismic excitation exceeds the energy absorption capacity of the structure, such a structure as that described above would reach displacement amplitudes corresponding to significant structural damage and possibly total collapse (Figure 1-6).

The effect of the duration of strong motion or number of cycles of strong inelastic response is not incorporated into the low-damped elastic response spectrum. Thus, a given elastic spectral response would correspond to greater damage capability for a long duration earthquake than for a short duration earthquake.

Furthermore, it was mentioned in the previous subsection that short duration earthquake records have narrower frequency content and greater differences between the spectral responses at peaks versus valleys than do longer duration records. These longer duration records are richer in a broad range of frequency content and tend to be smoother. The ability of structures to withstand earthquake ground motions which result in elastic response spectra substantially higher than the elastic design response spectrum is greater for spectra which have narrow frequency content and many peaks and valleys than it is for smooth, broad frequency content spectra. Basically, if the elastic structure is in resonance with the ground motion at a frequency of one of

the peaks of the elastic spectrum, small inelastic behavior of the structure will shift the structure frequency off the resonant peak and into a valley. As will be shown in subsequent chapters, the level of inelastic response is more consistently predicted by the average spectral response over a broad frequency range to the soft (lower frequency) side of the elastic natural frequency. The difference between this frequency averaged spectral response and the elastic natural frequency spectral response is significantly greater for narrow frequency band elastic spectra with large peaks and valleys than it is for broad frequency content, smooth elastic spectra of the type used in design.

When one ignores duration and considers only the elastic response spectra or the design acceleration defined by Equations 1-1 or 1-6 and 1-7, one would conclude that the Melendy Ranch record was more severe than the Taft record for structures with natural frequencies greater than 3 Hz (see Figure 1-7), and the 1966 Parkfield Cholame #2 record was more severe than the 1940 El Centro record at all frequencies (see Figure 1-8). Both conclusions would be incorrect and illustrate the inadequacy of the elastic response spectrum to define the damage capability of an earthquake. The problem is that the elastic response spectrum values are related primarily to the power of the earthquake (Equation 1-3), or the rms acceleration (Equation 1-4), or the design acceleration (Equations 1-1 or 1-6 and 1-7), while the damage capability is probably more related to the total energy fed into structures (Equation 1-2). Housner (1975) has proposed that this dilemma be solved by a two-parameter definition of the ground shaking in which one parameter could be any of the parameters relating to the power of the earthquake such as the design acceleration from Equations 1-1 or 1-6 and 1-7. the other parameter should be strong motion duration, T_D.

Short (1980a and 1980b) and Kennedy (1981a) have studied the effect of a high acceleration, short duration record such as the Melendy Ranch (1972, 0.52g corrected acceleration) record on a nuclear power plant structure designed for a long duration, much lower acceleration record like the Taft (1952, 0.18g corrected acceleration) record. The shear wall-type structure was designed to ultimate strength for a broad-banded design spectrum anchored to 0.2g. The structure was subjected to shaking characterized by the Melendy Ranch record. Concrete elements were defined to have highly degrading stiffness characteristics. The Melendy Ranch record shows maximum 5% damped spectral acceleration in excess of 1.5g in the 5 to 6 Hz frequency range and the structure was designed to have a fundamental frequency within this range. The nonlinear response of this structure was found to be highly stable with a single inelastic excursion followed by pseudo-elastic behavior with a slightly degraded stiffness. Thus, a highly degrading structure designed for a design response spectrum anchored to an "effective" ground acceleration of 0.2g shows perfectly satisfactory behavior when subjected to the Melendy Ranch record. Therefore, this record should be taken to have a design acceleration value of 0.2g or less as opposed to the nominal values of 0.5g. In summary, ignoring duration and considering only the elastic response spectrum would lead one to conclude that the Melendy Ranch record was more severe than the Taft record; however, this would be an incorrect conclusion which illustrates the inadequacy of the elastic response spectrum to alone define the damage capability of an earthquake.

1.2   CONCLUSIONS REACHED FROM A REVIEW OF STRUCTURAL DAMAGE FROM PAST EARTHQUAKES

Appendix A summarizes the results of a literature review on structural damage from past earthquakes. The primary purpose of this review was to summarize the available data on whether or not elastic computed forces could be used to estimate the onset of significant structural damage. Whenever possible, the elastic computed forces were compared with the design forces and/or the estimated ultimate capacity of the structures reviewed.

The conclusion of this review is that the inelastic energy absorption capability of the structure, and the duration of strong ground motion both influence structural performance and one cannot totally rely on the elastic computed forces in determining structural performance. The onset of significant structural damage for structures which had some seismic design was predominantly due to either:

1. Inadequate design, detailing, or construction necessary to achieve a ductile design. In other words, the structure had features which do not meet a strict interpretation of the intended provisions in the current Uniform Building Code for achieving a ductile design.

2. The structure contained "weak links" such that inelastic energy absorption was not spread throughout the structure but was very localized. In other words, the ratio of elastic computed forces (demand) to estimated ultimate capacity was far from uniform throughout the structure.

These factors appear to have at least as much and probably more influence on the ground motion level at which significant structural damage occurs than does the average ratio of elastic computed demand to estimated ultimate capacity.

As discussed in Appendix A, the ratio of elastic computed demand to capacity was evaluated for a number of structures for the 1971 San Fernando earthquake. So long as the structure did not suffer from one of the above two deficiencies, minor structural damage did not appear to occur at elastic demand to capacity ratios less than about 1.5. Similarly, significant structural damage did not appear to occur at elastic demand to capacity ratios less than about 2.5. These estimates represent lower bounds and were significantly exceeded in some cases without the corresponding damage. For instance, in the case of the Veterans Administration Hospital Building #41, the elastic demand to capacity ratio exceeded 3 with essentially no structural damage. However, this lack of even minor damage appears to be heavily influenced by beneficial nonlinear soil-structure interaction effects.

The ratio of elastic demand to capacity will be referred to as the reduction factor or the input scale factor, F, in subsequent chapters of this report. This factor F represents the factor by which the elastic computed response must be divided before being compared with the yielding capacity for the purpose of predicting a given level of structural damage. Alternately, F represents a scale factor by which the ground motion can be increased beyond that which corresponds to an elastic response equal to the structural yielding capacity.

The reduction factor, F, associated with the onset of significant structural damage appears to be influenced by the duration of strong shaking. The following statements are keyed to durations T_D' defined by Equation 1-5 for consistency. It was noted above that for the 1971 San Fernando records ($T_D' \approx 5$ to 6 seconds) the reduction factor, F, corresponding to the onset of significant structural damage was at least 2.5. Similarly, F corresponding to the onset of significant structural damage would also appear to have been at least 2.5 for the 1952 Kern County ($T_D' \approx 10$ seconds) and the 1972 Managua earthquakes. However, correlation with the onset of structural damage for well-designed buildings would appear to require larger F factors for the 1978 Santa Barbara ($T_D' \approx 3$ seconds), the 1979 Imperial Valley (generally T_D' between 3 and 5 seconds for records exceeding 0.2g), the 1966 Parkfield ($T_D' < 2$ seconds), and the 1972 Ancona ($T_D' < 2$ seconds) earthquakes. The sketchy nature of the data does not enable the increase in F to be quantitatively defined. However, the summation of damage data strongly suggest that F corresponding to the onset of significant structural damage is larger for records with strong durations less than about 5 seconds. Strong durations less than about 5 seconds reduce the damage potential of a given level of ground shaking.

In summary, the literature review clearly indicates that the characterization of ground motion by low-damped (10% and lesser damping) elastic response spectra is insufficient to define the structural damage potential of the ground motion. One must also consider the inelastic

energy absorption capability of the structure and the strong duration of the ground motion particularly for records with strong durations by Equation 1-5 of less than 5 seconds. The inelastic energy absorption reduction factor, F, appears to be at least 2.5 prior to the onset of significant structural damage for well-designed structures and earthquake strong durations greater than 5 seconds. These observations form the impetus for the analytical studies reported in subsequent chapters.

1.3   CHARACTERIZATION OF STRUCTURE DAMAGE

This study concentrates on predicting nonlinear response of stiffness degrading shear wall and braced frame structures with fundamental frequencies in the amplified spectral acceleration region from 1.8 to 10 Hz. These structure types and fundamental frequencies are typical of those found in nuclear power plants.

Representative shear force versus deformation diagrams for shear walls and braced frames undergoing multiple cycles of deformation are shown in Figure 1-9. The structural element retains its initial stiffness and strength characteristics up to the first nonlinear cycle. After the first nonlinear cycle, the structure loses stiffness and strength. Thus, each subsequent nonlinear cycle ratchets the structure to greater total nonlinear deformations. A short duration ground motion is likely to result in only one nonlinear cycle. With a long duration record, multiple nonlinear cycles occur and each subsequent cycle results in greater deformation. Thus, one effect of a longer duration ground motion is to result in greater total deformations than occur from a short duration ground motion for a stiffness and strength degrading structure.

For this study, a quantitative description of damage was required. Basically, damage can be generally related to:

1.   Displacement ductility which is defined as the ratio of maximum deformation to yield deformation.

2.   Total hysteretic energy absorbed during nonlinear cycles.

For moment frames and inelastic hinge rotations, the total hysteretic energy absorbed during nonlinear cycles probably best accounts for the cumulative damage that may occur as a result of reversed inelastic deformations.

However, for degrading stiffness and degrading strength shear walls and braced frames, the displacement ductility also describes cumulative damage because each nonlinear cycle results in increased deformation or displacement ductility over the previous nonlinear cycle (see Figures 1-5, 1-6 and 1-9). Thus, the maximum displacement ductility reached provides a measure of the cumulative damage up to that point. Furthermore, a study of multiple cycle force-deformation diagrams such as those shown in Figure 1-9 tends to indicate that strength degradation is minor until a certain displacement ductility is reached. Beyond the displacement ductility, strength degradation increases rapidly with additional nonlinear cycles. This displacement ductility at which strength degradation tends to increase rapidly with subsequent cycles can be considered to represent the onset of significant structural damage. Thus, if the onset of significant structural damage is considered to represent the limit of acceptable structural performance, the displacement ductility probably represents the better descriptor of permissible damage. Collapse would generally require additional nonlinear cycles resulting in substantial strength degradation after the permissible displacement ductility is reached. Therefore, hysteretic energy absorption for nonlinear cycles after the permissible displacement ductility is reached probably provides the best descriptor of collapse for shear walls and braced frames. Additional research is necessary on this subject.

For nuclear power plant structures, deformations beyond the onset of significant structural damage would generally not be considered acceptable. Therefore, within this study, a limit on permissible displacement ductility is used as a measure of acceptable structural performance.

The use of permissible displacement ductility as the descriptor of structural performance introduces some conservative bias to this study for short duration records. A short duration ground motion could result in the permisible displacement ductility being reached without the ground motion time history having sufficient remaining strong motion duration to lead to the rapid strength degradation from subsequent nonlinear cycles necessary for collapse. Thus, the short duration record could lead to the permissible displacement ductility being reached without the structure being at the onset of collapse because of insufficient duration to the ground motion record. On the other hand, for a long duration record, reaching the permissible displacement ductility would indicate the structure was at the onset of collapse from rapid strength degradation during subsequent nonlinear cycles.

In other words, the use of a permissible displacement ductility as a measure of damage may overemphasize the ability of short duration ground motion records to damage shear wall and braced-frame structures. However, this potential conservatism in evaluating the effect of short duration records was judged desirable because of the lack of understanding on the relative importance of hysteretic energy absorption versus displacement ductility in leading to damage. Even so, the reader should note that this study may overemphasize the ability of short duration earthquakes to damage shear wall and braced-frame structures.

The response of nonlinear systems can be best represented graphically by means of a modified response spectrum to reflect the effect of nonlinear behavior (called herein an <u>inelastic yield spectrum</u>).* Consider the structural <u>resistance function</u> (or primary load-deflection curve), as shown in Figure 1-10(a). In this case, the total deformation of the system is specified as a multiple of the yield deformation, $\delta_m = \mu \delta_y$.

---

* The term "inelastic yield spectrum" is somewhat of a misnomer but will be used herein because of its common usage in the literature.

The factor μ represents the displacement ductility. For the response of a single-degree-of-freedom system, the yield level spectral acceleration, $SA_y = \omega^2 \delta_y$, multiplied by the mass, gives the yield resistance level, $V_y = M\omega^2 \delta_y = K\delta_y$. The inelastic yield spectrum is a plot of the yield level spectral acceleration versus the corresponding system elastic frequency, as indicated in Figure 1-10(b). If the system had remained linear, then the system response would be the elastic deformation, δ_e, and the corresponding spectral acceleration level would be given by $SA = \omega^2 \delta_e$. The yield level spectral acceleration may then be considered as a reduced elastic level response or, $SA_y = SA/F$, where F is the reduction factor (Application A). If δ_y is considered to be the elastic response level associated with the input motion $\ddot{y}$, then $\delta_m = \mu\delta_y$ is the response level which results from the scaled input motion, $\ddot{y} \times F$ (Application B). Thus, F may be viewed as either an input scale factor (Application B) or as a reduction factor (Application A) depending upon application viewpoint. It should be noted that the inelastic yield spectrum is associated with a given level of peak deformation as specified by the ductility ratio (Application A). Given a deformation damage measure, the inelastic yield spectrum or input scale factors provide the format for comparing input motions on the basis of equal inelastic structural response. Thus, for a permissible displacement of ductility, the inelastic yield spectrum represents the "effective" response spectrum. The definition of equal-damage response spectra allows two records with the same effective spectral acceleration at a structural natural frequency to cause the same level of nonlinear structural response.

1.4   OBJECTIVE OF THIS STUDY

In the previous subsections it was shown that the low-damped elastic spectral response does not provide a consistent descriptor of damage for short duration versus long duration ground motion records. The elastic spectral response would indicate much greater damage to a 5 Hz structure from the very short duration Melendy Ranch record than from the long duration Taft record (see Figure 1-7). Yet, a detailed nonlinear analyses of a nuclear power plant structure showed that if this plant was

designed for the 0.18g Taft record, the structure would not be seriously
damaged by the 0.52g Melendy Ranch record because it only undergoes one
cycle of nonlinear deformation. There is insufficient energy content in
the short duration record to ratchet a degrading stiffness structure to
failure.

The objective of this study was to determine what ground motion
characteristics do provide a good descriptor of damage for degrading
stiffness ductile structures such as those found in nuclear power plants.
Thus, this study will define a procedure for developing "effective"
spectral responses such that two ground motion records with the same
"effective" spectral responses at the structures natural frequency will
lead to the same displacement ductility. Thus, using the "effective"
response spectra as input to an elastic analysis and design will result
in the permissible system displacement ductility being reached for both
actual time histories.

These "effective" response spectra then serve as a means of
describing the relative damage capability of different ground motion time
histories and thus serve as a means of providing an engineering character-
ization of the ground motion. The characterization of the ground motion
by "effective" spectral responses provides a better engineering character-
ization of the ground motion than does the instrumental peak acceleration,
or the elastic spectral responses.

It will be shown that the "effective" spectral responses can be
approximated by the highly-damped average spectral acceleration over a
frequency range to the soft (flexible) side of the elastic natural
frequency. Thus, the highly-damped spectral acceleration within this
frequency range can serve as a method of providing an engineering charac-
terization of the ground motion. Details will be presented in subsequent
chapters.

This study is concerned with the inelastic response of structural systems (braced frames and shear walls) and the concept of "effective" spectral response is considerd valid for such systems. The results of this study can also probably be extrapolated to ductile passive equipment whose fragility is governed by structural failure modes. However, the study is probably not appropriate for active equipment.

1.5   STUDY APPROACH

The study effort was subdivided into three major subtasks: (1) analytical studies to develop an estimation procedure for inelastic yield spectra; (2) a demonstration of "effective" ground motion comparisons on the basis of equal damage; and (3) a literature review to document and evaluate the observed performance of structures during past damaging earthquakes. The major study effort was associated with the analytical subtask. The analytical studies were further subdivided into the following study increments:

(a)   The selection and evaluation of a group of strong motion records which encompass a wide range of possible free-field input motions.

(b)   A review of the inelastic behavior of primary power plant structural configurations and components.

(c)   The definition of a set of representative structural system models with the overall nonlinear response behavior attributed to power plant structural types.

(d)   The development of an analysis procedure for determination of reduction factors based upon input scaling.

(e)   The determination and evaluation of a set of input scale factors (reduction factors) which correspond to two different damage (deformation) levels.

(f)   The development and correlation of an input scale factor or reduction factor estimation procedure.

(g)   The development of "effective" spectra using this reduction factor procedure.

1.6   REPORT OUTLINE

The ground motion records used in this study are described in Chapter 2. Engineering characterization defining both the time and frequency characteristics of these records are presented and discussed. Minimum engineering characterizations to define elastic response of these records are discussed.

The structural models and analytical approach used in this study are presented in Chapter 3. The primary structural model used consisted of a degrading stiffness, degrading strength, pinched behavior shear wall model developed to closely approximate the shear wall behavior shown in Figure 1-9. This model was specified as having 7 percent elastic damping. Nonlinear response of such models with initial (elastic) natural frequencies of 2.1, 3.2, 5.3, and 8.5 Hz was studied. These natural frequencies are approximately equally-spaced within the frequency range from 1.8 to 10 Hz which covers the range of fundamental frequencies for the majority of nuclear power plant building structures. The study concentrated on predicting the nonlinear reduction factor, F, associated with ductility ratios of 1.85 and 4.3. These ductility ratios were considered to represent lower bounds on the onset of minor structural damage and the onset of significant structural damage, respectively.

Model parameter variation studies were also conducted (Appendix D). For a few cases, damping was reduced to 3 percent elastic damping to determine the effect of elastic damping on the reduction factor. The nonlinear force-deformation characteristics were modified to study the effect of such characteristics. Lastly, a few cases were also analyzed for a nonlinear model representing the braced-frame characteristics in Figure 1-9.

The study results are presented in Chapter 4 in terms of response reduction factors, F, obtained from a series of nonlinear analyses using the ground motions and structure models described in Chapters 2 and 3. Statistical studies performed on these reduction

factors are presented. A method to derive these reduction factors from the characteristics of the elastic response spectra and the structural model is presented.

A method to define an "effective" response spectrum using the results of Chapter 4 is presented in detail in Chapter 5. This method requires only a knowledge of the nonlinear characteristics of the structure model and the elastic response spectra. "Effective" response spectra are presented for the ground motion time histories studied.

The relative strengths of the ground motion records used in this study in terms of elastic ($\mu = 1.0$) and inelastic ($\mu = 1.85$ and 4.3) structural response for stiff structures ($f = 1.8$ to 10 Hz) are described in Chapter 6.

Lastly, conclusions from these analytical studies are summarized in Chapter 7.

TABLE 1-1

INSTRUMENTAL PEAK VERSUS DESIGN ACCELERATIONS

Earthquake Records		Instrumental Peak Accel.[*] A_{IP} (g)		Elastic Response Design Accel. A_D (g)		Strong Duration T_D''(Sec)
		Uncorrected	Corrected	$1.25*A_{3F}$	K_p*RMS	
Melendy Ranch	N61E	.50	.48	0.40	0.36	1.2
	N29W	.70	.52	0.45	0.34	1.5
Parkfield, Cholame #2	N65E	.51	.49	0.50	0.41	4.4
Temblor	S25W	.41	.35	0.26	0.26	4.2
Pacoima Dam	N76W	1.25	1.07	0.78	0.78	5.7
Hollywood Storage	S00W	.19	.17	0.15	0.15	9.3
PE Lot	N90E	.22	.21	0.21	0.19	9.0
El Centro 1940	NS	.37	.35	0.30	0.28	13.1
Olympia	N86E	.31	.28	0.21	0.21	13.1
Taft	S69E	.20	.18	0.14	0.14	16.1

* As reported by California Institute of Technology
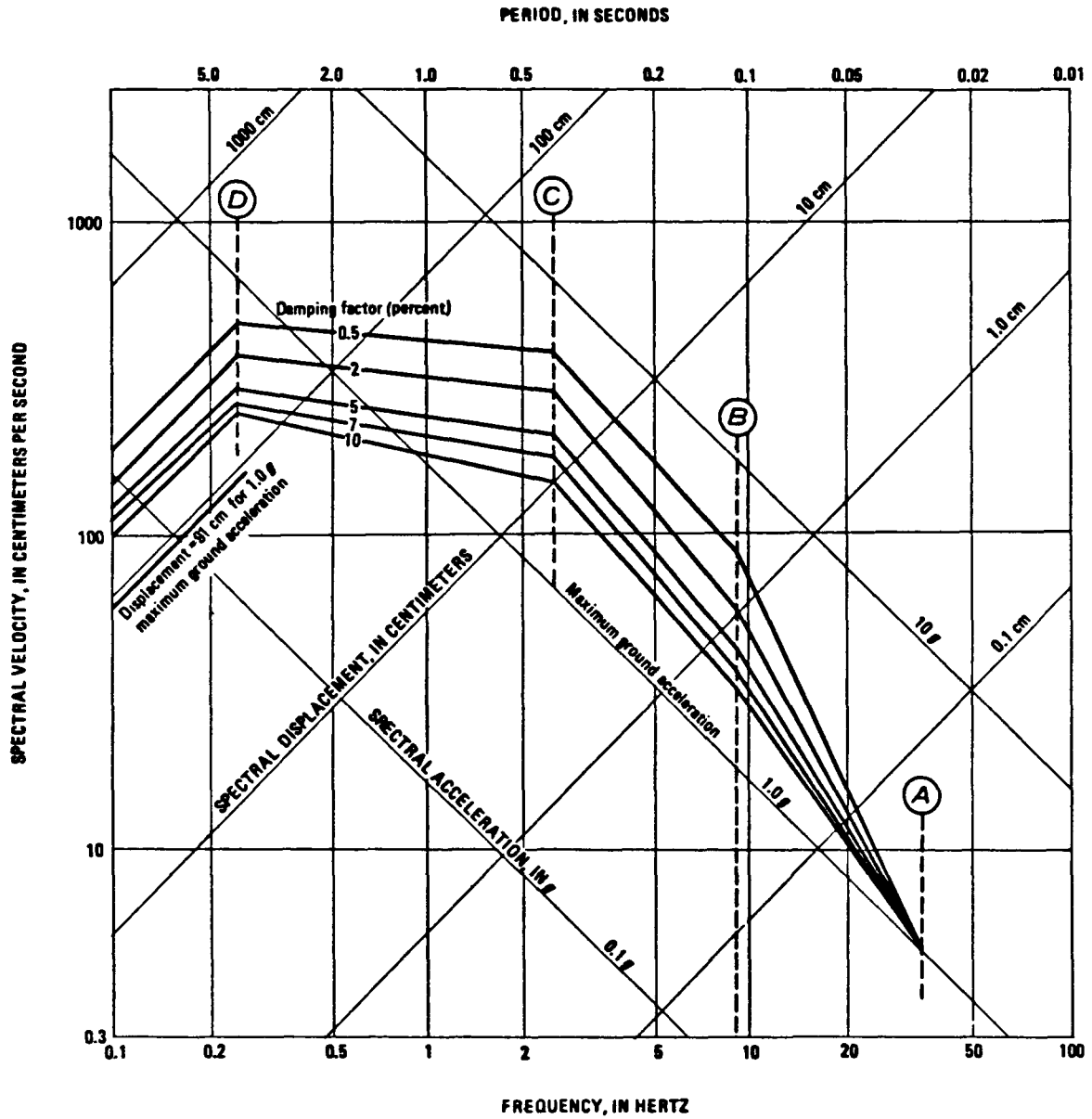
FIGURE 1-1.   SITE-INDEPENDENT HORIZONTAL RESPONSE
SPECTRUM SCALED TO 1.0g [USNRC (1973a)]
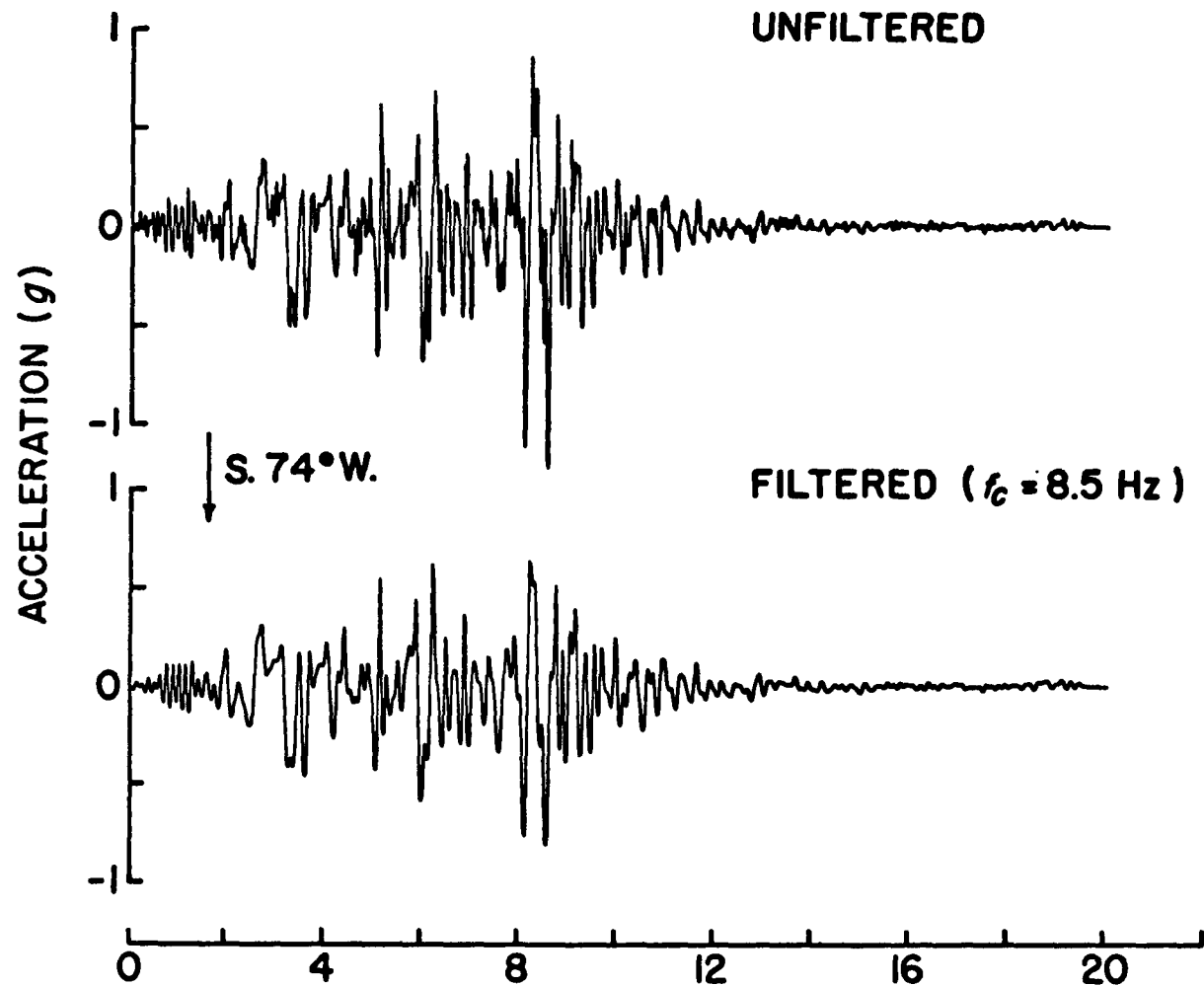
FIGURE 1-2. UNFILTERED AND FILTERED ACCELEROGRAMS OF THE 1971 SAN FERNANDO EARTHQUAKE FROM THE S. 74° W. ACCELEROGRAPH COMPONENT AT PACOIMA DAM. RESPONSE OF FILTER IS 1.0 AT FREQUENCIES LESS THAN 8 HZ AND 0.0 AT FREQUENCIES GREATER THAN 9 HZ WITH A HALF-WAVE COSINE TAPER FROM 8 TO 9 HZ. (PAGE AND OTHERS, 1972).
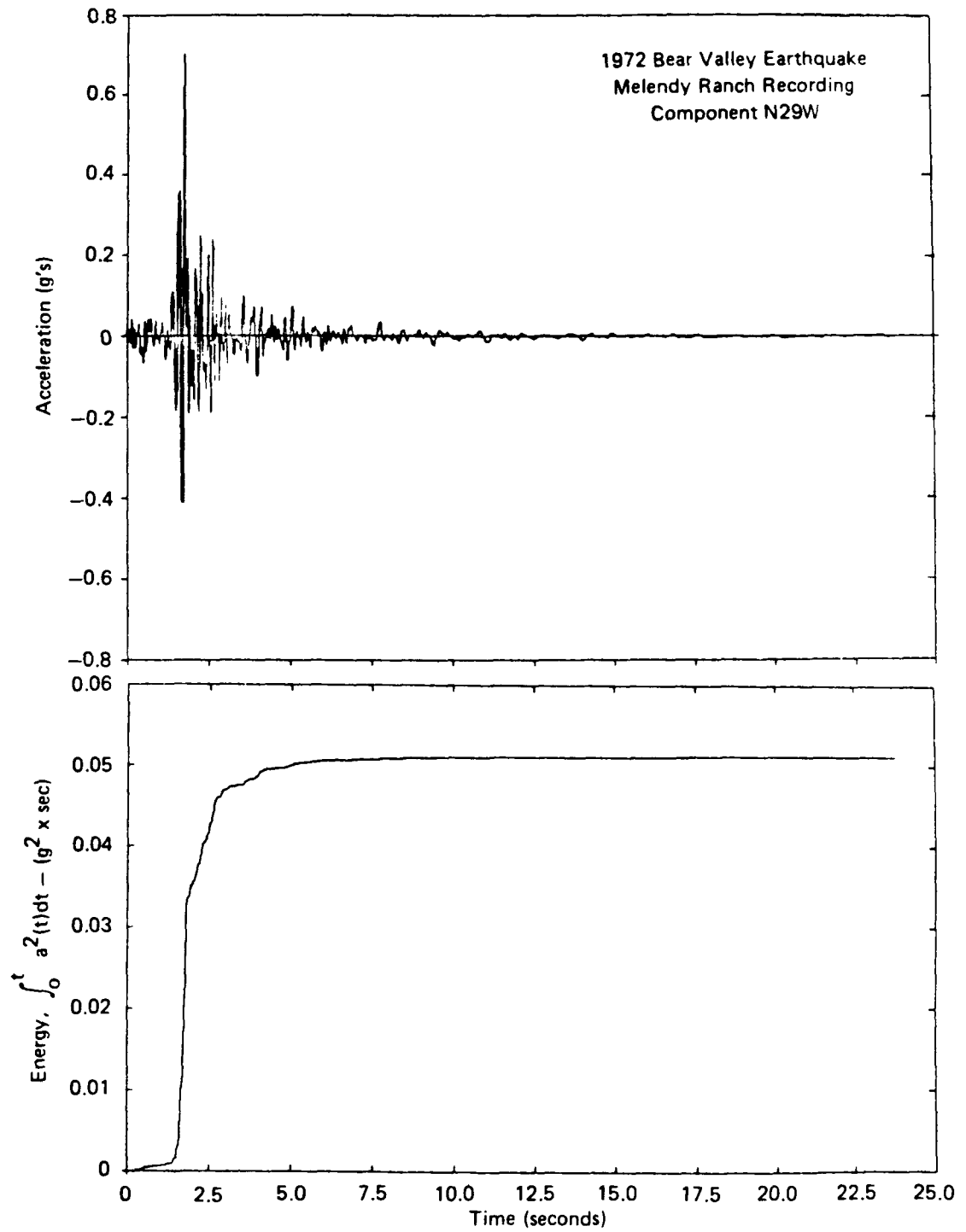
FIGURE 1-3.   ACCELERATION AND VARIATION OF CUMULATIVE ENERGY
WITH TIME FOR THE 1972 BEAR VALLEY EARTHQUAKE
RECORDING AT MELENDY RANCH
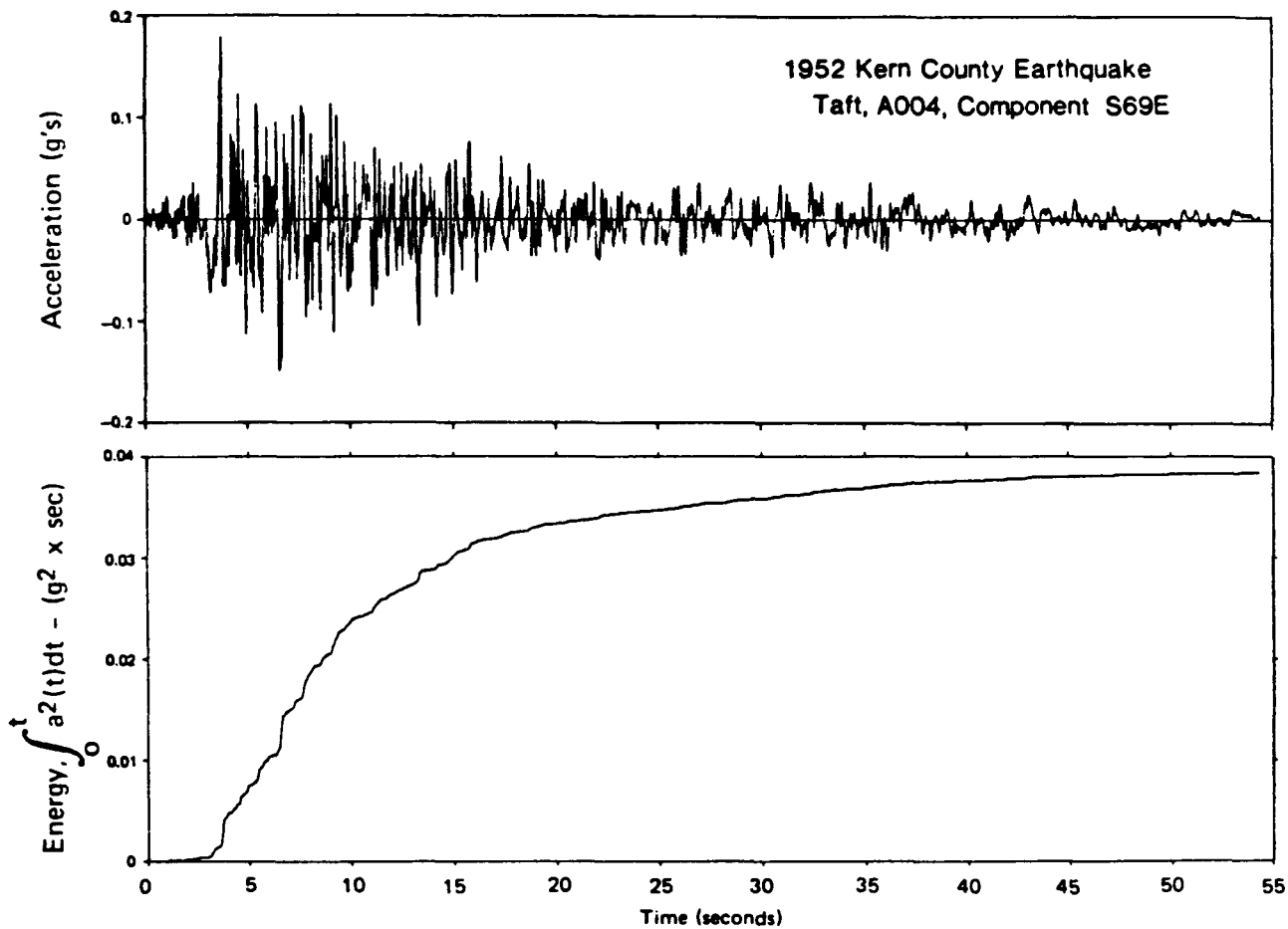
FIGURE 1-4. ACCELEROGRAM AND VARIATION OF CUMULATIVE ENERGY WITH
TIME FOR THE 1952 KERN COUNTY EARTHQUAKE RECORDING AT TAFT
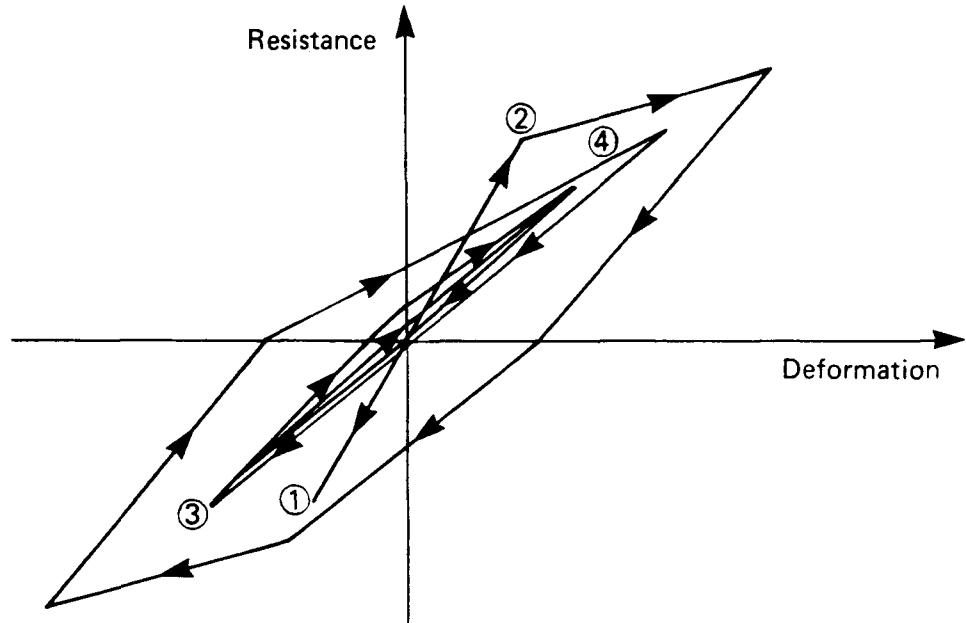
FIGURE 1-5.   SEISMIC SHEAR FORCE-DISPLACEMENT RELATION FOR STRUCTURAL
MEMBER WHICH SHAKES DOWN TO PSEUDO-ELASTIC BEHAVIOR
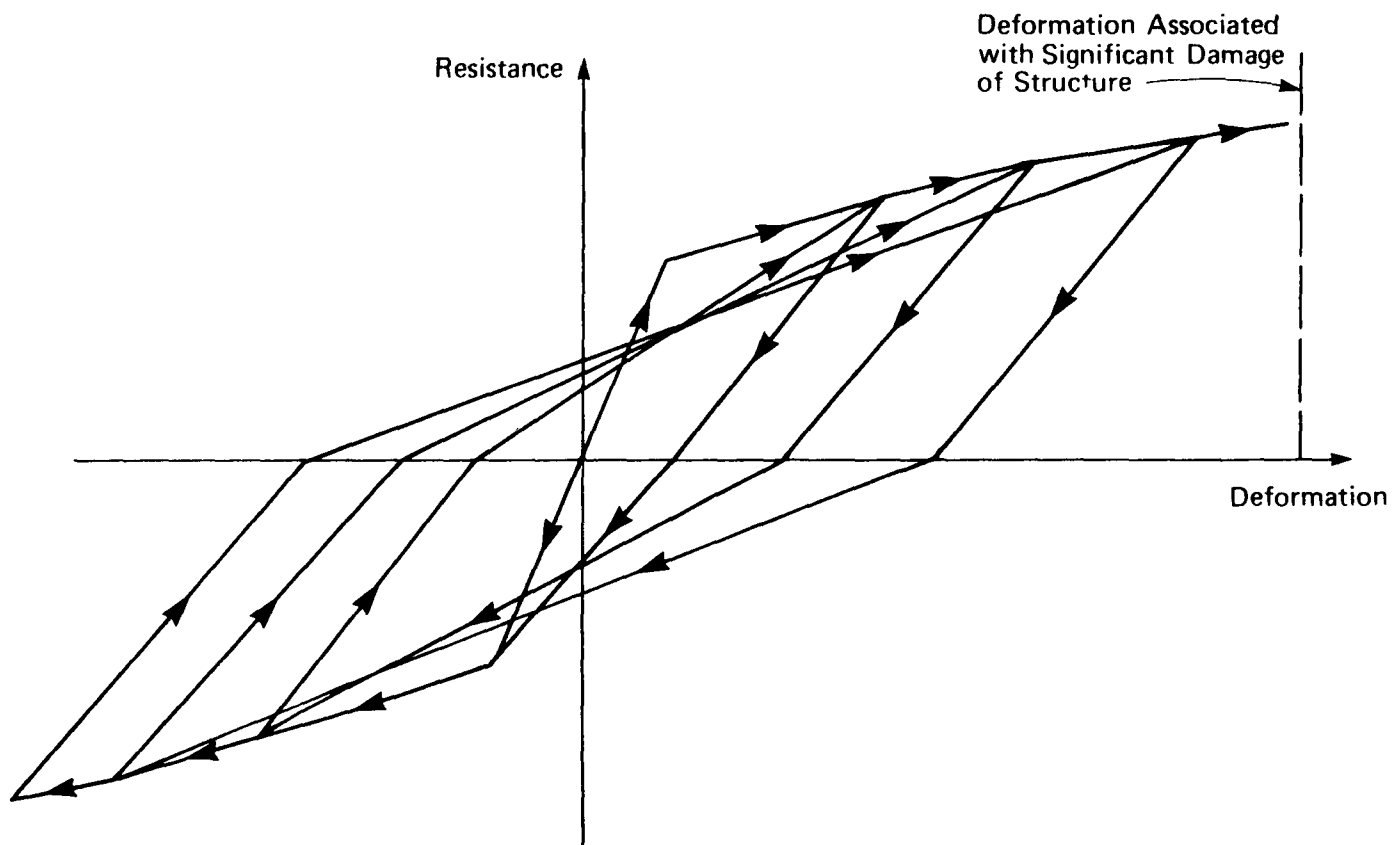
FIGURE 1-6.   SEISMIC SHEAR FORCE-DISPLACEMENT RELATION FOR STRUCTURE MEMBER WHICH
               PROGRESSIVELY CYCLES TO DEFORMATION CORRESPONDING TO SIGNIFICANT DAMAGE
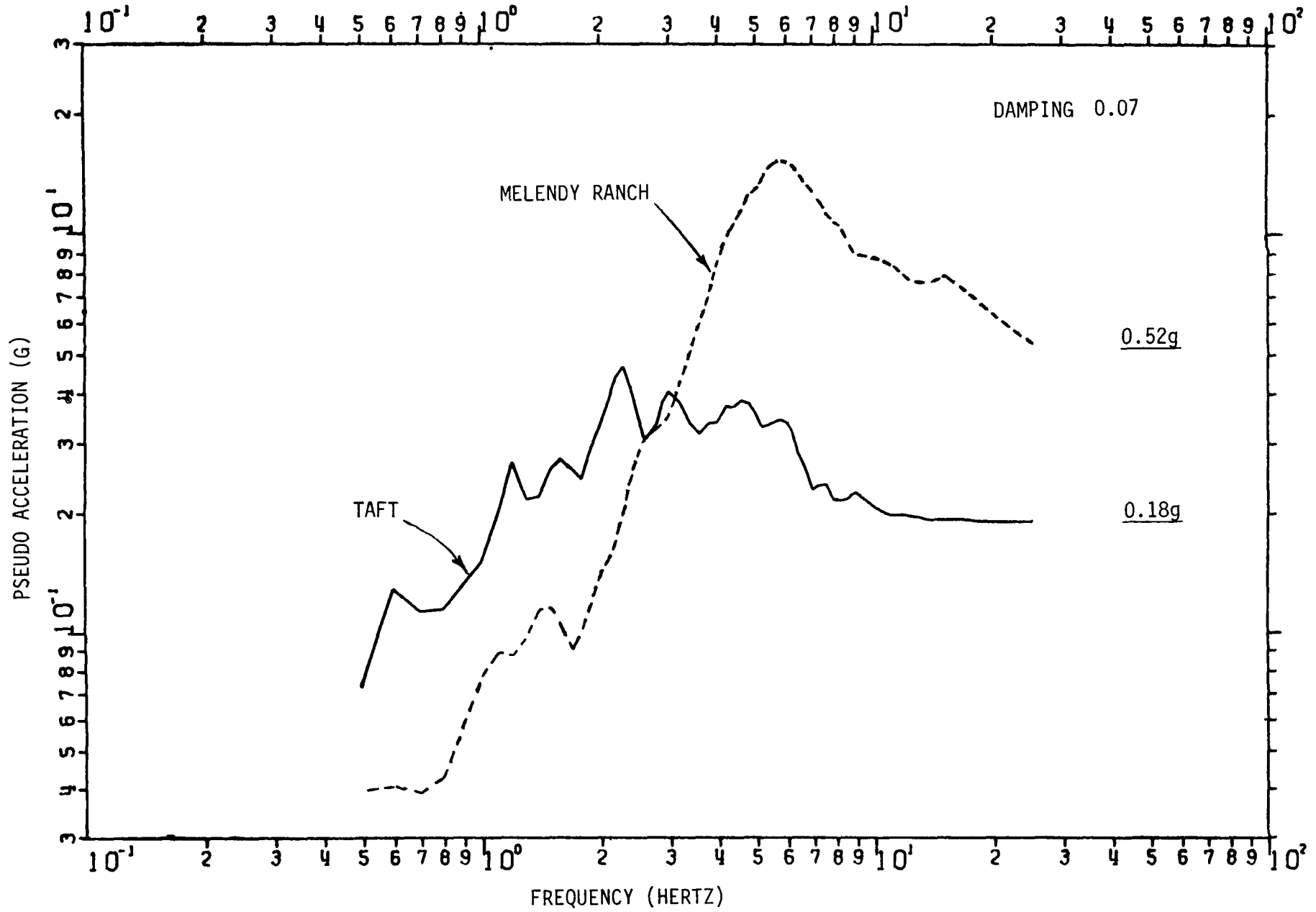
FIGURE 1-7. COMPARISON OF MELENDY RANCH AND TAFT RESPONSE SPECTRA
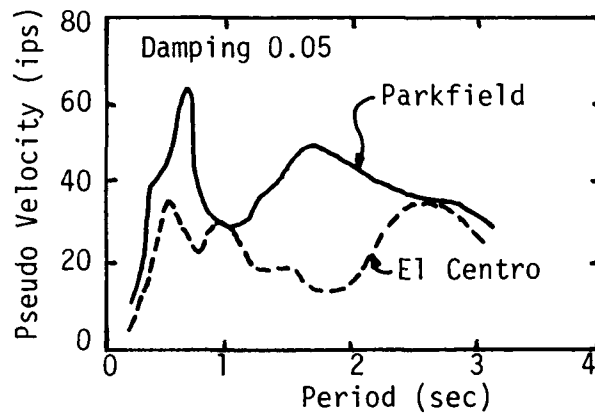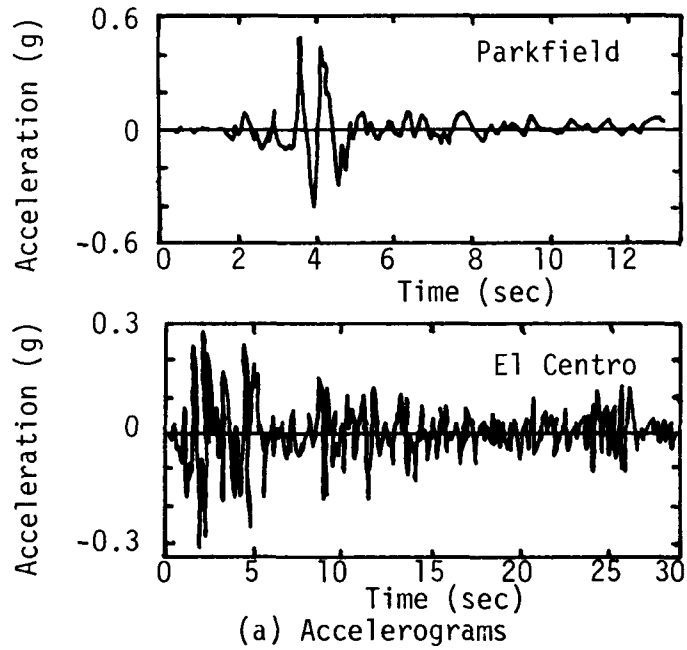
FIGURE 1-8.   GROUND RESPONSE CHARACTERISTICS FROM PARKFIELD CHOLAME #2
(1966) AND EL CENTRO (1940) EARTHQUAKE RECORDS
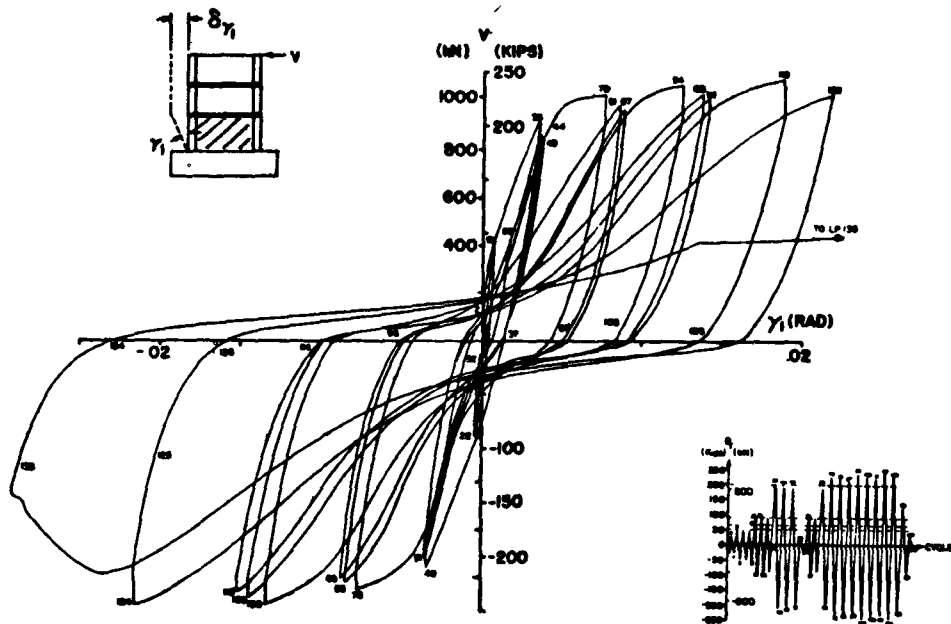
(a) Shear force-shear distortion diagram for structural concrete wall test (Wang, Bertero, Popov; 1975)
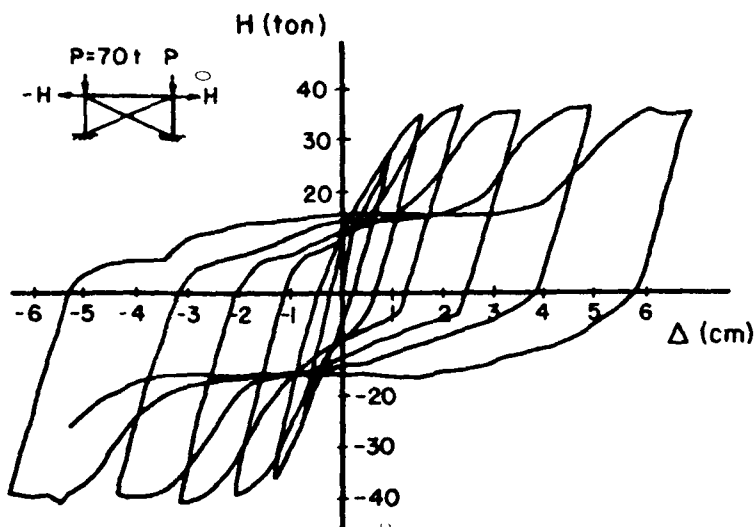
(b) Lateral force-displacement diagram for braced-steel frame (Wakabayashi; 1973)

FIGURE 1-9. CYCLIC LOAD-DEFLECTION BEHAVIOR OF REPRESENTATIVE POWER PLANT STRUCTURAL ELEMENTS

$$\omega^2 = \frac{K}{M}$$

Factored Seismic Input

Application (B)

$$M\ddot{u} + K\,u = -M\ddot{y} \times 1 \longrightarrow \delta_y$$

$$M\ddot{u} + K\,u = -M\ddot{y} \times F \longrightarrow \delta_e$$

$$M\ddot{u} + V(u) = -M\ddot{y} \times F \longrightarrow \mu\delta_y$$

Application (A)

$$M\ddot{u} + K\,u = -\frac{M\ddot{y}}{F} \longrightarrow \delta_y$$

$$M\ddot{u} + K\,u = -M\ddot{y} \longrightarrow \delta_e$$

$$M\ddot{u} + V(u) = -M\ddot{y} \longrightarrow \mu\delta_y$$

$V_e = M\,SA$

$V_y = M\,SA_y$
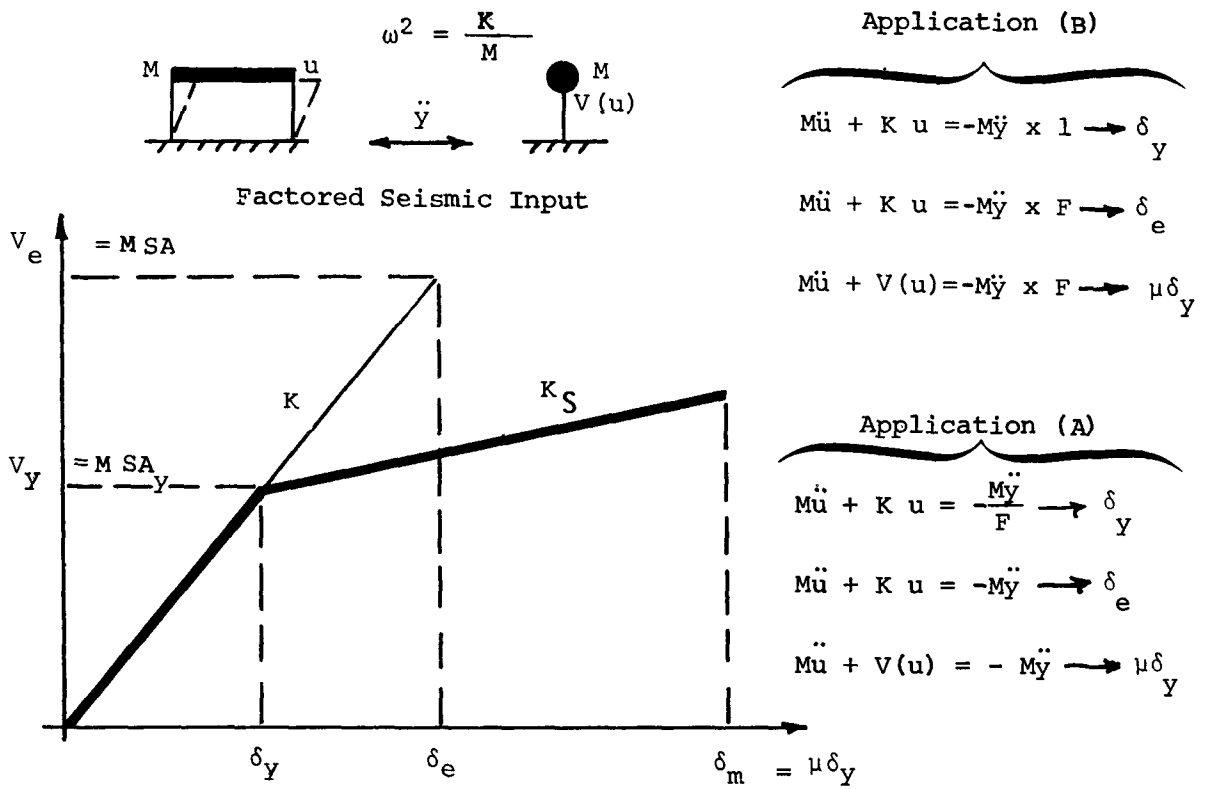
(a) Structural Resistance Function for Single-Degree-of-Freedom Representation of Overall Structural Behavior

$$SA = FSA_y \quad \text{(Application B)}$$
$$SA = \omega^2\delta_e \quad \text{(Application A)}$$

$$SA_y = \omega^2\delta_y \quad \text{(App. B)}$$

$$SA_y = \frac{SA}{F} \quad \text{(App. A)}$$

Elastic Spectrum

Inelastic Yield Spectrum

$SA = \omega^2 \delta \cdot (\log SA)$

$(\log f)$

$f_1 = 1.8\ \text{Hz}$ $f_2 = 10\ \text{Hz}$ f_{rigid}

Range of Interest for Nuclear Structures
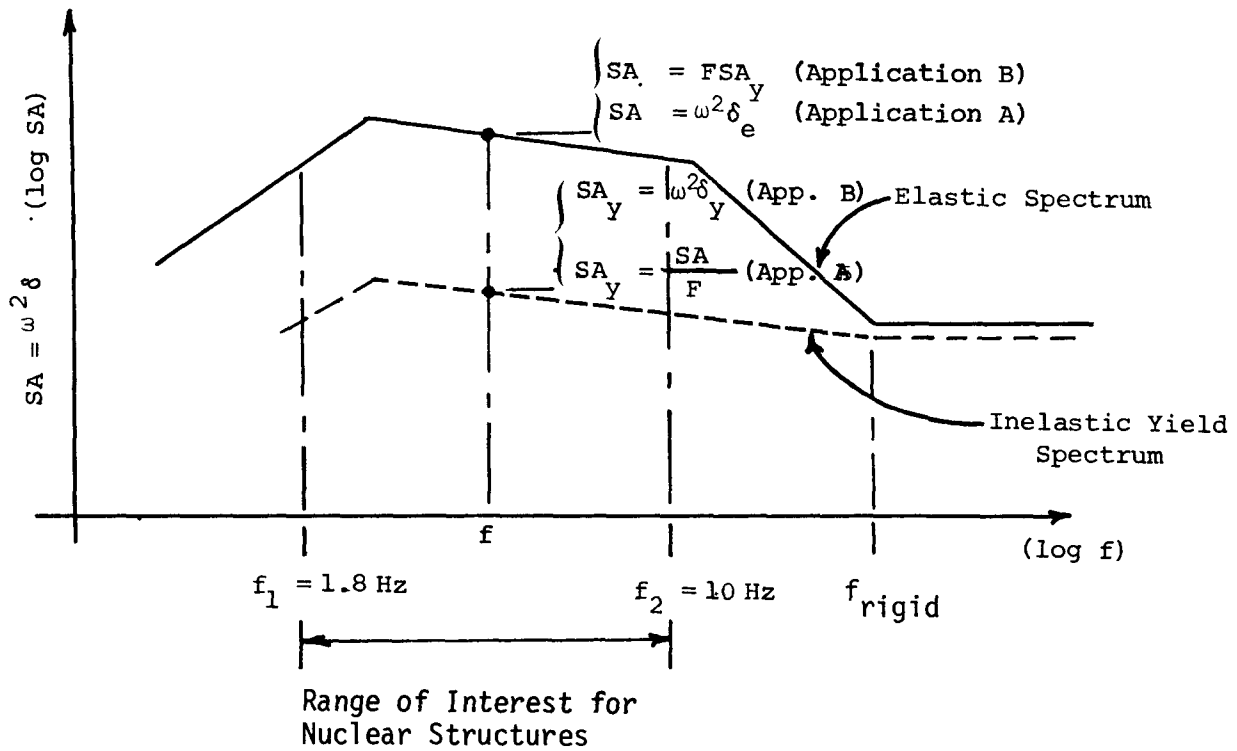
(b) Inelastic Yield Spectrum

FIGURE 1-10.   DEFINITION OF STRUCTURAL RESISTANCE FUNCTION AND CORRESPONDING INELASTIC YIELD SPECTRUM

2. ENGINEERING CHARACTERIZATION OF GROUND MOTION
FOR RECORDS STUDIED

Eleven real earthquake ground motion time histories and one artificial earthquake time history were used in this study. The eleven real records used are defined in Table 2-1. Throughout the study, the record will be designated by the underlined name in Table 2-1. On some figures, an abbreviated symbol will be used for each record. The names and symbols used for these 11 records are: Taft (T), Olympia (O), El Centro No. 12 (EC12), El Centro No. 5 (EC5), Pacoima Dam (PD), Hollywood Storage (HS), Coyote Lake (CL), Parkfield (PA2), Gavilan College (GC), Goleta (G), and Melendy Ranch (MR). The Artificial (A) time history was a 0.2g ground motion which approximated, at low damping, the NRC Regulatory Guide 1.60 response spectrum anchored to 0.2g and had a duration of approximately 20 seconds. It is typical of some of the more realistic artificial time histories used in nuclear power plant dynamic analyses.

Table 2-1 presents the earthquake name and date, the local magnitude, M_L, the surface-wave magnitude, M_S, the recording station, its distance from the fault trace on which the earthquake was located, and the corrected peak ground acceleration, a, and velocity, v. All time history inputs utilized herein have been corrected and processed using the routine processing procedures outlined by Hudson (1979). The corrected peak ground velocity reported was obtained by integrating the corrected acceleration record.

These real earthquake records were selected in order to have a wide variation in ground motion characteristics. Local magnitudes range from 4.7 to 7.2 with fault rupture distances ranging from less than 1 Km to 40 Km. The corrected peak accelerations vary between 0.14 and 1.17g with corrected peak velocities ranging from 1.6 to 44.6 in/sec. Figure 2-1 presents acceleration time history plots of these 11 real records

plus the artificial record. All time histories have been normalized to a peak acceleration of 0.5g in Figure 2-1 in order to make duration comparisons easier. These plots are ordered by decreasing duration of strong motion. The Olympia, Taft, El Centro #12, and Artificial records represent long strong motion duration records. The Pacoima Dam, Hollywood Storage, El Centro #5, and Goleta records are of moderate duration. The Coyote Lake, Parkfield, Gavilan College and Melendy Ranch records have short strong motion durations. The generally expected range of strong motion durations of earthquakes with magnitudes from 4.5 through somewhat over 7.0 are covered by the 12 time histories used in this study. The very long strong motion durations which might occur from great earthquakes with surface wave magnitudes greater than 8.0 are not covered by this study.

Plots of the following detailed ground motion characteristics are presented in Appendix B for each of these 12 records:

1. Acceleration time history

2. Cumulative energy

3. 7, 10, 15, 20 and 25% damped-elastic response spectra

4. Elastic response time histories for 2, 5, and 8 Hz, 7% damped oscillator

5. Fourier spectra for the strong motion portion of the accelerogram

6. Cumulative spectral density functions for the strong motion portion of the records.

These plots fully define the time duration, frequency characteristics, elastic response characteristics, and energy characteristics of these records. A careful study of these plots will show the wide variation of ground motion characteristics in the 2 to 8 Hz frequency range included in this study. All of these plots are ordered in descending order from the longest duration record (Olympia) to the shortest duration record (Melendy Ranch). Data presented in these plots will be discussed in subsequent subsections.

2.1   ENERGY, POWER, AND DURATION CONTENT

The total energy E_m (more correctly defined as the Fourier energy) of the record is defined by Equation 1-2 integrated over the full duration of the record. A cumulative energy plot is simply a plot of E(T) versus time, T, where E(T) is defined by Equation 1-2 integrated from time zero to time T.

Housner and Jennings (1977), have demonstrated that $\frac{\pi}{2} E_m$ may be interpreted as the "frequency ensemble work" and is a measure of the capacity of the ground motion to do work on an idealized <u>uniform</u> population of structures of <u>all</u> natural frequencies. For this reason, Arias (1970 suggested using $\frac{\pi}{2g} E_m$ as a measure of seismic intensity and such is defined as the Arias Intensity. One might thus consider E_m or Arias Intensity to be a measure of the damage potential of a ground motion record for a uniform population of structures over all frequencies. As can be seen from the plots in Appendix B, the total energy, E_m, is very poorly correlated with the peak ground acceleration, a. This is one of the reasons why peak ground acceleration alone does not provide a good measure of damage. For instance, Figure 2-2 compares the Olympia and Melendy Ranch records. Melendy Ranch has a corrected peak acceleration 1.85 times that of Olympia. Yet, the total energy for Melendy Ranch is only 56% of that for Olympia.

The most common definition of strong motion duration is that due to Trifunac and Brady (1975). By this definition, the strong motion duration is defined as:

$$T_D = T_{0.95} - T_{0.05} \qquad\qquad (2-1)$$

where $T_{0.95}$ represents the time at which $E(T)/E_m = 0.95$ and $T_{0.05}$ represents the time at which $E(T)/E_m = 0.05$. Thus, this duration window includes 90% of the total cumulative energy. The time T_f can be defined as the f-fraction Husid time since it represents the time at which the f-fraction of the total energy has occurred.

However, for stiff structures (1.8 to 10 Hz) such as those in nuclear power plants, Equation 2-1 provides too long of an estimate of strong motion duration for many records. Many records contain a long tail of oscillatory ground motion with lesser accelerations at the end of the record which continues to input energy but at a substantially lesser rate than the earlier portion of the record. This situation is illustrated for the Taft record in Figure 2-3. Based upon Equation 2-1, the duration of the Taft record would be considered to be 28.1 seconds. Yet, 70% of the total energy is input in a duration T_D of only 9.9 seconds. Reporting the duration of the Taft record as 28.1 seconds would severely misrepresent its effective duration at least for stiff structures with frequencies over 2 Hz. Figure 2-4 compares the time history acceleration response of an example set of simple, damped-elastic oscillators (7% damping) obtained for representative long and short duration input motions. The example oscillators were tuned to 2, 5 and 8 Hz to encompass the range of elastic structure frequency considered in the study. The time of peak response, T_{max}, and the times, $T_{0.05}$ and $T_{0.75}$ are indicated for each example oscillator response shown in Figure 2-4. For the records and frequencies considered in Figure 2-4, the time of peak response, T_{max}, falls between $T_{0.05}$ and $T_{0.75}$. Thus, at least for stiff structures, a more appropriate and shorter definition of strong duration than that given by Equation 2-1 is needed.

In order to determine a more appropriate definition of strong duration, a study of the time of maximum response was conducted for all twelve earthquake time histories considered herein. The time of maximum response for both elastic and nonlinear structures representative of degrading stiffness and degrading strength shear walls was considered. Shear wall structure models with initial (elastic) natural frequencies of 2.14, 3.20, 5.34, and 8.54 Hz and 7% elastic damping were used. The time of maximum displacement response, T_{max} for elastic response ($\mu = 1.0$) and two levels of nonlinear response ($\mu = 1.9$ and $\mu = 4.3$) was determined for all four natural frequencies. The upper bound of maximum response time, $\overline{T}_{max}$, noted for the entire set of oscillators within a frequency range from 2.14 to 8.54 Hz (i.e., $\overline{T}_{max} = \max \left\{ T_{max} \right\}_i$) can be compared to

various Husid ratio times as tabulated in Table 2-2 for each of the 12 selected earthquake records. In Table 2-2, the time $T_{0.95}$, $T_{0.85}$, $T_{0.75}$, $T_{0.05}$ are the times associated with 95%, 85% 75% and 5% of the total cumulative energy. The time, T_{pa}, is the time associated with the first zero crossing of the accelerogram following the maximum positive or negative acceleration, whichever occurs later in time. From Table 2-2, it can be seen that an upper bound on the time of maximum response can be reasonably approximated by:

$$T_M = \max \left\{ \begin{array}{c} T_{0.75} \\ T_{pa} \end{array} \right\} \qquad (2\text{-}2)$$

In no case, was the actual upper bound on the time of maximum response more than 6% greater than that given by Equation 2-2.

Thus, Equation 2-1 was modified to provide the following definition of effective strong motion duration for stiff structures:

$$T_D' = T_M - T_{0.05} \qquad (2\text{-}3)$$

Equation 2-3 provides a better definition of the relative length of strong duration for stiff structures than does Equation 2-1.

With the strong duration defined by Equation 2-3, the Housner power (average rate of energy input) during this time can be defined by:

$$P = \frac{\Delta E}{T_D'} \qquad (2\text{-}4)$$

where ΔE represents the cumulative energy between time $T_{0.05}$ and T_M. Except for Olympia and Pacoima Dam, ΔE is equal to 70% of E_m since $T_m = T_{0.75}$. For Olympia and Pacoima Dam, T_{pa} exceeds $T_{0.75}$ and thus T_m exceeds $T_{0.75}$. For Olympia and Pacoima Dam, ΔE equals 85%, and 82%, respectively, of E_m.

The durations, T_D' and T_D, peak ground accelerations, a, peak ground velocity, v, effective total energy, ΔE, and average power, P, are tabulated in Table 2-3 for all 12 records studied. The records are ordered in terms of decreasing duration, T_D'. One should note the reasonably poor correlation between T_D' and T_D. These records would have been in a substantially different order if they had been ordered by T_D rather than T_D'. Thus, T_D does not serve as a good measure for the effective duration of strong shaking for stiff structures.

If the power of the cumulative energy plot is assumed to be approximately constant during the effective duration window, then the root-mean-square-acceleration, a_{rms}, is also approximately constant during this interval and can be given by:

$$a_{rms} = \sqrt{P} \qquad\qquad (2\text{-}5)$$

A review of the cumulative energy plots given in Appendix B for the 12 records considered in this study indicate that the assumption of constant power during the interval defined by Equation 2-3 is reasonable. The rms accelerations are tabulated in Table 2-3.

For stiff structures, the quantities T_D', a, v, ΔE, and P listed in Table 2-3 are judged to provide an adequate characterization of the ground motion in the time domain. It should be noted that only two of the quantities T_D', ΔE, and P need be defined. The third quantity follows automatically from Equation 2-4.

2.2   FREQUENCY CONTENT

2.2.1   Response Spectra
Structural analysts are most familiar with the frequency content of ground motion records being defined by their low-damped elastic response spectra. Elastic response spectra for all 12 records are presented in Figures B-2 of Appendix B. It is most informative to group these records into the following three groups in accordance with their effective duration:

1. Long Duration: $T_D' > 9$ sec.

2. Intermediate Duration: 2.5 sec. $\leq T_D' \leq 9$ sec.

3. Short Duration: $T_D' < 2.5$ sec.

This study considers four records in each group. The 7% damped elastic response spectra normalized to 1g ground acceleration are plotted in Figure 2-5 for each of the four records in each of the three groups and compared to the Regulatory Guide 1.60 response spectrum.

Table 2-4 lists the 7% damped spectral accelerations at 2.14, 3.20, 5.34, and 8.54 Hz for each of the records. In addition, Table 2-5 lists the v/a ratios, the maximum 7% damped spectral acceleration amplification factor (SA_m/a) and the frequency (f_a) at which this amplification occurs, the maximum 7% damped velocity amplification factor (SV_m/v) and the frequency (f_v) at which it ocurs, and the corner frequency* (f_{av}) between the amplified acceleration and amplified velocity regions. This corner frequency was defined by:

$$ f_{av} = \frac{SA_m}{2\pi SV_m} \tag{2-6} $$

The relationship between the corner frequency and the frequencies at which the spectral acceleration and spectral velocity peak is shown schematically in Figure 2-6. For short duration records such as Melendy Ranch, the spectral acceleration and spectral velocity peak at the same frequency. In this case, the corner frequency is equal to the frequency at which both spectral responses peak. For the longer duration records, the frequency, f_a, at which the spectral acceleration peaks is generally a factor of 2 or more greater than the frequency f_v at which the spectral velocity peaks. In these cases, the corner frequency is not as distinctly located. The corner frequency estimated by Equation 2-6 lies about midway between f_a and f_v.

---

* As used herein, the term "corner frequency" refers to the interaction of the amplified spectral acceleration and amplified spectral velocity regions. This definition is not the same as that used by seismologists.

Equation 2-3. Such spectra are presented in Figure B-4 through B-5 of Appendix B for the 12 time histories studied. The single-sided Power Spectral Density function, G'(f), is related to the Fourier amplitude, F'(f), by:

$$G'(f) = \frac{2|F'(f)|^2}{T'_D} \qquad (2-7)$$

where the primes are used to indicate that these functions are only evaluated within the time window defined by Equation 2-3. The Cumulative Spectral Density function (Cum G(f)) is obtained by integrating G'(f) from zero to the frequency f.

The differing frequency characteristics of the short duration records versus the long duration records is clearly indicated by the Fourier spectra in Figure B-4 or the Cumulative Spectral Density plots of Figure B-5. Table 2-6 lists the frequencies, f_{10}, f_{50}, and f_{90}, at which 10, 50, and 90%, respectively, of the cumulative power occurs for the 12 records studied. The range from f_{10} to f_{90} represent the frequency range within which 80% of the power is located. The frequency f_{50} represents the median frequency.

The five records with durations T'_D from 9.6 seconds to 3.4 seconds (El Centro #12 through El Centro #5) all have median frequencies between 2.15 and 3.3 Hz and contain significant power between at least 0.8 and 6.55 Hz. The two longest duration records (Olympia and Taft) have similar median frequencies but do have slightly lesser frequency bandwidths. Even so, these records cover frequency bands from at least 1.2 to 5.5 Hz.

As shown in Table 2-6, all five of the records with strong durations T'_D of 3.0 seconds and less are missing some of the frequency content of the longer duration records. Coyote Lake, Gavilan College,

2-10

and Melendy Ranch are missing frequency content below the 2.5 to 3.6 Hz
range. Parkfield is missing frequency content below 1.2 Hz. Both Goleta
and Parkfield are missing high frequency content above about 3 Hz.
Because of either missing low or high frequency content, Goleta, Coyote
Lake, Parkfield, and Melendy Ranch have very narrow amplified regions for
their response spectra as demonstrated in the previous section. The
breadth of the frequency bandwidth for Gavilan College is nearly as large
as those for Olympia and Taft but is much less than for the other longer
duration records. Furthermore, the median frequency for this record
differs substantially from that of the longer records having a much
higher median frequency because low frequency content is missing from
this record.

2.2.3   Moments of the Spectral Density Function

Vanmarcke (1972, 1975) has suggested that the moments of the
spectral density function can be utilized to provide a measure of the
frequency content of a given input motion. The terms λ_0', λ_1' and λ_2'
denote, respectively, the zero, first, and second moment of the spectral
density function as given by:

$$\lambda_0' = \text{zero moment} = \int_0^\infty G'(\omega)\,d\omega \tag{2-8}$$

$$\lambda_1' = \text{1st moment} = \int_0^\infty \omega G'(\omega)\,d\omega \tag{2-9}$$

$$\lambda_2' = \text{2nd moment} = \int_0^\infty \omega^2 G'(\omega)\,d\omega \tag{2-10}$$

It should be noted that $(\lambda_0'/2\pi)$ serves as an alternate means of
describing the power P listed in Table 2-3. Given the zero, first, and
second moments, the central frequency (mean frequency), Ω', and
dispersion (coefficient of variation), δ', are given by:

$$\Omega' \equiv \text{central frequency (Hz)} = \frac{1}{2\pi}\sqrt{\lambda_2'/\lambda_0'} \tag{2-11}$$

$$\delta' \equiv \text{dispersion parameter} = \sqrt{1-(\lambda_1')^2/\lambda_2'\lambda_0'} \tag{2-12}$$

Thus the frequency standard deviation, σ_f', is:

$$\sigma_f' = \delta' \ \Omega' \tag{2-13}$$

The mean frequency and frequency standard deviations for each of the 12 records are also listed in Table 2-6.

The mean frequencies, Ω', all exceed the median frequencies, f_{50}, as one would expect. For the 7 longer duration records, the mean frequencies lie between 3.6 and 4.7 Hz. The lower frequency f_{10} lies 1.25 to 1.45 standard deviations below the mean while f_{90} lies from 0.95 to 1.20 standard deviations above the mean. Thus, for records with durations T_D' greater than about 3 seconds, the records can be described as having 80% of their power within a range from -1.35 to +1.05 standard deviations from the mean. In these cases, Ω' and σ_f' serve as good descriptors of the frequency content. However, it should also be noted that one may not need to describe the specific frequency content of these records. All of these records can be reasonably fit in the 1.8 to 10 Hz range by a single design spectrum such as Reg. Guide 1.60 anchored to a design acceleration. Thus, their frequency content is not sufficiently different from each other to require a record specific description of the frequency content.

For the 5 short duration records ($T_D' < 3.0$ seconds), the mean frequency, Ω', tends to serve as a reasonable description of the central frequency. However, the dispersion statistic (either σ_f' or δ') appears to overpredict the breadth of frequencies from f_{10} to f_{90} in some cases. For instance, f_{10} lies at only -1.06, -1.1, and -0.92 standard deviations below the mean frequency for Goleta, Coyote Lake, and Parkfield, respectively, rather than at the -1.25 to -1.45 standard deviation range applicable for the longer records. Similarly, f_{90} lies at only 0.49, 0.85 and 0.33 standard deviations above the mean frequency for Goleta, Coyote Lake and Parkfield, respectively, rather than at the 0.95 to 1.20 standard deviation range applicable for the longer records. Thus, one must be cautious in using this dispersion statistic for the short duration records with T_D' of 3 seconds or less.

2-12

2.2.4 Frequency Content Summary and Conclusions

The seven long duration spectra can be reasonably approximated at about an 84th percent non-exceedance probability by a Reg. Guide 1.60 spectrum or some other "smooth-design" spectrum without introducing undue conservatism. Thus, the concept of a smooth design spectrum is compatible with these records. The problems with a "smooth-design" spectrum become serious with the four short duration ($T_D' < 2.5$ seconds) records. These four records apparently do not have sufficient duration to develop broad frequency content. Each record shows high spectral amplification only within a narrow frequency range. They cannot be fit over any broad frequency range by any Reg. Guide 1.60 spectrum anchored to any design ground acceleration. In fact, the ensemble of these four records cannot be fit by any "smooth-design" spectrum. If the four spectra were averaged, a smooth broad spectrum would result. However, this resulting smooth spectrum would be unrepresentative of any one of the four individual spectra which contain only narrow frequency content. Each spectrum shows high amplification in a different frequency range so that averaging the four would lead to a broad frequency content and the loss of the frequency characteristics of the individual records.

It will be shown that breadth of the amplified response region of the elastic response spectra has a major influence on both linear and nonlinear response of structures. A narrow frequency spectrum will only strongly excite one or two modes of a structure while a broad frequency design spectrum excites many modes. Use of a broad frequency design spectrum is likely to overpredict elastic response because of this combination of modes. As a structure goes nonlinear, its "effective" frequency is lowered. With a broad response spectrum, this shifting of frequency has only a small effect on the nonlinear response. On the other hand, with a narrow response spectrum, this shifting of frequency often has a major effect in reducing the nonlinear response. Artificial broadening of the frequency content will lead to an overprediction of the damage capability of this record. The most significant single conclusion of the entire study is that any engineering characterization of these

short duration records must retain the record's narrow frequency content. Hopefully, this conclusion will not be lost because of the maze of data presented herein.

The most apparent solution to the above dilemma for records with strong durations, T'_D, less than about 3 seconds is to define a narrow-frequency content design spectrum and then to vary the frequency at which this spectrum peaks over the range of frequency uncertainty for the site.

An engineering characterization of the frequency content of the records can be provided by the frequency range from f_{10} to f_{90} over which 80% of the power is distributed and by a mean frequency Ω'. All seven of the records with durations T'_D greater than 3.0 seconds contained frequency content between at least 1.2 to 5.5 Hz. The elastic response spectra for all of these records can be reasonably fit by a single design spectrum within the 1.8 to 10 Hz range. Thus, for these records, it appears to be unnecessary to specify the frequency content except in terms of a standard design spectrum.

On the other hand, all short duration records, with T'_D less than about 3.0 seconds included in this study are missing frequency content in either the high or low range of frequencies between 1.2 and 5.5 Hz. All of these records either do not contain power below 2.5 Hz or above 3.1 Hz. A single broadbanded design spectrum cannot be used even within the 1.8 to 10 Hz range to adequately approximate these records which miss frequency content either below 2.5 Hz or above 3.1 Hz. These records with durations less than about 3 seconds should be represented by narrow frequency content design spectra based upon ground motion record with similar frequency content as defined by the frequency range from f_{10} to f_{90}. Thus, Coyote Lake, Gavilan College, and Melendy Ranch could probably be approximated in the 1.8 to 10 Hz range by a single narrow frequency design spectrum which does not contain power below about 2.6 Hz. Parkfield and Goleta could probably be approximated in the 2 to 8 Hz range by a different narrow frequency design spectrum which doesn't contain power above about

3.0 Hz. For these records, uncertainty in the central frequency should be accommodated by the use of multiple narrow frequency content design spectra with differing central frequencies rather than by a single broad-banded spectrum which will result in overcomputing damage.

2.3   ENGINEERING CHARACTERIZATION NEEDED FOR ELASTIC RESPONSE

In order to define a design spectrum for elastic response of structures in the 1.8 to 10 Hz frequency range, records should be classified as having either broad or narrow frequency content. A record classified as having a broad frequency content should have at least a frequency range from 1.2 Hz to 5.5 Hz needed to develop 80% of the cumulative power of the record. All of the records considered in this study with effective durations, T_D', from Equations 2-2 and 2-3 of greater than 3.0 seconds meet this requirement. The elastic response spectra within the 1.8 to 10 Hz frequency range for these records can be approximated by a single broad frequency content design spectrum such as Reg. Guide 1.60 anchored to an "effective" acceleration. The shape of the design spectrum and the specification of an "effective" acceleration is sufficient to provide an engineering characterization of these records for computing elastic response of structures in the 1.8 to 10 hz frequency range. The concept of an "effective" acceleration is valid for elastic response with these records. Such statements cannot be made for the five records with T_D' durations of 3.0 seconds or less. None of these records can be fit over the 1.8 to 10 Hz frequency range by a broad frequency content design spectrum such as Reg. Guide 1.60. For these records, the concept of an "effective" anchor acceleration is not very meaningful until narrow frequency content design spectra are developed and specified.

To demonstrate these points, the 7% damped Reg. Guide 1.60 spectrum anchored at an "effective" acceleration is compared with the 7% damped spectra for the 11 real earthquake time histories over the frequency range from 1.8 to 10 Hz in Figures 2-7(a) through 2-7(c). The "effective" acceleration , A_{DE}, for anchoring the elastic Reg. Guide 1.60

spectrum was set so that 84% of the actual records spectral accelerations between 1.8 and 10 Hz would lie below the Reg. Guide spectra. In other words, the Reg. Guide spectra is exceeded at 16% of the frequencies between 1.8 and 10 Hz. Based upon this definition, the "effective" elastic anchor accelerations, A_{DE}, were determined and are shown in Table 2-7 for the 11 real records. Table 2-7 also presents the maximum, median, and minimum ratios of the actual spectral accelerations to Reg. Guide 1.60 spectral acceleration within the frequency range from 1.8 to 10 Hz. These ratios are defined as $(SA_a/SA_{1.60})_{max}$, $(SA_a/SA_{1.60})_{median}$, and $(SA_a/SA_{1.60})_{min}$, respectively. All of these ratios are reported for the Reg. Guide spectrum being anchored at the "effective" elastic design acceleration, A_{DE}.

The six real ground motion records with T_D' greater than 3.0 seconds (Olympia through El Centro #5) are all reasonably fit by the Reg. Guide 1.60 spectrum anchored at A_{DE}. For these 6 records, the maximum amount by which the actual spectral acceleration exceeds the Reg. Guide spectral accelerations between 1.8 and 10 Hz varies from 1.08 to 1.23 with a median-maximum value of 1.12. The median ratio of actual spectral acceleration to Reg. Guide spectral acceleration varies from 0.84 to 0.90 with a median-median of 0.88. Thus on the average, the Reg. Guide spectrum introduces a factor of conservatism of (1/0.88) = 1.14. The minimum ratio of actual spectral acceleration to Reg. Guide spectral acceleration varies from 0.45 to 0.70. Thus, for these 6 records, between 1.8 and 10 Hz the Reg. Guide spectrum anchored to A_{DE} ranges from 1.23 unconservative to (1/0.45) = 2.22 conservative with a median factor of conservatism of 1.14. The Reg. Guide spectrum anchored to A_{DE} represents an adequate characterization of these 6 records for elastic structural response.

The four short duration records with T_D' less than 3.0 seconds (Coyote Lake through Melendy Ranch) are clearly inadequately represented by the Reg. Guide spectrum anchored to A_{DE}. The maximum-maximum factor of unconservatism is 1.66 while the minimum-minimum factor of conserva-tism is (1/0.08) = 12.5 while the median-median factor of conservatism is

(1/0.64) = 1.56. The scatter band is simply too large when those records are attempted to be fit by the Reg. Guide spectrum even within the 1.8 to 10 Hz frequency range. The Reg. Guide spectrum does not serve as an adequate representation of these records.

The Goleta record ($T_D' = 3.0$ seconds) could be placed in either group. The fit to the Reg. Guide spectrum is better than for the four shorter duration records but not as good as for the six longer duration records. It is judged that the fit is not adequate and the Goleta record is placed with the four shorter duration records.

Development of narrow frequency design spectra would require the consideration of many more records than the five short duration records used in this study. However, these five records can be utilized to illustrate some problems. If all five of these short duration records were used to develop a design spectrum, the resulting spectrum would have a broad frequency content and would represent each individual record nearly as poorly as does the Reg. Guide 1.60 spectrum. In order to develop narrow frequency content design spectrum, one must separate these short duration records by their frequency content. The frequency range f_{10} to f_{90} over which 80% of the cumulative power is contained can probably be used for this purpose. It might be appropriate to segregate these records into a high frequency group of records in which f_{10} exceeds 2.5 Hz (Coyote Lake, Gavilan College, and Melendy Ranch would belong to this group) and a low frequency group in which f_{90} is less than 3.5 Hz (Parkfield and Goleta would belong to this group). A mid-frequency group of short duration records would probably also be needed to cover those records which do not fall into either the high or low frequency group. Once narrow frequency design spectra are developed for these records with T_D' less than about 3.0 seconds, the resulting design spectrum needs to be compared to the spectrum of the individual records similar to the comparisons made in this study for the longer duration records and the Reg. Guide 1.60 spectrum. It is believed that these narrow frequency design spectrum will provide an adequate engineering characterization for

elastic response of those short duration records when anchored to an appropriate "effective" acceleration. Uncertainties in frequency content should be covered by requiring the central frequency of these narrow frequency design spectrum to be varied over the range of uncertainty rather than by broadening the design spectrum.

It should be noted from the 11 real records in this study that the characteristics of narrow frequency content appears to be directly correlated to short durations T_D' of about 3.0 seconds and less as defined by Equation 2-2 and 2-3. Furthermore, the duration T_D' also appears to be highly correlated with the local magnitude, M_L, for records with ground accelerations of 0.14g and greater. The five records with T_D' of 3.0 seconds and less all have M_L of 5.7 and less. The six records with T_D' greater than 3.0 seconds all have M_L of 6.4 and greater. Thus, one might tentatively conclude that the Reg. Guide 1.60 spectrum provides an acceptable engineering characterization for elastic response for records from earthquakes with M_L of about 6.0 and greater and does not provide an adequate characterization for records with M_L less than about 6.0. It appears likely that records with both ground accelerations of 0.14g and greater and M_L of 6.0 or less can only be characterized by narrow frequency design spectrum and the standard usage of broad design spectra anchored at the 84th percentile will likely lead to substantial inaccuracy and generally excessive conservatism in these cases. Note that the SSE ground motion for nuclear power plants east of the Rocky Mountains generally corresponds to records with ground accelerations of 0.14g or greater and M_L of 6.0 or less and thus falls into this category.

For records with broad frequency content (at least 1.2 to 5.5 Hz), it was shown that the Reg. Guide 1.60 spectrum anchored to A_{DE} provides an adequate characterization for elastic response. The next step is to define A_{DE} in terms of characteristics of the ground motion. Several likely candidates exist for defining A_{DE}. These are corrected peak ground acceleration, a, rms acceleration, a_{rms}, and spectrum intensity, SI.

The rms acceleration over the duration T_D' is reported in Table 2-3. A median estimate of the design acceleration for elastic response is then provided by Equation 1-6 and 1-7 where the duration T_D' is substituted for T_D and the predominant period, T_o, is given by:

$$T_o = 1/\Omega'$$ (2-14)

in which Ω' represents the central frequency from Equation 2-11 and is listed in Table 2-6. The result is an effective elastic rms based anchor acceleration A_{DE1} given by:

$$A_{DE1} = \left(\sqrt{2 \ln(2.8T_D'\Omega')}\right) a_{rms}$$ (2-15)

Housner (1952) has suggested that spectrum intensity could serve as a measure of the ground motion severity. Within the frequency domain, spectrum intensity is defined by:

$$SI(\beta, f_1-f_2) = \int_{f_1}^{f_2} \frac{S_v(\beta, f)}{f^2} \, df$$ (2-16)

where S_v represents the spectral velocity, β represents the appropriate damping, f represents frequency, and f_1 to f_2 represents the frequency range of interest. For elastic response of nuclear power plant structures, an elastic spectrum intensity SI_e will be defined by the 7% damped spectrum between 1.8 and 10.0 Hz. Thus:

$$SI_e = SI (0.07, 1.8 - 10.0)$$ (2-17)

With this definition, an effective elastic SI based anchor acceleration A_{DE2} for anchoring the Reg. Guide 1.60 spectra can be defined as:

$$A_{DE2} = \frac{SI_e}{18}$$

(2-18)

where A_{DE2} is in fraction of gravity units, SI_e is obtained from integrating spectral velocities in inch-per-second units over a frequency range in Hz units. The factor in the denominator of Equation 2-18 has been empirically determined by this study to achieve a mean A_{DE}/A_{DE2} ratio near unity.

Table 2-7 presents, for each of the 11 records studied, the corrected ground acceleration, a, the rms based acceleration, A_{DE1}, and SI_e based acceleration, A_{DE2} for comparison with A_{DE} obtained from fitting the Reg. Guide Spectrum to actual ground motion spectra from 1.8 to 10 Hz. All three definitions for "effective" elastic design acceleration agree closely with A_{DE} for the six records (Olympia through El Centro #5) which can be represented by the Reg. Guide spectrum. For these six records:

Ratio	Max.	Mean	Min.	COV
A_{DE}/a	1.10	0.87	0.73	0.15
A_{DE}/A_{DE1}	1.17	1.06	0.96	0.08
A_{DE}/A_{DE2}	1.17	0.99	0.85	0.12

All mean ratios are close to unity and have low coefficients of variation (COV). The use of corrected ground acceleration, a, introduces a mean factor of conservatism of $(1/0.87) = 1.15$ and has the largest COV. Introduction of added conservatism in defining A_{DE} is undesirable since the use of the Reg. Guide 1.60 already generally introduces conservatism in the 1.8 to 10 Hz frequency range when compared with spectra from the actual records. The rms based "effective" acceleration, A_{DE1}, introduces a mean factor of unconservatism of 1.06 and has the lowest COV. This mean unconservatism is negligible when one considers the conservatism introduced by the use of the Reg. Guide 1.60 spectrum. The SI_e based "effective" acceleration, A_{DE2}, tends to overemphasize the importance of the lower frequencies (near 1.8 Hz) while underemphasizing the importance of the higher frequencies (near 10 Hz). For this reason, it has a slightly higher COV than does A_{DE1}.

It is concluded that an rms based effective acceleration, A_{DE1}, defined by Equation 2-15 provides a good definition of the anchor acceleration for the Reg. Guide 1.60 spectrum for the six longer duration real records studied. When the Reg. Guide 1.60 spectrum is anchored to A_{DE1}, within the 1.8 to 10 Hz frequency range of interest, the maximum ratio of $(SA_a/SA_{1.60})$ ranges from 1.29 to 1.05 with a median-maximum ratio of 1.20 for the six records studied. Similarly, the median ratio ranges from 1.05 to 0.83 with a median-median of 0.88 while the minimum ratio ranges from 0.76 to 0.49 with a median-minimum of 0.59. This performance is just as good as that obtained from the empirically determined A_{DE}.

For broad frequency content records (frequency content from 1.2 to 5.5 Hz) associated with duration T_D' greater than 3.0 seconds, the elastic response characteristics of the ground motion for structures with frequencies from 1.8 to 10 Hz can be adequately characterized by the Reg. Guide 1.60 spectra anchored to an rms based "effective" acceleration defined by Equation 2-15. For the six records studied, the maximum factor of unconservatism introduced was only 1.29, the median factor of

conservatism was (1/0.88) = 1.14 and the largest factor of conservatism was (1/0.49) = 2.04. These uncertainties are certainly tolerable considering the simplicity of this engineering characterization of the ground motion.

2.4   ENGINEERING CHARACTERIZATION OF GROUND MOTION SUMMARY

Eleven real earthquake ground motion time histories and one artificial earthquake time history have been considered. Characteristics of these ground motion records have been evaluated including energy, power and duration as well as frequency content by means of frequency breadth and a central frequency. Section 2.1 recommends that the strong motion duration, T_D', for stiff structures be computed from Equations 2-2 and 2-3 using cumulative energy plots (Figure 2-3). It is shown that this duration corresponds to the time of steepest slope (i.e., greatest power and greatest rms acceleration) from these energy plots. It is also shown that T_D' correlates well with the longest time to reach maximum structural response (both for elastic and inelastic response) for stiff structures (1.8 to 10 Hz). The breadth of the range of frequency content can be defined by the frequency range from f_{10} to f_{90} where 10% of the cumulative power lies at frequencies below f_{10} and 90% of the cumulative power lies at frequencies below f_{90}. Thus, the frequency range from f_{10} to f_{90} contains the central 80% of the cumulative power of the strong motion portion (T_D' duration) of the record. Central frequency, Ω' is defined in accordance with Equation 2-11 in terms of moments of the spectral density function.

The 11 real earthquake ground motions can be divided into two groups (Group 1: Taft, Olympia, El Centro #12, El Centro #5, Pacoima Dam and Hollywood Storage; Group 2: Coyote Lake, Parkfield Cholame #2, Gavilan College, Goleta and Melendy Ranch) as follows:

1.   Strong duration, T_D'. All the Group 1 records have strong durations of 3.4 seconds and greater while all the Group 2 records have durations of 3.0 seconds and less.

2. Local magnitude, M_L. All the Group 1 records are from earthquakes with local magnitudes of 6.4 and greater while all the Group 2 records are from earthquakes with local magnitudes of 5.7 and less.

3. Frequency breadth. All the Group 1 records have motions rich in frequency content (f_{10} to f_{90}) from at least 1.2 to 5.5 Hz. Each of the Group 2 records has narrower frequency content than the above range (i.e., f_{10} to f_{90} does not cover the range from 1.2 to 5.5 Hz).

An adequate engineering characterization for elastic structural response for stiff structures (1.8 to 10 Hz) subjected to any of the 6 longer duration (Group 1) records is provided by the Reg. Guide 1.60 spectrum anchored to an "effective" peak acceleration. It is shown in Section 2.3 that this "effective" peak acceleration, A_{DE1}, can be defined as an rms based acceleration given by Equation 2-15. This conclusion is not applicable to the 5 shorter duration (Group 2) records. Elastic response from any of the five Group 2 records cannot be adequately approximated by the Reg. Guide 1.60 spectrum or by any other broad frequency content spectrum. The most adequate way to characterize these records is by a narrow-banded design spectrum obtained by averaging records with similar central frequencies, Ω', and frequency bands, f_{10} to f_{90}. Uncertainties in central frequency, Ω', should be covered by shifting the central frequency of a narrow-banded design spectrum throughout the range of uncertainty and not by the use of a broad frequency content design spectrum for stiff structures subjected to Group 2 type records.

TABLE 2-1

CHARACTERISTICS OF THE SELECTED ACCELEROGRAMS

EARTHQUAKE	MAGNITUDE		RECORDING STATION AND COMPONENT	SYMBOLS	FAULT DISTANCE (km)	a (g)	v (in/sec)
	M_L	M_S					
21 July 1952 Kern County, CA	7.2	7.7	Taft Lincoln School (S69E)	T	40	0.180	7.0
13 April 1949 Olympia, WA	7.0	7.0	Highway Test Lab (N86E)	O	29	0.281	6.7
15 Oct. 1979 Imperial Valley,CA	6.6	6.9	El Centro Array No.12(140)	EC12	18	0.142	6.9
15 Oct. 1979 Imperial Valley, CA	6.6	6.9	El Centro Array No.5 (140)	EC5	1	0.530	17.3
09 Feb. 1971 San Fernando, CA	6.4	6.6	Pacoima Dam (S14W)	PD	3	1.170	44.6
09 Feb. 1971 San Fernando, CA	6.4	6.6	Hollywood Stg.P.E.Lot(N90E)	HS	21	0.211	8.3
06 Aug. 1979 Coyote Lake, CA	5.7	5.6	Gilroy Array No.2 (050)	CL	7	0.191	4.0
27 June 1966 Parkfield, CA	5.6	6.4	Cholame-Shandon No.2 (N65E)	PA2	< 1	0.490	10.4
28 Nov. 1974 Hollister, CA	5.2	4.5	Gavilan College (S67W)	GC	13	0.138	1.6
13 Aug. 1978 Santa Barbara, CA	5.1	5.6	UCSB Goleta (180)	G	4	0.347	15.7
04 Sept. 1972 Bear Valley, CA	4.7	4.3	Melendy Ranch (N29W)	MR	6	0.520	5.4

TABLE 2-2

COMPARISON OF UPPER BOUNDS ON PEAK ELASTIC AND INELASTIC DEFORMATION
RESPONSE TIME WITH HUSID RATIO TIMES

	Earthquake Record (Component)	$T_{0.95}$ (sec)	$T_{0.85}$ (sec)	$T_{0.75}$ (sec)	$T_{0.05}$ (sec)	T_{pa} (sec)	Elastic (μ=1.0) $\overline{T}_{max}$(sec)	Nonlinear (μ=1.9&4.3) $\overline{T}_{max}$(sec)
1	Olympia, WA., 1949 (N86E)	21.7	19.8	19.2	4.4	20.0	19.9	19.9
2	Taft, Kern Co., 1952 (S69E)	31.8	18.3	14.0	3.7	6.7	9.9	9.2
3	El Centro Array No. 12 Imperial Valley, 1979, (140)	25.0	18.3	16.0	6.4	11.0	12.0	16.6
4	Artificial (R.G. 1.60)	15.0	13.2	11.4	2.0	10.3	11.5	10.6
5	Pacoima Dam San Fernando, 1971 (S14W)	10.0	8.5	8.2	2.6	8.7	8.6	8.6
6	Hollywood Storage PE Lot, San Fernando, 1971 (N90E)	13.5	8.9	7.2	1.8	3.4	5.1	7.6
7	El Centro Array No. 5 Imperial Valley, 1979, (140)	12.7	8.7	7.9	4.5	5.7	8.2	8.3
8	UCSB Goleta Santa Barbara, 1978 (180)	13.6	8.7	6.9	3.9	4.9	5.1	5.1
9	Gilroy Array No., 2, Coyote Lake 1979, (050)	10.0	6.9	4.7	2.5	3.1	4.5	3.5
10	Cholame Array No. 2, Parkfield 1966 (N65E)	12.4	5.3	4.6	3.2	4.0	4.5	4.8
11	Gavilan College Hollister, 1974 (S67W)	3.4	3.0	2.9	1.8	2.3	3.0	2.9
12	Melendy Ranch Barn, Bear Valley 1972 (N29W)	4.1	2.6	2.3	1.5	1.9	2.3	2.1

$\overline{T}_{max}$ = Upper bound on time of maximum response throughout frequency range, f = 2.1-8.5 Hz, at 7% damping and for the following ductilities: Elastic (μ = 1.0) and Nonlinear (μ = 1.9 and 4.3)

TABLE 2-3

COMPARISON OF DURATION MEASURES, PEAK GROUND ACCELERATION, PEAK GROUND VELOCITY, ENERGY, AVERAGE POWER AND RMS ACCELERATION OF SELECTED INPUT ACCELERATIONS

	Earthquake Record (Component)	T_D' (sec)	T_D (sec)	a (g)	v (in/sec)	ΔE (ft^2/sec^3)	P (g^{2}x10^{-3})	RMS Acc. a_{rms}(g)
1	Olympia, WA., 1949 (N86E)	15.6	17.3	0.281	6.7	64.2	3.97	.063
2	Taft, Kern Co., 1952 (S69E)	10.3	28.1	0.180	7.0	27.4	2.57	.051
3	El Centro Array No. 12 Imperial Valley, 1979, (140)	9.6	18.6	0.142	6.9	18.6	1.88	.043
4	Artificial (R.G. 1.60)	9.4	13.0	0.200	11.3	44.2	4.54	.067
5	Pacoima Dam San Fernando, 1971 (S14W)	6.1	7.4	1.170	44.6	466.8	74.0	.272
6	Hollywood Storage PE Lot, San Fernando, 1971 (N90E)	5.4	11.7	0.211	8.3	30.0	5.37	.073
7	El Centro Array No. 5 Imperial Valley, 1979, (140)	3.4	8.2	0.530	17.3	78.1	22.2	.149
8	UCSB Goleta Santa Barbara, 1978 (180)	3.0	9.7	0.347	15.7	57.3	18.5	.136
9	Gilroy Array No. 2, Coyote Lake, 1979, (050)	2.2	7.5	0.191	4.0	13.3	5.86	.077
10	Cholame Array No. 2, Parkfield 1966 (N65E)	1.4	9.2	0.490	10.4	86.1	59.4	.244
11	Gavilan College Hollister, 1974 (S67W)	1.1	1.6	0.138	1.6	2.1	1.80	.042
12	Melendy Ranch Barn, Bear Valley 1972 (N29W)	0.8	2.6	0.520	5.4	29.8	36.0	.190

$T_D' \equiv$ Strong Duration (from Equation 2-3) T_D = Trifunac-Brady Duration = 5-95% Range for $\int a^2 dt$

$\Delta E \equiv$ Fourier Input Energy $E(T_m) - E(T_{.05})$, $E(T) = \int_0^T a^2 dt$

$P \equiv$ Average Fourier Input Power = $\Delta E / T_D'$

TABLE 2-4

ELASTIC 7 PERCENT DAMPED SPECTRAL ACCELERATION

	Earthquake Record (Component)	SA(g)			
		2.14 Hz	3.20 Hz	5.34 Hz	8.54 Hz
1	Olympia, WA., 1949 (N86E)	0.487	0.595	0.443	0.440
2	Taft, Kern Co., 1952 (S69E)	0.395	0.375	0.323	0.214
3	El Centro Array No. 12 Imperial Valley, 1979, (140)	0.218	0.270	0.327	0.248
4	Artificial (R.G. 1.60)	0.430	0.549	0.477	0.454
5	Pacoima Dam San Fernando, 1971 (S14W)	1.623	1.614	1.673	1.589
6	Hollywood Storage PE Lot, San Fernando, 1971 (N90E)	0.263	0.431	0.626	0.512
7	El Centro Array No. 5 Imperial Valley, 1979, (140)	0.741	0.880	1.136	1.106
8	UCSB Goleta Santa Barbara, 1978 (180)	0.641	0.642	0.585	0.490
9	Gilroy Array No., 2, Coyote Lake 1979, (050)	0.203	0.443	0.656	0.390
10	Cholame Array No. 2, Parkfield 1966 (N65E)	1.404	0.813	0.533	0.557
11	Gavilan College Hollister, 1974 (S67W)	0.088	0.118	0.204	0.241
12	Melendy Ranch Barn, Bear Valley 1972 (N29W)	0.158	0.435	1.491	0.951

TABLE 2-5

COMPARISON OF RESPONSE SPECTRA PARAMETERS

	Earthquake Record (Component)	$v/_a$ in/sec/g	$\dfrac{SA_m}{a}$	f_a (Hz)	$\dfrac{SV_m}{v}$	f_v (Hz)	f_{av} (Hz)
1	Olympia, WA., 1949 (N86E)	24.0	2.24	3.12	2.52	1.61	2.3
2	Taft, Kern Co., 1952 (S69E)	38.7	2.58	2.30	1.97	1.18	2.1
3	El Centro Array No. 12 Imperial Valley, 1979, (140)	48.5	2.42	5.00	2.29	0.45	1.3
4	Artificial (R.G. 1.60)	(56.5)	2.83	2.50	1.91	0.45	1.6
5	Pacoima Dam San Fernando, 1971 (S14W)	38.1	2.13	2.60	1.74	0.83	2.0
6	Hollywood Storage PE Lot, San Fernando, 1971 (N90E)	39.4	3.06	5.50	2.78	0.25	1.7
7	El Centro Array No. 5 Imperial Valley, 1979, (140)	32.7	2.16	5.88	2.29	0.36	1.8
8	UCSB Goleta Santa Barbara, 1978 (180)	45.4	2.44	1.33	2.57	1.20	1.3
9	Gilroy Array No., 2, Coyote Lake 1979, (050)	21.0	3.45	5.26	2.18	3.30	4.6
10	Cholame Array No. 2, Parkfield 1966 (N65E)	21.3	2.96	2.30	5.34	1.52	1.6
11	Gavilan College Hollister, 1974 (S67W)	11.4	2.79	10.5	1.83	2.60	8.3
12	Melendy Ranch Barn, Bear Valley 1972 (N29W)	10.4	3.03	5.50	3.19	5.50	5.5

SA_m = Max. Spectral Acceleration 7% Damping

SV_m = Max. Spectral Velocity, 7% Damping

TABLE 2-6

COMPARISON OF FREQUENCY DOMAIN PARAMETERS

	Earthquake Record (Component)	Frequency Range (Hz)			Mean Freq. Ω' (Hz)	Std. Dev. σ_f' (Hz)
		f_{10}	f_{50}	f_{90}		
1	Olympia, WA., 1949 (N86E)	1.20	3.05	6.10	3.90	1.99
2	Taft, Kern Co., 1952 (S69E)	1.10	2.70	5.50	3.61	1.89
3	El Centro Array No. 12 Imperial Valley, 1979, (140)	0.55	3.05	7.50	4.52	2.80
4	Artificial (R.G. 1.60)	0.60	2.15	6.55	3.91	2.58
5	Pacoima Dam San Fernando, 1971 (S14W)	0.75	2.60	6.70	4.19	2.56
6	Hollywood Storage PE Lot, San Fernando, 1971 (N90E)	0.75	3.30	7.90	4.68	2.71
7	El Centro Array No. 5 Imperial Valley, 1979, (140)	0.80	2.75	6.75	4.12	2.51
8	UCSB Goleta Santa Barbara, 1978 (180)	0.80	1.40	3.05	2.34	1.45
9	Gilroy Array No., 2, Coyote Lake 1979, (050)	2.70	4.70	6.90	5.12	2.10
10	Cholame Array No. 2, Parkfield 1966 (N65E)	1.20	1.80	2.75	2.34	1.24
11	Gavilan College Hollister, 1974 (S67W)	2.55	6.35	11.35	7.67	3.30
12	Melendy Ranch Barn, Bear Valley 1972 (N29W)	3.55	5.60	8.20	6.11	2.08

TABLE 2-7

"EFFECTIVE" ELASTIC DESIGN ACCELERATION

	Earthquake Record (Component)	$(SA_a/SA_{1.60})$*			Effective Elastic Acceleration A_{DE} (g)	Ground Accel. a (g)	RMS Based Accel. A_{DE1} (g)	Spectral Intensity Based Accel. A_{DE2} (g)
		Max.	Median	Min.				
1	Olympia, WA., 1949 (N86E)	1.12	0.90	0.70	0.219	0.281	0.202	0.253
2	Taft, Kern Co., 1952 (S69E)	1.23	0.89	0.61	0.149	0.180	0.155	0.175
3	El Centro Array No. 12 Imperial Valley, 1979, (140)	1.09	0.86	0.61	0.128	0.142	0.133	0.128
4	Pacoima Dam San Fernando, 1971 (S14W)	1.08	0.84	0.55	0.856	1.170	0.795	0.879
5	Hollywood Storage PE Lot, San Fernando, 1971 (N90E)	1.14	0.86	0.45	0.233	0.211	0.213	0.200
6	El Centro Array No. 5 Imperial Valley, 1979, (140)	1.11	0.90	0.60	0.471	0.530	0.404	0.442
7	UCSB Goleta Santa Barbara, 1978 (180)	1.33	0.82	0.69	0.283	0.347	0.332	0.324
8	Gilroy Array No., 2, Coyote Lake 1979, (050)	1.15	0.77	0.25	0.233	0.191	0.202	0.154
9	Cholame Array No. 2, Parkfield 1966 (N65E)	1.16	0.48	0.37	0.562	0.490	0.514	0.564
10	Gavilan College Hollister, 1974 (S67W)	1.66	0.58	0.26	0.105	0.138	0.106	0.060
11	Melendy Ranch Barn, Bear Valley 1972 (N29W)	1.14	0.69	0.08	0.573	0.520	0.435	0.221

* Ratios of Actual to Reg. Guide 1.60 Spectral Accelerations are reported for the frequency range of 1.8 to 10 Hz.
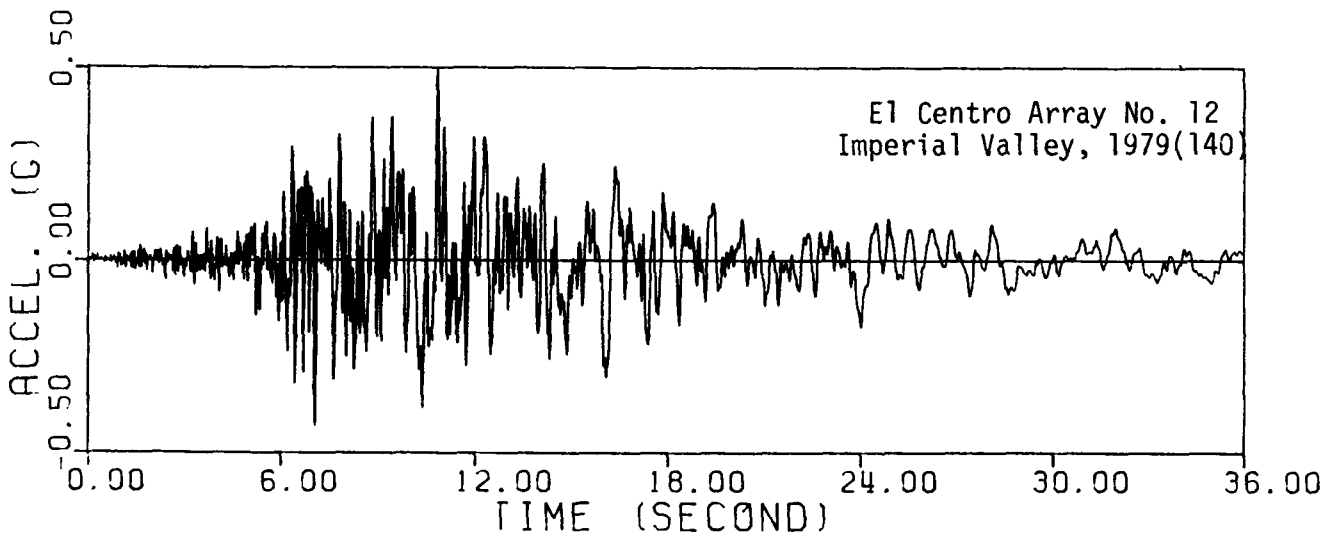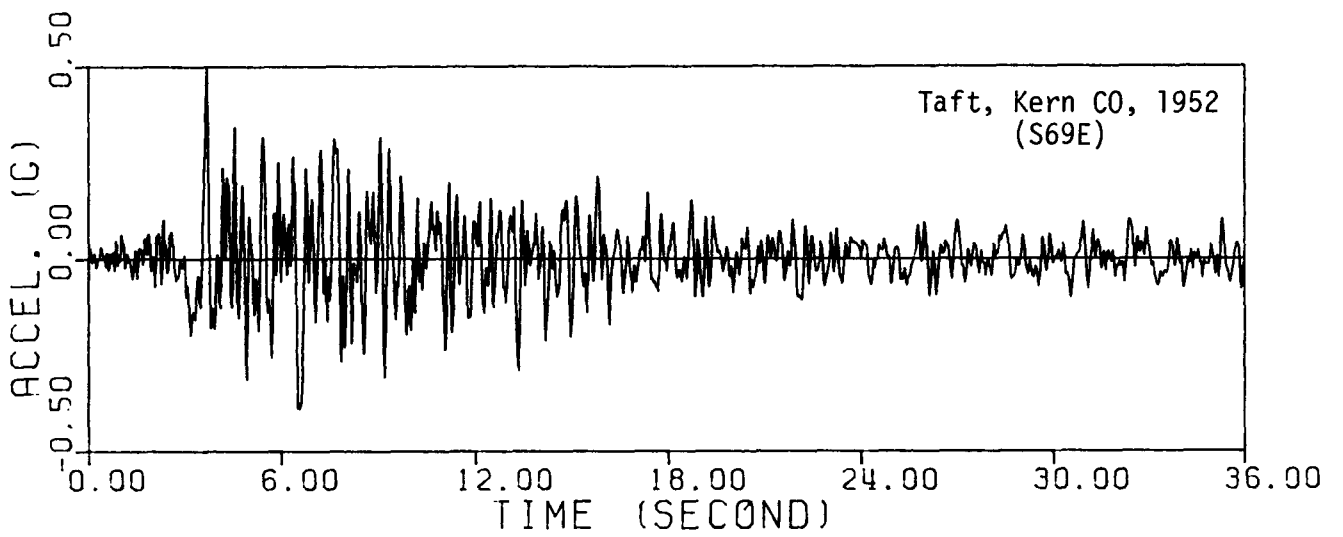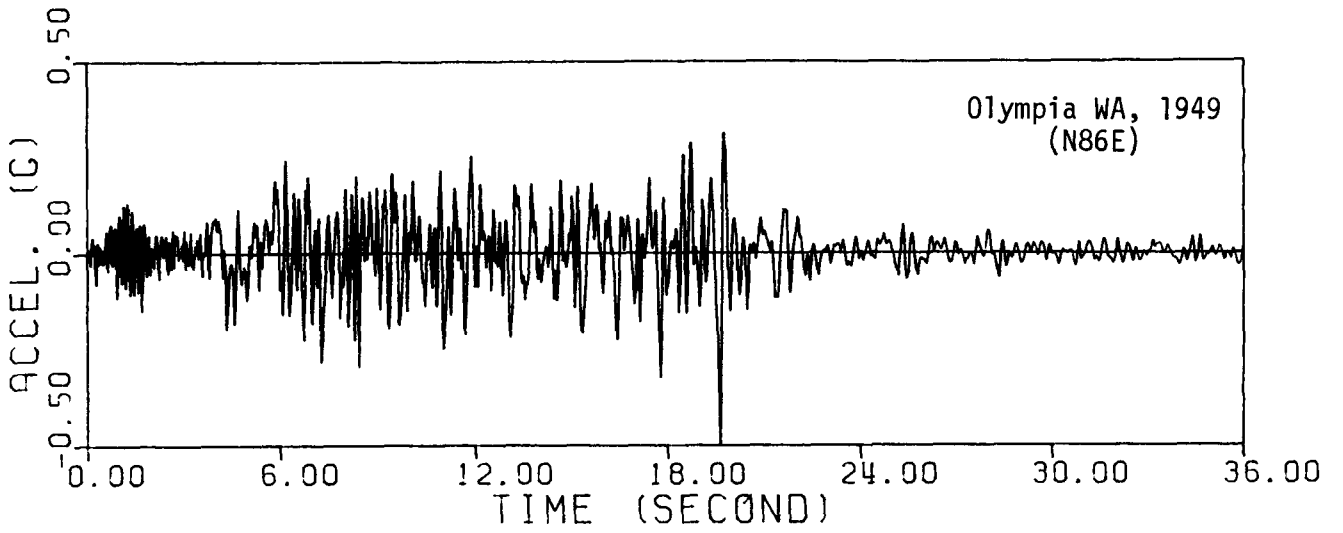
FIGURE 2-1. EARTHQUAKE TIME HISTORY RECORDS (NORMALIZED TO 0.5g)

FIGURE 2-1.   EARTHQUAKE TIME HISTORY RECORDS (NORMALIZED TO 0.5g)
(Continued)

2-32
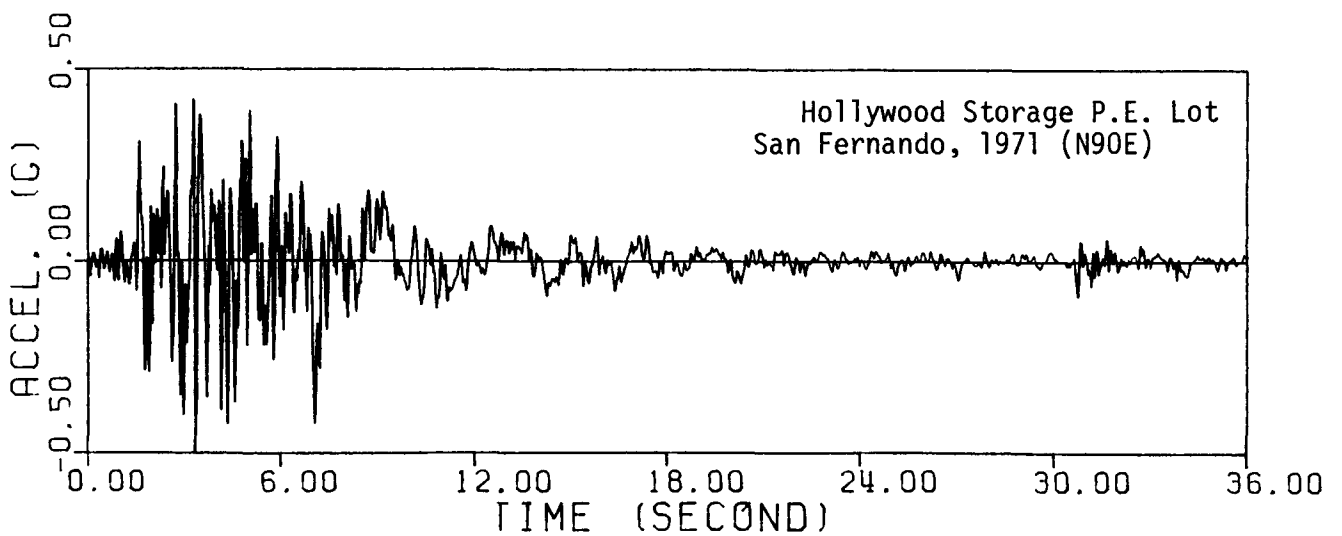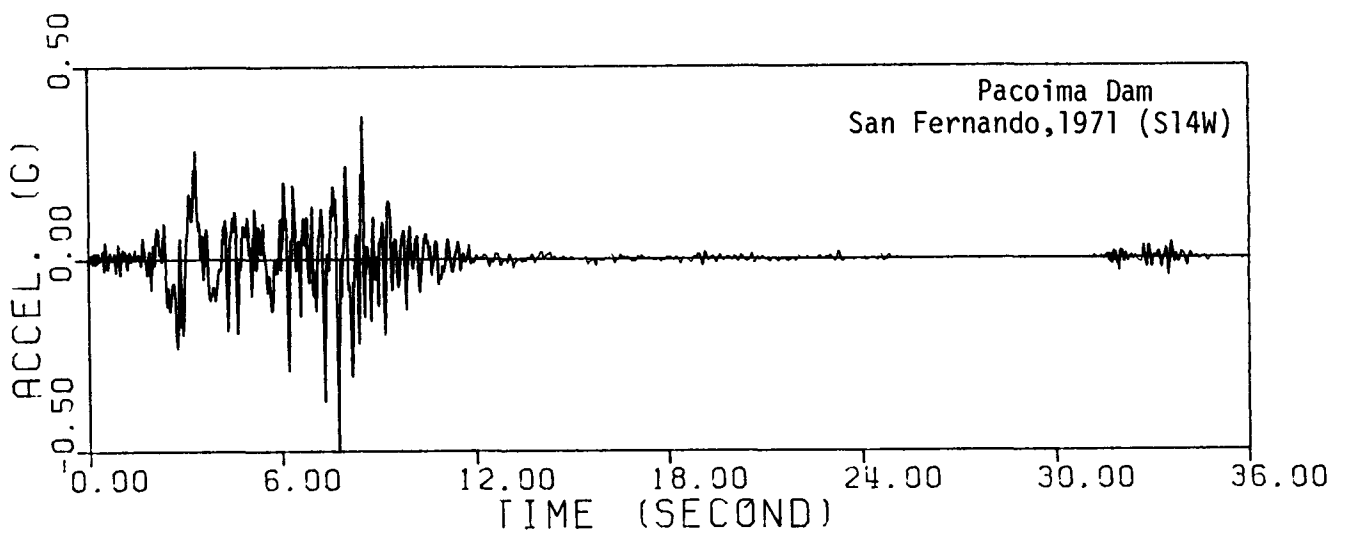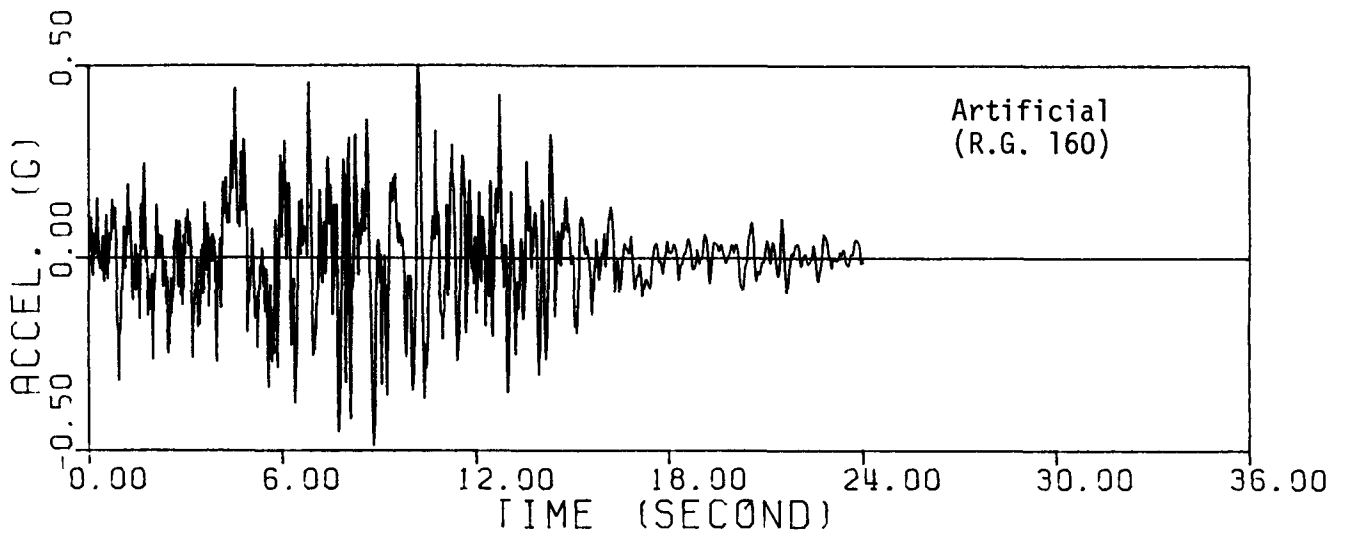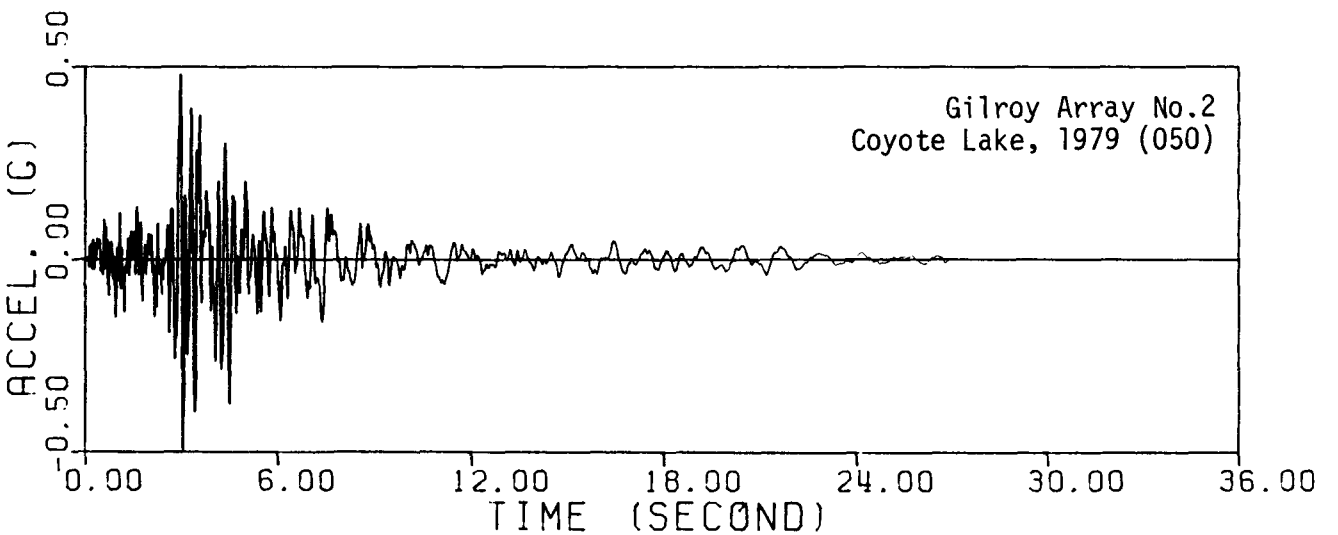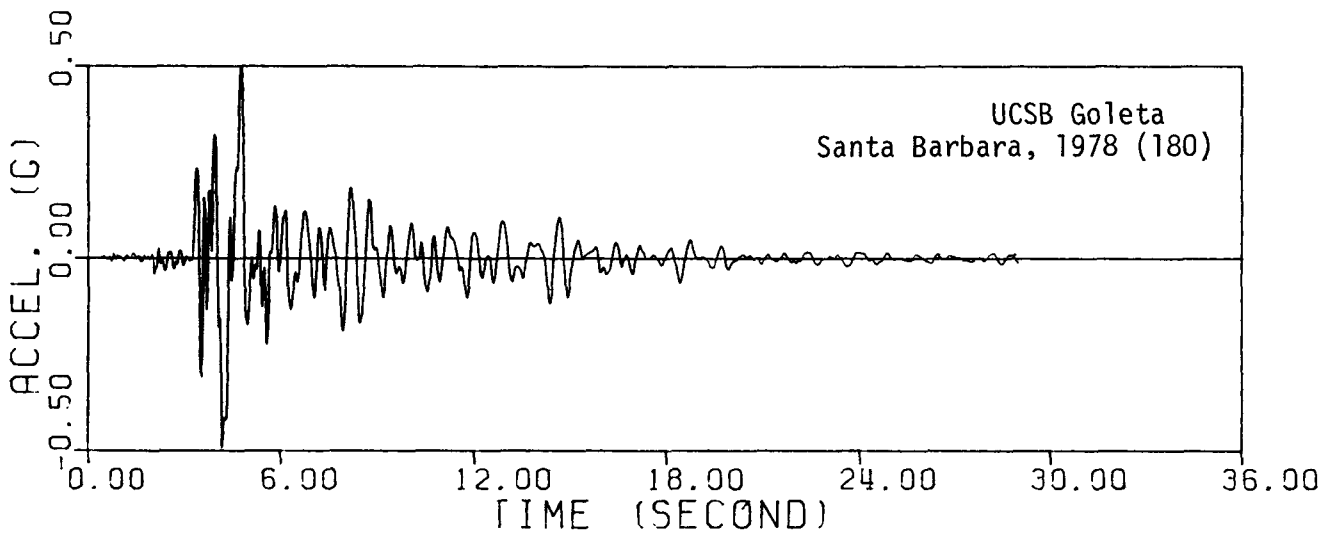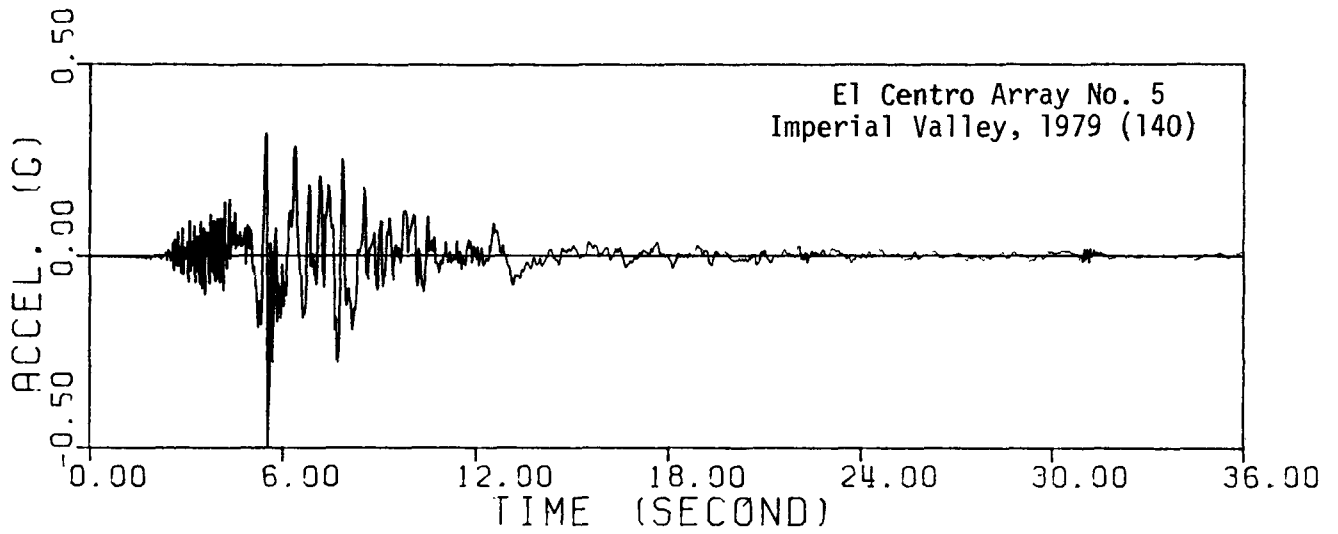
FIGURE 2-1. EARTHQUAKE TIME HISTORY RECORDS (NORMALIZED TO 0.5g)
(Continued)
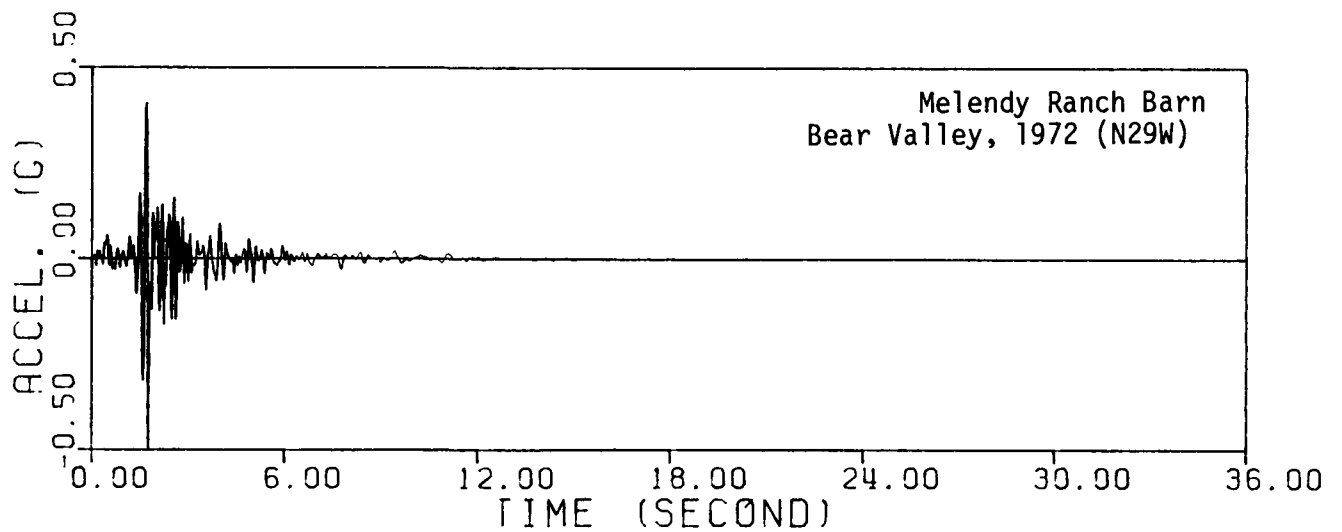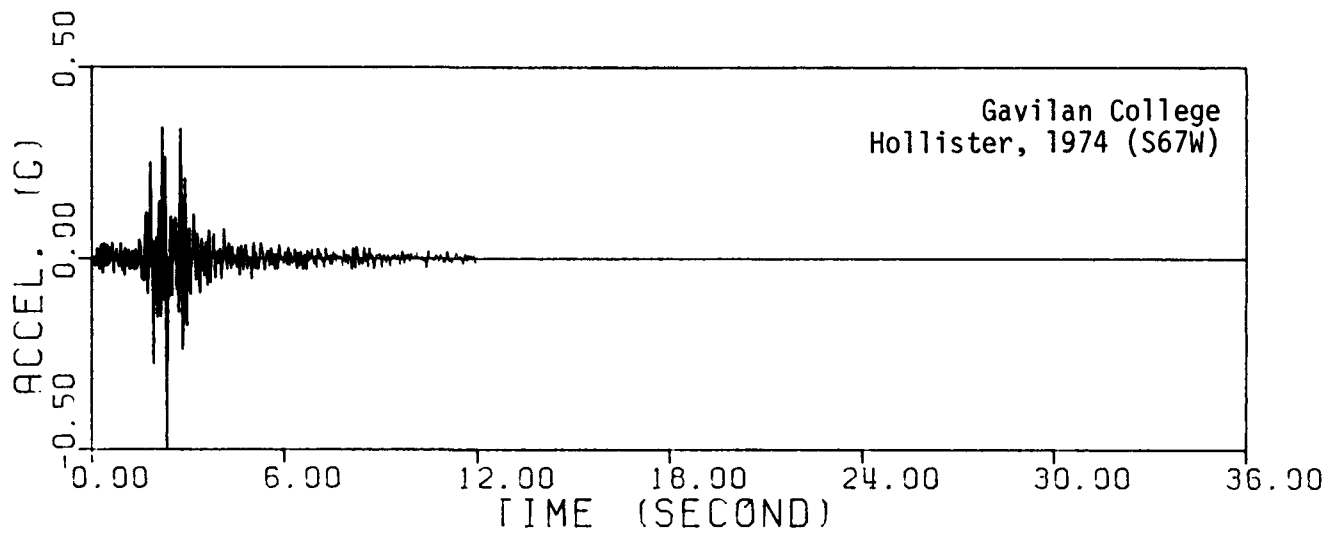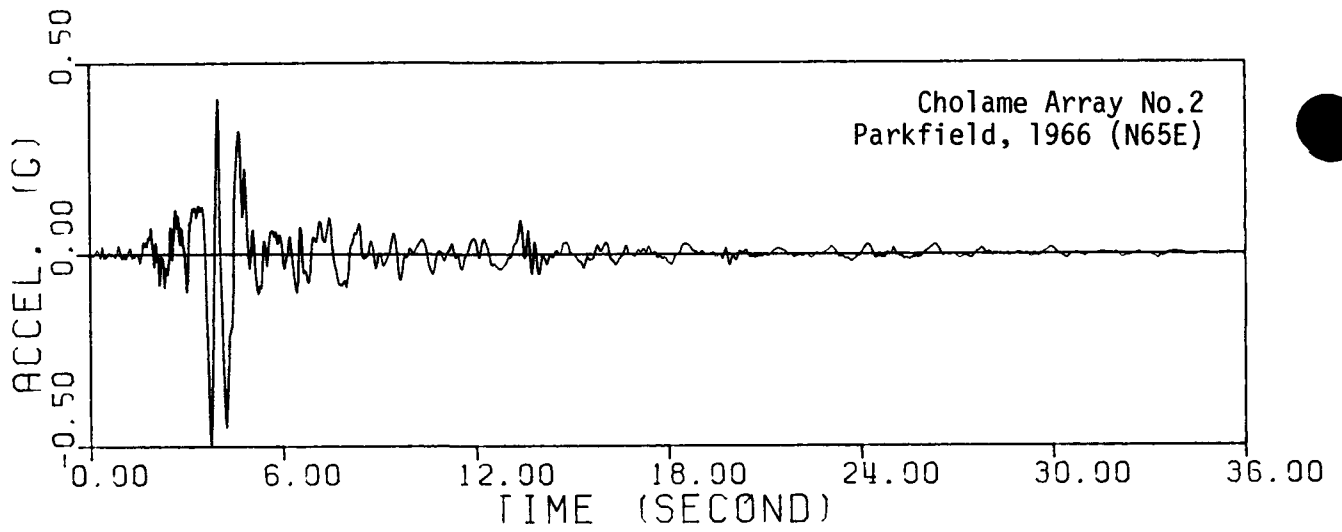
FIGURE 2-1.   EARTHQUAKE TIME HISTORY RECORDS (NORMALIZED TO 0.5g)
(Continued)
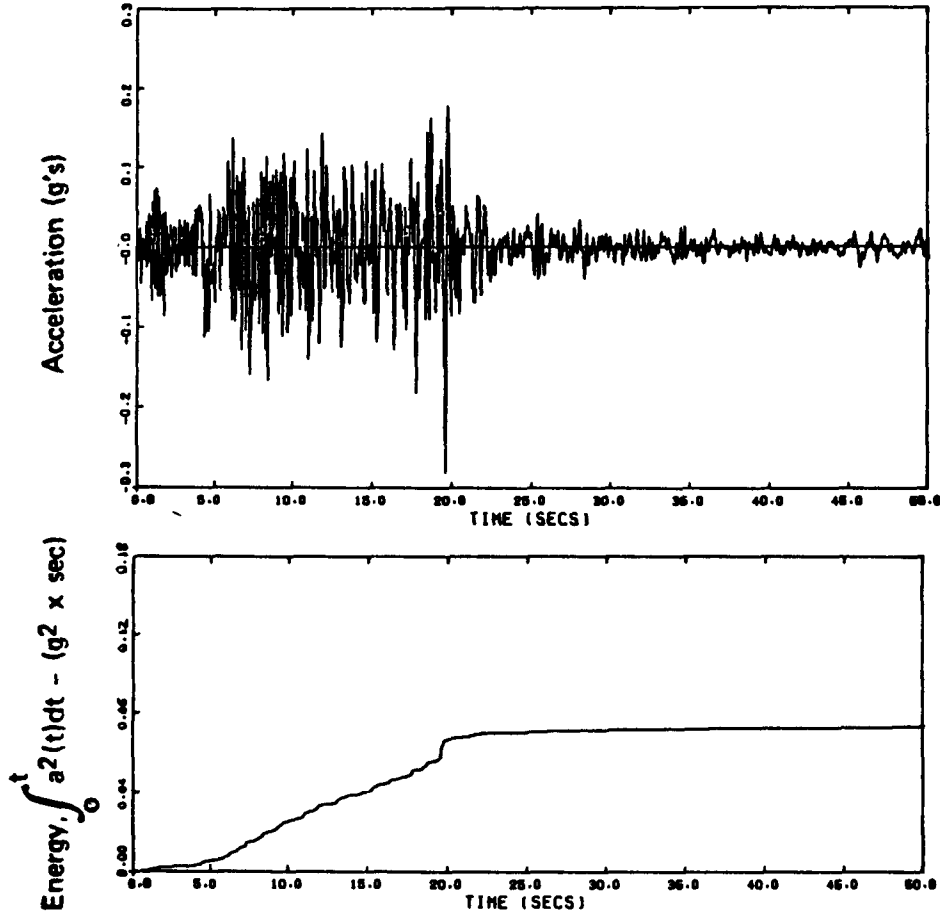
OLYMPIA, WASHINGTON HIGHWAY
TEST LAB, N86E
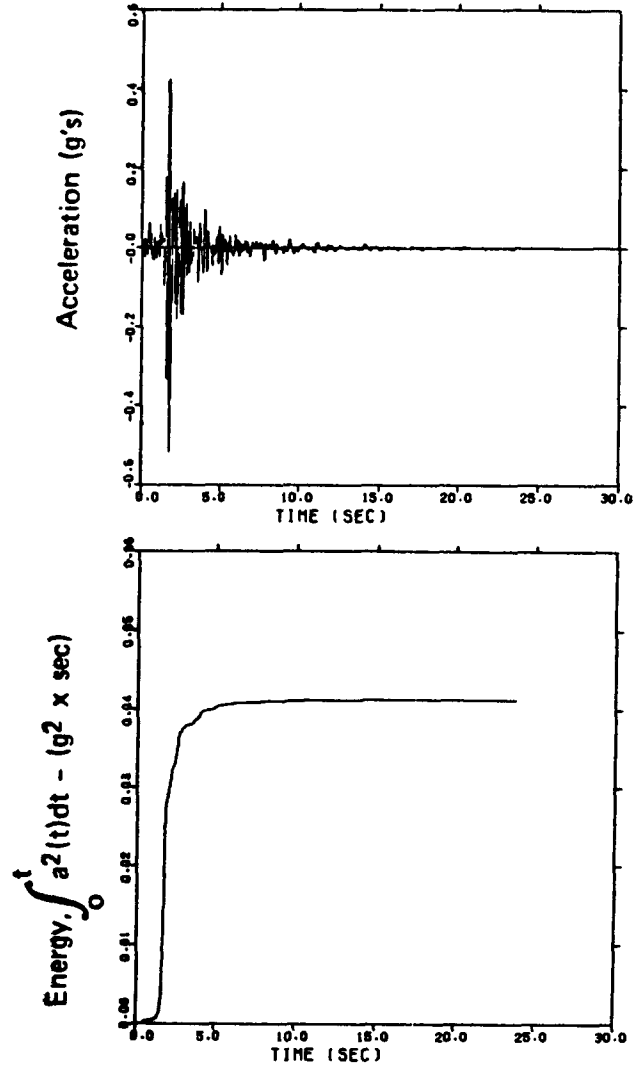
MELENDY RANCH N29W

FIGURE 2-2. COMPARISON OF ACCELEROGRAM AND VARIATION OF CUMULATIVE ENERGY
WITH TIME FOR REPRESENTATIVE LONG AND SHORT DURATION MOTIONS
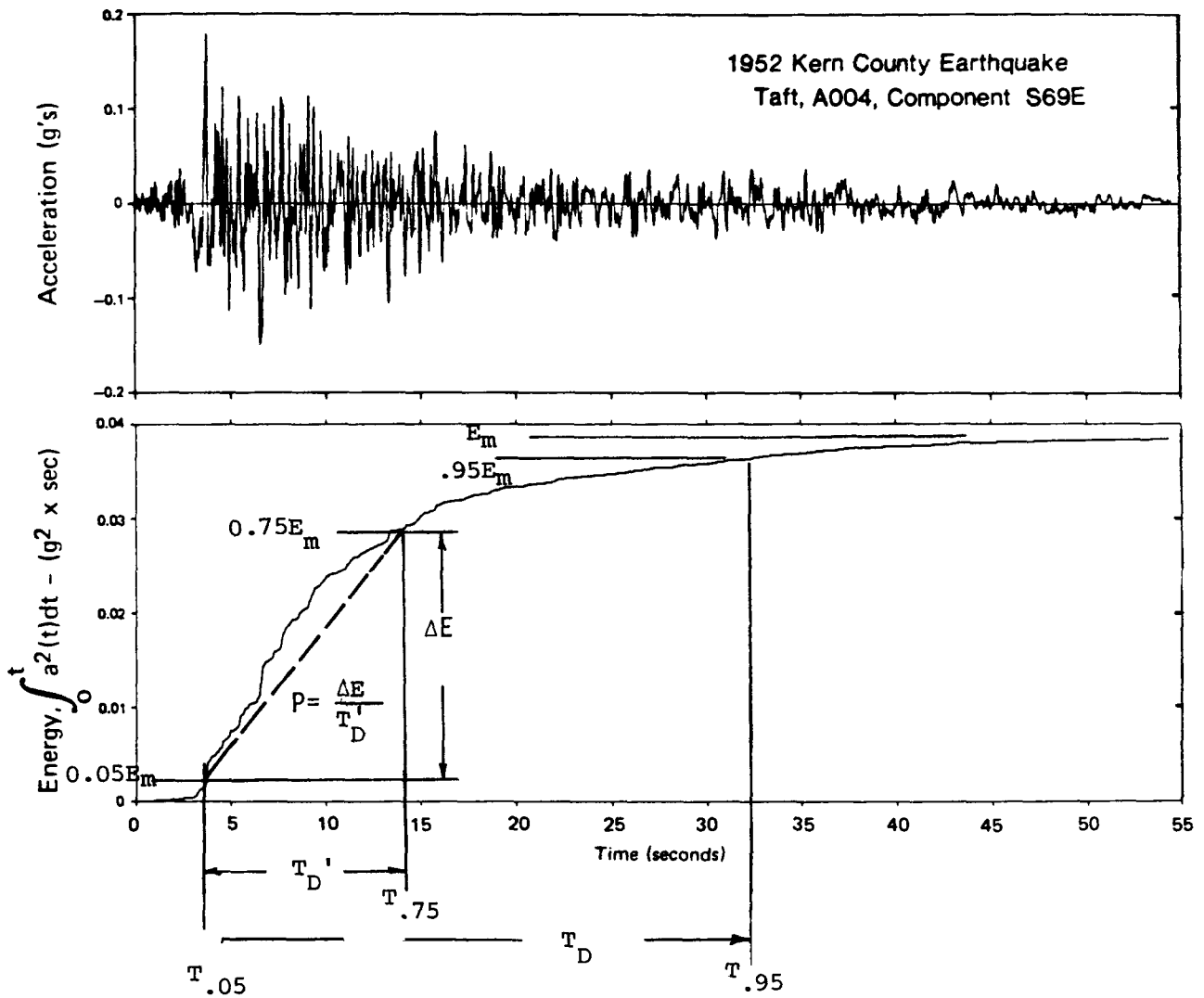
FIGURE 2-3. ACCELEROGRAM AND VARIATION OF CUMULATIVE ENERGY WITH TIME
FOR THE 1952 KERN COUNTY EARTHQUAKE RECORDING AT TAFT
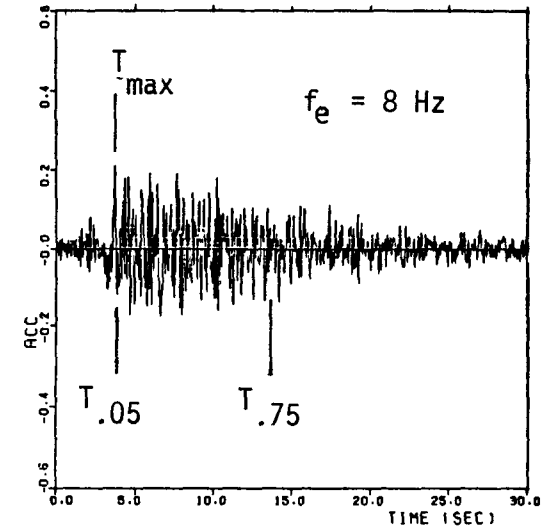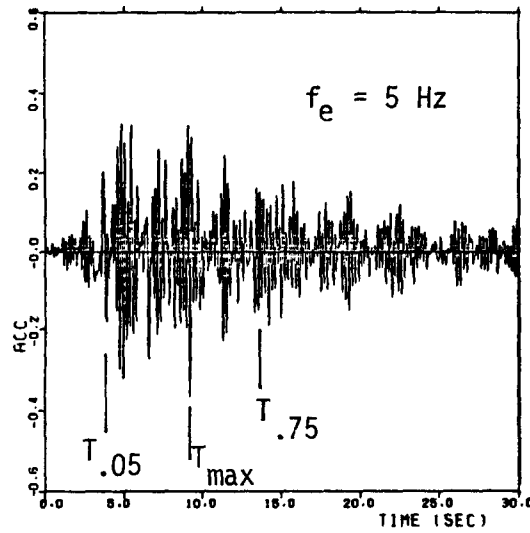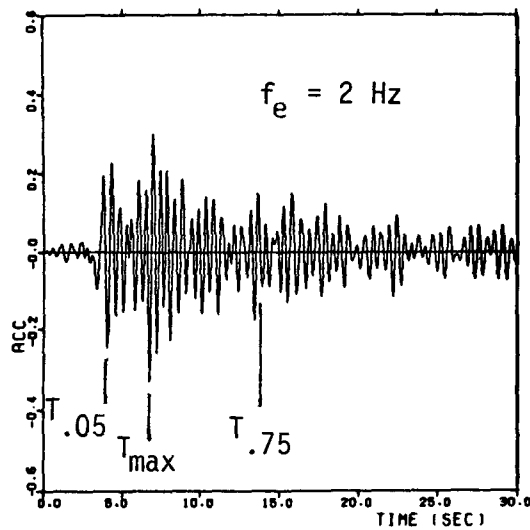
(a) SDOF Oscillator (7% Damping) Response Due to Taft Record
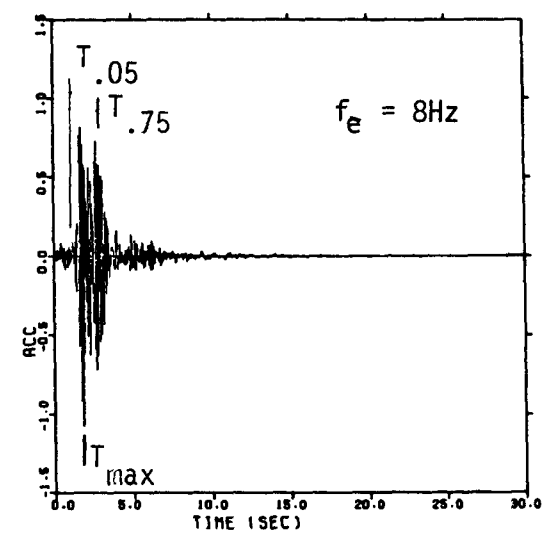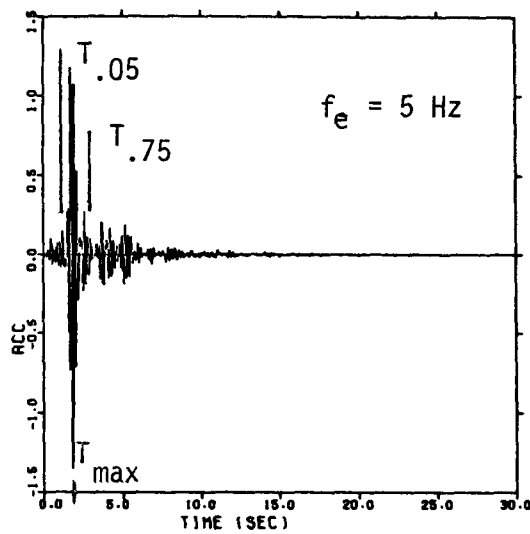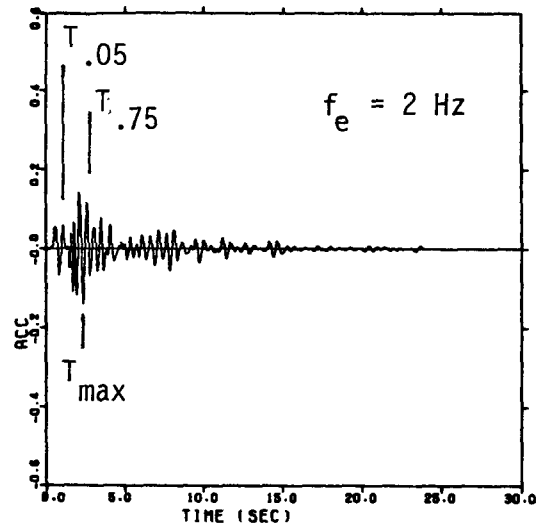
(b) SDOF Oscillator (7% Damping) Response Due to Melendy Ranch Record

FIGURE 2-4.   ELASTIC RESPONSE OF DAMPED OSCILLATOR DUE TO REPRE-
SENTATIVE LONG AND SHORT DURATION MOTIONS
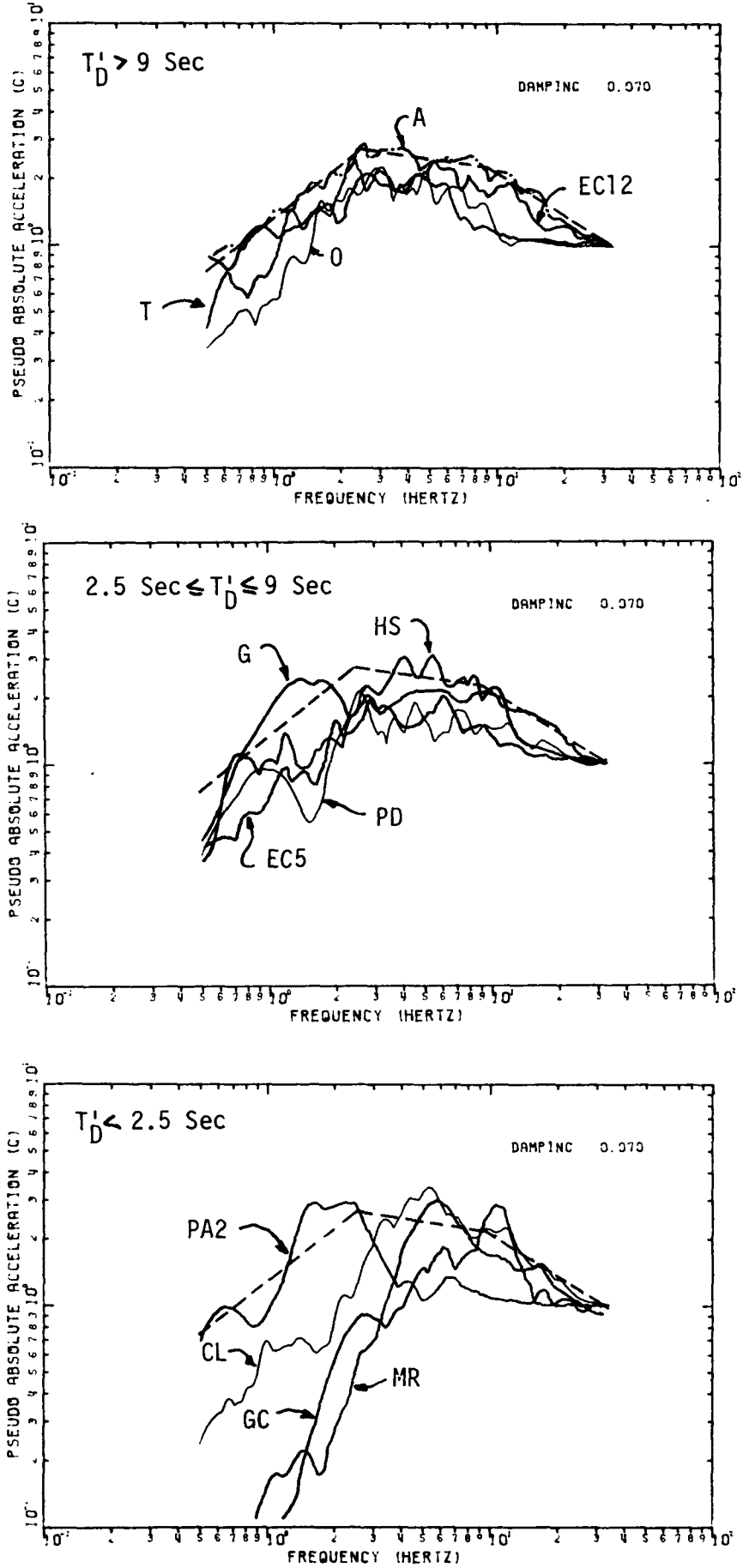
FIGURE 2-5.   COMPARISON OF NORMALIZED (1.0g) RESPONSE
               SPECTRA SHAPES AS A FUNCTION OF DURATION
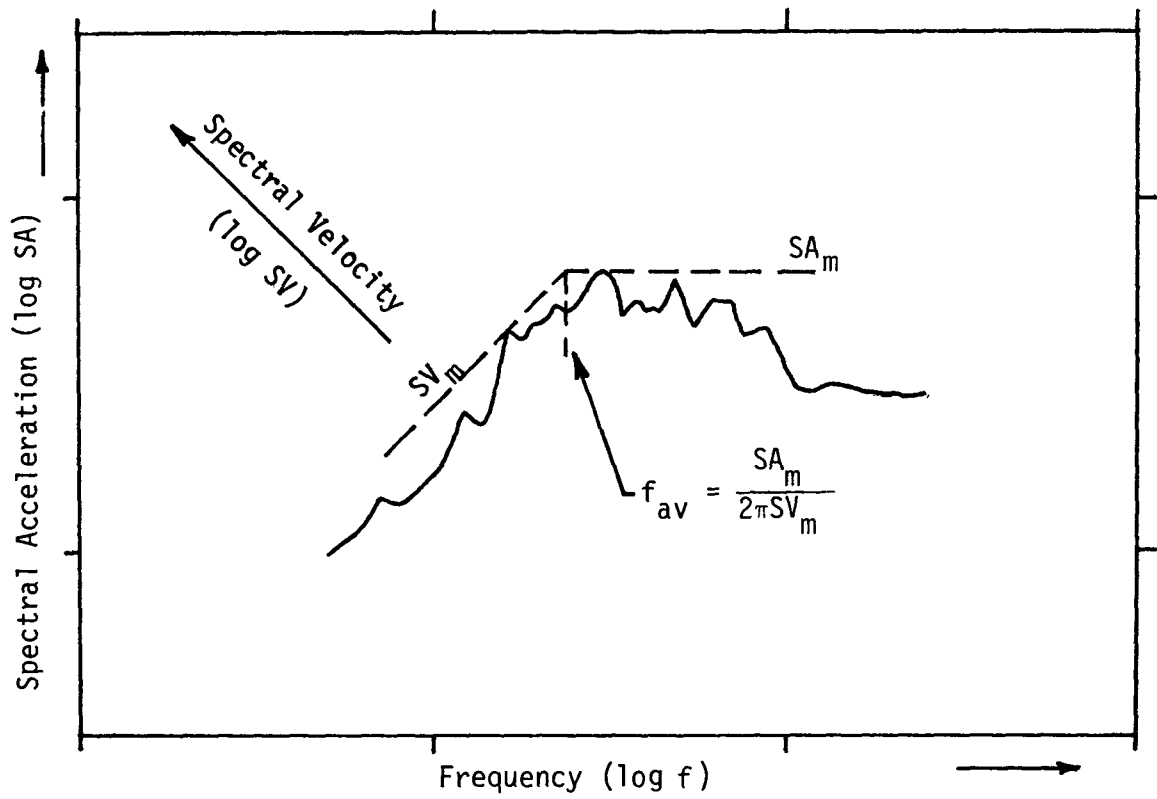
(a) Representative Long Duration Input Motion
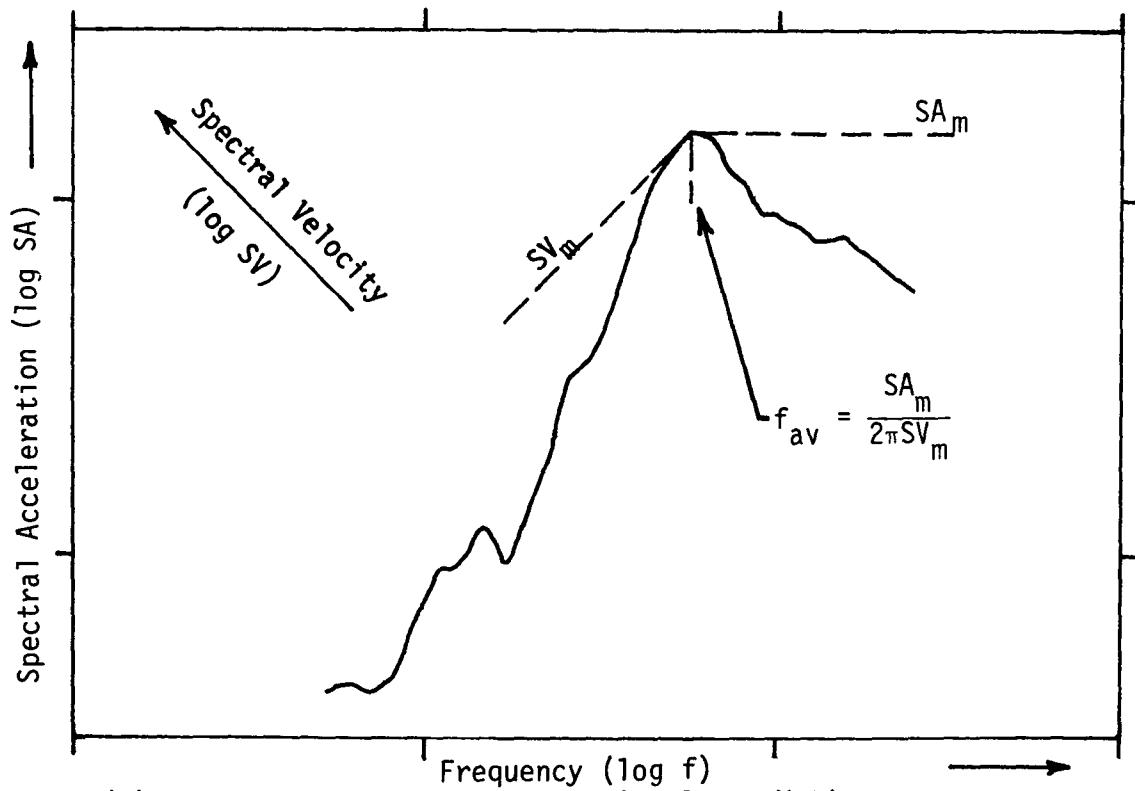
(b) Representative Short Duration Input Motion

FIGURE 2-6. GROUND MOTION PARAMETERS
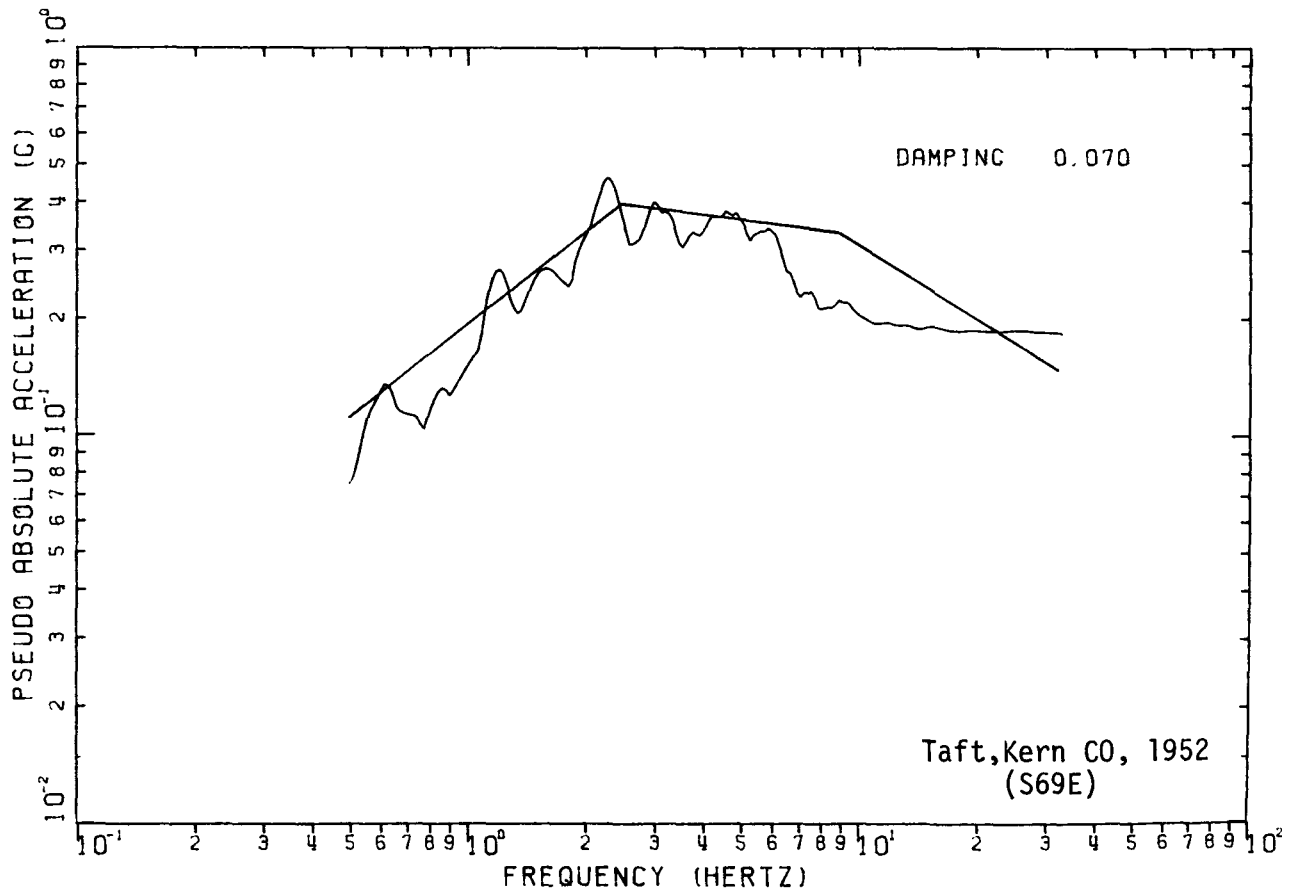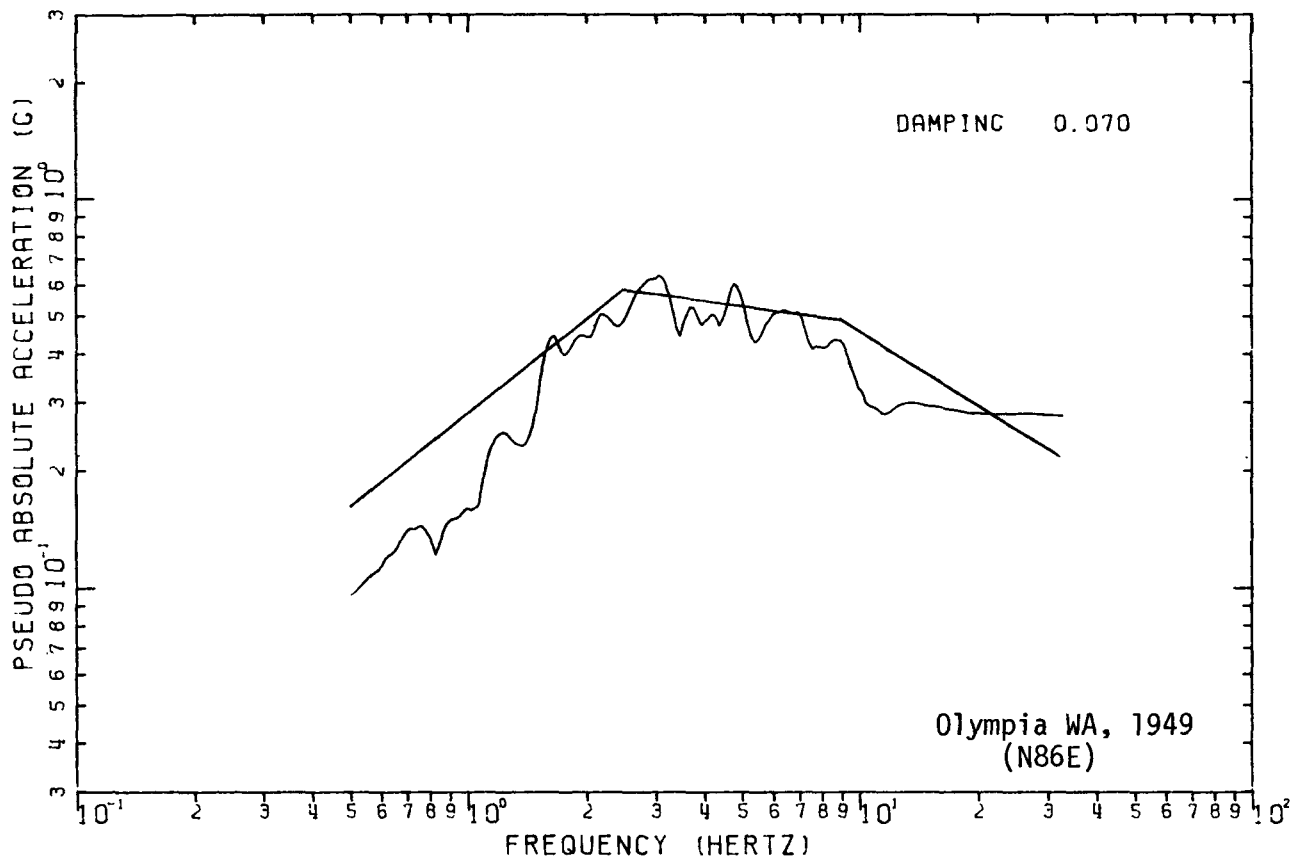
(a) Long Duration Records ($T'_D > 9.0$ Sec)

FIGURE 2-7a. COMPARISON OF REAL GROUND MOTION SPECTRA WITH REG.GUIDE 1.60
SPECTRA ANCHORED TO "EFFECTIVE" ACCELERATION, A_{DE}
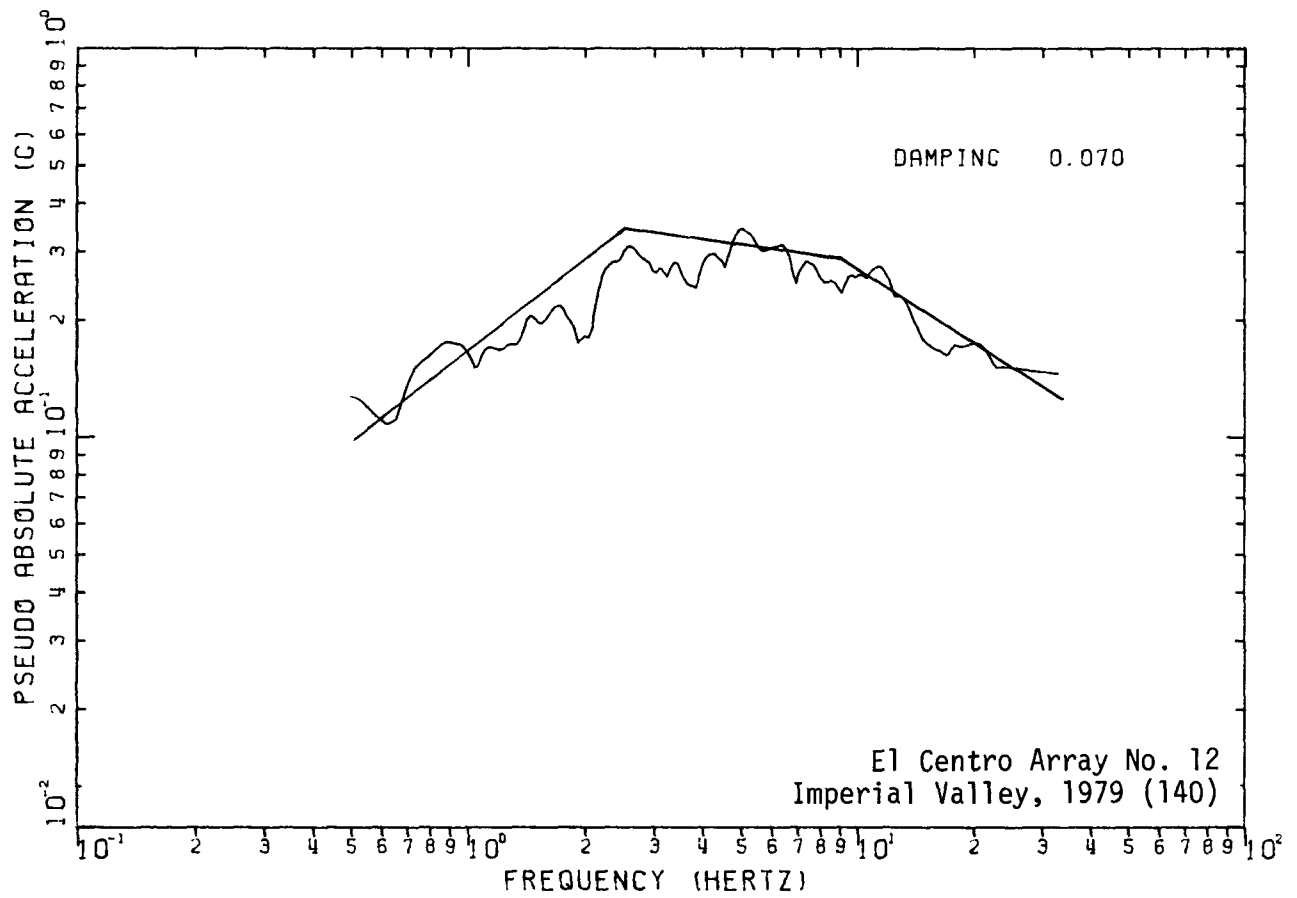
(a) Long Duration Records $(T_D' > 9.0$ Sec)
(Continued)

FIGURE 2-7a. COMPARISON OF REAL GROUND MOTION SPECTRA WITH REG. GUIDE 1.60
SPECTRA ANCHORED TO "EFFECTIVE" ACCELERATION, A_{DE}

DAMPING 0.070

Pacoima Dam
San Fernando, 1971 (S14W)

DAMPING 0.070

Hollywood Storage P.E. Lot
San Fernando, 1971 (N90E)
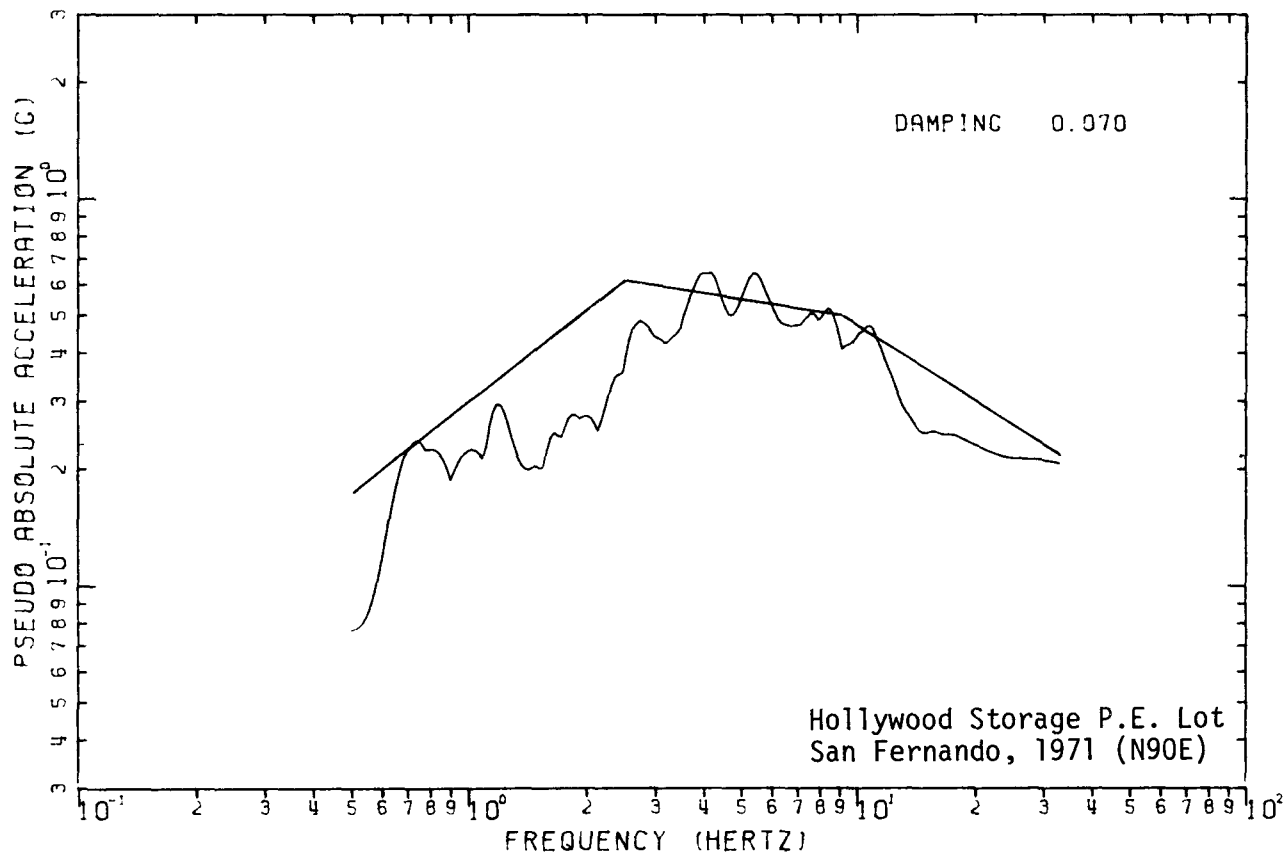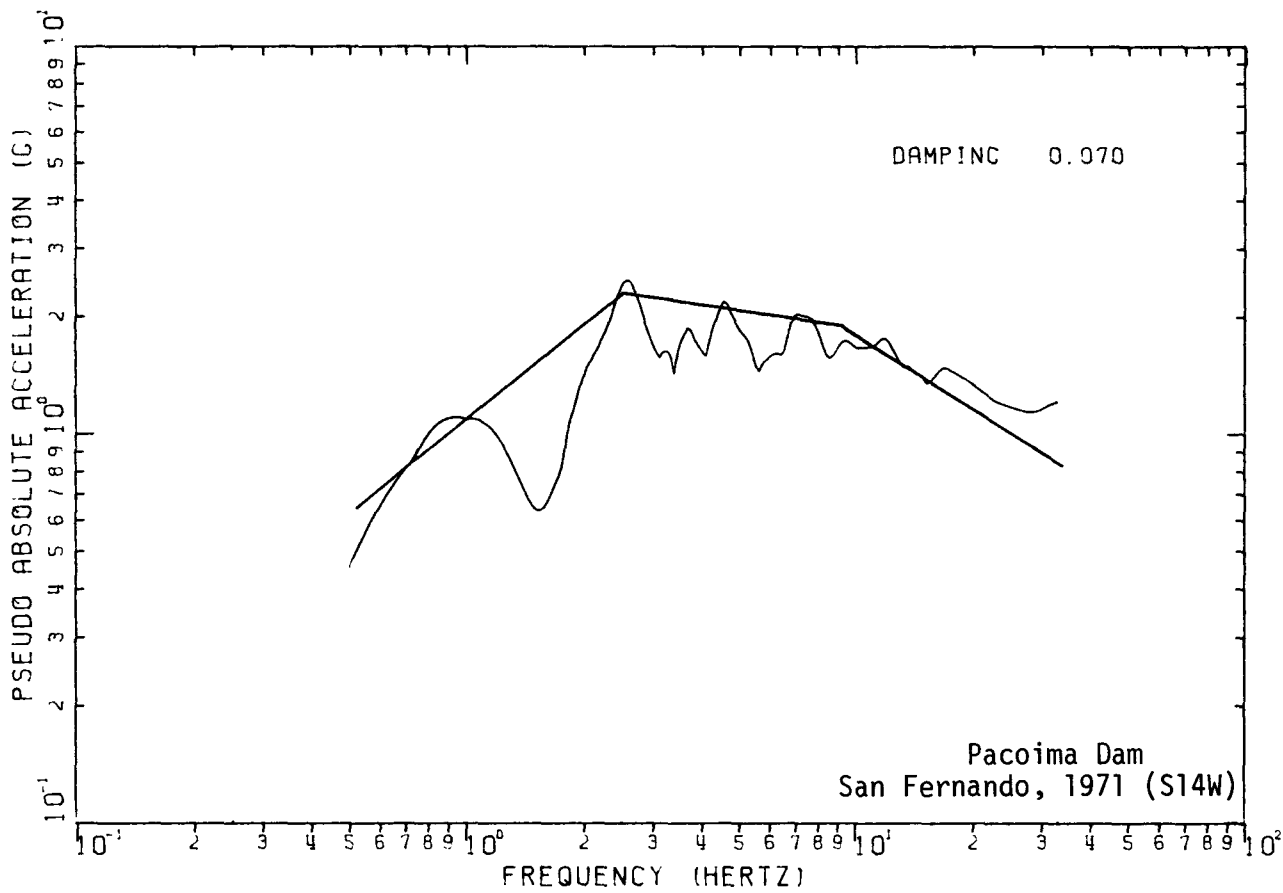
(b) Mid Duration Records (2.5 Sec $\leq T_D \leq$ 9.0 Sec)

FIGURE 2-7b. COMPARISON OF REAL GROUND MOTION SPECTRA WITH REG. GUIDE 1.60
SPECTRA ANCHORED TO "EFFECTIVE" ACCELERATION, A_{DE}

El Centro Array No.5
Imperial Valley, 1979(140)

DAMPING 0.070

PSEUDO ABSOLUTE ACCELERATION (G)

FREQUENCY (HERTZ)

UCSB Goleta
Santa Barbara, 1978 (180)

DAMPING 0.070

PSEUDO ABSOLUTE ACCELERATION (G)

FREQUENCY (HERTZ)
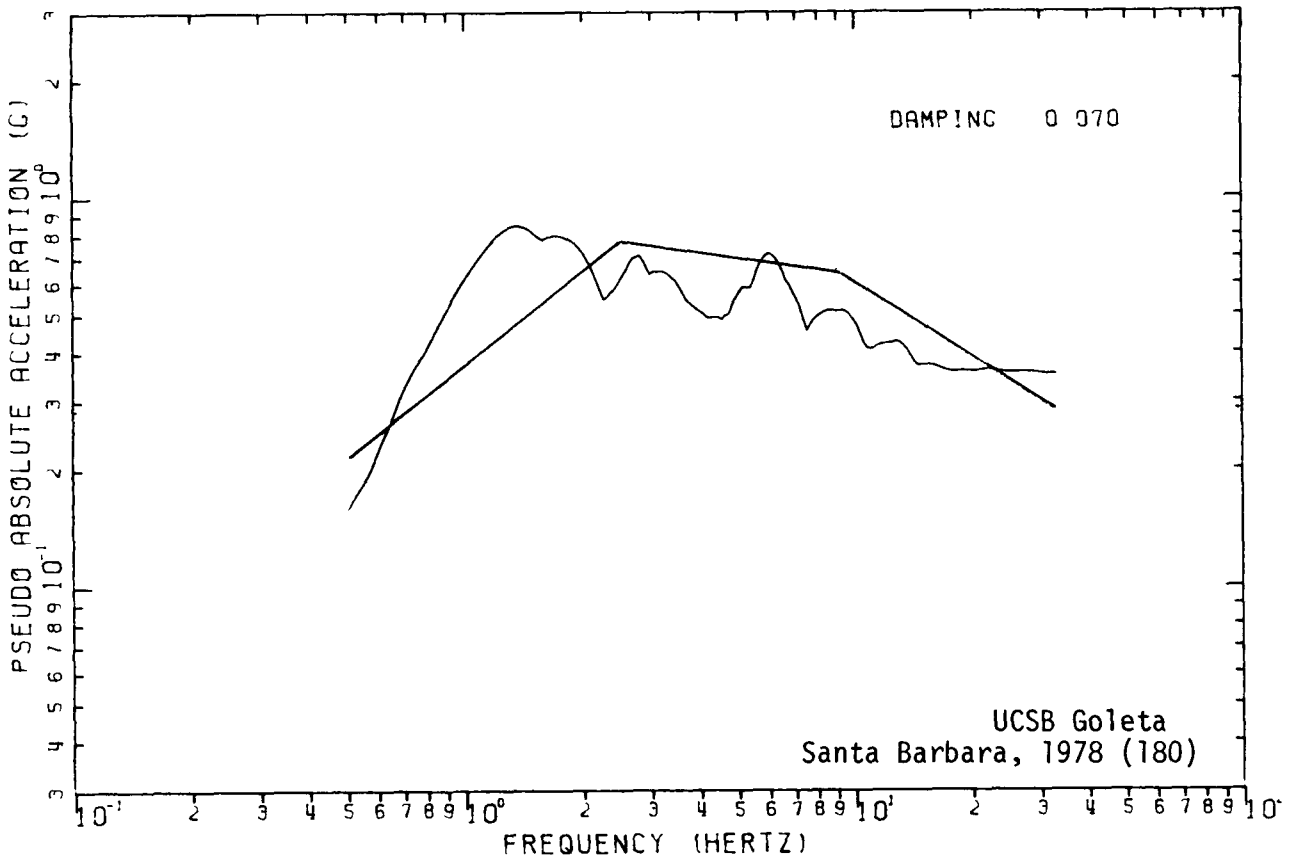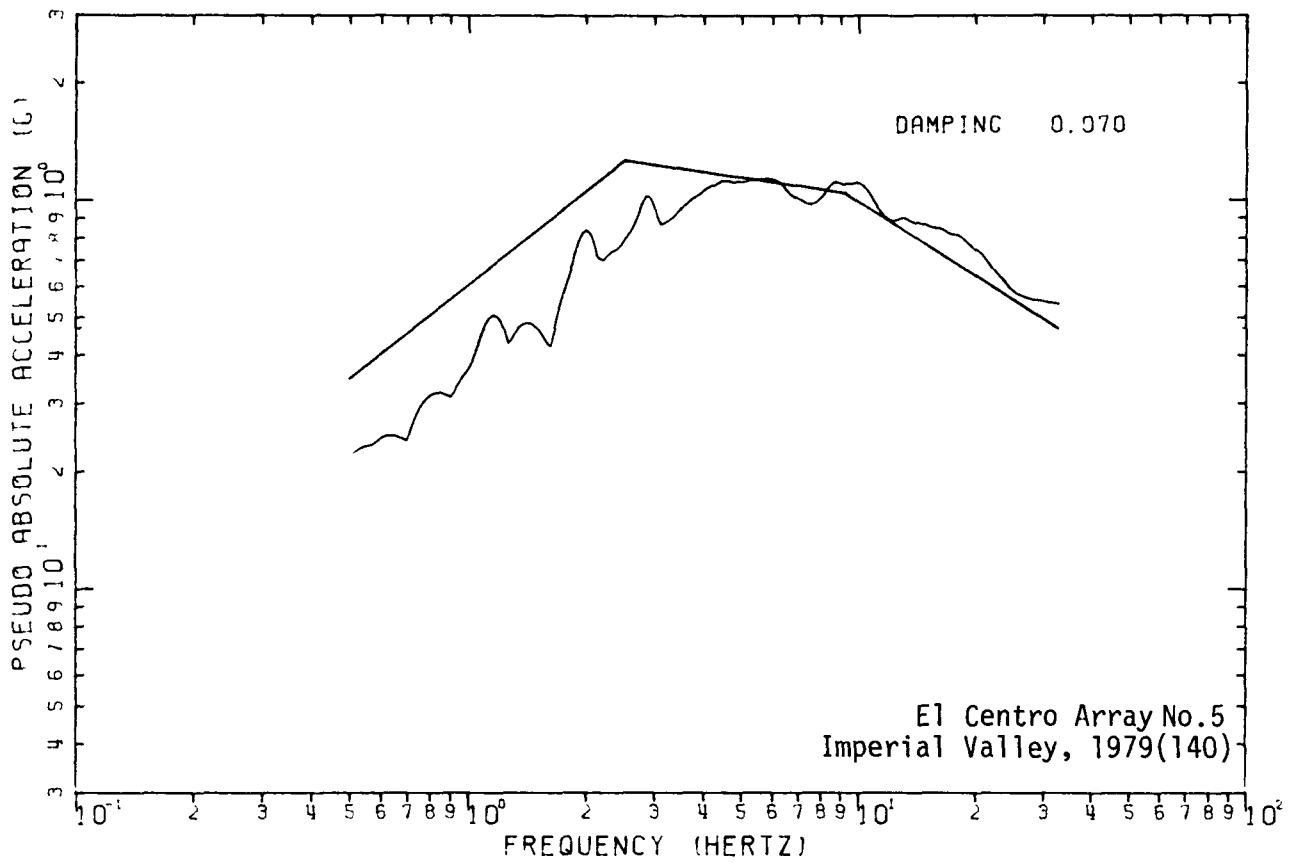
(b) Mid Duration Records (2.5 Sec$\leq T_D' \leq$ 9.0 Sec)
(Continued)
FIGURE 2-7b. COMPARISON OF REAL GROUND MOTION SPECTRA WITH REG. GUIDE 1.60
SPECTRA ANCHORED TO "EFFECTIVE" ACCELERATION, A_{DE}
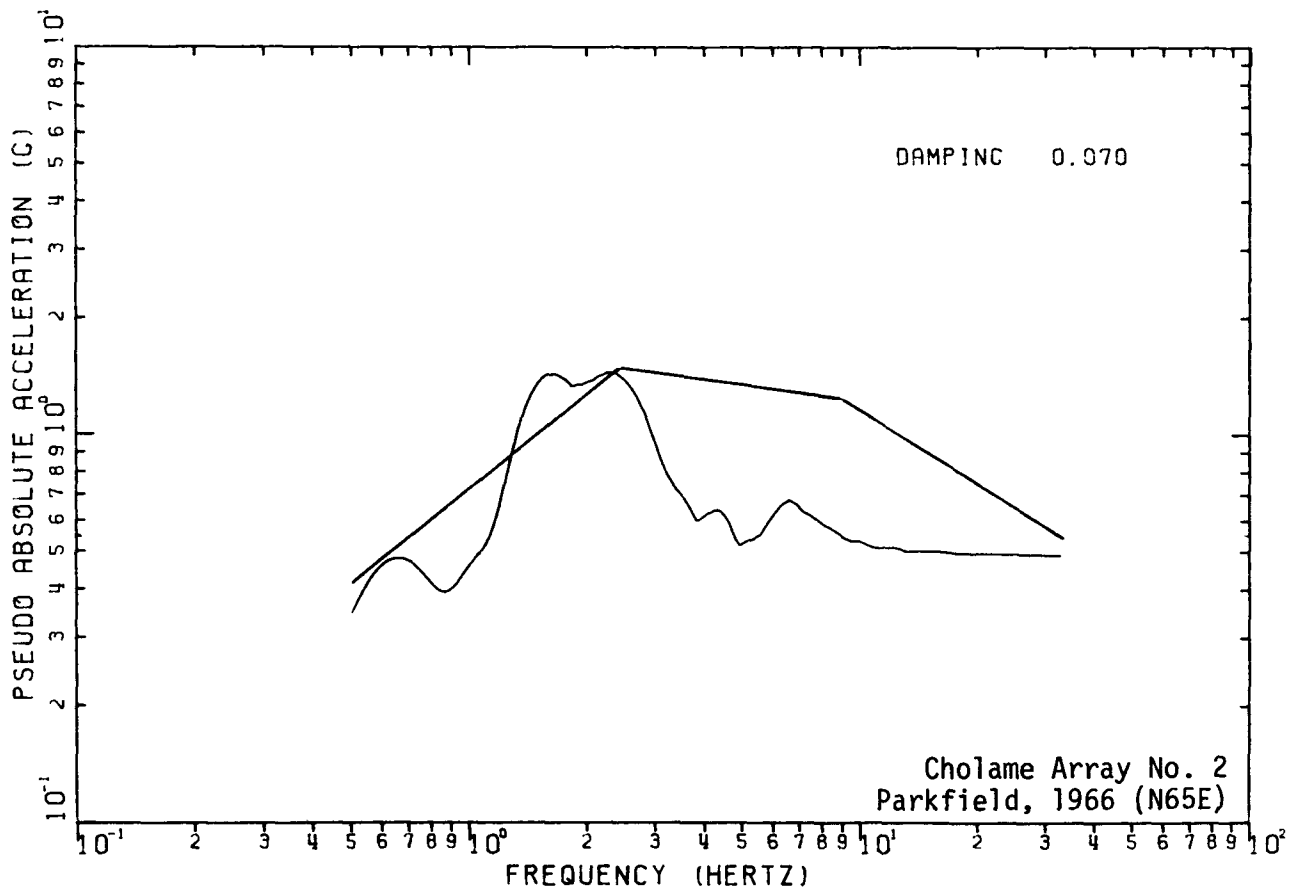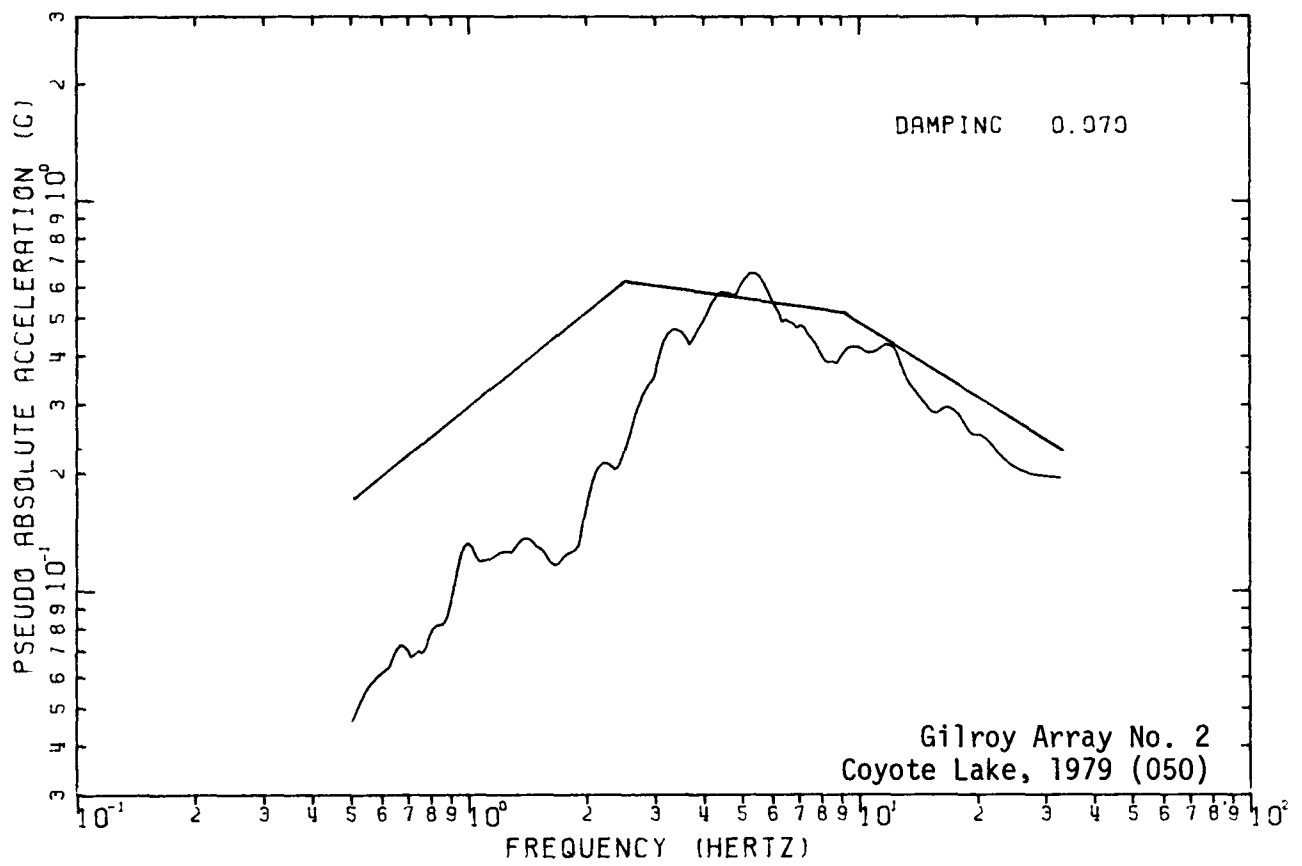
(c) Short Duration Records ($T_D' < 2.5$ Sec)

FIGURE 2-7c. COMPARISON OF REAL GROUND MOTION SPECTRA WITH REG. GUIDE 1.60
SPECTRA ANCHORED TO "EFFECTIVE" ACCELERATION, A_{DE}

DAMPING 0.070

Gavilan College
Hollister, 1974 (S67W)

DAMPING 0.070

Melendy Ranch Barn
Bear Valley, 1972 (N29W)
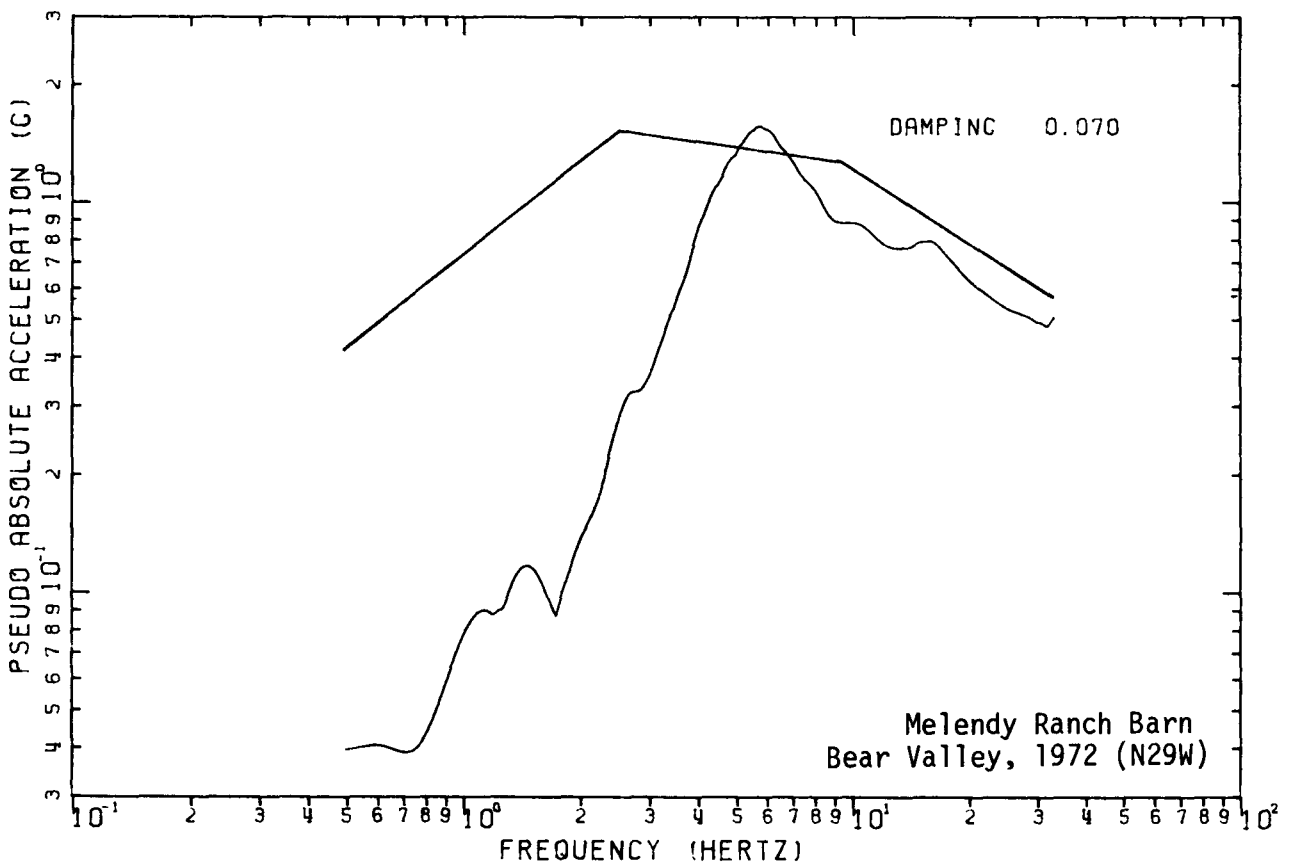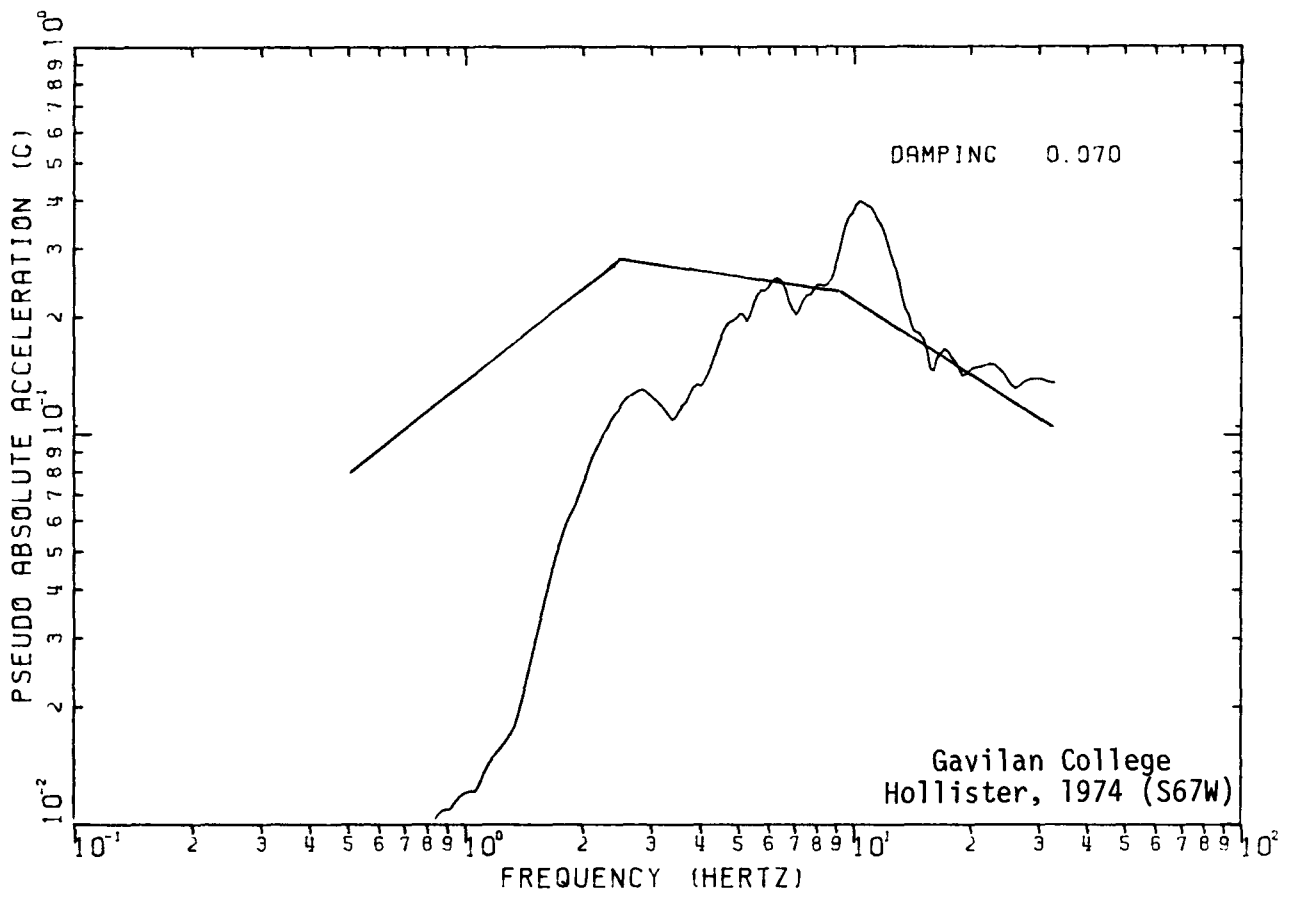
(c) Short Duration Records ($T_D' < 2.5$ Sec)
(Continued)
FIGURE 2-7c. COMPARISON OF REAL GROUND MOTION SPECTRA WITH REG. GUIDE 1.60
SPECTRA ANCHORED TO "EFFECTIVE" ACCELERATION, A_{DE}

3. TECHNICAL APPROACH FOR NONLINEAR STRUCTURAL RESPONSE ANALYSES

Chapter 2 presented the minimum engineering characterization of the ground motion required for the determination of elastic structural response. However, as noted in Chapter 1, elastic structural response does not provide a good measure of structural damage. Potential quantitative measures of structural damage and their relative pros and cons were presented in Section 1.3. Throughout this study, the ratio of peak displacement to elastic yield displacement (ductility ratio, μ) is used as a measure of damage for the reasons given in Section 1.3. Again, it should be noted that this measure of damage may overstate the damage capability of short duration ground motions. However, this damage measure is used because of uncertainty concerning other measures of damage and because it serves as a conservative damage measure.

The purpose of this chapter is to provide technical background material for the computation and prediction of inelastic structural response. Results of inelastic structural response analyses will be presented in Chapter 4. Ground motion characterizations for inelastic response will be described in Chapter 5.

3.1 REPRESENTATIVE NONLINEAR STRUCTURAL RESPONSE RESISTANCE FUNCTIONS

Several representative nonlinear structural response resistance functions are shown in Figure 3-1. These are a) Bilinear, b) Takeda, and c) Shear Wall.

The bilinear model represents the resistance function for intrinsically ductile, nondeteriorating systems such as shear members and unbraced moment-resisting steel frames primarily deforming in flexure with only moderate axial loads. In this model, the structure loads with an initial stiffness, K, until the yield capacity, V_y, is reached. Further loading occurs along a reduced stiffness, sK. Unloading occurs on the

initial stiffness, K. Cycles are stable without any dependence on the number of previous nonlinear cycles. The elasto-plastic model represents a subset of this bilinear model in which the second slope, sK, is zero.

The Takeda model generally represents the appropriate model for properly reinforced concrete structures primarily loaded in flexure. Initially, the Takeda model loads and unloads in the same manner as the bilinear model. However, nonlinear deformations are accompanied by concrete cracking. Upon returning to zero force, the presence of these cracks softens reloading in either direction. Future loading cycles are always toward the point of maximum previous deformation. The Takeda model thus incorporates stiffness degradation due to concrete cracking.

Experimentally determined resistance functions (Figure 1-9a) for low-rise concrete shear walls predominantly deforming in shear exhibit certain characteristics not incorporated into the previously described Takeda model. These are:

a) Unloading on a softer stiffness, K_u, than the initial loading stiffness.

b) A substantial pinched behavior upon loading in the opposite direction until displacements return to zero.

c) After zero displacements are reached, further loading is toward a point of greater displacement than that reached in any prior deformation cycle.

d) Once a certain ductility level, μ_{max}, is reached, future loading cycles are accompanied by rapid strength degradation.

The shear wall model shown in Figure 3-1c incorporates Items (a) through (c). Strength degradation should be precluded by limiting the permissible upper bound ductility, μ_{max}, to levels less than that at which substantial strength degradation occurs. Thus, it was judged to be unnecessary to incorporate strength degradation into this shear wall model.

Low-rise shear walls predominantly deforming in shear represent the primary seismic load carrying elements for most nuclear plant structures. Thus, the shear wall resistance function model is used for most of the nonlinear analyses in this study. This model was chosen because:

1. It is more representative of the majority of nuclear plant structures.

2. Its use is conservative relative to either the bilinear or Takeda models.

The shear wall model has less hysteretic energy dissipation per cycle than does either the bilinear or Takeda model. Thus, for a given ground motion time history, the maximum computed ductility level, μ, will be larger from this model than from either the Takeda or bilinear model. A short parametric analysis is presented in Appendix D to demonstrate that this shear wall model does lead to greater ductility levels than does the Takeda model.

The other primary lateral load carrying systems often found in nuclear plants are steel-braced frames. A representative nonlinear resistance function for such braced frames was shown in Figure 1-9b. This braced frame resistance function also shows pinched behavior similar to that for shear walls. However, the pinching is not generally as severe so that a typical braced frame nonlinear response cycle will generally contain more hysteretic energy dissipation than does a similar shear wall nonlinear response cycle. Thus, again, the shear wall model will generally conservatively overestimate the ductility level, μ, for a braced frame subjected to a given ground motion when both models have the same yield capacity and elastic stiffness, K. This point is also demonstrated by a short braced frame parametric analysis presented in Appendix D.

In summary, it is judged that results and conclusions presented in this study based upon the shear wall model can be conservatively used for structures exhibiting bilinear, Takeda, shear wall, or braced-frame resistance functions.

3.2   DETAILED DESCRIPTION OF SHEAR WALL MODEL

3.2.1   Rules for Constructing Shear Wall Resistance Function Model

Reinforced concrete walls resist shear through various mechanisms. Initially, the wall is elastic and shear resistance is developed according to elastic beam theory. Inclined shear cracks develop when the principal tensile stresses exceed the concrete tensile strength. Once shear cracks open, the shear force is resisted mainly by the reinforcing bars and aggregate interlock. Other mechanisms such as dowel action, truss action, and the flexural compression zone also contribute to the shear resistance. The opening and closing of cracks under load reversals causes the pinching behavior noted in the hysteresis loops. Also, as shear cracks open wider and damage to the concrete increases, the contribution of concrete, through aggregate interlock, to shear resistance decreases. This effect causes strength degradation under large displacement cycles. A shear force-shear distortion diagram obtained during a structural wall test was shown in Figure 1-9a which illustrates the reverse cycle loading behavior characterized by stiffness degradation and pinching of the hysteresis loops. Relatively few reversing load tests of low-rise walls have been reported. Fiorato and Corley (1977) have summarized the laboratory testing conducted on low-rise walls with typical reinforcement ratios, in the range of 0.25 - 0.5%, which are more typical of commerical building construction (Shiga, 1973; Barda, 1976; Cardenas, 1973; Paulay, 1977; Park, 1975; Alexander, 1973). Much of the structural wall testing (Wang, 1975) conducted at the University of California, Berkeley, provides useful information on the behavior of low-rise wall segments which has been recently summarized by Bertero (1977) and Popov (1980). Cyclic load testing of low-rise box structures with

3-4

reinforcement ratios in the range of 0.6 - 1.6% has been limited to model structures and conducted primarily in Japan (Umemura, 1977, 1980: Uchido, 1980; Fukada, 1981).

The primary or envelope loading curve assumed for inelastic shear elements representing the shear flexibility of low-rise reinforced concrete walls is defined by a bilinear approximation of the deformation behavior of low aspect ratio walls under monotomically increasing load. The consideration of a bilinear curve consisting of two linear segments is based on the work by Umemura (1977, 1980) interpreted in terms of the Arakawa formula (Kubota, 1978) for shear strength of reinforced concrete members. The slope of the first segment represents the effective shear stiffness of the uncracked concrete wall section, while the slope of the second segment represents the effective stiffness of the reinforcing steel after cracking has occurred.

The hysteresis behavior for the shear element is defined by a set of 10 rules. These rules are described below, and they are also shown by their corresponding numbers in Figure 3-2.

Rule 1:   The shear deformation curve, defined by a linear stiffness, K, is elastic up to the yield shear force, V_y.

Rule 2:   Once the yield point in any direction is exceeded, loading continues on the second slope defined by a softer linear stiffness parameter, sK.

Rule 3:   Unloading is initiated when the direction of loading changes. A degrading unloading stiffness feature is built into the model. This is shown in Figure 3-3a. Therefore, if the system unloads from Rule 2, instead of unloading parallel to the elastic stiffness, K, to a recovery point such as δ_r', unloading is towards a new recovery point, δ_r, such that

$$\delta_r = (1-\alpha)\delta_r' \qquad\qquad (3-1)$$

where α is the unloading stiffness parameter. The reduced unloading slope is used for subsequent unloading as long as the maximum deformation is not exceeded. If the recovery point, δ_r, is reached, loading in the opposite direction is according to Rule 4. Reloading from this part is according to Rule 8.

Rule 4: Once the unloading is finished, the system would initially exhibit a low stiffness in the opposite direction. This is a typical pinching behavior which is observed in shear wall tests. The pinched behavior is due to opening and closing of cracks under cyclic loads. Loading stiffness for this point is assumed to be the same as the second slope of the primary curve, sK. Once zero deformation is reached, loading will be according to Rule 7. Unloading from this part is according to Rule 5.

Rule 5: Unloading from Rule 4 is parallel to the unloading (Rule 3) slope on the same deformation side. Once zero shear force is reached, loading in the opposite direction is according to Rule 8. If the direction of loading changes, loading is according to Rule 6.

Rule 6: If the direction of loading changes while in Rule 5, loading will be on the same line until the point where unloading was initiated is reached (Point A in Figure 3-2c). Loading is according to Rule 4 thereafter. On the other hand, unloading from this part is according to Rule 5.

Rule 7: Once the cracks are closed ($\delta = 0$ in Rule 4), loading begins toward the previous point of maximum deformation. In addition, a strength degrading feature is built into the model. This is shown in Figure 3-3b. Thus, instead of loading towards the previous point of maximum (Point $\tilde{A}$ in Figure 3-3b), a new target point such as $\tilde{B}$ is defined such that

$$\delta_{\tilde{B}} = \delta_{\tilde{A}}/\gamma \qquad (3-2)$$

where γ is the strength degradation parameter. Once point $\tilde{B}$ is reached, loading starts on the second slope again (Rule 2). Unloading from this part is according to Rule 3.

Rule 8:   This rule assures that any loading from Rule 3 will be
           towards the previous intermediate point (Points B and
           C in Figure 3-2c). Once this point is reached, loading
           is according to Rule 7 (Point C in Figure 3-2c).
           However, for a point such as B in Figure 3-2c, loading
           from Rule 8 is on the second slope (Rule 2).
           Unloading from this part is according to Rule 9.

Rule 9:   Unloading from Rule 8 is parallel to the last minimum
           unloading slope (Rule 3). Once unloading is finished,
           loading in the other direction is according to Rule 4.
           A change of direction in load would cause the system
           to follow Rule 10.

Rule 10:   Loading from Rule 9 is on the same slope until the
           previous intermediate point (Point D in Figure 3-2c)
           is reached. Loading is according to Rule 8 thereafter.
           Unloading from this part is according to Rule 9. The
           small amplitude or shakedown behavior of the shear
           hysteresis model is shown in Figure 3-3c.

The 10 rule hysteretic model defined above is based on quasi-static cyclic load tests of shear wall elements representative of nuclear plant box-type reinforced concrete structures. The model is similar to the shear models used by Banon (1981) and Saiidi (1979). Except for shear pinching and strength degradation, the model is very similar to the modified Takeda model (Kanaan, 1975) used to represent the hysteretic behavior of reinforced concrete in flexure. Comparison of the model behavior with available cyclic load test data indicates that the model provides good agreement with test results when large displacement cycles are considered up to displacements associated with the onset of substantial strength degradation (typically occurring at ductility levels ranging from 4.3 to 6.0). The shakedown behavior (i.e., behavior after peak deformation is reached as shown in Figure 3-3c) used in this model is unverified because of insufficient experimental data on cyclic behavior after peak response is reached. However, proper modeling of this shakedown behavior is unimportant so long as a peak displacement (ductility ratio) criteria is used as a measure of damage. The proper modeling of this shakedown behavior is very important if a total hysteretic energy absorption criterion had been used as a measure of damage. The lack of experimental data on shakedown behavior is one of the primary drawbacks to the use of a total hysteretic energy absorption criteria as a measure of damage.

3.2.2 Resistance Function Properties Used in this Study

The following resistance function parameters were used in this study:

a) Slope parameter of post-yield loading curve, $s = 0.1$
b) Unloading stiffness parameter, $\alpha = 0.35$
c) Strength degradation parameter, $\gamma = 0.95$

The second slope of the loading curve is shallow compared to the initial stiffness, K, for most structural elements, with s typically ranging from about 0.03 to 0.15. The value chosen for this study ($s = 0.1$) is considered representative for shear walls with large reinforcement ratios (approximately one percent steel) typical of nuclear plant structures. The second slope increases with steel percentage and s would be less than 0.1 for steel percentages less than about one percent. A very limited parameter study is presented in Appendix D to show that the computed ductility level, μ, decreases slightly as s is increased above 0.1. The results presented herein are reasonable for the case of $0 < s < 0.1$ and become conservative for cases where $s \gg 0.1$.

The unloading stiffness and strength degradation parameters, α and γ, respectively, have been chosen to be realistic (slightly conservative) for ductility levels up to about 4.3 which is the maximum ductility level considered in this study. The unloading stiffness parameter, $\alpha = 0.35$, results in an unloading stiffness, K_u, of approximately two-thirds of the initial loading (elastic) stiffness at a ductility level of 3.0 which is slightly greater unloading softening than shown by most experimental data. However, Appendix D shows results are not sensitive to α. Similarly, the strength degradation parameter, $\gamma = 0.95$, is representative of the very slight strength degradations which occur at ductility levels less than 4.3. However, this strength degradation is substantially too small if the ductility level is increased significantly beyond about 4.3.

The elastic yield capacity, V_y, for each analysis was established by:

$$V_y = mS_a(f,\beta) \quad *$$ (3-3)

where m is the mass of the structural element, and $S_{a(f,\beta)}$ is the spectral acceleration for the given ground motion at the elastic natural frequency, f, and the elastic damping ratio, β, where:

$$f = \frac{1}{2\pi}\sqrt{\frac{K}{m}}$$ (3-4)

represents the frequency at the initial (elastic) stiffness, K. In other words, all structures were placed at the onset of yielding when subjected to the ground motions defined in Chapter 2.

This study was conducted at the following two ductility levels:

Low: $\mu_L = 1.85$

High: $\mu_H = 4.27$

Inelastic response of shear walls begins as soon as extensive concrete cracking occurs. For heavily reinforced shear walls (steel percentages of about one percent) typical of those found in nuclear plants, this inelastic behavior occurs before the code specified minimum ultimate capacity is reached. Based upon our review of a number of shear wall designs, a ductility level of about 1.85 represents our best estimate of the inelastic deformations which would occur in a shear wall designed for static lateral loads to the ACI-349 code capacity. The current elastic design analysis method when carried to code ultimate capacities is judged to lead to roughly this level of inelastic deformation for

---

* S (f,β) used here is equivalent to SA_y in Chapter 1 and Figure 1-10 for Application B (determination of input scale factors).

static lateral loads. In other words, μ_L of 1.85 is judged to correspond to code capacity pseudo-elastic behavior. This situation is illustrated in Figure 3-4. This means that the recommendations and conclusions of this study for the low ductility case (μ = 1.85) are considered to be appropriate for shear wall structures designed to remain essentially elastic for the design earthquake.

The high ductility level, μ_H = 4.27, represents a conservative lower bound on the deformations which correspond to significant strength degradation under a small number (3 to 5) of strong nonlinear response cycles which might occur during strong ground shaking. In other words, this ductility level represents our best judgment of a conservative lower bound on the onset of significant structural damage.

Thus, the low (1.85) and high (4.27) ductility levels considered in this study are believed to bound the ductility range of interest for nuclear plant shear wall type structures.

3.2.3   Dynamic Properties Used in this Study

This study is concerned with the engineering characterization of ground motion responses of stiff structures representative of those in nuclear plants. Such structures tend to have fundamental elastic frequencies in the 1.8 to 10 Hz range, i.e., the amplified acceleration response range. Therefore, this study is intended to cover structures, with fundamental elastic frequencies from 1.8 to 10 Hz. Results of this study can probably be extrapolated to frequencies beyond this range but this was not verified by studying structures with elastic frequencies outside of this range. Shear wall structural elements with the following elastic natural frequencies were used in this study:

$$f = 2.14 \text{ Hz};\quad 3.20 \text{ Hz};\quad 5.34 \text{ Hz};\quad 8.54 \text{ Hz}$$

to represent the frequency range from 1.8 to 10 Hz. Elastic stiffnesses, K, for the shear wall resistance function were then computed from Equation 3-4.

Energy dissipation due to the elastic component of response was modeled by a viscous damping coefficient, c, given by:

$$c = \left(\frac{\beta}{\pi f}\right) K_T \qquad\qquad (3\text{-}5)$$

where β represents the fraction of critical damping within the elastic range of response, and K_T represents the tangent stiffness at any point on the resistance function. The damping coefficient, c, was made proportional to the tangent stiffness as opposed to the initial stiffness to avoid double-counting the hysteretic energy dissipation within the inelastic range. Energy dissipation primarily occurs during nonlinear response due to the hysteresis loop of the resistance function. This energy dissipation is already accounted for by the use of resistance functions with hysteretic loops and would be double-counted to some extent if the damping coefficient, c, were not reduced during nonlinear response.

Damping is a term which is utilized to account for various mechanisms of energy dissipation which occur when a structure is subjected to dynamic loads. Within the elastic range, damping is normally considered to be viscous and it is defined as a percentage of critical damping. It is usually difficult to estimate the viscous damping in a structure, because it depends on many factors such as material type (i.e., reinforced concrete or steel) and stress level. Damping values used in structural analyses are usually conservative estimates based upon experimental data. A detailed survey of studies on damping in nuclear facilities has been recently compiled by Stevenson (1980). Test results indicate that a conservative estimate of damping in concrete structures (mainly shear walls) varies from 5 percent for stress values below 0.5 yield to 10 percent for stress values close to yield. Regulatory Guide 1.61 (USNRC, 1973) suggests a 7 percent damping value be used for shear wall type structures under SSE conditions. This value has been used in this study. Thus:

$$\beta = 0.07$$

A small parametric study was performed with a lower elastic damping value of $\beta = 0.03$ and the results are presented in Appendix D. This study shows that the results and conclusions of this study on reduction factors to be applied to elastic spectra to obtain inelastic spectra are slightly conservative when the elastic damping value used for the elastic spectra is less than 7 percent. Thus, the results of this study are usable for elastic spectra with 7 percent and less damping.

This study is not intended to address the question of what value of damping should be used when performing nonlinear analyses of shear wall structures. There are advocates of damping values ranging from about 3% to 10% as well as advocates for both initial stiffness and tangent stiffness proportional damping. More research needs to be performed on these issues. However, the conclusions of this study are insensitive to these issues.

3.3   SIMPLIFIED METHODS TO APPROXIMATE NONLINEAR STRUCTURAL RESPONSE

Simplified methods to predict nonlinear structural response from elastic response spectra consist generally of one of the following approaches:

1.   Replace the nonlinear resistance function by an equivalent linear resistance function which has a lesser stiffness, K_e, and increased damping, β_e. This equivalent linear resistance function is then used with the elastic response spectra to compute maximum displacement response, $\delta_m = \mu\delta_y$.

2.   Modify the elastic response spectra to create reduced equivalent inelastic response spectra for use with the initial elastic stiffness, K, and elastic range damping, β, to compute the yield displacement response, δ_y and V_y.

Each of these general methods is discussed in greater detail in the following subsections.

3.3.1 Equivalent Linear Resistance Function Models

An equivalent linear resistance function model is developed to replace the actual resistance functions (Figure 3-1). This equivalent model should be capable of approximating the average reduced stiffness (or frequency) and average increased damping which occur during the nonlinear response cycles which occur prior to peak response. The secant stiffness represents the minimum effective stiffness during nonlinear response and for the resistance functions shown in Figure 3-1 this stiffness is given by:

$$K_s/K = \frac{1 + s(\mu-1)}{\mu} \tag{3-6}$$

The secant frequency, f_s, is obtained from Equation 3-4 by substituting K_s for K. Thus:

$$f_s/f = \sqrt{K_s/K} \tag{3-7}$$

The effective frequency, f_e', represents the frequency associated with some "average" nonlinear response cycle and the effective damping, β_e', represents the sum of elastic, β, and hysteretic, β_H, damping associated with this "average" nonlinear response cycle. Appendix C provides technical background suggesting that the effective frequencies and damping can be approximated by:

$$f_e'/f = (1-A) + A(f_s/f)$$

$$\beta_e' = \left(\frac{f_s}{f_e'}\right)^2 [\beta + \beta_H] \tag{3-8}$$

$$\beta_H = C_N(1-f_s/f)$$

where A and C_N are empirically determined coefficients selected to provide a good fit of the peak responses computed by nonlinear time history analyses. One would expect A to be approximately 0.5 for the case of N=1 (one strong nonlinear response cycle) and to increase toward 1.0 as N became large with the pinched shear wall resistance function. Furthermore, the coefficient A should increase with increasing ductility, i.e., with reducing (f_s/f) ratios. The coefficient C_N is expected to be less than 0.55 for N=1, less than 0.38 for N=2, and less than 0.32 for N=3 and 4 for the pinched shear wall resistance function (See Appendix C). However, both A and C_N will be empirically determined.

Previous investigators have made attempts to estimate the average effective frequency and damping for nonlinear structural response. Based upon a study of Takeda resistance function models for reinforced concrete structures, Sozen (Gulkan and Sozen, 1974; and Shibata and Sozen, 1976) has suggested:

$$\text{(Sozen)} \quad f'_e \approx f_s$$

$$\beta'_e \approx \beta + 0.2(1 - f_s/f) \tag{3-9}$$

Note that Equation 3-8 would be identical to Equation 3-9 if A=1.0 and $C_N = 0.20$.

Similarly, based upon a study of bilinear resistance functions and of resistance functions which approximate those for braced frames (Figure 1-9b), Iwan (1980) has suggested the effective frequency be given by:

$$\text{(Iwan)} \quad f'_e = \frac{f}{1 + 0.121(\mu-1)^{0.939}}$$

$$\beta'_e = \beta + 0.0587(\mu-1)^{0.371} \tag{3-10}$$

3-14

The equivalent linear response coefficients, A and C_N, will be determined in Chapter 4 to provide a good fit of the nonlinear time history maximum response results. Then, Equations 3-8, 3-9, and 3-10 will each be used to predict the nonlinear response factor, F, which will be compared with the actual computed nonlinear response factor for all 12 earthquake time histories and 4 elastic frequencies at $\mu_L = 1.85$ and $\mu_H = 4.27$ in the next chapter. F is the scale factor by which the ground motion must be increased over that corresponding to structure yield capacity in order to achieve a given level of nonlinear response, μ.

With each of these equivalent linear models, the maximum nonlinear structural response displacement, δ_m, is given by:

$$\delta_m = \frac{F_\mu S_a(f'_e, \beta'_e)}{(2\pi f'_e)^2} \tag{3-11}$$

whereas, the yield displacement, δ_y, is given by:

$$\delta_y = \frac{\delta_m}{\mu} \tag{3-12}$$

or

$$\delta_y = \frac{S_a(f, \beta)}{(2\pi f)^2} \tag{3-13}$$

Thus, the input scale factor, F_μ, is given by:

$$F_\mu = \mu (f'_e/f)^2 \left\{ \frac{S_a(f,\beta)}{S_a(f'_e,\beta'_e)} \right\} \tag{3-14}$$

in order to achieve a ductility level μ. It is these predicted factors, F_μ, which will be compared with the actual nonlinear analysis computed factors, F, in the next chapter.

3.3.2   Inelastic Spectra* Deamplification Factors

In lieu of constructing an equivalent elastic structure model to account for inelastic response, one can simply modify the elastic spectrum to obtain an inelastic response spectrum for use with the elastic structure model. The inelastic spectral response to use at the elastic frequency is obtained by dividing the elastic spectral response at that frequency by an inelastic deamplification factor, F_μ, i.e.:

$$S_{a\mu(f,\beta)} = \frac{S_a(f,\beta)}{F_\mu}^{**} \tag{3-15}$$

Then the required yield capacity, V_{yR}, of the structure to achieve a given ductility level, μ, is obtained by using the inelastic spectral acceleration, $S_{a\mu}$, in Equation 3-3 in lieu of the elastic spectral acceleration, S_a.

---

*   Modified spectra to reflect nonlinear behavior

** For the purpose of computing spectra deamplification factors (Application A), $S_a(f,\beta)$ as used in this section corresponds to SA of Chapter 1 and Figure 1-10.

One method to predict the inelastic deamplification factor is through the use of Equation 3-14. If this equation is used, the technique of using an inelastic response spectrum and an elastic structure model will produce identical results as are obtained from the use of an equivalent elastic structure model with the elastic response spectrum so long as the same effective frequency and effective damping are used in Equation 3-14 to determine F_μ.

Alternately, investigators have developed estimates of F_μ directly from a combination of theoretical considerations and empirical studies. The inelastic deamplification factor is different in the amplified spectral acceleration frequency range (generally about 2 to 8 Hz) than it is in the amplified spectral velocity frequency range (generally about 0.25 to 2 Hz). Newmark (1978) has suggested that:

Acceleration Region

$$F_\mu = F_{\mu a} = \sqrt{2\mu-1} \tag{3-16}$$

Velocity Region

$$F_\mu = F_{\mu v} = \mu \tag{3-17}$$

More recently, Riddell and Newmark (1979) have suggested the following improvement on these factors:

$$F_\mu = \left((q+1)\mu-q\right)^r \tag{3-18}$$

where:

Acceleration Region

$$q = q_a = 3.0\beta^{-0.30}$$

$$r = r_a = 0.48\beta^{-0.08} \tag{3-19}$$

Velocity Region

$$q = q_v = 2.7\beta^{-0.40}$$

$$r = r_v = 0.66\beta^{-0.04} \tag{3-20}$$

When using Equation 3-19 or 3-20, β is elastic damping in percent of critical. For $\mu = 1.85$ and 4.27, these two approaches yield ($\beta = 7\%$):

μ	Acceleration, $F_{\mu a}$		Velocity, $F_{\mu v}$	
	Newmark	Riddell	Newmark	Riddell
1.85 4.27	1.64 2.75	1.63 2.55	1.85 4.27	1.92 3.65

The Riddell equations will be used herein for comparison with the time history computed F_μ factors.

An inelastic spectral response corner frequency is specified by:

$$f_{sav} = \left(\frac{F_{\mu v}}{F_{\mu a}}\right) f_{av} \tag{3-21}$$

where f_{av} represents the corner frequency between elastic spectral velocity and acceleration as listed in Table 2-5 for each of the ground motions considered in this study. At frequencies below f_{sav}, the velocity deamplification factor, $F_{\mu v}$, is used to specify the inelastic spectral acceleration, $S_{a\mu}$ by Equation 3-15. At frequencies above f_{sav} the acceleration deamplification factor, $F_{\mu a}$, is used. However, within the amplification acceleration region, the inelastic spectral acceleration is not allowed to drop below:

Acceleration Region

$$S_{a\mu}(f,\beta) \geq \frac{a}{\mu^{0.13}} \tag{3-22}$$

as per the suggestion of Riddell and Newmark (1979).

a) Bilinear

b) Takeda
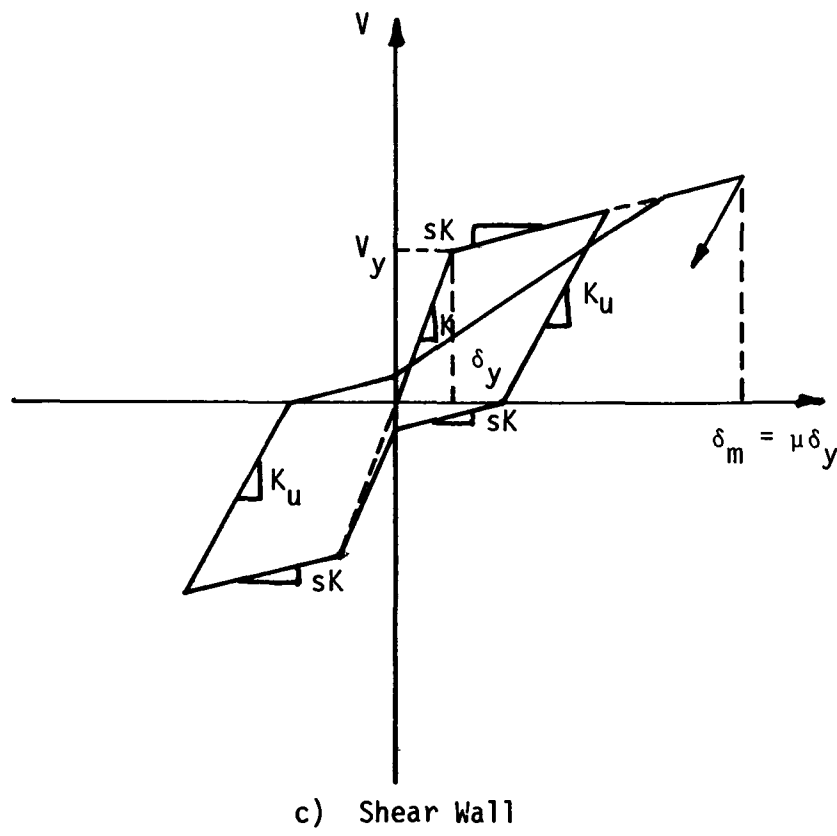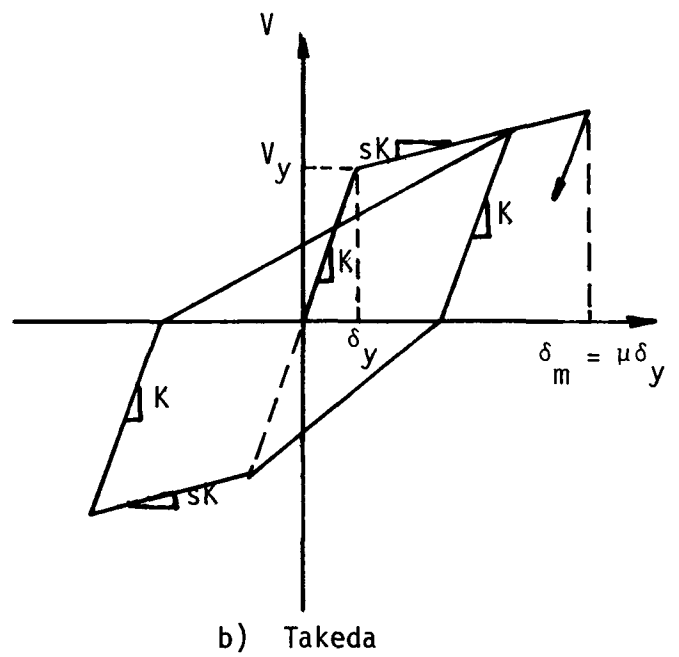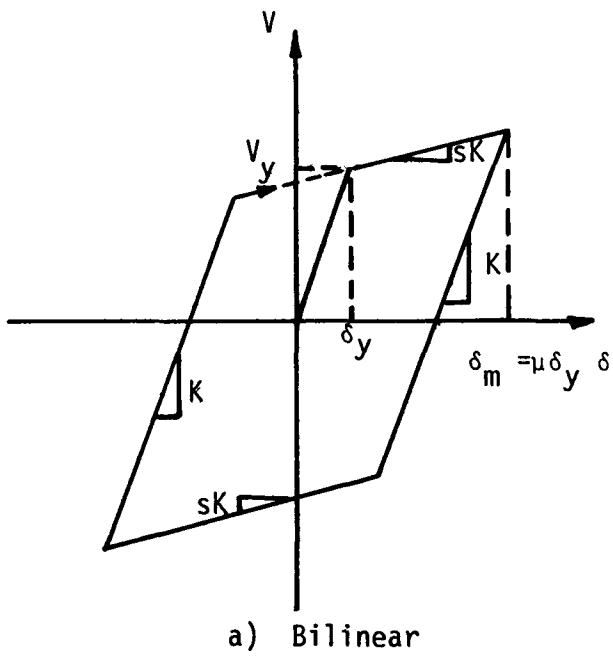
c) Shear Wall

FIGURE 3-1. REPRESENTATIVE NONLINEAR RESISTANCE FUNCTIONS
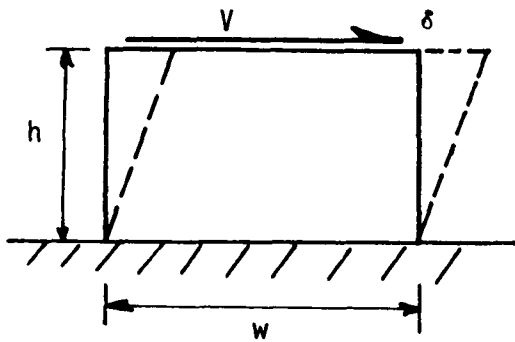
(a) Reinforced Concrete Shear Wall
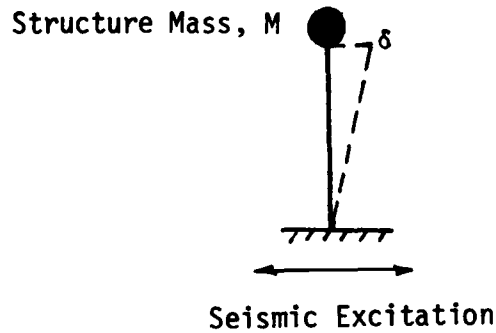
(b) Structure Model
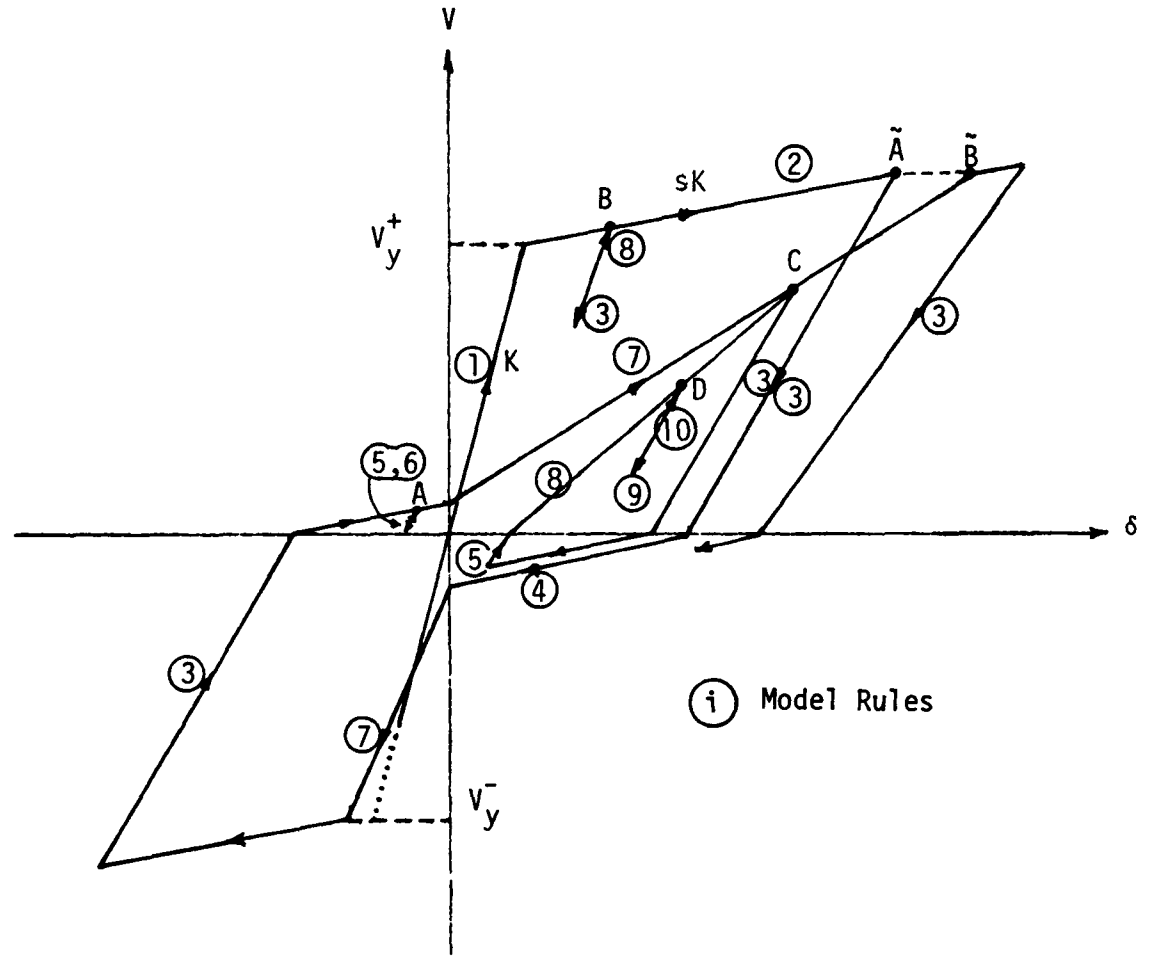
(c) Shear Deformation Hysteretic Behavior

FIGURE 3-2. SHEAR WALL STRUCTURE MODEL AND CORRESPONDING
HYSTERETIC DEFORMATION BEHAVIOR

$$\delta_r = (1-\alpha)\delta'_r$$
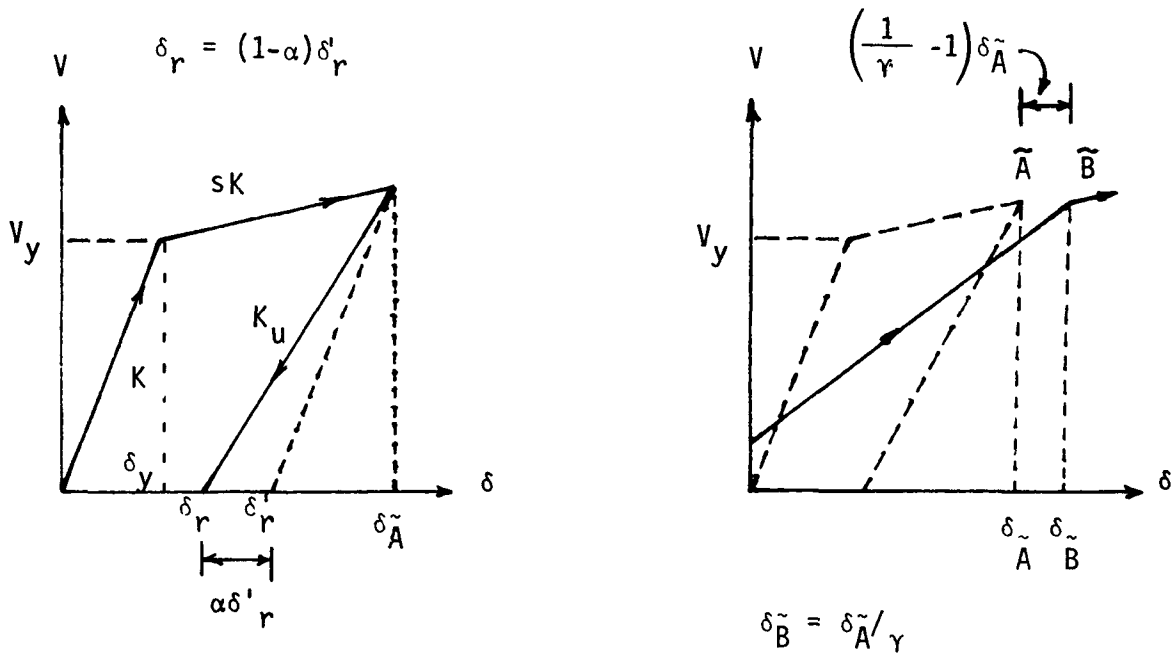
(a) Unloading stiffness parameter α

$$\delta_{\tilde{B}} = \delta_{\tilde{A}}/\gamma$$

(b) Strength degradation parameter γ
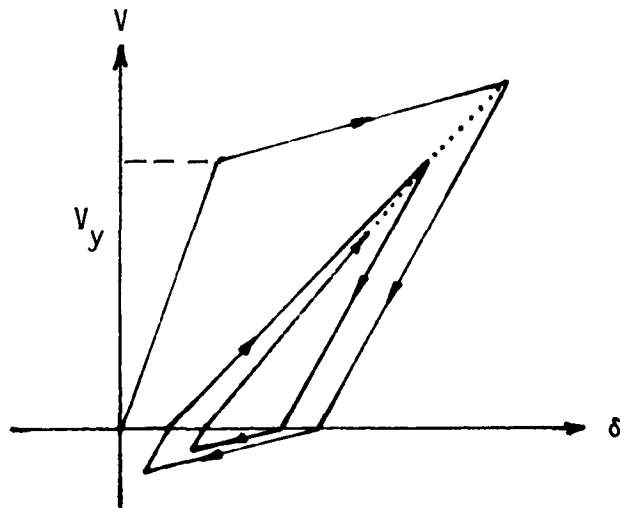
(c) Shakedown behavior

FIGURE 3-3. CHARACTERISTICS OF THE HYSTERESIS MODEL AND IDENTIFICATION OF MODEL PARAMETERS
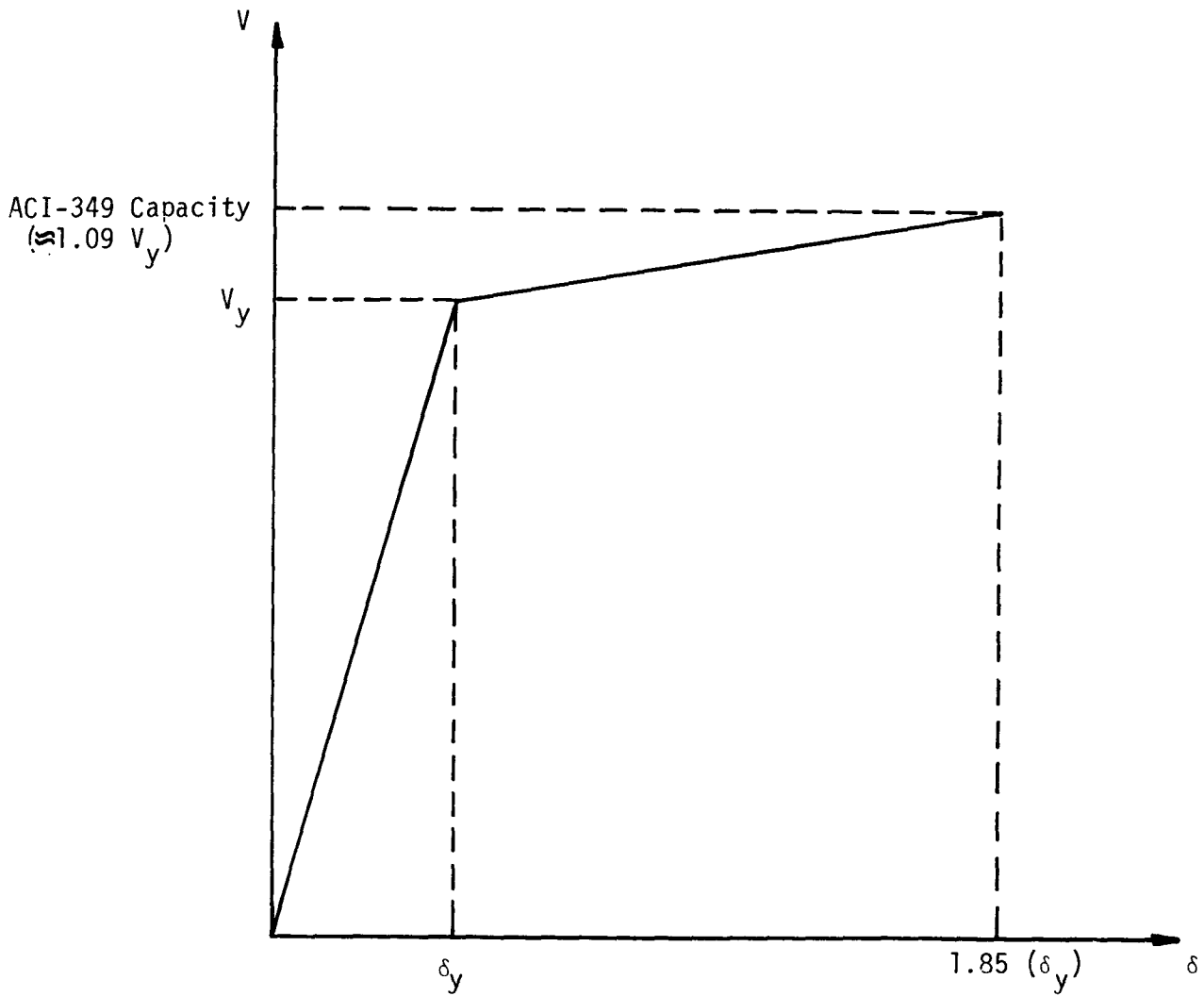
FIGURE 3-4.   REPRESENTATIVE RELATIONSHIP BETWEEN ACTUAL NONLINEAR RESISTANCE FUNCTION AND ACI-349 CODE CAPACITY FOR SHEAR WALL WITH ABOUT ONE PERCENT REINFORCEMENT STEEL

4. NONLINEAR STRUCTURAL RESPONSE ANALYSIS RESULTS AND COMPARISON TO PREDICTION EQUATIONS

As noted in Chapter 3, the structural model yield capacities, V_y, were determined from the elastic spectral acceleration, $S_a(f,\beta)$, at the models elastic frequency, f, and elastic damping β, of 7 percent. Next, the input ground motion was scaled by an input amplitude scale factor, F, and the maximum inelastic response (ductility factor, μ) was computed by time history nonlinear structural response analyses. Note that with a scale factor of unity, the elastic yield response ($\mu = 1.0$) will occur and with F factors greater than unity, inelastic response ($\mu > 1.0$) will occur. A sufficient number of analyses were performed with different F factors to enable the F factors corresponding to $\mu_L = 1.85$ and $\mu_H = 4.27$ to be accurately determined by interpolation for each ground motion time history and elastic natural frequency, f, considered.

Thus, F represents an input scale factor by which the ground motion must be increased over that corresponding to the structure yield capacity in order to achieve a given level of nonlinear response, μ. Alternately, F is also equal to the spectral deamplification factor needed to convert an elastic spectral acceleration to a ductility of μ. This inelastic spectral acceleration then defines the yield capacity, V_{yR}, required in order to limit the ductility level to μ when the structure is subjected to the actual unscaled time history. Both definitions for F are equivalent to each other. Thus, the input scale factors, F, corresponding to $\mu_L = 1.85$ and $\mu_H = 4.27$ as computed by time history nonlinear structural response analyses can be directly compared to the inelastic deamplification factors, F_μ, predicted by Equations 3-14 and 3-16 through 3-20 to evaluate the accuracy of these prediction methods.

4.1　INPUT SCALE FACTOR RESULTS FOR GROUND MOTION STUDIED

Table 4-1 presents the input scale factors, F_H and F_L, corresponding to $\mu_H = 4.27$ and $\mu_L = 1.85$, respectively, for the time histories and elastic frequencies studied. Mean values, standard deviations, and coefficients of variation of these scale factors are also presented for each earthquake ground motion and for each frequency studied as well as overall composite values. The trends for the high ductility and low ductility scale factors are similar. Therefore, only the high ductility scale factor results will be discussed.

One should not infer that the mean F_H and F_L values shown in Table 4-1 of 2.62 and 1.54, respectively, can be used as average inelastic scale factors. The inelastic scale factor is sensitive to duration, frequency, and the smoothness of the elastic spectrum and a single average number should not be used for any particular case.

4.1.1　Duration Effects

The high ductility scale factor, F_H, is plotted in Figure 4-1 against strong motion duration, T_D', for each of the cases studied. Very large data scatter exists. In fact, the coefficient of variation for F_H is 0.49. This large data scatter tends to mask strong motion duration effects. For durations T_D' greater than 2.5 seconds, the scatter band on F_H is from 1.25 to slightly less than 4.0 with a mean of 2.28 and a coefficient of variation of 0.29. For durations less than about 2.5 seconds, the lower bound on F_H remains about 1.25 while the upper bound rapidly increases with decreasing duration. The result is that the mean increases for these short duration records to 3.29 but the coefficient of variation also increases to 0.57 or approximately double what it was for the longer duration records.

The only conclusion which can be reached from the comparison is that in some cases F_H is substantially greater for the short duration records than it is for the long duration records but in some other cases, F_H does not appear to be increased by short duration.

4.1.2 Frequency Effects

Table 4-1 shows a definite trend of increasing F_H with decreasing elastic natural frequency. However, there is substantial data scatter which also tends to increase with decreasing natural frequency. Obviously, there is a frequency effect but it is being partially masked by some other important effects.

4.1.3 Influence of Frequency Shift from Elastic to Secant Frequency

As structures go nonlinear, their effective frequency gradually shifts from the elastic frequency toward the softer secant frequency (see Section 3.3.1 for a discussion of this effect). As this effect occurs, energy is fed into the structure over the frequency range from f to f_s and thus one could postulate that the average spectral acceleration over this frequency range is a better descriptor of nonlinear structural response than is the elastic spectral acceleration. Thus, if the average spectral acceleration within this frequency range is less than the spectral acceleration at the elastic frequency then F_H would be high, while if the average spectral acceleration is less than the spectral acceleration at the elastic frequency, then F_H would be low (see Figure 4-2 for a schematic picture of the concept).

Figures 4-3a through 4-3c plot the relationship between average spectral acceleration and elastic frequency spectral acceleration for each of the 12 records and 4 frequencies considered. F_H exceeds 2.7 in each of the following cases:

$$F_H \geq 2.7$$

Olympia - 2.14 Hz
Taft - 2.14 Hz
Artificial - 3.20, 2.14 Hz
Pacoima Dam - 2.14 Hz
El Centro #5 - 2.14 Hz
Coyote Lake - 5.34, 3.20, 2.14 Hz
Gavilan College - 8.54, 5.34, 3.20, 2.14 Hz
Melendy Ranch - 5.34, 3.20, 2.14 Hz

All of these 16 cases have average spectral accelerations between f and f_s less than the spectral acceleration at f. Similarly, F_H is less than or equal to 1.7 in each of the following cases:

$F_H \leq 1.7$

Olympia - 8.54, 5.34 Hz

Taft - 8.54, 5.34 Hz

El Centro #12 - 8.54 Hz

Pacoima Dam - 8.54 Hz

Goleta - 8.54 Hz

Coyote Lake - 8.54 Hz

Parkfield - 8.54, 5.34, 3.20 Hz

All of these 11 cases have average spectral accelerations between f and f_s greater than the spectral acceleration at f.

It is clear that the average spectral acceleration between f and f_s has a more significant influence on inelastic response than does the spectral acceleration at the elastic frequency, f. This factor accounts for the large variation in F_H. This spectral averaging effect is the overriding dominant effect influencing inelastic structural response.

The spectral averaging effect is much more important than the apparent duration effect described in Subsection 4.1.1. In fact, it is this spectral averaging effect which creates most of the apparent duration effect on F_H. As noted in Chapter 2, short duration records (T_D' < 3.0 seconds) appear to have narrow frequency content with a narrow frequency range of highly amplified spectral accelerations. When the elastic frequency lies from about 1.4 to 2.0 times the frequency at which these narrow frequency content spectra have maximum spectral acceleration, the F_H factor is low (less than 1.70). On the other hand, when the elastic frequency is less than 1.2 times the frequency of maximum spectral acceleration, the F_H factor is higher (greater than 3.0). Thus, one should expect very large data scatter on the F_H factor for these short duration records.

The conclusion is that one must retain the narrow frequency
content band-width on spectral amplification for these short duration
records in any engineering characterization of the record for nonlinear
structural response. All of the comments made in Chapter 2 on the
importance of frequency content band-width are even more important for
nonlinear structural response. Short duration records ($T_D' < 3.0$
seconds) should not be averaged together in a way which increases their
frequency content band-width in order to obtain a design spectrum. Such
averaging will destroy ones ability to accurately compute nonlinear
structure response using the averaged design spectrum.

4.2   NUMBER OF STRONG NONLINEAR RESPONSE CYCLES

So long as the ductility level, μ, is used as a measure of
damage, the spectral averaging effect described in the previous subsection
will have the predominant influence on the ductility level reached and
thus on damage. The strong motion duration, T_D', primarily effects the
spectral averaging process because short duration records have narrower
frequency content. However, duration also has a very direct influence on
the number of strong nonlinear cycles, N, and thus the hysteretic energy
dissipation per cycle (see Subsection 3.3.1 for a technical discussion of
this effect). This number of strong nonlinear cycles appears to have
only a minor influence on the maximum ductility level, μ, reached. Thus,
so long as the ductility level is used to describe damage, this duration
effect on damage will be much less important than the spectral averaging
effect described previously. However, if the total hysteretic energy
dissipation were used to describe damage, then this duration effect on
the number of strong nonlinear cycles would be very important. Thus, the
following discussions on the number of strong nonlinear cycles is
warranted even though N has only a minor effect on the ductility level
reached.

Figure 4-4 shows a plot of nonlinear structural response versus
time for a 5.34 Hz structure subjected to the Olympia record scaled to an
input level to produce a ductility level of 4.35. Initially, the

structure oscillates at an elastic frequency of about 5.3 Hz. Just prior to (1) the first nonlinear excursion occurs. Due to the strong nonlinear cycle (1) - (2) , the effective frequency is reduced to about 4.1 Hz. A second strong nonlinear cycle is associated with (3) - (4) - (5). Due to this cycle, f_e is further reduced to about 3.7 Hz. The next strong nonlinear cycle is (6) - (7). During this time, the effective frequency gradually lowers from 3.6 to 3.1 Hz. The last nonlinear cycle is (8) - (9) and peak ductility, μ = 4.35, is reached at (9). Olympia results in essentially 4 strong nonlinear cycles through the time of peak displacement. The effect of previous nonlinear cycles is to reduce the hysteretic energy dissipation during the last cycle (8) - (9) below that which would have occurred at this ductility if the preceding cycles had not occurred. Thus, the peak ductility, μ, is somewhat greater than would have occurred with this same factor, F, if the preceding cycles had not occurred.

The influence of strong duration, T_D', on the number of strong nonlinear cycles is illustrated by comparisons of the nonlinear resistance versus deformation plots for Taft (T_D' = 10.3 seconds), Parkfield (T_D' = 1.4 seconds), and Melendy Ranch (T_D' = 0.8 seconds). These resistance versus deformation plots are shown in Figures 4-5 through 4-7 for a 5.34 Hz structure at ductility levels of approximately 1.9 and 4.3. Note that the number of strong nonlinear cycles does not appear to be sensitive to the ductility level. This conclusion was found to be generally true for all cases studied. Next, Figures 4-8 and 4-9 present the resistance deformation diagrams for Taft and Melendy Ranch scaled to produce ductility levels of approximately 4.3 for elastic frequencies of 2.14, 5.34, and 8.54 Hz. These plots show that the number of strong nonlinear response cycles does vary somewhat with frequency. However, no consistent trends were observed. Sometimes N increased as f decreased and sometimes N decreased as f decreased. Generally, the differences were one cycle.

Table 4-2 presents the relationship between strong duration, T_D', and the number of strong nonlinear response cycles, N, generally observed in this study. Also presented in this table are frequency and damping coefficients, C_F and C_N, which will be discussed in the next section.

4.3 COMPARISON OF COMPUTED SCALE FACTORS WITH THOSE PREDICTED BY EQUIVALENT LINEAR RESPONSE MODELS

The scale factors, F, by which the ground motion amplitudes must be increased to achieve a ductility ratio of $\mu_L = 1.85$ or $\mu_H = 4.28$ are listed in Table 4-1. These factors were computed by performing nonlinear time history analyses. It would be desirable to be able to predict these scale factors simply from characteristics of the elastic response spectra without having to perform nonlinear time history analyses. One method to achieve this goal would be to convert the nonlinear resistance function for the structure to an equivalent linear resistance function with an effective frequency, f_e', and effective damping, β_e'. This equivalent linear model is used with the elastic spectral acceleration at frequency f_e' and damping β_e' to compute peak response. By this approach, the predicted scale factor, F_μ, is given by Equation 3-14. Then, the ratio, R, given by:

$$R = \frac{F_\mu}{F} \tag{4-1}$$

represents the ratio of the predicted to time history computed scale factor. If R exceeds 1.0, the equivalent linear model overpredicts (unconservative) the scale factor. Conversely, if R is less than unity, the equivalent linear model underpredicts (conservative) the scale factor. The desire is to find a method to define the equivalent linear model so that the mean value of R will be close to unity with a small coefficient of variation.

Subsection 3.3.1 suggested that the effective frequency, f_e', and effective damping, β_e', could be defined by Equation 3-8 in terms of two empirical coefficients, A and C_N. The coefficient A was varied from 0 to 1.0 in 0.1 increments while the coefficient C_N was varied from 0 to 0.5 in 0.1 increments. For each specific set of A and C_N coefficients, the ratio R of predicted to computed scale factors was determined for the four elastic frequencies, f, the two ductilities, μ , and the twelve time histories studied. It was found that a mean R value close to unity with a low coefficient of variation could be achieved when A was defined by:

$$A = C_F (1 - (f_s/f)) \leq 0.85 \qquad (4-2)$$

with the coefficients C_F and C_N defined in Table 4-2 as functions of the number of strong nonlinear cycles N.

One should note that as A increases, the effective frequency, f_e', is shifted closer to the secant frequency (A = 1.0) and away from the elastic frequency (A = 0). It was found that A increases with increases in the number of strong nonlinear cycles and with decreases in the ratio (f_s/f), i.e., increases in the ductility ratio, μ . However, A should not exceed 0.85. Thus, the effective frequency (Equation 3-8) does not shift more than 85% of the difference from the elastic frequency to the secant frequency. The lowest A found in this study was 0.35 for Melendy Ranch (N=1) at the low ductility μ= 1.85 (f_s/f = 0.77). Thus, in this study, the effective frequency was found to range from 35% to 85% of the difference from the elastic frequency to the secant frequency. Table 4-3 lists the ratio of (f_e'/f) as obtained from Equations 3-8 and 4-2 and the C_F values in Table 4-2 for N=1 through 4 for the low and high ductility cases studied.

The hysteretic damping coefficients, C_N, listed in Table 4-2 range from 32% to 55% of the values listed in Equation C-10 of Appendix C for C_{NN} associated with the <u>largest</u> nonlinear response cycle. This coefficient C_N decreases substantially as N is increased from 1 to 2 and only slightly with further increases in N. Table 4-3 presents the effective damping percentages β_e', which results from the use of these C_N values in Equation 3-8 for the cases studied. Damping percentages are rounded to the closest 0.5%. One should note that the effective damping percentages, β_e', are only slightly increased over the elastic damping ($\beta = 7\%$) for the low ductility ($\mu_L = 1.85$) case with N of 2 and greater. Significantly higher effective damping percentages result for the high ductility cases ($\mu_H = 4.27$) and for the case of N=1.

Also shown in Table 4-3 are effective frequency and damping percentages as defined by the Sozen procedure (Equation 3-9) and the Iwan procedure (Equation 3-10). The effective frequencies obtained by the method recommended in this study generally lie between those obtained by the Sozen and Iwan methods. For N=1, the method recommended herein gives an effective frequency very similar to that from the Iwan method. However, as N increases, the recommended method produces an effective frequency lower than that from the Iwan method and higher than that from the Sozen method.

The effective damping percentages obtained from the recommended method are substantially lower than those obtained from the Sozen and Iwan methods. The reasons for this lower effective damping are twofold:

1. The shear wall resistance functions used in this study have a more extreme pinched behavior (more conservative) than the resistance functions used in the Sozen and Iwan studies. It is believed that the resistance functions used in this study are more realistic for shear wall structures and are conservative for other structural systems where the resistance functions used by Sozen and Iwan are likely to be more realistic.

2. The elastic damping, β, was made proportional to the tangent stiffness at any time in this study whereas the elastic damping was held proportional to the initial stiffness in the Sozen and Iwan studies. Thus, within this study, the effective elastic damping was much reduced during nonlinear response. The reasons for making elastic damping proportional to the tangent stiffness are given in Subsection 3.2.3.

Tables 4-4 through 4-6 present the ratios R of predicted to computed scale factors obtained from effective linear models defined by the recommended, Sozen, and Iwan methods, respectively.

Table 4-4 shows that an effective linear model with effective frequency and effective damping defined by the recommended procedure accurately predicts the scale factor. The ratio of predicted to computed scale factors has a mean of 0.98 (2% conservative) for the high ductility case and a mean of 1.02 (2% unconservative) for the low ductility case. Furthermore, the COV about these means are only 0.12 and 0.09 for the high and low ductility cases, respectively. At the worst extremes, the ratio of predicted to computed scale factors ranged from 0.75 to 1.29 for the high ductility case and from 0.85 to 1.26 for the low ductility case. This agreement is considered to be exceptionally good. Furthermore, no consistent errors are observed. The agreement is equally good throughout the frequency range covered (approximately 1.8 to 10 Hz). The agreement is good for all 12 time histories considered. Figure 4-10 demonstrates that the ratio R of predicted to computed scale factors is independent of the strong motion duration, T_D', and the ductility level, μ. In other words, no consistent bias exists with either of these parameters. The worst COV are for the Coyote Lake record but are only 0.20 and 0.15 for the high and low ductility cases, respectively. The most severe unconservatism occurs for the Taft and El Centro #12 records where the predicted scale factors are 6 to 10% unconservative on the average. The most severe conservatism occurs for the El Centro #5 and Pacoima Dam records where the predicted scale factors are 5 to 12% conservative on the average.

4-10

The Sozen method (Table 4-5) also performs well on the average for defining an effective linear structure model to be used to predict peak response. However, it does not perform as well as the recommended procedure. On the average, the Sozen model introduces slight conservatism (2% for the high ductility case, and 6% for the low ductility case). However, the COV are from 150% to 200% of those for the recommended procedure. Thus, the scatter band is larger with the ratio of predicted to computed scale factors ranging from 0.66 to 1.43 for the high ductility case and from 0.60 to 1.37 for the low ductility case. Furthermore, consistent errors are observed. The method tends to introduce consistent conservative bias (ratios of predicted to computed scale factors less than unity) when the elastic frequency lies to the stiff side of the frequency at which the elastic spectra peak. The basic problem appears to be that the method overpredicts the softening of the structure. Thus, the method tends to overpredict the peak displacement (ductility) response of the structure for a given level of ground motion. On the other hand, the method also tends to overestimate the effective damping for the shear wall resistance functions used in this study and this tends to underpredict peak response. On the average, this overprediction and underprediction cancel each other and thus the mean ratio of predicted to computed scale factors is close to unity. However, for structures with an elastic frequency on the stiff side of the frequency at which spectral accelerations peak, the overprediction of displacement (ductility) due to too large a frequency shift is substantially greater than the underprediction due to the use of too large of an effective damping and the net result is significant overprediction of peak response.

The Iwan method (Table 4-6) does not perform well in defining an effective linear structure model for the shear wall resistance functions used in this study. The ratio of predicted to computed scale factors for a given ductility ratio is consistently greater than unity. This means that for a given ground motion level, the Iwan method will consistently unconservatively underpredict the peak displacement (ductility) response. This unconservatism results from both an underestimate of frequency shift

and an overestimate of the effective damping. This unconservatism is significantly greater for the long duration records (N=3 and 4) than for Melendy Ranch (N=1) for which the Iwan method works reasonably well. In general, the Iwan method should not be used to generate effective linear structure models for shear wall type structures.

The conclusion is that an equivalent linear model can be used to accurately predict peak nonlinear response of structures at least within the elastic frequency range from 1.8 to 10 Hz studied herein. For shear wall type structures, the procedure recommended herein should be used to define the effective frequency, f_e', and effective damping, β_e', of the equivalent linear model. This procedure requires that the number of strong nonlinear response cycles, N, be defined. Table 4-2 can be used to define N as a function of the strong duration T_D'. This procedure will be conservative for other types of structural resistance functions where the pinching behavior is less severe than for the shear wall resistance function models used in this study.

4.4   COMPARISON OF COMPUTED SCALE FACTORS WITH THOSE PREDICTED BY INELASTIC RESPONSE SPECTRA

As noted in Section 3.3.2, in lieu of constructing an equivalent elastic structure model to account for inelastic response, one can simply modify the elastic spectrum to obtain an inelastic response spectrum for use with the elastic structure model. The inelastic spectral response associated with the elastic frequency, f, and elastic damping, β, is obtained by dividing the elastic spectral response at this frequency and damping by an inelastic deamplification factor, F_μ, as shown in Equation 3-15.

One method to define F_μ is through the use of Equation 3-14 together with the effective elastic frequency, f_e', and effective damping β_e', defined in the preceding section for the equivalent elastic structure model. Another method to define F_μ is through the use of the Riddell procedure described in Subsection 3.3.2. Lastly, F_μ might be

defined by some average spectral acceleration within a frequency range
bounded by the elastic frequency, f, and the secant frequency, f_s.
Thus:

$$F_\mu = \mu \left(\frac{f'_{ea}}{f} \right)^2 \left\{ \frac{S_a(f,\beta)}{\overline{S_a(f_u - f_s, \beta'_{ea})}} \right\} \tag{4-3}$$

where $\overline{S_a(f_u - f_s, \beta'_{ea})}$ represents the average spectral acceleration
between an upper frequency, f_u, and the secant frequency, f_s, at an
average effective damping, β'_{ea}, and f'_{ea} represents an average
effective frequency within the frequency band from f_u to f_s. Intui-
tively, it would seem that this averaging process would provide a more
accurate estimate of F_μ than that obtained by Equation 3-14 wherein only
a single effective frequency, f'_e, is used.

Many different forms of spectral averaging were tried. These
included:

1. Averaging spectral accelerations with a uniform weighting
    of spectral accelerations at all frequencies between f_u and
    f_s.

2. Averaging spectral accelerations with a linear increase in
    weighting of spectral accelerations as frequencies were
    decreased from f_u (zero weighting) to f_s (unity weighting).

3. Uniform weighted averaging of spectral velocities at all
    frequencies between f_u and f_s.

It was found that Methods (2) and (3) did not produce better accuracy in
estimating F_μ than could be obtained with Method (1). Therefore, only
the method based on uniform weighted averaging of spectral accelerations
will be described herein.

The upper frequency, f_u, was defined by:

$$\left(\frac{f_u}{f}\right) = (1-B) + B\left(\frac{f_s}{f}\right) \tag{4-4}$$

and for uniform weighted averaging, the average effective frequency within the frequency band from f_u to f_s is:

$$f'_{ea} = \frac{f_u + f_s}{2} \tag{4-5}$$

Then the average effective damping was defined by:

$$\beta'_{ea} = \left(\frac{f_s}{f'_{ea}}\right)^2 [\beta + \beta_H]$$
$$\beta_H = C_N\left(1-(f_s/f)\right) \tag{4-6}$$

Note that Equations 4-4 and 4-6 are identical in format to Equation 3-8 which was recommended for developing a single frequency equivalent elastic structural model. The coefficient, B, was varied from $0(f_u = f)$ to $1(f_u = f_s)$ in 0.1 increment intervals while the coefficient C_N was varied from 0 to 0.5 in 0.1 increments. For each specific set of B and C_N coefficients, the ratio R of predicted to computed deamplification factors was determined for the four elastic frequencies, f, the two ductilities, μ, and the 12 time histories studied.

Mean R values close to unity with a low coefficient of variation could be achieved when:

$$B = \left[2C_F(1-(f_s/f))\right] - 1 \qquad (4-7)$$

except
$$0 \leq B \leq 0.70$$

with the coefficients C_F and C_N being identical to those defined for the effective elastic structural model in Table 4-2. It should be noted that with B defined by Equation 4-7, the average effective frequency, f'_{ea}, is identical to the equivalent elastic frequency, f'_e, defined by Equations 3-8 and 4-2 for all cases where A from Equation 4-2 exceeds 0.5 since B = (2A-1). However, when A is less than 0.5, B is limited to a lower bound of zero ($f_u = f$) and f'_{ea} is less than f'_e. For those cases where f'_{ea} is less than f'_e, the average effective damping, β'_{ea}, from Equation 4-6 is slightly greater than β'_e from Equation 3-8. Otherwise, these two effective damping ratios are identical. Table 4-7 lists the frequency ratios (f_u/f), and (f'_{ea}/f) and the average effective damping percentage, β'_{ea}, found from Equation 4-4 through 4-7 together with Table 4-2 for all cases studied. Note that average effective damping has been rounded to the nearest 0.5 percent.

The ratio of the predicted inelastic deamplification factor (identical to scale factor) using Equation 3-14 together with the effective frequency, f'_e, and effective damping, β'_e, to the computed factor has already been given in Table 4-4 since this method is identical to the use of an equivalent elastic structure model. The ratio of the predicted inelastic deamplification factor using the spectral averaging approach defined by Equations 4-3 through 4-7 to the computed factor is given in Table 4-8. The ratio of the predicted inelastic deamplification factor obtained by the Riddell method (Equations 3-18 through 3-22) to the computed factor is given in Table 4-9.

By comparing Table 4-8 and Table 4-4, one notes that the spectral averaging approach recommended in this section does only trivially better than the simpler equivalent elastic frequency approach of the previous section. The mean ratios of predicted to computed deamplification factors are essentially identical from the two approaches. The spectral averaging approach shows only a negligible reduction in an already low coefficient of variation. However, the spectral averaging approach does reduce the extreme bounds of this ratio of predicted to computed deamplification factors. Whereas, for the high ductility case the equivalent elastic model produced a scatter band for this ratio ranging from 0.75 to 1.29, the spectral averaging approach reduces this band to a range from 0.75 to 1.19. Similarly, for the low ductility case, the equivalent elastic model scatter band ranged from 0.85 to 1.26 while the spectral averaging approach scatter band ranged from 0.85 to 1.14. Response spectra contain a number of small local peaks and valleys even at damping ratios as high as 12%. The equivalent elastic model approach can place the effective frequency at one of these local valleys or peaks. The spectral averaging approach smooths these local valleys and peaks and thus reduces the possible extremes in the ratio of predicted to computed deamplification factors. This smoothing represents a minor improvement. It is unclear whether this minor improvement warrants the substantial increase in computational work entailed by the spectral averaging approach.

The mean ratio of the predicted to computed inelastic deamplification factor for the Riddell method is 1.10 (10% unconservative) for both the high and low ductility cases studied. This mean unconservatism is due to the extreme pinched behavior of the shear wall resistance functions used in this study. Such pinching was not considered in the Riddell study. This slight unconservatism of the Riddell method could be accommodated in design by the use of slightly lower acceptable ductility levels in design. However, the Riddell method also shows COV for the ratio of predicted to computed deamplification factors which range from 140% to 200% of those obtained for the spectral averaging method recommended in this study. For the high ductility case, the scatter band ranges from

0.43 to 1.78 which is judged to be excessively large when compared to a scatter band of 0.75 to 1.19 for the spectral averaging method. The problem of a large scatter band is not as severe for the low ductility case where it ranges from 0.88 to 1.47 for the Riddell method as compared with 0.85 to 1.14 for the spectral averaging method. The Riddell method is a very easy method to generate an inelastic response spectrum. However, this study shows it should be used with some caution because of the potentially large uncertainties as expressed by the wide scatter bands demonstrated herein. It should be noted that the Newmark method described in Subsection 3.3.2 would be slightly less accurate than the Riddell method so these same comments apply to the Newmark method.

4.5   CONCLUSIONS ON PREDICTING INELASTIC RESPONSE

It is concluded that the inelastic spectral response, $S_{a_\mu}(f,\beta)$, associated with an elastic structural frequency, f, elastic damping, β, and ductility factor, μ, can be accurately approximated by either:

Point Estimate Approach

$$S_{a_\mu}(f,\beta) = \frac{S_a(f'_e,\beta'_e)}{\mu(f'_e/f)^2} \qquad (4\text{-}8)$$

Spectral Averaging Approach

$$S_{a_\mu}(f,\beta) = \frac{\overline{S_a(f_u\text{-}f_s,\beta'_{ea})}}{\mu(f'_{ea}/f)^2} \qquad (4\text{-}9)$$

where f'_e and β'_e represent the best estimate effective frequency and effective damping ratios as defined by Equations 3-8, and 4-2 with coefficients defined by Table 4-2. Similarly, $\overline{S_a(f_u\text{-}f_s,\beta'_{ea})}$ represents the average spectral acceleration between frequencies f_u and f_s for an average effective damping, β'_{ea}, and f'_{ea} represents the midpoint frequency between f_u and f_s where these terms are defined by Equations 4-4 through 4-7 with coefficients from Table 4-2.

Within this study, the spectral averaging approach shows only a slight improvement in accuracy over the point estimate approach. Both approaches are very accurate with a COV of only 0.12 at μ_H = 4.27, and a COV of only 0.09 at μ_L = 1.85 for the point estimate approach with slightly lower COV for the spectral averaging approach. The spectral averaging approach requires substantially greater computational effort. However, it does smooth out local peaks and valleys in the spectral responses and this smoothing is desirable. Therefore, for an elastic response spectrum which contains significant local peaks and valleys at damping values of 7.5 to 12.5%, the spectral averaging approach would be slightly preferable. If the elastic response spectrum does not contain significant local peaks and valleys at these higher damping levels, the point estimate approach would be equally accurate.

It should be noted that both approaches require knowledge of the elastic response spectrum at the appropriate damping values which range from 7.5 to 12.5% for the ductility levels considered in this study. In addition, both methods require an approximate knowledge of strong motion duration, T_D', since the frequencies f_e', f_{ea}', and f_u and the effective damping values, β_e' and β_{ea}' depend slightly on T_D' particularly when T_D' becomes moderately short (7 seconds and less). These properties represent the minimum engineering characterization of the ground motion required for predicting inelastic structural response.

The approaches defined by Equation 4-8 and 4-9 for predicting inelastic spectral response and the approach described in the previous section for defining an equivalent elastic structural model were developed for shear wall type resistance functions with elastic damping of 7%. However, based upon the parameter studies described in Appendix D, these approaches can be conservatively used for braced frames and other structural or equipment systems so long as the structural system does not have a resistance-deformation function which shows greater stiffness degradation and pinching behavior than that used in this study for shear walls.

The brief parametric studies in Appendix D demonstrate:

1. Equation 4-6 can be used to estimate the average effective
    damping equally well for an elastic damping of 3% as for an
    elastic damping of 7%. The prediction procedure works
    equally well at 3% elastic damping as at 7% elastic damping.

2. The frequency shift and hysteretic damping coefficient, C_F
    and C_N, in Table 4-2 were developed for a shear wall
    resistance function model. Use of these coefficients will
    introduce only a slight conservatism for the Takeda model.
    The shear wall model overestimates the stiffness degradation
    and pinching behavior for braced-frame and bilinear
    resistance function models. Therefore, these coefficients
    overemphasize the importance of N and T_D' for such
    models. The input scale factor (inelastic spectral
    deamplification factor) for the braced-frame and bilinear
    resistance function models studied in Appendix D lay midway
    between the scale factors predicted using the C_F and C_N
    given in Table 4-2 for the appropriate T_D' and the scale
    factor predicted using $C_F = 1.5$ and $C_N = 0.30$ which are
    given for N=1. Averaging the results obtained from the use
    of these two different sets of C_F and C_N values will
    improve the prediction accuracy for braced-frame and
    bilinear models when T_D' is greater than 1.0 seconds.

TABLE 4-1

STATISTICAL EVALUATION OF SCALE FACTOR DATA

(a) Scale Factors (F_H) for High Ductility Ratio (μ = 4.27)

Earthquake Record (Comp)		Model Structure Frequency				Mean $<F>$	Std. Dev. σ	C.O.V. $\sigma/<F>$
		8.54 Hz	5.34 Hz	3.20 Hz	2.14 Hz			
1	Olympia, WA., 1949 (N86E)	1.56	1.54	2.61	3.75	2.37	1.05	0.44
2	Taft, Kern Co., 1952 (S69E)	1.25	1.65	2.05	3.38	2.08	0.92	0.44
3	El Centro Array No. 12 Imperial Valley, 1979, (140)	1.56	2.29	2.10	2.14	2.02	0.32	0.16
4	Artificial (R.G. 1.60)	1.89	1.88	2.84	2.75	2.34	0.53	0.23
5	Pacoima Dam San Fernando, 1971 (S14W)	1.70	1.86	2.67	3.89	2.53	1.00	0.40
6	Hollywood Storage PE Lot, San Fernando, 1971 (N90E)	1.94	2.50	2.60	2.05	2.27	0.33	0.15
7	El Centro Array No. 5, Imperial Valley, 1979, (140)	2.38	2.66	2.33	3.45	2.71	0.52	0.19
8	UCSB Goleta Santa Barbara, 1978 (180)	1.52	2.05	2.05	1.96	1.90	0.25	0.13
9	Gilroy Array No. 2, Coyote Lake, 1979, (050)	1.56	3.85	4.36	3.03	3.20	1.22	0.38
10	Cholame Array No. 2, Parkfield 1966 (N65E)	1.55	1.29	1.48	2.65	1.74	0.61	0.35
11	Gavilan College Hollister, 1974 (S67W)	2.84	2.97	2.71	8.49	4.25	2.83	0.67
12	Melendy Ranch Barn, Bear Valley, 1972 (N29W)	1.89	5.48	5.16	3.36	3.97	1.67	0.42

	8.54 Hz	5.34 Hz	3.20 Hz	2.14 Hz
Mean, $<F>$	1.8	2.5	2.75	3.41
Std. Dev., σ	0.43	1.17	1.03	1.73
C.O.V., $\sigma/<F>$	0.24	0.47	0.37	0.51

Overall:
$<F>$ = 2.62
σ = 1.28
C.O.V. = 0.49

(b) Scale Factors (F_L) for Low Ductility Ratio (μ_L = 1.85)

Earthquake Record (Comp)		Model Structure Frequency				Mean $<F>$	Std. Dev. σ	C.O.V. $\sigma/<F>$
		8.54 Hz	5.34 Hz	3.20 Hz	2.14 Hz			
1	Olympia, WA., 1949 (N86E)	1.36	1.11	1.49	1.70	1.41	0.25	0.18
2	Taft, Kern Co., 1952 (S69E)	1.20	1.25	1.50	1.78	1.43	0.27	0.19
3	El Centro Array No. 12 Imperial Valley, 1979, (140)	1.34	1.56	1.29	1.48	1.42	0.12	0.08
4	Artificial (R.G.,1.60)	1.50	1.33	1.60	1.73	1.54	0.17	0.11
5	Pacoima Dam San Fernando, 1971 (S14W)	1.25	1.38	1.26	2.19	1.52	0.45	0.29
6	Hollywood Storage PE Lot, San Fernando, 1971 (N90E)	1.45	1.65	1.58	1.39	1.52	0.12	0.08
7	El Centro Array No. 5, Imperial Valley, 1979, (140)	1.58	1.60	1.34	1.51	1.51	0.12	0.08
8	UCSB Goleta Santa Barbara, 1978 (180)	1.35	1.65	1.41	1.49	1.48	0.13	0.09
9	Gilroy Array No. 2, Coyote Lake, 1979, (050)	1.36	1.93	2.00	1.86	1.79	0.29	0.16
10	Cholame Array No. 2, Parkfield 1966 (N65E)	1.22	1.21	1.21	1.59	1.31	0.19	0.15
11	Gavilan College Hollister, 1974 (S67W)	1.61	1.55	1.62	1.93	1.68	0.17	0.10
12	Melendy Ranch Barn, Bear Valley, 1972 (N29W)	1.45	1.96	2.18	1.98	1.89	0.31	0.16

	8.54 Hz	5.34 Hz	3.20 Hz	2.14 Hz
Mean, $<F>$	1.39	1.52	1.54	1.72
Std. Dev., σ	0.13	0.27	0.29	0.24
C.O.V., $\sigma/<F>$	0.09	0.18	0.19	0.14

Overall:
$<F>$ = 1.54
σ = 0.26
C.O.V. = 0.17

TABLE 4-2

CORRELATION BETWEEN DURATION (T_D'), EFFECTIVE NUMBER OF STRONG NONLINEAR CYCLES (N), FREQUENCY SHIFT COEFFICIENT (C_F), AND HYSTERETIC DAMPING COEFFICIENT (C_N)*

Strong Duration T_D' (Sec.)	Effective Number of Strong Nonlinear Cycles, N	Frequency Shift Coefficient, C_F	Hysteretic Damping Coefficient, C_N
less than 1.0	1	1.5	0.30
1.0 - 7.0	2	1.9	0.15
9.0 - 11.0	3	2.3	0.11
greater than 15.0	4	2.7	0.11

* These frequency shift and hysteretic damping coefficients were developed for a shear wall resistance function model. However, based upon parameter studies in Appendix D, they can also be conservatively used for bilinear, Takeda, and braced-frame resistance function models. Use of these coefficients will introduce only a slight conservatism for the Takeda model. The shear wall model overestimates the stiffness degradation and pinching behavior for braced-frame and bilinear resistance function models. Therefore, these coefficients overemphasize the importance of N and T_D' for such models. The input scale factor (inelastic spectral deamplification factor) for the braced-frame and bilinear resistance function models studied in Appendix D lie midway between the scale factors predicted using the C_F and C_N given in Table 4-2 for the appropriate T_D and the scale factor predicted using C_F = 1.5 and C_N = 0.30 which are given for N=1.

TABLE 4-3

COMPARISON OF EFFECTIVE FREQUENCY AND EFFECTIVE DAMPING AS OBTAINED BY VARIOUS METHODS

Ductility μ	Secant Frequency Ratio, (f_s/f)	N*	Recommended Method		Sozen Method		Iwan Method	
			(f_e'/f)	β_e' (%)	(f_e'/f)	β_e' (%)	(f_e'/f)	β_e' (%)
1.85	0.77	1	0.92	10	0.77	11.5	0.91	12.5
		2	0.90	7.5				
		3	0.87	7.5				
		4	0.85	7.5				
4.27	0.56	1	0.71	12.5	0.56	16	0.73	16
		2	0.63	10.5				
		3	0.62	9.5				
		4	0.62	9.5				

* Number of Strong Nonlinear Cycles

TABLE 4-4

RATIO OF PREDICTED TO COMPUTED SCALE FACTOR FOR RECOMMENDED METHOD TO DEFINE EFFECTIVE LINEAR MODEL

High Ductility Case ($\mu_H = 4.27$)

	Earthquake Record (Comp)	Model Structure Frequency				Mean <F>	Std. Dev. σ	C.O.V. σ/<F>
		8.54 Hz	5.34 Hz	3.20 Hz	2.14 Hz			
1	Olympia, WA., 1949 (N86E)	1.09	1.01	.93	1.01	1.01	.07	.06
2	Taft, Kern Co., 1952 (S69E)	1.01	.99	1.02	1.02	1.01	.01	.01
3	El Centro Array No. 12 Imperial Valley, 1979, (140)	.90	1.02	1.29	1.03	1.06	.16	.16
4	Artificial (R.G. 1.60)	1.00	.87	.92	.91	.93	.05	.06
5	Pacoima Dam San Fernando, 1971 (S14W)	1.01	1.13	.88	.90	.98	.12	.12
6	Hollywood Storage PE Lot, San Fernando, 1971 (N90E)	.84	1.11	1.17	1.05	1.04	.14	.14
7	El Centro Array No. 5, Imperial Valley, 1979, (140)	.75	.87	.99	.91	.88	.10	.11
8	UCSB Goleta Santa Barbara, 1978 (180)	1.11	.95	.84	.78	.92	.14	.16
9	Gilroy Array No. 2, Coyote Lake, 1979, (050)	.83	.77	1.19	1.01	.95	.19	.20
10	Cholame Array No. 2, Parkfield 1966 (N65E)	1.16	.98	.77	1.03	.99	.16	.16
11	Gavilan College Hollister, 1974 (S67W)	.84	1.09	1.13	1.01	1.02	.13	.13
12	Melendy Ranch Barn, Bear Valley, 1972 (N29W)	.90	1.02	1.06	1.01	1.00	.07	.07

Mean, <F>	.95	.98	1.02	.97	Overall:
Std. Dev., σ	.13	.11	.16	.08	<F> = .98
C.O.V., σ/<F>	.14	.11	.15	.08	σ = .12 C.O.V. = .12

Low Ductility Case ($\mu = 1.85$)

	Earthquake Record (Comp)	Model Structure Frequency				Mean <F>	Std. Dev. σ	C.O.V. σ/<F>
		8.54 Hz	5.34 Hz	3.20 Hz	2.14 Hz			
1	Olympia, WA., 1949 (N86E)	.97	1.05	.93	.95	.98	.05	.05
2	Taft, Kern Co., 1952 (S69E)	1.10	1.01	1.09	1.20	1.10	.08	.07
3	El Centro Array No. 12 Imperial Valley, 1979, (140)	.96	1.04	1.04	1.09	1.03	.05	.05
4	Artificial (R.G. 1.60)	.89	1.17	1.00	.85	.98	.14	.15
5	Pacoima Dam San Fernando, 1971 (S14W)	.96	.90	1.00	.94	.95	.04	.04
6	Hollywood Storage PE Lot, San Fernando, 1971 (N90E)	1.07	1.11	.89	1.05	1.03	.10	.09
7	El Centro Array No. 5, Imperial Valley, 1979, (140)	1.06	.95	1.00	.98	1.00	.05	.05
8	UCSB Goleta Santa Barbara, 1978 (180)	1.16	1.06	1.01	.85	1.02	.13	.13
9	Gilroy Array No. 2, Coyote Lake, 1979, (050)	1.00	.90	1.02	1.26	1.05	.15	.15
10	Cholame Array No. 2, Parkfield 1966 (N65E)	1.13	1.19	.92	.99	1.06	.12	.12
11	Gavilan College Hollister, 1974 (S67W)	1.01	1.03	.85	1.07	.99	.10	.10
12	Melendy Ranch Barn, Bear Valley, 1972 (N29W)	1.00	1.05	.97	1.05	1.02	.04	.04

Mean, <F>	1.03	1.04	.98	1.02	Overall:
Std. Dev., σ	.08	.09	.07	.12	<F> = 1.02
C.O.V., σ/<F>	.08	.09	.07	.12	σ = .09 C.O.V. = .09

TABLE 4-5

RATIO OF PREDICTED TO COMPUTED SCALE FACTOR FOR SOZEN METHOD TO DEFINE EFFECTIVE LINEAR MODEL

High Ductility (μ = 4.27')

	Earthquake Record (Comp)	Model Structure Frequency				Mean \<F\>	Std. Dev. σ	C.O.V. σ/\<F\>
		8.54 Hz	5.34 Hz	3.20 Hz	2.14 Hz			
1	Olympia, WA., 1949 (N86E)	.91	.87	.96	1.13	.97	.11	.12
2	Taft, Kern Co., 1952 (S69E)	.95	.98	1.31	.91	1.04	.18	.18
3	El Centro Array No. 12 Imperial Valley, 1979, (140)	1.12	.98	1.11	1.05	1.07	.06	.06
4	Artificial (R.G. 1.60)	.93	.92	.97	1.18	1.00	.12	.12
5	Pacoima Dam San Fernando, 1971 (S14W)	.82	.90	1.15	.67	.89	.20	.23
6	Hollywood Storage PE Lot, San Fernando, 1971 (N90E)	.84	1.11	1.11	.91	.99	.14	.14
7	El Centro Array No. 5, Imperial Valley, 1979, (140)	.68	.90	1.19	.86	.91	.21	.23
8	UCSB Goleta Santa Barbara, 1978 (180)	1.09	.77	.68	.74	.82	.18	.22
9	Gilroy Array No. 2, Coyote Lake, 1979, (050)	.82	.92	1.43	.96	1.03	.27	.26
10	Cholame Array No. 2, Parkfield 1966 (N65E)	.88	.66	.78	1.32	.91	.29	.32
11	Gavilan College Hollister, 1974 (S67W)	.80	.93	1.33	1.13	1.05	.23	.22
12	Melendy Ranch Barn, Bear Valley, 1972 (N29W)	.79	1.30	1.19	.90	.97	.17	.18

	8.54 Hz	5.34 Hz	3.20 Hz	2.14 Hz
Mean, \<F\>	.89	.94	1.10	.98
Std. Dev., σ	.13	.16	.22	.19
C.O.V., σ/\<F\>	.14	.17	.20	.19

Overall:
\<F\> = .98
σ = .19
C.O.V. = .19

Low Ductility (μ = 1.85)

	Earthquake Record (Comp)	Model Structure Frequency				Mean \<F\>	Std. Dev. σ	C.O.V. σ/\<F\>
		8.54 Hz	5.34 Hz	3.20 Hz	2.14 Hz			
1	Olympia, WA., 1949 (N86E)	.85	1.04	1.00	.89	.95	.09	.09
2	Taft, Kern Co., 1952 (S69E)	.91	.96	.88	1.15	.98	.12	.12
3	El Centro Array No. 12 Imperial Valley, 1979, (140)	.82	1.09	1.02	.90	.96	.12	.13
4	Artificial (R.G. 1.60)	.81	.89	.86	1.01	.89	.09	.10
5	Pacoima Dam San Fernando, 1971 (S14W)	.91	.91	.82	1.17	.95	.15	.16
6	Hollywood Storage PE Lot, San Fernando, 1971 (N90E)	.91	.82	1.08	1.06	.97	.12	.13
7	El Centro Array No. 5, Imperial Valley, 1979, (140)	.76	.81	1.11	1.37	1.01	.28	.28
8	UCSB Goleta Santa Barbara, 1978 (180)	.74	.85	.98	.68	.81	.13	.16
9	Gilroy Array No. 2, Coyote Lake, 1979, (050)	.80	.85	1.30	1.16	1.03	.24	.24
10	Cholame Array No. 2, Parkfield 1966 (N65E)	.85	.80	.62	.86	.78	.11	.14
11	Gavilan College Hollister, 1974 (S67W)	.84	1.15	.83	1.35	1.04	.25	.24
12	Melendy Ranch Barn, Bear Valley, 1972 (N29W)	.60	1.12	.97	.90	.90	.22	.24

	8.54 Hz	5.34 Hz	3.20 Hz	2.14 Hz
Mean, \<F\>	.82	.94	.96	1.04
Std. Dev., σ	.09	.13	.17	.21
C.O.V., σ/\<F\>	.11	.14	.18	.20

Overall:
\<F\> = .94
σ = .17
C.O.V. = .18

TABLE 4-6

RATIO OF PREDICTED TO COMPUTED SCALE FACTOR FOR IWAN METHOD TO DEFINE EFFECTIVE LINEAR MODEL

High Ductility (μ = 4.27)

Earthquake Record (Comp)		Model Structure Frequency				Mean \<F\>	Std. Dev. σ	C.O.V. σ/\<F\>
		8.54 Hz	5.34 Hz	3.20 Hz	2.14 Hz			
1	Olympia, WA., 1949 (N86E)	1.83	1.72	1.38	1.11	1.51	.33	.22
2	Taft, Kern Co., 1952 (S69E)	1.88	1.68	1.48	1.49	1.63	.19	.12
3	El Centro Array No. 12 Imperial Valley, 1979, (140)	1.64	1.90	1.60	1.52	1.67	.16	.10
4	Artificial (R.G. 1.60)	1.63	1.47	1.30	1.62	1.51	.16	.10
5	Pacoima Dam San Fernando, 1971 (S14W)	1.54	1.64	1.14	1.42	1.44	.22	.15
6	Hollywood Storage PE Lot, San Fernando, 1971 (N90E)	1.55	1.42	1.65	1.60	1.56	.10	.06
7	El Centro Array No. 5, Imperial Valley, 1979, (140)	1.14	1.19	1.63	1.42	1.35	.23	.17
8	UCSB Goleta Santa Barbara, 1978 (180)	1.53	1.59	1.44	1.26	1.46	.14	.10
9	Gilroy Array No. 2, Coyote Lake, 1979, (050)	1.62	1.15	1.43	1.68	1.47	.24	.16
10	Cholame Array No. 2, Parkfield 1966 (N65E)	1.55	1.61	1.23	1.39	1.45	.17	.12
11	Gavilan College Hollister, 1974 (S67W)	1.21	1.45	1.34	.81	1.20	.28	.23
12	Melendy Ranch Barn, Bear Valley, 1972 (N29W)	1.10	1.10	1.12	1.15	1.12	.02	.02

	8.54 Hz	5.34 Hz	3.20 Hz	2.14 Hz
Mean, \<F\>	1.52	1.49	1.40	1.37
Std. Dev., σ	.25	.25	.18	.25
C.O.V., σ/\<F\>	.16	.17	.13	.18

Overall:
\<F\> = 1.44
σ = .23
C.O.V. = .16

Low Ductility (μ = 1.85)

Earthquake Record (Comp)		Model Structure Frequency				Mean \<F\>	Std. Dev. σ	C.O.V. σ/\<F\>
		8.54 Hz	5.34 Hz	3.20 Hz	2.14 Hz			
1	Olympia, WA., 1949 (N86E)	1.37	1.33	1.22	1.21	1.28	.08	.06
2	Taft, Kern Co., 1952 (S69E)	1.32	1.42	1.39	1.35	1.37	.04	.03
3	El Centro Array No. 12 Imperial Valley, 1979, (140)	1.35	1.37	1.43	1.37	1.38	.03	.03
4	Artificial (R.G. 1.60)	1.15	1.53	1.31	1.23	1.31	.16	.13
5	Pacoima Dam San Fernando, 1971 (S14W)	1.13	1.12	1.28	1.20	1.18	.07	.06
6	Hollywood Storage PE Lot, San Fernando, 1971 (N90E)	1.32	1.25	1.19	1.28	1.26	.05	.04
7	El Centro Array No. 5, Imperial Valley, 1979, (140)	1.14	1.09	1.41	1.35	1.25	.16	.13
8	UCSB Goleta Santa Barbara, 1978 (180)	1.22	1.30	1.30	1.01	1.21	.14	.11
9	Gilroy Array No. 2, Coyote Lake, 1979, (050)	1.18	1.15	1.32	1.41	1.27	.12	.10
10	Cholame Array No. 2, Parkfield 1966 (N65E)	1.27	1.25	1.13	1.21	1.22	.06	.05
11	Gavilan College Hollister, 1974 (S67W)	1.26	1.27	1.03	1.25	1.20	.12	.10
12	Melendy Ranch Barn, Bear Valley, 1972 (N29W)	1.02	1.17	1.03	1.12	1.09	.07	.07

	8.54 Hz	5.34 Hz	3.20 Hz	2.14 Hz
Mean, \<F\>	1.23	1.27	1.25	1.25
Std. Dev., σ	.11	.13	.14	.11
C.O.V., σ/\<F\>	.09	.10	.11	.09

Overall:
\<F\> = 1.25
σ = .12
C.O.V. = .10

TABLE 4-7

EFFECTIVE FREQUENCY RANGES AND AVERAGE EFFECTIVE DAMPING

Ductility μ	Secant Frequency Ratios, (f_s/f)	Number of Strong Nonlinear Cycles, N	(f_u/f)	(f'_{ea}/f)	β'_{ea} (%)
1.85	0.77	1	1.00	0.88	10.5
		2	1.00	0.88	8
		3	0.98	0.87	7.5
		4	0.94	0.85	7.5
4.27	0.56	1	0.86	0.71	12.5
		2	0.70	0.63	10.5
		3	0.69	0.62	9.5
		4	0.69	0.62	9.5

TABLE 4-8

RATIO OF PREDICTED TO COMPUTED INELASTIC DEAMPLIFICATION FACTOR FOR RECOMMENDED SPECTRAL AVERAGING METHOD

High Ductility Case (μ = 4.27)

	Earthquake Record (Component)	Model Structure Frequency				Mean $<F>$	Std. Dev. σ	C.O.V. σ/$<F>$
		8.54 Hz	5.34 Hz	3.20 Hz	2.14 Hz			
1	Olympia, WA., 1949 (N86E)	1.04	1.00	.92	.98	.99	.05	.05
2	Taft, Kern Co., 1952 (S69E)	.96	1.02	1.03	.94	.99	.04	.04
3	El Centro Array No. 12 Imperial Valley, 1979, (140)	.92	1.04	1.17	1.01	1.04	.10	.10
4	Artificial (R.G. 1.60)	.99	.88	.91	.93	.93	.05	.05
5	Pacoima Dam San Fernando, 1971 (S14W)	1.01	1.06	.89	.90	.97	.08	.09
6	Hollywood Storage PE Lot, San Fernando, 1971 (N90E)	.87	1.05	1.17	1.02	1.03	.12	.12
7	El Centro Array No. 5, Imperial Valley, 1979, (140)	.75	.87	1.05	.90	.89	.12	.14
8	UCSB Goleta Santa Barbara, 1978 (180)	1.06	.91	.82	.76	.89	.13	.15
9	Gilroy Array No. 2, Coyote Lake, 1979, (050)	.86	.81	1.19	1.01	.97	.17	.18
10	Cholame Array No. 2, Parkfield 1966 (N65E)	1.15	.96	.77	1.05	.98	.16	.16
11	Gavilan College Hollister, 1974 (S67W)	.80	1.07	1.11	.95	.98	.14	.14
12	Melendy Ranch Barn, Bear Valley, 1972 (N29W)	.95	1.00	1.02	1.09	1.02	.06	.06

	8.54 Hz	5.34 Hz	3.20 Hz	2.14 Hz	Overall:
Mean, $<F>$	.95	.97	1.00	.96	$<F>$ = .97
Std. Dev., σ	.11	.09	.14	.09	σ = .11
C.O.V., σ/$<F>$	.12	.09	.14	.09	C.O.V. = .11

Low Ductility Case (μ = 1.85)

	Earthquake Record (Component)	Model Structure Frequency				Mean $<F>$	Std. Dev. σ	C.O.V. σ/$<F>$
		8.54 Hz	5.34 Hz	3.20 Hz	2.14 Hz			
1	Olympia, WA., 1949 (N86E)	.96	1.02	.95	.92	.96	.04	.04
2	Taft, Kern Co., 1952 (S69E)	1.11	1.04	1.03	1.12	1.08	.05	.04
3	El Centro Array No. 12 Imperial Valley, 1979, (140)	1.00	.99	1.06	1.07	1.03	.04	.04
4	Artificial (R.G. 1.60)	.90	1.12	.95	.89	.97	.11	.11
5	Pacoima Dam San Fernando, 1971 (S14W)	1.00	.95	.95	.98	.97	.02	.03
6	Hollywood Storage PE Lot, San Fernando, 1971 (N90E)	1.08	1.00	.94	1.09	1.03	.07	.07
7	El Centro Array No. 5, Imperial Valley, 1979, (140)	1.00	.94	1.12	1.10	1.04	.08	.08
8	UCSB Goleta Santa Barbara, 1978 (180)	1.04	1.02	1.05	.85	.99	.09	.10
9	Gilroy Array No. 2, Coyote Lake, 1979, (050)	.99	.88	1.05	1.14	1.02	.11	.11
10	Cholame Array No. 2, Parkfield 1966 (N65E)	1.09	1.12	.89	.97	1.02	.11	.11
11	Gavilan College Hollister, 1974 (S67W)	1.01	1.09	.87	1.08	1.01	.10	.10
12	Melendy Ranch Barn, Bear Valley, 1972 (N29W)	.89	1.06	.95	1.04	.99	.08	.08

	8.54 Hz	5.34 Hz	3.20 Hz	2.14 Hz	Overall:
Mean, $<F>$	1.01	1.02	.98	1.02	$<F>$ = 1.01
Std. Dev., σ	.07	.07	.08	.10	σ = .08
C.O.V., σ/$<F>$	.07	.07	.08	.09	C.O.V. = .08

TABLE 4-9

RATIO OF PREDICTED TO COMPUTED SCALE FACTOR FOR RIDDELL METHOD TO DEFINE EFFECTIVE LINEAR MODEL

High Ductility Case (μ = 4.27)

	Earthquake Record (Component)	Model Structure Frequency				Mean <F>	Std. Dev. σ	C.O.V. σ/<F>
		8.54 Hz	5.34 Hz	3.20 Hz	2.14 Hz			
1	Olympia, WA., 1949 (N86E)	1.21	1.23	1.40	.97	1.20	.18	.15
2	Taft, Kern Co., 1952 (S69E)	1.15	1.32	1.23	1.08	1.20	.10	.08
3	El Centro Array No. 12 Imperial Valley, 1979, (140)	1.35	1.11	1.10	.86	1.10	.20	.18
4	Artificial (R.G. 1.60)	1.35	1.36	.90	1.33	1.24	.22	.18
5	Pacoima Dam San Fernando, 1971 (S14W)	.96	.93	.63	.94	.86	.16	.19
6	Hollywood Storage PE Lot, San Fernando, 1971 (N90E)	1.31	1.02	.95	1.78	1.26	.38	.30
7	El Centro Array No. 5, Imperial Valley, 1979, (140)	1.06	.96	.86	1.06	.98	.10	.10
8	UCSB Goleta Santa Barbara, 1978 (180)	1.13	1.00	1.09	1.14	1.09	.06	.06
9	Gilroy Array No. 2, Coyote Lake, 1979, (050)	1.58	.95	.84	1.20	1.14	.33	.29
10	Cholame Array No. 2, Parkfield 1966 (N65E)	.88	1.02	1.35	1.38	1.16	.25	.22
11	Gavilan College Hollister, 1974 (S67W)	1.29	1.23	1.35	.43	1.08	.43	.40
12	Melendy Ranch Barn, Bear Valley, 1972 (N29W)	1.17	.67	.71	1.09	.91	.26	.29

	8.54 Hz	5.34 Hz	3.20 Hz	2.14 Hz	
Mean, <F>	1.20	1.07	1.03	1.10	Overall:
Std. Dev., σ	.19	.19	.26	.32	<F> = 1.10
C.O.V., σ/<F>	.16	.18	.25	.29	σ = .25 C.O.V. = .23

Low Ductility Case (μ = 1.85)

	Earthquake Record (Component)	Model Structure Frequency				Mean <F>	Std. Dev. σ	C.O.V. σ/<F>
		8.54 Hz	5.34 Hz	3.20 Hz	2.14 Hz			
1	Olympia, WA., 1949 (N86E)	1.20	1.47	1.09	1.13	1.22	.17	.14
2	Taft, Kern Co., 1952 (S69E)	1.08	1.30	1.09	1.08	1.14	.11	.10
3	El Centro Array No. 12 Imperial Valley, 1979, (140)	1.22	1.04	1.26	1.10	1.16	.10	.09
4	Artificial (R.G. 1.60)	1.09	1.23	1.02	.94	1.07	.12	.11
5	Pacoima Dam San Fernando, 1971 (S14W)	1.18	1.12	1.19	.88	1.09	.14	.12
6	Hollywood Storage PE Lot, San Fernando, 1971 (N90E)	1.12	.99	1.03	.97	1.03	.07	.07
7	El Centro Array No. 5, Imperial Valley, 1979, (140)	1.03	1.02	1.22	1.01	1.07	.10	.09
8	UCSB Goleta Santa Barbara, 1978 (180)	1.13	.99	1.16	1.09	1.09	.07	.06
9	Gilroy Array No. 2, Coyote Lake, 1979, (050)	1.20	.99	.96	1.03	1.04	.11	.11
10	Cholame Array No. 2, Parkfield 1966 (N65E)	1.01	.98	1.35	1.03	1.09	.17	.16
11	Gavilan College Hollister, 1974 (S67W)	1.19	1.24	1.19	.99	1.15	.11	.10
12	Melendy Ranch Barn, Bear Valley, 1972 (N29W)	1.12	.98	.88	.97	.99	.10	.10

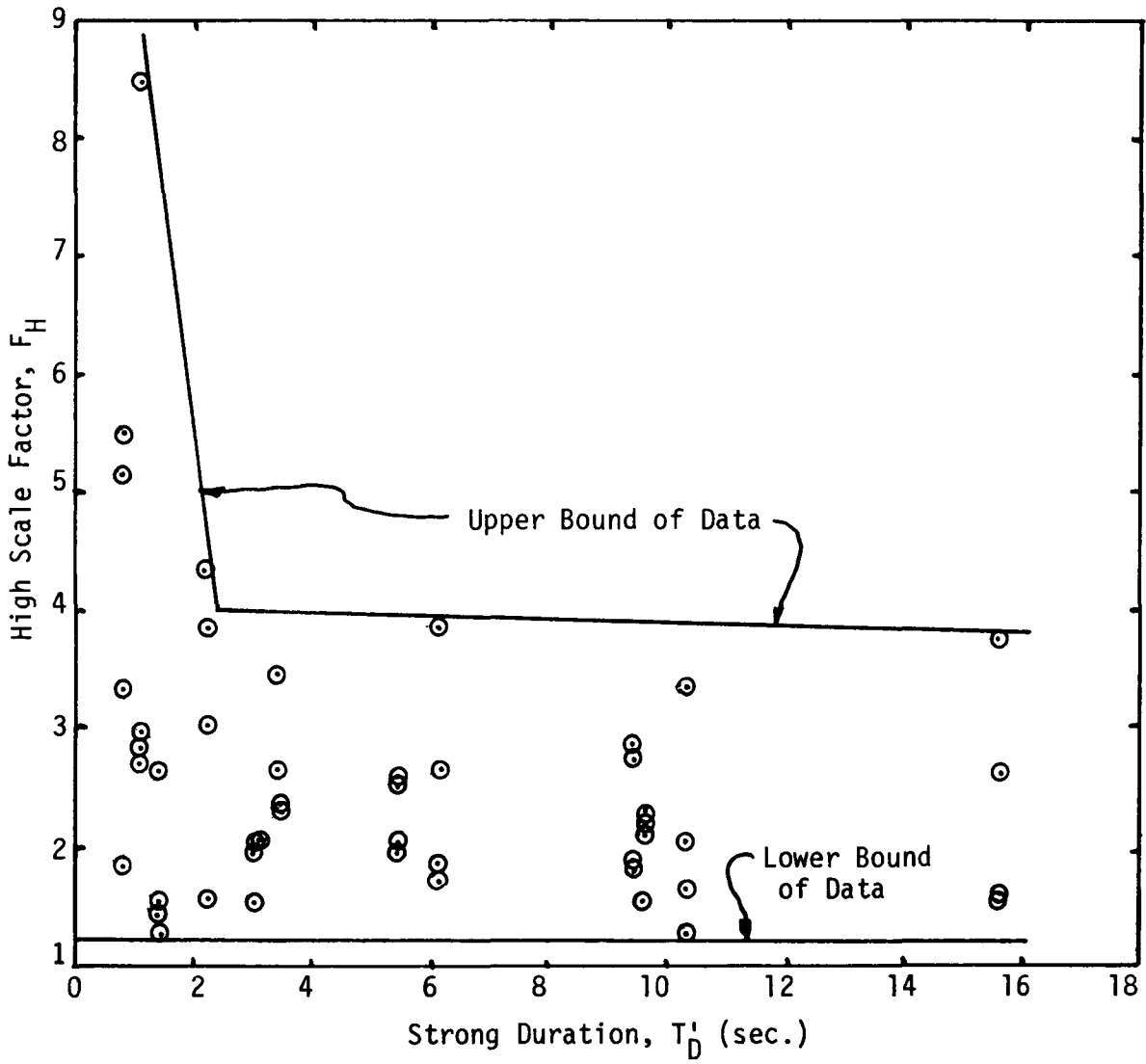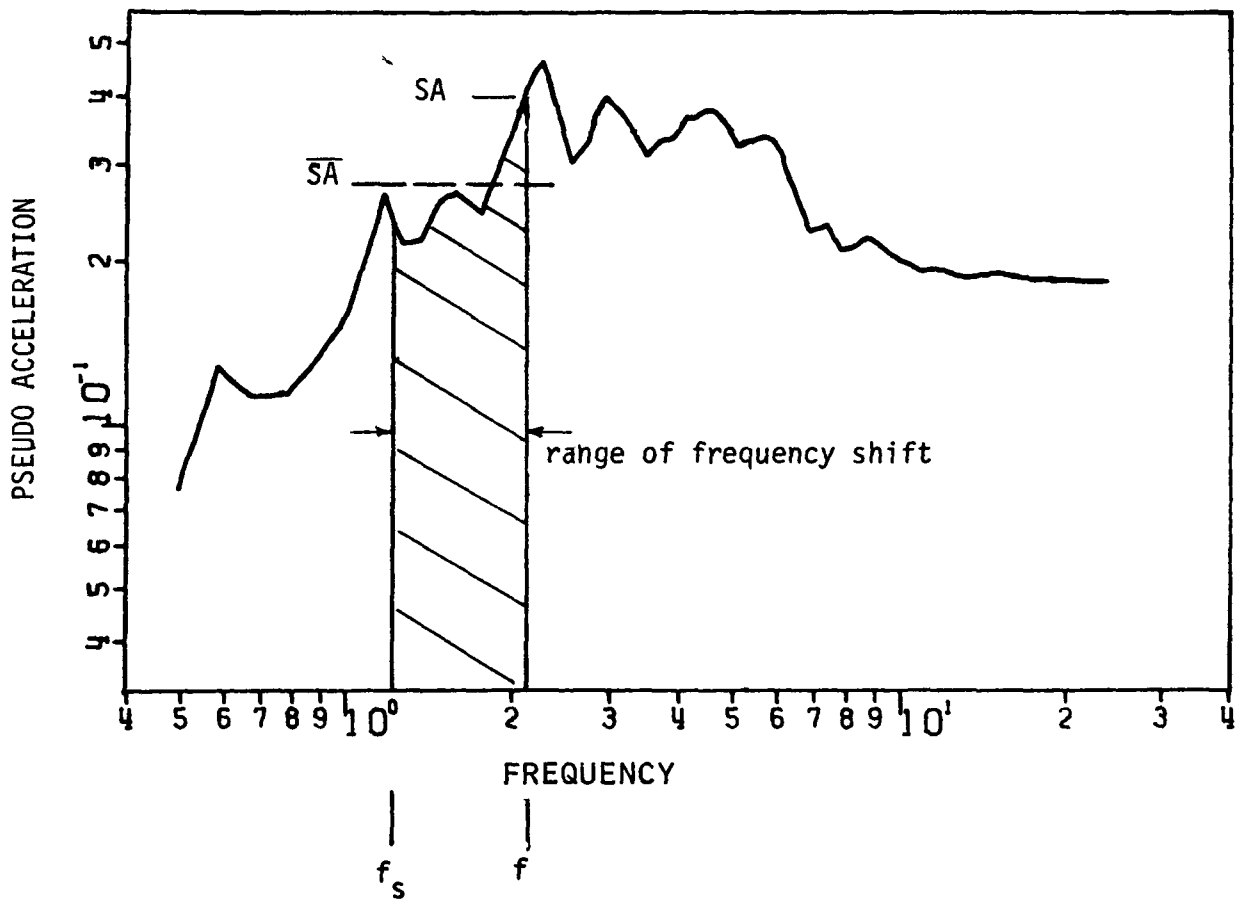|	8.54 Hz	5.34 Hz	3.20 Hz	2.14 Hz	
Mean, <F>	1.13	1.11	1.12	1.02	Overall:
Std. Dev., σ	.07	.16	.13	.07	<F> = 1.10
C.O.V., σ/<F>	.06	.14	.12	.07	σ = .12 C.O.V. = .11

FIGURE 4-1.   SCALE FACTOR, F_H VERSUS DURATION, T_D'

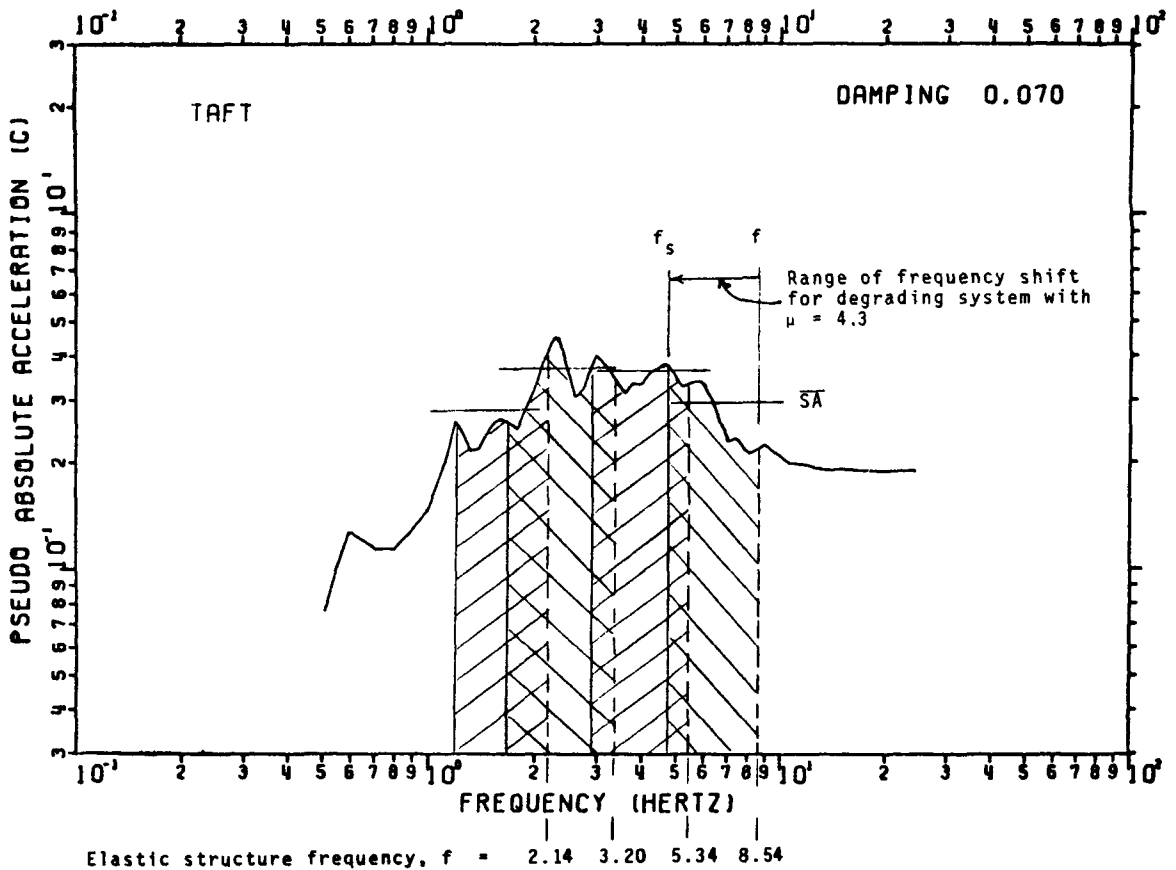FIGURE 4-2. EFFECT OF FREQUENCY SHIFT DUE TO NONLINEAR RESPONSE

FIGURE 4-3a.   ELASTIC RESPONSE SPECTRA FOR 7% DAMPING ($T_D^1 \geq 9$ Sec)

FIGURE 4-3a.   ELASTIC RESPONSE SPECTRA FOR 7% DAMPING ($T_D^1 > 9$ Sec)
(Continued)

4-32
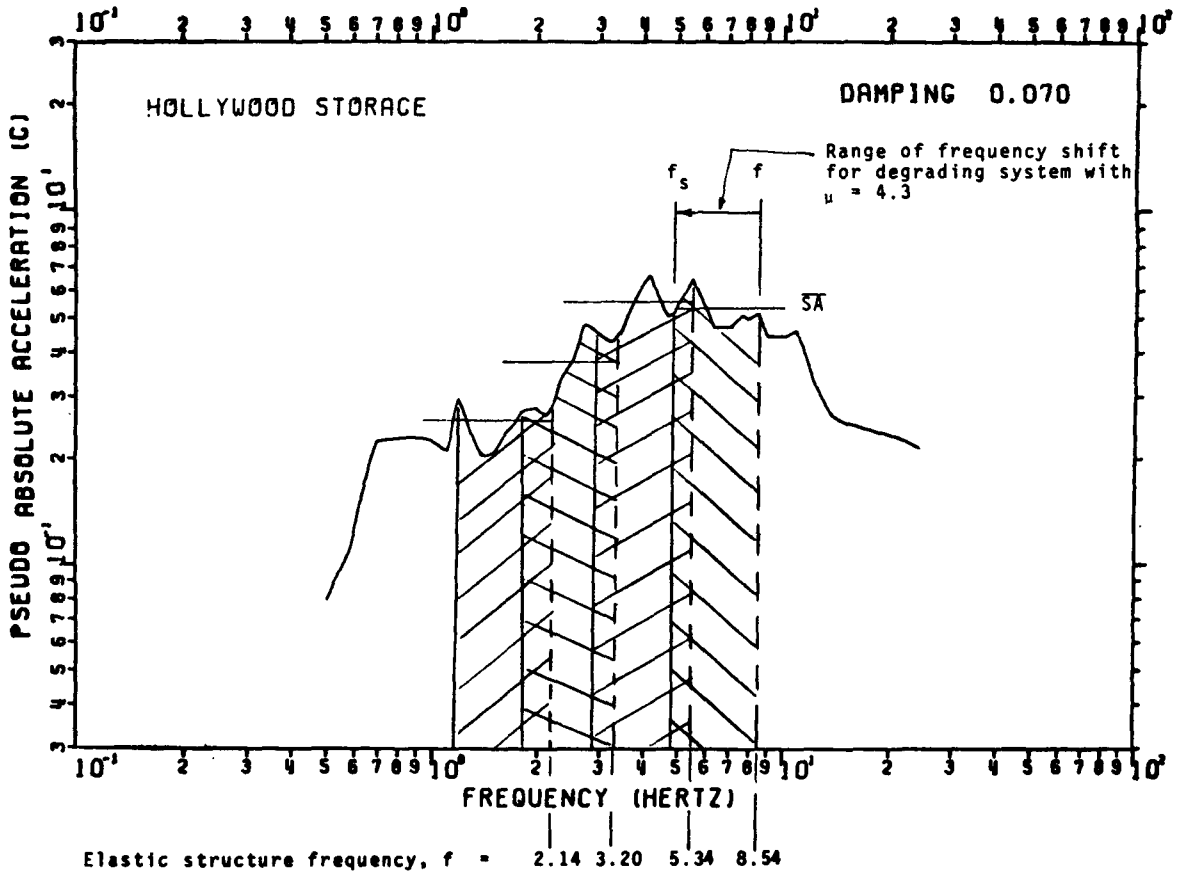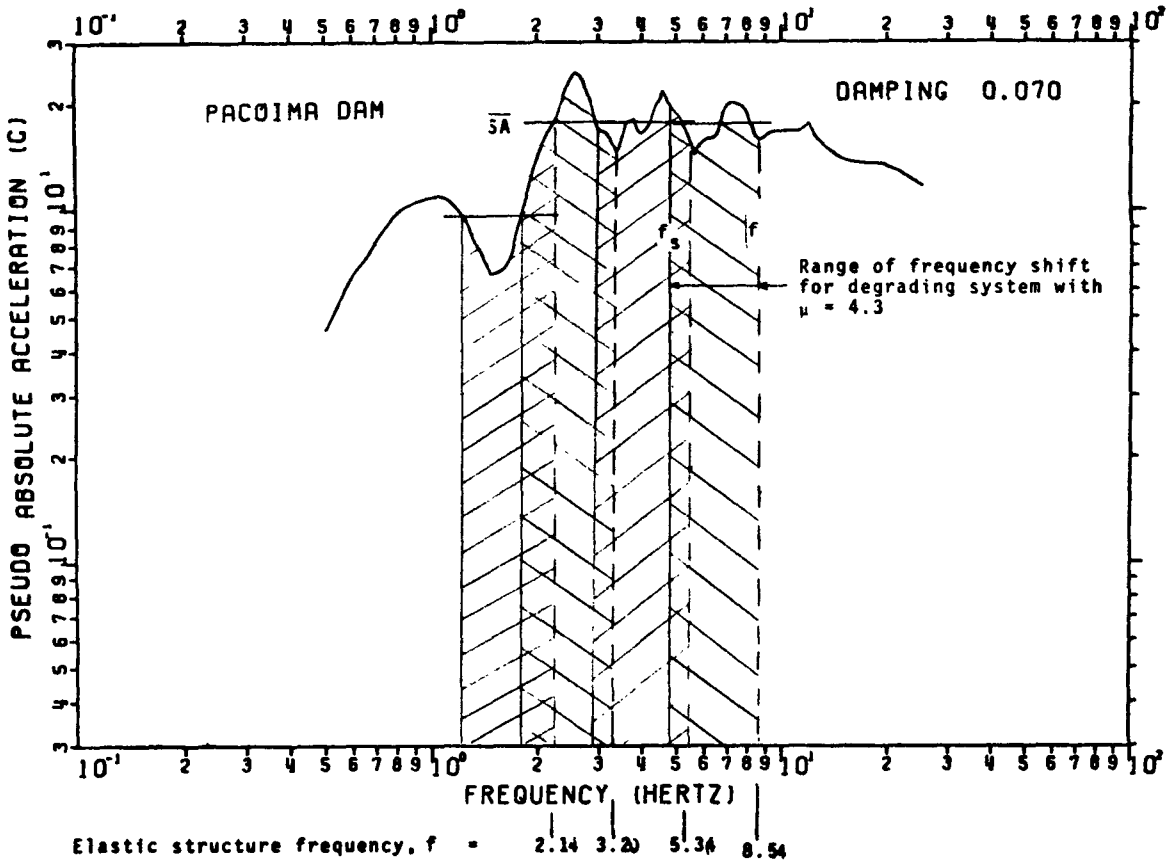
FIGURE 4-3b. ELASTIC RESPONSE SPECTRA FOR 7% DAMPING $(2.5 \; Sec \leq T_D' \leq 9 \; Sec)$
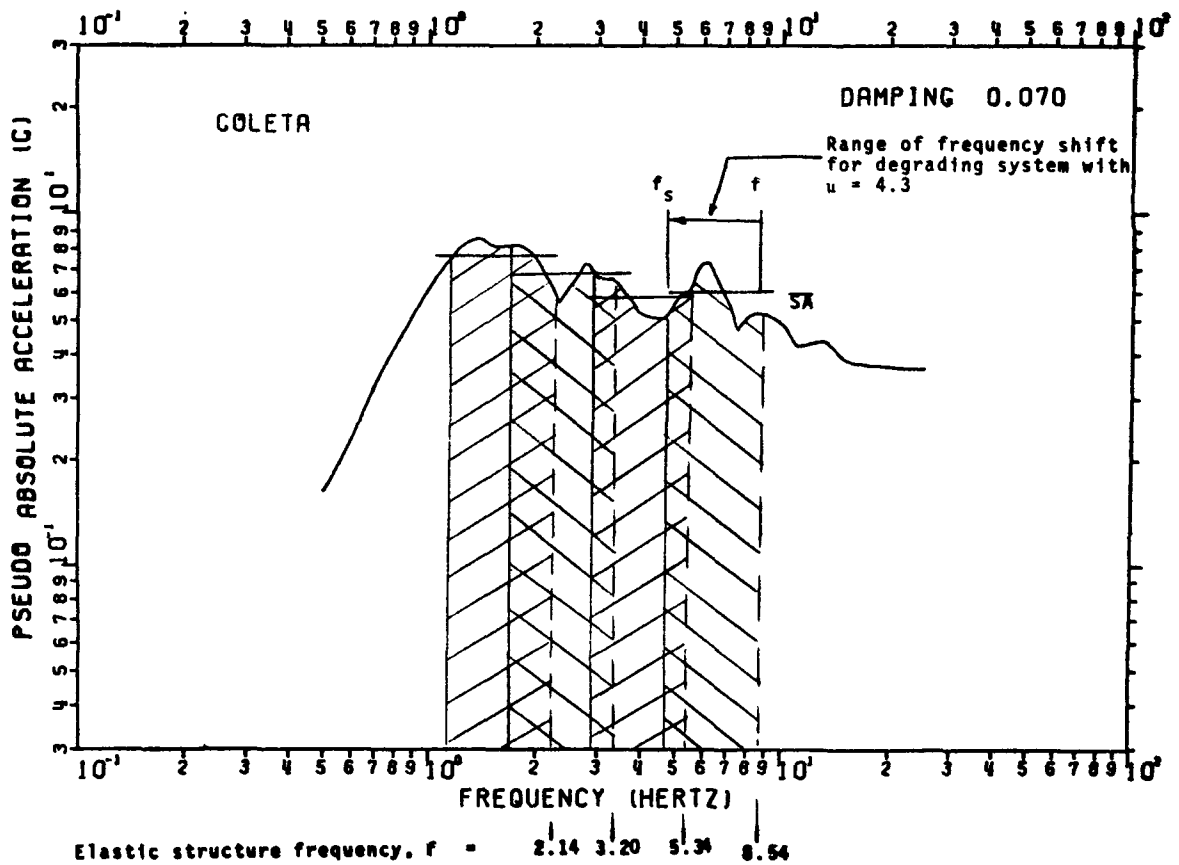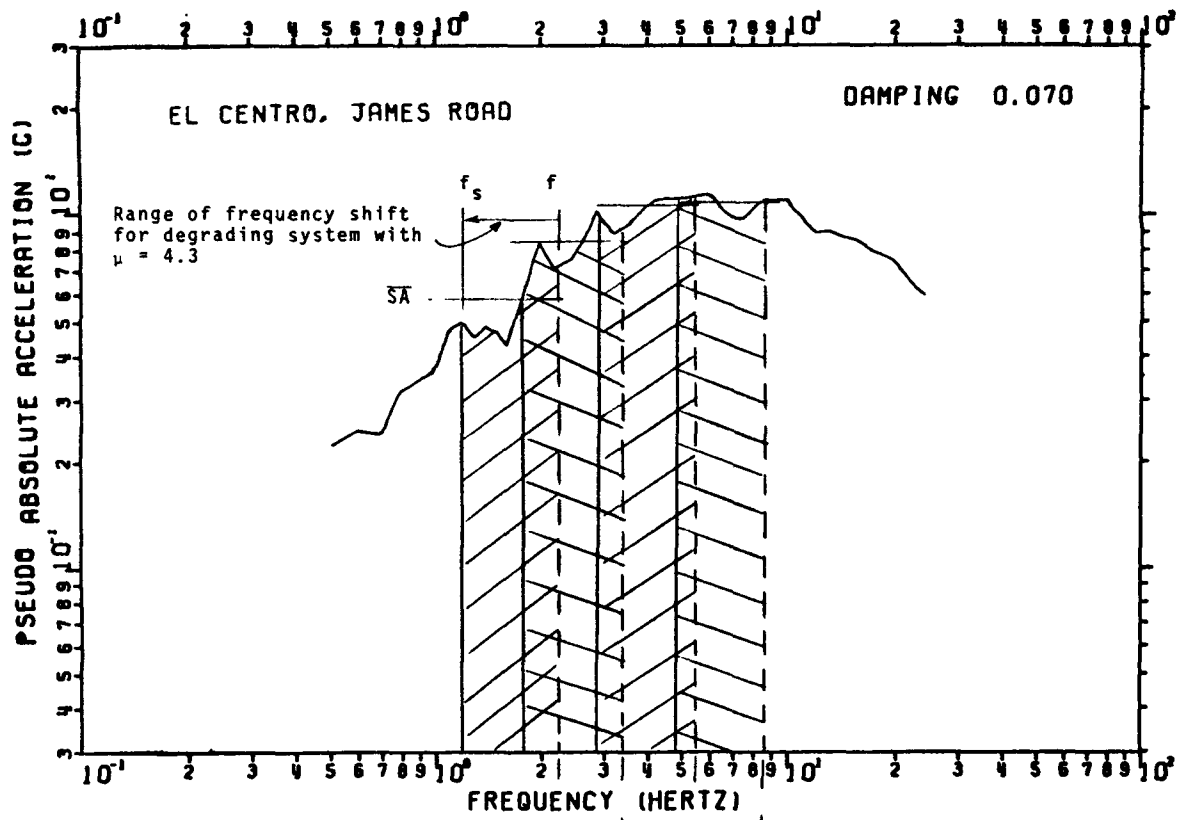
FIGURE 4-3b.   ELASTIC RESPONSE SPECTRA 7% DAMPING (2.5 Sec≤T_D^1≤9 Sec)
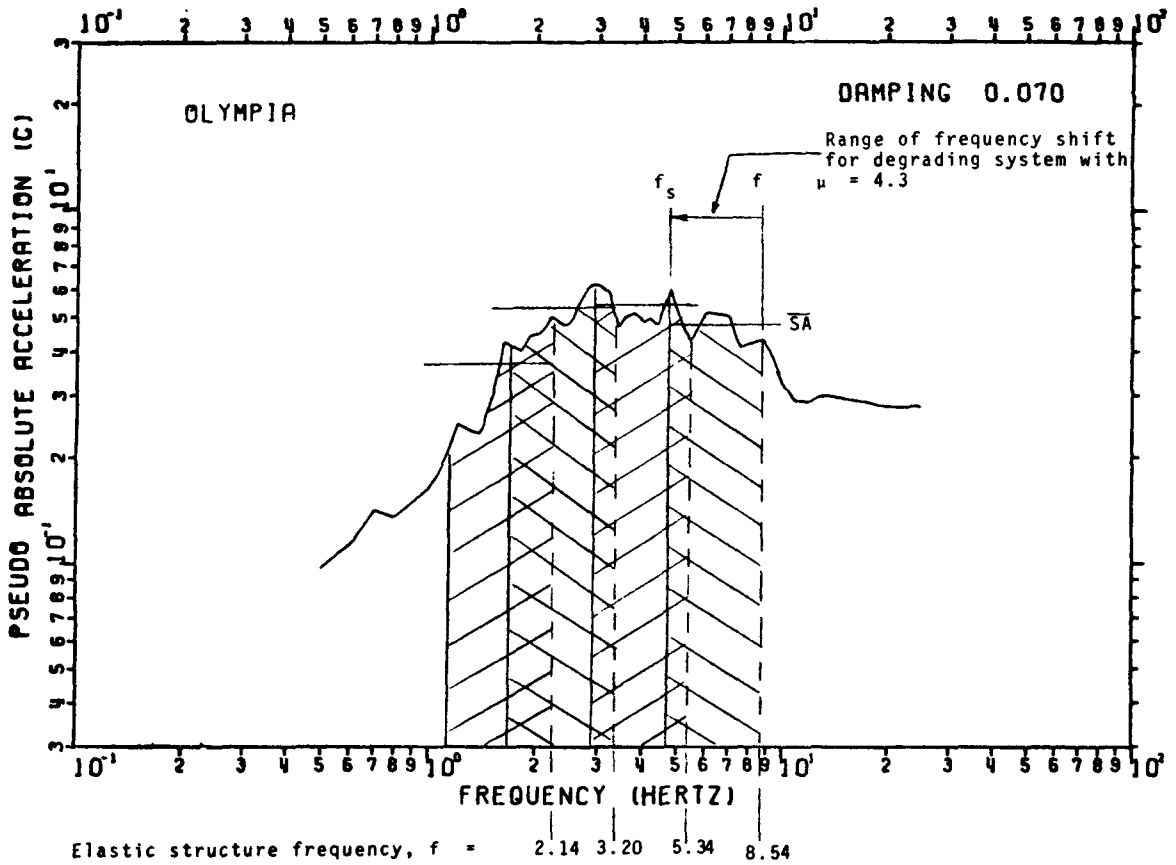(Continued)

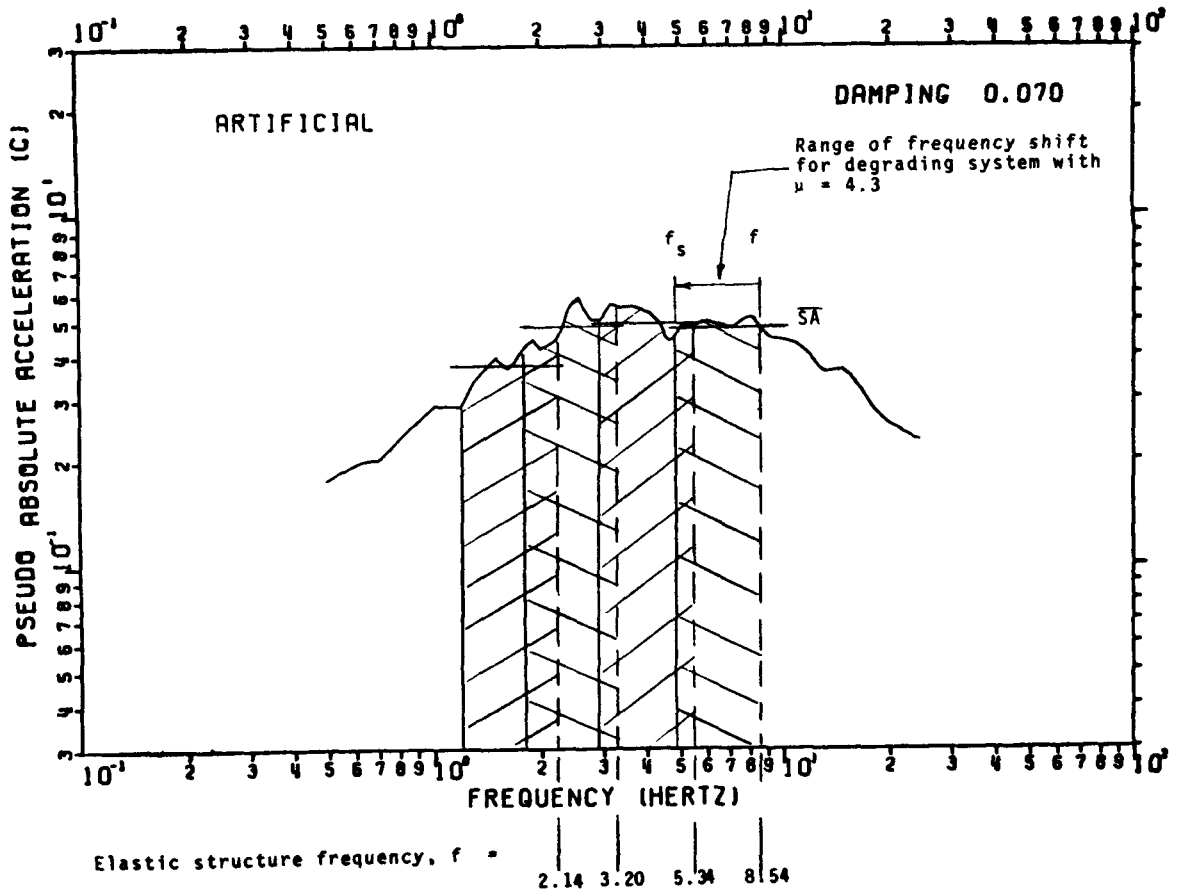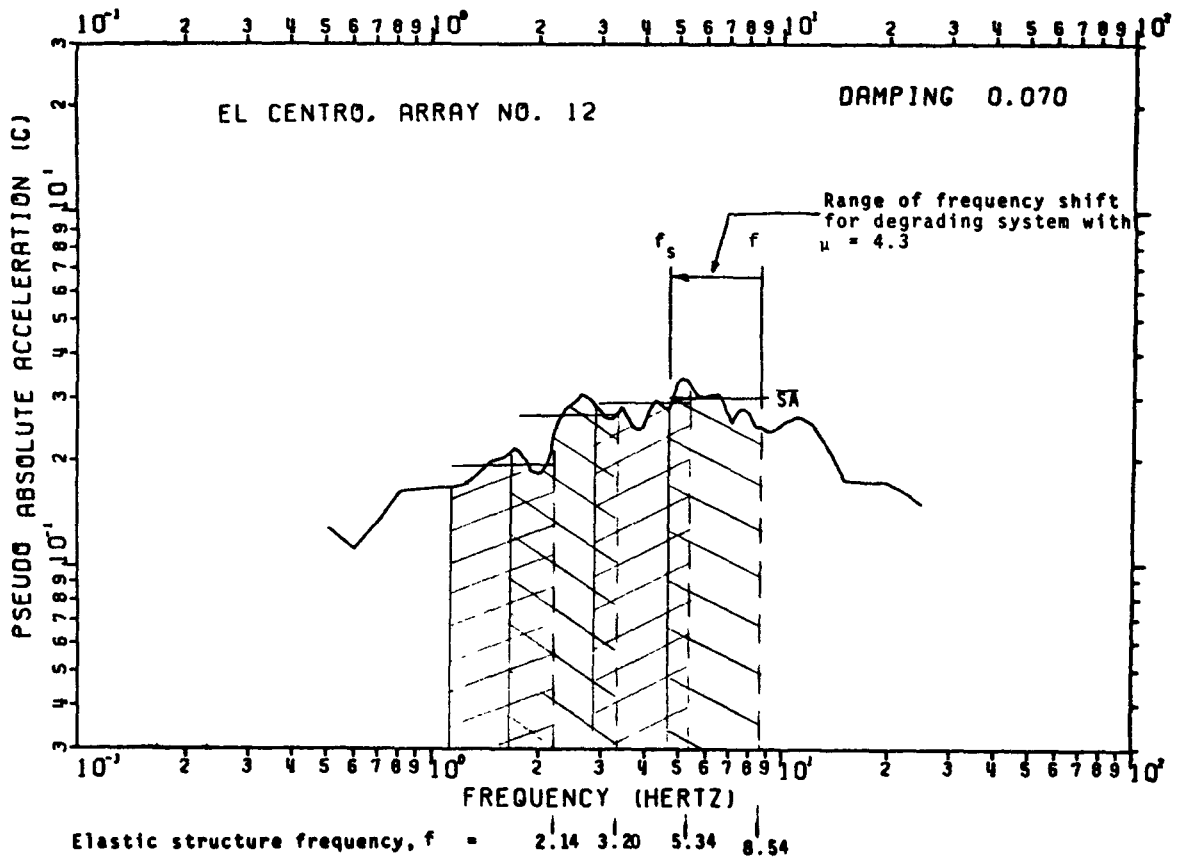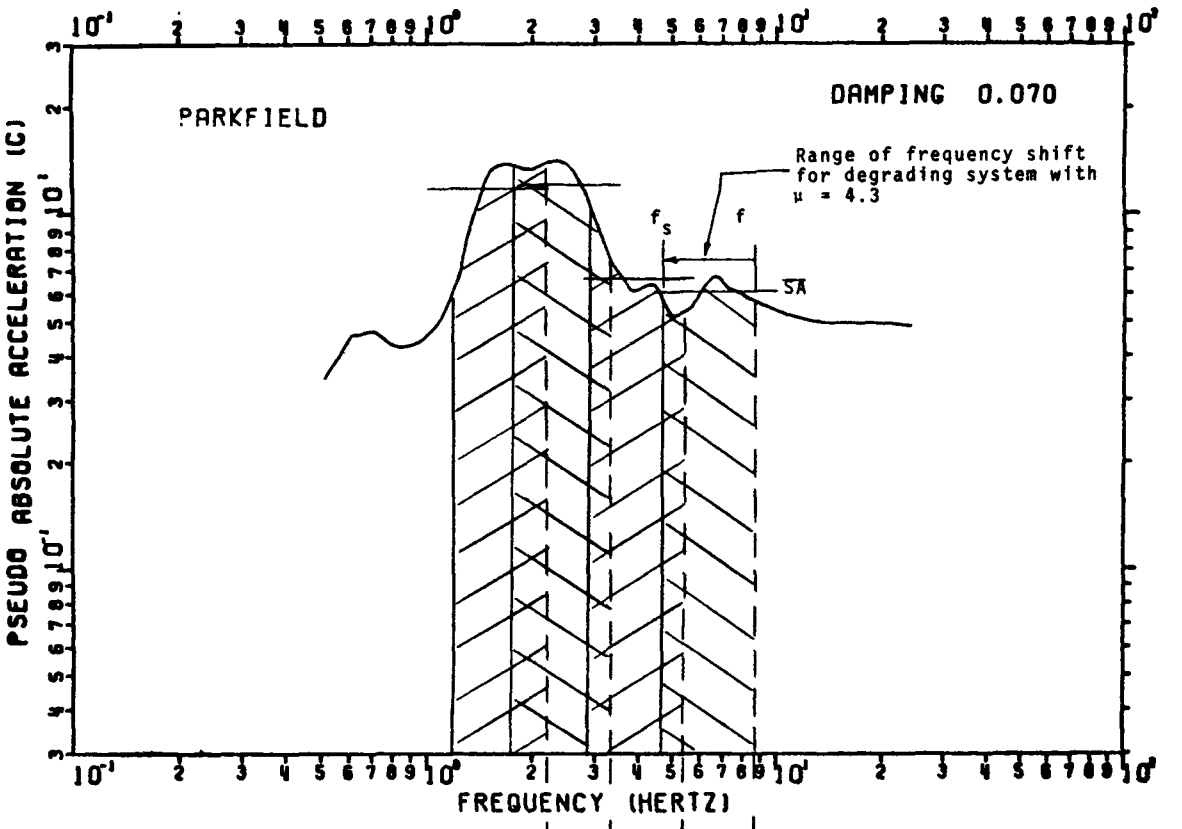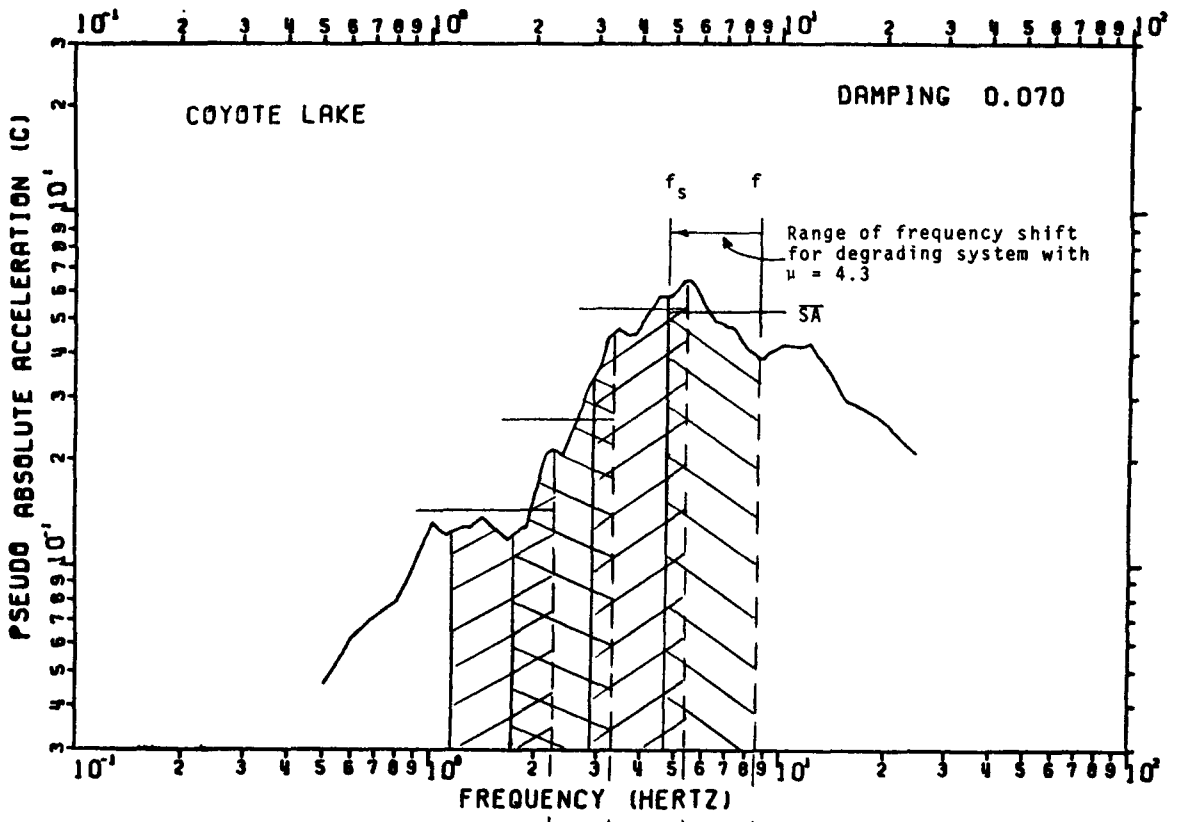FIGURE 4-3c.   ELASTIC RESPONSE SPECTRA FOR 7% DAMPING ($T_D' < 2.5$ Sec)
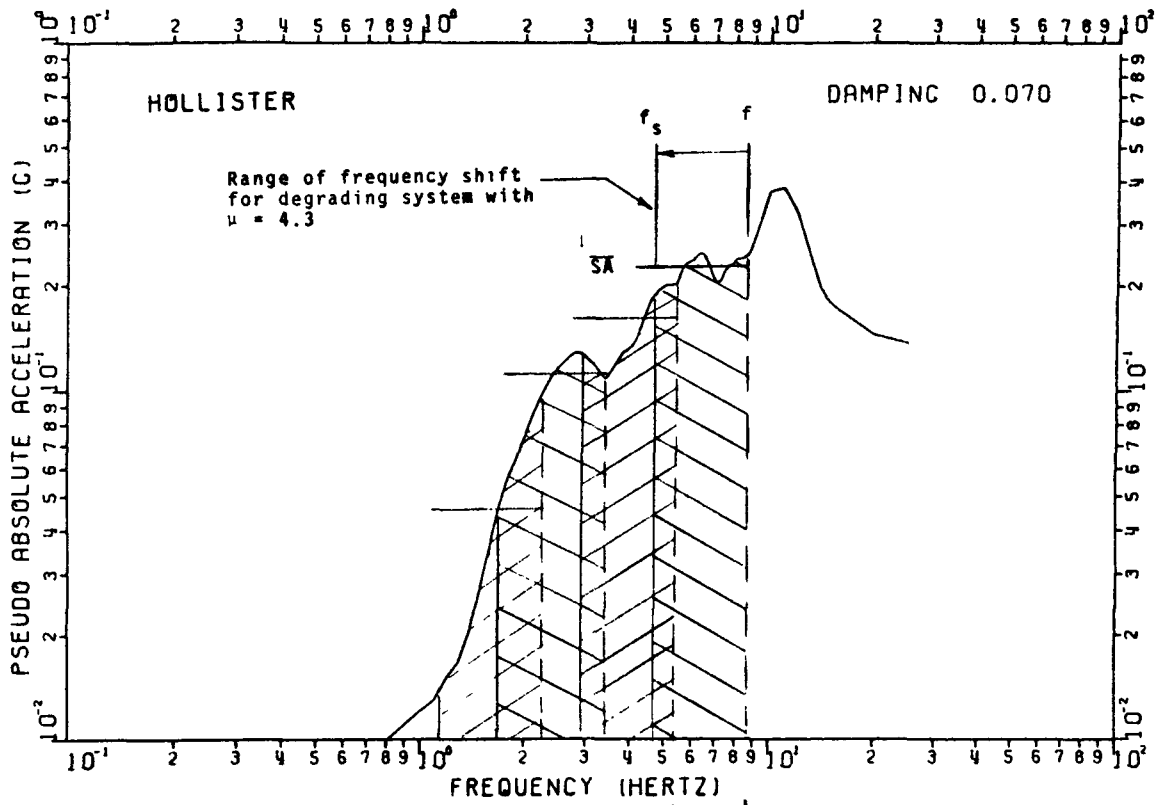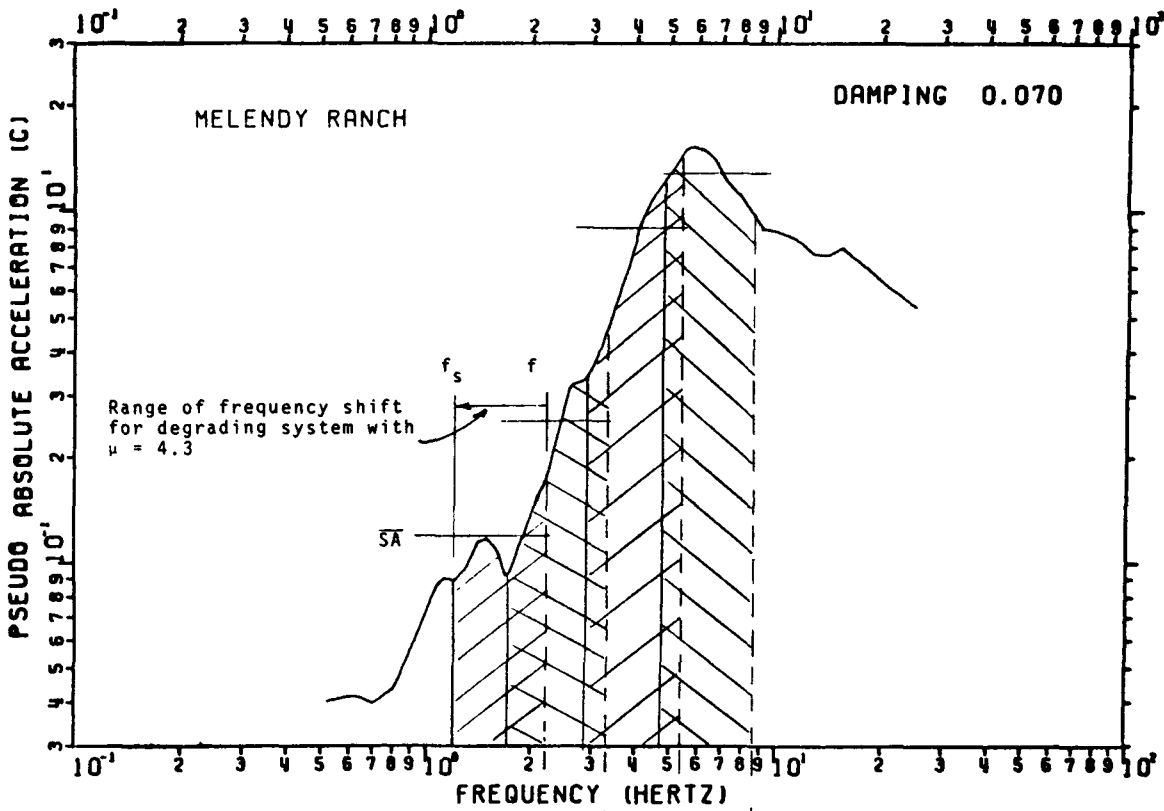
FIGURE 4-3c.   ELASTIC RESPONSE SPECTRA FOR 7% DAMPING ($T_D' < 2.5$ Sec)
(Continued)
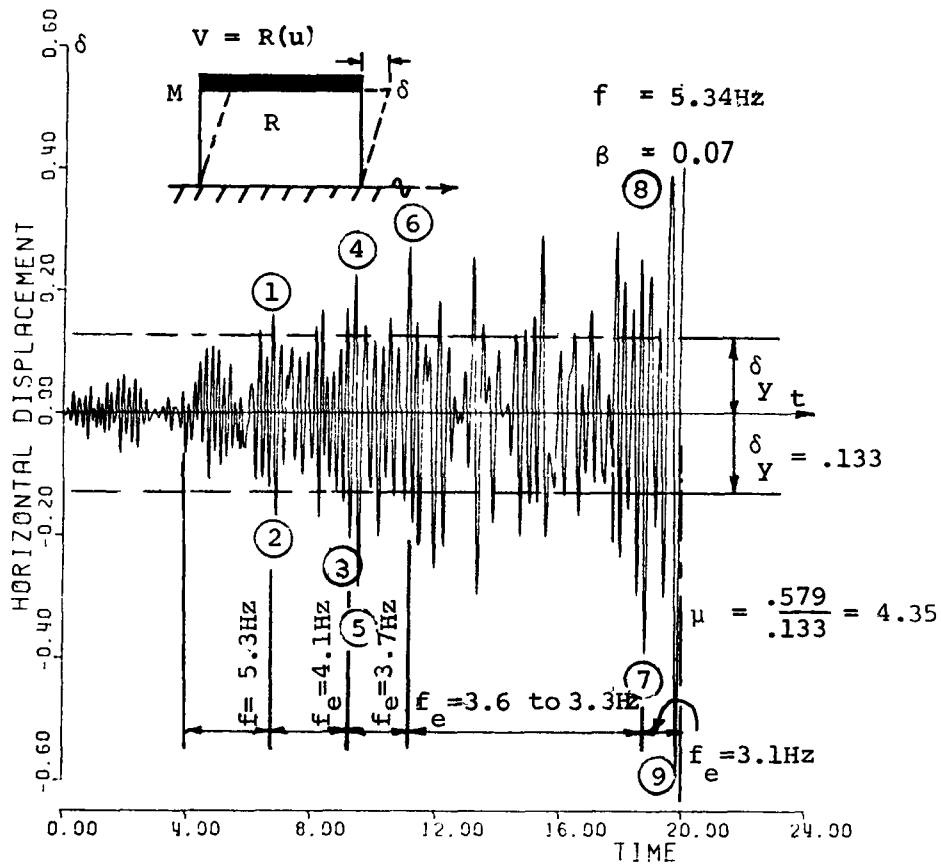
(a) Time History Response
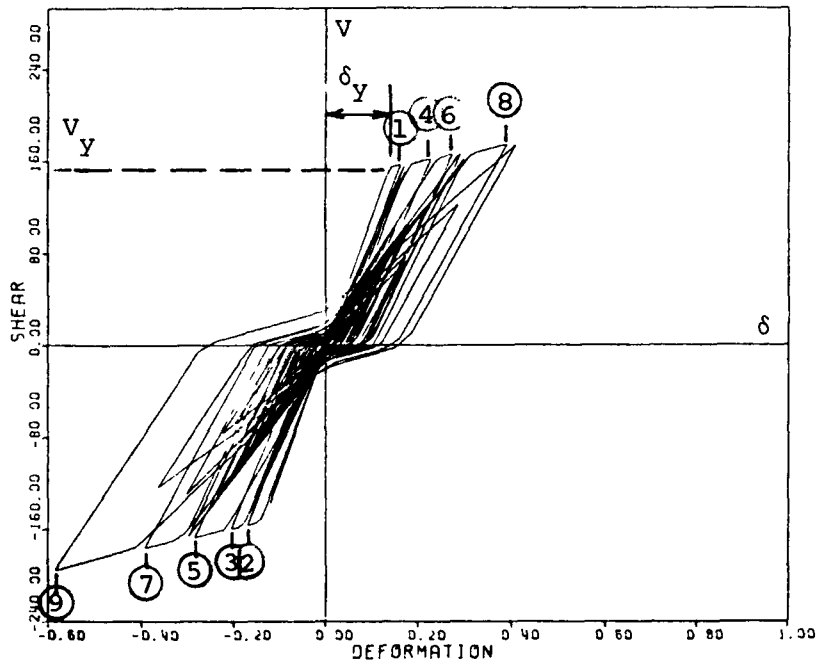
(b) Reaction Force - Displacement Response

FIGURE 4-4. MODEL STRUCTURE RESPONSE FOR OLYMPIA EARTHQUAKE
(N86E, 1949) FOR f = 5.34 Hz, μ = 4.35
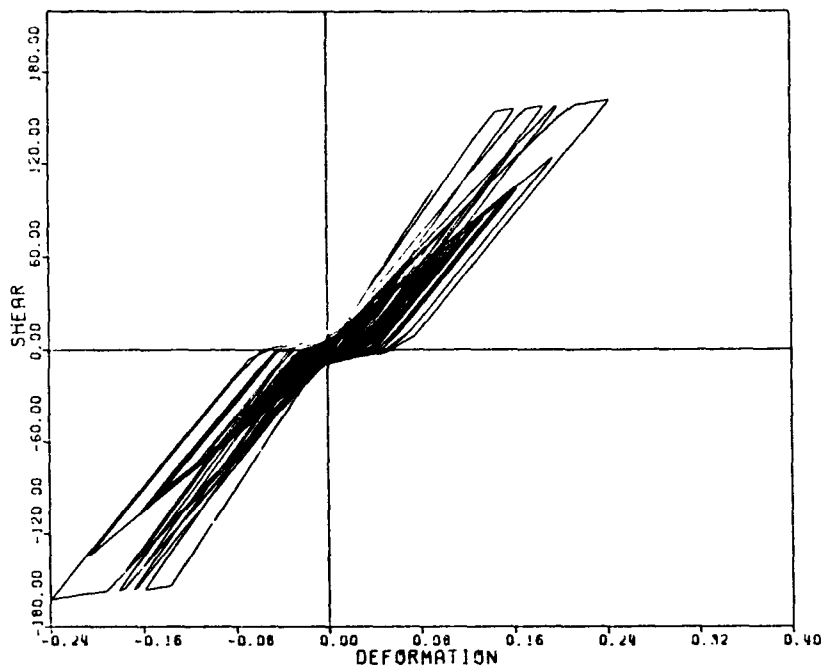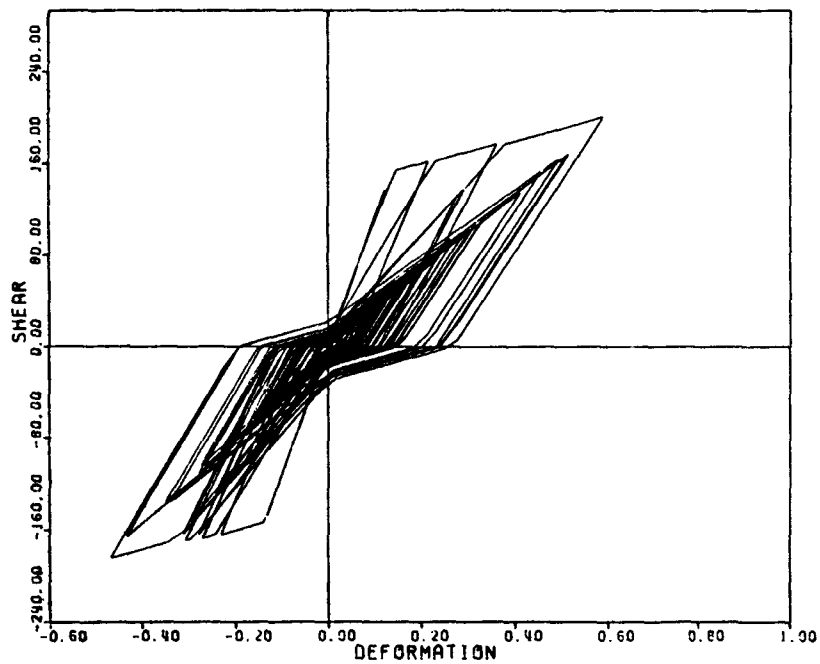
(a) f = 5.34 Hz
     β = 0.07
     μ = 1.9

(b) f = 5.34 Hz
     β = 0.07
     μ = 4.3

FIGURE 4-5.   MODEL STRUCTURE RESPONSE TO KERN CO. EARTHQUAKE
              (TAFT, S69E, 1952) for f = 5.34 Hz, μ = 1.9-4.3

4-38
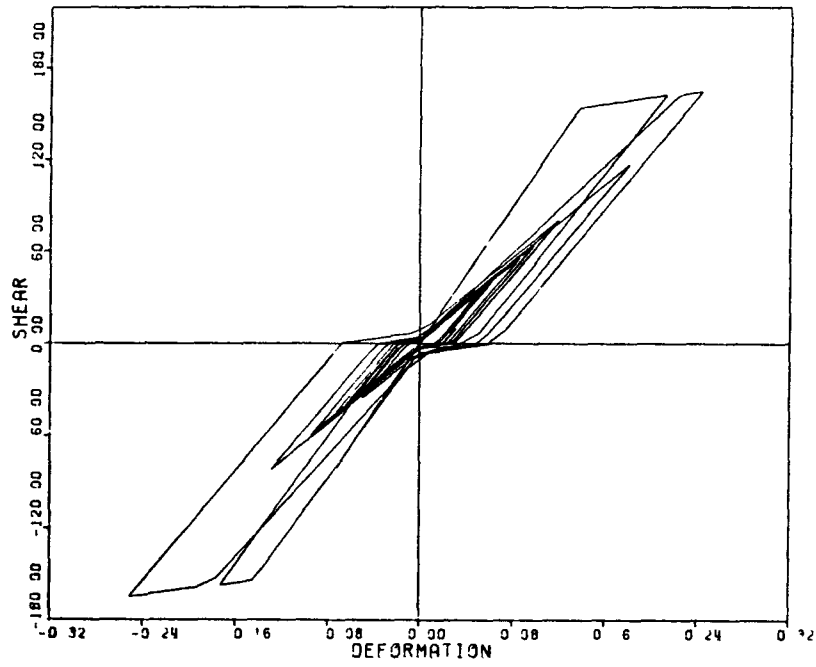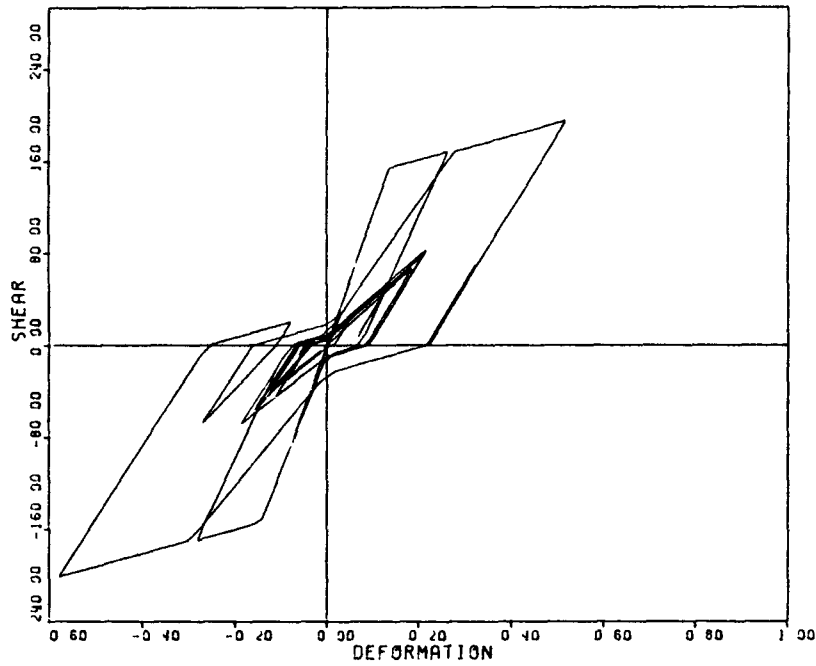
(a) f = 5.34 Hz
     β = 0.07
     μ = 1.9

(b) f = 5.34 Hz
     β = 0.07
     μ = 4.3

FIGURE 4-6.   MODEL STRUCTURE RESPONSE TO PARKFIELD EARTHQUAKE (CHOLAME
               ARRAY NO. 2, N65E, 1966) for f = 5.34 Hz, μ = 1.9-4.3
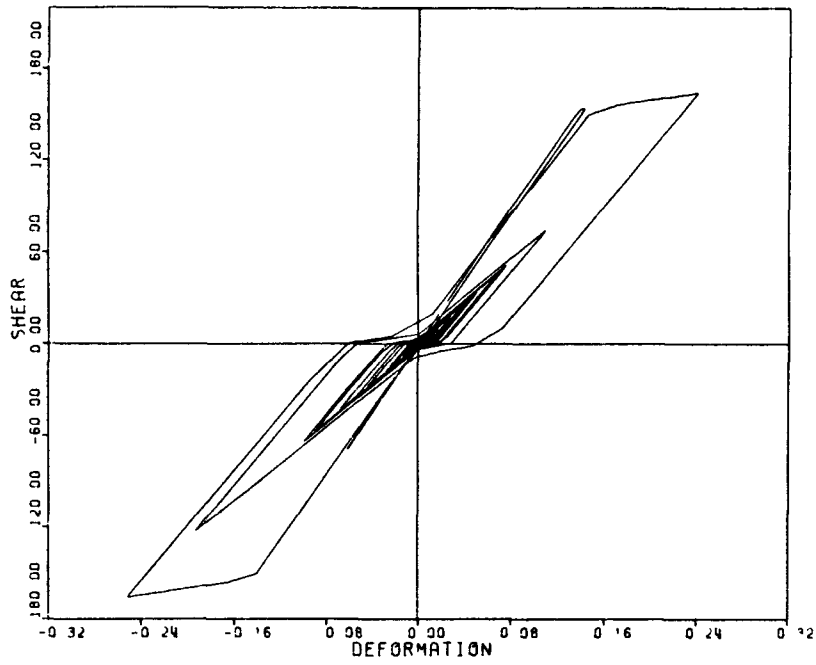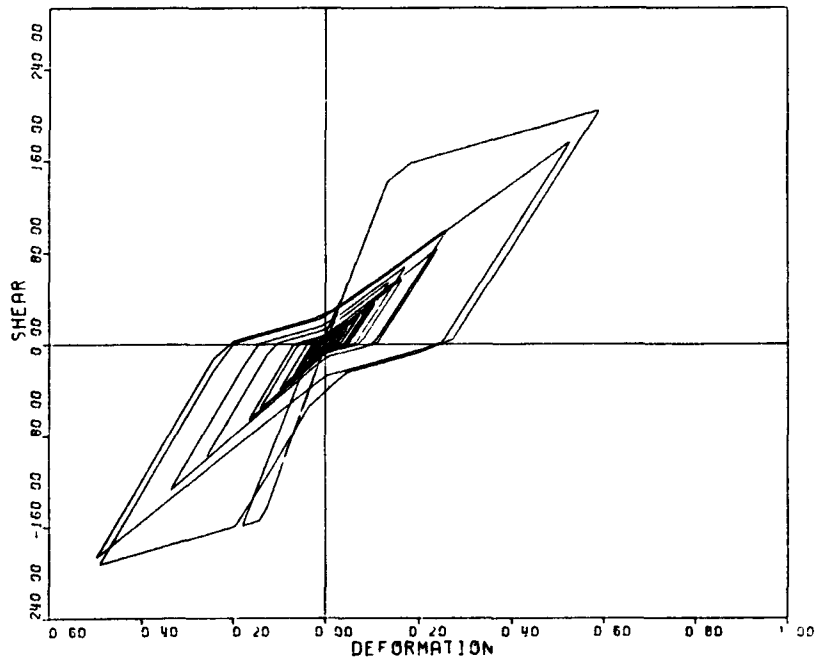
(a) f = 5.34 Hz
     β = 0.07
     μ = 1.9

(b) f = 5.34 Hz
     β = 0.07
     μ = 4.3

FIGURE 4-7. MODEL STRUCTURE RESPONSE TO BEAR VALLEY EARTHQUAKE (MELENDY
             RANCH, N29W, 1972) for f_e = 5.34 Hz, μ = 1.9-4.3

4-40
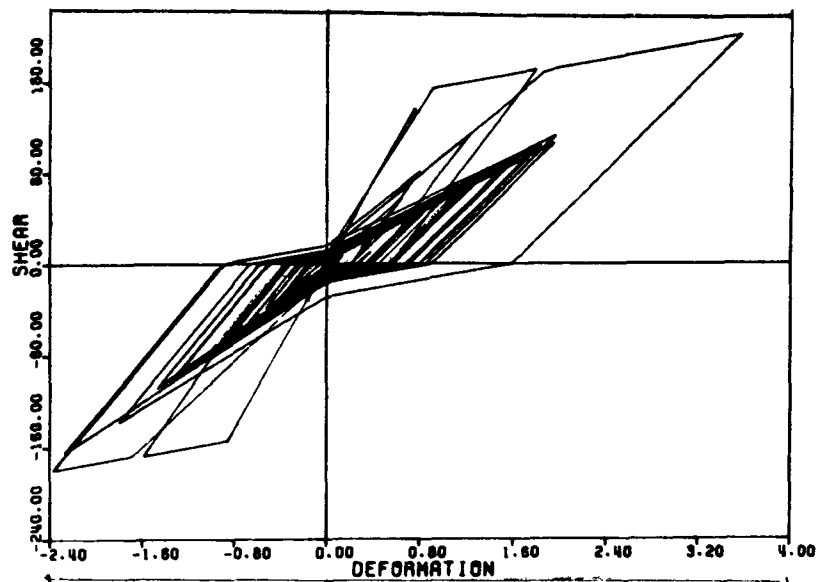
(a) f = 2.14 Hz
    β = 0.07
    μ = 4.3
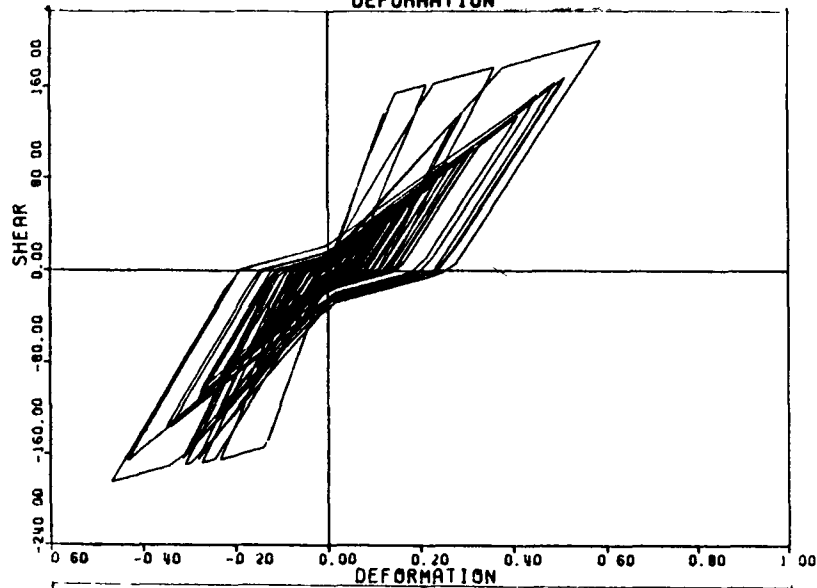
(b) f = 5.34 Hz
    β = 0.07
    μ = 4.3
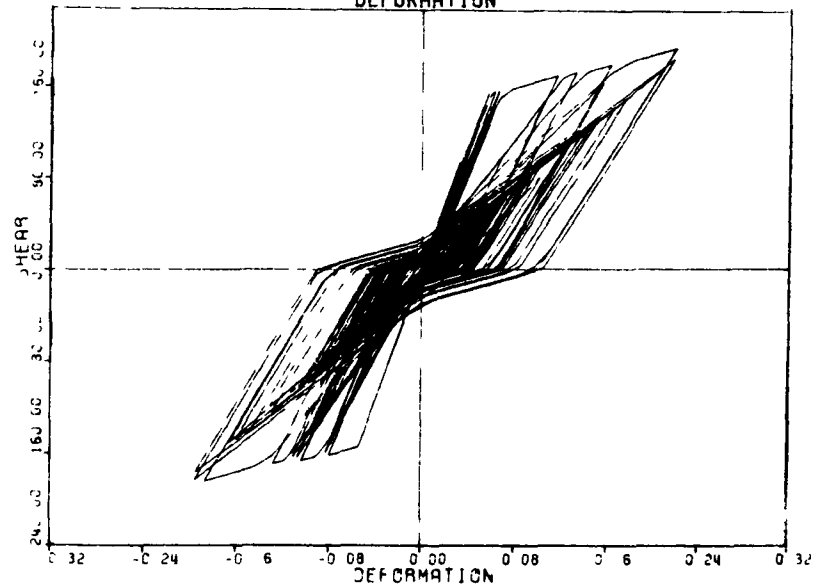
(c) f = 8.54 Hz
    β = 0.07
    μ = 4.1

FIGURE 4-8.   STRUCTURE RESPONSE TO KERN CO. EARTHQUAKE (TAFT,
              S69E, 1952) for f = 2-9 Hz, μ = 4.1 - 4.3
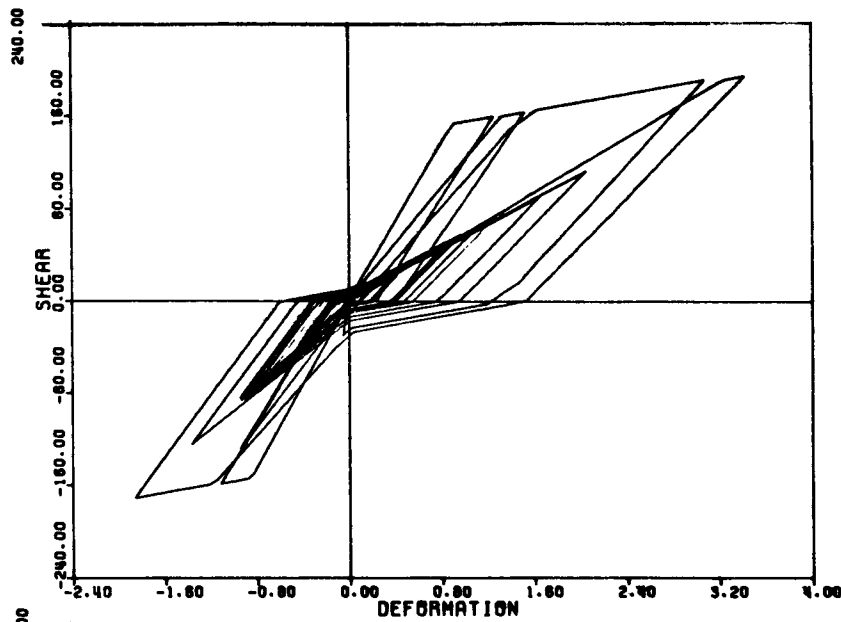
(a) $f_e = 2.14$ Hz

$\beta_e = 0.07$

$\mu = 4.3$
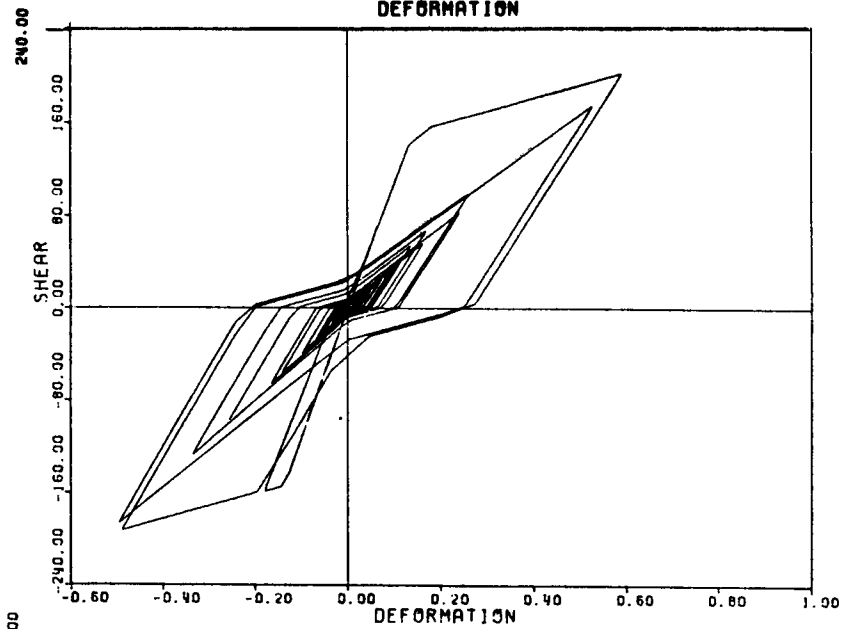
(b) $f_e = 5.34$ Hz

$\beta_e = 0.07$

$\mu = 4.3$
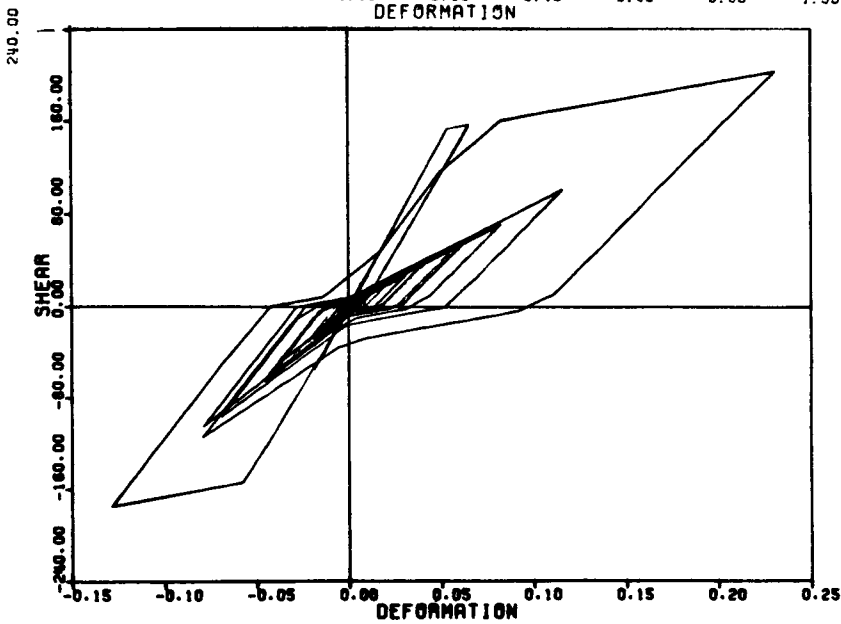
(c) $f_e = 8.54$ Hz

$\beta_e = 0.07$

$\mu = 4.3$

FIGURE 4-9. MODEL STRUCTURE RESPONSE TO BEAR VALLEY EARTHQUAKE (MELENDY RANCH, N29W, 1972) for f_e = 2-9 Hz, μ = 4.3

4-42
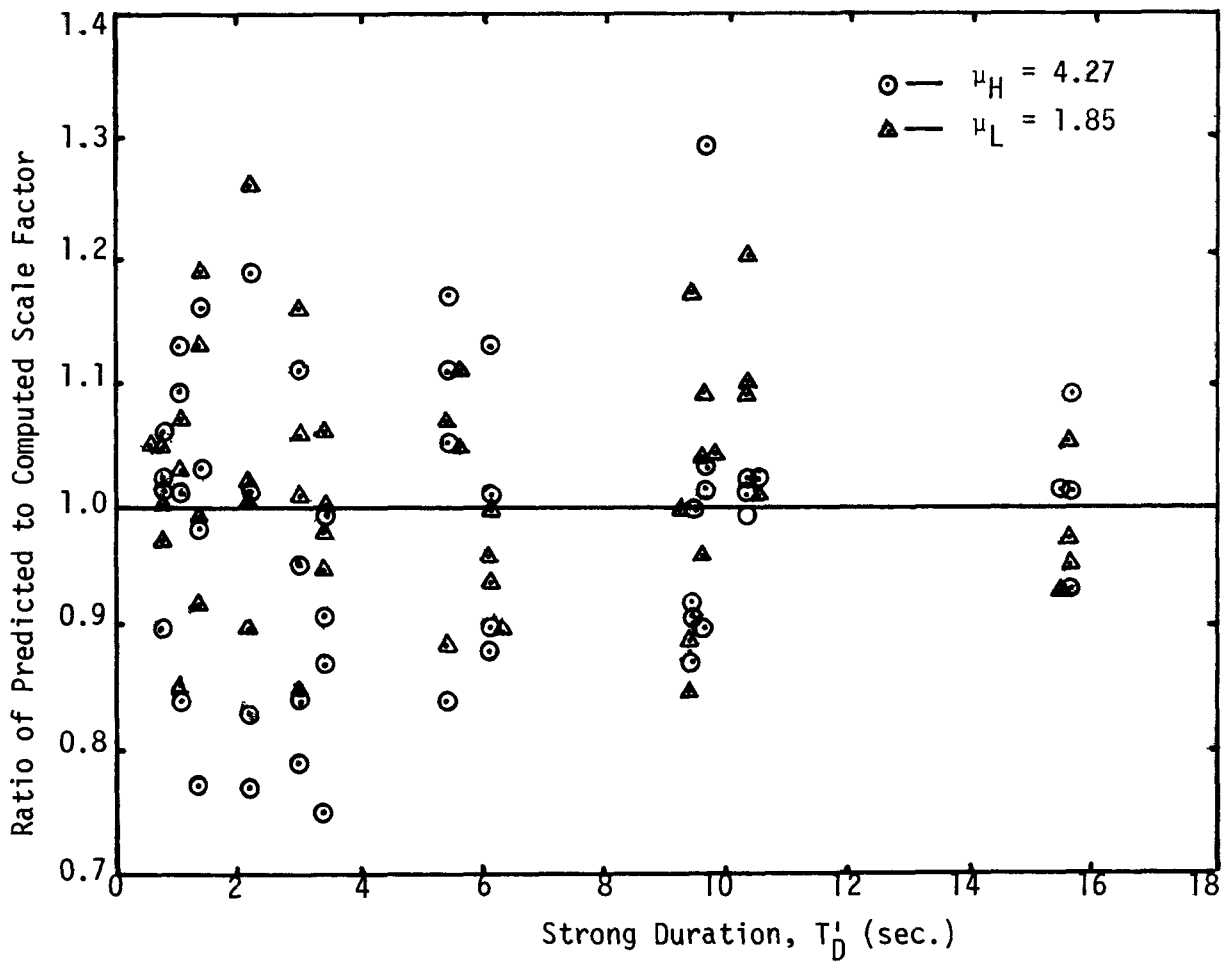
FIGURE 4-10.   RATIO OF PREDICTED TO COMPUTED SCALE FACTOR VERSUS DURATION, T_D'

5. GROUND MOTION CHARACTERIZATION FOR NONLINEAR RESPONSE

Chapter 2 described the engineering characterization of ground motion for elastic structural response. This chapter will extend that engineering characterization of ground motion to the prediction of nonlinear structural response using the procedure recommended by Chapter 4 for predicting nonlinear response.

The nonlinear response characterization of ground motion can be defined in terms of the inelastic spectral response, $S_{a\mu}(f,\beta)$, which can be obtained by the spectral averaging approach of Equation 4-9. This inelastic spectral response can be obtained for either an average design spectrum such as R.G. 1.60 or for actual earthquake spectra. It was shown in Chapter 2 that the R.G. 1.60 spectrum anchored to an "effective" acceleration could be used as an engineering characterization of the ground motion for longer duration $(T_D' > 3.0$ records) broad frequency content (1.2 to 5.5 Hz) records when predicting the elastic response of stiff structures (natural frequencies of 1.8 to 10 Hz). Therefore, the inelastic spectral responses will first be shown for the R.G. 1.60 spectrum.

5.1   INELASTIC R.G. 1.60 SPECTRA

Figures 5-1 and 5-2 show the inelastic response spectra from 1.0 to 10.0 Hz corresponding to $\mu = 1.85$ and $\mu = 4.27$ for the 7% damped R.G. 1.60 spectrum. All spectra are anchored to a 1.0g ground acceleration. The inelastic spectra were developed using Equations 4-4 through 4-7 and 4-9 together with the coefficients of Table 4-2. The inelastic deamplification factors for a given ductility are a constant throughout the amplified acceleration frequency range and another constant throughout the amplified spectral velocity region. These constants are a function of the number of strong inelastic cycles (i.e., a function of the strong duration) decreasing with an increasing number of cycles. One can compare

these constant F_μ factors found from this study for shear wall resistant function models with the Riddell factors reported in Section 3.3.2 as follows:

μ	N	Inelastic Deamplification Factor for Acceleration Region, $F_{\mu a}$		Inelastic Deamplification Factor for Velocity Region, $F_{\mu v}$	
		Recommended	Riddell	Recommended	Riddell
1.85	1	1.74		1.92	
	2	1.52	1.63	1.69	1.92
	3	1.44		1.63	
	4	1.36		1.58	
4.27	1	3.68		3.60	
	2	1.93	2.55	2.91	3.65
	3	1.81		2.75	
	4	1.81		2.75	

One should note that the Riddell F_μ values are greater than the F_μ values found in this study for the longer duration records (N=2 through 4) for which the R.G. 1.60 spectrum was an adequate characterization of the ground motion. The shear wall resistance function models used in this study have significantly lower effective damping β'_e than the models used in the Riddell study for the same elastic damping of 7%.

The conclusion is that the inelastic deamplification factors
proposed by Riddell are unconservative for the shear wall resistance
function models used in this study. This unconservatism increases with
ductility level from a factor of about 1.15 at μ = 1.85 to about 1.37 at
μ = 4.27.

Secondly, one should note that for T_D' > 3.0 seconds (N=2
through 4), the F_μ factor is rather insensitive to N. One could use the F_μ
values for N=3 with a maximum error of about $\pm$ 6%. Therefore, for broad
frequency content ground motions associated with T_D' > 3.0 seconds for
which the R.G. 1.60 spectrum is a reasonable characterization of the
ground motion, it is unnecessary to estimate T_D' or N. It is adequate
to assume N=3 for the purpose of predicting the ductility level μ.

5.2   PREDICTED INELASTIC SPECTRA FOR REAL TIME HISTORIES

Figures 5-3 through 5-13 present the inelastic spectra predicted
within the frequency range from 1.0 to 10.0 Hz for the 11 real time
histories included in this study using the prediction methods of Chapter 4
and ductilities of 1.85 and 4.27. Several points should be noted from
these figures:

1.   The peak inelastic spectral accelerations always occur at
      frequencies higher than those at which the peak elastic
      spectral accelerations occur. This situation occurs because
      inelastic response of these higher frequency structures
      shifts the effective frequency downward into the range of
      peak elastic response.

2.   The inelastic deamplification factors associated with
      frequencies equal to or less than that at which the elastic
      spectrum peaks are much greater than those for higher
      frequencies.

These points are most dramatically illustrated by the Parkfield
Cholame Array #2 spectra (Figure 5-11). The elastic spectral amplifica-
tions are very high from 1.2 to 3.0 Hz and drop off very rapidly at both
higher and lower frequencies. The largest inelastic deamplification

5-3

factors are associated with elastic frequencies less than 3.0 Hz since inelastic response will shift these frequencies lower and markedly reduce response. Structures with frequencies of 3.0 Hz and less could be designed to yield at spectral accelerations much less than those indicated by the elastic spectra for Parkfield without severe damage. However, for the Parkfield record one must be very careful not to reduce the elastic spectral accelerations for structures in about the 3.5 to 5.0 Hz range. These structures should be designed to remain elastic for the Parkfield record. Inelastic response of such structures will shift their effective frequencies into the frequency range (1.2 to 3.0 Hz) within which the power of the input is predominantly concentrated. For such structures, inelastic responses would rapidly increase because of this frequency shift. For records with narrow frequency content, such as Parkfield, one should be very careful about taking any credit for inelastic response for structures which lie slightly to the stiff side of the predominant frequency range of the record. On the other hand, for even stiffer structures (elastic frequencies greater than 5.0 Hz) the inelastic deamplification factors are again significant although not as large as for structures with frequencies below 3.0 Hz.

5.3   COMPARISON OF INELASTIC SPECTRA TO R.G. 1.60 INELASTIC SPECTRA

In Section 2.3, the 7% damped elastic R.G. 1.60 spectrum anchored at an "effective" acceleration was compared to the 7% damped elastic spectra for the 11 real earthquake time histories over the frequency range from 1.8 to 10 Hz. The "effective" acceleration, A_{DE}, was set so that 84% of the actual spectral accelerations between 1.8 and 10 Hz would lie below the R.G. 1.60 spectrum. In other words, the R.G. 1.60 spectrum was exceeded at 16% of the frequencies between 1.8 and 10 Hz. This process has been repeated for the inelastic spectra corresponding to μ = 1.85 and 4.27. The corresponding "effective" acceleration, $A_{D\mu}$, for inelastic response are shown in Table 5-1.

Figures 5-3 through 5-13 compare the μ = 1.0, 1.85, and 4.27 spectra for the 11 actual records studied to the corresponding R.G. 1.60 spectra anchored to the effective design accelerations, A_{D_μ}, for these same ductility levels for frequencies from 1.0 to 10 Hz. The R.G. 1.60 spectrum used depends upon the number of strong nonlinear cycles, N. The N = 4 spectrum was used for Olympia; N = 3 for Taft and El Centro #12; N = 1 for Melendy Ranch; and N = 2 for the other 7 records. Table 5-2 presents the maximum, median, and minimum ratio of actual inelastic spectral acceleration to R.G. 1.60 inelastic spectral acceleration $\left(SA_{\mu_a} / SA_{\mu_{1.60}} \right)$ for the frequency range from 1.8 to 10 Hz considered in this study.

The six real ground motion records with $T_D' > 3.0$ seconds (Olympia through El Centro #5) are all reasonably fit by the R.G. 1.60 spectrum anchored at A_{D_μ} for μ = 1.0 (elastic), 1.85, and 4.27. Actually, the fit is even better for the inelastic Reg. Guide spectra to the inelastic actual spectra than it is for elastic spectra (μ = 1.0). There-fore, the conclusion of Section 2.3 that the R.G. 1.60 spectrum anchored to an "effective" acceleration provides an adequate engineering character-ization of the ground motion for the six longer duration records for elastic response of structures with elastic frequencies between 1.8 and 10 Hz can be easily extended to inelastic response at least up to ductility levels of 4.3. The reason that the R.G. 1.60 spectrum works even better for inelastic response than for elastic response is that inelastic response spectra are smoother than elastic spectra and thus can be better fit by a smooth, broad frequency design spectrum such as R.G. 1.60.

Similarly, the conclusion of Section 2.3 that the elastic R.G. 1.60 spectrum does not provide an adequate engineering characterization for the 5 shorter duration records ($T_D' \leq 3.0$ seconds) for elastic response can also be extended to inelastic response.

For the six records with broad frequency content and $T_D' > 3.0$ seconds (Olympia through El Centro #5), the "effective" design accelerations, $A_{D\mu}$, for $\mu = 1.0$, 1.85, and 4.27 are compared in Table 5-1 to the corrected instrumental ground acceleration, a, the rms based design acceleration, A_{DE1}, and the Spectral Intensity based design acceleration, A_{DE2}, described in Section 2.3. For these six records, all three accelerations could serve as a basis for defining "effective" acceleration to anchor the R.G. 1.60 spectrum. For these six records:

μ	Ratio	Max.	Mean	Min.	COV
1.0	$A_{D\mu}/a$	1.10	0.87	0.73	0.15
	$A_{D\mu}/A_{DE1}$	1.17	1.06	0.96	0.08
	$A_{D\mu}/A_{DE2}$	1.17	0.99	0.85	0.12
1.85	$A_{D\mu}/a$	1.13	0.87	0.71	0.17
	$A_{D\mu}/A_{DE1}$	1.21	1.06	0.94	0.09
	$A_{D\mu}/A_{DE2}$	1.19	0.99	0.83	0.14
4.27	$A_{D\mu}/a$	1.19	0.91	0.70	0.19
	$A_{D\mu}/A_{DE1}$	1.31	1.10	0.95	0.12
	$A_{D\mu}/A_{DE2}$	1.26	1.03	0.85	0.16

The rms-based "effective" acceleration, A_{DE1}, has the lowest COV. However, it also introduces a mean factor of unconservatism of between 1.06 at the lower ductilities to 1.10 at $\mu = 4.27$. Considering the conservative bias introduced by use of the R.G. 1.60 spectrum (see Table 5-2), this slight factor of unconservatism is unimportant. When the R.G. 1.60 spectrum is anchored to A_{DE1}, within the 1.8 to 10 Hz range, the following ratio of $(SA_{\mu_a}/SA_{\mu_{1.60}})$ are obtained for the 6 records considered:

5-6

	$(SA_{\mu_a}/SA_{\mu_{1.60}})$					
	Maximum		Medium		Minimum	
μ	Range	Median	Range	Median	Range	Median
1.0	1.29-1.05	1.20	1.05-0.83	0.88	0.76-0.49	0.59
1.85	1.24-1.00	1.10	1.15-0.85	0.99	0.88-0.51	0.64
4.27	1.32-1.03	1.12	1.06-0.84	0.98	0.82-0.56	0.67

For broad frequency content records (frequency content at least throughout the range from 1.2 to 5.5 Hz) associated with durations T_D' greater than 3.0 seconds, both the elastic ($\mu = 1.0$) and inelastic response chararacteristics of the ground motion for structures with elastic frequencies from 1.8 to 10 Hz can be adequately characterized by the R.G. 1.60 spectra anchored to an rms based "effective" acceleration defined by Equation 2-15. For the six records studied with these characteristics, the maximum factor of unconservatism obtained at any frequency from 1.8 to 10 Hz for ductilities from 1.0 to 4.3 was 1.32 while the maximum factor of conservatism was (1/0.49) = 2.04. The median factor of conservatism ranged from (1/0.88) = 1.14 for elastic response ($\mu = 1.0$) to (1/0.99) = 1.01 for inelastic response. In other words, at the worst, this method of defining the engineering characterization of ground motion can range from a 1.3 factor of unconservatism to a 2.0 factor of conservatism with a slight conservative bias on the average. Considering the uncertainties in the ground motion, this range of accuracy is very tolerable.

5.4   GROUND MOTION CHARACTERIZATION FOR NONLINEAR RESPONSE SUMMARY

In this chapter, inelastic spectra are predicted by the spectral averaging approach presented in Chapter 4 for the 11 real earthquake ground motion records considered in this study. In addition, inelastic Reg. Guide 1.60 spectra have been constructed by the same approach. The actual earthquake spectra and the Reg. Guide spectra are utilized to establish "effective" acceleration, $A_{D\mu}$, for inelastic response as the value the Reg. Guide spectrum must be anchored such that 84 percent of the actual earthquake inelastic response spectral accelerations between 1.8 and 10 Hz would lie below the Reg. Guide 1.60 spectrum. It is shown in Table 5-2 that the inelastic spectra for all the longer duration records studied are reasonably fit by the Reg Guide 1.60 spectra anchored to $A_{D\mu}$ but this is not the case for the 5 shorter duration records. It is also shown in this chapter that the rms based definition for "effective" acceleration, A_{DE1} as given by Equation 2-15 provides a good match with the empirically determined "effective" acceleration, $A_{D\mu}$.

In Chapter 2 it was demonstrated that an adequate engineering characterization for elastic structural response for stiff structures (1.8 to 10 Hz) subjected to any of the six real ground motion records with $T_D' > 3.0$ seconds is provided by the Reg. Guide 1.60 spectrum anchored to an "effective" peak acceleration, A_{DE1} as given by Equation 2-15. In this chapter, it is demonstrated that this conclusion can be extended to inelastic response at least up to ductility levels of 4.3. Similarly, the conclusion of Chapter 2 that the elastic Reg. Guide 1.60 spectrum does not provide adequate engineering characterization for the 5 shorter duration records ($T_D' \leq 3.0$ seconds) for elastic response can also be extended to inelastic response.

TABLE 5-1

"EFFECTIVE" DESIGN ACCELERATIONS FOR INELASTIC RESPONSE

	Earthquake Record (Component)	"Effective" Design Acceleration, $A_{D\mu}$ (g)			Ground Accel. a (g)	RMS-Based Accel. A_{DE1} (g)	Spectral Intensity Based Accel. A_{DE2} (g)
		$\mu = 1.0$	$\mu = 1.85$	$\mu = 4.27$			
1	Olympia, WA., 1949 (N86E)	0.219	0.216	0.223	0.281	0.202	0.253
2	Taft, Kern Co., 1952 (S69E)	0.149	0.145	0.148	0.180	0.155	0.175
3	El Centro Array No. 12 Imperial Valley, 1979, (140)	0.128	0.129	0.135	0.142	0.133	0.128
5	Pacoima Dam San Fernando, 1971 (S14W)	0.856	0.825	0.820	1.170	0.795	0.879
6	Hollywood Storage PE Lot, San Fernando, 1971 (N90E)	0.233	0.238	0.251	0.211	0.213	0.200
7	El Centro Array No. 5, Imperial Valley, 1979, (140)	0.471	0.487	0.528	0.530	0.404	0.442
8	UCSB Goleta Santa Barbara, 1978 (180)	0.283	0.272	0.402	0.347	0.332	0.324
9	Gilroy Array No. 2, Coyote Lake, 1979, (050)	0.233	0.241	0.243	0.191	0.202	0.154
10	Cholame Array No. 2, Parkfield 1966 (N65E)	0.562	0.516	0.625	0.490	0.514	0.564
11	Gavilan College Hollister, 1974 (S67W)	0.105	0.101	0.093	0.138	0.106	0.060
12	Melendy Ranch Barn, Bear Valley, 1972 (N29W)	0.573	0.631	0.620	0.520	0.435	0.221

TABLE 5-2

COMPARISON OF ACTUAL SPECTRAL ACCELERATIONS TO R.G. 1.60 SPECTRAL ACCELERATIONS ANCHORED TO $A_{D\mu}$

Earthquake Record (Component)	$(SA_{\mu_a}/SA_{\mu_{1.60}})*$								
	$\mu = 1.0$			$\mu = 1.85$			$\mu = 4.27$		
	Max.	Median	Min.	Max.	Median	Min.	Max.	Median	Min.
1 Olympia, WA., 1949 (N86E)	1.12	0.90	0.70	1.08	0.94	0.82	1.07	0.94	0.61
2 Taft, Kern Co., 1952 (S69E)	1.23	0.89	0.61	1.12	0.92	0.68	1.10	0.95	0.86
3 El Centro Array No. 12 Imperial Valley, 1979, (140)	1.09	0.86	0.61	1.03	0.88	0.70	1.01	0.83	0.70
5 Pacoima Dam San Fernando, 1971 (S14W)	1.08	0.84	0.55	1.02	0.93	0.49	1.03	0.91	0.54
6 Hollywood Storage PE Lot, San Fernando, 1971 (N90E)	1.14	0.86	0.45	1.02	0.91	0.51	1.02	0.87	0.50
7 El Centro Array No. 5 Imperial Valley, 1979, (140)	1.11	0.90	0.60	1.03	0.95	0.54	1.01	0.81	0.51
8 UCSB Goleta Santa Barbara, 1978 (180)	1.33	0.82	0.69	1.65	0.89	0.76	1.35	0.64	0.53
9 Gilroy Array No. 2, Coyote Lake 1979 (050)	1.15	0.77	0.25	1.04	0.80	0.27	1.01	0.77	0.27
10 Cholame Array No. 2, Parkfield 1966 (N65E)	1.16	0.48	0.37	1.40	0.53	0.46	1.15	0.49	0.42
11 Gavilan College Hollister, 1974 (S67W)	1.66	0.58	0.26	1.26	0.84	0.18	1.09	0.57	0.11
12 Melendy Ranch Barn, Bear Valley 1972 (N29W)	1.14	0.69	0.08	1.03	0.80	0.09	1.01	0.61	0.10

* Ratios of Actual to Reg. Guide 1.60 Spectral Accelerations are reported for the frequency range of 1.8 to 10 Hz

7% Damping

$\mu = 1.0$

$\left.\begin{array}{l} N = 4 \\ N = 3 \\ N = 2 \\ N = 1 \end{array}\right\} \mu = 1.85$

PSEUDO ABSOLUTE ACCELERATION (G)

FREQUENCY (HERTZ)

T'_D (Sec)	N	F_μ	
		1.75 Hz	6.0 Hz
< 1.0	1	1.92	1.74
1.0 - 7.0	2	1.69	1.52
9.0 - 11.0	3	1.63	1.44
>15.0	4	1.58	1.36
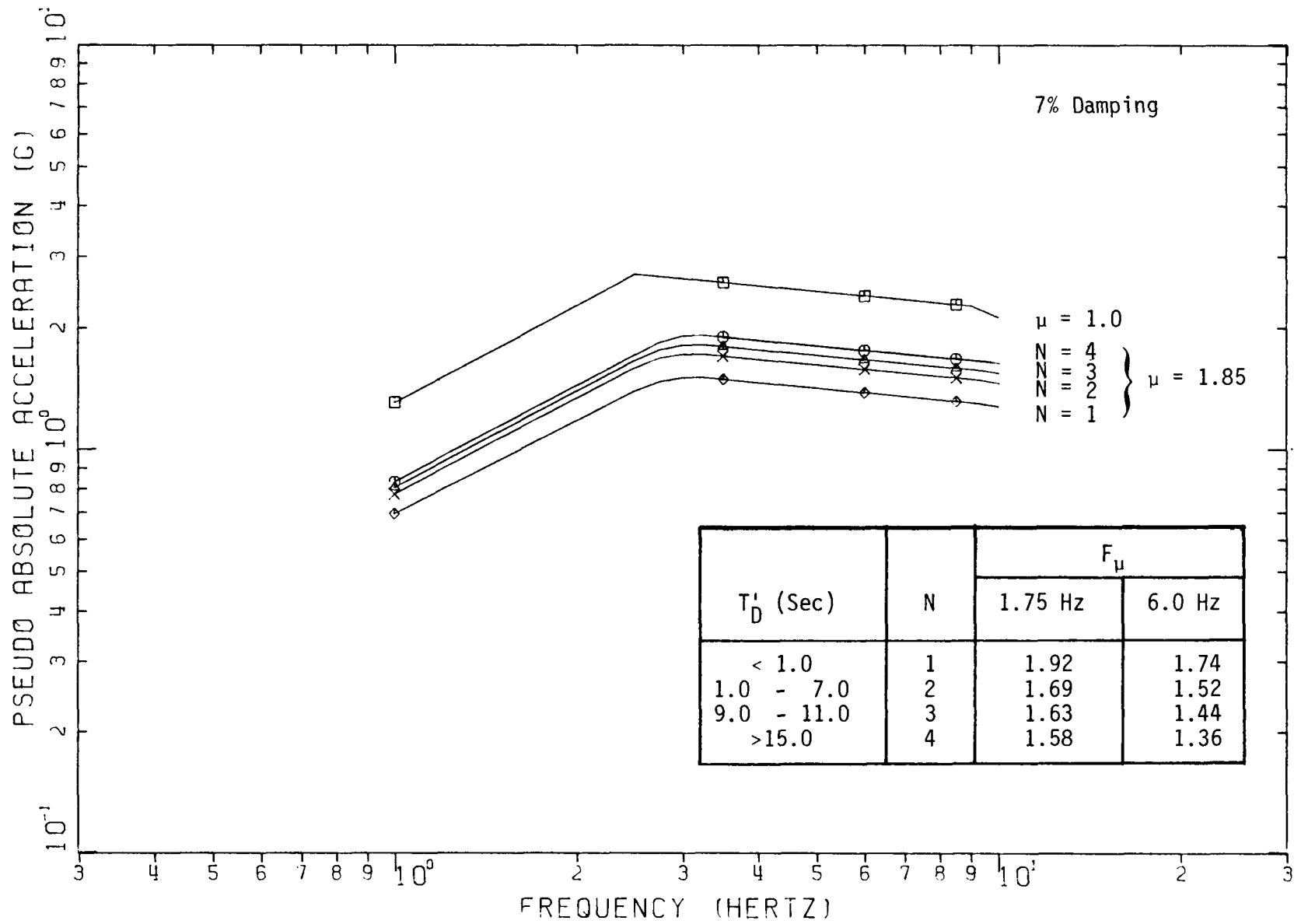
FIGURE 5-1.   INELASTIC REG. GUIDE 1.60 RESPONSE SPECTRA - LOW DUCTILITY

7% Damping

$\mu = 1.0$

N = 3 & 4
N = 2   } $\mu = 4.27$

N = 1

T_D' (Sec)	N	F_μ	
		1.75 Hz	6.0 Hz
< 1.0	1	3.60	2.68
1.0 - 7.0	2	2.91	1.93
9.0 - 11.0	3	2.75	1.81
>15.0	4	2.75	1.81

PSEUDO ABSOLUTE ACCELERATION (G)

FREQUENCY (HERTZ)
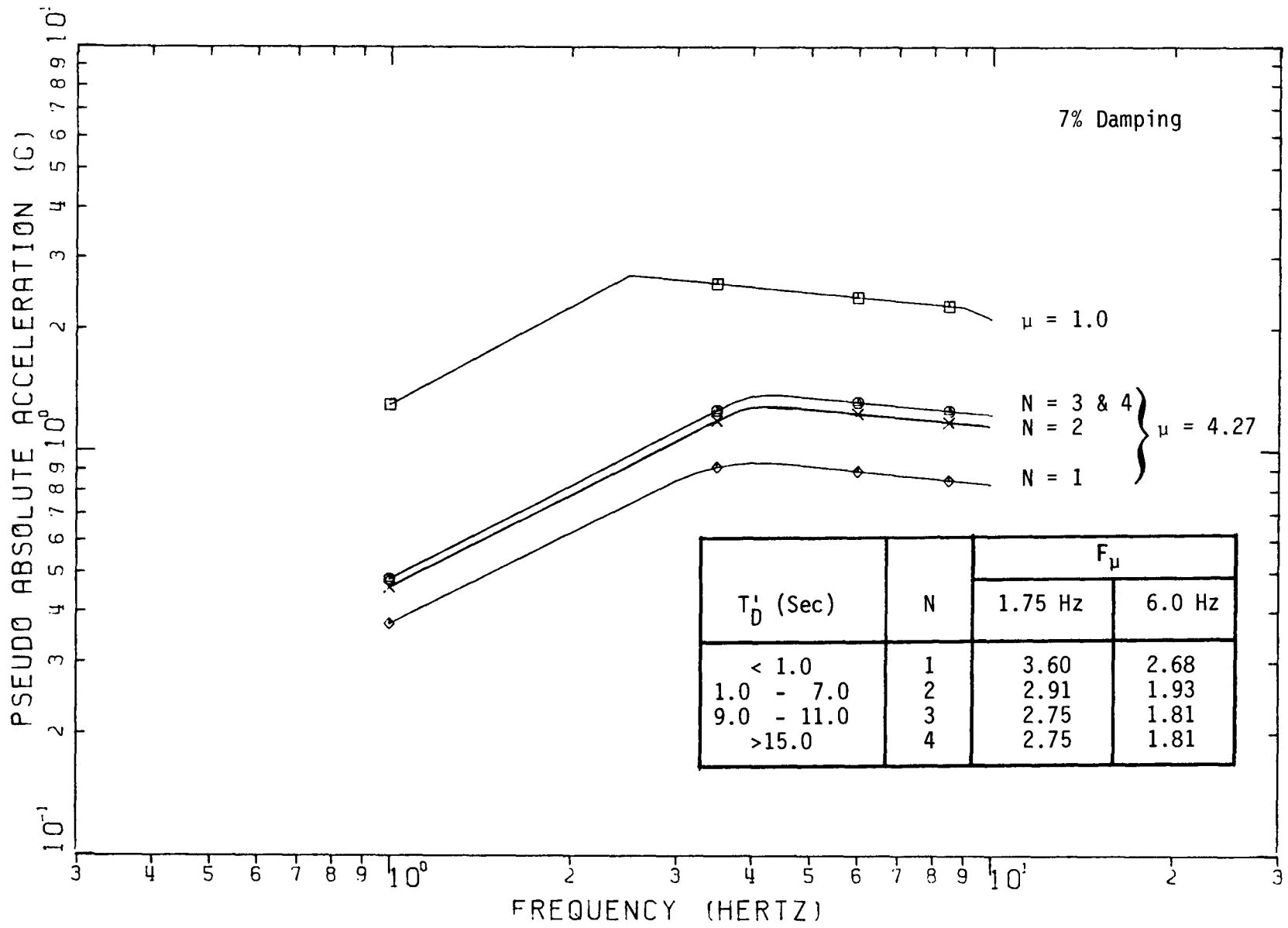
FIGURE 5-2.   INELASTIC REG. GUIDE 1.60 RESPONSE SPECTRA - HIGH DUCTILITY

FIGURE 5-3.   COMPARISON OF OLYMPIA SPECTRA WITH REG. GUIDE 1.60 SPECTRA
ANCHORED TO "EFFECTIVE" DESIGN ACCELERATION, $A_{D\mu}$
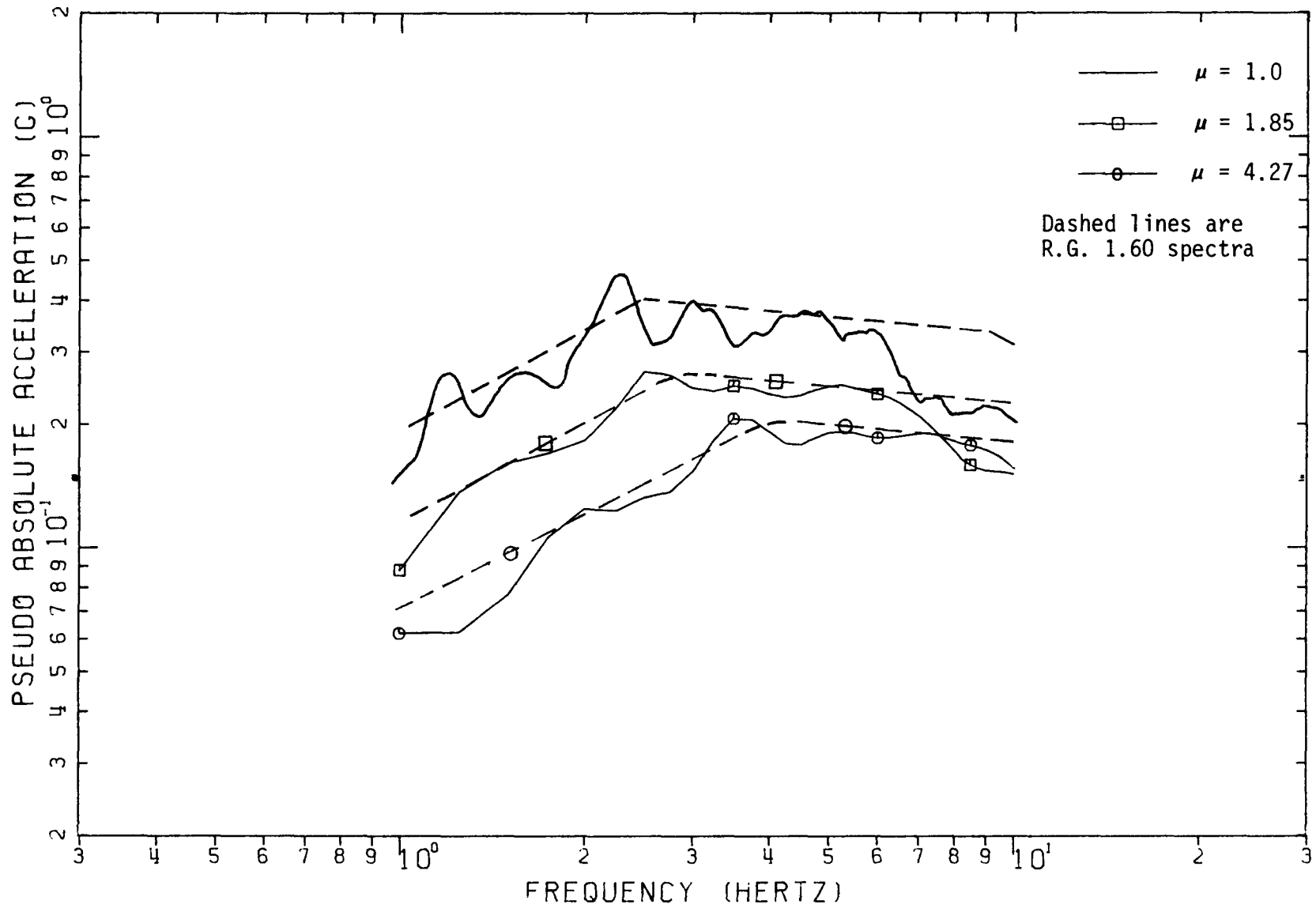
FIGURE 5-4.   COMPARISON OF TAFT SPECTRA WITH REG. GUIDE 1.60 SPECTRA
ANCHORED TO "EFFECTIVE" DESIGN ACCELERATION, $A_{D\mu}$
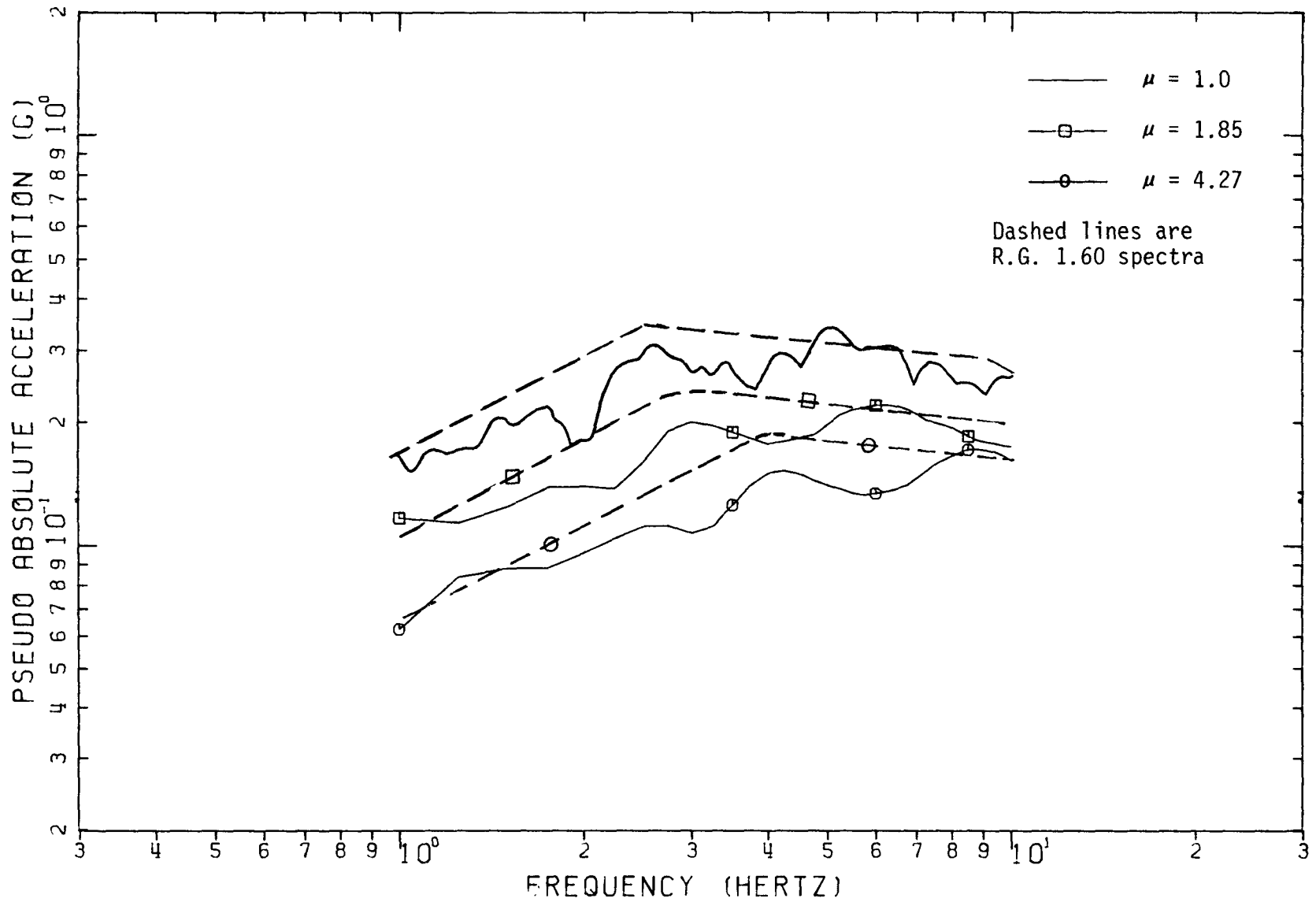
FIGURE 5-5. COMPARISON OF EL CENTRO #12 SPECTRA WITH REG. GUIDE 1.60 SPECTRA ANCHORED TO "EFFECTIVE" DESIGN ACCELERATION, $A_{D\mu}$
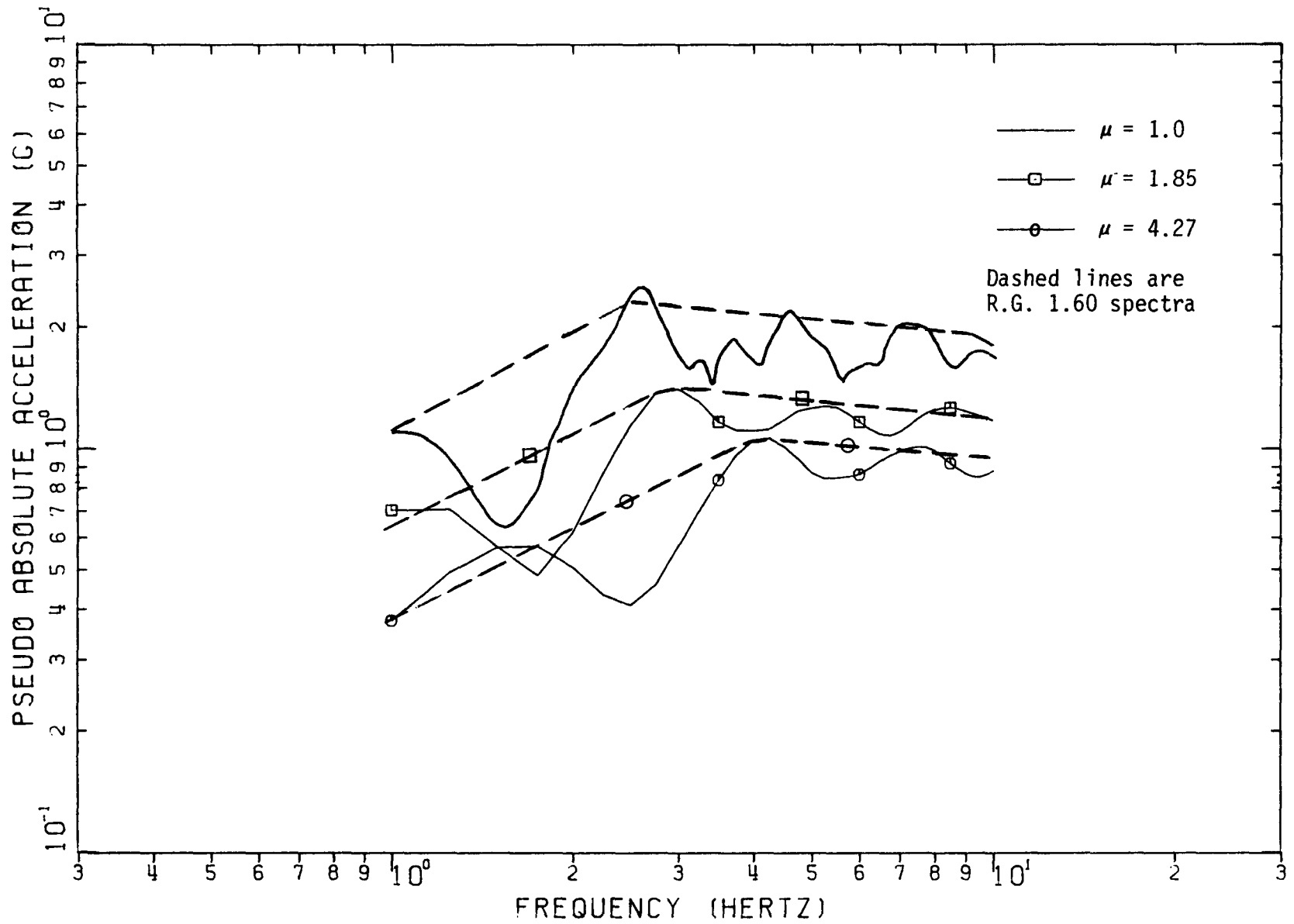
FIGURE 5-6.   COMPARISON OF PACOIMA DAM SPECTRA WITH REG. GUIDE 1.60 SPECTRA
ANCHORED TO "EFFECTIVE" DESIGN ACCELERATION, $A_{D\mu}$
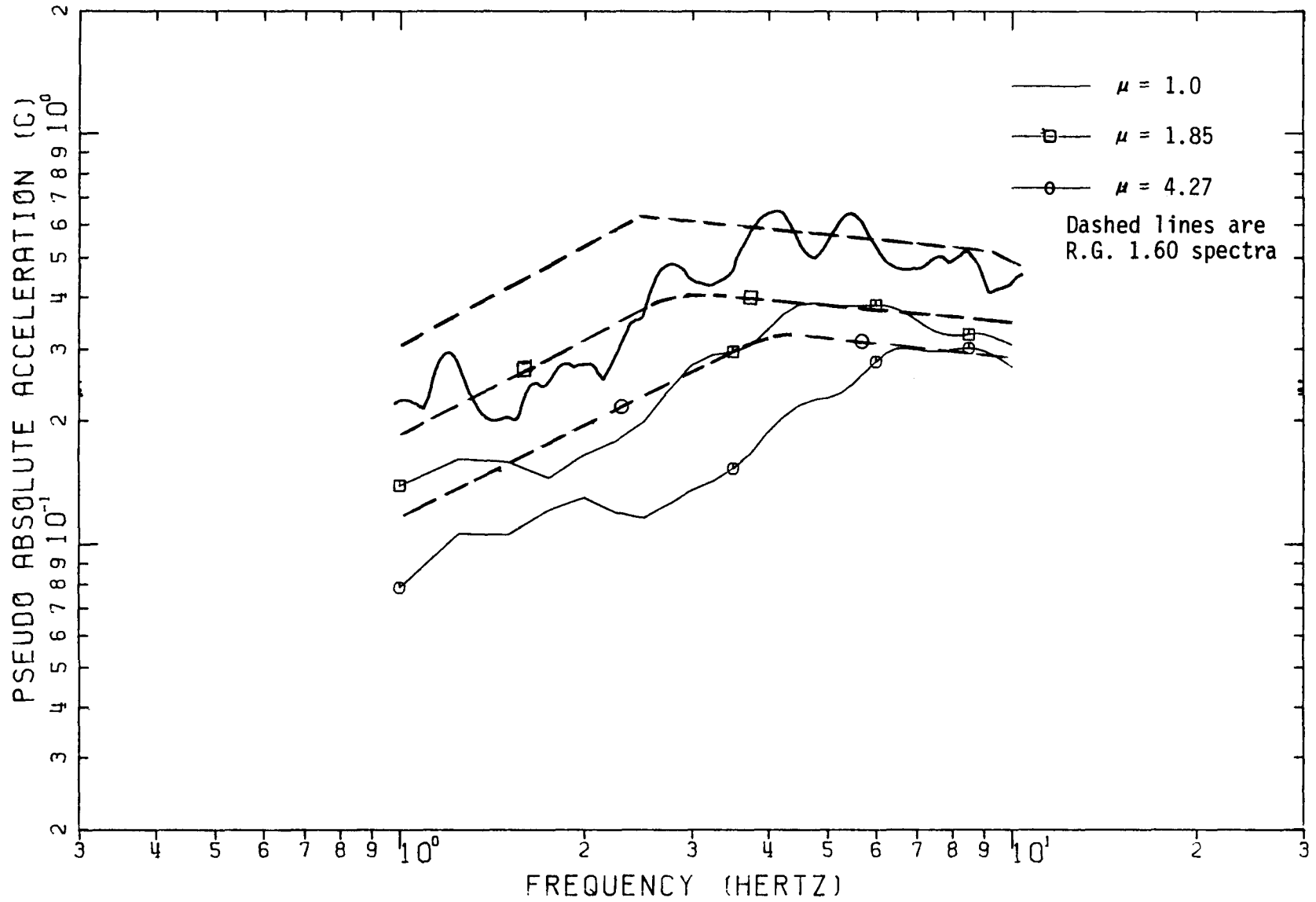
FIGURE 5-7. COMPARISON OF HOLLYWOOD STORAGE SPECTRA WITH REG. GUIDE 1.60
SPECTRA ANCHORED TO "EFFECTIVE" DESIGN ACCELERATION, $A_{D\mu}$
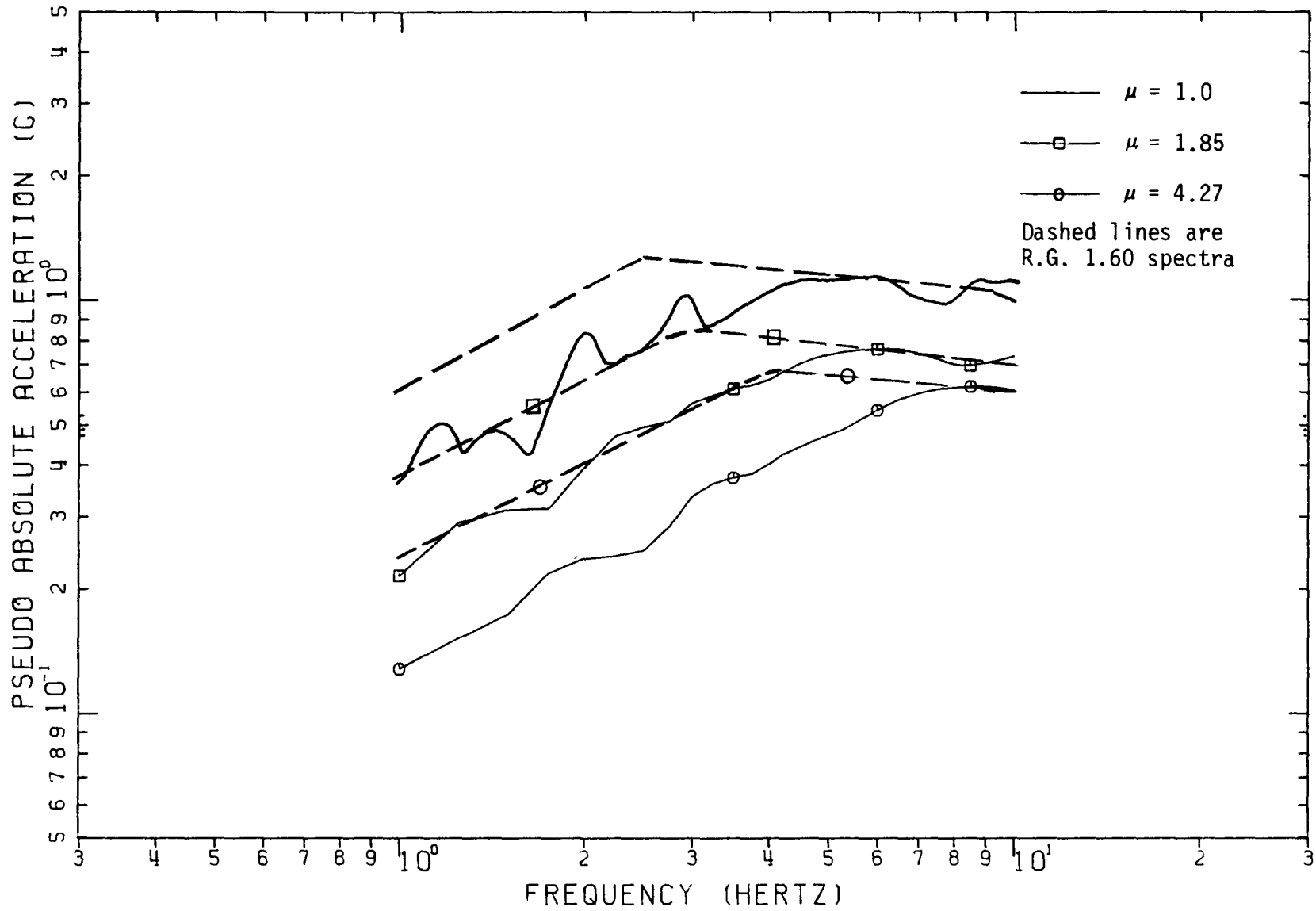
FIGURE 5-8. COMPARISON OF EL CENTRO #5 SPECTRA WITH REG. GUIDE 1.60 SPECTRA ANCHORED TO "EFFECTIVE" DESIGN ACCELERATION, $A_{D\mu}$
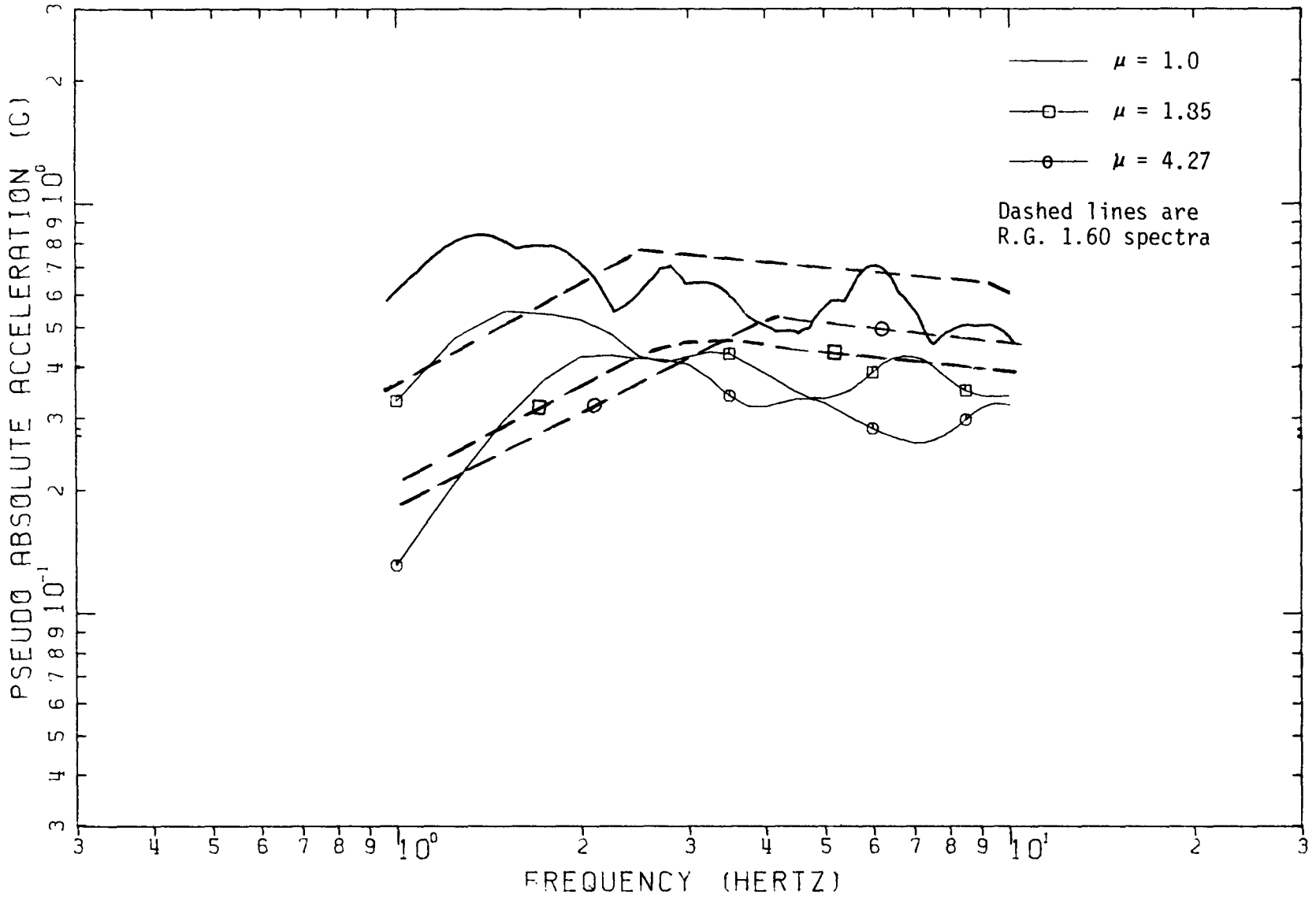
FIGURE 5-9.   COMPARISON OF GOLETA SPECTRA WITH REG. GUIDE 1.60 SPECTRA
ANCHORED TO "EFFECTIVE" DESIGN ACCELERATION, $A_{D\mu}$
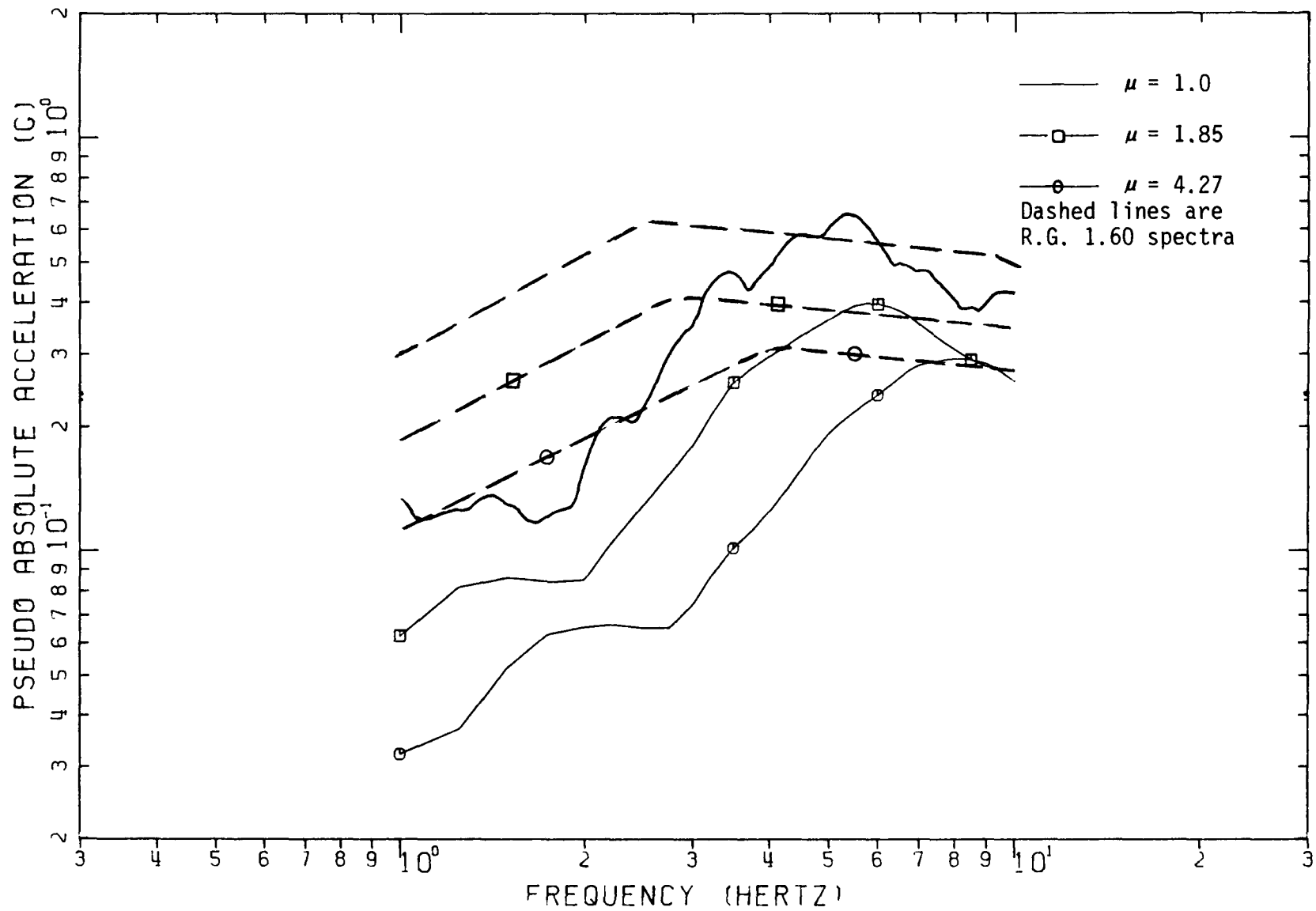
FIGURE 5-10.   COMPARISON OF COYOTE LAKE, GILROY SPECTRA WITH REG. GUIDE 1.60
SPECTRA ANCHORED TO "EFFECTIVE" DESIGN ACCELERATION, $A_{D\mu}$
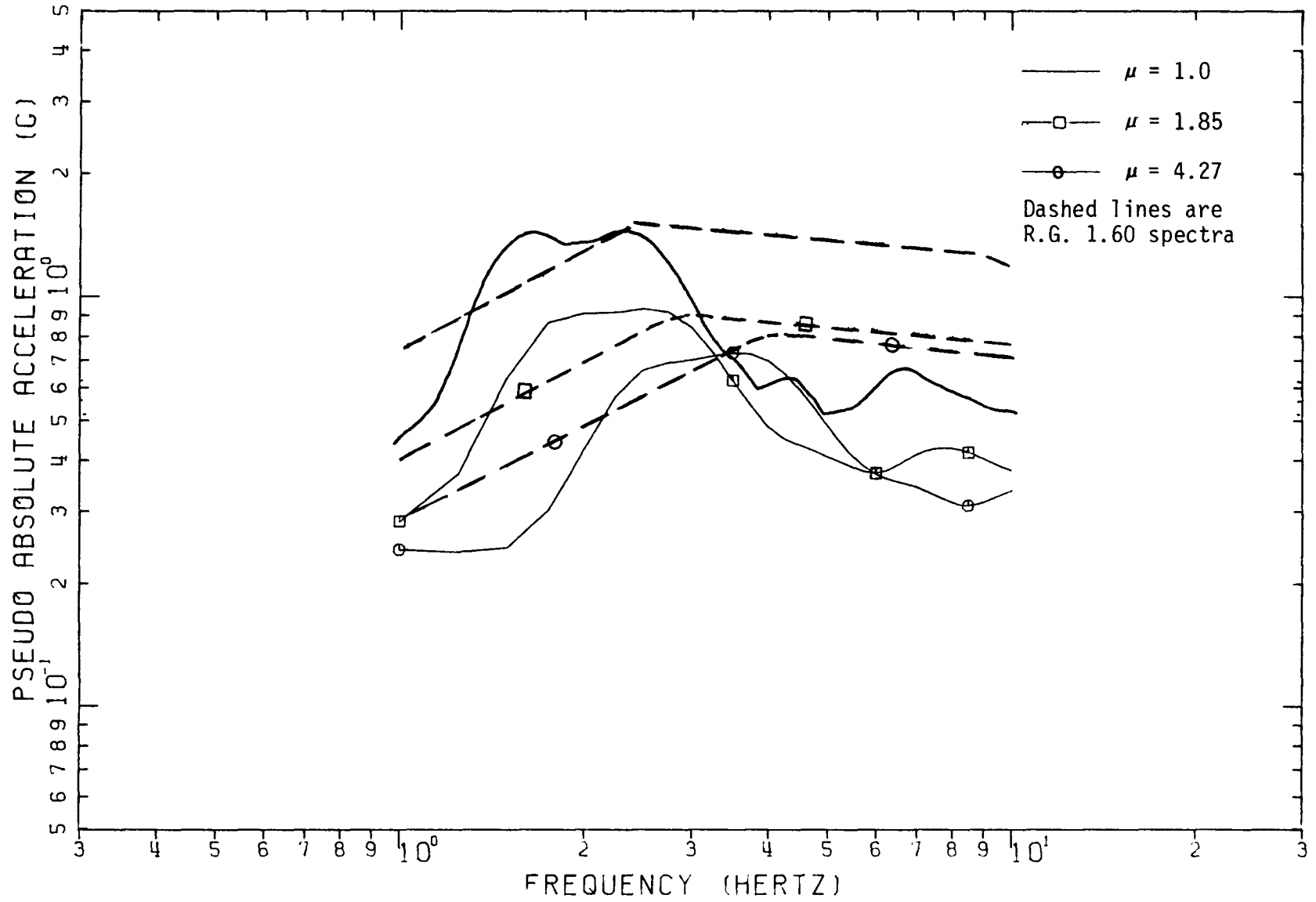
FIGURE 5-11. COMPARISON OF PARKFIELD, CHOLAME SPECTRA WITH REG. GUIDE 1.60
SPECTRA ANCHORED TO "EFFECTIVE" DESIGN ACCELERATION, $A_{D\mu}$
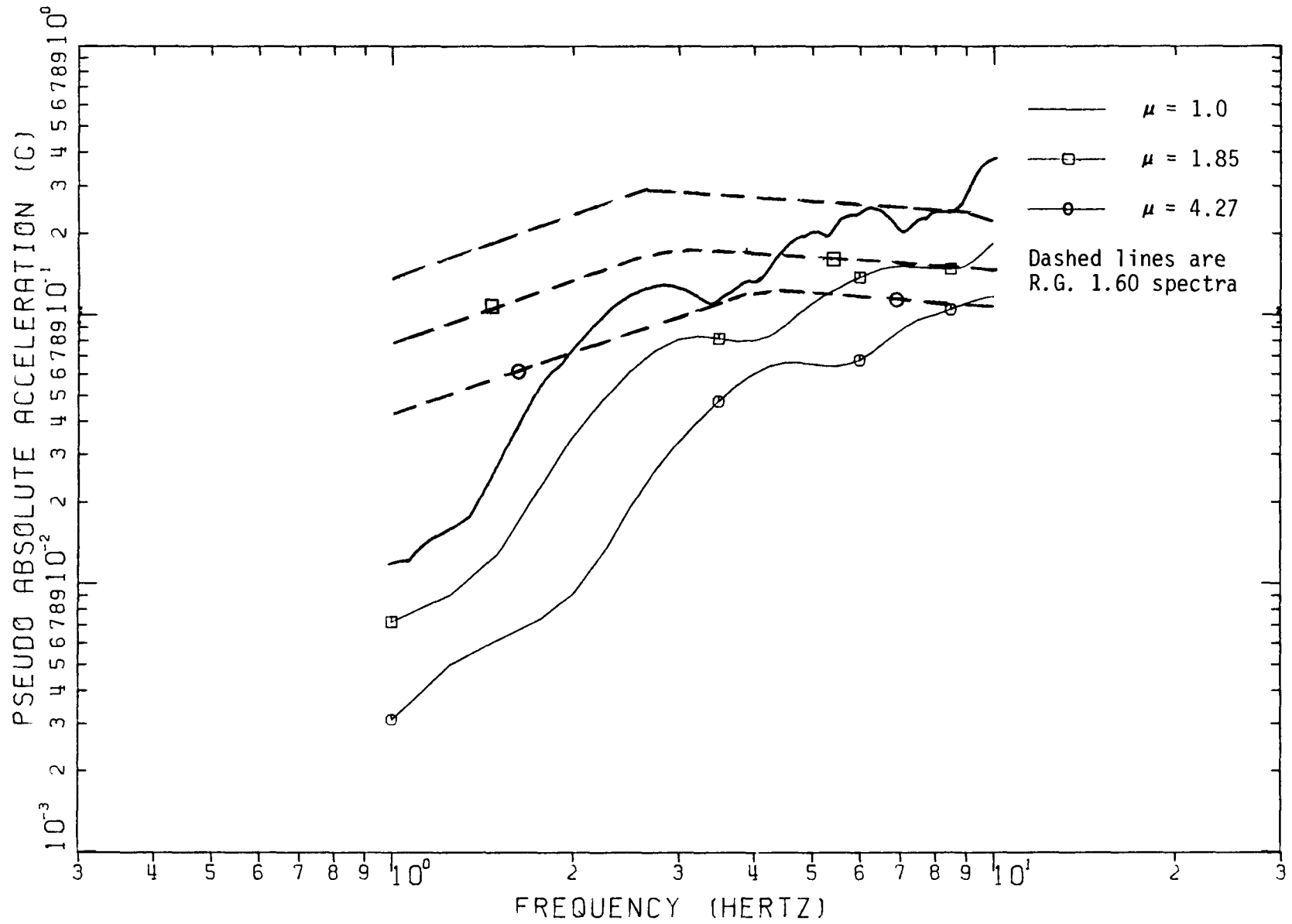
FIGURE 5-12.   COMPARISON OF GAVILAN COLLEGE SPECTRA WITH REG. GUIDE 1.60 SPECTRA
ANCHORED TO "EFFECTIVE" DESIGN ACCELERATION, $A_{D\mu}$
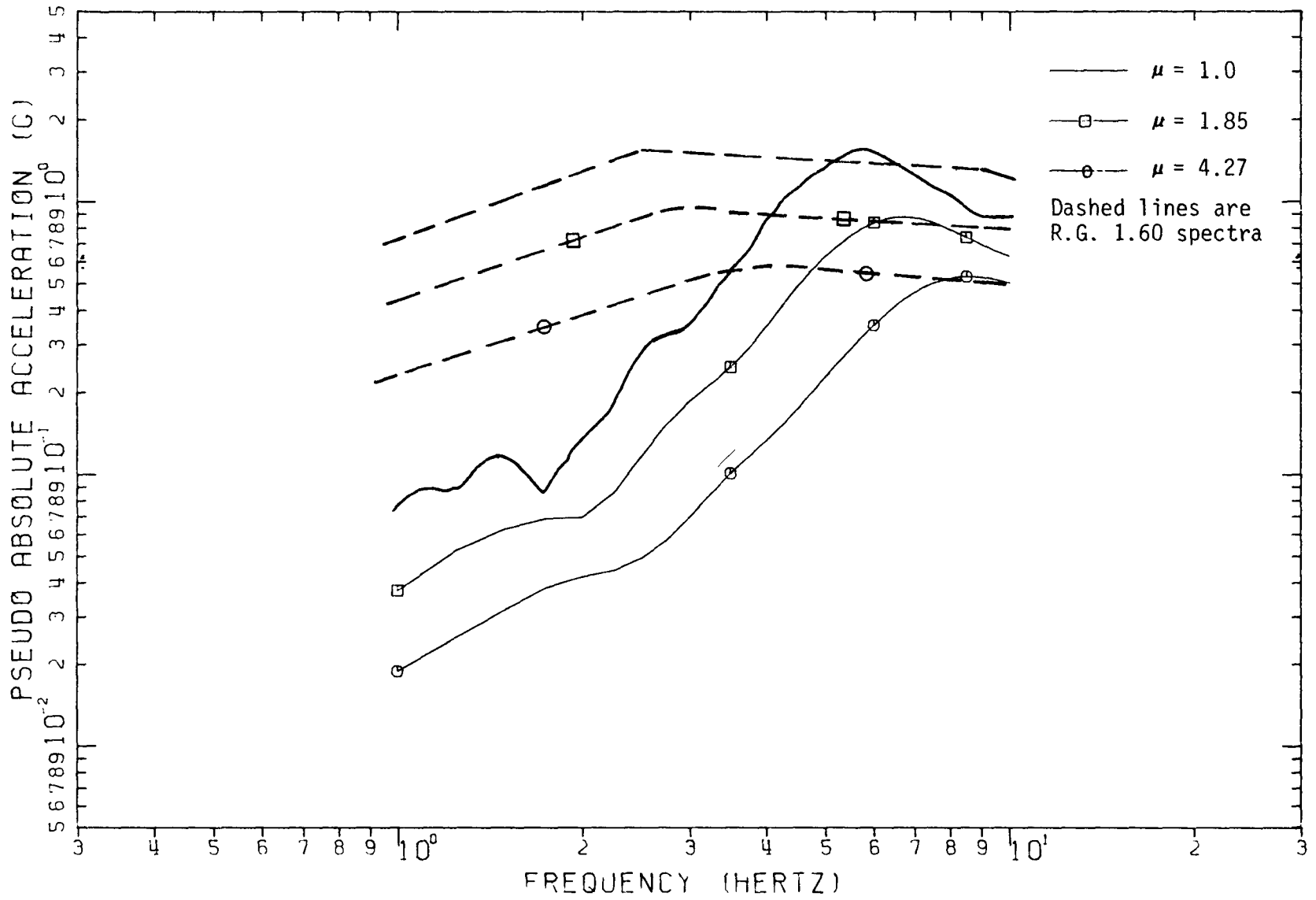
FIGURE 5-13.   COMPARISON OF MELENDY RANCH SPECTRA WITH REG. GUIDE 1.60
SPECTRA ANCHORED TO "EFFECTIVE" DESIGN ACCELERATION, $A_{D\mu}$

6. MEASURE OF RELATIVE STRENGTH OF GROUND MOTION RECORDS

6.1 APPROACH

One method to define the relative strength of a ground motion record is in terms of the resulting maximum structural response. Within this study, the maximum structural response is defined in terms of ductility levels reached. The study has considered shear wall resistance function structures with elastic behavior ($\mu = 1.0$), nearly elastic behavior ($\mu = 1.85$), and a conservative lower bound on the onset of significant structural strength degradation ($\mu = 4.27$). The relative strength of a ground motion record can then be defined by the inelastic spectral acceleration, $S_{a\mu(f,\beta)}$, corresponding to an appropriate ductility level, μ, for a structure with an elastic frequency, f, and elastic damping, β.

Figures 6-1a through 6-1d present the relative strengths of each of the 12 records studied as defined by $S_{a\mu(f,\beta)}$ for ductilities of 1.0, 1.85, and 4.27 for 7% damping and elastic frequencies of 8.54, 5.34, 3.20, and 2.14 Hz, respectively. These frequencies are considered representative of the frequency range from 1.8 to 10 Hz which is typical for stiff, nuclear power plant structures.
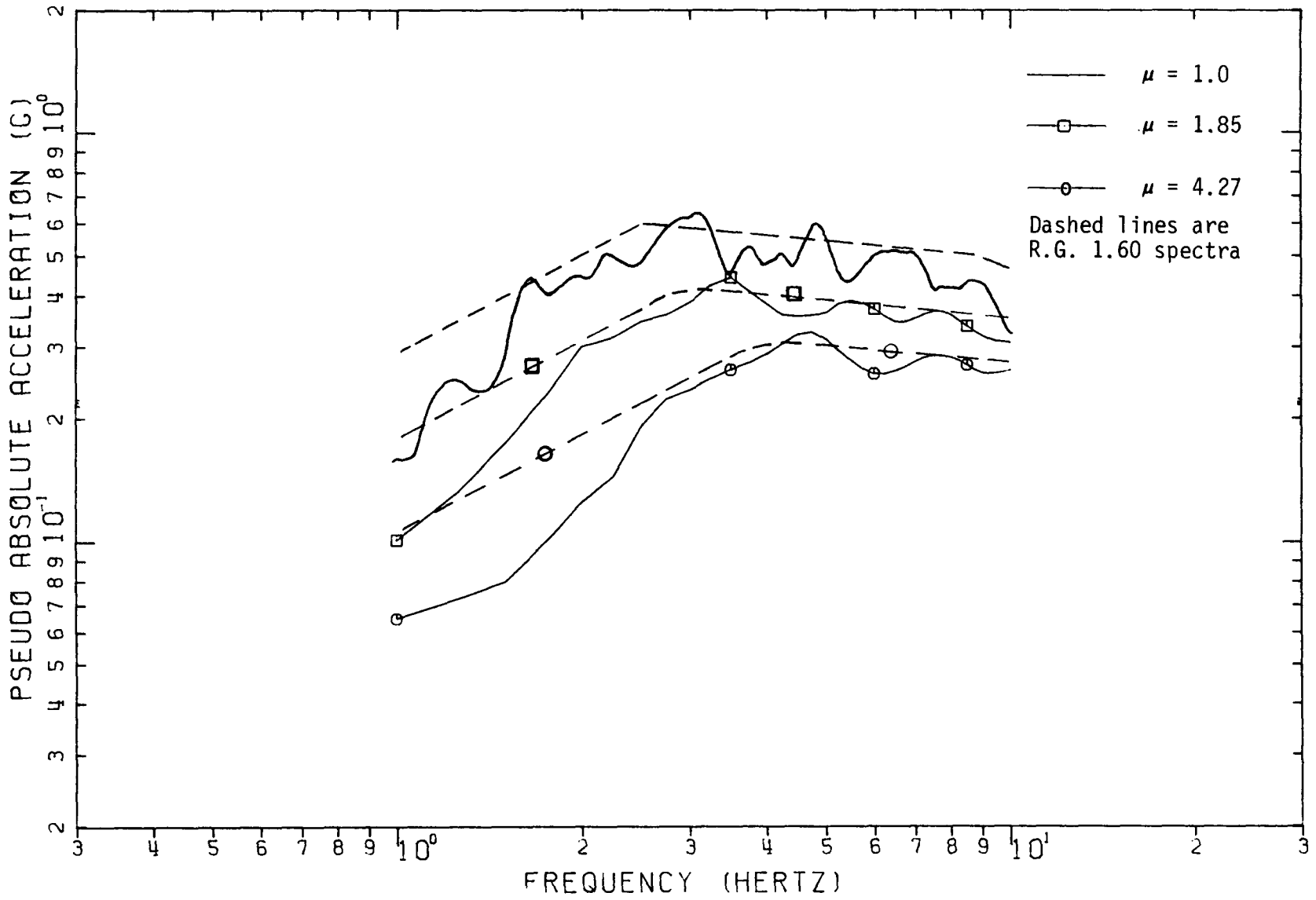
Several ground motion relative strength zones are defined on Figures 6-1a through 6-1d. These zones are defined in terms of the zero period ground acceleration (ZPA) for which a plant must be designed to remain elastic using the R.G. 1.60 spectrum in order to prevent the ductility level from exceeding 4.27 (conservative lower bound for onset of significant strength degradation) when subjected to the actual record. For $\mu = 4.27$ these zones are defined by:

Zone	Required Elastic Design ZPA Range (g)
Very Severe	> 0.3
Severe	0.2 - 0.3
Moderate	0.1 - 0.2
Low	< 0.1

In other words, if the plant must be designed to remain elastic for a R.G. 1.60 spectrum anchored at a ZPA greater than 0.3g in order to prevent the ductility from exceeding 4.27 for the actual record, this record is considered to be very severe. Similarly, if the elastic design ZPA must be between 0.2 and 0.3g to prevent the ductility from exceeding 4.27 for the actual record, the record is considered to be severe. For $\mu = 1.0$ and $\mu = 1.85$ these zones are defined in terms of a multiple of the spectral acceleration at $\mu = 4.27$. The following multiples are used:

$$Sa_{1.0} = 1.9 \, Sa_{4.27} \qquad f > 4 \text{ Hz}$$

$$Sa_{1.0} = 2.7 \, Sa_{4.27} \qquad f < 4 \text{ Hz}$$

$$Sa_{1.85} = 1.4 \, Sa_{4.27} \qquad f > 4 \text{ Hz}$$

$$Sa_{1.85} = 1.7 \, Sa_{4.27} \qquad f < 4 \text{ Hz}$$

These intercepts were selected so as to enable these lesser ductility spectral accelerations to be a reasonable prediction of the severity of the ground motion at $\mu = 4.27$.

As an example, at a frequency of 8.54 Hz, the Reg. Guide 1.60 spectral amplification factor is 2.29. Therefore, the intercept between the very severe and the severe zones for $\mu = 4.27$ at f = 8.54 Hz is 2.29 times 0.30g = 0.69g. The other intercepts for $\mu = 4.27$ and f = 8.54 Hz are at 0.46g and 0.23g. These zone intercepts for $\mu = 4.27$ are drawn on

Figure 6-1a (f = 8.54 Hz). The intercepts for μ = 1.0 and μ = 1.85 are then at 1.9 and 1.4 times, respectively, the corresponding intercept at μ = 4.27. Thus, the intercept between the very severe and severe zones is at 1.31g and 0.97g for μ = 1.0 and 1.85, respectively, on Figure 6-1a. A similar approach was used to define these intercepts on the figures for other frequencies.

6.2   RELATIVE STRENGTHS OF GROUND MOTION RECORDS STUDIED

The Pacoima Dam record represents a very severe ground motion by this definition for structures with elastic frequencies greater than about 4 Hz. This record represents severe ground motion for structures with natural frequencies of about 2.5 to 4 Hz and only moderate ground motion for structures with natural frequencies less than about 2.5 Hz. The elastic spectral acceleration (μ = 1.0) properly describes the relative severity of this record for structures with natural frequencies greater than about 2.5 Hz but overstates the relative severity of the record for structures with natural frequencies less than 2.5 Hz.

The elastic spectral accelerations (μ = 1.0) would lead one to believe that the Melendy Ranch and El Centro #5 records would be severe to very severe records for structures with natural frequencies from about 4 to 10 Hz. However, the severity of these records based upon the onset of significant strength degradation is seriously overstated by the elastic spectral acceleration. Based upon significant strength degradation, both records are barely severe records for structures with elastic frequencies of about 8.5 Hz. El Centro #5 is only a moderate record for structures with natural frequencies from about 2.2 to 8.0 Hz and is a low severity record for structures with frequencies below 2.2 Hz despite its high elastic spectral acceleration. The severity of Melendy Ranch drops off even more rapidly as the structure frequencies are reduced. Melendy Ranch is a moderately severe record for structures with natural frequencies of 5 to 8 Hz and has low severity for structures with natural frequencies less than 5 Hz despite its very high elastic spectral acceleration at frequencies above 4 Hz.

The Parkfield record shows elastic spectral accelerations
(μ = 1.0) of 0.5 to 0.6g for frequencies above about 5 Hz. These
elastic spectral accelerations increase to about 0.8g at a frequency of
3.2 Hz and increase to 1.4g at 2.1 Hz. Thus, based upon the elastic
spectral acceleration, one would judge the Parkfield record to be of
moderate severity for structures with natural frequencies above about 2.5
Hz increasing to a severe record for structures with natural frequencies
less than about 2.5 Hz. The elastic spectral accelerations appear to
underestimate the relative severity of the Parkfield record for structures
in the 2.5 to 3.5 Hz range. Based upon the onset of significant strength
degradation, the Parkfield record represents a severe ground motion for
structures with natural frequencies of 1.8 to 3.5 Hz.

El Centro No. 12, Taft, and Gavilan College represent low
severity ground motions throughout the frequency range from 1.8 to 10 Hz
whether defined by the elastic spectral acceleration or by the onset of
significant strength degradation. However, Gavilan College is of partic-
ularly low severity for ductilities associated with the onset of signifi-
cant strength degradation (μ = 4.27) and this particularly low severity
is not fully indicated by the elastic (μ = 1.0) spectral accelerations.

Because of its high frequency content, Coyote Lake is of moderate
severity for frequencies above about 7.5 Hz. For frequencies between 4.5
and 7.5 Hz, the elastic (μ = 1.0) spectral accelerations would indicate
moderate severity for Coyote Lake. However, because of its short
duration, this record has a narrow frequency content and is missing the
lower frequency content. Thus, based on the onset of significant strength
degradation, this record has low severity for structures with elastic
frequencies less than 7.5 Hz despite the high elastic spectral accelera-
tions down to 4.5 Hz.

Based on the onset of significant strength degradation, Goleta
represents a moderate severity ground motion for structures throughout
the frequency range from 1.8 to 10 Hz because of its low frequency content
(similar to Parkfield in this regard) and moderately high ground accelera-
tion.

For structures with elastic frequencies between about 1.8 and 3.5 Hz, only Pacoima Dam, Parkfield, El Centro #5, and Goleta represent moderate or severe ground motions based upon the onset of significant strength degradation. Pacoima Dam and El Centro #5 are in this category because of their broad frequency content (at least 0.8 to 6.7 Hz), longer, strong durations (greater than 3.0 seconds), and high ground accelerations (greater than 0.5g). Goleta and Parkfield are in this category despite their shorter durations (3.0 seconds or less) because of their predominately low frequency content (essentially no frequencies above 3.0 Hz) and yet moderately high ground acceleration (at least 0.35g). To obtain this high a ground acceleration without frequency content above 3.0 Hz requires substantial velocity content in the 1.8 to 3.5 Hz range.

In summary, from this study only Pacoima Dam is clearly capable of causing very severe structural damage (possibly collapse) for structures with natural frequences greater than 4 Hz that have been designed to remain elastic for the R.G. 1.60 spectrum anchored to 0.2g. This damage capability is due to the high acceleration (1.17g), longer strong duration (6.1 seconds), and broad frequency content (0.75 to 6.7 Hz) associated with this record. Even so, this record would be expected to result in only severe damage (ductilities slightly greater than 4.3 and some significant strength degradation) for structures with frequencies between 1.8 and 2.5 Hz when these structures are designed to remain elastic for a 0.2g R.G. 1.60 spectrum.

In addition, Parkfield might result in severe damage (ductilities slightly greater than 4.3 but no collapse) for such structures with elastic frequencies from 2.0 to 4.0 Hz because of its low frequency content (approximately 1.0 to 3.0 Hz) and high acceleration (0.5g). Similarly, El Centro #5 and Melendy Ranch might result in severe damage to similarly designed structures with frequency content above 7.5 Hz because of their high ground acceleration (0.5g) and higher frequency content (up to at least 7 Hz). None of the other records are capable of resulting in more than moderate damage (ductilities less than 4.3) for a 0.2g R.G. 1.60 designed structure.

Basically, this study indicates that 0.5g short duration records such as Parkfield and Melendy Ranch are capable of causing severe damage (short of collapse) to 0.2g designed structures within a narrow frequency range from about 1.8 f_a to 1.3 f_v where f_a is the frequency at which the spectral acceleration peaks and f_v is the frequency at which the spectral velocity peaks (see Table 2-5 for these frequencies). Outside this narrow frequency range which lies on the stiff side of the peak elastic spectral responses, these short duration records should not result in severe damage despite their ground accelerations being 2.5 times the elastic design acceleration.

Even the above may overestimate the damage capability of these high acceleration ground motions. This phase of this study has not considered the reduced structural responses which might result from soil-structure interaction, wave passage effects and wave scattering effects. Secondly, in this study, damage is defined in terms of the maximum ductility factor rather than total hysteretic energy absorption. The ductility descriptor of damage results in less benefit of short duration than would a hysteretic energy descriptor of damage. Thirdly, only single-degree-of-freedom structural response is considered in the measures of relative strength presented herein which tends to overestimate the damage capability of narrow frequency content records as compared to broad frequency content records capable of exciting multiple frequencies simultaneously in multi-degree-of-freedom structures. Lastly, potential overcapacity of the structure has been ignored. Generally, a structure has greater capacity than indicated by the minimum design requirements.

6.3 RELATIVE STRENGTH SUMMARY

If a structure of elastic frequency, f, and elastic damping, β, is designed to be at the onset of yielding for spectral acceleration $S_{a\mu}$ (f,β) which is the inelastic spectral acceleration for any ground motion considered, then the structure will respond to ductility level, μ, when subjected to that ground motion record. Thus, comparing $S_{a\mu}$ (f,β) for the various ground motion records considered in this study provides a

measure of the relative strength of the records. A ground motion record with a large $S_{a\mu}$ (f,β) requires the structure to be designed at a large yield level to limit response to a given ductility and is more severe than a record with a small $S_{a\mu}$ (f,β) which requires the structure to be designed at a small yield level to limit response to the same ductility level. In this chapter, the inelastic spectral acceleration values are compared for the 12 ground motion records considered in this study at 3 ductility levels (μ = 1.0, 1.85 and 4.27) at 4 frequencies (f = 8.54, 5.34, 3.20 and 2.14 Hz and one damping value (β = 7 percent)).

Relative strength zones (i.e., very severe, severe, moderate and low strengths) are defined in terms of the acceleration level for which a structure must be designed to remain elastic using the Reg. Guide 1.60 spectrum in order to prevent seismic response exceeding ductility levels of 4.27 when subjected to the actual earthquake ground motion. Similar relative strength zones for μ = 1.85 and 1.0 are obtained by scaling the zone levels for μ = 4.27. The inelastic spectral accelerations and relative strength zones are presented in Figures 6-1a through 6-1d for the 4 frequencies considered.

Based upon the data presented in Figures 6-1a through 6-1d, it is concluded that only the Pacoima Dam record is a very severe ground motion in terms of potential damage for structures with frequencies greater than 4 Hz. At below 4 Hz, this record is a severe ground motion at about 3 Hz and a moderate ground motion at about 2 Hz. At 8.5 Hz, the Melendy Ranch and El Centro #5 records are in the severe category. At below 4 Hz, the Parkfield record is within the severe category. All other ground motion records fall in the low or moderate categories at all frequencies. Note that reasons are outlined in this chapter as to why the damage capability of high acceleration, short duration earthquakes such as Melendy Ranch and Parkfield may be overstated by the methods used to assess relative strengths of the ground motion.

6-8

PD ─┼─ 1.59*   PD ─┼─ 1.27*   PD ─┼─ 0.94*   ↑
                                                                Very Severe
EC5 ─┼─ 1.11
                                                                ↕
MR ─┼─ 0.95   EC5 ─┼─ 0.70   MR ─┼─ 0.50   Severe
                       MR ─┼─ 0.65   EC5 ─┼─ 0.47

                                             PA2 ─┼─ 0.37
PA2 ─┼─ 0.56   PA2 ─┼─ 0.47   G ─┼─ 0.32   Moderate
HS ─┼─ 0.51   O ─┼─ 0.28
G ─┼─ 0.49   G ─┼─ 0.36   HS ─┼─ 0.27
A ─┼─ 0.45   HS ─┼─ 0.35   CL ─┼─ 0.25
O ─┼─ 0.44   O ─┼─ 0.32   A ─┼─ 0.24
CL ─┼─ 0.39   A ─┼─ 0.30
                       CL ─┼─ 0.29
                                             T ─┼─ 0.17
EC12 ─┼─ 0.25   EC12 ─┼─ 0.16
GC ─┼─ 0.24   EC12 ─┼─ 0.19
T ─┼─ 0.21   T ─┼─ 0.18
                       GC ─┼─ 0.15   GC ─┼─ 0.09   Low

μ = 1.0   μ = 1.85   μ = 4.27

LEGEND

A: Artificial (0.2g)
CL: Coyote Lake
EC5: El Centro #5
EC12: El Centro #12
G: Goleta
GC: Gavilan College
HS: Hollywood Storage
MR: Melendy Ranch
O: Olympia
PA2: Parkfield
PD: Pacoima Dam
T: Taft

*Values shown are inelastic spectral acceleration $S_{a\mu}$ for μ = 1.0, 1.85, and 4.27

f = 8.54 Hz
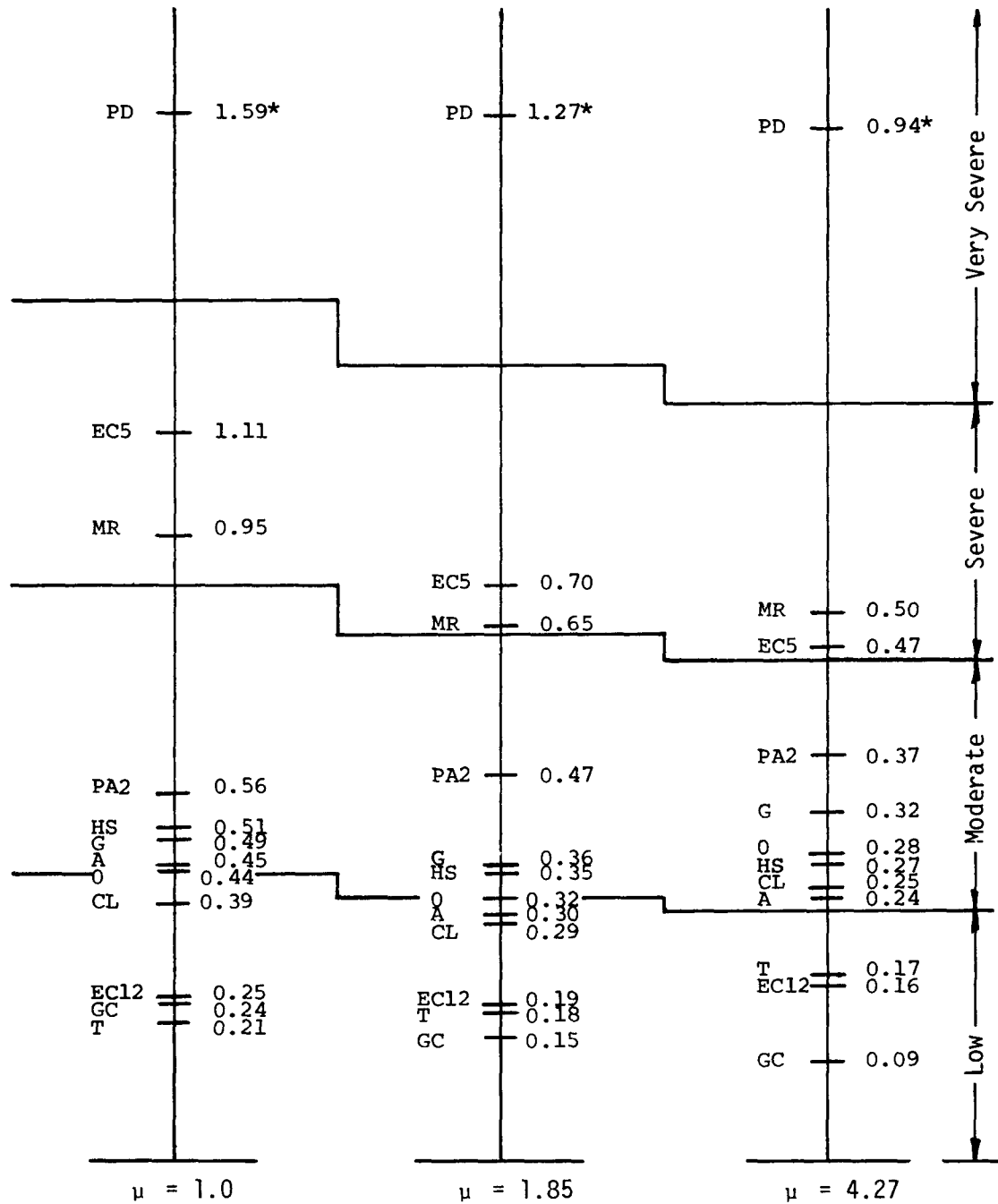
FIGURE 6-1a.   MEASURE OF RELATIVE STRENGTH OF GROUND MOTION RECORDS AS DEFINED BY $S_{a\mu}(f,7\%)$
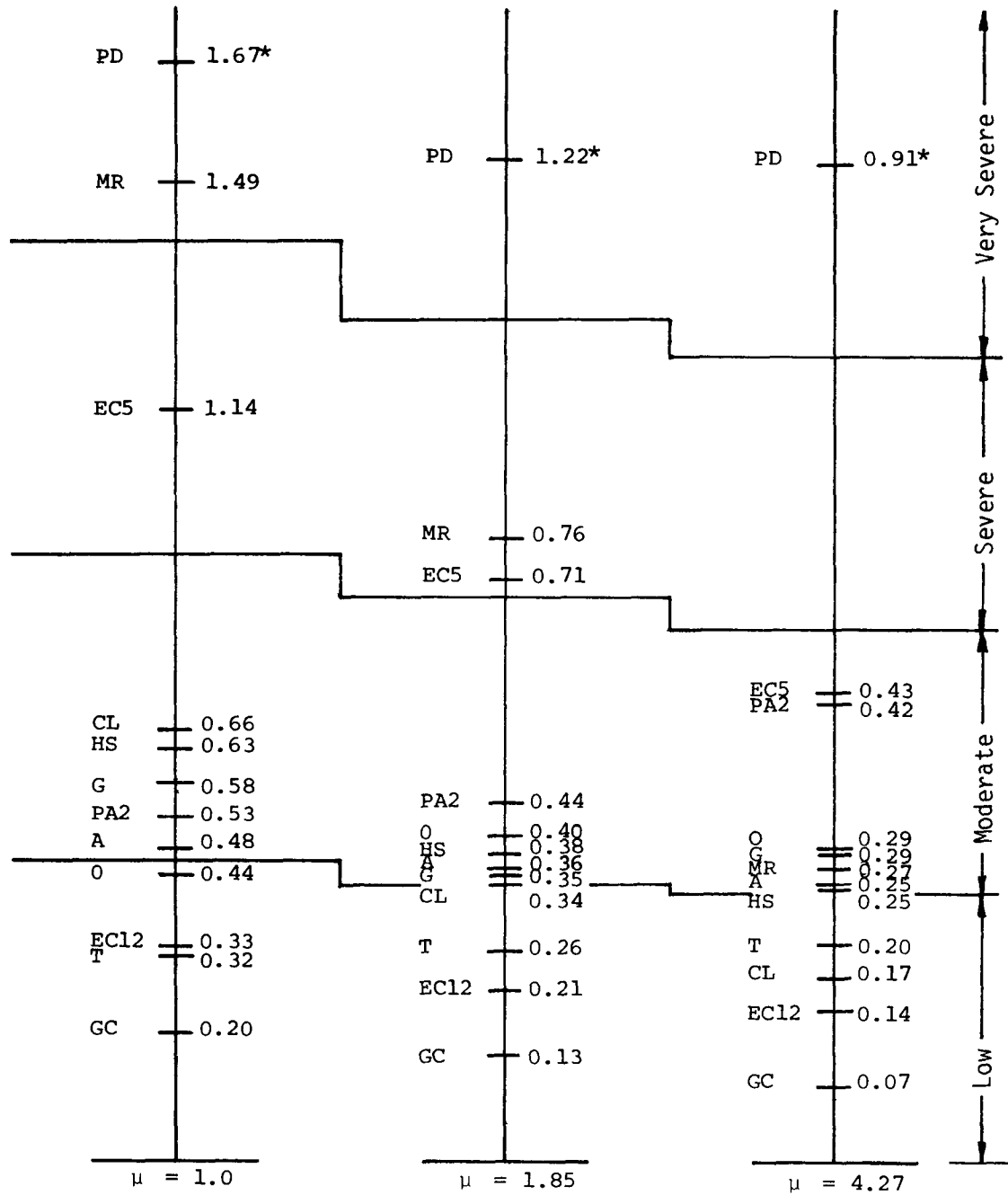
Column μ = 1.0:

PD — 1.67*

MR — 1.49

EC5 — 1.14

CL — 0.66
HS — 0.63

G — 0.58
PA2 — 0.53
A — 0.48

O — 0.44

EC12 — 0.33
T — 0.32

GC — 0.20

μ = 1.0

Column μ = 1.85:

PD — 1.22*

MR — 0.76
EC5 — 0.71

PA2 — 0.44
O — 0.40
HS — 0.38
A — 0.36
G — 0.35
CL — 0.34

T — 0.26

EC12 — 0.21

GC — 0.13

μ = 1.85

Column μ = 4.27:

PD — 0.91*

EC5 — 0.43
PA2 — 0.42

O — 0.29
G — 0.29
MR — 0.27
A — 0.25
HS — 0.25

T — 0.20
CL — 0.17

EC12 — 0.14

GC — 0.07

μ = 4.27

Very Severe

Severe

Moderate

Low

LEGEND

A: Artificial (0.2g)
CL: Coyote Lake
EC5: El Centro #5
EC12: El Centro #12
G: Goleta
GC: Gavilan College
HS: Hollywood Storage
MR: Melendy Ranch
O: Olympia
PA2: Parkfield
PD: Pacoima Dam
T: Taft

*Values shown are inelastic spectral accelerations $S_{a\mu}$ for μ = 1.0, 1.85 and 4.27

f = 5.34 Hz

FIGURE 6-1b.   MEASURE OF RELATIVE STRENGTH OF GROUND MOTION RECORDS AS DEFINED BY $S_{a\mu}(f,7\%)$
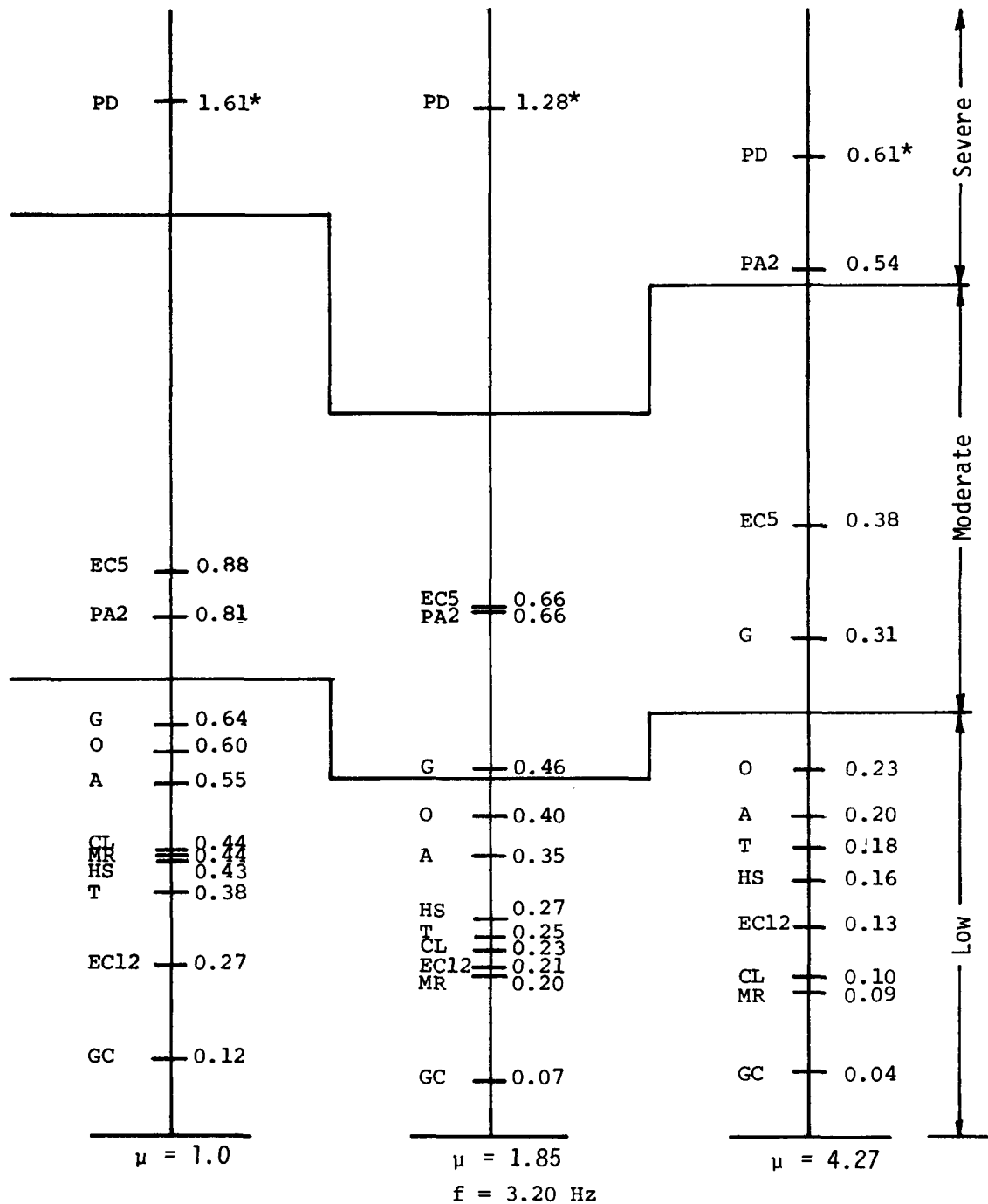
FIGURE 6-1c.   MEASURE OF RELATIVE STRENGTH OF GROUND MOTION RECORDS AS DEFINED BY $S_{a\mu}(f, 7\%)$

7. CONCLUSIONS

Many conclusions are reached in the individual sections as data are presented. Only the more significant conclusions will be summarized here.

7.1 ENGINEERING CHARACTERIZATION OF GROUND MOTION

The 11 real earthquake ground motion time histories studied (listed in Table 2-1) can be divided into two groups. Group 1 consists of the 6 longer duration records (Taft, Olympia, El Centro #12, El Centro #5, Pacoima Dam, and Hollywood Storage) while Group 2 consists of the 5 shorter duration records (Coyote Lake, Parkfield Cholame #2, Gavilan College, Goleta, and Melendy Ranch). Both elastic and inelastic structural response of stiff structures (1.8 to 10 Hz) subjected to the Group 1 records can be adequately approximated by the use of the Reg. Guide 1.60 spectrum anchored to an "effective" peak acceleration. In fact, it is shown in Section 2.3 that for elastic response between 1.8 and 10 Hz, the maximum ratio of actual spectral acceleration to Reg. Guide 1.60 spectral acceleration $(SA_a/SA_{1.60})$ ranges from 1.29 to 1.05 with a median maximum ratio of 1.20 for the six records studied. In other words, the Reg. Guide 1.60 spectrum anchored to an "effective" peak acceleration never introduces more than a factor of 1.29 unconservatism. The median ratio ranges from 1.05 to 0.83 with a median median of 0.88, or a factor of $(1/0.88) = 1.14$ conservatism. The minimum ratio ranges from 0.76 to 0.49 with a median minimum of 0.59. Thus, the Reg. Guide 1.60 spectrum anchored to an "effective" peak acceleration never introduces more than a factor of $(1/0.49) = 2.04$ conservatism for these six records. Section 5.3 shows similar results for inelastic response out to ductility ratio of 4.3 (the highest ratio studied). The maximum factor of unconservatism never exceeded 1.32 for ductilities from 1.0 to 4.3 and elastic frequencies from 1.8 to 10 Hz. Within this same range, the factor of conservatism never exceeded 2.04 and the median factor of conservatism

7-1

ranged from 1.14 for elastic response (μ = 1.0) to 1.01 for inelastic response (μ = 1.8 to 4.3). Considering the uncertainties in the ground motion, this performance is excellent.

In other words, an adequate engineering characterization for both elastic and inelastic structural response for stiff structures (1.8 to 10 Hz) subjected to any of the 6 longer duration (Group 1) records is provided by the Reg. Guide 1.60 spectrum anchored to an "effective" peak acceleration. It is shown in both Section 2.3 (elastic response) and 5.3 (inelastic response) that this "effective" peak acceleration, A_{DE1}, can be defined as an rms-based acceleration given by Equation 2-15. It can be seen from Equation 2-15 that the "effective" acceleration increases with increasing strong motion duration, T_D', and increasing mean (central) frequency, Ω'. In addition, the rms acceleration, a_{rms}, used to define A_{DE1} is heavily influenced by the method used to define the strong motion duration, T_D' (see Section 1.1.1 for a further discussion). Thus, to establish an "effective" acceleration, one must define a method to quantify T_D' and one must define a central frequency, Ω'. The central frequencies computed for each of the 11 real records and for an artificial Reg. Guide 1.60 time history are given in Table 2-6. The central frequency for the six Group 1 (longer duration) records plus the artificial record ranges from 3.6 to 4.7 Hz. For all of these records, this central frequency can be approximated as 4.0 Hz without introducing more than a 6% error in the computed "effective" peak acceleration.

Section 2.1 recommends that the strong motion duration, T_D', for stiff structures be computed from Equations 2-2 and 2-3 using cumulative energy plots (Figure 2-3). It is shown that this duration corresponds to the time of steepest slope (i.e., greatest power and greatest RMS acceleration) from these energy plots. It is also shown that T_D' correlates well with the longest time to reach maximum structural response (both for elastic and inelastic response) for stiff structures (1.8 to 10 Hz). The strong motion durations, T_D', given by Equations 2-2 and 2-3

are tabulated in Table 2-3 for the 11 real and one artificial record studied. It should be noted that Equations 2-2 and 2-3 often lead to much shorter estimates of strong duration than do other commonly used methods. However, it is recommended that the short durations given by Equations 2-2 and 2-3 correlate better with the longest time of maximum response for stiff structures and with the duration of maximum rms acceleration. The strong duration for the six Group 1 records range from 15.6 seconds (Olympia) to 3.4 seconds (El Centro #5). The strong duration for the five Group 2 records range from 3.0 seconds (Goleta) to 0.8 seconds (Melendy Ranch). Increasing strong duration from 3.4 seconds to 15.6 seconds increases the "effective" peak acceleration by a factor of 1.50 given identical rms accelerations. Therefore, strong duration has a moderately significant influence on the "effective" peak acceleration and must be reasonably approximated.

The previous conclusion that the Reg. Guide 1.60 spectrum anchored to an "effective" acceleration provides an adequate characterization of both elastic and inelastic structural response for stiff structures (1.8 to 10 Hz) is not applicable to the five Group 2 records. Neither elastic nor inelastic response from any of these five records can be adequately approximated by the Reg. Guide 1.60 spectrum or by any other broad frequency content spectrum. Thus, one must define the distinguishing differences between the Group 1 and Group 2 records. The most obvious differences are:

1. Strong duration, T_D'. All the Group 1 records have strong durations of 3.4 seconds and greater while all the Group 2 records have durations of 3.0 seconds and less.

2. Local magnitude, M_L. All the Group 1 records are from earthquakes with local magnitudes of 6.4 and greater while all the Group 2 records are from earthquakes with local magnitudes of 5.7 and less.

However, these differences do not appear to be the primary reason why the Reg. Guide 1.60 spectrum is inadequate for predicting the response of stiff structures. The primary reason is related to differ-

ences in the breadth of the range of frequency content. This breadth of the range of frequency content can be defined by the frequency range from f_{10} to f_{90} where 10% of the cumulative power lies at frequencies below f_{10} and 90% of the cumulative power lies at frequencies below f_{90}. Thus, the frequency range from f_{10} to f_{90} contains the central 80% of the cumulative power of the strong motion portion (T_D' duration) of the record. Table 2-6 defines the frequency range from f_{10} to f_{90} for the 11 real records and one artificial record studied. The six Group 1 records for which the Reg. Guide 1.60 spectrum provides an adequate engineering characterization from 1.8 to 10 Hz all have frequency bands (f_{10} to f_{90}) from at least 1.2 to 5.5 Hz. None of the five Group 2 records for which the Reg. Guide 1.60 spectrum does not provide an adequate engineering characterization cover the entire frequency band from 1.2 to 5.5 Hz. Coyote Lake, Gavilan College, and Melendy Ranch are missing frequency content below about 3 Hz. Goleta and Parkfield-Cholame #2 are missing frequency content above about 3 Hz. This missing frequency content and resultant narrow-banded response spectra has a strong influence on both elastic and inelastic structural response even for these stiff structures.

The conclusion is that the Reg. Guide 1.60 spectrum or other broad frequency content spectra anchored to an "effective" acceleration should only be used even for stiff structures (1.8 to 10 Hz) to characterize ground motion records which contain significant power between at least 1.2 to 5.5 Hz as defined by the range from f_{10} to f_{90}. Records which do not contain significant power throughout this frequency range should be characterized by narrower frequency design spectra.

The standard practice of averaging a number of real records together irrespective of their relative frequency content to produce a design spectrum will always lead to a broad frequency content design spectrum even when all the individual records are narrow banded. For instance, averaging the five Group 2 spectra will lead to an average spectrum which contains frequency content from at least 1.3 to 7 Hz.

Such a spectrum will be narrower than the Reg. Guide 1.60 spectrum which contains frequency content from 0.6 to 6.4 Hz, but for stiff structures (1.8 to 10 Hz) the differences will be minor. These differences would only be significant for structures with frequencies less than 1.8 Hz. Thus, a design spectrum obtained by averaging the five Group 2 spectra would not provide an adequate engineering characterization for either elastic or inelastic response of stiff structures subjected to any one of these five records. The only adequate way to characterize these records is by a narrow-banded design spectrum obtained by averaging records with similar central frequencies, Ω', and frequency bands, f_{10} to f_{90}. For instance, Parkfield Cholame #2 and Goleta can be averaged to obtain a narrow-banded, low-frequency spectrum representative of either record. Possibly, Melendy Ranch, Gavilan College, and Coyote Lake could be averaged to obtain a representative high frequency spectrum. Uncertainties in central frequency, Ω', should be covered by shifting the central frequency of a narrow-banded design spectrum throughout the range of uncertainty and not by the use of a broad frequency content design spectrum for stiff structures subjected to Group 2 type records.

A strong correlation appears to exist between local magnitude and strong duration, T_D', for records with instrumental accelerations, a, of 0.14g and greater. Records with M_L of 5.7 and less and values of a of 0.14g and greater all had T_D' of 3.0 seconds and less. Conversely, the records with M_L of 6.4 and greater all had T_D' greater than 3.0 seconds. It appears that earthquakes with M_L less than about 6.0 may not have sufficient energy content to be capable of producing both high accelerations (greater than 0.14g) and longer durations ($T_D' > 3.0$ seconds). Secondly, a strong correlation exists between T_D' and the breadth of the frequency band of significant power. None of the records with $T_D' \leq 3.0$ seconds had significant power throughout the frequency range from 1.2 to 5.5 Hz while all of the records with $T_D' > 3.0$ seconds contained power throughout this frequency range. A tentative conclusion would be that the design response spectrum for earthquakes with $M_L < 6.0$ and ground accelerations of 0.14g and greater should be a narrow-banded

spectrum obtained by averaging only records with similar central frequencies, Ω', and similar frequency bands, f_{10} to f_{90}. This conclusion would have wide ranging effects since the SSE design earthquake for nuclear plants east of the Rocky Mountains would generally correspond to these conditions. The conclusion is only tentative because not enough records were studied.

7.2 PREDICTION OF INELASTIC SPECTRAL DEAMPLIFICATION FACTORS AND INELASTIC RESPONSE SPECTRA

A representative nonlinear lateral force-deformation resistance function for shear wall type structures was presented in Chapter 3. In each analysis, the yield capacity of this model was set equal to the capacity associated with the elastic spectral acceleration at the structure's elastic natural frequency for each earthquake record. Thus, the structure was at the onset of yielding (ductility, μ, of unity) when subjected to the ground motion record. Next, a series of nonlinear time history analyses were performed in which the record time history had amplitudes scaled up by an input scale factor, F. For a given F, the maximum resultant ductility, μ, was determined. By this means, the input scale factors, F, corresponding to a low ductility ($\mu_L = 1.85$) and a high ductility ($\mu_H = 4.27$) were determined. Table 4-1 presents these input scale factors for the 12 records studied at four natural frequencies between 1.8 and 10 Hz. The low ductility is intended to correspond to minor inelastic behavior while the high ductility corresponds to a conservative estimate of the onset of significant strength degradation.

It should be noted that these input scale factors, F, are equal to the inelastic spectral deamplification factor by which the elastic spectral acceleration must be divided to obtain an inelastic spectral acceleration. If the structure were designed to have a yield capacity corresponding to this inelastic spectral acceleration at the elastic natural frequency, then the structure would undergo a ductility, μ, when subjected to the actual recorded time history. As illustrated in Figure

3-4, a shear wall elastically designed to ACI-349 code ultimate capacities for static lateral loads is permitted some inelastic deformation. Input scale factors or inelastic spectral deamplification factors are based on the yield capacity which is less than the code ultimate capacity.

It was found that these input scale factors (inelastic spectral deamplification factors) were not constant for a given ductility factor, μ. The F factors were heavily influenced by the ratio of spectral accelerations on the soft (lower frequency) side of the elastic frequency to the spectral accelerations at the elastic frequency. When the spectral accelerations on the lower frequency side were much less than the spectral acceleration at the elastic frequency, F was high. Conversely, when these lower frequency spectral accelerations were much higher than the elastic frequency spectral accelerations, F was low. This effect can be considered to be either a spectral averaging effect or can be considered to be an effective frequency shift to lower frequencies. For simplicity, it will be called a spectral averaging effect. This effect is discussed in more detail in Section 4.1.3.

This spectral averaging effect was by far the most substantial factor influencing the computed F factors. For the broad frequency content Group 1 records ($T_D' > 3.0$ seconds), the F factors were fairly uniform and showed a gradual increase as frequencies were reduced. On the other hand, the F factors for the narrow frequency Group 2 records ($T_D' \leq 3.0$ seconds) were far from uniform. Thus, for the short duration records, the F factor could be either very large or could be low depending upon where the structure's elastic frequency lay relative to the frequency of maximum spectral acceleration. Except within a narrow frequency band, the F factors for these short duration records are greater than for the longer duration records. However, within this narrow frequency band, the F factors for the short duration records are about equal to or may be slightly less than those for the longer duration records. Figure 4-1 shows this increase in scatter for F as T_D' is reduced.

In addition to the spectral averaging effect, a smaller duration effect was also noted. The predominant duration effect is accounted for by the spectral averaging. The lesser duration effect is related to the number of strong nonlinear response cycles. It is clear that the number of strong nonlinear response cycles inceases with duration and ranges from 1 for Melendy Ranch ($T_D' = 0.8$ seconds) to 4 for Olympia ($T_D' = 15.6$ seconds). Other than for Olympia and Melendy Ranch, the records generally showed 2 or 3 strong nonlinear response cycles. In every case, the total number of strong nonlinear response cycles was low (4 or less). On the average, the duration effect on the F factors was small once the spectral averaging effect was accounted for.

One effect of increasing the number of strong nonlinear response cycles from 1 to 4 was to reduce the effective structural natural frequency toward the secant frequency and away from the elastic frequency. With one strong nonlinear cycle, the effective frequency lay about midway between the secant and the elastic frequencies. With more nonlinear response cycles, the effective frequency more closely approached the secant frequency. However, the effective frequency was never as low as the secant frequency. A second effect was to reduce the effective damping percentage with increasing numbers of nonlinear cycles for the shear wall resistance functions. The technical basis for this reduced damping is described in Appendix C. Both the frequency shift and effective damping reduction were most noticeable when increasing the number of strong nonlinear cycles from 1 to 2. These effects were much smaller when increasing the number of strong nonlinear cycles from 2 to 4 (see Table 4-3). Thus, within about 10% accuracy on the predicted F_μ factor, one could assume 3 strong nonlinear response cycles when evaluating the effective frequency and effective damping except when T_D' is less than one second in which case, one should assume 1 strong nonlinear response cycle. Therefore, other than for the spectral averaging effect, it is really only necessary to estimate whether T_D' is greater or less than one second for predicting the inelastic spectral deamplification factor, F_μ. The effect of T_D' and the number of strong nonlinear response cycles, N, on the F_μ factor is shown for the Reg. Guide 1.60 spectrum in Figures 5-1 and 5-2.

It was found that the inelastic structural response of single-degree-of-freedom structural models, the inelastic spectral deamplification factor (F_μ), and the inelastic spectral acceleration ($S_{a\mu}$) could all be accurately predicted from characteristics of the moderately damped (7 to 15% damping) elastic response spectrum and an approximate knowledge of T_D'. Either of two methods could be used.

1. The nonlinear resistance function model can be replaced by an equivalent linear resistance function with a lesser effective frequency (lesser effective stiffness) and increased effective damping than the elastic frequency (elastic stiffness) and elastic damping. This equivalent linear model is then used with the elastic response spectrum to compute maximum displacement responses, $\delta_m = \mu\delta_y$.

2. The elastic response spectrum is reduced to obtain an inelastic response spectrum for use with the elastic frequency and damping in order to compute the yield displacement, δ_y, and required yield capacity, V_y, needed to hold the structure to a ductility, μ. At a given frequency and damping value, the inelastic spectral acceleration is given by:

$$S_{a\mu}(f,\beta) = \frac{S_a(f,\beta)}{F_\mu} \qquad (7\text{-}1)$$

where F_μ is the predicted inelastic spectral deamplification factor.

In the first method, and effective frequency, f_e', and an effective damping ratio, β_e', must be estimated. It is recommended that Equations 3-8 and 4-2 be used together with coefficients from Table 4-2 to make these estimates. This effective frequency and effective damping estimate can also be used together with the elastic response spectra to predict F_μ by Equation 3-14 for use in the second method. This approach for predicting F_μ is called a point estimate approach since it is based upon a single point estimate of f_e', and β_e'. When this point estimate approach is used to predict F_μ, the first and second approximate nonlinear analysis methods described above produce identical results. Therefore, further comparisons can be made based upon the accuracy with which F_μ is predicted compared to the time history computed F factors.

It was found that the recommended point estimate approach (based on an estimated f_e' and β_e') provided an excellent estimate of F_μ. The ratio of predicted to time history computed scale factors (F_μ/F) are shown in Table 4-4 to have mean values of 0.98 and 1.02 and coefficients of variations (COV) of only 0.12 and 0.09 for ductility levels of μ_H = 4.27 and μ_L = 1.85, respectively. At the worst extremes, the ratio F_μ/F ranged from 0.75 to 1.29 for μ_H and from 0.85 to 1.26 for μ_L.

Other methods also exist for predicting an effective frequency f_e', and an effective damping ratio, β_e'. Two common methods defined as the Sozen method and the Iwan method are described in Section 3.3.1. These methods were not developed for shear wall type resistance functions but were used in this study for comparison with the recommended method for predicting an effective frequency and an effective damping. Table 4-3 compares the effective frequencies and effective damping percentages predicted by the three methods. One should note that the Sozen method predicts lower effective frequencies while the Iwan method predicts higher effective frequencies than does the recommended method. In other words, the Sozen method softens the structure more while the Iwan method softens the structure less than the method recommended by this study. Both the Sozen and the Iwan methods predict substantially higher effective damping percentages than the method recommended by this study for shear wall resistance functions. The reasons for this difference are given in Section 4.3. Tables 4-5 and 4-6 compare the predicted to computed scale factors (F_μ/F) when the effective frequencies and effective damping are computed by the Sozen and Iwan methods, respectively. The Sozen method introduces a slight conservative bias while the Iwan method introduces a significant unconservative bias for the mean ratios. Both methods result in substantially higher COV than the recommended method. The conclusion is that the recommended procedure provides a better estimate of the effective frequency and effective damping for shear wall type structures than does either the Sozen or Iwan methods.

It was judged that a spectral averaging approach should provide a better estimate of F_μ than the best point estimate approach. Spectral averaging smooths out local peaks and valleys in the response spectrum and is expected to be more stable. Therefore, a number of spectral averaging approaches to estimate F_μ were also investigated. A simple approach given by Equations 4-3 through 4-7 together with Table 4-2 is recommended. This approach averages the spectral accelerations between f_u and the secant frequency, f_s, where f_u lies between the elastic and secant frequencies as shown in Table 4-7. The ratios of predicted to computed scale factors (F_μ/F) as obtained by this spectral averaging approach are shown in Table 4-8. One should note that the spectral averaging approach provides only marginal improvement over the recommended point estimate approach (Table 4-4). It is not clear that this marginal improvement is worth the considerable increase in computational effort required. However, if the elastic response spectrum contains significant local peaks and valleys at about 10% damping, the spectral averaging approach would be expected to provide some improvement over the point estimate approach. The data indicates that the spectral averaging approach does reduce the maximum factor of unconservatism (maximum ratio of F_μ/F). This maximum ratio of F_μ/F is 1.29 for the point estimate approach and only 1.19 for the spectral averaging approach at $\mu_H = 4.27$, and is lowered from 1.26 to 1.14 for $\mu_L = 1.85$.

Other commonly used approaches for estimating F_μ are the Newmark method and the Riddell method described in Section 3.3.2. These methods give similar results for F_μ with the Riddell method being a slight improvement over the Newmark method. Table 4-9 shows the predicted to computed scale factors (F_μ/F) when the Riddell method is used. One should note that for the shear wall resistance function model used in this study, the Riddell method introduces a slight factor of unconservatism on the average. Furthermore, the COVs range from 140% to 200% larger than those obtained for the spectral averaging approach recommended in this study (Table 4-8). For $\mu_H = 4.27$, the extreme range of (F_μ/F) ranges from 0.43 to 1.78 for the Riddell approach as compared to a range of 0.75 to

1.19 for the recommended spectral averaging method. At $\mu_L = 1.85$, the extreme range for the Riddell method is not as severe but still ranges from 0.88 to 1.47 as compared to 0.85 to 1.14 for the recommended spectral averaging method.

It is concluded that either the point estimate approach or the spectral averaging approach recommended in this study provide excellent predictions for F_μ out to ductilities of at least 4.3. Either approach provides significantly more accurate estimates for F_μ than do other commonly used approaches for shear wall type resistance functions. It should be noted that F factors presented in this report are not intended to be specifically used for the design of facilities. These factors have been evaluated on the basis of a limited number of ground motion records and at a limited number of structural frequencies and ductility levels. Instead, the purpose of this work is to present the methodology by which inelastic spectral deamplification factors may be developed such that permissible levels of inelastic deformation may be incorporated into designs using simplified elastic analytical techniques.

Although this study was predominantly concerned with shear wall resistance functions, other inelastic resistance functions and the influence of various parameter variations were also studied and the results are summarized in Appendix D. The basic conclusion of these parameter variation studies was that the approaches recommended in this study can be conservatively used for braced-frames and other structural or equipment systems so long as these systems do not have resistance-deformation functions which show greater stiffness degradation and pinching behavior than that used in this study for shear walls. The authors do not know of any other structural system used in nuclear power plants which would have more severe stiffness degradation or pinching behavior and so they generally believe that the recommended approaches from this study could be conservatively applied to all structural and equipment systems in a nuclear power plant. Some other conclusions of these parametric studies are:

1. Equation 4-6 can be used to estimate the average effective damping equally well for an elastic damping of 3% as for an elastic damping of 7%. The prediction procedure works equally well at 3% elastic damping as at 7% elastic damping.

2. The frequency shift and hysteretic damping coefficient, C_F and C_N, in Table 4-2 were developed for a shear wall resistance function model. Use of these coefficients will introduce only a slight conservatism for the Takeda model. The shear wall model overestimates the stiffness degradation and pinching behavior for braced-frame and bilinear resistance function models. Therefore, these coefficients over-emphasize the importance of N and T_D for such models. The input scale factor (inelastic spectral deamplification factor) for the braced-frame and bilinear resistance function models studied in Appendix D lay midway between the scale factors predicted using the C_F and C_N given in Table 4-2 for the appropriate T_D and the scale factor predicted using $C_F = 1.5$ and $C_N = 0.30$ which are given for N=1. Averaging the results obtained from the use of these two different sets of C_F and C_N values will improve the prediction accuracy for braced-frame and bilinear models when T_D is greater than 1.0 seconds and thus will reduce the conservatism introduced by the recommended approach for these models.

Figures 5-3 through 5-13 present the inelastic spectra predicted within the frequency range from 1.0 to 10.0 Hz for the 11 real time histories included in this study using the spectral averaging prediction methods of Chapter 4 and ductilities of 1.85 and 4.27. Several points should be noted from these figures:

1. The peak inelastic spectral accelerations always occur at frequencies higher than those at which the peak elastic spectral accelerations occur. This situation occurs because inelastic response of these higher frequency structures shifts the effective frequency downward into the range of peak elastic response.

2. The inelastic deamplification factors associated with frequencies equal to or less than that at which the elastic spectrum peaks are much greater than those for higher frequencies.

These points are most dramatically illustrated by the Parkfield-Cholame Array #2 spectra (Figure 5-11). The elastic spectral amplifications are very high from 1.2 to 3.0 Hz and drop off very rapidly at both higher and lower frequencies. The largest inelastic deamplification factors are associated with elastic frequencies less than 3.0 Hz since inelastic response will shift these frequencies lower and markedly reduce response. Structures with frequencies of 3.0 Hz and less could be designed to yield at spectral accelerations much less than those indicated by the elastic spectra for Parkfield without severe damage. However, for the Parkfield record, one must be very careful not to reduce the elastic spectral accelerations for structures in about the 3.5 to 5.0 Hz range. These structures should be designed to remain elastic for the Parkfield record. Inelastic response of such structures will shift their effective frequencies into the frequency range (1.2 to 3.0 Hz) within which the power of the input is predominantly concentrated. For such structures, inelastic responses would rapidly increase because of this frequency shift. For records with narrow frequency content, such as Parkfield, one should be very careful about taking any credit for inelastic response for structures which lie slightly to the stiff side of the predominant frequency range of the record. On the other hand, for even stiffer structures (elastic frequencies greater than 5.0 Hz) the inelastic deamplification factors are again significant although not as large as for structures with frequencies below 3.0 Hz.

This study is concerned with the inelastic response of structural systems (braced frames and shear walls) and the concept of "effective" spectral response is considered valid for such systems. The results of this study can also probably be extrapolated to ductile passive equipment whose fragility is governed by structural failure modes. However, the study is probably not appropriate for active equipment.

This study was conducted using single-degree-of-freedom (SDOF) structural models. It is believed that the results should also be applicable for multi-degree-of-freedom (MDOF) models. However, when used with MDOF models, one must keep in mind these results are to be used with a system ductility. In the case of localized nonlinear behavior, the story drift ductility is often about twice the system ductility and element ductility will exceed story drift ductility. Thus, if one needs a specific control on either element or story drift ductility, the system ductility must be held to lesser limits. This topic will be discussed further in a follow-on study which extends the SDOF results to MDOF models.

7.3 MEASURE OF RELATIVE STRENGTH OF GROUND MOTION RECORDS

If a structure of elastic frequency, f, and elastic damping, β, is designed to be at the onset of yielding for spectral acceleration $S_{a\mu}$ (f,β) which is the inelastic spectral acceleration for any ground motion considered, then the structure will respond to ductility level, μ, when subjected to that ground motion record. Thus, comparing $S_{a\mu}$ (f,β) for the various ground motion records considered in this study provides a measure of the relative strength of the records. A ground motion record with a large $S_{a\mu}$ (f,β) requires the structure to be designed at a large yield level to limit response to a given ductility and is more severe than a record with a small $S_{a\mu}$ (f,β) which requires the structure to be designed at a small yield level to limit response to the same ductility level. In Chapter 6, the inelastic spectral acceleration values are compared for the 12 ground motion records considered in this study at 3 ductility levels (μ = 1.0, 1.85 and 4.27) at 4 frequencies (f = 8.54, 5.34, 3.20 and 2.14 Hz and one damping value (β = 7 percent)).

Relative strength zones (i.e., very severe, severe, moderate and low strengths) are defined in terms of the acceleration level for which a structure must be designed to remain elastic using the Reg. Guide 1.60 spectrum in order to prevent seismic response exceeding ductility levels of 4.27 when subjected to the actual earthquake ground motion. Similar

relative strength zones for μ = 1.85 and 1.0 are obtained by scaling the zone levels for μ = 4.27. The inelastic spectral accelerations and relative strength zones are presented in Figures 6-1a through 6-1d for the 4 frequencies considered.

Based upon the data presented in Figures 6-1a through 6-1d, it is concluded that only the Pacoima Dam record is a very severe ground motion in terms of potential damage for structures with frequencies greater than 4 Hz. At below 4 Hz, this record is a severe ground motion at about 3 Hz and a moderate ground motion at about 2 Hz. At 8.5 Hz, the Melendy Ranch and El Centro #5 records are in the severe category. At below 4 Hz, the Parkfield record is within the severe category. All other ground motion records fall in the low or moderate categories at all frequencies. Note that reasons are outlined in Chapter 6 as to why the damage capability of high acceleration, short duration earthquakes such as Melendy Ranch and Parkfield may be overstated by the methods used to assess relative strengths of the ground motion.

8. REFERENCES

Alexander, C. M., Heiderbrecht, A. C., and Tso, W. K. (1973), "Cyclic Load Tests on Shear Wall Panels", Proceedings of the Fifth World Conference on Earthquake Engineering, Rome, pp. 1116-1119.

Arias, A. (1970), "A Measure of Earthquake Intensity", Seismic Design for Nuclear Power Plants, MIT Press, Cambridge, Massachusetts.

Banon, H., Biggs, J. M., and Irvine, H. M. (1981), "Seismic Damage in Reinforced Concrete Frames", Journal Structural Division, ASCE, Vol. 107, ST 9, pp. 1713-1729, September.

Barda, F., Hanson, J. M., and Corley, W. G. (1976), "Shear Strength of Low-Rise Walls with Boundary Elements", Proceedings of the Sixth World Conference on Earthquake Engineering, New Delhi.

Bertero, V. V., et. al., (1977), "Seismic Design Implications of Hysteretic Behavior of R/C Structural Walls", Proceedings of the Sixth World Conference on Earthquake Engineering, New Delhi.

Blume, J. A., (1979), "On Instrumental versus Effective Acceleration and Design Coefficients", Proceedings of the Second U.S. National Conference on Earthquake Engineering", Stanford, California, August.

Cardenas, A. E., Hanson, J. M. Corley, W. G., and Hognestad, E. (1973), "Design Provisions for Shear Walls", ACI Journal, Proc. Vol. 70, No. 3, pp. 221-230, March.

Dobry, R., Idriss, I. M., Ng, E. (1978), "Duration Characteristics of Horizontal Components of Strong-Motion Earthquake Records", Bulletin of the Seismological Society of America, Vol. 68, No. 5, pp. 1487-1520, October.

Fiorato, A. E. and Corley, W. G. (1977), "Laboratory Tests of Earthquake-Resistant Structural Wall Systems and Elements", Workshop on Earthquake-Resistant Reinforced Concrete Building Construction, University of California, Berkeley, pp. 1388-1429, July.

Fukada, Y., Hirashima, S. and Shobara, R. (1981), "Experimental Study on One-Thirtieth Scale Model of Reinforced Concrete Reactor Build-Under Cyclic Lateral Loading", Trans. Sixth International Conference of Structural Mechanics in Reactor Technology, Volume K, paper K15/1, August.

Gugerli, H. and Goel, S. C. (1980), "Large Scale Tests for the Hysteresis Behavior of Inclined Bracing Members", Proceedings of the Seventh World Conference on Earthquake Engineering, Istanbul, pp. 87-94.

Gulkan, P. and Sozen, M. A. (1974), "Inelastic Responses of Reinforced Concrete Structures to Earthquake Motions", ACI Journal, Vol. 71, No. 12, pp. 604-610, December.

Hoffman, R. B. (1974), "State-of-the-Art for Assessing Earthquake Hazards in the United States; Factors in the Specification of Ground Motions for Design Earthquakes in California", Miscellaneous Paper S-63-1, U.S. Army Engineers Waterways Experiment Station, Vicksburg, Mississippi, June.

Housner, G. W. (1952), "Spectrum Intensities of Strong-Motion Earthquakes", Proceedings of the Symposium on Earthquake and Blast Effects on Structures", Earthquake Engineering Research Institute, Los Angeles, California, June.

Housner, G. W. (1975), "Measures of Severity of Earthquake Ground Shaking", Proceedings of the U.S. National Conference on Earthquake Engineering, EERI, Ann Arbor, Michigan, pp. 25-33., June.

Housner, G. W., and Jennings, P. C. (1977), "Earthquake Design Criteria for Structures", Report No. EERL 77-06, EERL, California Institute of Technology, Pasadena, November.

Housner, G. W. (1979), "Statistics of Pulses on Strong Motion Accelerograms", Proceedings of the NSF Seminar Workshop on Strong Ground Motion.

Hudson, D. E. (1979), Reading and Interpreting Strong Motion Accelerograms, EERI Monograph, EERI, Berkeley.

Husid, R. (1973), Terremotos-Earthquakes, Editorial Andres Bello, Santiago, Chile.

Iwan, W. D. and Gates, N. C. (1979), "Estimating Earthquake Response of Simple Hysteretic Systems", Journal of the Engineering Mechanics Division, ASCE, Vol. 105, No. EM3, pp. 391-405, June.

Iwan, W. D. (1980), "Estimating Inelastic Response Spectra from Elastic Spectra", Earthquake Engineering & Structural Dynamics, Vol. 8, pp. 375-399.

Jain, A. K. and Goel, S. C. (1978a), "Hysteresis Models for Steel Members Subjected to Cyclic Buckling or Cyclic End Moments and Buckling (User's Guide for Drain - 2D: EL9 and EL10)", Report No. UMEE 78R6, Department of Civil Engineers, University of Michigan, December.

Jain, A. K., Goel, S. C. and Hanson, R. D. (1978b), "Inelastic Response of Restrained Steel Tubes", Journal of Structural Division, ASCE, ST6, Vol. 104, pp. 897-910, June.

Jain, A. K. and Goel, S. C. (1979), "Cyclic End Moments and Buckling in Steel Members", Proceedings of the Second U.S. National Conference on Earthquake Engineering, Stanford, pp. 413-422.

Jain, A. K., Goel, S. C. and Hanson, R. D. (1980), "Hysteretic Cycles of Axially Loaded Steel Members", Journal Structural Division, ASCE, ST8, Vol. 106, pp. 1777-1795, August.

Jennings, P. C. and Housner, G. W. (1977), "The Capacity of Extreme Earthquake Motions to Damage Structures", Structural and Geotechnical Mechanics, Prentice-Hall, Englewood Cliffs, New Jersey, pp. 102-116.

Kanaan, A. E. and Powell, G. H. (1973, 1975), "DRAIN-2D, General Purpose Computer Program for the Dynamic Analysis of Inelastic Plane Structures", EERC Report No. 73-6, Earthquake Engineering Research Center, University of California, Berkeley, April, 1973 (Revised 1975).

Kennedy, R. P. (1980), "Ground Motion Parameters Useful in Structural Design", presented at Conference on Evaluation of Regional Seismic Hazards and Risk, Santa Fe, New Mexico, October.

Kennedy, R. P., Short, S. A. and Newmark, N. M. (1981a), "The Response of a Nuclear Power Plant to Near-Field Moderate Magnitude Earthquakes", Sixth International Conference on Structural Mechanics in Reactor Technology, Paris, France, August 17-21.

Kennedy, R. P. (1981b), "Peak Acceleration as a Measure of Damage", presented at Fourth International Seminar on Extreme-Load Design of Nuclear Power Facilities, Paris, France, August.

Mahin, S. A. and Bertero, V. V., "An Evaluation of Inelastic Seismic Design Spectra", Journal Structural Division, ASCE, Vol. 107, ST9, pp. 1777-1795, September.

Maison, B. F. and Popov, E. P. (1980), "Cyclic Response Prediction for Braced Steel Frames", Journal Structural Division, ASCE, Vol 106, ST7, pp. 1401-1416, July.

McCann, M. W., Jr. and Shah, H. C. (1979), "RMS Acceleration for Seismic Risk Analysis: An Overview", Proceedings of the Second U.S. National Conference on Earthquake Engineering, Stanford University, pp. 883-897, August 22-24.

Mortgat, C. P. (1979), "A Probabilistic Definition of Effective Acceleration", Proceedings of the Second U.S. National Conference on Earthquake Engineering, Stanford University, pp. 743-752, August 22-24,

Newmark, N. M. (1970), "Current Trends in the Seismic Analysis and Design of High Rise Structures, Chapter 16, in Earthquake Engineering, edited by R. Wiegel, Prentice-Hall, Inc., Englewood Cliffs, New Jersey, pp. 403-424.

Newmark, N. M. (1973a), "A Study of Vertical and Horizontal Earthquake Spectra", WASH-1255, Directorate of Licensing, U.S. AEC, Washington.

Newmark, N. M. and Hall, W. J., (1973b), "Procedures and Criteria for Earthquake Resistant Design", Building Practices for Disaster Mitigation, National Bureau of Standards (Washington, D.C.), Building Sciences Series 46, Vol. 1, pp. 209-236, February.

Newmark, N. M. (1975), "Seismic Design Criteria for Structures and Facilities: Trans-Alaska Pipeline System", Proceedings of the U.S. National Conference on Earthquake Engineering, Ann Arbor, Michigan.

Newmark, N. M. (1976), "A Rationale for Development of Design Spectra for Diablo Canyon Reactor Facility", N. M. Newmark Consulting Engineering Services, Urbana, Illinois, September.

Newmark, N. M. and Hall, W. J. (1978), "Development of Criteria for Seismic Review of Selected Power Plants", NUREG/CR-0098, Newmark Consulting Engineering Services, Urbana, Illinois, May.

Newmark, N. M., and Hall, W. J. (1982), "Earthquake Spectra and Design", Earthquake Engineering Research Institute Monograph.

Nuttli, O. W. (1979), "State-of-the-Art for Assessing Earthquake Hazards in the United States: The Relation of Sustained Maximum Ground Acceleration and Velocity to Earthquake Intensity and Magnitude", Miscellaneous Paper S-73-1, Report 16, November, 1979, U.S. Army Engineers Waterways Experiment Station, Vicksburg, Mississippi.

Page, R. A., Boore, D. M., Joyner, W. B., and Coulter, H. W. (1972), "Ground Motion Values for Use in the Seismic Design of the Trans-Alaska Pipeline System", USGS Circular No. 672, Washington.

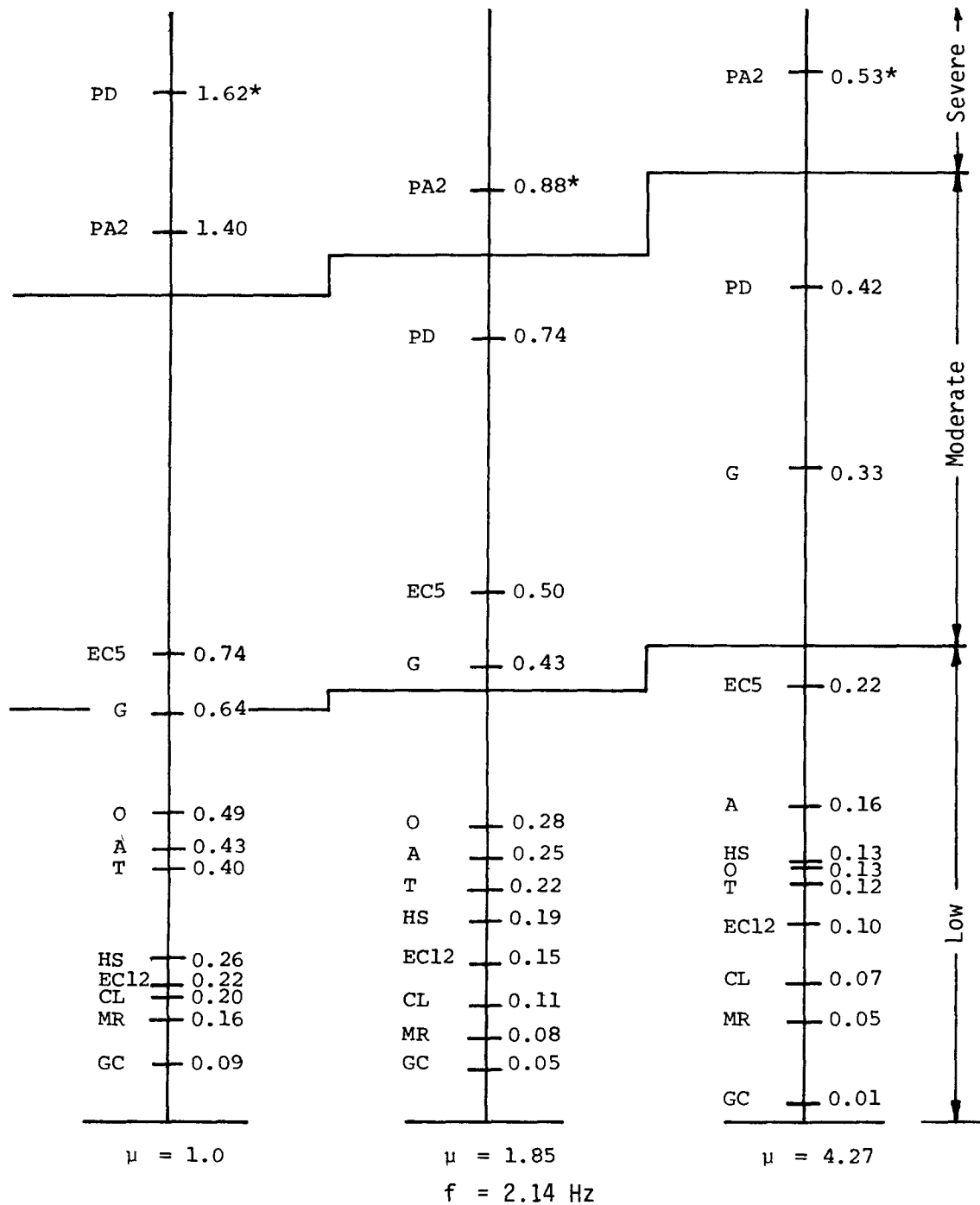Park, R. and Paulay, T. (1975), Reinforced Concrete Structures, John Wiley and Sons, New York, pp. 610-662.

Paulay, T. (1975), "Earthquake Resistant Structural Walls", Workshop on Earthquake-Resistant Reinforced Concrete Building Construction, University of California, Berkeley, pp. 1339-1365, July.

Ploessel, M. R., and Slosson, J. E. (1974), "Repeatable High Ground Accelerations from Earthquakes", California Geology, Vol. 27, No. 9, pp. 195-199, September.

Popov, E. P., Zayas, V. A. and Mahin, S. A. (1979a), "Cyclic Inelastic Buckling of Thin Tubular Columns", Journal Structural Division, ASCE, Vol. 105, ST11, pp. 2261-2277, November.

Popov, E. P. (1979b), "Inelastic Behavior of Steel Braces Under Cyclic Loading", Proceedings of the Second U.S. National Conference on Earthquake Engineering, Stanford, pp. 923-932.

Popov, E. P. (1980), "Update on Simulated Seismic Tests on Reinforced Concrete and Structural Steel Assemblies", Proceedings of the 1980 Annual Convention of the Structural Engineering Association of California, Monterey, pp. 15-35, October.

Popov, E. P. and Black, R. G. (1981), "Steel Structures Under Severe Cyclic Loadings", Journal Structural Division, ASCE, Vol. 107, ST9, pp. 1857-1881, September.

Riddell, R. and Newmark, N. M. (1979), "Statistical Analysis of the Response of Nonlinear Systems Subjected to Earthquakes", SRS 468, Department of Civil Engineering, University of Illinois, Urbana, August.

Saiidi, M. and Sozen, M. A. (1979), "Simple and Complex Models for Nonlinear Seismic Response of Reinforced Concrete Structures", Civil Engineering Studies, Structural Research Series, No. 465, University of Illinois, Urbana, August.

Schnabel, P. B. and Seed, H. B. (1973), "Accelerations in Rock for Earthquakes in the Western United States", Bulletin of the Seismological Society of America, Vol. 62, April.

Shibata, A. and Sozen, M. A. (1976), "Substitute-Structure Method for Seismic Design in R/C", Journal Structural Division, ASCE, Vol. 102, ST1, pp. 1-18, January.

Shiga, T., Shibata, A. and Takahashi, J. (1973), "Experimental Study on Dynamic Properties of Reinforced Concrete Shear Walls", Proceedings of the Fifth World Conference on Earthquake Engineering, Rome, Paper 142.

Short, S. A., Kennedy, R. P., and Newmark, N. M. (1980a), "PWR Reactor Building Response from High Acceleration, Short Duration Earthquakes", Seventh World Conference on Earthquake Engineering, Istanbul, Turkey, September.

Short, S. A., Kennedy, R. P., Newmark, N. M., and Sozen, M. A. (1980b), "Nonlinear Response of Nuclear Plant to Moderate Magnitude, Near Field Earthquake", ASCE Specialty Conference on Civil Engineering and Nuclear Power, Knoxville, Tennessee, September.

Singh, P. (1977), "Seismic Behavior of Braces and Braced Steel Frames", UMEE 77R1, Department of Civil Engineering, University of Michigan, July.

Stevenson, J. D. (1980), "Structural Damping Values as a Function of Dynamic Response Stress and Deformation Levels", Nuclear Engineering and Design, Vol. 60, pp. 211-237.

Trifunac, M. D. and Brady, A. G. (1975), "A study of the Duration of Strong Earthquake Ground Motion", Bulletin of the Seismological Society of America, Vol. 65, pp. 581-626.

Uchida, T. et. al., (1980), "Structural Test and Analysis on the Seismic Behavior of the Reinforced Concrete Reactor Building", Proceedings of the Seventh World Conference on Earthquake Engineering, Istanbul, pp. 217-224.

Umemura, H. and Tanaka, H. (1977), "Elasto-Plastic Dynamic Analysis of Reactor Buildings", Proceedings of the Sixth World Conference on Earthquake Engineering., New Delhi, India, pp. 8-51/8-56.

Unemura, H. et. al., (1980), "Restoring Force Characteristics of R.C. Walls with Openings and Reinforcing Methods", Proceedings of the Seventh World Conference on Earthquake Engineering, Istanbul, pp. 209-216.

USNRC (1973a), "Design Resonse Spectra for Seismic Design of Nuclear Power Plants', Regulatory Guide 1.60 (Revision 1), Office of Standards Development, USNRC, Washington, D.C., December.

USNRC (1973b), "Damping Values for Seismic Design of Nuclear Power Plants", Regulatory Guide 1.61, Office of Standards Development, USNRC, Washington, D.C., October.

USNRC (1980), "Part 100 - Reactor Site Criteria", Rules and Regulations, Title 10, Chapter 1, Code of Federal Regulations - Energy.

REFERENCES (Continued)

Vanmarcke, E. H. (1972), "Properties of Spectral Moments with Applications to Random Vibration", Journal of the Engineering Mechanical Division, ASCE, Vol. 98, No. EM2, pp. 425-446, April.

Vanmarcke, E. H. (1975), "Structural Response to Earthquakes", Chapter 8 in Seismic Risk and Engineering Decisions, C. Lomnitz and E. Rosenblueth, eds., Elsevier Publishing Co., New York.

Vanmarcke, E. H., and Lai, S. P. (1980), "Strong Motion Duration and RMS Amplitude of Earthquake Records", Bulletin of the Seismological Society of America, Vol. 70, No. 4, pp. 1293-1307, August.

Wang, T. Y., Bertero, V. V. and Popov, E. P. (1975), "Hysteretic Behavior of Reinforced Concrete Framed Walls", Report No. EERC 75-23, EERC, University of California, Berkeley.

Wakabayashi, M. et. al., (1973), "Inelastic Behavior of Steel Frames Subjected to Constant Vertical and Alternating Horizontal Loads", Proceedings of the Fifth World Conference on Earthquake Engineering, Rome, Vol. I, pp. 1194-1197.

Wakabayashi, M. et. al., (1977), "Hysteretic Behavior of Steel Braces Subjected to Horizontal Load due to Earthquakes", Proceedings of the Sixth World Conference on Earthquake Engineering, New Delhi, India, Vol. III, pp. 3188-3193.

Whitman, R. V. (1978), "Effective Peak Acceleration", Proceedings of the Second International Conference on Microzonation, San Francisco, California, Vol. III, pp. 1247-1255, November 26 - December 1.

μ = 1.0

PD	1.62*
PA2	1.40
EC5	0.74
G	0.64
O	0.49
A	0.43
T	0.40
HS	0.26
EC12	0.22
CL	0.20
MR	0.16
GC	0.09

μ = 1.85
f = 2.14 Hz

PA2	0.88*
PD	0.74
EC5	0.50
G	0.43
O	0.28
A	0.25
T	0.22
HS	0.19
EC12	0.15
CL	0.11
MR	0.08
GC	0.05

μ = 4.27

PA2	0.53*
PD	0.42
G	0.33
EC5	0.22
A	0.16
HS	0.13
O	0.13
T	0.12
EC12	0.10
CL	0.07
MR	0.05
GC	0.01

Severe → Moderate → Low

LEGEND

A: Artificial (0.2g)
CL: Coyote Lake
EC5: El Centro #5
EC12: El Centro #12
G: Goleta
GC: Gavilan College
HS: Hollywood Storage
MR: Melendy Ranch
O: Olympia
PA2: Parkfield
PD: Pacoima Dam
T: Taft

*Values shown are inelastic spectral accelerations $S_{a\mu}$ for μ = 1.0, 1.85 and 4.27

FIGURE 6-1d.   MEASURE OF RELATIVE STRENGTH OF GROUND MOTION RECORDS AS DEFINED BY $S_{a\mu}(f, 7\%)$

LITERATURE REVIEW: EARTHQUAKE STRUCTURAL DAMAGE

Seismic design criteria for nuclear power plants are normally expressed in the form of elastic response spectra anchored to an instrumental peak acceleration or some "reference acceleration for seismic design" coupled with an elastic structural analysis. Numerous studies have suggested that the predicted performance (i.e., damage or lack of damage) of structures obtained using such design spectra anchored to instrumental peak ground motion and elastic analysis does not correlate well with the observed performance of real structures. Namely, the analyses generally overestimate earthquake force levels and thus predict that damage would be more severe than is actually observed. One such investigation has been performed as part of this study for the El Centro Steam Plant subjected to the 1979 Imperial Valley earthquake. The results of the steam plant evaluation are reported in Appendix E. These studies indicate that in order to better correlate both design conditions and predicted structural response with the actual observed performance (i.e., damage or lack of damage) of structures, design parameters must not only reflect peak acceleration and the frequency characteristics of the earthquake motion, but also must consider factors such as duration of strong motion, the number of peak cycles, etc., as well as the energy absorption capacity of the structures and soil-structure interaction effects. It has also been suggested that the problem is further complicated when dealing with near-source ground motions due to low-to-moderate magnitude earthquakes whose motions are characterized by very high peak accelerations, and short duration of strong shaking.

The purpose of this task was to conduct a literature review of available data and document the performance of real structures subjected to strong ground shaking from past earthquakes. The primary objective was

to use the assembled information to judge how well the predicted struc-
tural performance, based on design motions such as those currently defined
for nuclear power plants (namely, design motions based on elastic spectra
anchored to peak acceleration from recorded motions coupled to an elastic
response analysis) correlates with the actual observed behavior of real
structures in past earthquakes. A second objective was to identify, from
the cases reviewed, ground motion and structural characteristics that
strongly influenced the actual observed response behavior of the
structure.

A.1   SCOPE

There are many papers describing damage to structures resulting
from earthquakes. By far, most of these papers focus on architectural
and cosmetic damage. There are only a limited number that discuss
performance (i.e., structural damage or lack of structural damage) where
the level of ground shaking is known. This review focuses on such papers
as much as possible. The review concentrates on the performance of
structures subjected to near-source, strong ground motions from low-to-
moderate size earthquakes. It also emphasizes the structural performance
of those structures located in close proximity to recorded motion. For
completeness and comparisons sake, the review includes data from larger-
size earthquakes and for structures located at more distant ranges. In
all cases, structures which had dynamic response characteristics similar
to those of nuclear power plant structures were sought.

The review addresses and documents in detail the performance of
a wide variety of structure-types subjected to strong motion from ten
different earthquakes. The damage noted in 18 additional earthquakes is
addressed in brief. Table A-1 lists all of the earthquakes reviewed and
structure-types reported. Table A-2 provides additional details on these
earthquakes and distance to pertinent structures. The earthquakes cover
a wide Richter magnitude range, 2.7 to 8.3. The majority fall in the low-
to-moderate range of 4.5 to 6.5. Essentially, all structures discussed
are located near-source and thus, were subjected to high accelerations.

The performance of a wide range of structure-types is noted and includes residential, commercial, and industrial buildings. Discussed, for example, are older to newer structures; low-rise to high-rise buildings; office buildings; mobile homes and office trailers; private and commercial housing; schools; bridges; and general commercial buildings. Industrial facility structures include those associated with refineries, steam plants, pumping stations, cycling plants, water tanks (elevated and ground level), a research/experimental laboratory, a thermal plant, steel stacks, hydro/geothermal plants, and nuclear power plants. The review focused on the performance of engineered structures where attempts were made to reconcile predicted response behavior with actual observed behavior.

Earthquake design considerations of the reported structures covered a wide range. On the one extreme, there were structures which incorporated the latest concepts in earthquake resistance design. Such structures employed good provisions for accommodating both lateral and vertical earthquake forces, had good load-carrying continuity between major structural elements (e.g., beams, floors, walls, etc.), were well-anchored to well-designed foundations, were designed to be flexible, and had good energy absorbing capacity. Well-designed structures were built under quality control guidelines. Schools, hospitals, and nuclear power plants have even more strict earthquake provisions placed on them than conventional facilities designed to the Uniform Building Code. At the other extreme, many reported structures did not incorporate any earthquake design provisions, lacked any structural continuity between major load-carrying members, and had few or no quality control or quality assurance requirements.

A detailed study of the El Centro Plant subjected to the 1979 Imperial Valley earthquake was conducted for this project. This plant was designed for a horizontal force coefficient of 0.2 and was subjected to actual earthquake ground motion estimated to be about 0.5g and experienced no significant structural damage. It was also a case in

which building drawings as well as measured ground motion close to the
site was available. The results of the El Centro Steam Plant evaluation
are summarized in Section A.3.5 and presented in detail in Appendix E.

A.2   ASSESSMENT PROCEDURE

The following is a brief description of the assessment procedure
employed to meet the review objectives. For each earthquake, the litera-
ture was reviewed to identify structures that were subjected to strong
ground shaking and whose observed structural performance is reported.
The structure's capacity was then established by defining the earthquake
force level associated with the onset of structural damage and/or the
force level associated with the onset of collapse. At the lower capacity
level, one would expect only minor yielding and inelastic behavior of
structural members. At the higher capacity level, one would expect sig-
nificant damage, yielding and inelastic behavior. Next, the earthquake
force level in the structure was estimated by means of an elastic response
analysis using either recorded or estimated ground motion to define the
structure input. The estimated force level was then compared with the
structure's capacity in order to predict performance. This final compar-
ison was employed to assess how well the predicted structural performance,
using elastic structural analysis methods based on elastic response spec-
tra and peak accelerations from recorded motion, correlated with actual
observed behavior.

Most published observations of performance focus on conventional
structures designed to Uniform Building Code (UBC) provisions. For such
structures, the expected performance can be expressed as a function of
code design level. For example, past observations suggest that on the
average, a properly designed structure should survive major shaking to
earthquake force levels more than 4 to 6 times design values. Under such
force levels, the structure can be expected to behave inelastically,
exhibiting large, plastic deformations and some structural damage, but
without collapse. At force levels at about 2 to 3 times code design
levels, onset of yielding can be expected with some inelastic behavior but
only minor structural damage.

Figure A-1 taken from Reference A-60, gives an example of observed data from the 1971 San Fernando earthquake for multi-story reinforced concrete structures constructed since 1964. The figure supports the above capacity level of 2 to 3 times code design levels for the onset of damage. The authors suggest that margin of safety against collapse of these structures was not tested by the San Fernando earthquake, but the data suggests that responses equivalent to five or more times design base shear could have been resisted without collapse, though severe damage would probably have resulted.

A.3   RESULTS OF REVIEW

Over 150 papers (listed at the end of this Appendix) have been reviewed; most of which describe the nature of structural damage resulting from past earthquakes. Based on information presented in these papers, the performance of structures during ten different earthquakes is reported in more detail. Published data from the other earthquakes is generally too limited to draw significant conclusions. Table A-1 lists the earthquakes chronologically and identifies the types of structures which are discussed along with cited references. Other earthquakes investigated but not discussed in any detail are the 1933 Long Beach, 1949 Olympia (A-140, A-152, A-155)*, 1964 Alaska (A-55), 1967 Caracas, Venezuela (A-110, A-148), 1974 Lima Peru (A-65, A-146), 1976 Friuli, Italy (A-80, A-145) 1977 Romania, 1980 Mammoth Lakes (A-156) and 1980 Trinidad-Offshore (Eureka) (A-123, A-124).

For each of the cases presented, a brief description of the size and location of the earthquake and the general extent of strong ground shaking is first included. Next, the types of affected structures are identified and the level of ground motion to which they were subjected is estimated. The actual performance of the structures is then described and compared with that which would be predicted using elastic dynamic analysis procedures.

---

*   Numbers in parentheses refer to the Research Bibliography reference number.

A.3.1   San Fernando, California Earthquake, 1971 (A-58, A-60, A-66, A-67, A-76, A-84, A-87, A-157, A-159, A-162, A-163)

The San Fernando earthquake occurred on February 9, 1971 at the northern edge of the Los Angeles metropolitan area. The earthquake was of moderate magnitude (M_L = 6.4, M_S = 6.6). Its hypocenter was located at the southern edge of the San Gabriel Mountains at a depth of 8.4 km. The focal mechanism for the San Fernando fault consists of thrust with a significant left-lateral movement along a fault dipping north-northeast at an angle between 35° and 50°. The aftershock locations indicate that rupture was limited to a disc-shaped region approximately 20 km across. The rupture extended to the surface along an irregular fault zone.

The San Fernando earthquake occurred near the center of the largest concentration of strong motion recording instruments in the world. As a result, more usable strong-motion accelerometers were recorded than from all previous earthquakes combined. The highest ground motion was 1.2g horizontal motion recorded on the Pacoima Dam abutment located on the upthrust block 8 km from the epicenter. Peak horizontal accelerations from 0.15 to 0.40g were recorded in the area surrounding the fault rupture. Strong motion lasted some 12 seconds. The majority of the recordings were obtained in the Los Angeles area approximately 30 km to the south of the rupture zone. Many of these instruments were installed at various levels of high-rise buildings. The site conditions at the recording stations range from crystalline basement rocks to the north and east through older sedimentary rocks to deep deposits of unconsolidated and consolidated alluvium in the valleys to the south. The majority of the recordings obtained in the Los Angeles area are from buildings founded on thick, Pliocene deposits.

Modified Mercalli (MM) intensities ranging from VIII to XI occurred in a 190 square mile area in the region surrounding the fault rupture. Extensive damage to residential buildings, streets and utilities occurred along the zone of surface faulting. Two hospitals suffered major collapses due to ground shaking. Forty-nine people were

killed in the collapse of older, unreinforced masonry buildings at the San Fernando Veterans Administration Hospital and three additional people were killed (2 due to to life support failure; 1 due to structural failure) in a modern reinforced concrete hospital. Severe damage to other residential and commerical buildings and highway bridges occurred in this area. Major landslides were caused by ground shaking, including the near failure of the Lower Van Norman Dam and severe damage to the Upper Van Norman Dam.

Outside of the immediate area of strongest shaking, damage was mainly restricted to older structures. Most of the urban areas were constructed since 1933 when the first earthquake design requirements were incorporated into the local building codes and most modern buildings performed well.

Although only of moderate size, the earthquake provided a real test for many types of building structures. Many engineering studies were conducted of earthquake-resistant structures to determine the adequacy of present design criteria. These studies included (a) tall buildings that contained three strong-motion instruments (b) major structures in the heavily shaken areas, most which happened to be medical facilities (c) modern one-story industrial and commercial structures, (d) public schools because these represented both non-earthquake and earthquake resistant designs and (e) some old, unreinforced masonry structures (e.g., the Veterans Administration Hospitals).

The majority of the structures studied (except for tall buildings in downtown Los Angeles) suffered moderate to severe damage and even collapse. Engineering studies focused on damaged structures rather than undamaged structures subjected to strong motions. The discussion included herein of Building 41 of the Veterans Administration Hospital complex is an exception.

<u>Veterans Administration Hospital Building 41</u> - The Veterans
Administration Hospital Buildings 41 and 43 provide what is probably the
best example in the San Fernando earthquake of structures designed to
resist nominal loads, yet surviving intense shaking and suffering only
minor structural damage. A study (A-163) was conducted of Building 41 to
reconcile the observed behavior with the level of strong shaking experi-
enced during the earthquake.

Building 41 and the Olive View Hospital (which was severely
damaged) were located near the major surface faulting and about 1-1/4
miles southwest of the Pacoima Dam where peak accelerations over 1g were
recorded. Other buildings at the Veterans Administration site, which
accounted for most of the earthquake's casualties, were not designed to
resist earthquakes.

There were no actual strong-motion accelerometers in the vicinity
of the building site and thus, it is impossible to reconstruct the high-
frequency components of the ground motion which are important towards the
response of the building. The range of peak acceleration values measured
or inferred from nearby sites is rather wide; 0.5g to 1.2g. Moreover,
the peak acceleration is not as important as the frequency content of the
record in the range of structural frequencies. Reasonable estimates of
spectral amplitudes in the period range of interest are 0.7g to 1.5g.

Building 41 was designed in 1937 and built in 1938. It was four
stories high, about 51 x 200 feet in plan with a centrally-located
penthouse. The vertical and lateral load-carrying system consisted mainly
of reinforced concrete shear walls supported on spread footings. There
were six shear walls in the transverse direction and three longitudinal
walls. Due to the sloping terrain, the ground story (or basement) was
half-buried on the north side, whereas, it was nearly on grade on the
south elevation. The basement floor slabs were cast on grade, and, as
such, were not load-carrying. The other three floor slabs and the roof
slabs were ribbed. These slabs were supported on beams spanning between
columns and bearing walls. The building had structural symmetry.

The building was designed for a lateral load coefficient of approximately 10 percent its weight (at working stresses). The UBC code in force today would lead to a base shear coefficient of 0.28.

In view of the apparent strength of the longitudinal walls, the study focused on the transverse response only. The lateral load capacity was first estimated on the basis of conventional code (current) oriented procedures. The results indicated that with a fixed base, the structure could resist lateral loads implied by a lateral load coefficient of about 0.4g; the limiting factor being the tensile strength of concrete in the walls.

A complete three-dimensional model of the entire structure was dynamically analyzed for a flat acceleration spectrum. The most important result from the analysis was that the inferred level of ground acceleration as indicated by a spectral acceleration of about 0.5g is still quite low compared with credible lower bound estimates of the spectral acceleration to which this building was subjected. This implies that the structure had a capacity significantly in excess of that revealed by the fixed-base elastic analysis. Considering linear soil-structure interaction in the analysis does not necessarily lower the level of internal forces in the structure compared with the fixed-base analysis (i.e., spectral acceleration may rise steeply with increasing period even though damping is increased. Thus, a nonlinear soil-structure interaction analysis was performed to help resolve the discrepancy between observed behavior and capacity estimates.

The need for a nonlinear analysis stemmed mainly from the fact that at relatively low levels of excitation, partial uplift of the structure was already suggested. The reduced contact area between the base and the soil leads to lowering the rocking and lateral rigidities of the foundation, and with increasing separation, may lead to partial yielding of the soil. A two-dimensional analysis was conducted using the 1971 Pacoima Dam (S16E) and the Holiday Inn (Orion Blvd., N00W) records

normalized to a 0.5g peak acceleration. This level is compatible with the lower estimates of ground motion at the site. Both records gave a base shear of approximately 0.9g.

The results clearly show that nonlinear soil-structure interaction effects lead to lower shear forces and moments and to higher compressive axial forces in the concrete walls. All these effects tend to increase the ability of the structure to survive strong shaking. The key to the successful response of the buildings was found to be in the combined effects of two factors: (a) the large strength built into the structure attained through proper detailing and (b) the beneficial effects of nonlinear soil-structure interaction.

Earthquake forces based on linear elastic analysis estimate forces greater than 10 times design or at least 3 times the estimated capacity. At such force levels, yielding and inelastic response behavior leading to severe damage would be predicted. The actual performance of the building was one of essentially no damage. Therefore, the linear analysis overestimated the actual earthquake forces by a significant amount.

Thus, VA Building 41 represents a structure which, at linear elastic calculated forces of at least 3 times the estimated capacities, experienced essentially no damage.

High-Rise Buildings - There were 66 high-rise buildings in the major Los Angeles area that were instrumented with strong-motion accelerometers at the time of the February 9, San Fernando earthquake. Engineering studies were conducted and are reported on 11 of these buildings (A-60). All had three strong-motion instruments and were designed by applicable building codes. Study results were used to review earthquake design procedures and evaluate actual safety factors in the minimum design requirements specified by the building code.

The buildings are the Sheraton-Universal Hotel, Bank of
California, two Holiday Inns, Bunker Hill Tower, KB Valley Center, Muir
Medical Center, Kajima International Building, Certified Life Building,
Union Bank (Los Angeles), and 1901 Avenue of the Stars Building. All of
the buildings were located 13 to 26 miles from the epicenter.

The buildings ranged from 7 to 42 stories in height. Construc-
tion materials were either reinforced concrete or structural steel.
Lateral force systems employed ductile moment resisting frames, moment-
resisting frames, flat slab and parameter frame, ductile frame (tube
system), shear wall, and X-braced frame.

Fundamental periods of the buildings ranged from 0.7 seconds to
over 4.0 seconds. Design base shear values varied from 2.6 to 7.3 percent
of gravity. Peak record ground acceleration values at the different
building sites ranged from 10 to 26 percent gravity.

All of the 11 buildings experienced calculated force levels
greater than code design values. For the Sheraton-Universal Hotel, KB
Valley Center, Union Bank, Muir Medical Center, Kajima International
Building, Certified Life Building and the 1901 Avenue of Stars Building,
dynamic elastic analyses using the recorded ground motion would predict
forces from about 1 to 2 times their design levels. Even so, no damage
was observed. For the Bunker Hill Tower and the Bank of California
building, calculated forces were 2.5 to 3.0 times their design loads and
therefore, some yielding, inelastic behavior and minor strutural damage
might be expected. However, no significant structural damage was
observed in these buildings. Minor damage to structural elements was
observed in the form of cracking and spalling of concrete and local
yielding of reinforcement. The structural response of the Bunker Hill
Tower was nonlinear and could not be described or modeled very well by
linear-elastic dynamic analysis techniques. The analysis of the two
Holiday Inns indicated earthquake force levels 4 to 5 times design
values. Thus, predicted performance would suggest significant yielding,
inelastic behavior and structural damage. Beam and slabs would be

expected to yield and columns to remain within elastic limits. Observations did show signs of beam yielding and substantial nonstructural damage. No serious column damage was observed. Beam damage was less severe than would be predicted from the calculated forces.

Thus, for these 11 high-rise buildings, no damage was observed at elastic calculated forces up to 2 times their design levels. Only minor cracking, concrete spalling, and reinforcement yielding was observed for elastic calculated forces up to 3 times the design levels. Structural yielding and substantial nonstructural damage was observed at elastic calculated forces 5 times design, but without significant structural damage.

Olive View Hospital (A-162) - An extensive field and analytical investigation of the structural performance of the main building of the Olive View Hospital Medical Treatment and Care Facility was conducted. This modern, engineered building suffered such severe structural and nonstructural damages that it had to be demolished after the earthquake. The observed structural damages were compared with those predicted by elastic and nonlinear dynamic analysis.

The main building was a relatively massive, 6-story reinforced concrete structure. The building's ground story was considerably larger in plan than the upper five stories; approximately 1/3 of the building's total weight was concentrated at the first floor. The upper portion consisted of four rectangular structures connected to each other at right angles and enclosing an open courtyard. A stairtower appendage was located at the end of each wing.

The entire Olive View Medical Center was designed according to the provision of the 1964 UBC for a lateral base shear of approximately 8 percent gravity. The main building had a complex structural system incorporating a wide variety of structual elements. The primary vertical load-carrying system used in the building consisted of columns and flat slabs with drop panels.

Two different types of lateral load-resisting structural systems were used. In the upper four stories, numerous shear walls were provided to resist lateral loads. These walls, however, did not extend through the first and ground stories, so that the slabs and columns of the lower two stories formed a relatively flexible, moment-resisting space frame.

Essentially all observed damage is attributed to ground shaking (i.e., none due to permanent ground displacements). No ground motion records were obtained near the building site. Several accelerograms were numerically simulated or taken from recordings obtained at other sites in order to perform the analyses. The Olive View facility was located about six miles southwest of the epicenter, a MM intensity of XI has been assigned to the site. According to Reference A-162, the duration of the severe ground motion in the general vicinity of the site was estimated to be about 8 seconds and the peak ground acceleration was estimated to be 0.65g. Acceleration time history used in the elastic analysis was the Pacoima Dam base rock motion normalized to 0.65g. The nonlinear dynamic analysis used several different acceleration time histories scaled to peak values ranging from 0.4g to 1.0g.

Damage to the building was particularly severe in the bottom two stories. Very large, permanent deformations were observed, including substantial inelastic deformation in slabs and columns, and the failure of numerous tied-columns. The tied-columns generally failed in shear, resulting in the collapse of three of the stairtowers and much of the single-story portion of the ground story. Interstory deformation in the upper stories were small due to the presence of the shear walls. In general, damage to upper stories was relatively minor.

Elastic analysis results were able to detect brittle failures of the tied-columns (when the results were compared with estimated shear capacities) and the concentration of deformation in the bottom two stories. However, identification of many of the details of the response, such as the severity and distribution of inelastic deformations, and the significant increase in lateral displacements when an inelastic mechanism formed, was not possible from the results of the various elastic analysis performed.

The inelastic analyses revealed that the building was designed to be very strong in comparison with building code specifications, but that for some members (notably, the tied-columns and flat slabs in the bottom two stories) the required inelastic deformations were larger than they could develop according to their detailing. The inelastic analyses also indicated that the relatively small strength and stiffness of the bottom two stories resulted in a partial sidesway collapse mechanism which concentrated drifts and inelastic deformations in these two stories. The displacements predicted by the inelastic analyses, although generally larger than those predicted by the elastic analyses, were smaller than the permanent displacements observed in the building. On the other hand, the inelastic response was found to be very sensitive to the ground motion record used, and, in particular, to records that contain severe, long-duration acceleration pulses.

Base shears of the building were calculated using elastic analysis with results indicating values at least 12 times design value. From such a large calculated base shear, one would generally predict total collapse of the main building particularly, when one considers the local concentration of nonlinearities at the bottom two stories. Maximum story shears were also calculated from nonlinear dynamic analyses for different ground acceleration time histories and found to be similar in magnitude despite of the fact that the time histories were scaled to peak acceleration values ranging from 0.4g to 1.0g. From nonlinear analysis, the base shear in the bottom two stories were calculated to be 4 times larger than the working stress levels used in the design of the building. The inelastic shears were significantly smaller than the story shear forces predicted using elastic methods. This base shear value of 4 times design appeared to be more compatible with the observed behavior, namely, significant damage, yielding and inelastic behavior resulting in near collapse.

Thus, the Olive View Hospital represents a case where elastic computed forces were at least 12 times their design values. Furthermore, nonlinearities were concentrated at the lower two stories. Very severe damage resulted.

Holy Cross Hospital - The Holy Cross Hospital was located in the area heavily shaken by the earthquake approximately nine miles from the epicenter. The main building has a 7-story tower, a 3-story wing to the north and 1-story wings to the east and west. A single-story basement was built under the main tower. The main framing of the 7-story tower consisted of concrete joists framed to beams or to walls along interior column lines and to spandrels on the exterior column lines. On the north and south exterior walls, spandrels were located on the inside edge of the columns. The 1-story and 3-story wings were of similar joist and beam construction for floors and roofs. The lateral force system consisted of concrete shear walls in each direction. As most shear walls were not continuous from top to bottom, reliance also was placed on the concrete floor joist and slab system acting as a diaphragm to transfer shears at points of discontinuity. The hospital was designed to a base shear of approximately 8 percent gravity.

Damage to the structural system of the main building was quite general, but more pronounced on the first 4 stories. The west shear walls were discontinuous below the second floor. The diaphragms were inadequate to redistribute horizontal loads on the 2nd, 3rd and 4th floors, and were damaged severely in this area. One of the west wall columns was shattered at the third floor. Each of the west shear wall elements exhibited cracking. The longitudinal shear walls had numerous X-pattern failures over door openings. Excessive nonelastic movement of shear walls produced deformations large enough to cause portions of the vertical load framing system to act as a moment frame so that columns were carrying earthquake shears and moments. Due to deformations in the transverse directions, the columns exhibited shear cracking. In the longitudinal direction, many exterior spandrels were crushed in flexural compression and the column covers were shattered.

There were no accelerometers in or near the Holy Cross Hospital complex. However, its location indicates that the ground shaking would be between the instrumental motion at the Pacoima Dam and at the Holiday

Inn on Orion Blvd. Peak ground acceleration at these sites were 1.2g and 0.25g, respectively. Using this information plus the observed performance of the building itself, a peak ground acceleration of 0.4g to 0.5g was estimated for the site (Reference A-67).

Calculated earthquake forces for the main building using an elastic model of the building indicate a base shear of approximately 0.55g. As with the Indian Hills Medical Center, response spectra of the Pacoima Dam (S74W) and the Holiday Inn, Orion Blvd. (NS) records were scaled to the peak ground acceleration estimates and were used to account for spectral amplification. In addition, ultimate capacities of several critical shear walls were computed in the main tower structure. These capacity calculations suggest a 15 percent gravity base shear would be associated with major cracking.

Elastic calculated earthquake forces were 3 to 4 times ultimate capacity and 6 to 8 times design. From such high forces, one would predict significant yielding, inelastic behavior, and structural damage. Although significant damage was observed, collapse was not imminent. The building met the basic intent of the code (i.e., no collapse under heavy shaking). The shattered columns gave indication that damage would have been greater had the high intensity of shaking occurred over a longer time interval.

Thus, the Holy Cross Hospital represents a case where significant damage, but no collapse occurred for elastic calculated forces 6 to 8 times design and 3 to 4 times ultimate capacity.

<u>Indian Hills Medical Center</u> - The Indian Hills Medical Center was located in the heavily shaken area, some nine miles from the epicenter. The building is a reinforced concrete structure of seven stories, about 80 x 170 feet in plan, with a complete load-carrying frame. Concrete beams run north and south across the building. Typical floor slabs span between girders. The exterior walls are light, curtain-wall

construction except where concrete shear walls are located. These shear walls are concentrated toward the ends of the building. The building was designed per the 1966 edition of the Los Angles code for a lateral base shear of 4.5 percent gravity.

Some damage to shear walls was observed as cracks forming at the horizontal construction joints of floor lines. There was evidence of slight horizontal movement although these cracks were not related directly to shear. The slabs, in some cases, also showed cracks. The ends of shear walls were designed as columns and thus, were subjected to both shear and axial loads. Concrete in the splice area crumbled. All shear walls in lower levels cracked in the typical X-pattern indicating high shear stress. Damage was noted at intersections of girders and walls.

No strong-motion records were available at the building site. However, based on the building location relative to the epicenter, the nearby buildings studied, and its own observed performance, the peak ground motion was estimated to be between 0.4 and 0.5g (Reference A-67).

A linear elastic dynamic analysis was conducted of the building to estimate earthquake forces. Time history motions considered were the Pacoima Dam (S74W) and the Holiday Inn, Orion Blvd. (NS) records scaled to the peak estimated acceleration for the site. This analysis, accounting for spectral effects, resulted in a calculated base shear of 35 percent gravity. In addition, ultimate capacities of several of the critical shear walls in compression, tension and shear were computed establishing an ultimate capacity limit of about 10 percent gravity or 2 times the design values.

Thus, elastic calculated earthquake forces are 3.5 times ultimate capacity and 7 times design. From such high forces, one would predict significant yielding, inelastic behavior, structural damage, and possibly the onset of collapse. However, observations suggest the building was not near collapse.

Medical Buildings Near Hansen Lake - Four medical buildings located near Hansen Lake were studied. These are the Foothill Medical Center, the Pacoima Lutheran Medical Center, the Golden State Community Mental Health Center and the Pacoima Memorial Lutheran Hospital. All are located about 8 to 9 miles from the earthquake epicenter and less than 1 mile south of the nearest fault break. There were no strong motion instruments at any of the building sites. However, peak ground motion is estimated to be about the same as that at Holy Cross Hospital and Indian Hills Medical Center (i.e., in the 0.4 to 0.5g range).

All four facilities were designed to a base shear of about 13 percent gravity. Except for the Golden State Center, all of the medical buildings included design and construction features not considered adequate under strict interpretation of the Los Angeles Building Code. These features were directly responsible for the type of damage observed in the structures. For example, a closer study of the Foothill Medical Center showed that a 7 percent gravity lateral load would be sufficient to cause the first failure of its bracing system.

The Golden State Center is considered to be properly designed in that it met the intent of the building code. Calculated forces (via elastic analysis and peak ground acceleration) would result in an earthquake force level perhaps 2 to 3 times the Golden State Center design value. One would, thus, predict onset of yielding, minor inelastic behavior, and negligible structural damage except at the location of improper design and construction features. This prediction is consistent with the observed performance.

Low-Rise Industrial and Commercial Buildings - The performance of fifteen low-rise industrial and commercial buildings were studied. Thirteen are one-story buildings with wood roof systems, one is a five-story monolithic concrete building, and one is a one-story building with precast concrete roof and walls. All fifteen buildings were located between 8 and 17 miles from the epicenter and were built since 1958. All were designed by applicable building codes. No recordings of the motion

at the building sites were made. Peak ground motion was estimated to have been between 20 and 40 percent gravity with most buildings subjected to 40 percent gravity (Reference A-67). Principal damage was due to heavy vibration although there was some permanent ground displacement. The lateral design forces for most buildings was about 13 percent of dead load. Calculated forces using elastic analysis procedure (i.e., response spectra anchored to the peak acceleration estimates) would suggest earthquake forces at least 3 to 6 times design. Thus, significant yielding, inelastic behavior, and significant damage would be predicted from the calculated loads. Observed performance varied from moderate damage to complete collapse of the structures. Much of the damage was the result of lack of continuity (i.e., strength capacity) between the wall and the roof systems. Several wall shear failures were caused by lack of ability to resist out-of-plane earthquake forces. Performance of the buildings was strongly influenced by their capacity for energy absorption and ductility.

Implications - The San Fernando earthquake subjected a variety of structures to ground accelerations that equaled or exceeded their design values. Many engineering analyses were performed to compare both calculated and actual responses. In those cases where an elastic analysis calculated base shear forces only moderately greater than the structures design values, good correlation was seen between predicted and observed behavior. Both predicted and actual performances of these structures ranged from no damage to moderate cracking and yielding of structural elements.

In those cases where an elastic analysis calculated base shear forces much greater than the structure's design value, the predicted extent of damage significantly exceeded observed response. Total collapse would be predicted for some structures, yet actual performance ranged from no damage (VA Building 41) to significant yielding and inelastic response (Olive View, Holy Cross, Indian Hills).

Inelastic analysis incorporating nonlinear material properties were performed on several structures in an effort to reconcile the differences between calculated elastic response and actual behavior. The inelastic analysis method produced lower base shear forces and gave a better correlation with observed structural performance.

In the absence of design or construction deficiencies which would result in reduced ductility or energy absorption capability, the following general observations could be made:

1. For the Veterans Administration Hospital Building #41, essentially no structural damage occurred even though the fixed base, linear elastic calculated forces exceeded design forces by a factor greater than 10 and exceeded the estimated ultimate capacities by a factor greater than 3. This structure was a stiff structure (similar to many nuclear power plant structures) subject to substantial nonlinear soil structure interaction effects. The beneficial effect of nonlinear soil-structure interaction effects and particularly good structural detailing have been judged to be responsible for the very good performance at high force levels.

2. High-rise buildings (not similar to nuclear power plants) tended to show no damage at elastic calculated force levels up to 2 times their design levels; minor structural damage at elastic calcuated forces up to 3 times design; and structural yielding and substantial non-structural damage but no substantial structural damage at elastic calculated forces 5 times design. It should be noted that the design capacity is based on working stress design and that the estimated actual ultimate capacity is generally about twice the design capacity. Thus, minor structural damage might be expected at 1.5 times the ultimate capacity, while no substantial structural damage would be expected at 2.5 times ultimate capacity. The Holy Cross Hospital showed significant structural damage but no collapse at elastic calculated forces 3 to 4 times the ultimate capacity. However, collapse is likely to have resulted if the duration of strong shaking had been longer.

3. Very significant structural damage occurred at the Olive View Hospital at elastic calculated forces greater than 12 times design. However, this damage was heavily influenced by the fact that nonlinear behavior was concentrated at the lower two floors as opposed to being spread uniformly throughout.

The San Fernando data illustrate the importance of designing adequate ductility into the structural system and the importance of not overdesigning the strength of a portion of the structure so as to concentrate the nonlinearities into localized "weak-link" regions. So long as these principles are observed, these data illustrates that the onset of significant structural damage should not occur at elastic calculated force levels less than 2.5 times the ultimate capacity for ground motion similar to that recorded for the San Fernando earthquake. Because of nonlinear soil-structure interaction, the actual performance might be substantially better than indicated by this 2.5 factor. These data clearly illustrate that elastic response cannot be correlated with damage unless the inelastic energy absorption capability (ductility) of properly designed structures is considered. The elastic computed response must be reduced by a factor of approximately 2.5 or greater if it is to be compared with the ultimate capacity for the purposes of predicting the onset of significant structural damage for a properly designed structure subjected to San Fernando type ground motion.

A.3.2   Managua, Nicaragua, Earthquake, 1972
         (A-26, A-30, A-40, A-42, A-111, A-112, A-113)

On December 23, 1972, a moderate magnitude earthquake (M_S = 6.2) occurred in Managua. Loss of life approached 10,000, approximately 57 percent of the city's 450,000 occupants were rendered homeless, property damages are estimated to be about $1 billion. The hypocenter of the main shock was located in an area approximately coinciding with downtown Managua at a depth of 2 to 8 kilometers. Only one accelerometer record was obtained at the ESSO refinery which was approximately 3 miles from the fault traces and the city of Managua. Peak recorded accelerations were 0.39g EW, 0.33g NS and 0.31g vertical.

From the results of seismoscope records throughout the city, observation of damage, and the estimated location of the hypocenter, it follows that the ground motion in central Managua was more intense than that recorded at the refinery. Peak accelerations have been estimated at

0.5 to 0.6g. A maximum MM intensity of nearly IX was estimated in the central downtown area where much damage was observed. Other areas of concentrated damage were the heavily populated northwestern part of the city and in the populated, industrial areas to the northeast. In the vicinity of the ESSO refinery, intensity values of V to VI were estimated.

Structures in Managua were predominantly one-to-two stories with some taller buildings up to eight stories in height. The type of construction in the city can be described according to height rather than function. Low-rise structures were dominated by taquezal type construction - adobe bricks filling a light timber framework. Suburban housing typically consisted of reinforced masonry or concrete walls with heavy reinforced concrete roof slabs. One-story factories and warehouses were also constructed in this manner. Taller structures consisted primarily of reinforced concrete. The range of actual base shear strength coefficients was wide. On one extreme were institutional buildings, heavy but with considerable wall area. At the other extreme were light, modern buildings.

Severe damage and collapse were generally confined to those structures with taquezal, concrete, and unreinforced masonry construction that lacked adequate lateral force resistance. These buildings are inherently quite weak and heavy enough to generate large lateral forces under earthquake shaking. There were examples of moment resisting unbraced frame structures for which the structure endured the earthquake without severe damage but experienced motions great enough to cause extensive property losses and loss of functionality. Shear wall frame buildings were much stiffer; the limited deformations resulted in very little property loss or loss of functionality. However, some of these showed sufficient structural damage to question their safety for an earthquake of equal intensity but longer duration.

A variety of industrial facilities were located in Managua. Damage to these facilities varied with distance from the fault, type of construction, and the extent to which earthquake-resistive details were engineered into their design.

ESSO Refinery - The ESSO Refinery was designed and built in two different stages in the mid 1950's and early 1960's. Plant structures include vertical vessels of various heights and slenderness, pumps, generators, heat exchangers, piping systems, tanks, foundations, etc. The design met requirements of the Uniform Building Code. All detailing reflected the U.S. design procedures in effect at the time of design. All equipment was tied to its foundation, piping systems were braced, etc. In 1968, a smaller earthquake caused some difficulties at the plant. Consequently, portions of the plant were redesigned to withstand a peak ground acceleration of 0.2g. On the average, however, the design base shear coefficient at the facility was about 0.10 to 0.13g.

The peak recorded acceleration at the site was 0.39g. The high amplitude portion of the motion lasted for about five seconds with a nominal acceleration value of about 0.2g. Ground motion of a long-period nature followed. Much of the equipment and low-height structures at the site have relatively high natural frequencies. The tall fractionating towers, reactors, and oil heaters are characterized by low frequencies. The nature of the ground shaking was such that most structures and equipment would see some response amplification over the ground acceleration. The peak ground acceleration was over 3 times the average design base shear coefficients. Considering spectral amplification, the elastic computed forces would be expected to have been at least 6 times the average design base shear and at least 3 times the yield capacity.

Damage at the refinery was minimal and limited primarly to grouted pads, concrete block walls, and some steel cross bracing. After performing analyses, Blume (A-26) noted that even when the earthquake demand on the plant was over three times yield capacity, damage was insignificant.

ENALUF Thermal Plant - The ENALUF facility is a three unit, oil-fired plant with a total capacity of 90 MW(e). At the site were modern turbine generators, a group of six diesel generators of approximtely 1 MW(e) each, a 138/69-KV transmission substation, a 69/13.8-KV distribution station and an indoor switching station. The plant was reportedly designed to a lateral force of 0.10g.

The ENALUF facility was located within 0.15 miles of the principal fault. A peak ground acceleration at the site was estimated at 0.6g - six times the design level. Any elastic analysis techniques based on the ground excitation would give calculated forces much greater than yield capacity. Significant yielding would be predicted.

Overall damage to the plant was slight. Some of the worst damage occurred to unanchored equipment which was free to displace or fall. Equipment attached to the floor was not affected by the earthquake. Piping throughout the plant struck platforms or equipment. Usually, the pipe's lagging and thermal insulation were crushed, but the pipe itself was undamaged.

Implications - Both the ESSO Refinery and the ENALUF thermal plant provides examples of engineered structures subjected to strong ground shaking. Calculated earthquake forces based on ground accelerations would far exceed estimated capacities (by factors of 3 to 6 or more). Again, elastic analysis without accounting for the inelastic energy absorption capability would result in a poor correlation between predicted and observed structural performance.

A.3.3   Kern County, California Earthquake, 1952
          (A-32, A-137, A-138, A-139, A-140)
          The Kern County area of California was subjected to strong ground shaking from the major July 21, 1952 Kern County (Arvin-Tehachapi) earthquake (M_L = 7.2, M_S = 7.7) and a series of related earthquakes and aftershocks that followed. The epicenter was located about 26 miles

south of Bakersfield and 4 miles west of Wheeler Ridge. The shock was felt over 160,000 square miles. Another strong shock, August 22, 1952, had a more local effect. It caused considerable damage to Bakersfield and immediate vicinity and was felt over 40,000 square miles.

There were no strong motion accelerometer stations in the central area to record the ground motion. The nearest station was at Taft about 25 miles from the fault rupture. The maximum peak acceleration was 0.20g. Strong motion (>0.1g) lasted more than 12 seconds. The instrument site has been assigned a MM intensity of VII. In areas of higher intense shaking (MM intensity VIII and IX), closer to the fault rupture, the ground motion is estimated to be significantly greater than 0.20g.

The earthquake occurred near a populated area. Consequently, a large variety of residential, public, commercial and industrial structures were affected. Construction material used in these structures included wood, both reinforced and unreinforced masonry and concrete, and steel. In general, damage to buildings, elevated water tanks, and other structures followed the pattern that structures performed well when earthquake provisions were incorporated in their design. Poorly designed and constructed buildings were the first to suffer severe damage or collapse.

Relatively few wood frame structures were seriously damaged. Those that were heavily damaged were thrown off foundations because of a lack of bracing or sufficient bolting to foundation walls. In the region of strongest shaking, unreinforced brick, concrete block and adobe structures were severely damaged; however, the performance of reinforced concrete block and reinforced, grouted brick was good. Small steel structures such as gasoline stations suffered no damage, although some high-rise steel structures suffered minor damage.

There were several refineries subjected to strong shaking. The overall behavior of refineries was good and damage was slight. This can be attributed to the general use of steel piping and good anchorage of

equipment. Most piping breaks occurred due to lack of flexibility or use of cast iron. Breakage in steel underground piping was limited to a few cases in very poor soil.

Kern County Steam Plant - The Kern County Steam Plant was built in 1947-48 and has a capacity of 175 MW in two units. The principal building is constructed of steel frames and concrete walls. The plant building and associated equipment represent a wide range of fundamental frequencies. All structures within the plant were designed for a lateral force of 20 percent gravity. For this design level, the onset of yielding is estimated at base shears of 40 to 60 percent of its weight.

This plant is located about 15 miles from the fault rupture. At this location, peak ground motion was estimated to be between 0.3 and 0.4g. The fundamental frequencies of the plant structures should cover a wide range. Estimated earthquake forces using elastic response (spectrum) analysis should result in some plant structures having a calculated force of at least two to three times greater than the above estimated yield levels. Yielding of major structural elements in the plant would then be predicted. However, damage to the buildings was negligible suggesting that if an elastic analysis had been used to calculate earthquake forces, the loads would have been significantly overestimated.

Elevated Water Tanks - A water tank at the Maricopa Seed Farms, 100,000 gallons in capacity and 100 feet in height, was subject to strong shaking estimated to be about 0.25 to 0.3g. This tank was located about 20 miles from the fault rupture. The tank was designed to a value of 0.1g. Even ignoring possible spectral amplification elastic analysis would result in calculated forces in the tank far greater than its design capacity. Significant damage would be predicted; yet, none occurred. A similar tank at nearby Di Giorgio Farms, designed to 0.12g and subjected to strong shaking also suffered little damage. For both tanks, elastic analysis would overestimate earthquake forces actually seen by the structures.

Implications - The overall performance of structures during this earthquake points to the importance of energy absorption and ductility in the response behavor of structures (e.g., brittle structures suffered the greatest damage). The observed performance of the Kern County steam Plant and elevated tanks show that calculated earthquake forces based on elastic analysis overestimate actual forces. Thus, their predicted performance did not correlate with observed behavior.

A.3.4   Santa Barbara, California Earthquake, 1978
         (A-64, A-119, A-120, A-160)

A moderate earthquake (M_L = 5.1, M_S = 5.6) struck the Santa Barbara-Goleta area on August 13, 1978. The earthquake was centered in the Santa Barbara Channel, 5 to 8km south of downtown Santa Barbara. The resulting ground motion displayed a marked directional asymmetry which had an important bearing on overall effects of the earthquake. This asymmetry caused the most intense ground motion in the Goleta area even though Santa Barbara is closer to the epicenter. A maximum MM intensity of VII is reported near the University of California Santa Barbara (UCSB) campus located in Goleta. The focal depth was estimated at about 13km. The fracture apparently propagated from the epicenter laterally west-northwest toward Goleta for a rupture length of about 8km with a terminus about 4km from the UCSB campus.

Several strong motion accelerometers recorded the ground motion. In Santa Barbara, strong motion was recorded at the base of the Freitas Building and also the Santa Barbara Courthouse. A peak value of 0.23g was recorded. A Goleta Substation of the Southern California Edison Company recorded 0.29g. Two recordings were made on the UCSB campus near Building 340 and at the base of North Hall. The recorded acceleration at North Hall had a peak value of 0.42g. Duration of strongest shaking was about 2 to 3 seconds.

As would generally be expected because of the more severe
shaking, structures in Goleta suffered more damage than those in Santa
Barbara. Most of the major structures located in Goleta are on or near
the UCSB campus. These included a number of reinforced concrete shear
wall buildings up to 8 stories in height located on the campus, several
large steel frame hangars and a control tower at the adjacent municipal
airport, a pair of high-rise reinforced concrete shear wall dormitories
west of campus, and a number of long low-rise (1-3 stories) commercial
buildings north of campus. The major remaining buildings in the Goleta
area consist of conventional 1-3 story wood frame apartment buildings and
duplexes located in the area west of campus. Finally, there are several
mobile home parks in the area located east, north and west of campus.
Except for a few old wood frame and adobe structures (mostly farm houses)
the buildings in Goleta are relatively modern. The majority have been
constructed within the last 20 to 30 years.

Several of the multi-story, reinforced concrete buildings on the
UCSB campus received moderate diagonal cracking of shear walls in the
lower stories. Some of the roof-top mechanical equipment were severely
affected, and instruments and supplies were destroyed in some
laboratories. Damage to light fixtures, ceilings, and plaster occurred
throughout the campus. The total earthquake damage to structures and
buildings on the UCSB campus was estimated at $3.4 million. Of this
total, only approximately $300,000 was attributed to structural damage.

Just north of the UCSB campus there are nearly 100 buildings.
The buildings comprise a mixture of hangars and single story office
service buildings. The majority of the buildings are wooden and of World
War II vintage. Most of the damage was architectural. The most notable
structural damage was limited to two hangars and the airport control
tower. Both are steel frame structures. They suffered permanent
deformations. With these exceptions., the remaining structural damage
consisted of cracked concrete floor slabs in two buildings and shifted
wood columns in one of them. There was essentially no damage to

electrical service facilities. Structures in the Santa Barbara area display a wider variation of architecture, and construction than those in Goleta. However, damage to these structures was comparatively minor.

North Hall (UCSB) - North Hall is a rectangular three-story reinforced concrete shear wall structure originally built with a deficiency in its lateral resistance. Thus, concrete shear walls were added to make the structure meet the 1976 edition of the Uniform Building Code. As previously indicated, the building was instrumented with strong-motion accelerometers during the earthquake. The base acceleration in the transverse direction was about .40g. There was also another intrument which measured approximately .65g on the third floor, and the roof record reached 1g. These motions imply a base shear of 50 to 70 percent of the weight of the structure; yet the damage to the building consisted only of light-to-moderate X-cracking in the concrete shear walls.

Implications - Although the level of ground shaking was quite high, little structural damage occurred to engineered structures. Performance predictions based on earthquake forces levels from elastic analysis would have predicted much greater damage. In particular, calculated earthquake forces at North Hall based on the measured acceleration would clearly have predicted damage, yet none was observed.

Secondly, the damage was less at Goleta for 0.25 to 0.45g ground accelerations than occurred in San Fernando within these same ground acceleration regions. Thus, the inelastic energy absorption effects indicated by the San Fernando data, would have to be even greater at Goleta to account for the small amount of observed damage. In other words, the shorter duration Goleta records resulted in less damage than the longer duration San Fernando records, for the same ground acceleration.

A.3.5   Imperial Valley, California, Earthquake, 1979
         (A-35, A-36, A-37, A-38, A-125, A-127, A-128, A-129)

On October 15, 1979, a moderate earthquake (M_L = 6.6, M_S = 6.9) shook the Imperial Valley of California. The central region of Imperial Valley extending from Brawley to Calexico is estimated to have had ground motion associated with a maximum MM VII. The distribution of strong ground shaking was about the same in El Centro, Imperial, Calexico, and Brawley, the four communities most affected by the earthquake.

The area was well instrumented by a network of strong-motion accelerometers. In several instances, peak vertical accelerations were considerably higher than horizontal acceleration values (for example, at Station No. 2, a 1.74g vertical acceleration was recorded). The maximum peak recorded horizontal acceleration was 0.81g at Bonds Corners which is located about 2km from the epicenter and causative fault. El Centro experienced ground motion in the 0.2 to 0.5g range, Imperial Valley College 0.52g, Brawley 0.22g, Holtville 0.26 and Calexico 0.28. Station No. 9 in El Centro is the same location where the 1940 El Centro record was taken. It is 6km west of the Imperial Fault and also 1km from the El Centro Steam Plant. Peak accelerations were 0.40g NS, 0.27g EW, and 0.38 vertical. About 0.83km SE of the plant another strong-motion instrument recorded 0.51g NS, 0.37g EW and 0.93 vertical. With only a few exceptions, particularly that at Bonds Corners, the duration of strong shaking (i.e., greater than 0.1g) was very short. Bonds Corners strong shaking lasted about 13 seconds.

Earthquake damage and effects in the Imperial Valley varied greatly in their occurrence and distribution. The damage consisted of partially collapsed unreinforced brick walls; cracked cornices, parapets and gables; a few damaged chimneys; display windows broken or shattered; plaster cracked and fallen; sections of suspended ceiling tiles displaced or fallen; shelves, and considerable quantities of glassware, dishes, and small objects fallen and broken.

Wood frame stucco dwellings, some as close as 30 to 150 meters from the fault rupture had very minor damage. The most heavily damaged modern building was the Imperial County Services Building in El Centro, a six-story reinforced concrete frame shear wall structures designed under the 1967 provisions of the UBC. Excluding this building, the most severe damage in Brawley, Calexico, El Centro, and Imperial was to low-rise unreinforced brick buildings and to a few low-rise reinforced concrete frame buildings constructed before the 1940 El Centro earthquake.

The Imperial Valley College had a recording of 0.52g. The majority of buildings on campus are low, one-story structures with reinforced concrete block walls and metal deck roofs. Buildings are of recent construction, probably less than 10 years old. Structural damage was minor and typical of damage observed in previous earthquakes.

There was some elevated water storage tanks in or near the cities of Brawley, Imperial, El Centro and Calexico. Most experienced no damage. Two suffered minor to moderate damage in the form of buckled braces and torn gusset plates; one tank collapsed and ruptured. Ground supported steel storage tanks, in general, performed very well except for those with height to diameter ratios greater than one. As these tanks were not anchored down, they rocked and lifted off their foundation pads resulting in seam ruptures, piping failures, and compression buckling.

Imperial County Services Building - Although the intensity of shaking in El Centro was VII, the Imperial County Services Building was assigned an intensity IX. Completed in 1971, the six-story reinforced concrete frame and shear-wall structure was designed per UBC (probably for a base shear of about 13 percent gravity). Although severely damaged, the building did not collapse but was subsequently demolished because of the earthquake damage. The major damage to the building was the failure of the four reinforced concrete support columns on the east side of the building. The concrete at the base of the columns on one side of the building was shattered and the vertical reinforced beams were severely bent. The partial collapse of the support columns allowed

the eastern extremity of the building to sag about 1 foot. In the upper
levels of the building, the south exterior wall was extensively cracked
near the window frames. Also, there was partial separation between
floors, walls, and ceilings; fallen suspended ceiling tiles; damage to
interior walls; and office furniture shifted or overturned. A shear wall
system was used to resist NS motion and a frame system used for EW
forces. At the east and west ends of the building above the second
floor, the exterior consisted of reinforced concrete shear walls. The
ground story had four walls resisting NS forces. The second floor slabs
transferred shear forces from the end walls in the second story to
interior walls in the ground story. A thicker slab at the second floor
was used to aid the shear transfer. The foundation consisted of pile
caps resting on tapered piles.

Sixteen acceleration records were obtained at the building
site. Three were free-field. Peak ground accelerations were 0.29g NS
and 0.32g EW. Motion measurements indicated building periods were 0.62
seconds in the EW direction, 0.44 seconds in the NS direction and a
torsion mode period at 0.35 seconds. Much inelastic behavior was also
noted. Peak measured roof acceleration was 0.48g EW.

El Centro Steam Plant (See Appendix E) - The El Centro Steam
Plant is located in the northeast portion of El Centro, about 25km from
the epicenter and 5km from the causative fault for the 1979 earthquake.
The NS component of the acceleration record from USGS recording station
5165 which was located less than 1km from the steam plant had a peak
recorded acceleration of 0.49g NS. In spite of the high ground
accelerations at the plant site, no significant structural damage
occurred to the plant.

The El Centro Steam Plant has four units that burn oil or
natural gas. Units 1, 2, and 3 were designed by Gibbs and Hill and built
in 1949, 1952 and 1957, respectively. Unit 4, the newest and largest
with a 80-MW electric output, was designed by Fluor corporation, Ltd.,

and built in 1968. Combined output of all four units is 174 MW. Each
unit of the plant is structurally independent and contains three struc-
tures: a turbine building, a turbine pedestal and a boiler structure.
Soil at the site consists of very deep alluvial deposits composed of
stiff to hard clays interlain with laminations of silty clay loam.

Units 3 and 4 were operating when the earthquake occurred.
Units 1 and 2 were down for maintenance. The operating units tripped off
line when station power was lost. Unit 3 was restored to service within
15 minutes after the main shock. Unit 4 was restored to service within
two hours. Several of the references cited report the detailed earth-
quake effects on the plants. In general, only minor damage was observed.
There was a great deal of motion at the site, and various traces of the
motion were observable, e.g., skid marks of reheater feet, bent seismic
stops, etc. There were some equipment failures; leaks occurred in the
water supply for the hydrogen coolers; a two-inch pipe failed; a buckling
failure occurred in an oil storage tank; old wooden forced draft cooling
towers sustained damage to the wooden structure; and a lightning arrester
broke off a transformer. Structural damage was limited to buckling of
bracing members in the boiler structures.

The seismic design basis of Units 1, 2 and 3 is unknown. Review
of the project specifications for Unit 4 indicates that the steel framing
was designed for a lateral static equivalent seismic loading of 0.2g
(dead and live loads). The Unit 4 turbine building is a moment-resisting
steel frame with reinforced concrete shear walls on 3 sides. The boiler
structure is a braced steel frame while the turbine pedestal is a rein-
forced concrete frame that supports the turbine generator. The pedestal
shares a box-girder foundation with the turbine building and boiler
structure.

Analyses of Unit 4 of the steam plant have been reported in
References A-37 and A-128. Both analyses of the Unit 4 structure were not
conducted for the expressed purpose of correlating predicted structural

damage with observed structural damage. The analysis presented in Reference A-37 was conducted for the purpose of estimating equipment response levels, thus, the structural model was greatly simplified. The analysis presented in Reference A-128 utilized a general three-dimensional representation of the Unit 4 structure, but considered the foundation to be fixed-base, thus, ignoring soil-structure interaction effects. It should be noted that the purpose of the analysis conducted in Reference A-128 was to demonstrate that a particular set of conservative design criteria would yield analysis results which would greatly overpredict the observed structural response levels of the Unit 4 structure.

Since portions of the Unit 4 structure were designed for a static 0.2g lateral force and yet the observed damage for a recorded ground motion, characterized by a 0.5g peak acceleration, was slight, the Unit 4 structure was selected to be investigated in detail as part of this study. This investigation is described in Appendix E. In general, the results of this study indicate that the concrete shear walls, which were not considered as part of the design lateral force system, actually carried much of the lateral force. Thus because of the presence of these shear walls, the basic response of the turbine building remained within code limits for the 0.5g ground motion due to the participation of these walls in the overall lateral response. However, there were local regions in which the calculated seismic response of the turbine building steel frame was nearly double the plastic moment capacity and in which horizontal diagonal bracing members exceeded yield by a factor of 4 due to the lack of effective diaphragms in some regions. In the boiler structure, elastically calculated seismic response would also indicate more damage than was actually observed. For members damaged during the earthquake, the ratio of calculated seismic response to ultimate capacity is 4.0 or greater. For the members with no observed buckling following the earthquake, the ratio of calculated seismic response to ultimate capacity is 4.9 or less. Hence, it may be concluded that for the Imperial Valley earthquake and the steam plant structure, the onset of significant structural damage should not occur at elastically calculated force levels less than about 4 times the code specified ultimate capacity. The

investigation of the El Centro Steam Plant demonstrates that the plant had significantly more capacity than the design level of 0.2g due to the additional turbine building shear walls as well as other factors such that it may be concluded that seismic capacity cannot be directly inferred from the design level earthquake acceleration. In addition, this investigation also demonstrates that elastic analyses using instrumental earthquake ground motion predicts much more damage than actually occurs during an earthquake even if all seismic resistant mechanisms for the structure and code specified ultimate capacities are accounted for. This investigation points out the need for including inelastic energy absorption capability, wave scattering phenomena, repeatable acceleration peaks, duration of strong shaking, etc., in design analyses of critical facilities such that analytical results realistically reflect potential levels of structural damage.

1940 versus 1979 Earthquakes - There are many similarities between the May 18, 1940 and the October 15, 1979 Imperial Valley earthquakes. Ground rupture from the 1979 event followed the same pattern as the 1940 event, and showed many of the same features and characteristics. The similarity also extends to the distribution and types of damage. Their magnitude, about 6.5, and felt areas are approximately the same, yet damage from the 1940 earthquake was much greater if damage to the Imperial County Services Building in El Centro is excluded in the comparison.

It should be noted that the maximum acceleration recorded at the same site in El Centro during the 1940 and 1979 earthquakes were 0.36 and 0.40g, respectively. This suggests that the levels of maximum horizontal acceleration in El Centro, were not markedly different in the two earthquakes, but the duration of strong shaking differs by a factor of at least three. The difference in damage levels suggest that the greater duration of shaking during the 1940 shock might be the reason for the greater damage.

Implication - The general lack of damage (excluding the Imperial County Services Building) during the 1979 Imperial Valley earthquake for 0.3 to 0.6g ground motion indicates the importance of ground motion duration in estimating damage potential and the need for inelastic energy absorption capability in the design of structures to mitigate damage. Certainly, one would have expected greater damage if these strong ground accelerations had been associated with longer duration records such as those recorded in the 1971 San Fernando or in the 1952 Kern County earthquake.

A.3.6   Parkfield, California Earthquake, 1966
         (A-32, A-33, A-115 through A-118)

The Parkfield-Cholame area of California was subjected to very high ground accelerations from a moderate earthquake (M_L = 5.6, M_S = 6.4) on June 27, 1966. The epicenter was located on the San Andreas fault approximately 5 miles northwest of Parkfield or 20 miles northwest of Cholame. A maximum intensity VII was assigned to a small area in and near the San Andreas fault zone, extending southeasterly from a few miles north of Parkfield to a few miles south of Cholame. Five strong motion instruments and fifteen seismoscopes recorded the ground motion. The maximum recorded acceleration was 51 percent gravity (Station 2) located about 200 feet of the fault trace. Other peak acceleration values were 47 (Station 5), 28 (Station 8) and 7 (Station 12) percent gravity at distance of 3, 6 and 9 miles, respectively. The accelerometer at Temblor also located about 6 miles from the fault recorded 41 percent gravity. Although 0.5g was recorded at the fault, the ground motion attenuated rapidly with distance and at 10 miles from the fault the maximum acceleration was reduced to about one-tenth of its near fault value. At Cholame Station 2, the motion consisted primarily of a single pulse with strong motion less than 2 seconds. However, ground motion recorded at further distance lost this pulse-like characteristic.

Despite the large accelerations, very little damage was caused by the earthquake. In general, the area was sparsely populated and there were no multi-story buildings. However, there were a number of small structures, a couple of oil company pumping plants, an electrical transformer station, several bridges, and houses, etc. A pump station near Shandon was subjected to ground motion estimated at 25 percent gravity. No damage occured to the building or to a steel stack. Another pump station located closer to the fault and subjected to higher ground shaking also saw no damage.

In Cholame and vicinity, a domestic water tank containing approximately 4500 gallons of water saw an estimated 0.4g acceleration. Although there was evidence of slight base movement, no damage was observed. At a Standard Oil Station, some metal forms buckled.

The fire station building in Parkfield is located within limits of the fault and was subjected to an estimated acceleration greater than 0.4g. The station is a one-story, reinforced brick building presumably constructed according to UBC requirements. A conservative estimate of the design base shear would be about 0.15g. Given the high level of ground motion, some yielding would have been predicted. The station, however, was not damaged.

Implications - The observed performance of the Parkfield fire station indicates that elastic calculated earthquake forces would substantially overestimate actual forces. Correlation between elastic predicted and observed behavior would not be good.

Reference A-33 states in general, judging from the effects of the main shock on structures, the recorded maximum acceleration apparently lacked damage potential. Probable reasons are (a) short duration of the maximum ground acceleration, (b) predominent period of the ground acceleration out of range of the natural periods of existing structures, and (c) few structures of engineering significance located in the vicinity of the maximum recorded accelerations.

A.3.7 Bear Valley Earthquake, 1972 (A-34)

The Bear Valley earthquake occurred on September 4, 1972 in San Benito County, California. The earthquake was of small size (m_b = 4.6, M_L = 4.7). The hypocenter was located at a depth of 5km, approximately 1km southwest of the most recently active trace of the San Andreas fault. The aftershock locations define a vertical plane 3km in width and 4km in length parallel to the San Andreas fault. Recent work indicates that there may be a systematic bias to the west for the location of the earthquake in the region. Movement of the aftershock zone, a few kilometers to the east, would place the zone directly on the San Andreas.

Three strong motion instruments were located within 10km of the calculated epicenter. The stations, recorded peak horizontal accelerations and calculated epicentral distances are: the Stone Canyon Geophysical Observatory, peak acceleration 0.23g, distance 3km; Melendy Ranch Barn, peak recorded acceleration 0.70g, (0.52g corrected), distance 9km; Bear Valley Fire Station, peak acceleration 0.17g, distance 10km. Eastward movement of the rupture zone to place it on the San Andreas fault would result in the distance from the rupture zone to each of the three stations being only a few kilometers. All three instruments are located on relatively shallow deposits of recent alluvium.

The earthquake occurred in a sparsely populated region. The principal effect of the earthquake pertained to numerous rockfalls along the steep banks of the San Benito River. The epicentral region was assigned an intensity VI with only slight damage reported. The damage was reported at the Bear Valley Fire Station at a distance of approximately 9km from the epicenter. At the fire station, cinder block walls developed fine cracks, a fire truck rocked noticeably from side-to-side, and a vertical pipe from a water heater extending through the ceiling crushed the sheet rock. At Melendy Ranch, approximately 8km from the epicenter, small landslides occurred, small objects fell and vehicles rocked.

Implications - As no major engineered structures were located within the region affected by the Bear Valley earthquake (the design basis for the Bear Valley Fire Station is unknown) no significant statement can be made concerning the effect of high ground acceleration earthquake motions on engineered structures from this earthquake.

A.3.8   Coyote Lake Earthquake, 1979
         (A-105, A-106, A-107, A-108, A-109)
         On August 6, 1979, a magnitude, M_L = 5.7, earthquake occurred at a depth of 10km in the Calaveras fault zone at Coyote Lake approximately 50 km southeast of San Jose or 10km north-northeast of Gilroy, California.

Because of the high seismic activity in the Gilroy-Hollister area, there were a number of strong motion instruments in the area which recorded the ground motions. All stations in the Gilroy array are within 16km of the epicenter and extend from a rock site through an alluvial valley to another rock site. The stations in the Bear Valley array located between 50 and 75km from the epicenter recorded accelerations greater than 0.05g. A maximum horizontal acceleration of 0.42g was recorded at station 6 located on rock within 1km of the fault trace and to the southeast of the epicenter.

The earthquake caused very little damage in the epicentral area, which is mountainous and sparsely populated. A strong motion instrument at Coyote Dam recorded a horizontal acceleration of 0.23g. The highest MM intensity values of VII were observed in the Gilroy and San Felipe Lake areas. Intensities were higher in these areas due to deep, alluvial-filled valleys and the direction of earthquake energy propagation.

Reports from Gilroy and Hollister indicated no significant structural damage. Minor cosmetic damage consisting of plaster cracking, some pounding between adjacent buildings, and glass breaking occurred. In general, the level of damage was very low.

Implications - Although the earthquake affected a variety of commercial structures in both Gilroy and Hollister, insufficient published data describing the performance of specified structures exists. Consequently, no correlation between predicted and observed structural performance can be made.

A.3.9   Oroville, California Earthquake, 1975 (A-147)

The Oroville earthquake occurred on August 1, 1975, near Oroville, California. The earthquake was of medium size (M_L = 5.7, M_S = 5.6) with a hypocenter depth of 8km.

Five strong motion instruments were located within 35Km of the earthquake epicenter. The Oroville Dam seismograph station, a rock site, recorded a peak horizontal acceleration of 0.11g and a peak vertical acceleration of 0.14g. Two instruments were on alluvium and recorded peak accelerations of 0.08g and 0.07g while the remaining two instruments were on rock, one recording a peak acceleration of 0.03g and the other not being triggered.

Twelve strong motion instruments were installed in the epicentral area after the occurrence of the main shock. Over 100 strong motion recordings were obtained for aftershocks in the magnitude range M_L = 3.0 to 5.0 at epicentral distances generally less than 12km.

The Oroville Medical Center is a one-story wood frame structure with a two-story portion on a side hill. The building is located on approximately 100 feet of Cenozoic terrace gravels. Peak horizontal accelerations between 0.04g and 0.39g were recorded for aftershocks in the magnitude range M_L = 4.0 to 4.9 at hypocentral distances of 7km to 11km. Damage consisted primarily of nonstructural plaster damage.

Within the city of Oroville, where the peak horizontal accelerations may have been of the order of 0.10g to 0.15g, building damage consisted primarily of broken windows, cracked plaster and broken ceiling

tiles. Very little structural damage occurred in modern buildings. Only minor damage was observed in any of the several State Water project facilities in the area, including the Oroville Dam and the associated power plant.

Implications - The only engineered structures of significance in the epicentral area were the State Water Project facilities at Oroville Dam and Thermalito Afterbay. These facilities experienced peak horizontal accelerations of the order of 0.1g during the main shock with only slight damage. This low level of shaking did not allow an effective assessment of the correlation between predicted and observed behavior.

A.3.10   Greenville, California Earthquake, 1980
         (A-141, A-142, A-143)

In January, 1980, the Livermore Valley area of California was shaken by a series of earthquakes. Most of the damage was the result of shocks which occurred on January 24th. The largest shock was a M_L = 5.5 located 12km north of the Livermore Valley and 20km northwest of the Lawrence Livermore National Laboratory (LLNL) along the Greenville fault. In addition to the main shock, there was a foreshock M_L = 2.7 a minute and a half earlier and an aftershock M_L = 5.2, located again on the Greenville fault 14km to the south of the first principal shock. The second principal shock caused essentially no damage.

There were no strong motion instruments in the Livermore Valley or at LLNL. The closest instruments were at Del Valle Dam and Veteran's Hospital, south of General Electric Vallecitos Plant (Pleasanton), Kodak Facility (Dublin), and Tracy. Peak ground acceleration recorded were 0.26g, 0.18g, 0.11g, 0.15g and 0.09g. Estimates for ground motion at the LLNL Site were 0.2 to 0.3g.

In general, damage to structures in the Livermore vicinity was very light. A few chimneys were cracked and several unreinforced brick serpentine walls were toppled. The abutment on Greenville Road Overpass on Interstate 580 which passes almost directly over the Greenville fault

had one abutment drop 6 to 10 inches interrupting traffic. There was
some insignificant minor cracking in the concrete structure. The
Livermore City Hall, a fairly new reinforced concrete building, had no
structural damage; however, there was extensive damage to the suspended
T-bar ceilings. Elsewhere in Livermore, there was very little damage to
structures except for occasional broken glass.

Most of the damage was concentrated in the eastern portion of
the valley, damage was noted principally to a mobile home park. A high
percentage of mobile homes fell off their stands and sustained damage.
No damage was reported to an electrical substation or any equipment which
was located 1 mile west of Greenville fault. Two wineries are located
about 2 to 3 kilometers southeast of Livermore. One suffered no damage
to any structure, while extensive damage was sustained by an elevated
water tank and wine tanks in the other. An elastic estimated base shear
coefficient of 35 percent of gravity was estimated to have caused the
observed damage. Typical damage to the small wind fiberglass lined steel
tanks was toppling due to broken legs. No ruptures occurred and damage
was not significant. The larger tanks (stainless steel) suffered more
damage. There were failures to anchorage, local buckling, concrete
spalling of support base, and permanent overall deformations. Only one
tank ruptured. Total dollar value for repairs was estimated at $1 to 1.5
million.

The Lawrence Livermore National Laboratory occupies an area of
approximately one square mile located about 2 miles east of downtown
Livermore. It contains some 147 buildings and 975 trailer units (repre-
senting about 3.5 million square feet of floor area). Design criteria
for LLNL facilities varies considerably. Critical facilities (i.e., those
with radioactive materials) were designed or evaluated using dynamic
analysis with peak ground motion values of 0.5 to 0.8g; laser and magnetic
fusion experimental facility (with high capital cost) employs a 0.25g
ground acceleration with a dynamic analysis; office buildings vary from
no seismic design to the Uniform Building Code with an equivalent static
coefficient of about 0.2; equipment and furnishing also varies from no

seismic design to a greater than 1.0g static coefficient. Damage to equipment and facilities were estimated at $10 million. A large part of the cost was for structural repairs to three administrative buildings, for the repair of architectural-type damage, and for essential improvement to meet upgraded seismic safety standards. The total dollar cost for both repair and improvements was estimated at between $15 and $20 million.

There was no structural damage to critical facilities at LLNL and only minor cosmetic or architectural damage. These facilities are typically of very stiff low rise shear wall type of construction. In general, building facility damage was primarily to five non-critical buildings all of which are moment resisting structures. The interior furnishings were most affected. Connections between tilt-up concrete slabs and their supporting structural steel frames were affected. Core walls had considerable cracking in some buildings.

The 975 individual trailer units at LLNL are assembled into 216 complexes. Eighty-seven were tied down. In general, there was little damage to trailers. In complexes not tied down, one trailer was badly damaged (walls cracked, etc.) and four were moderately damaged (interior ceiling tiles and light fixtures displaced). No structural damage occurred to trailers tied down.

In general, much of the actual cost of repair at LLNL resulted from cosmetic damage. Tall bookcases that were not anchored tipped over, damaging walls and breaking interior glass. Sheetrock partitions were cracked in many buildings. Ceiling tiles, light fixtures, and air diffusers (not anchored) fell to the floor and broken water pipes caused water damage.

Implications - The engineered structures behaved as would be expected of structures designed in accordance with UBC code design provisions which resist moderate earthquakes without structure damage but allow nonstructural damage.

A.3.11 Other Earthquakes

In addition to the above included cases, numerous other examples exist where observations have been made of structures subjected to relatively strong ground motions. Although not included in detail, they are worth citing.

The lack of damage in the vicinity of the ground accelerations due to the 1972 Ancona, Italy earthquakes is noted in Reference A-13. The 1972 earthquakes magnitude of 4 to 5.0 produced recorded maximum accelerations of 0.6g at Rocca (rock) and 0.4g at Palombina (sediment). Epicentral distances to these stations were about 7 and 15km, respectively. Italian seismologists and engineers (A-39) report the relatively small damage and the fact that buildings designed with seismic coefficients of about 0.07g in accordance with the recently adopted Italian earthquake code, suffered no damage. This conclusion again indicates that short duration records and inelastic energy absorption capability of structures limit actual damage. Without accounting for these factors, elastic computed forces compared to ultimate capacities would greatly overpredict damage.

References A-140, A-154 describe briefly structural performance during the 1940 Imperial Valley (El Centro) earthquake which caused considerable damage. References A-152, A-155 describe effects from the 1949 Olympia earthquake. Reference A-55 describes the damage to structures caused by the 1964 Alaska earthquake. There were no recorded motions for the 1964 Alaska earthquake.

References A-26 and A-40 address the damage that the 1906 San Francisco earthquake (magnitude 8.3) brought on the City of San Francisco. The epicenter of the 1906 earthquake was about 17km from downtown San Francisco on the San Andreas fault. There were no ground motion recordings. References A-26 and A-40 suggest that current procedures would estimate peak accelerations exceeding 1.0g in downtown. Further, spectral accelerations, if based on the peak acceleration value, with reasonable damping ratios and at the fundamental frequencies of major buildings of

the era, would be 2.0g or more. The papers indicate that there were 52 major buildings in San Francisco, none of which were specifically designed to resist earthquakes. Their resistance to earthquakes was a by-product of their wind design and non-structural facades and partitions. None of the buildings collapsed and all but seven were repaired and returned to use. Most are still in use today. A few of the surviving buildings include the 19-story Central Tower, the Fairmont Hotel, the old portion of the St. Francis Hotel, the post office at Seventh and Mission Streets and the Ferry Building. None of these buildings would meet current code requirements. The references indicate that an average base shear coefficient of 0.4 would be a generous estimate of the yield-level stress capacity for these buildings.

A number of observations have been made regarding the effect of more distant earthquakes on structures. References A-110, A-146, A-148, A-149, and A-150 discuss the 1967 Caracus, Venezuela, 1974 Lima, Peru, and the 1977 Romania earthquakes whose epicenters were far removed from its highly affected areas. Structures with longer periods were more influenced and soil conditions played a larger role.

Another more distant earthquake series, the 1960 Chile earthquakes, caused considerable damage and is fairly well-documented in References A-151, A-26, A-40, A-43, and A-88. Of particular note, is the behavior of the Huachipato Steel Plant located near Concepcion in Central Chile. This plant was subjected to strong motions. The plant was built in 1947-1960. The facility includes a blast furnace, steel production plant and blooming, merchant and reversing mills and a fabricating shop. There are also many vertical stacks and several elevated water tanks. In general, the plant was designed using allowable stress values associated with static lateral coefficients believed to be in the range of 0.10 to 0.30. An extensive study of the plant was conducted in order to develop the most likely spectral response accelerations. The actual damage, or lack of damage, was then used to reconstruct the probable response pattern and then to determine the base shears and an approximate spectral diagram for the plant. The probable spectral acceleration at the period and

damping of the most critical structures is 1.2g. Damage predictions based on earthquake forces developed from such spectral accelerations clearly would suggest significant damage. Very little damage was observed.

Agadir, Morocco was severely damaged by an earthquake on February 29, 1960. The earthquake was assigned a magnitude of 5.8, with estimates ranging from 5.5 to 6.0. The epicenter of the earthquake was within 2 to 3 kilometers of the center of the city of Agadir. Damage observations suggest a depth of focus no more than 2 or 3 kilometers. The radius of significant damage was very confined, within a 5km radius of the epicenter. Intensities of X and XI were assigned to this central city area. No strong motion data are available. Damage evidence (A-110) strongly suggests that the ground motion consisted largely of a single primary acceleration pulse of short duration. There were several types of structures in Agadir at the time of the earthquake. The most prevalent was constructed with unreinforced or poorly reinforced masonry. Nearly all such structures nearest the quake epicenter collapsed or were damaged beyond repair.

Another principal type of structure employed reinforced concrete. Many had concrete columns and beams for carrying vertical loads; however, the joints between members lacked both moment and shear resistance capability. When subjected to lateral shaking, the beam-column connections failed. The lack of continuity between the various structural elements did not allow a redistribution of loads and many such structures collapsed. It was generally observed that even in cases where structures had significant static resistance to lateral forces, their earthquake performance was poor due to a lack of ductility and energy absorption capacity.

References A-44, A-121 and A-122 report on the June 8, 1975, earthquake (M_L = 5.2, M_S = 5.7) that occured in the Ferndale region of Northern California. The epicenter was located 4 miles south and slightly west of Ferndale. The Humboldt Bay Power Plant is located south of Eureka and adjacent to the bay. The plant consists of two units of fossil fuel

powered generators and a nuclear powered generator unit (Unit 3). Both fossil fuel units were operating at the time of the earthquake while the nuclear unit was out of service for a scheduled refueling, maintenance and modification. The only strong motion accelerograms recorded during the earthquake were those obtained at the power plant site located 12 miles from the epicenter of the earthquake. A MM intensity of V is assigned to the plant site. Unit 3 was instrumented with three strong motion instruments. At these sensor locations, the largest peak acceleration was recorded in the (transverse) EW direction. Peak (corrected) values were 0.35g, 0.25g and 0.16g, for free-field (storage building), ground level inside the refueling building and reactor caisson (78 feet below grade), respectively. Strong shaking was about 3 to 5 seconds. The corresponding acceleration response spectra for 2 percent damping indicates that maximum spectral values occurred for both instruments in the Refueling Building between 2 to 3Hz and for the Storage Building between 2 to 10Hz. The effect of the earthquake was to trip the generator oil circuit breakers and the auxiliary transformer for both fossil units. On the nuclear unit, the only abnormal condition caused by the earthquake involved spurious actions on one of a pair of redundant relays in the refueling building high differential pressure protection system. Small waves (9 to 12 inches) were observed in the spent fuel pool. No significant earthquake related damage was observed.

References A-114, A-123 and A-124 report the effect of a November 8, 1980 earthquake on the Humboldt plant. This earthquake had a surface wave magnitude of 7.0 and occured off the coast of California west of Eureka and the Humboldt plant. Free-field peak ground motion estimates were 0.15g to 0.25g. The effects of the earthquake on plant structure, piping, equipment and components were minimal. The only structural damage was permanent deformation of a reinforced masonry wall of the plant's one-story cold machine shop. The wall is 18 feet high and spans horizontally 70 to 80 feet between cross walls. Movement at the base of three water storage tanks was evidenced, but there was no damage to the tank or attached piping. Effects on piping and mechanical equipment were essentially nil.

References A-45, A-97 and A-144 discuss earthquake effects on two nuclear power plants. First is the Fukishima Nuclear Station which was subjected to strong motion from the 7.4 magnitude Miyagi-Ken-Oki, Japan earthquake of June 1978 located about 140km from the station. Peak ground motion was approximately 0.1g with a maximum response acceleration of about 0.25g. OBE design motion was 0.18g. The only damage reported for the power complex was breakage of some non-critical electrical insulators. The second is the Wm. H. Zimmer Station, Moscow, Ohio which was subjected to ground motion from the July 27, 1980 Sharpsburg, Kentucky earthquake. Magnitude of this event was 5.1 with its epicenter located 46 miles south-southeast of the station. Peak acceleration at the site was 0.04g, below the OBE of 0.1g. There was no visible damage to any structures at Zimmer.

References A-134, A-135 and A-136 indicate that the Virgil C. Summer Nuclear Station, located near Parr, South Carolina was subjected to ground motion from several nearby magnitude earthquakes in 1978. The strongest event occurred on August 27, 1978 and had a local magnitude of 2.8. The epicenter on this event, called Monticello Reservoir Earthquake, was about 6500 feet northwest of the nuclear station. The focal depth is estimated at 100 to 500 meters. The nearest recording instrument, a USGS strong motion accelerometer was located on a straight line between the plant and the epicenter and at a distance of about 4400 feet. Peak recorded horizontal components of the accelerations were 0.27g and 0.21g, and 0.08g for the vertical component. The duration of strong shaking was very short (less than 1 second). A conservative estimate of 0.10g to 0.18g is made for the ground motion at the plant site. No damage was observed. In fact, the event was essentially unfelt by personnel at the plant.

Cloud (A-41) discusses the seismic performance of power piping by examining the intrinsic characteristics of piping that are built-in due to designed construction practice and also by examining the performance of comparable piping in past earthquakes. Discussed are power plant

piping behavior during seven past earthquakes. These are the 1979
Imperial Valley, the 1978 Miyagi-Ken-Oki, the 1972 Managua, the 1971 San
Fernando, the 1964 Alaska, the 1952 Kern County (Taft) and the 1933 Long
Beach. Observations include the seismic performance of piping in the El
Centro Steam Plant in the Imperial Valley, the Fukushima Nuclear Power
Plant, and the ESSO Refinery Complex and the ENALUF Power Plant in
Managua, San Fernando Valley Power Plant, the Kern County Steam Station,
and the Long Beach Steam Station. In summary, Cloud indicates that based
on the available data and observations pertaining to the behavior of
power piping during actual earthquakes, even for power plants experiencing
severe ground motion the piping remains intact.

A.4   CONCLUSIONS

The objectives of the review effort were twofold. First, to
assess how well predicted structural performance, based on elastic
analysis procedures that employ elastic response spectra derived from
recorded ground motion, correlates with actual observed structural
behavior during past earthquakes. Second, to identify ground motion and
structural characteristics that strongly influence a structure's response
behavior.

To meet these objectives, an extensive literature review was
conducted and a data base established that documents the performance of
structures subjected to strong ground shaking from past earthquakes.
When possible, those cases were identified where a direct comparison
between observed behavior and predicted performance based on calculated
earthquake forces could be made.

The literature review and damage documentation presented,
herein, lead to the following conclusions:

1. When the level of ground motion was such that the observed
    overall structural behavior was essentially elastic, the
    predicted behavior based on calculated earthquake forces
    using elastic analysis correlated well with observation.
    Note, structures were observed to often exhibit such
    overall behavior and still exhibit local yielding.

2. When the level of ground motion caused the actual structure to respond inelastically, the elastic analysis method gave calculated earthquake forces which signficantly over-estimated the actual force level which occurred producing the observed damage. In these cases where the calculated elastic force levels would be generally indicative of significant structural damage, the predicted performance did not correlate with observed behavior.

3. Several factors were identified which influence the response behavior of well-designed structures. Among these are the duration of strong shaking, the energy absorption or ductility capacity of a given structural system, and the effects of soil-foundation interaction. In general, the documentation assembled qualitatively supports the belief that such factors must be included in the develoment of design ground motion criteria if predicted structural behavior is to accurately correlate with actual observed performance.

4. There are some documented cases where short duration motions have not caused any significant damage, even to non-engineered structures, in spite of the fact that the short duration motions had equal or higher peak accelerations than long duration motions which resulted in significant damage.

TABLE A-1

LIST OF EARTHQUAKE/STRUCTURE-TYPES

INCLUDED IN REVIEW/DAMAGE DOCUMENTATION

EARTHQUAKE	STRUCTURE-TYPE	REFERENCES
Cases with Damage Documentation		
1952 Kern County, CA	General, Kern County Steam Plant, Elevated Tanks	137-140, 32
1966 Parkfield, CA	General	32, 33, 115-118
1971 San Fernando, CA	General Medical Facilities, High-Rise Buildings, Industrial, O. View, VA	58, 60, 66, 67, 76, 84, 87, 157, 158, 159, 162, 163
1972 Bear Valley, CA	General	34
1972 Managua, Nicaragua	General, ESSO Refinery, ENALUF Thermal Plant	26, 30, 40, 42, 111-113
1975 Oroville, CA	General, State Water Project	147
1978 Santa Barbara, Ca	General	64, 119, 120, 160
1979 Coyote Lake, CA	General	105-109
1979 Imperial Valley, CA	General, El Centro Steam Plant	35-38, 125-129
1980 Greenville, CA	General, LLNL	141-143
Other Cases Reviewed		
1906 San Francisco, CA	Major High-Rise Buildings	26, 30, 99, 155
1940 Imperial Valley, CA	General	154, 140
1949 Olympia, WA	General	140, 152, 155
1960 Agadir, Morocco	General	110
1960 Chile	Huachipato Steel Plant	26, 40, 43, 88, 151
1964 Alaska	General	55, 110

LIST OF EARTHQUAKE/STRUCTURE-TYPES
INCLUDED IN REVIEW/DAMAGE DOCUMENTATION

EARTHQUAKE	STRUCTURE-TYPE	REFERENCES
Other Cases Reviewed (Continued)		
1967 Caracas, Venezuela	General, High-Rise	110, 148
1967 Koyna, India	Koyna Dam	130-133
1972 Ancona, Italy	General	13, 39
1974 Lima, Peru	General	65, 146
1975 Ferndale, CA	General, Humboldt Bay, Nuclear Power Plant	44, 121, 122, 85
1976 Friuli, Italy	General	80, 145
1977 Romania	General	62, 149, 150
1978 Miyagi-Ken-Oki, Japan	Fukushima Nuclear Power Plant	45, 97
1978 Monticellor Reservoir	Virgil C. Summer Nuclear Plant	134-136
1980 Mammoth Lake, CA	General	156
1980 Eureka, CA	General, Humboldt Bay, Nuclear Power Plant	114, 123, 124
1980 Sharpsburg	Wm. Zimmer Nuclear Power Plant	144

TABLE A-2

SUMMARY - EARTHQUAKES, MAXIMUM RECORDED ACCELERATIONS, STRUCTURE-TYPES AND
LEVEL OF MOTION AT STRUCTURE SITE

Earthquake		Magnitude		Maximum Recorded Acceleration	Distance Causative Fault	Structure-Type	Level of Motion Structure Site		Duration of Strong Shaking (>.1g)
		M_L	M_S						
18 April 1906	San Francisco	6.9	8.3	-	-	High Rise Buildings	Up to 1.0g EST	-	[long]
18 May 1940	Imperial Valley	6.4	7.1	0.39	10 km	General	-	IX-X	25 sec.
21 July 1952	Kern County	7.2	7.7	0.20	40	General	0.2 - 0.5 EST	VIII-IX	>12
29 Feb. 1960	Agadir, Morocco	-	5.8	-	-	General	-	X-XI	single pulse
21 May 1960	Chile	-	7.5	-	-	Hauchipato Steel Plant	>0.1	-	[short]
26 July 1963	Skopje, Yogoslavia	-	6.0	-	-	General	-	VII	short
27 June 1966	Parkfield	5.6	6.4	0.50	<1	General	0.06 - 0.50	VII	<2 single pulse
10 Dec. 1967	Koyna, India	6.0	6.5	0.63	7	Koyna Dam	0.63	-	6
9 Feb. 1971	San Fernando	6.4	6.6	1.2	3	General	Up to 0.5 (?)	VI-XI	[<7]
14/21 June 1972	Ancona, Italy	4.9/4.4	-	0.60/0.40	7/15	General	0.60/0.40	-	<2
4 Sept. 1972	Bear Valley	4.7	4.3	0.70	6	General	-	VI	<3
23 Dec. 1972	Managua, Nicaragua	-	6.2	0.39	5	General	<0.6 EST	IX	[>10]
						ESSO Refinery	0.39	V-VI	10
						ENALUF	0.6 EST	VII-VIII	[>10]
6 Oct. 1974	Acapulco, Mexico	-	4.8	0.53	35	General	0.53	-	1-2
7 June 1975	Ferndale	5.2	5.7	0.35	20	General	-	VI-VII	[<4]
						Humbolt Bay Power Plant	0.35	V	<4
12 June 1978	Miyagi-Ken-Oki	-	7.4	0.10	140	Fukushima Nuc. Power Plant	0.10	-	[short]
13 Aug. 1978	Sahta Barbara	5.1	5.6	0.45	4	General	0.45	VII	2-3
27 Aug. 1978	Monticello Reservoir	2.8	-	0.25	<1	Virgil C. Summer NPP	<0.1 EST	-	<1
15 Oct. 1979	Imperial Valley	6.6	6.9	0.81	2	General	0.2 - 0.4	VII	<13
						El Centro Steam Plant	0.49	VII	7
6 Aug. 1979	Coyote Lake	5.7	5.6	0.42	7	General	0.42	VII	<2
24 Jan. 1980	Greenville	5.9	5.9	0.17	16	Livermore Valley/LLNL	0.2 - 0.3 EST	-	[short]
27 July 1980	Sharpsburg	5.1	-	-	-	Wm. Zimmer NPP	<0.1	VI	[short]

A-53

Circles represent the maximum first-mode base shears
experienced during the earthquake, ticked circles represent
structures that had some damage; squares represent the nominal
code values of base shears for which the buildings were designed.
The periods are those of the fundamental modes of vibration.
Base shear coefficient is equal to base shear divided by total
weight of structure.

FIGURE A-1.   BASE SHEAR COEFFICIENTS OF MULTI-STORY CONCRETE BUILDINGS SUBJECTED
TO STRONG GROUND SHAKING DURING 1971 SAN FERNANDO EARTHQUAKE
(Reference A-60)

RESEARCH BIBLIOGRAPHY FOR THE EARTHQUAKE STRUCTURAL DAMAGE
LITERATURE REVIEW

A-1   J. A. Blume, The Effect of Arbitrary Variations in Peak Ground Acceleration on Spectral Response, Diablo Canyon Nuclear Power Plant, URS D-11 30, May 9, 1977.

A-2   P. B. Shnabel, and H. B. Seed, "Accelerations in Rock for Earthquakes in Western U.S.", Bulletin of the Seismological Society of America, Vol. 63, Nos. 2, 1973.

A-3   M. R. Ploessel, and J. E. Slosson, "Repeatable High Ground Accelerations from Earthquakes", California Geology, September, 1974.

A-4   R. A. Page, D. M. Boore, W. B. Joyner and H. W. Coulter, "Ground Motion Values for Use in the Seismic Design of the Trans-Alaska Pipeline System", Geological Survey Circular, 672, Washington, D.C., 1972.

A-5   R. B. Hoffman, "State-of-the-Art for Assessing Earthquake Hazards in the United States; Factors in the Specification of Ground Motions for Design Earthquakes in California", Miscellaneous Paper S-63-1, U.S. Army Engineers Waterways Experiment Station, Vicksburg, Miss., June, 1974.

A-6   O. W. Nuttli, "State-of-the-Art for Assessing Earthquake Hazards in United States; The Relation of Sustained Maximum Ground Acceleration and Velocity to Earthquake Intensity and Magnitude", Miscellaneous Paper S-73-1, Report 16, November, 1979, U.S. Army Engineer Waterways Experiment Station, Vicksburg, Miss., 1979.

A-7   C. P. Mortgat, and H. C. Shah, "A Bayesian Approach to Seismic Hazard Mapping; Development of Stable Design Parameters", The J. A. Blume Earthquake Engineering Center, Report No. 28, Dept. of Civil Engr., Stanford University, 1978.

A-8   C. P. Mortgat,, "A Probabilistic Definition of Effective Acceleration", Proceedings of the 2nd U.S. National Conference on Earthquake Engineering, Stanford University, August 22-24, 1979, pp. 743-752.

A-9   E. H. Vanmarcke and S. P. Lai, "Strong Motion Duration of Earthquakes", M.I.T. Dept. of Civil Engineering Research Report R77-16, 1977.

A-10   T. C. Hanks, "Measures of High-Frequency Strong Ground Motion", Proceedings of the NSF Seminary Workshop on Strong Ground Motion, 1978.

A-11   T. C. Hanks, "Seismological Aspects of Strong Motion Seismology",
        Proceedings of the 2nd U.S. National Conference on Earthquake
        Engineering, Stanford University, August 22-24, 1979, pp.
        898-912.

A-12   M. W. McCann, Jr., and H. C. Shah, "RMS Acceleration for Seismic
        Risk Analysis: An Overview", Proceedings of the 2nd U.S. National
        Conference on Earthquake Engineering, Stanford University,
        August 22-24, 1979, pp. 883-897.

A-13   N. M. Newmark, "A Rationale for Development of Design Spectra
        for Diablo Canyon Reactor Facility", N. M. Newmark Consulting
        Engineering Services, Urbana, Illinois, September, 1976.

A-14   R. P. Kennedy, "Ground Motion Parameters Useful in Structural
        Design", Structural Mechanics Associates, Inc., Presented at the
        Conference on Evaluation of Regional Seismic Hazards and Risk,
        Santa Fe, New Mexico, October 21, 1980.

A-15   H. Yamahara, "Ground Motion During Earthquake and the Input Loss
        of Earthquake Power to an Excitation of Buildings", Soils and
        Foundation, Vol. 10, No. 2, 1970, pp. 145-161, Tokyo.

A-16   N. M. Newmark, W. J. Hall and J. R. Morgan, "Comparison of
        Building Response and Free-Field Motion in Earthquakes",
        Proceedings of the 6th World Conference on Earthquake
        Engineering, New Delhi, India, 1977.

A-17   R. H. Scanlan, "Seismic Wave Effects on Soil-Structure-
        Interaction", Earthquake Engineering and Structural Dynamics,
        Vol. 4, 1976, pp. 379-338.

A-18   N. Ambraseys, "Character of Strong Ground Motion in the Near
        Field of Small Magnitude Earthquakes", Invited Lecture, 5 Conf.
        European Committee for Earthquake Engineering, Istanbul,
        September, 1975.

A-19   J. R. Whitely, J. R. Morgan, W. J. Hall, and N. M. Newmark "Base
        Response Arising from Free-Field Motions", Transactions of the
        4th SMiRT Conference, Vol. K(a), 1977.

A-20   D. Ray and D. P. Jhaveri, "Effective Seismic Input Through Rigid
        Foundation Filtering", Transactions of the 4th SMiRT Conference,
        Vol. K(a), 1977.

A-21   W. J. Hall, J. R. Morgan and N. M. Newmark, "Traveling Seismic
        Waves and Structural Response", Proceedings of the Second
        International Conference on Microzonation, Vol. III, San
        Francisco, California, November, 1978.

A-22   Reduction in Free-Field Ground Motion Due to the Presence of
        Structures, Submitted to: Southern California Edison Company by
        TERA Corporation, August, 1980.

A-23   C. B. Crouse, "Prediction of Free-Field Earthquake Ground
        Motions" Proceedings ASCE Conference on Earthquake Engr. & Soil
        Dynamics, 1978.

A-24   G. W. Housner, "Statistics of Pulses on Strong Motion Accelero-
        grams", Proceedings of the NSF Seminar Workshop on Strong Ground
        Motion, 1979.

A-25   G. W. Housner, "Spectrum Intensities of Strong Motion Earth-
        quakes", Proceedings of the Symposium on Earthquake and Blast
        Effects on Structures, EERI, June, 1975, pp. 20-36.

A-26   J. A. Blume, "Instrumental Versus Effective Acceleration",
        Report D-11 26, Final Safety Analysis Report, Units 1 and 2,
        Diablo Canyon Site, Amendment No. 50. "Seismic Evaluation for
        Postulated 7.5M Hosgri Earthquake", U.S. Nuclear Regulatory
        Commission Docket Nos. 50-275 and 50-232, 1977.

A-27   R. V. Whitman, "Effective Peak Acceleration", Proceedings of the
        2nd International Conference on Microzonation, San Francisco,
        Vol. III, 1978, pp. 1247-1255.

A-28   S. A. Short, R. P. Kennedy, et al, "Nonlinear Response of a
        Nuclear Plant to a Moderate Magnitude, Near-Field Earthquake",
        ASCE Specialty Conference on Civil Engineering and Nuclear Power,
        Knoxville, Tennessee, September, 1980.

A-29   G. W. Housner, "Measures of Severity of Earthquake Ground
        Shaking", Proceedings of the U.S. National Conference on
        Earthquake Engineering, EERI, Ann Arbor, Michigan, June, 1975,
        pp. 25-33.

A-30   J. A. Blume, "On Instrumental Versus Effective Acceleration and
        Design Coefficients", Proceedings of the 2nd U.S. National
        Conference on Earthquake Engineering, Stanford, California, 1979

A-31   S. H. Harzell, J. N. Brune and J. Prince, "The October 6, 1974, Acapulco Earthquake; An Example of the Importance of Short-Period Surface Waves in Strong Ground Motion", Bulletin of the Seismological Society of America, Vol. 68, December, 1978, pp. 1663-1677.

A-32   G. W. Housner, "Earthquake Research Needs for Nuclear Power Plants", Journal Power Division, Proceedings ASCE, Vol. 97, 1971, pp. 77-91.

A-33   W. K. Cloud, "Intensity Map and Structural Damage, Parkfield, California Earthquake of June 27, 1966", Bulletin of the Seismological Society of America, Vol. 57, No. 6, 1967, pp. 1161-1178.

A-34   J. F. Lander, Editor, Seismological Notes, Bulletin of the Seismological Society of America, Vol. 62, No. 5, January-February, 1972, pp. 1360-1362.

A-35   C. Rojahn, Selected Papers on the Imperial Valley, California Earthquake of October 15, 1979, U.S. Geological Survey, Open File Report 80-1094, 1980.

A-36   G. E. Brandow, et al, Reconnaissance Report, "Imperial County, California Earthquake of October 15, 1979", Earthquake Engineering Research Institute, February, 1980.

A-37   R. C. Murray, T. A. Nelson, et al, "Response of El Centro Steam Plant Equipment During the October 15, 1979, Imperial Valley Earthquake", Lawrence Livermore Laboratory, NUREG/CR-1665, UCRL-53005, September, 1980.

A-38   Reconnaissance Reports - Imperial Valley Earthquake, October 15, 1979, USNRC Earthquake Team Report, November, 1979.

A-39   R. Console, F. Peronaci, A. Sonaglia, Relazione Sue Fenomeni Sismica Dell 'Anconitano, 1972, Annali di Geofistica, Vol. 26, Supplement, 1973, Rome.

A-40   J. A. Blume, "Performance of Industrial and Power Facilities in Major Earthquakes", Report D-11 34, Final Safety Analysis Report, Units 1 and 2, Diablo Canyon Site, Amendment No. 50, "Seismic Evaluation for Postulated 7.5M Hosgri Earthquake", Nuclear Regulatory Commission, Docket Nos. 50-275, and 50-232, 1977.

A-41   R. L. Cloud, "Seismic Performance of Piping in Past Earthquakes",
        ASCE Specialty Conference on Civil Engineering and Nuclear Power,
        Knoxville, Tennesee, September, 1980.

A-42   J. F. Meehan, H. J. Degenkolb, et al, "Managua, Nicaragua
        Earthquake of December 23, 1972", Earthquake Engineering
        Research Institute, May, 1973.

A-43   J. A. Blume, A Structural Dynamic Analysis of Steel Plant
        Structures Subjected to the May, 1960, Chilean Earthquakes,
        Bulletin of the Seismological Society of America, Vol. 53,
        February, 1963, pp. 439-480.

A-44   O. Steinhardt, Report on Magnitude 5.7 Ferndale Earthquake of
        June 7, 1975, PG&E Company.

A-45   P. I. Yanev, T. A. Moore and J. A. Blume, "Fukushima Nuclear
        Power Station, Effect and Implications of the June 12, 1978,
        Miyagi-Ken-Oki, Japan, Earthquake", URS Reconnaissance Report,
        Copy 66, January, 1979.

A-46   R. P. Kennedy, W. H. Tong and S. A. Short, "Earthquake Design
        Ground Acceleration Versus Instrumental Peak Ground Accelera-
        tion", Report SMA 12501.01, Structural Mechanics Associates,
        Inc., Newport Beach, California, October, 1980.

A-47   J. A. Blume, "On the Attenuation of Ground Motion by Large
        Foundations", Report D-LL 39*, J. A. Blume, M. R. Somerville,
        and R. M. Czarnecki, "A Comparison of Observed and Estimated
        Peak Ground Accelerations and Their Probabilities", Report D-LL
        36*, J. A. Blume, A. S. Kiremedjiian, "Recurrence Relationships
        by Fault Units", Report D-LL 37*, 1977.

A-48   J. A. Blume, "A Busy Start for the New Decade", Newsletter,
        EERI, Vol. 14, No. 2, March, 1980.

A-49   J. A. Blume and M. H. Stauduhar, (eds.), "The Thessaloniki,
        Greece Earthquake of June 20, 1978", EERI, January, 1979.

---

*   Final Safety Analysis Report, Units 1 and 2, Diablo Canyon Site,
    Amendment No. 50, "Seismic Evaluation for Postulated 7.5M Hosgri
    Earthquake", 1977, USNRC, Docket Nos. 50-275 and 50-232.

A-50 J. A. Blume, "The Motion and Damping of Building Relative to Seismic Response Spectra", Bulletin of the Seismological Society of America, 60:231-249, February, 1970.

A-51 J. A. Blume, "Allowable Stresses and Earthquake Performance", Proceedings of the 6th World Conference on Earthquake Engineering, New Delhi, 1977.

A-52 J. A. Blume, "Structural Dynamics in Earthquake-Resistant Design",Journal of the Structural Division, ASCE, July, 1958.

A-53 B. A. Bolt and R. A. Hansen, "The Upthrow of Objects in Earthquakes", Bulletin of the Seismological Society of America, Vol. 67, No. 5, October, 1977, pp. 1415-1427.

A-54 R. L. Cloud, "How Nuclear Piping Code Rules Will Influence Piping Design Today and Tomorrow", Heating, Piping & Air Conditions, June, 1970, p. 69.

A-55 W. K. Cloud, The Great Alaska Earthquake of 1964, Engineering, National Academy of Sciences, Washington, D.C., 1973.

A-56 C. A. Cornell and N. M. Newmark, "On the Seismic Rehability of Nuclear Power Plants", Proc. Topical Mtg. on Probabilistic Analysis of Nuclear Reactor Safety, Vol. 3 ANS, 1978, pp. XXIVI-1 to 1-14.

A-57 N. C. Donovan, B. A. Bolt and R. V. Whitman, "Development of Expectancy Maps and Risk Analysis", Journal, Structural Division, Proceedings, ASCE, 1978.

A-58 K. V. Steinbrugge, et. al., "San Fernando Earthquake, February 9, 1971", Pacific Fire Rating Bureau, San Francisco, California, 1971.

A-59 W. J. Hall, B. Mohraz and N. M. Newmark, Statistical Studies of Vertical and Horizontal Earthquake Spectra, prepared for USNRC, Report NUREG-0003, January, 1976.

A-60 G. W. Housner, and P. C. Jennings,, "Earthquake Design Criteria for Structures", Report No. EERL 77-06, EERL, California Institute of Technology, Pasadena, November, 1977.

A-61 Jungmann, "Documentation of the Earthquake in the Schwabiache Alb on 3 September 1978", Kraftwerk Union, October 11, 1978.

A-62   D. L. Leeds, (ed.), "Earthquake in Romania, March 4, 1977",
        EERI, Vol. 11, No. 3B, May, 1977.

A-63   R. K. McGuire and T. P. Bernard, "The Usefulness of Ground
        Motion Duration in predicting the Severity of Seismic Shaking,"
        Proceedings of the 2nd U.S. National Conference on Earthquake
        Engineering, Stanford University, August 22-24, 1979.

A-64   R. K. Miller and S. F. Felszeghy, "Engineering Features of the
        Santa Barbara Earthquake of August 13, 1978", EERI, UCSB-ME-78-2,
        December, 1978.

A-65   D. Moran, G. Ferver, et al, "Engineering Aspects of The Lima,
        Peru Earthquake of October 3, 1974", EERI, May, 1975.

A-66   J. L. Mulloy, "San Fernando Earthquake of February 9, 1971",
        Effects on Power System Operation and Facilities, Department of
        Water and Power, City of Los Angeles, October 1974.

A-67   L. Murphy, "San Fernando, California Earthquake of February 9,
        1971", Sci-Coord., U.S. Dept. of Commerce, NOAA, 3 Vols.,
        Washington, D.C., 1973.

A-68   N. M. Newmark, Testimony Before the Atomic Licensing Appeal
        Board USNRC, Pacific Gas and Electric Company (Diablo Canyon
        Nuclear Power Plant Units Nos. 1 and 2), Docket Nos. 50-275 and
        50-323.

A-69   N. M. Newmark, W. J. Hall and B. Mohraz, "A Study of Vertical
        and Horizontal Earthquake Spectra," Directorate of Licensing,
        U. S. Atomic Energy Commission Report WASH-1255, April, 1973.

A-70   N. M. Newmark, J. R. Morgan and W. J. Hall, "Response Spectra of
        Combined Translation and Torsion For A Traveling Seismic Wave,
        Prepared for NRC, Contract NRC-04-058, September, 1978.

A-71   N. M. Newmark, "Interpretation of Apparent Upthrow of Objects in
        Earthquakes", Proceedings of the 5th World Conference on
        Earthquake Engineering, Rome, Vol. 2, 1974, pp 2338-2343.

A-72   N. M. Newmark, "Seismic Design Criteria for Structures and
        Facilities: Trans-Alaska Pipeline System", Proceedings of the
        U.S. National Conference on Earthquake Engineering, Ann Arbor,
        Michigan, 1975.

A-73   R. A. Page, J. A. Blume and W. B. Joyner, "Earthquake Shaking
        and Damage to Buildings", Science Vol. 189, No. 4203, August 22,
        1975.

A-74   C. Rojahn, B. J. Merrill, et. al, "The Island of Hawaii Earth-
        quake", EERI, Vol. 10, No. 18, February, 1976.

A-75   J. B. Savy, "Determination of Seismic Design Parameters: A
        Stochastic Approach", M.I.T., Cambridge, Massachusetts.

A-76   A. I. Snyder, "Damage to Mechanical Equipment as the Result of
        the February 9, 1971 Earthquake in San Fernando, California,"
        Seismic Design and Analysis, American Society of Mechanical
        Engineers, 1971.

A-77   O. W. Steinhardt, "Protecting A Power Lifeline Against
        Earthquakes", Journal of the Technical Councils of ASCE,
        November, 1978.

A-78   O. W. Steinhardt, "Low-Cost Seismic Strengthening of a Power
        System", ASCE Preprint 80-076, April, 1980.

A-79   J. M. Stephenson, "Earthquake Damage to Anchorage Area
        Utilities", U. S. Naval Civil Engineering Laboratory, June, 1954.

A-80   J. L. Stratta and L. A. Wyllie, Jr., "Reconnaissance Report,
        Friuli, Italy Earthquakes of 1976", EERI, January, 1979.

A-81   J. L. Stratta, T. J. Canon, et al, "Reconnaissance Report
        Mindanao, Phillippines Earthquake, August 17, 1976", EERI,
        August, 1977.

A-82   W. F. Swiger, "Notes on Plants Designed by Stone & Webster Which
        Have Experienced Large Earthquakes", 1979 (unpublished).

A-83   J. M. Tanaka, "Airports and Air Traffic Control Facilities",
        U.S. Army Corps of Engineers District, Alaska, 1967.

A-84   A. Rutenberg, P. C. Jennings and G. W. Housner, "The Response of
        Veterans Hospital Building 41 in the San Fernando Earthquake",
        EERI Report 80-03, May, 1980.

A-85   J. E. Valera, H. B. Seed, C. F. Tsai and J. Lysmer, "Seismic
        Soil-Structure Interaction Effects at Humboldt Bay Power Plant",
        Journal of the Geotechnical Engineering Division, ASCE, Vol.
        103, No. GT10, October, 1977.

A-86   E. H. Vanmarcke and S. P. Lai, "Strong-Motion Duration and RMS
        Amplitude of Earthquake Records", Bulletin of the Seismological
        Society of America, Vol. 70, No. 4, August, 1980, pp 1293-1307.

A-87   H. S. Lew, E. V. Leyendecker, and R. D. Dikkers, "Engineering
        Aspects of the 1971 San Fernando Earthquake", U.S. Department of
        Commerce, National Bureau of Standards, Washington, D.C., 1971.

A-88   R. Vignola and E. Arze, "Behavior of a Steel Plant Under Major
        Earthquakes", Proceedings of the 2nd World Conference on
        Earthquake Engineering, Japan, 1960.

A-89   H. M. Waldron, R. P. Miller and S. D. Werner, "Geotechnical
        Investigations at Nuclear Power Plant Sites", Nuclear
        Engineering and Design, North Holland Publishing Company, Vol.
        36, 1976, pp. 397-409.

A-90   S. D. Werner, "Engineering Characteristics of Earthquake Ground
        Motions," Nuclear Engineering and Design, North Holland
        Publishing Company, Vol. 36, 1976, pp.367-395.

A-91   S. D. Werner, "Procedures for Developing Vibratory Ground Motion
        Criteria at Nuclear Power Plant Sites", Nuclear Engineering and
        Design, North Holland Publishing Company, Vol. 36, 1976, pp.
        411-441.

A-92   P. I., Yanev, Draft Paper on "Behavior of Power Plants and Other
        Industrial Facilities in Past Earthquakes", URS, April 28, 1980.

A-93   T. Zsutty and M. Deherra, "A Statistical Analysis of Accelerogram
        Peaks Based Upon the Exponential Distribution Model", Stanford
        University, Palo Alto, California.

A-94   Letter, N. Hirata, San Francisco District Mgr., Toshiba Interna-
        tional Corporation, to T. McIlraith, Pacific Gas & Electric Co.,
        San Francisco, California, April 9, 1979.

A-95   Ministry of Power Engineering and Electriciation, "Provisional
        Design Standards for Nuclear Power Plants in Seismic Regions",
        Minehnergo, USSR.

A-96   CIT Reports Published 1951, Dynamics Laboratory Disaster
        Research Center, EERL, 1980.

A-97   P. I. Yanev, (ed.), "Reconnaissance Report, Miyagi-Ken-Oki,
        Japan Earthquake", EERI, June 12, 1978.

A-98   H. Bolton Seed and John Lysmer, "The Significance of Site
        Response in Soil-Structure Interaction Analyses for Nuclear
        Facilities", ASCE Specialty Conference on Civil Engineering and
        Nuclear Power, Knoxville, Tennessee, September, 1980.

A-99   Tall Building Criteria and Loading, Monograph on Planning and
        Design of Tall Buildings, Volume CL, ASCE, 1980.

A-100   D. E. Hudson, "Strong Motion Earthquake Measurements in
        Epicentral Regions", Proceedings of the 6th World Conference on
        Earthquake Engineering, New Delhi, 1977.

A-101   E. H. Vanmarcke, "Random Vibration Approach to Soil Dynamics
        Problems", The Use of Probabilities in Earthquake Engineering,
        ASCE Preprint 2913, ASCE Fall Convention, San Francisco,
        California, 1977.

A-102   "Damage to Pumping and Power Stations", California DWR Bulletin
        No. 166-3, June, 1967.

A-103   J. Prince and L. Alonso, "The Relatively Light Damage Produced
        by Two Strong Motion Earthquakes in Southern Mexico", Pro-
        ceedings of the 7th World Conference on Earthquake Engineering,
        September, 1980.

A-104   J. Prince, L. Alonso, and I. Navarro, "Procasamiento de
        Acelerogramas Obtenidos en 1974, "Reporte del Instituto de
        Ingenieria, Universidad Nacional Autonoma de Mexico, February,
        1976.

A-105   R. B. Matthiesen and J. Ragsdale, "Preliminary Report of Strong-
        Motion Data from the August 6, 1979 Coyote Lake Earthquake",
        USGS, 1979.

A-106   G. Dean, et al, "1979 Coyote Lake (Gilroy) Earthquake", EERI
        Newsletter, September, 1979.

A-107   R. K. Reitherman, "Notes on Non-Structural Features of the
        August 6, 1979 Coyote Lake Earthquake", EERI Newsletter,
        November, 1979.

A-108   F. L. Mellon, "Report of Post-Earthquake Investigation Team
         Coyote Lake Earthquake of August 6, 1979", CALTRANS Office of
         Structures Design.

A-109   C. F. Armstrong, "Coyote Lake Earthquake, 6 August 1979",
         California Geology, November, 1979.

A-110   Earthquakes - Agadir, Morocco, February 19, 1960, Skopje,
         Yugoslavia, July 26, 1963; Anchorage, Alaska, March 27, 1964;
         Caracas, Venezuela July 1967, American Iron and Steel Institute,
         1975.

A-111   Managua, Nicaragua Earthquake of December 23, 1972, EERI
         Conference Proceedings, San Francisco, California, Vol. I & II,
         November 29 & 30, 1973.

A-112   Building Performance in the 1972 Managua Earthquake, NBS
         Technical Note 807, U.S. Department of Commerce, November, 1973.

A-113   M. A. Sozen and R. B. Matthiesen, "Engineering Report on the
         Managua Earthquake of 23 December 1973", "National Academy of
         Sciences, Washington, D.C., 1975.

A-114   Herring, K. S. et al, "Reconnaissance Report: Effects of
         November 8, 1980 Earthquake on Humboldt Bay Power Plant and
         Eureka, California Area", NUREG-0766, USNRC, June, 1981.

A-115   G. W. Housner and M. D. Trifunac, "Analysis of Accelerogram -
         Parkfield Earthquake", Bulletin of the Seismological Society of
         America, Vol. 57, No. 6, December, 1967, pp. 1193-1220.

A-116   W. K. Cloud and V. Perez, "Accelerograms - Parkfield Earthquake",
         Bulletin of the Seismological Society of America, Vol. 57, No. 6,
         December, 1967, pp. 1179-1192.

A-117   United States Earthquakes 1966, U.S. Dept. of Commerce, ESSA,
         1968.

A-118   G. B. Oakeshott, "Geologic Hazards Parkfield Earthquakes",
         California Division of Mines and Geology, July 13, 1966.

A-119   J. F. Meehan, "Reconnaisance Report Santa Barbara Earthquake
         August 13, 1978", Office of the State Architect, Sacramento,
         California.

A-120   United States Earthquakes, 1978, U.S. Dept. of Interior Geologi-
         cal Survey and U.S. Department of Commerce, NOAA, Golden,
         Colorado, 1980.

A-121   J. H. Gates, "A Note on the Ferndale, California Area Earthquake
         of June 7, 1975", (personal correspondence).

A-122   United States Earthquakes, 1975, U.S. Department of Interior,
         Geological Survey and U.S. Department of Commerce, NOAA,
         Boulder, Colorado, 1977.

A-123   "Seismic Report Post-Earthquake Investigation Team, Eureka,
         California (Trinidad-Offshore) Earthquake of November 8, 1980",
         CALTRANS, Office of Structures Design.

A-124   "Trinidad-Offshore, California Earthquake November 8, 1980",
         EERI Newsletter, Vol. 15, Part B, January, 1981.

A-125   R. Nason, "Seismic Intensity Studies in the Imperial Valley",
         (draft report) U. S. Geological Survey, Menlo Park, California,
         1980.

A-126   "Seismic Report Post-Earthquake Investigation Team, "Imperial
         Valley, California, Earthquake of October 15, 1979", CALTRANS,
         Office of Structures Design.

A-127   C. Real, R. D. McJunkin, and E. Leivas, "Effects of Imperial
         Valley Earthquake 15 October 1979", Imperial County, California,
         California Geology, December, 1979.

A-128   "Analysis of the El Centro Steam Plant", (draft report) submitted
         to PG&E by URS/John A. Blume, May, 1981.

A-129   J. M. Pauschke, C. S. Oliveira, H. C. Shah and T. C. Zutty, "A
         Preliminary Investigation of the Dynamic Response of the Imperial
         County Services Building During the October 15, 1979 Imperial
         Valley Earthquake", J. A. Blume Earthquake Engineering Center,
         Stanford University, January, 1981.

A-130   A. K. Chopra and P. Chakrabarti, "Analysis of the Earthquake
         Performance of Koyna Dam", Paper No. 121, Bulletin ISET, Vol. 9,
         No. 2, June, 1972, pp. 49-60.

A-131   A. K. Chopra and P. Chakrabarti, "The Koyna Earthquake and the
         Damage to Koyna Dam", Bulletin of the Seismological Society of
         America, Vol. 63, No. 2, April, 1973, pp. 380-397.

A-132   G. V. Berg, Y. C. Das, K. Gokhale, and A., V. Setlur, "The
         Koyna, India Earthquakes", Proceedings of the 4th World
         Conference on Earthquake Engineering, Santiago, Chile, 1969.

A-133   UNESCO Committee of Experts, "Koyna Earthquake of December 11,
         1967", Report, New Delhi, 1968.

A-134   Dames and Moore Report: Comparison of August 27, 1978,
         Monticello Reservoir Earthquake Response Spectra to the
         Operating Basis Earthquake Response Spectra for the Virgil C.
         Summer Nuclear Station, submitted to South Carolina Electric &
         Gas Company, 1980.

A-135   "Final Report - Significance of the Monticello Reservoir
         Earthquake of August 27, 1978 to the Virgil C. Summer Nuclear
         Station", prepared for South Carolina Electric & Gas Company,
         Dames and Moore Report 5182-068-09, May, 1980.

A-136   Personal Communication with Robert Whorton, South Carolina
         Electric and Gas Company, May, 1981.

A-137   United States Earthquakes 1952, Serial No. 773, U. S. Department
         of Commerce, Coast and Geodetic Survey, Washington, 1954.

A-138   K. V. Steinbrugge and D. F. Moran, "An Engineering Study of the
         Southern California Earthquake of July 21, 1952 and Its After-
         shocks", Bulletin of the Seismological Society of America, Vol.
         44, No. 2b April, 1954.

A-139   Earthquakes in Kern County, California During 1952, State of
         California, Department of Natural Resources, Division of Mines,
         SF, Bulletin 171, 1955.

A-140   C. F. Richter, Elementary Seismology, W. H. Freeman and Company,
         San Francisco and London, 1958.

A-141   "The LLNL Earthquake", Impact Analysis Committee Report on the
         Livermore, California, Earthquakes of January 24 and 26, 1980,
         UCRL-52956, July 15, 1980.

A-142   Greenville (Diablo-Livermore) Earthquakes of January 1980, EERI
         Newsletter, Vol. 14, No. 2, March, 1980.

A-143   "Seismic Report Post-Earthquake Investigation Team, Greenville,
         California Earthquake of January 24, 1980", CALTRANS, Office of
         Structures Design.

A-144   "Effects of Sharpsburg, Kentucky Earthquake of July 27, 1980, on
         Wm. Zimmer Station Moscow, Ohio", Report prepared for the
         Cincinnati Gas and Electric Company, Cincinnati, Ohio, Sargent
         and Lundy Engineers and Fugro, Inc., January, 1981.

A-145   Contribution to the Study of Friuli Earthquake of May, 1976,
         CNEN-ENFL Commission on Seismic Problems Associated with the
         Installation of Nuclear Plants, November, 1976.

A-146   P. Repetto, I. Aranzo and H. B. Seed, "Influence of Site Condi-
         tions on Building Damage During the October 3, 1974 Lima Earth-
         quake", Report No. UCB/EERC-80/41, September, 1980.

A-147   "Oroville, California, Earthquake, August, 1975", Special Report
         124, California Division of Mines and Geology, 1975.

A-148   H. B. Seed, I. M. Idriss, and H. Dezfullian, "Relationship
         Between Soil Conditions and Building Damage in the Caracas
         Earthquake of July 19, 1967", Report No. EERC 70-2, February,
         1970.

A-149   S. S. Tezcon, V. Yerlic, and H. T. Durgunoglu, "A Reconnaissance
         Report for the Romanian Earthquake of 4 March 1977", Earthquake
         Engineering and Structural Dynamics, Vol. 6, 1978, pp. 397-421.

A-150   Earthquake in Romania, March 4, 1977, An Engineering Report,
         National Research Council and EERI, 1980.

A-151   "Special Issue - An Engineering Report on the Chilean Earthquakes
         of May, 1960", Bulletin of the Seismological Society of America,
         Vol. 53, No. 2, February, 1963.

A-152   United States Earthquakes 1949, Serial No. 748, U. S. Department
         of Commerce, U.S. Coast and Geodetic Survey, Washington, 1951.

A-153   United States Earthquakes 1928-1935, U.S. Department of Commerce,
         Environmental Science Services Administration, Coast and Geodetic
         Survey, Washington, 1969.

A-154   United States Earthquakes 1936-1940, U.S. Department of Commerce, Environmental Science Services Administration, Coast and Geodetic Survey, Washington, 1969.

A-155   Earthquakes and Blast Effects on Structures, Proceedings of Symposium, Los Angeles, June, 1952, Sponsored by EERI and University of California, September, 1952.

A-156   A. G. Sylvester, "The Mammouth Lakes, California, Earthquakes, 25-31 May 1980", Department of Geological Sciences, U.C. Santa Barbara, May 31, 1980.

A-157   P. C. Jennings, Engineering Features of the San Fernando Earthquake February 9, 1971, California Institute of Technology, EERL 71-02, 1971.

A-158   United States Earthquakes 1971, U.S. Department of Commerce, NOAA, Boulder, Colorado, 1973.

A-159   G. Howard, et al, "Earthquake Effects at Nuclear Facilities - San Fernando Earthquake of February 9, 1971", U.C. Los Angeles, UCLA ENG-7215, February, 1972.

A-160   S. H. Mendes, "Earthquake Resistance of Modern Buildings - A Case Study", The 50-Year Event, Proceedings of the 1980 SEADC Convention, Monterey, October 2-4, 1980.

A-161   M. A. Larson, "Needed Improvements in A Seismic Design", Structural Moments, SEAOC publication, February, 1980.

A-162   S. A. Mahin, et. al, "Response of the Olive View Hospital Main Building During the San Fernando Earthquake", EERC 76-22, University of California, Berkeley, October, 1976.

A-163   A. Ruthenberg, P. C. Jennings, and G. W. Housner, "The Response of the Veterans Hospital Building 41 in the San Fernando Earthquake", Earthquake Engineering Research Laboratory, Report EERL 79-03, California Institute of Technology, Pasadena, California, 1979.

APPENDIX B

INPUT GROUND MOTION DATA
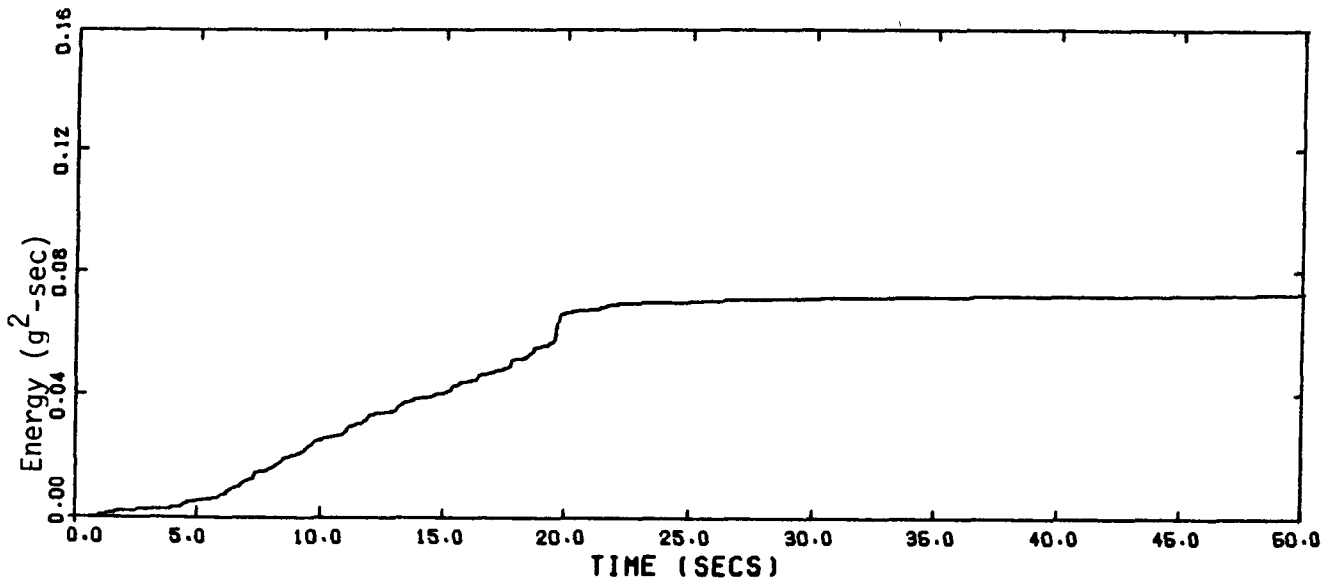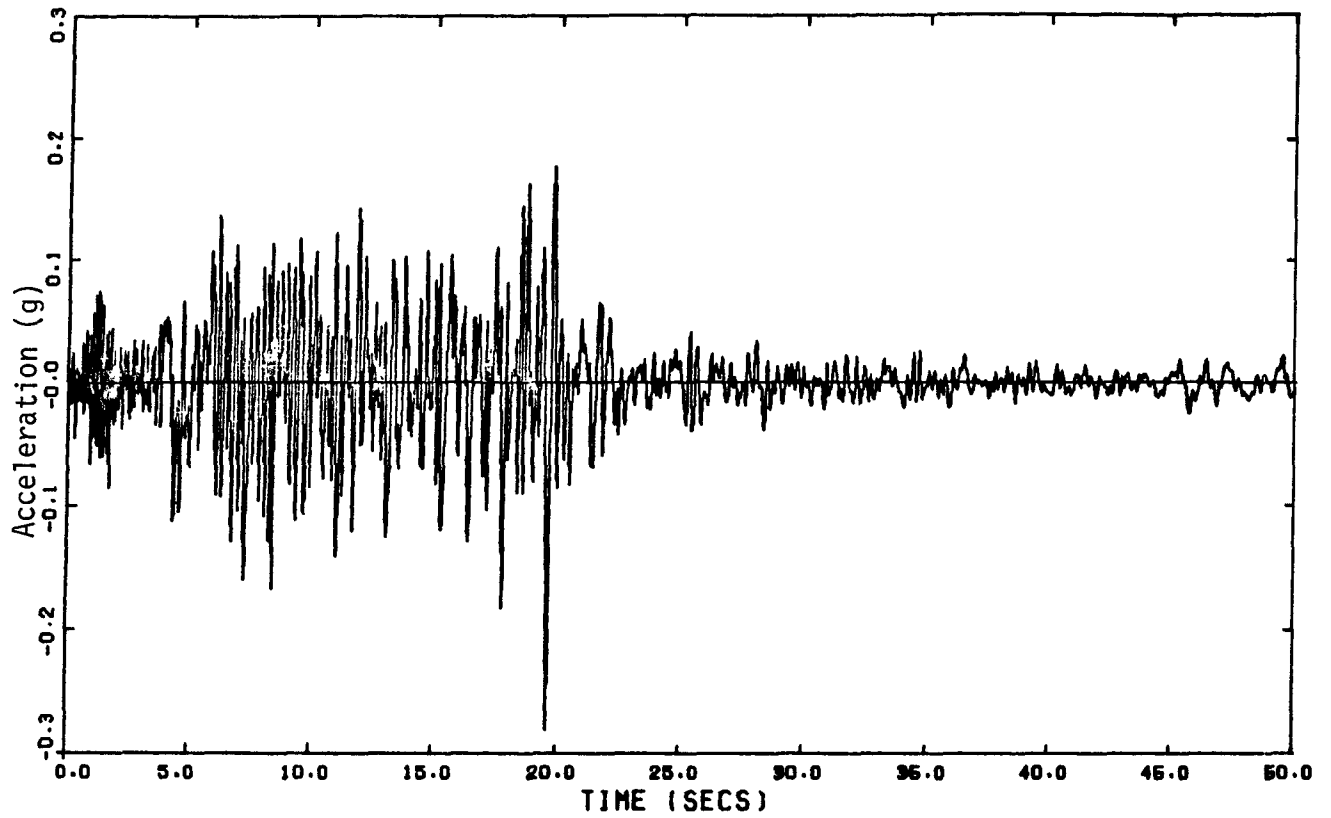
FIGURE B-1a.   ACCELEROGRAM AND CORRESPONDING CUMULATIVE ENERGY
FOR THE OLYMPIA, WA., 1949 (N86E) RECORD
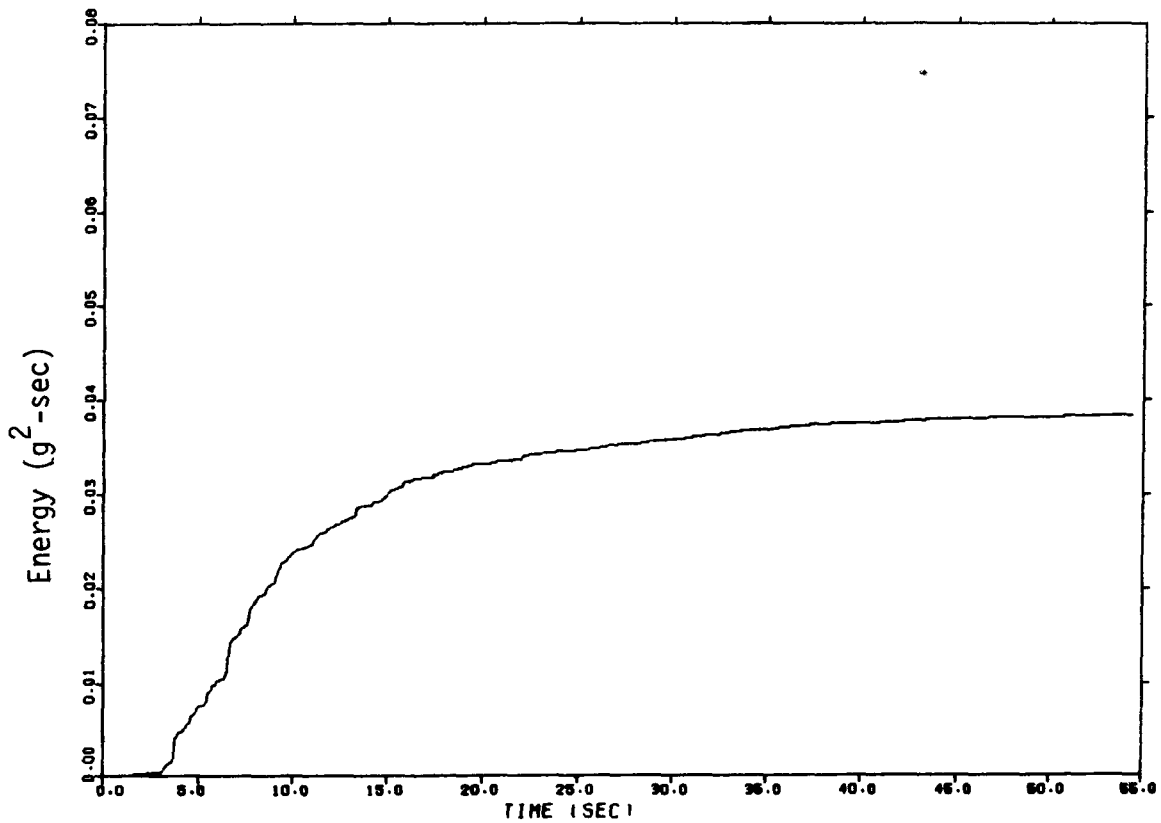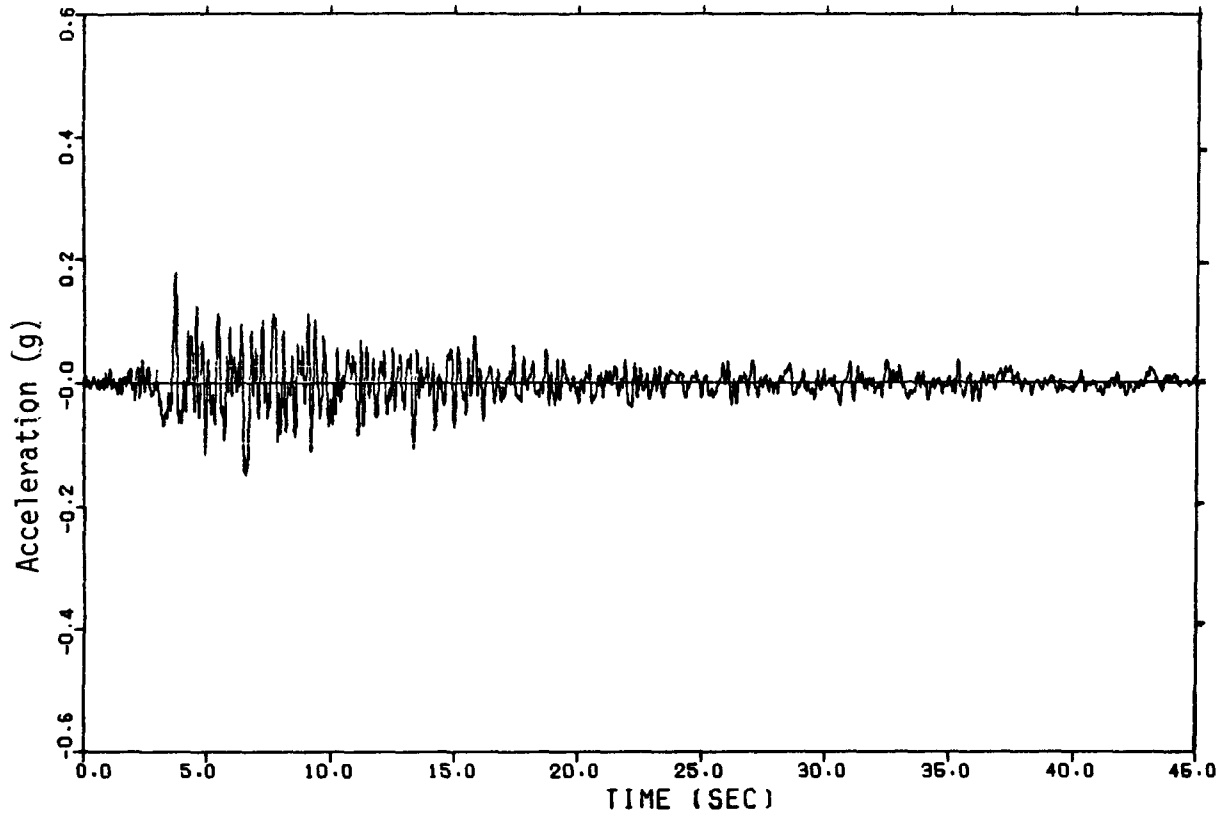
FIGURE B-1b.   ACCELEROGRAM AND CORRESPONDING CUMULATIVE ENERGY
FOR THE TAFT, KERN CO., 1952 (S69E) RECORD

B-2
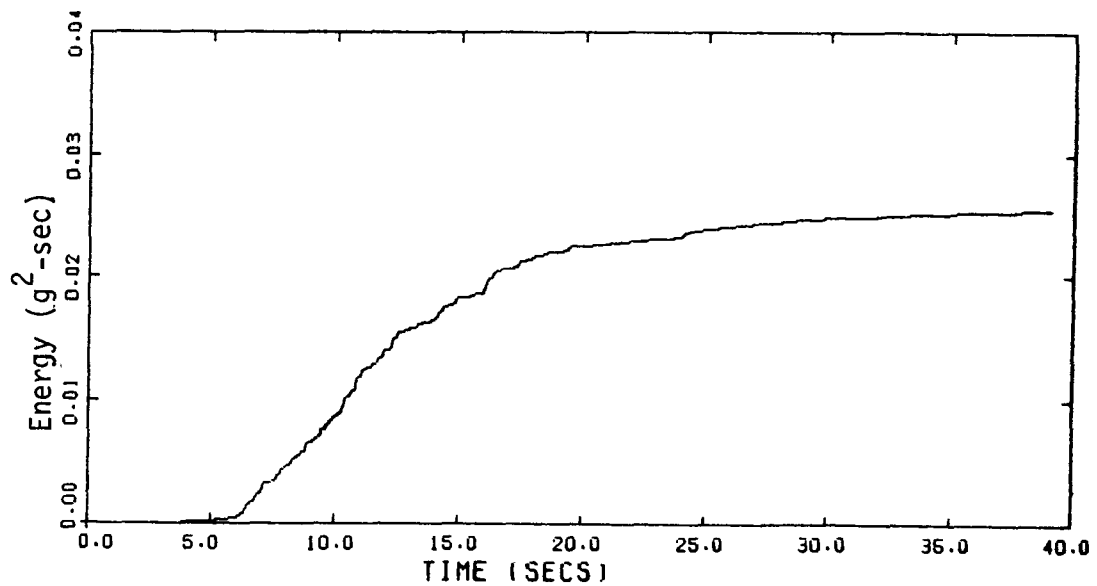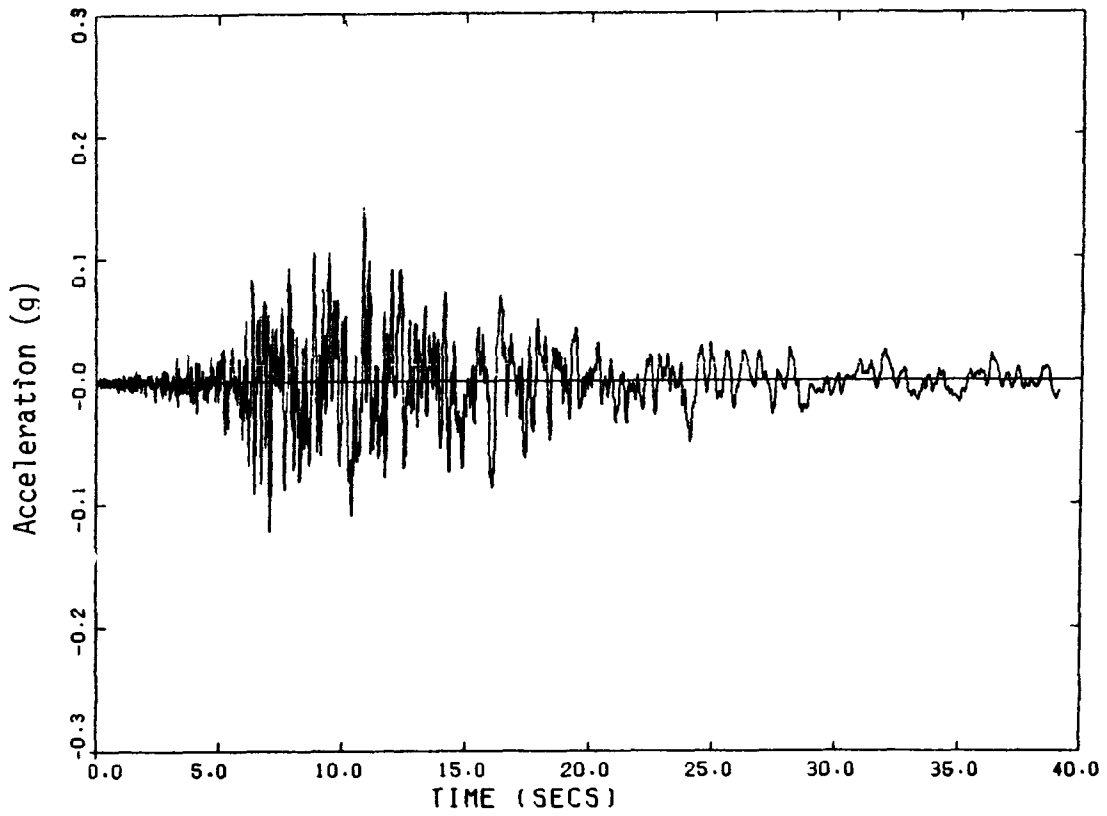
FIGURE B-1c.   ACCELEROGRAM AND CORRESPONDING CUMULATIVE ENERGY FOR THE
EL CENTRO, ARRAY NO. 12, IMPERIAL VALLEY 1979 (140) RECORD
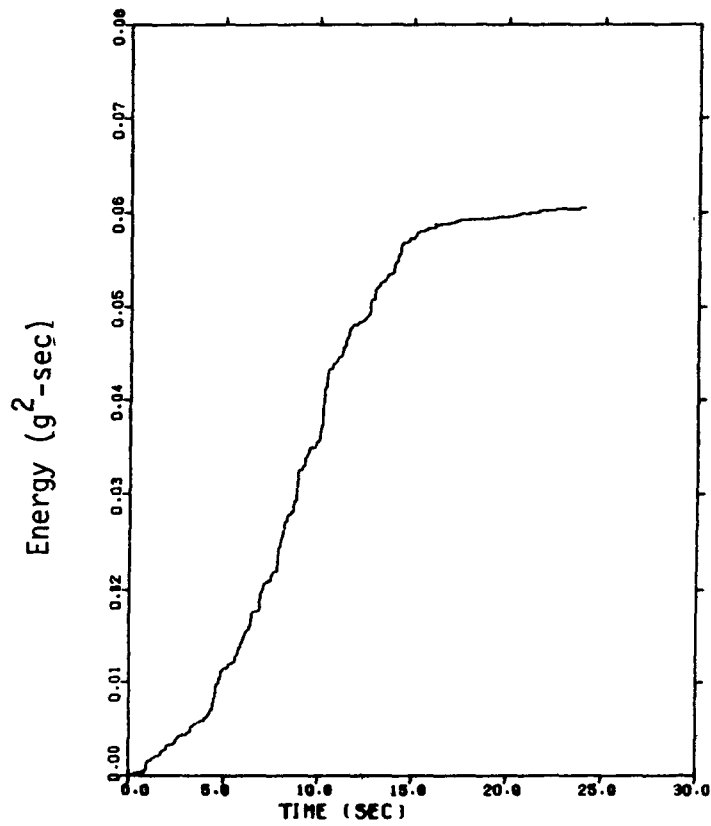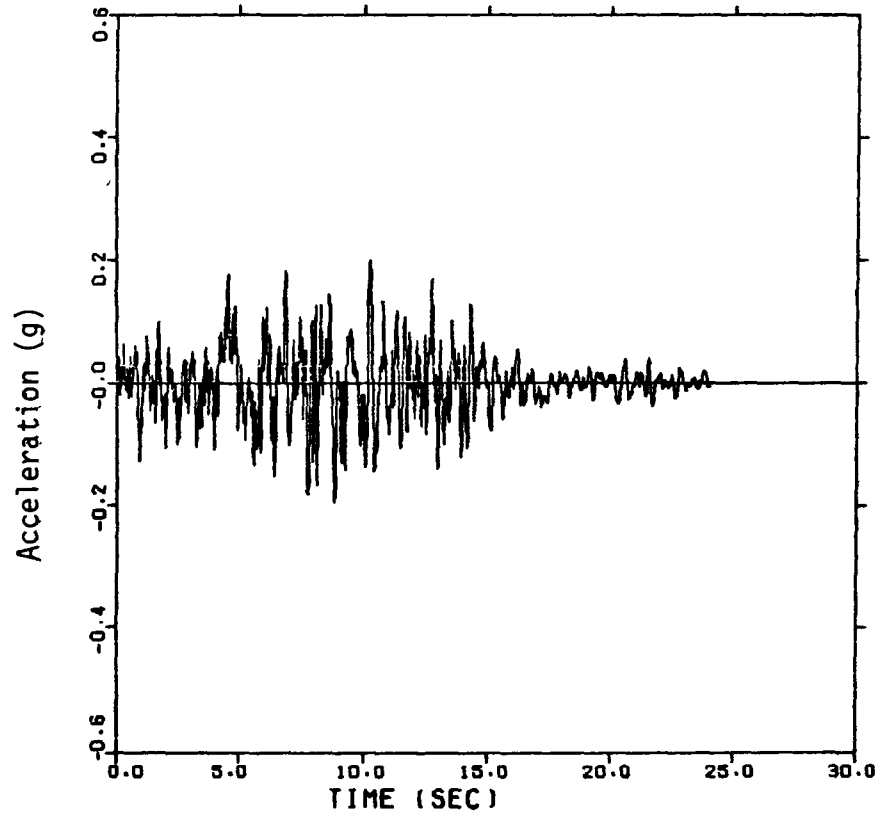
FIGURE B-1d.   ACCELEROGRAM AND CORRESPONDING CUMULATIVE ENERGY
FOR THE ARTIFICIAL (R.G. 1.60) RECORD

B-4
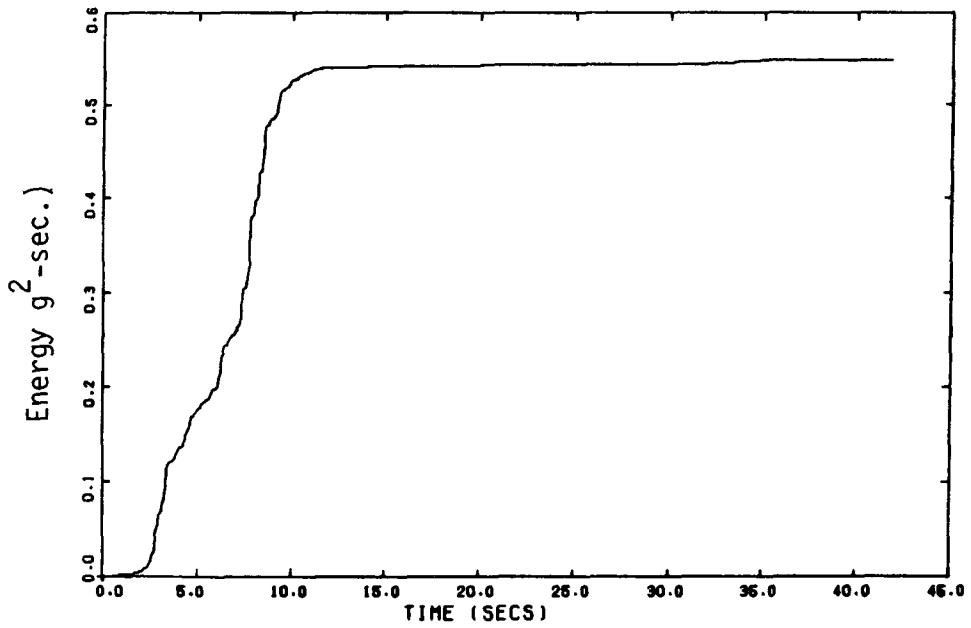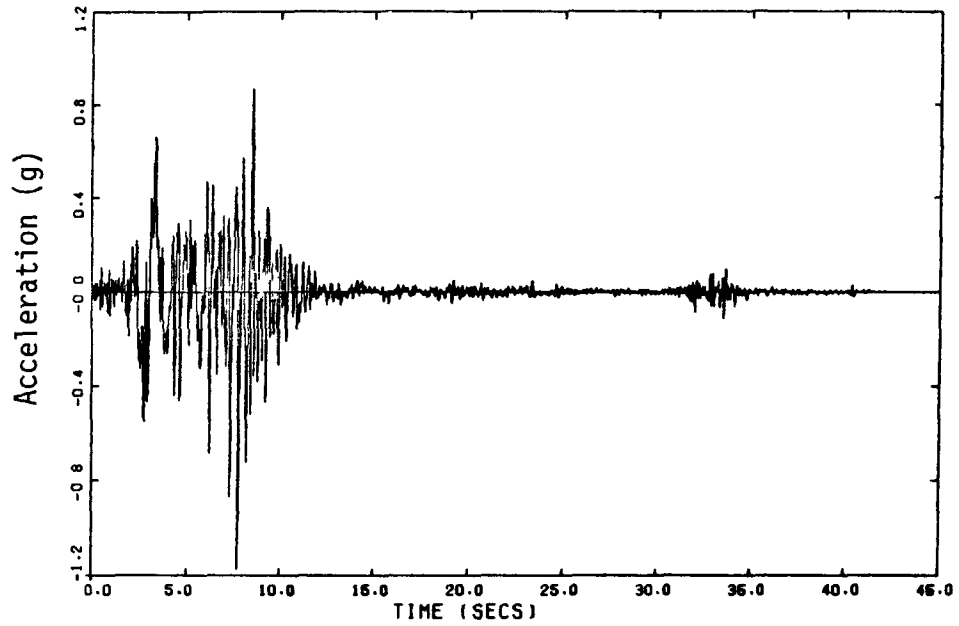
FIGURE B-1e.   ACCELEROGRAM AND CORRESPONDING CUMULATIVE ENERGY FOR
THE PACOIMA DAM, SAN FERNANDO, 1971 (S14W) RECORD
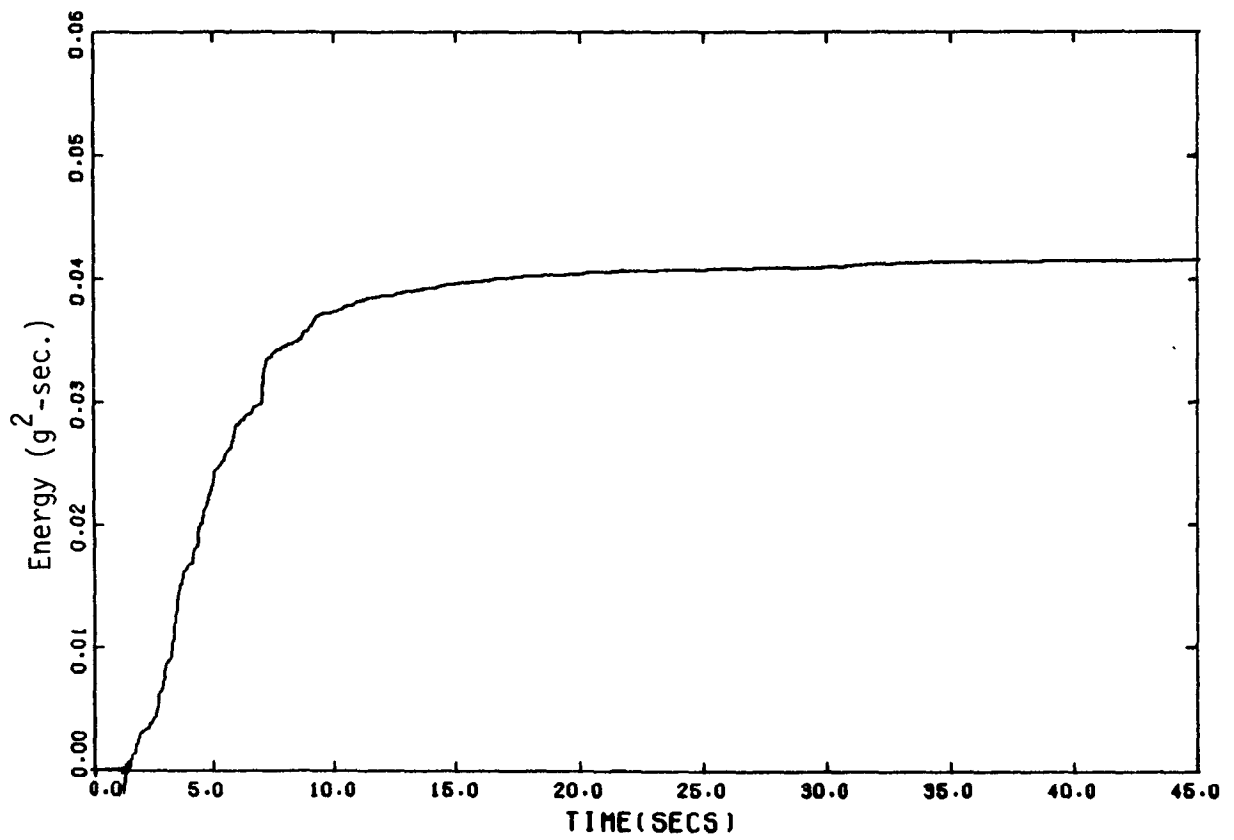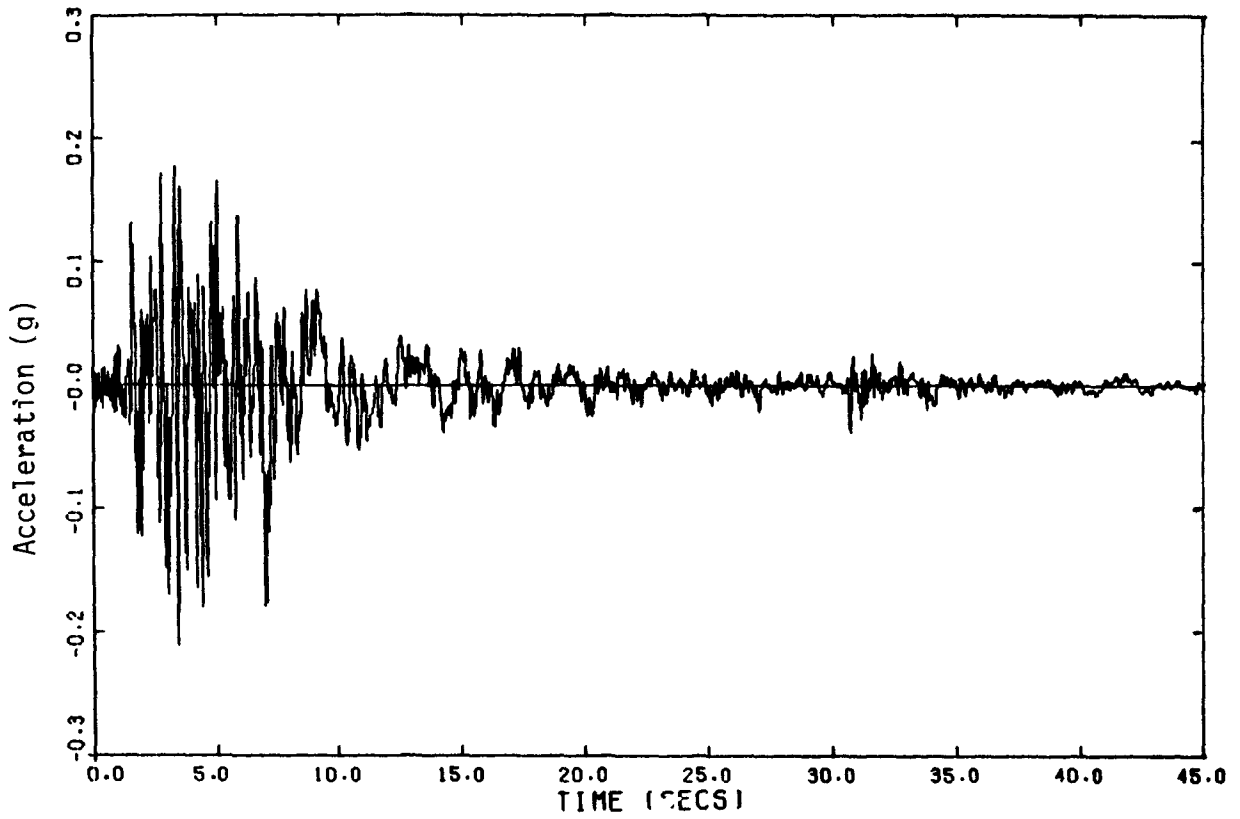
FIGURE B-1f. ACCELEROGRAM AND CORRESPONDING CUMULATIVE ENERGY FOR THE
HOLLYWOOD STORAGE P.E. LOT, SAN FERNANDO, 1971 (N90E) RECORD

B-6
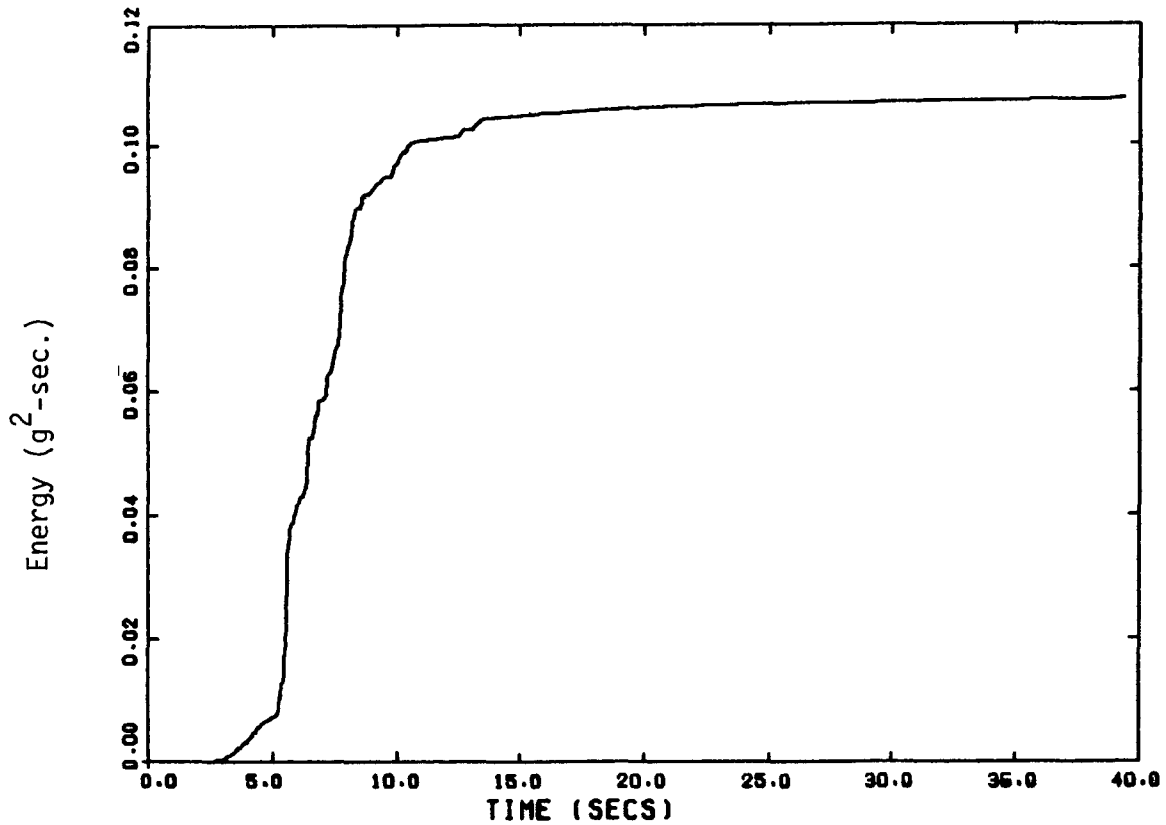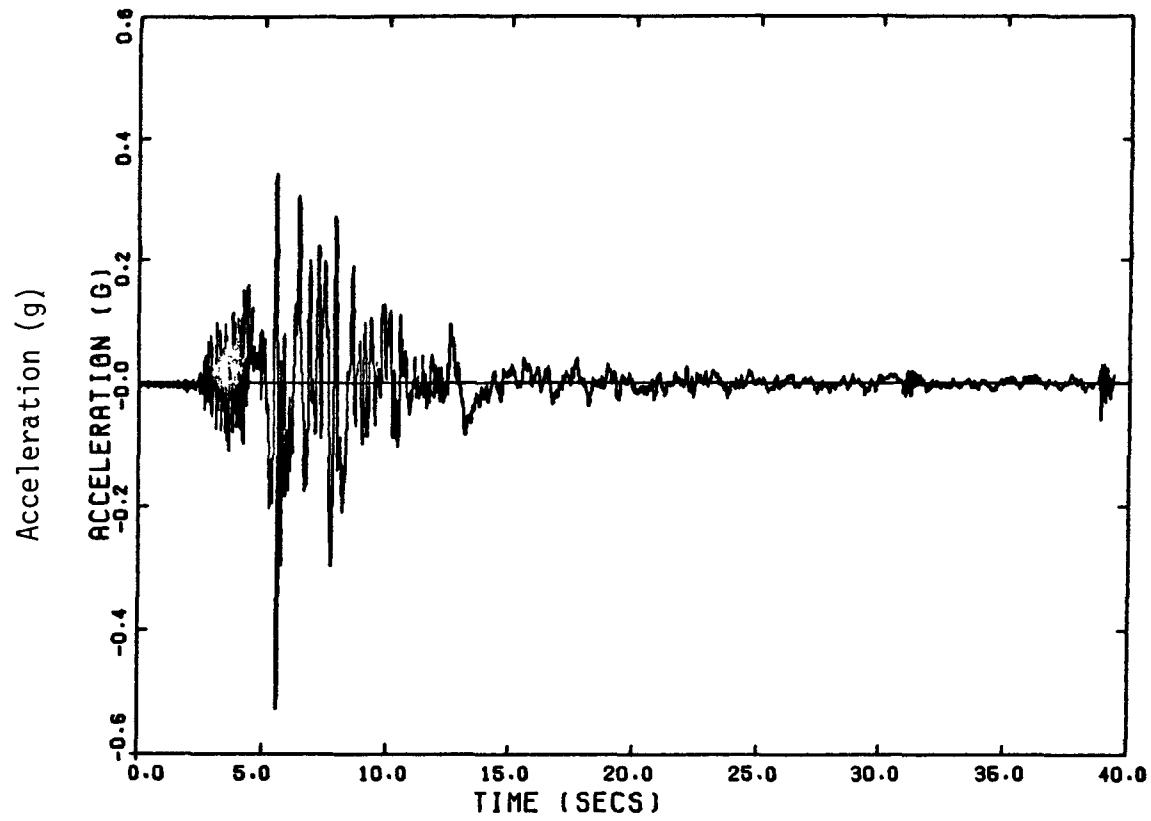
FIGURE B-1g.   ACCELEROGRAM AND CORRESPONDING CUMULATIVE ENERGY FOR THE
EL CENTRO ARRAY NO. 5 IMPERIAL VALLEY, 1979 (140) RECORD

B-7
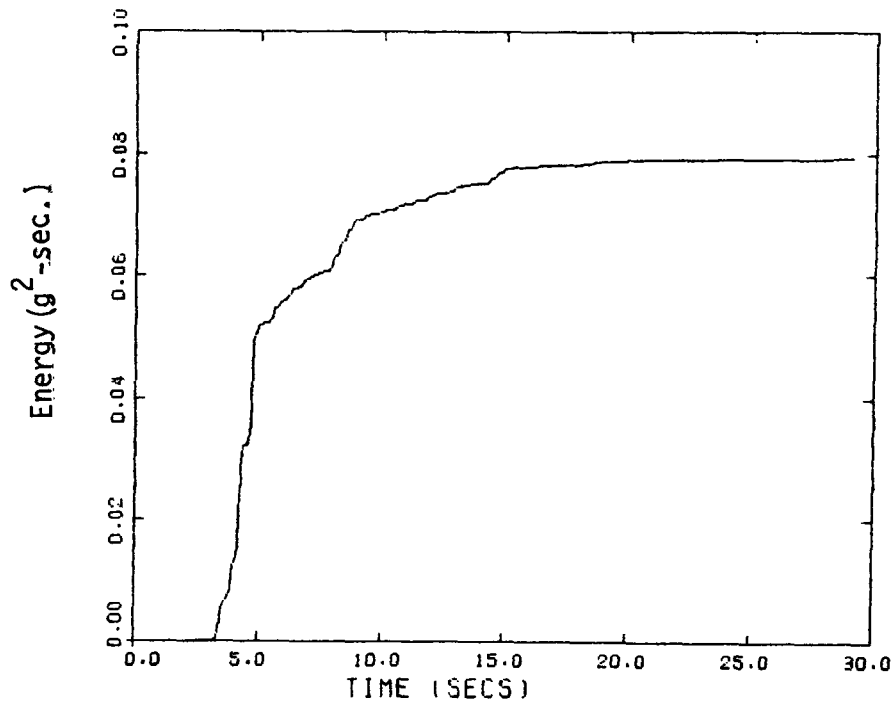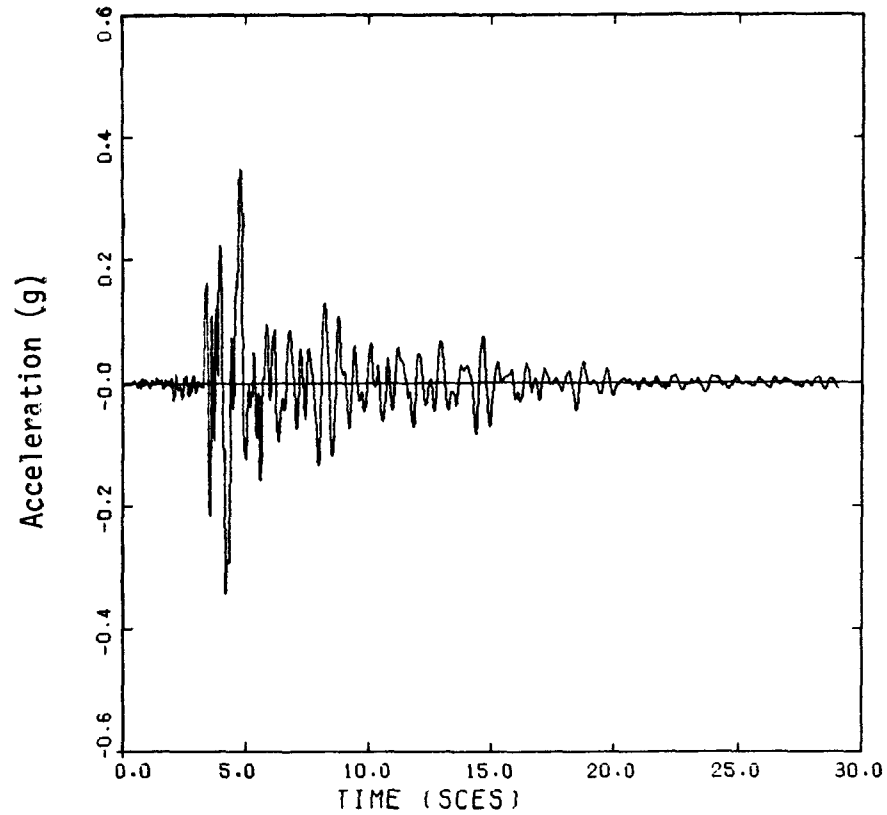
FIGURE B-1h. ACCELEROGRAM AND CORRESPONDING CUMULATIVE ENERGY FOR THE
UCSB GOLETA, SANTA BARBARA 1978 (180) RECORD

B-8
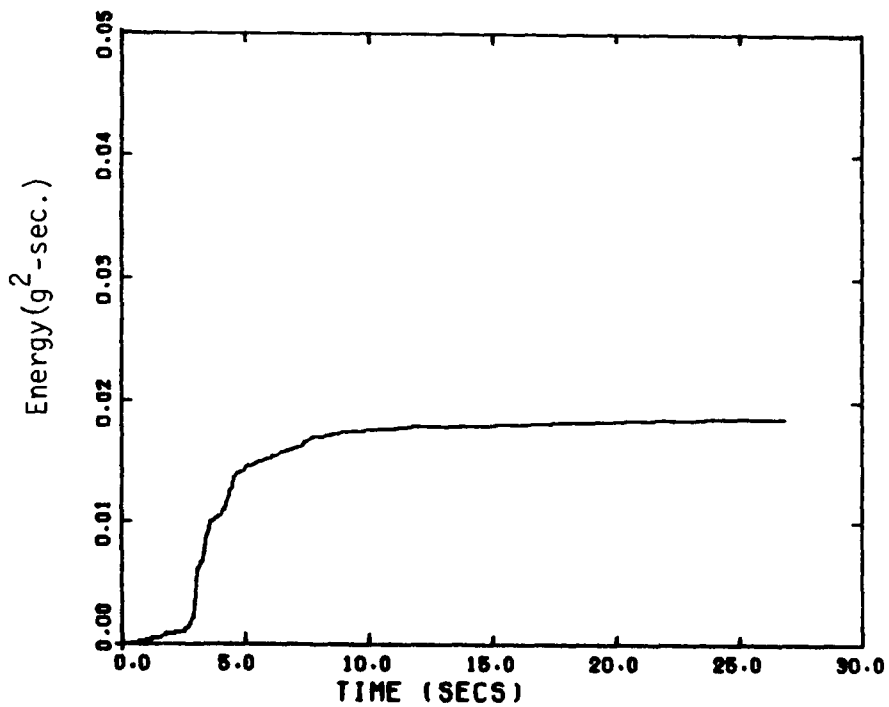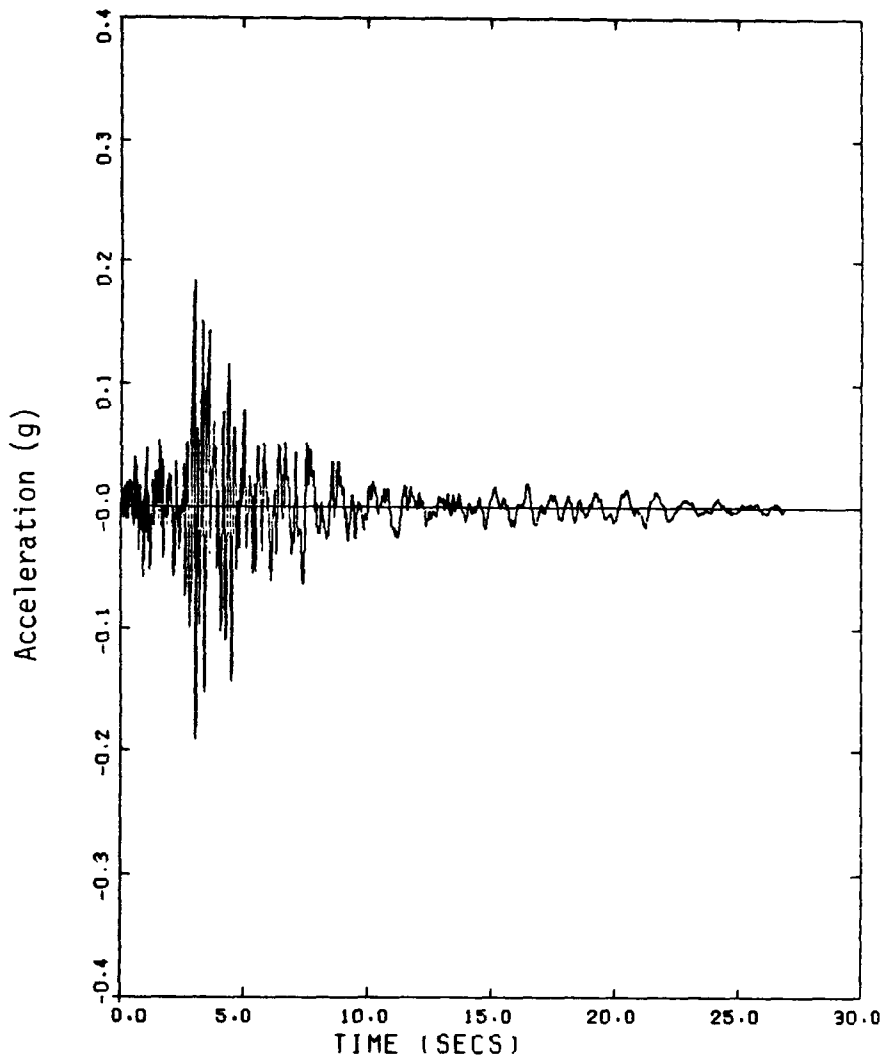
FIGURE B-1i.   ACCELEROGRAM AND CORRESPONDING CUMULATIVE ENERGY FOR
THE GILROY ARRAY NO. 2, COYOTE LAKE 1979 (050) RECORD

B-9
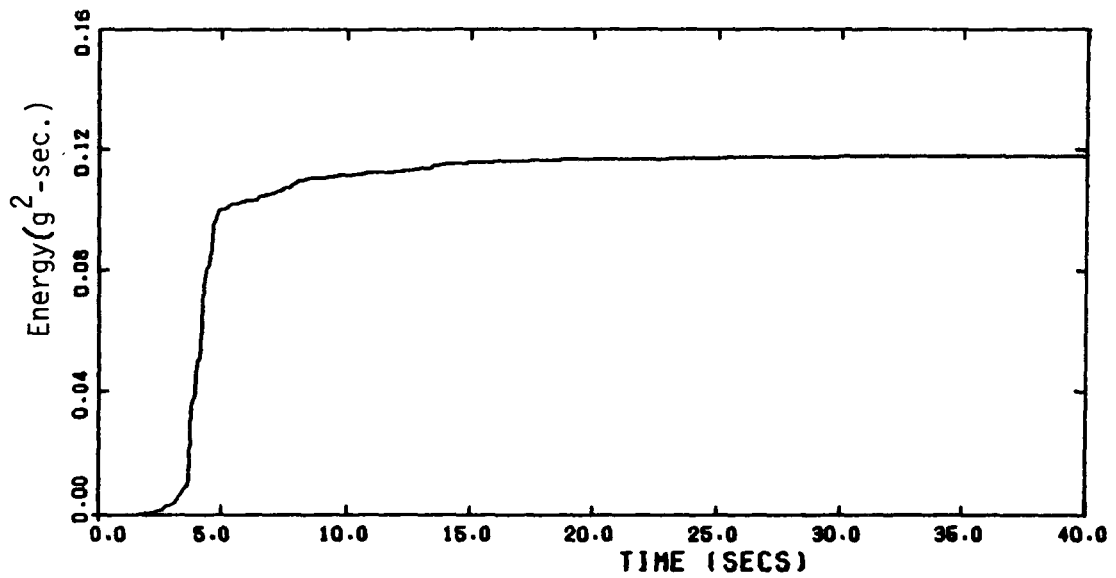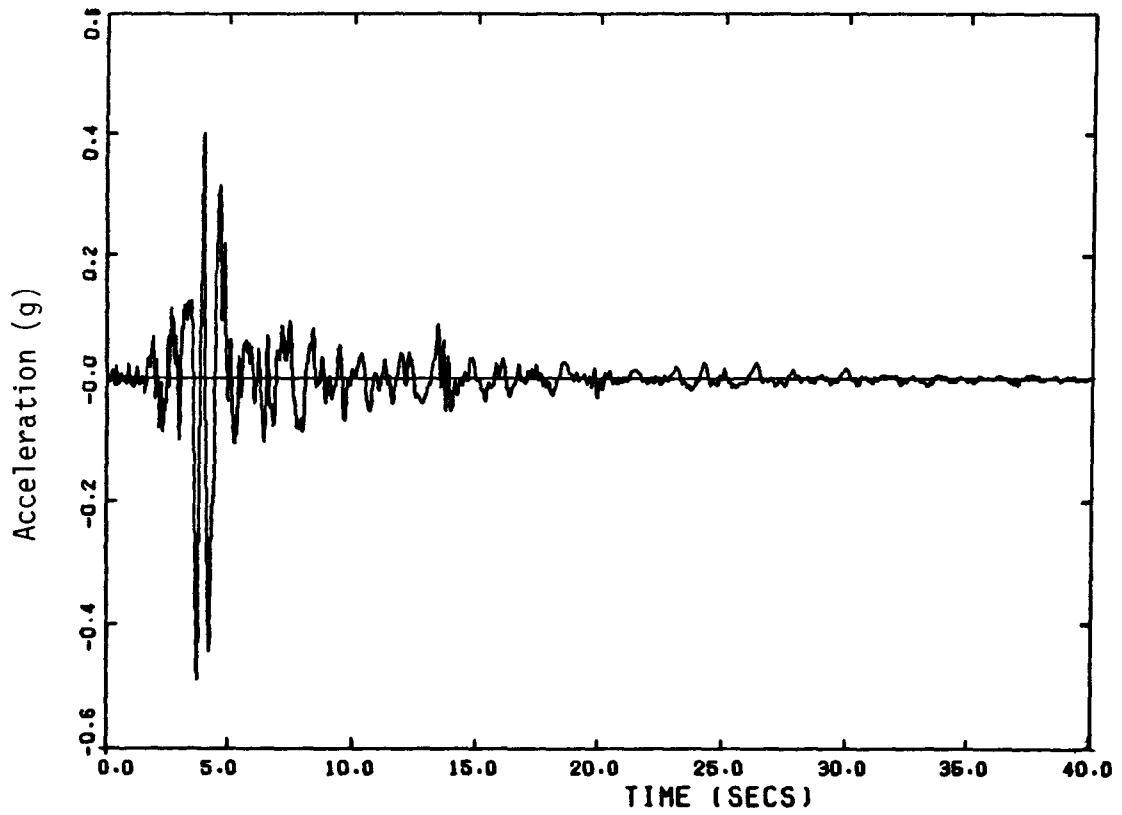
FIGURE B-1j.   ACCELEROGRAM AND CORRESPONDING CUMULATIVE ENERGY FOR THE
CHOLAME ARRAY NO. 2, PARKFIELD 1966 (N65E) RECORD
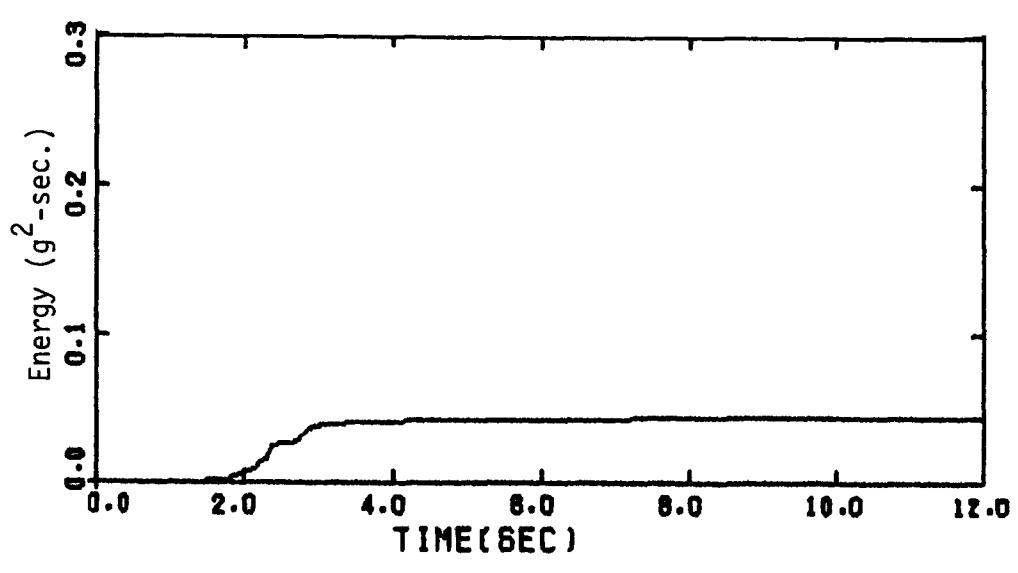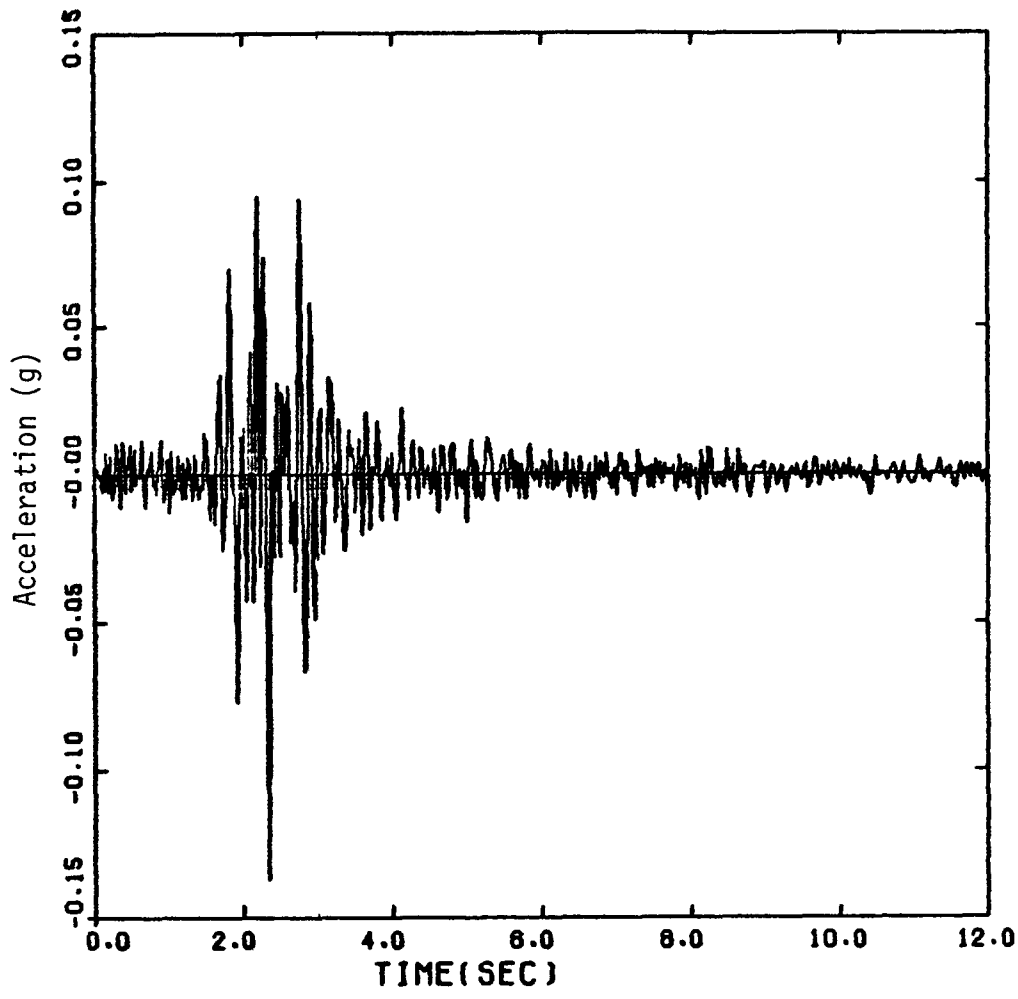
FIGURE B-1k.   ACCELEROGRAM AND CORRESPONDING CUMULATIVE ENERGY FOR
THE GAVILAN COLLEGE, HOLLISTER, 1974 (S67W) RECORD

B-11
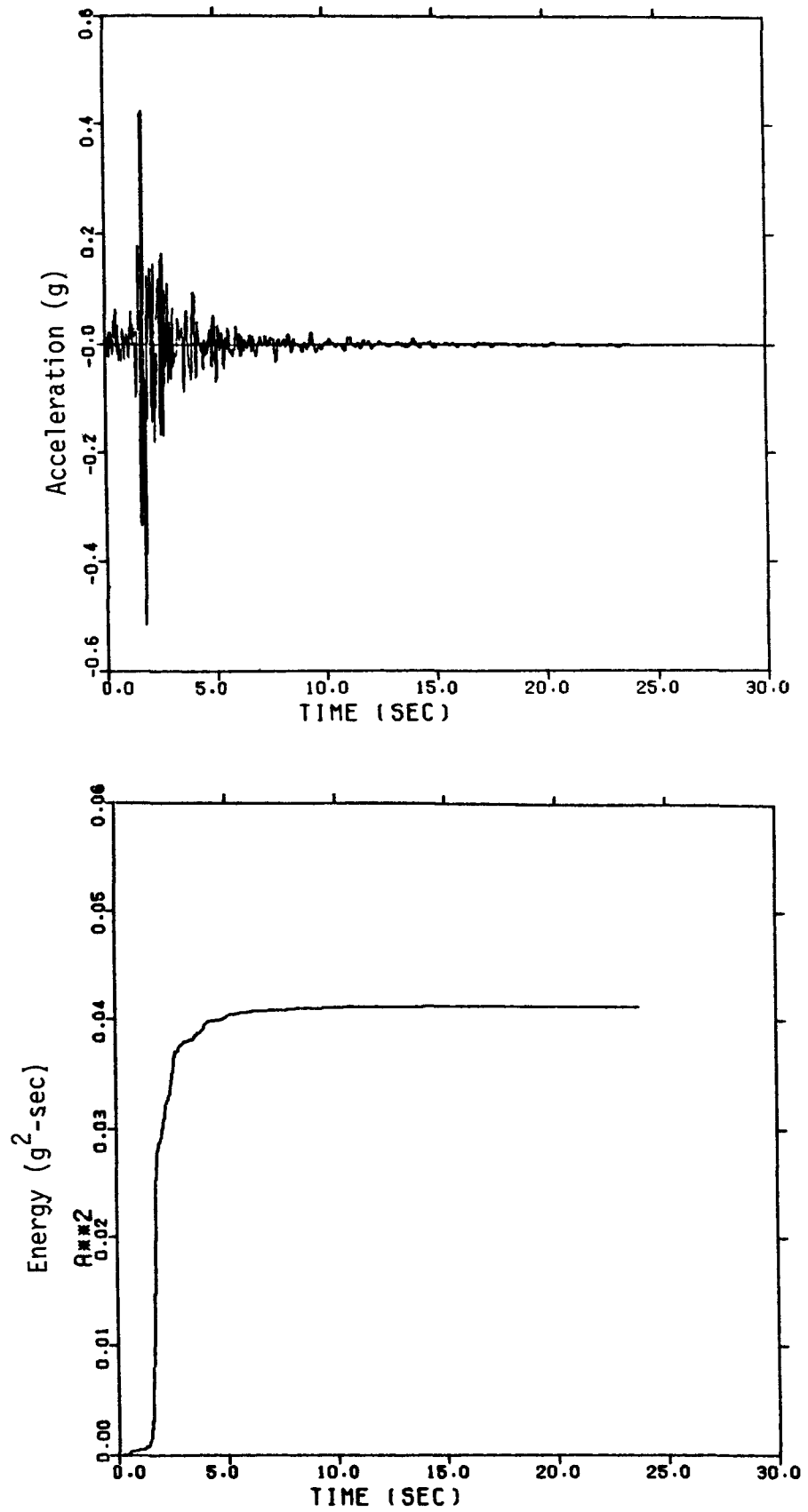
FIGURE B-11.   ACCELEROGRAM AND CORRESPONDING CUMULATIVE ENERGY FOR
THE MELENDY RANCH BARN, BEAR VALLEY 1972 (N29W) RECORD
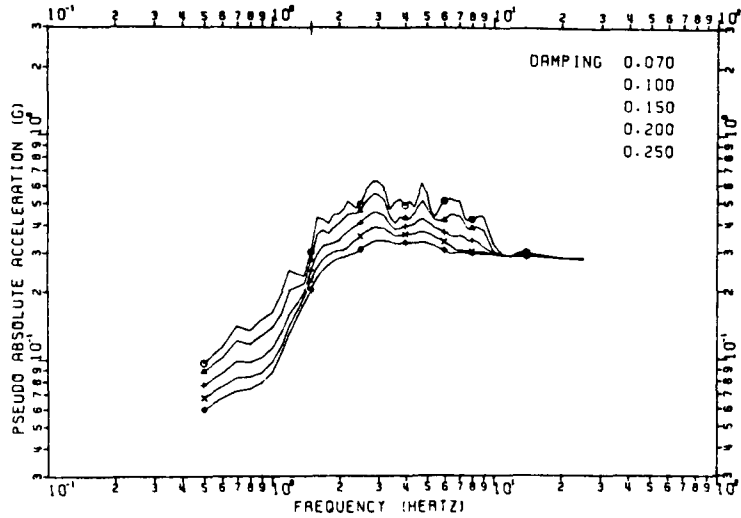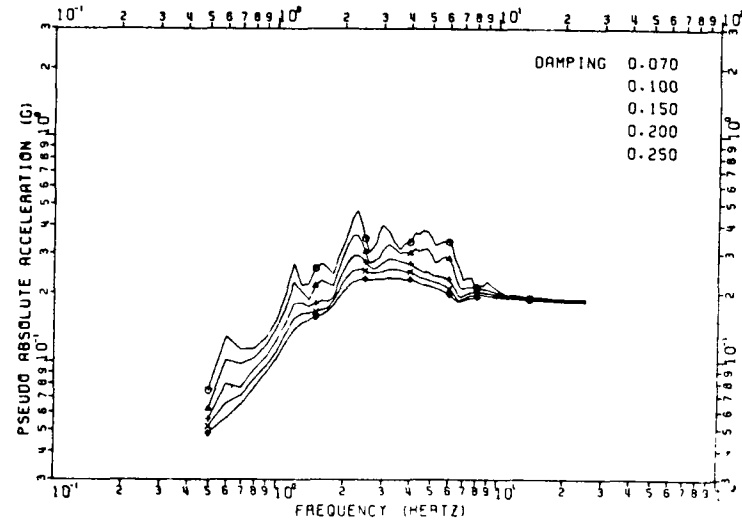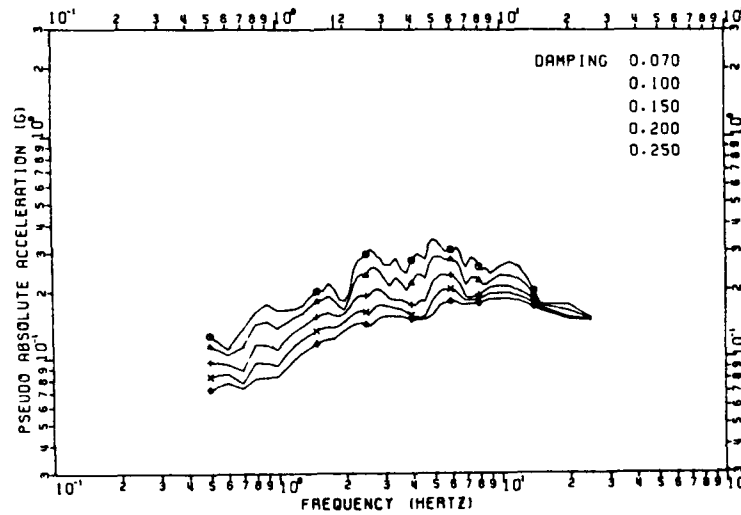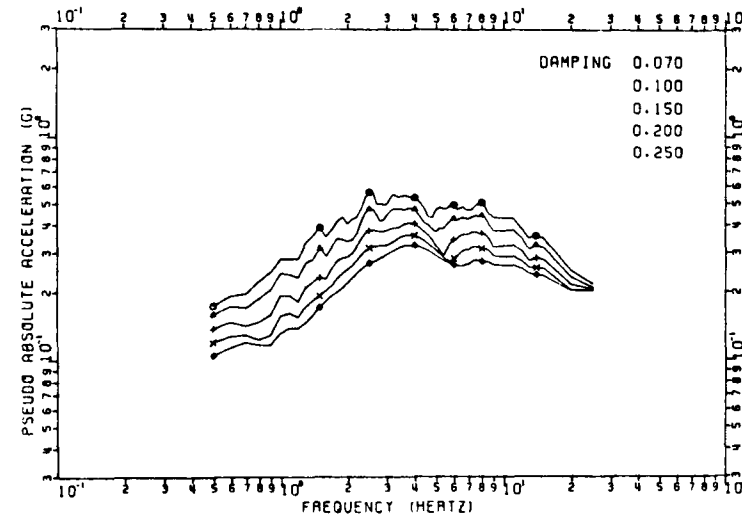
FIGURE B-2a.   ELASTIC RESPONSE SPECTRA ($T_D' > 9$ SEC.)

PSEUDO ABSOLUTE ACCELERATION (G)

FREQUENCY (HERTZ)

DAMPING 0.070
         0.100
         0.150
         0.200
         0.250

PACOIMA DAM

HOLLYWOOD STORAGE

EL CENTRO, ARRAY NO. 5

GOLETA
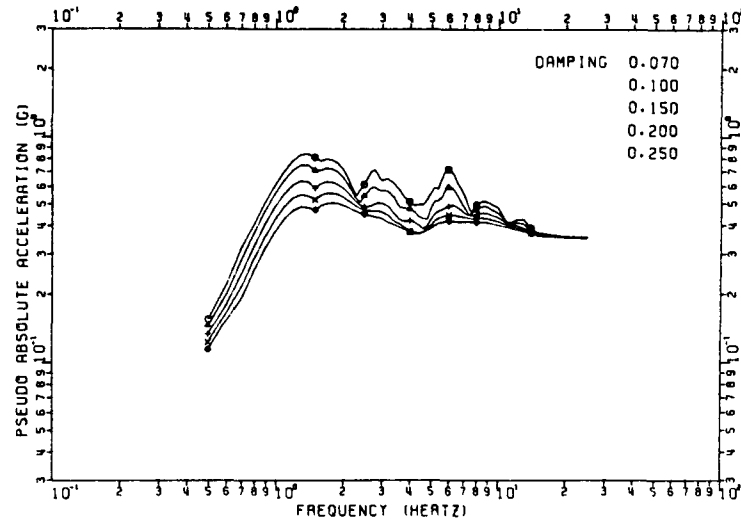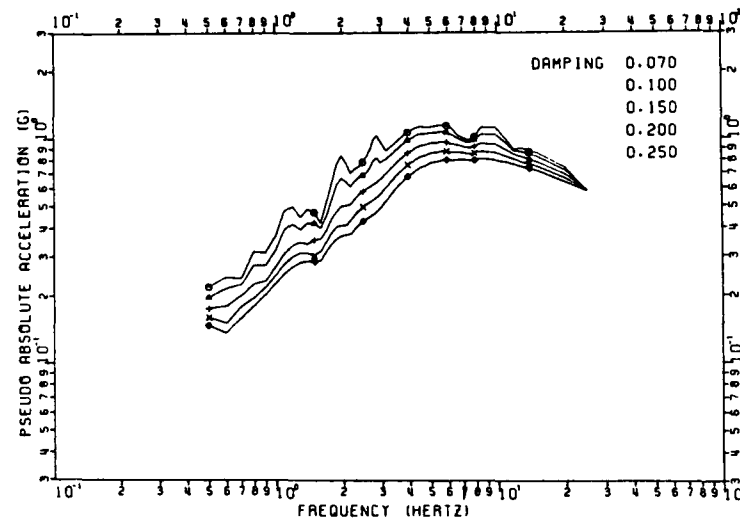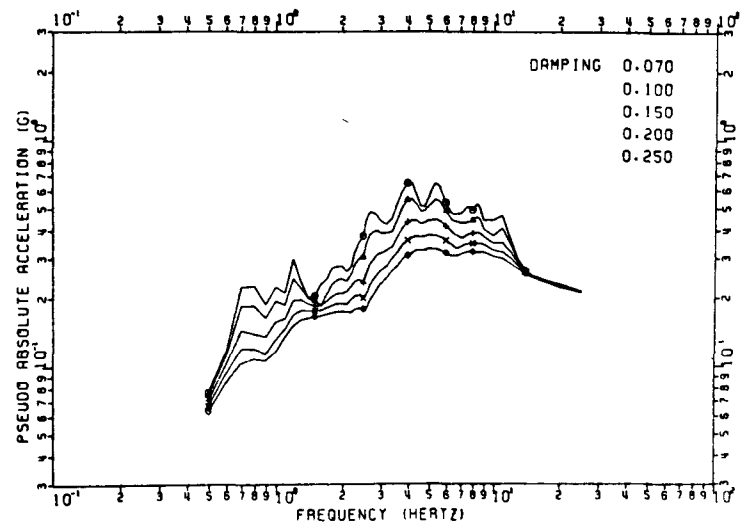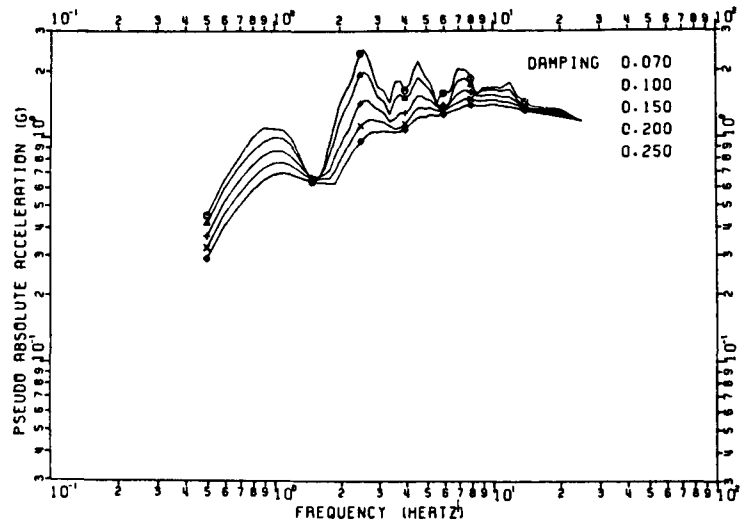
FIGURE B-2b.   ELASTIC RESPONSE SPECTRA (2.5 SEC. $< T_D' <$ 9 SEC.)
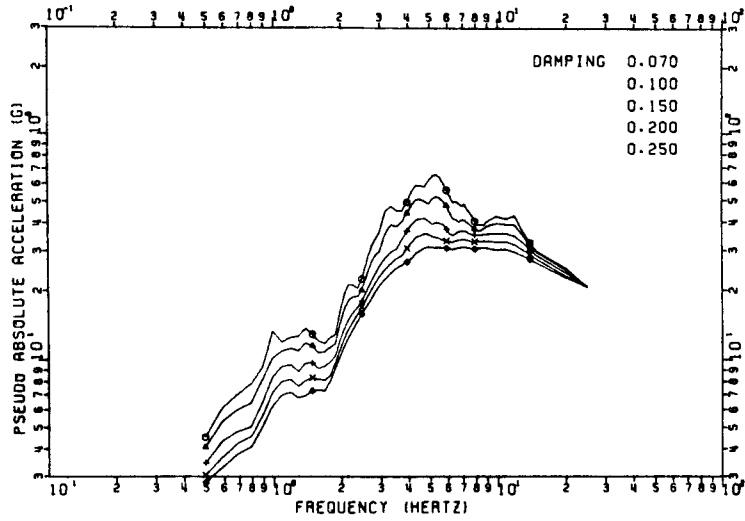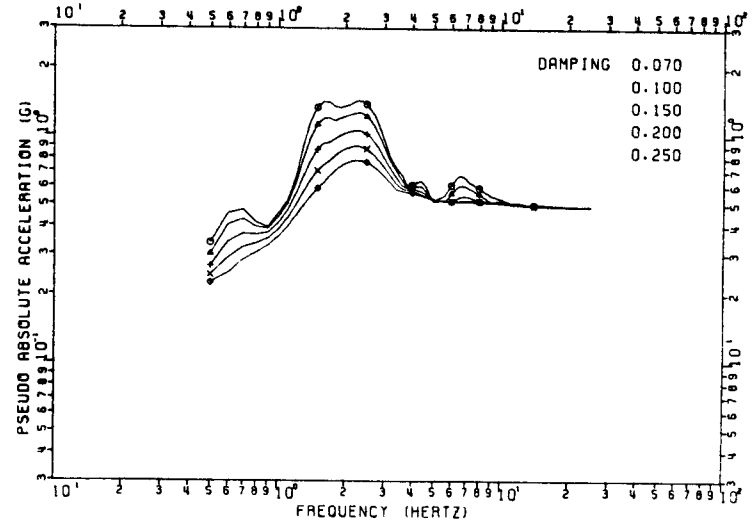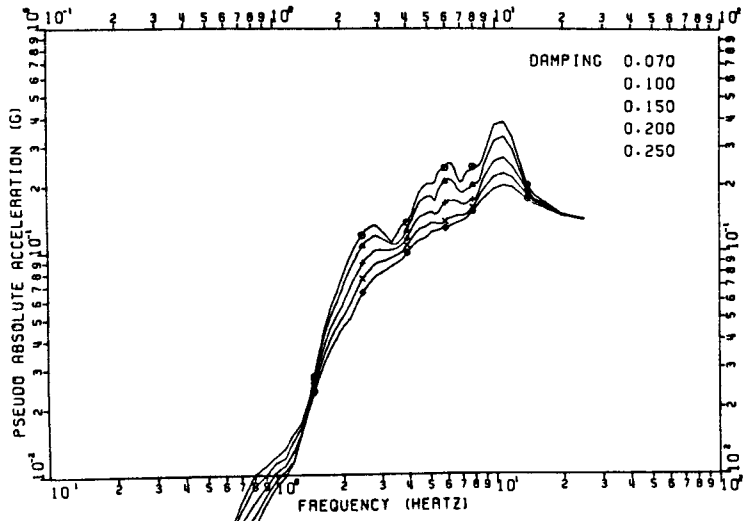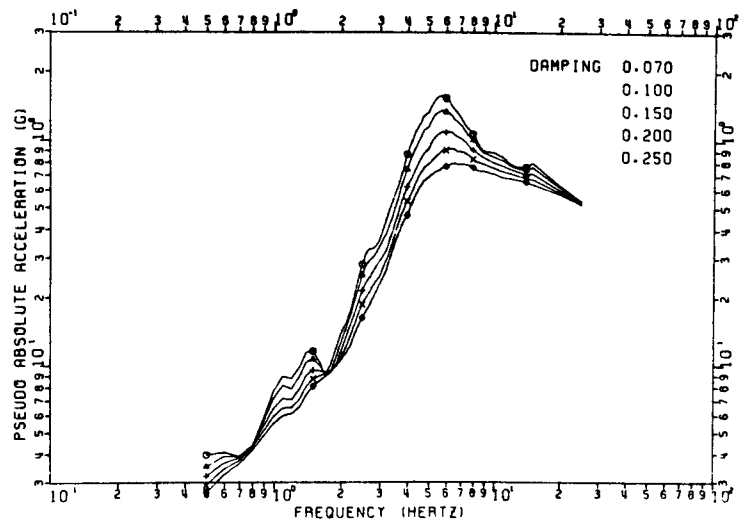
FIGURE B-2c.   ELASTIC RESPONSE SPECTRA ($T_D' < 2.5$ SEC.)
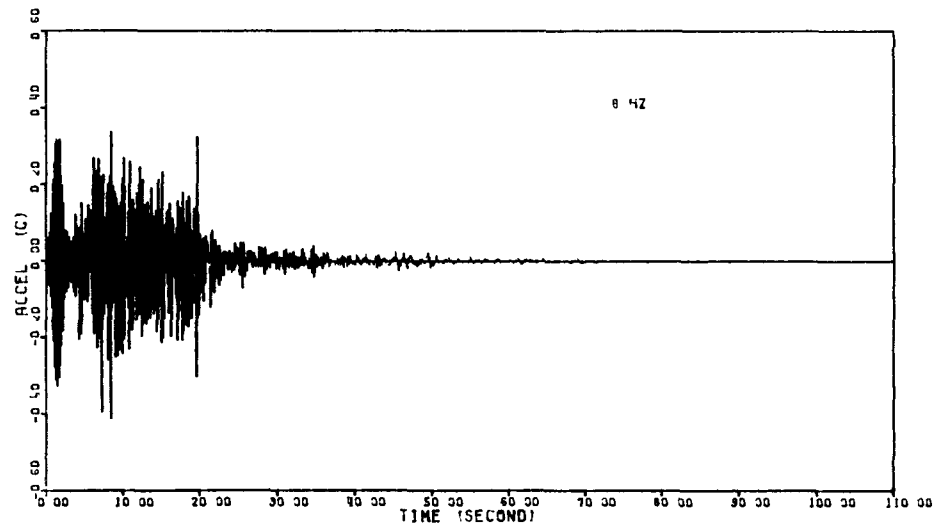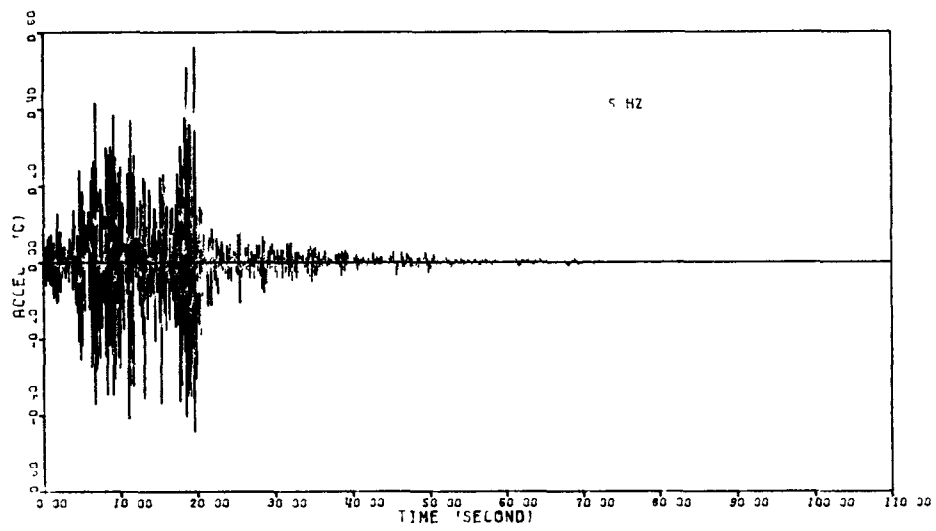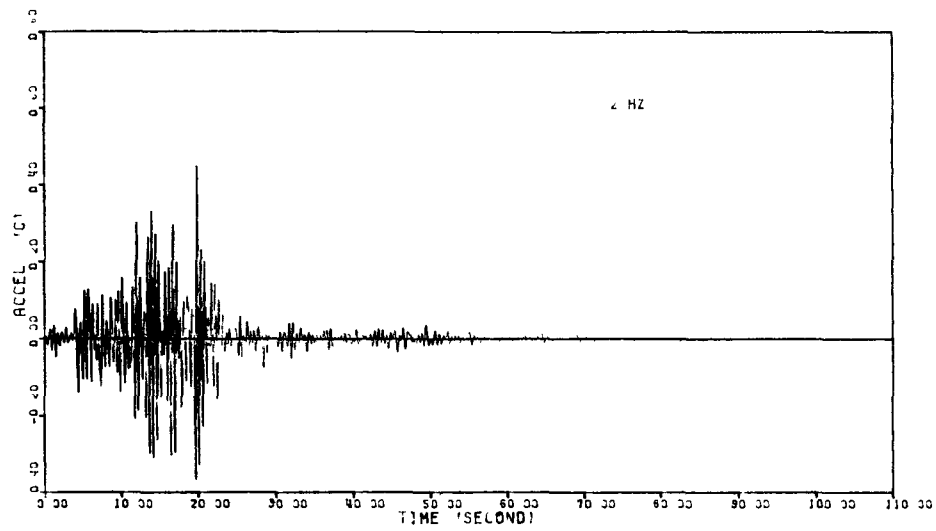
FIGURE B-3a.   ELASTIC RESPONSE OF 7% DAMPED, 2, 5 AND 8 HZ OSCILLATORS
   TO THE OLYMPIA, WA., (1949) EARTHQUAKE (N86E)

B-16
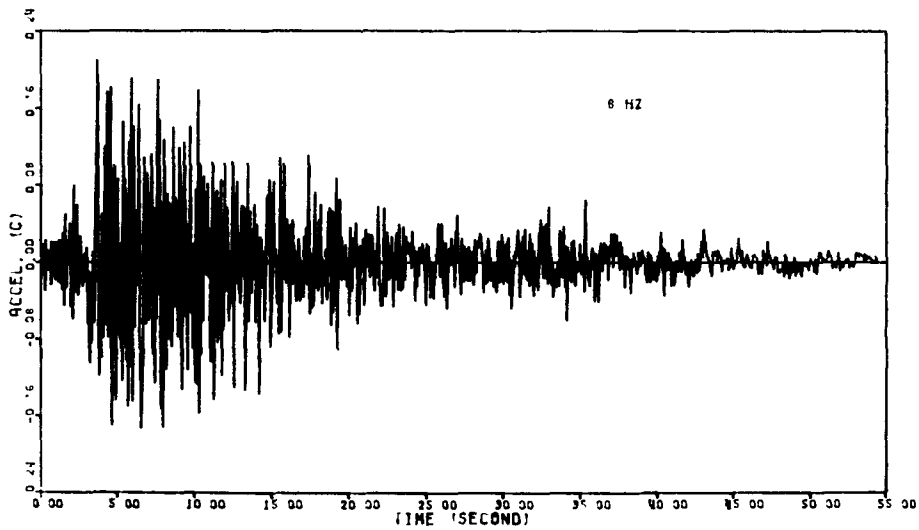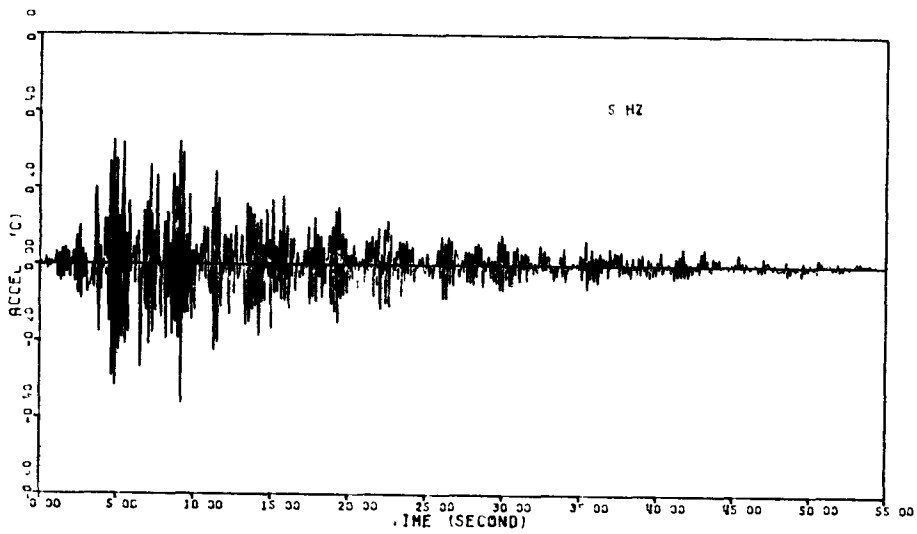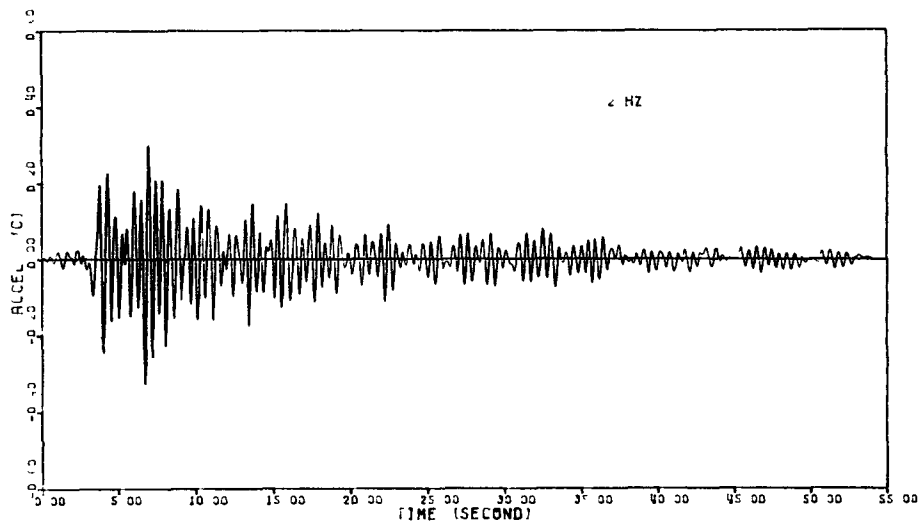
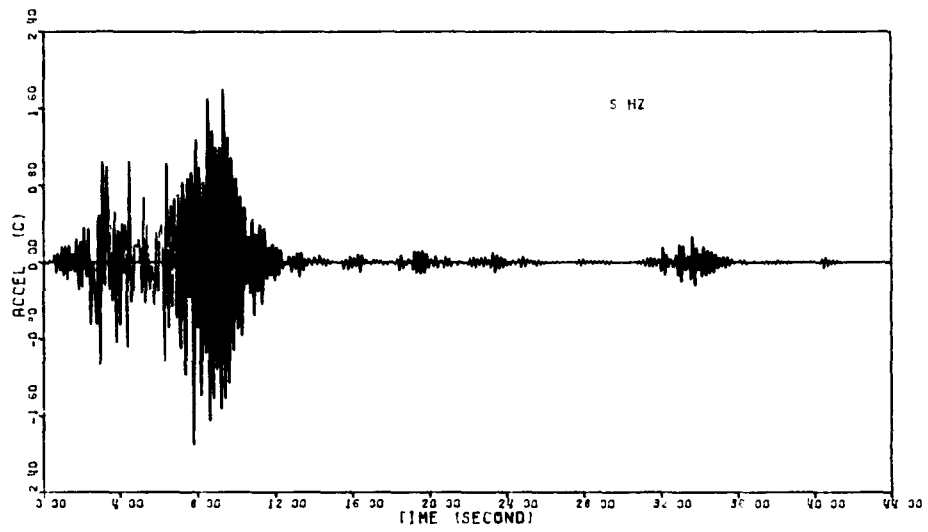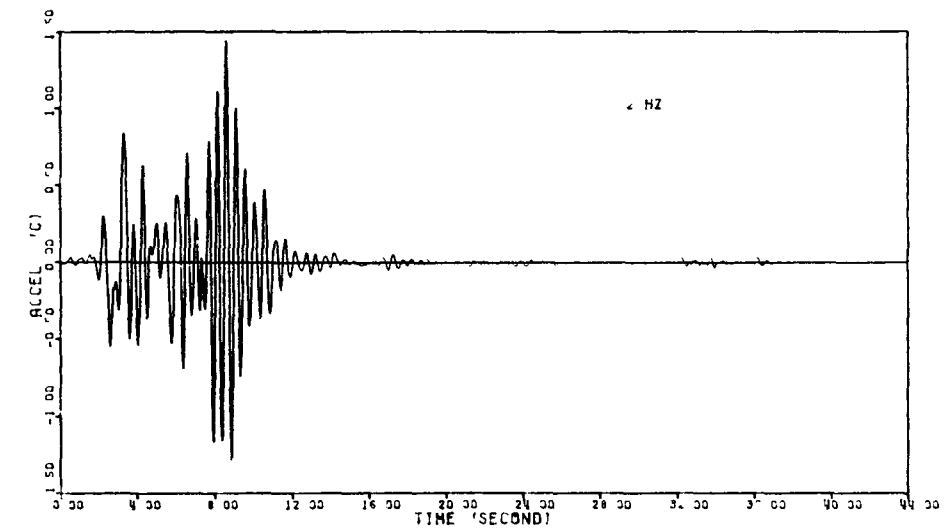FIGURE B-3b.   ELASTIC RESPONSE OF 7% DAMPED, 2, 5 AND 8 HZ OSCILLATORS
              TO THE TAFT, KERN CO., 1952 EARTHQUAKE (S69E)

B-17
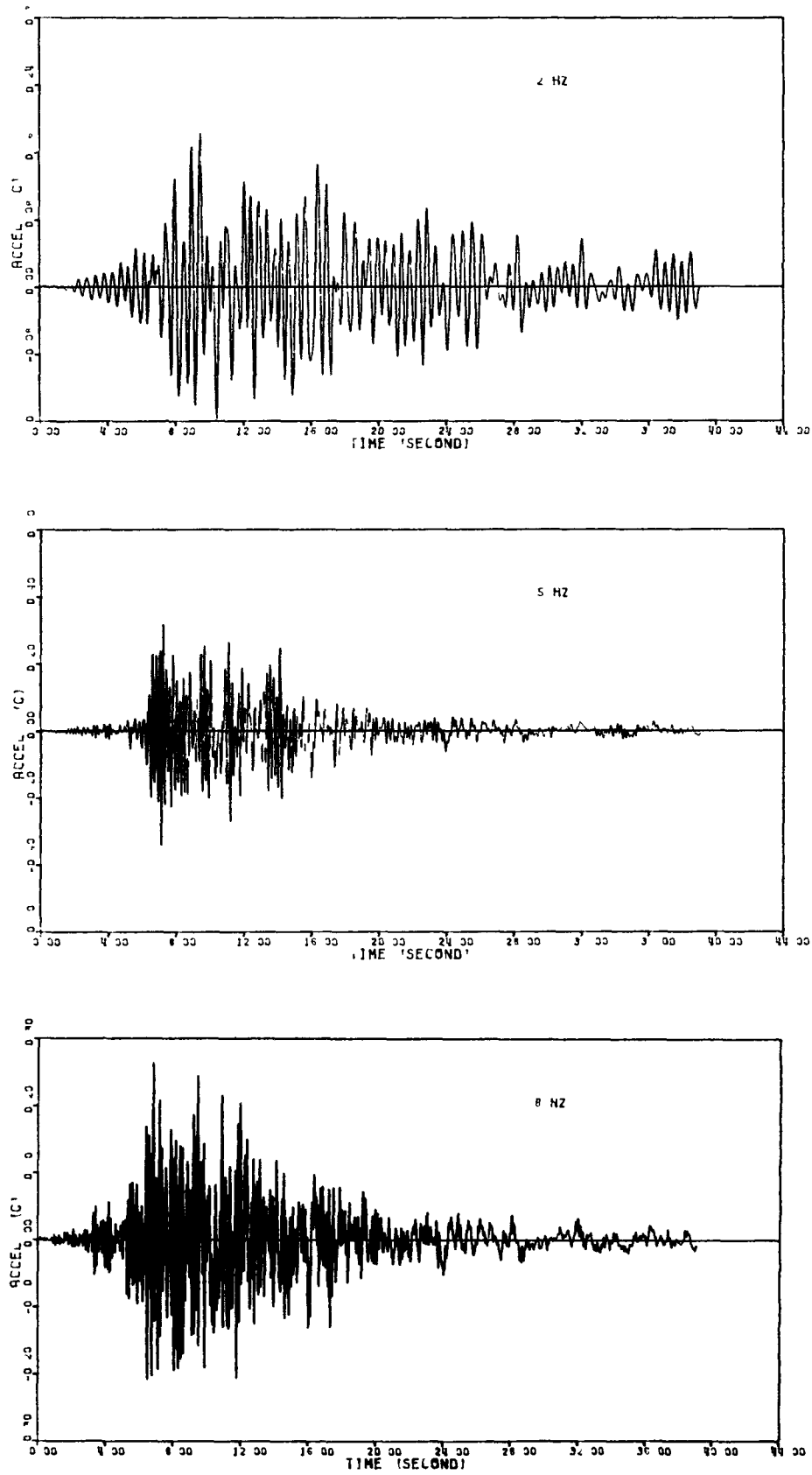
FIGURE B-3c.   ELASTIC RESPONSE OF 7% DAMPED, 2, 5 AND 8 HZ OSCILLATORS TO THE
EL CENTRO ARRAY NO. 12, IMPERIAL VALLEY, 1979 EARTHQUAKE (140)

B-18
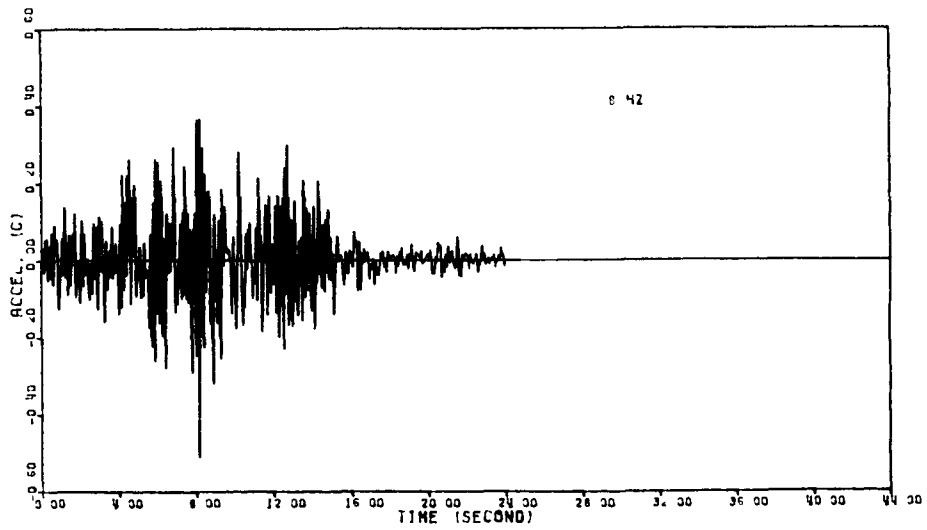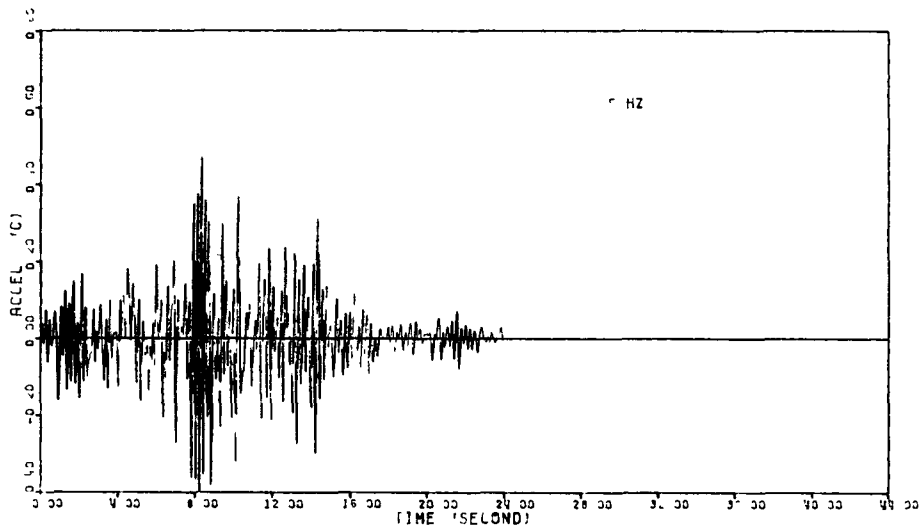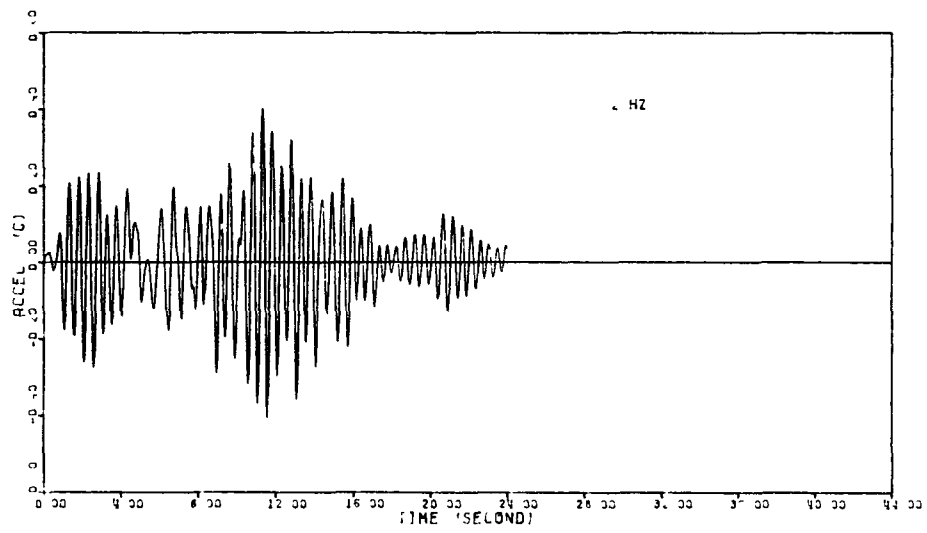
FIGURE B-3d. ELASTIC RESPONSE OF 7% DAMPED, 2, 5 AND 8 HZ
OSCILLATORS TO THE NRC ARTIFICIAL EARTHQUAKE

B-19
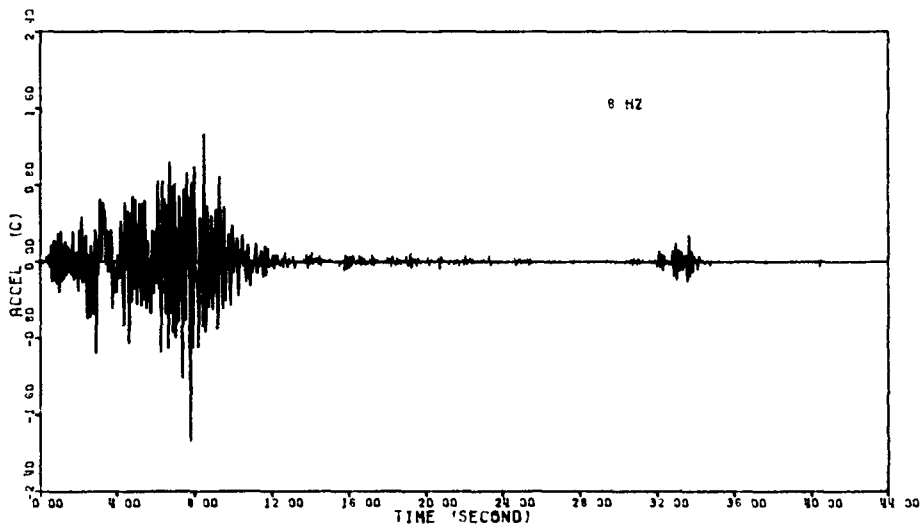
FIGURE B-3e.   ELASTIC RESPONSE OF 7% DAMPED, 2, 5 AND 8 HZ OSCILLATORS TO
THE PACOIMA DAM, SAN FERNANDO, 1971 EARTHQUAKE (S14W)
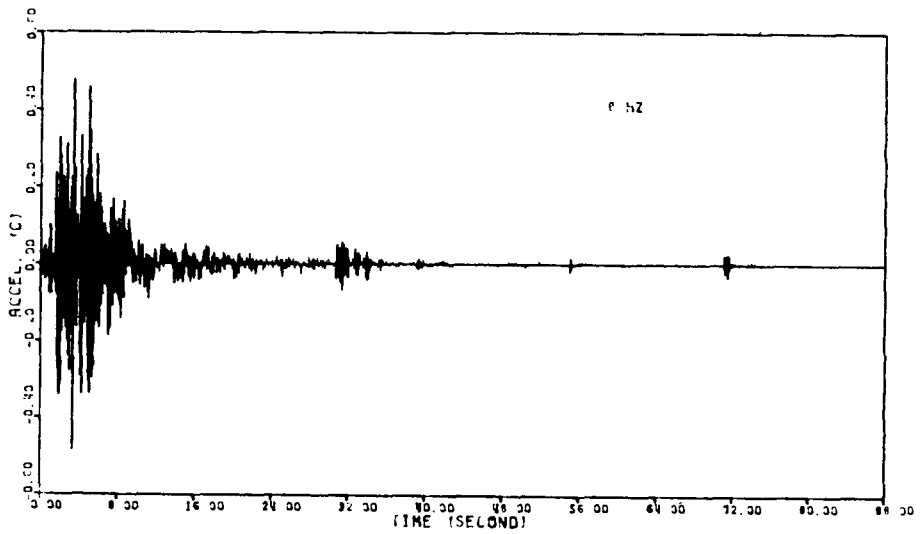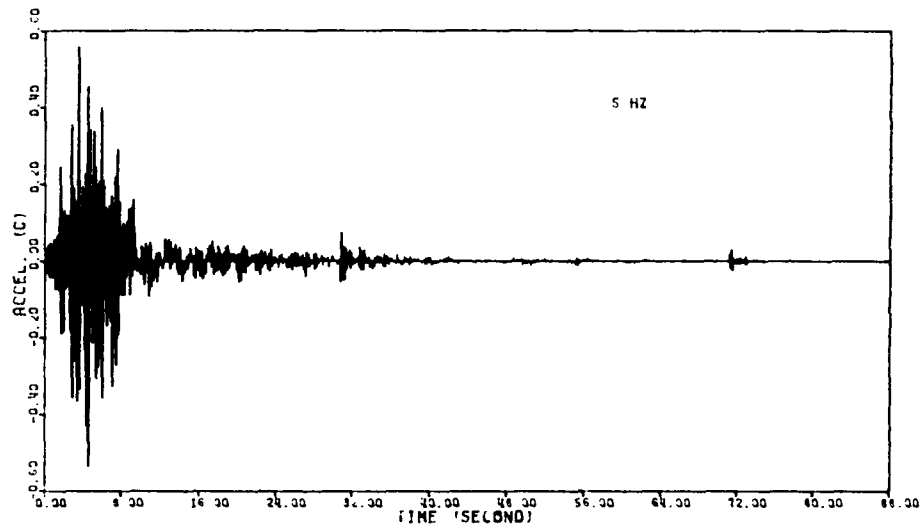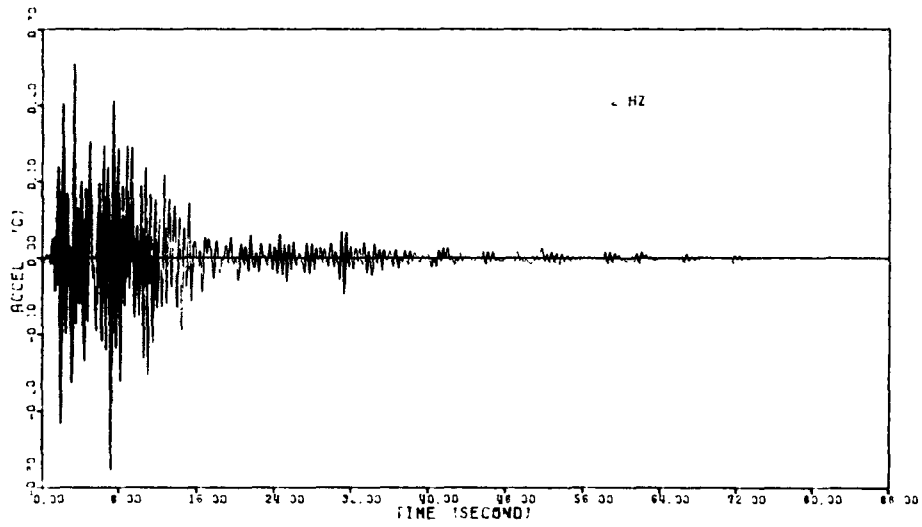
B-20

FIGURE B-3f.   ELASTIC RESPONSE OF 7% DAMPED, 2, 5 AND 8 HZ OSCILLATORS TO THE
                HOLLYWOOD STORAGE P.E. LOT, SAN FERNANDO, 1971 EARTHQUAKE (N90E)
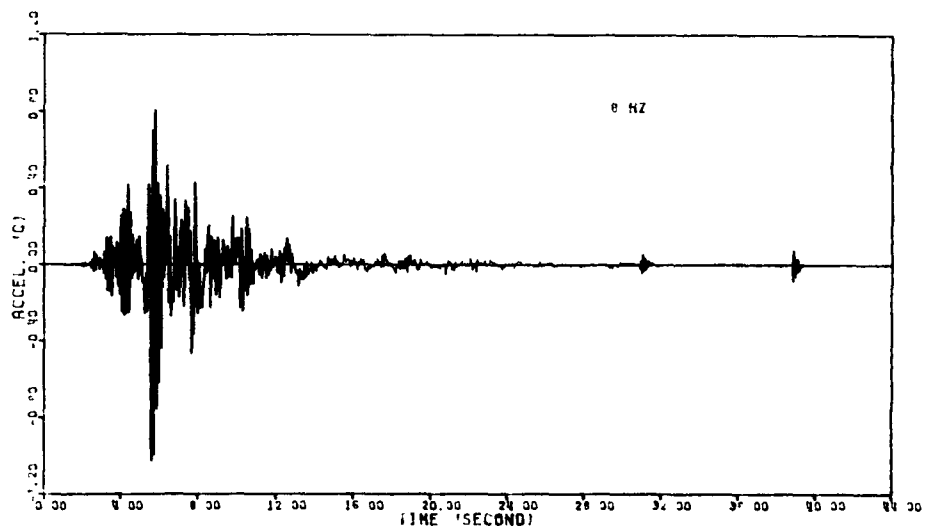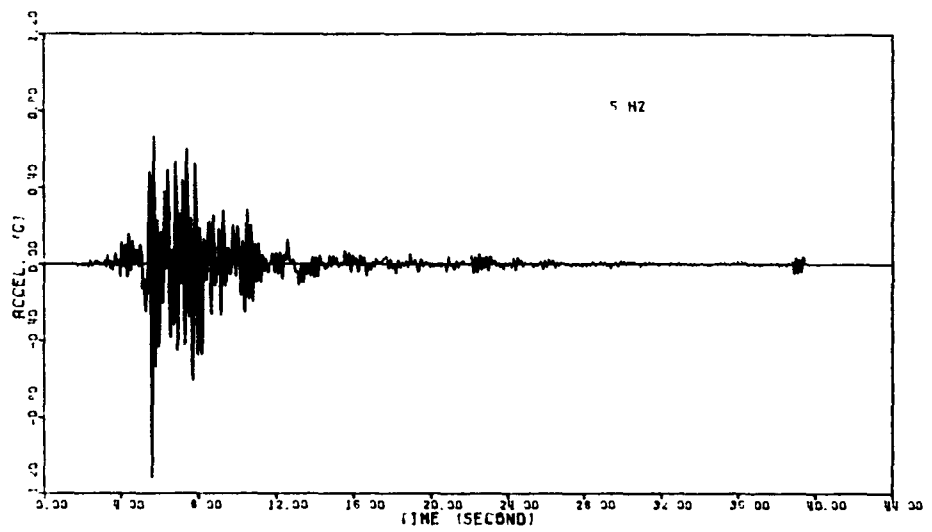
B-21

FIGURE B-3g.   ELASTIC RESPONSE OF 7% DAMPED, 2, 5 AND 8 HZ OSCILLATORS TO THE
EL CENTRO ARRAY NO. 5, IMPERIAL VALLEY, 1979 EARTHQUAKE (140)
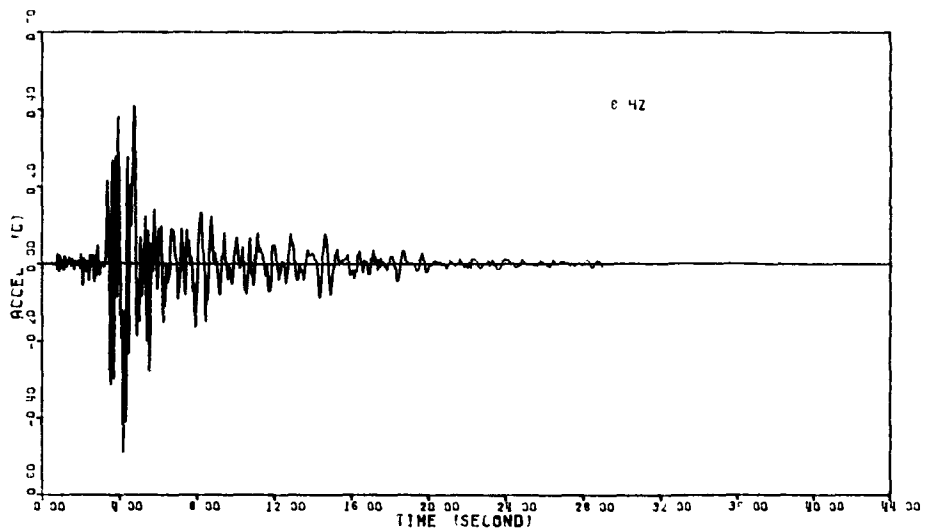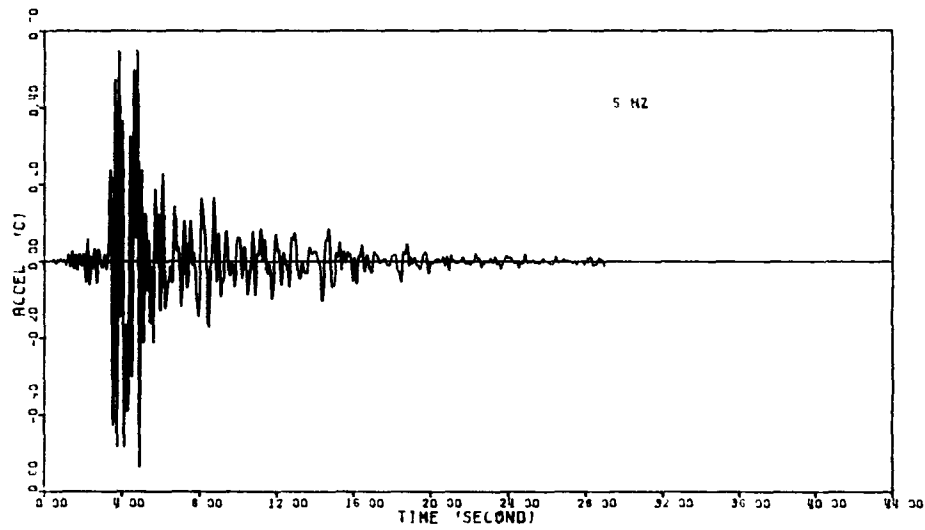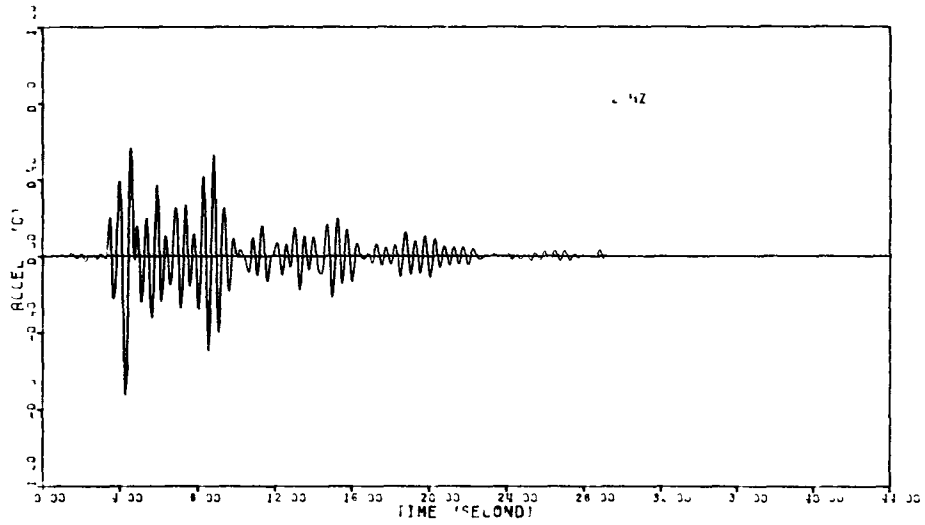
FIGURE B-3h.   ELASTIC RESPONSE OF 7% DAMPED, 2, 5 AND 8 HZ OSCILLATORS TO
THE UCSB GOLETA, SANTA BARBARA, 1978 EARTHQUAKE (180)

B-23
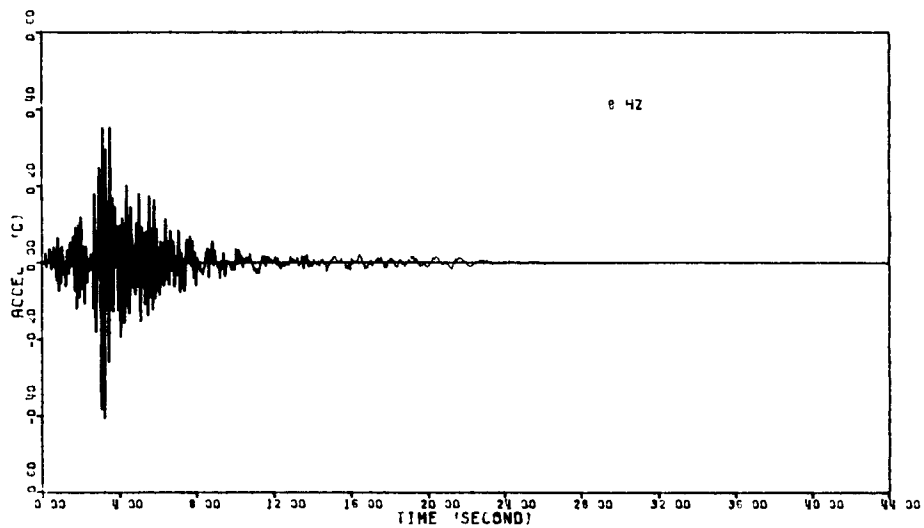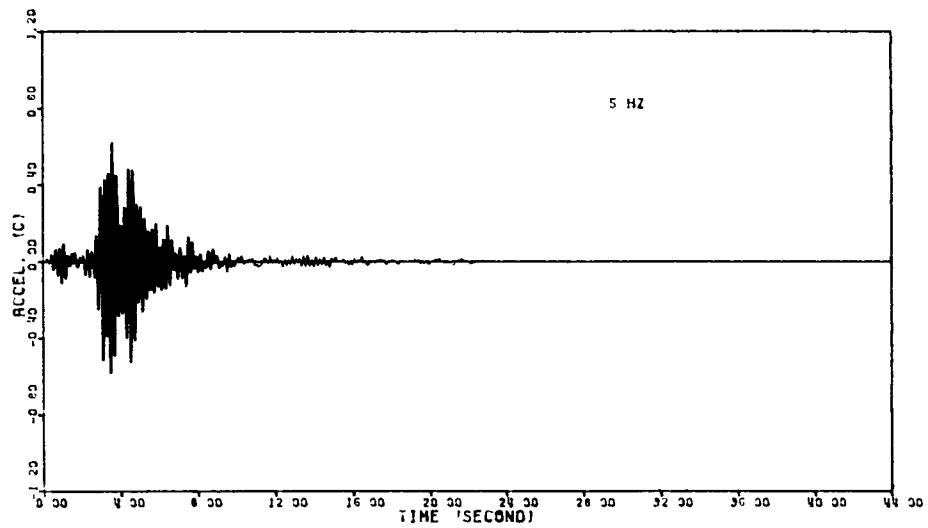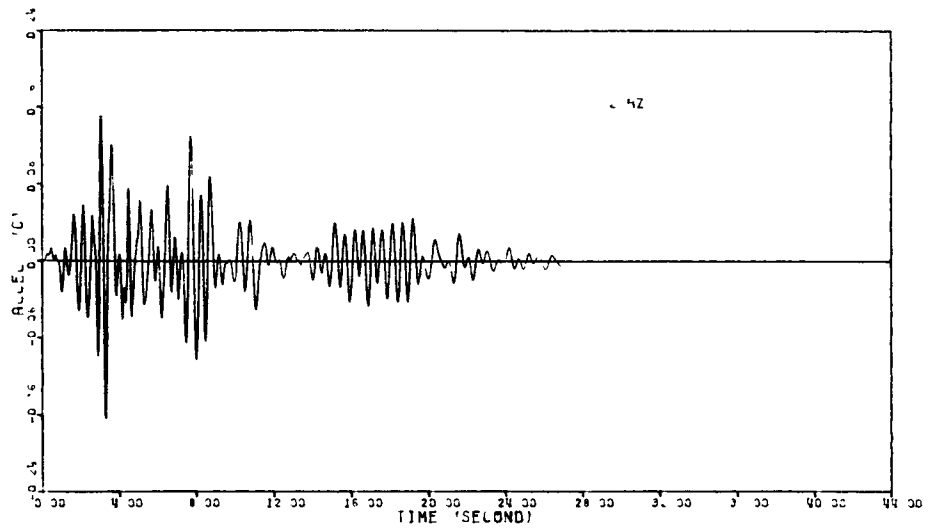
FIGURE B-3i.   ELASTIC RESPONSE OF 7% DAMPED, 2, 5 AND 8 HZ OSCILLATORS TO THE
GILROY ARRAY NO. 2, COYOTE LAKE, 1979 EARTHQUAKE (050)
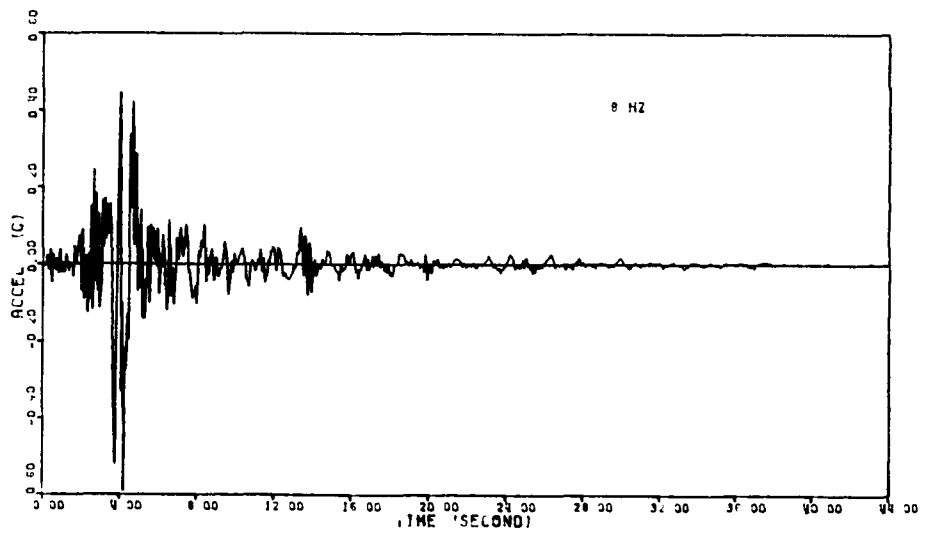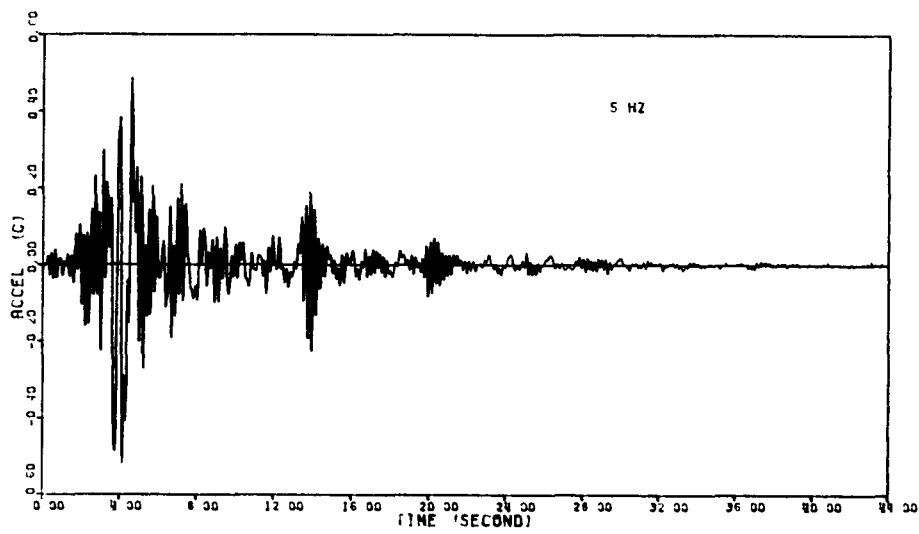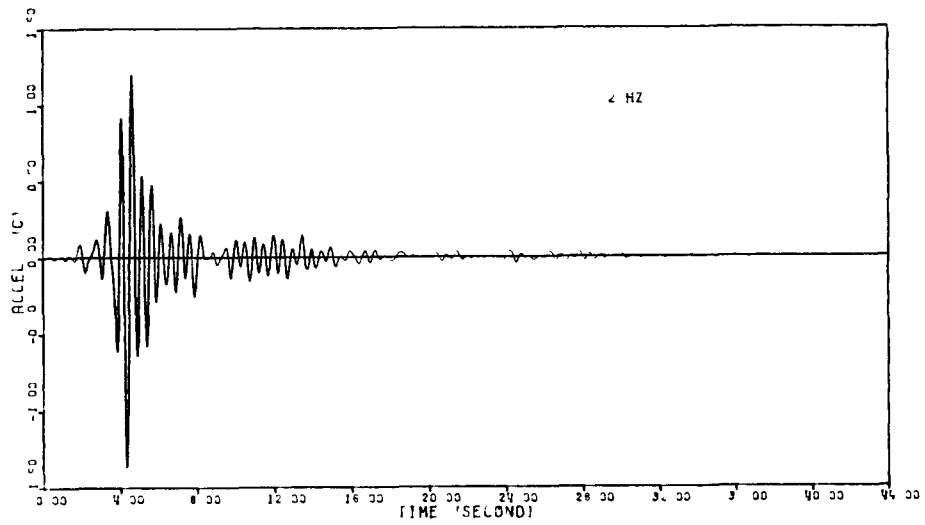
FIGURE B-3j.   ELASTIC RESPONSE OF 7% DAMPED, 2, 5 AND 8 HZ OSCILLATORS TO THE
CHOLAME ARRAY NO. 2, PARKFIELD, 1966 EARTHQUAKE (N65E)

B-25
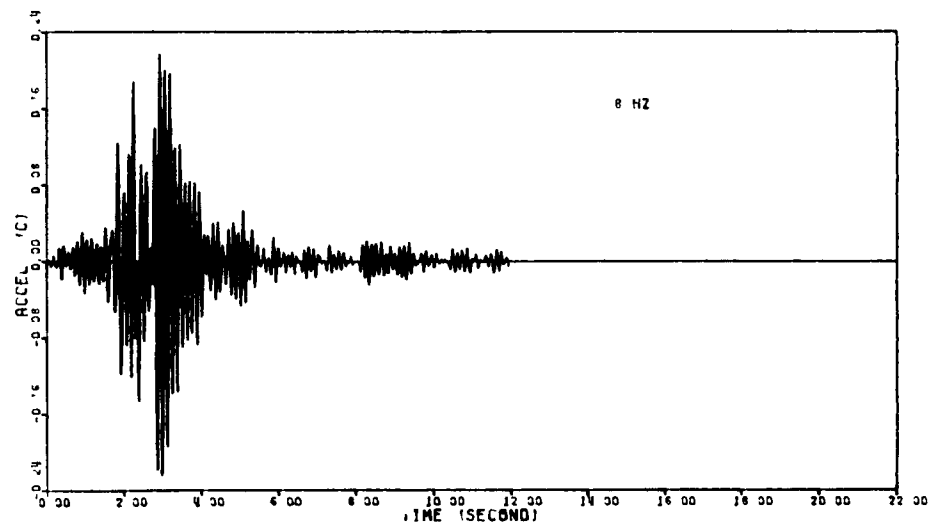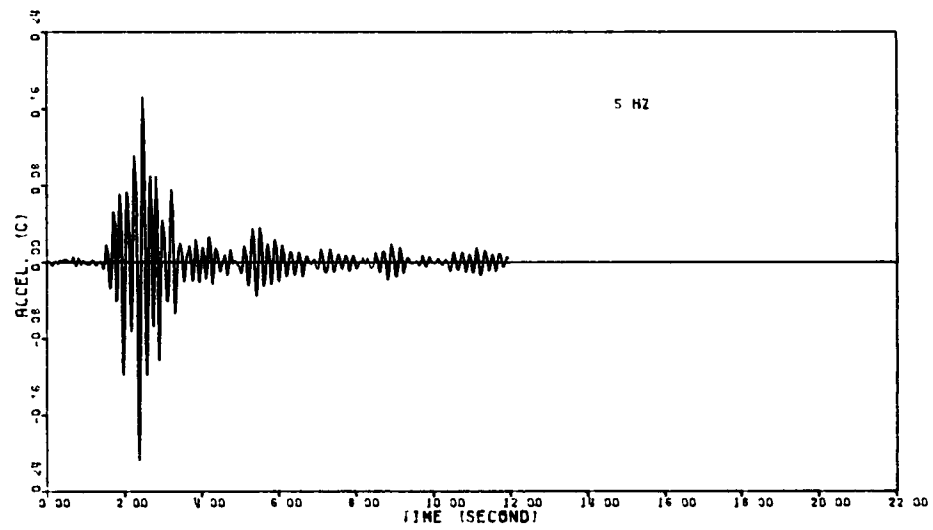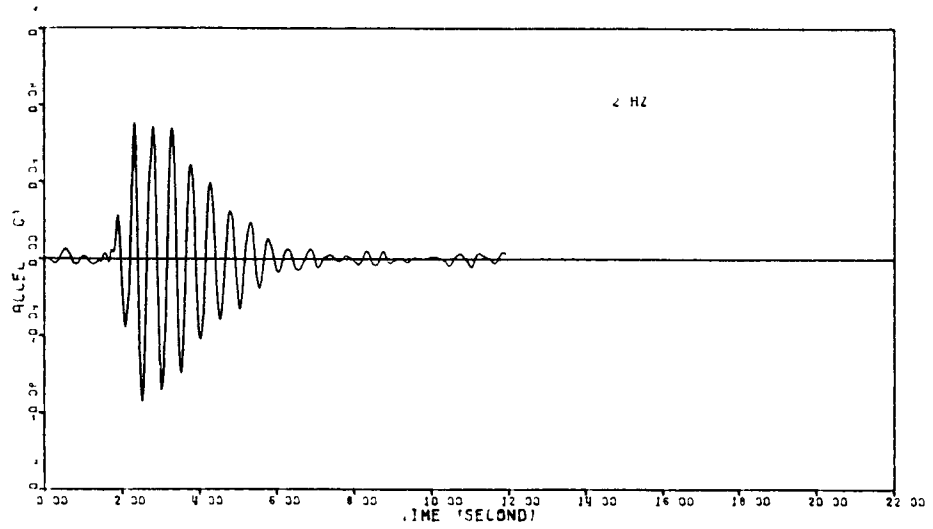
FIGURE B-3k.   ELASTIC RESPONSE OF 7% DAMPED, 2, 5 AND 8 HZ OSCILLATORS TO
THE GAVILAN COLLEGE, HOLLISTER, 1974 EARTHQUAKE (S67W)

B-26
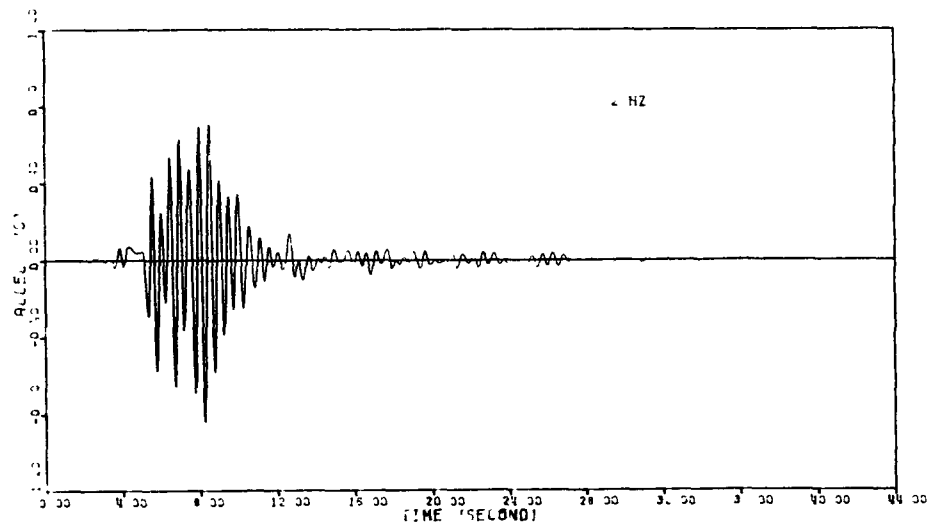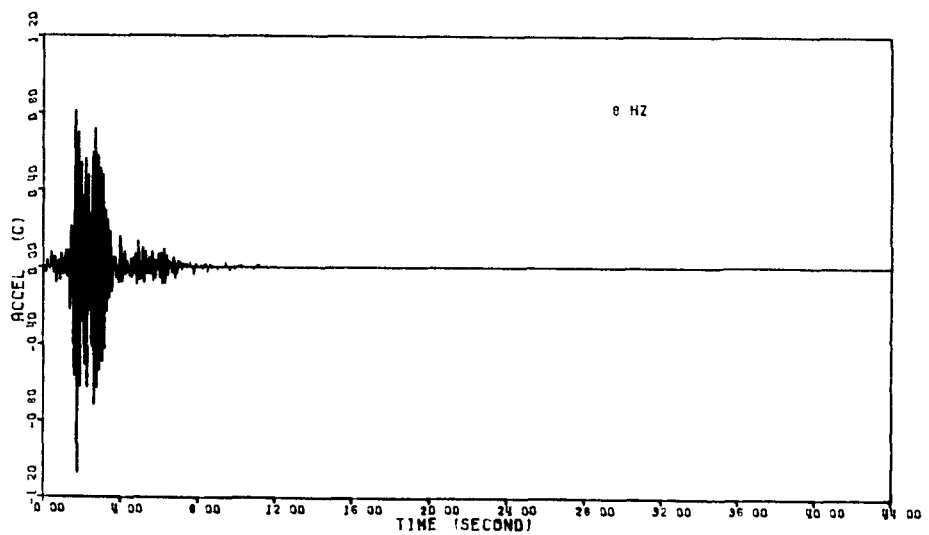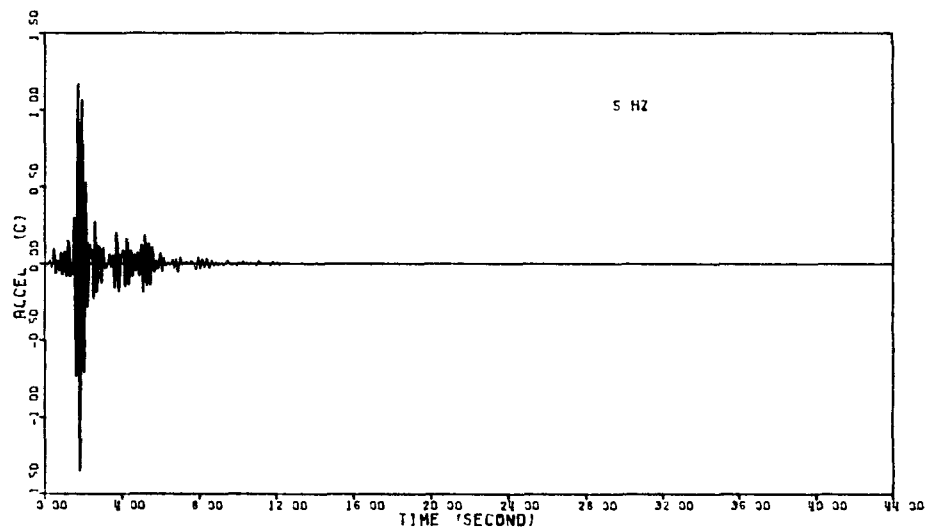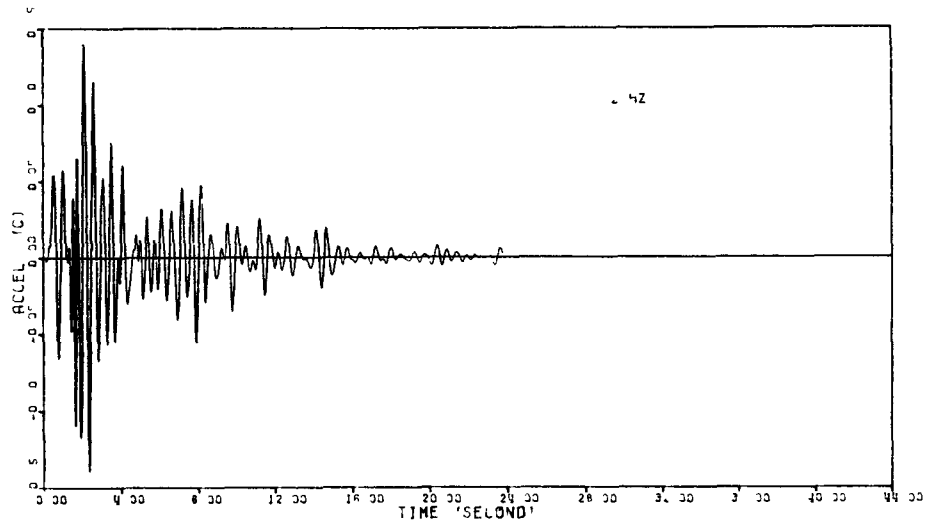
FIGURE B-3L.   ELASTIC RESPONSE OF 7% DAMPED, 2, 5 AND 8 HZ OSCILLATORS TO
THE MELENDY RANCH BARN, BEAR VALLEY, 1972 EARTHQUAKE (N29W)
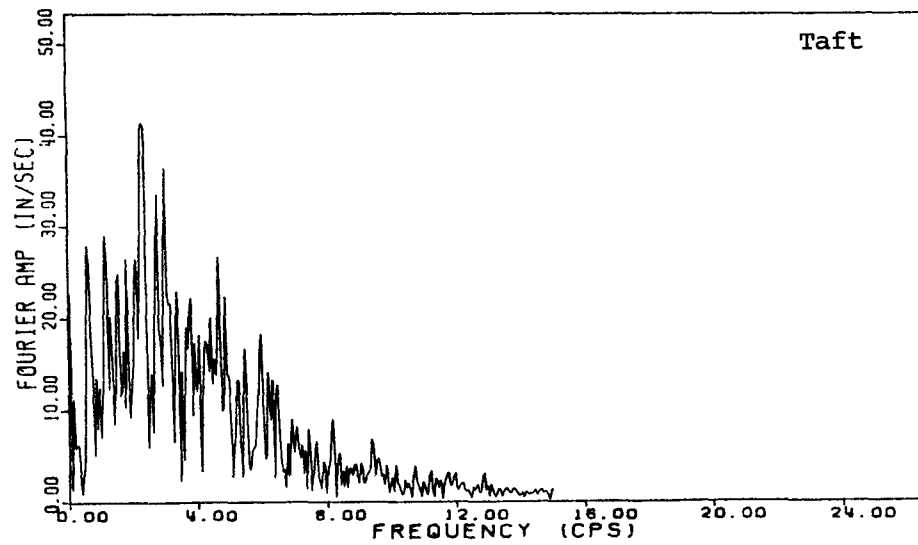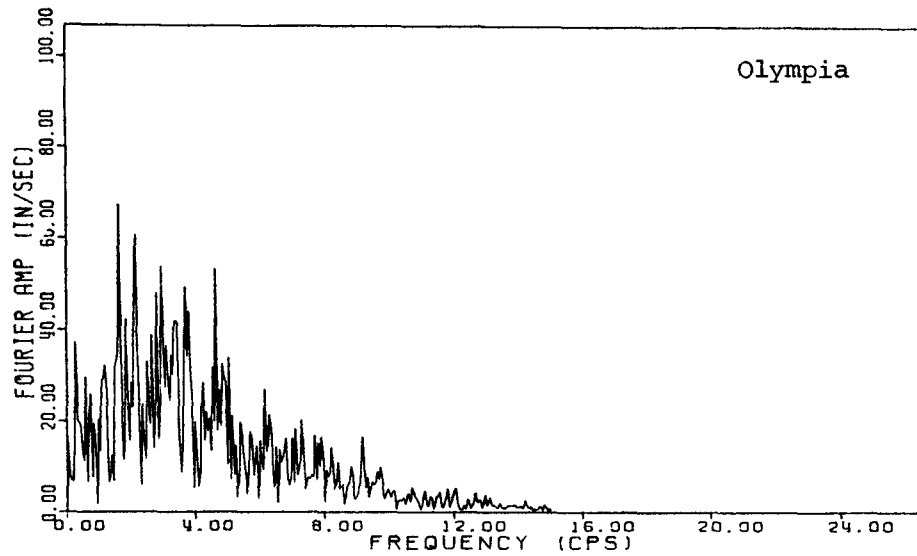
(a) $T_D' > 9$ sec.

FIGURE B-4a.   FOURIER SPECTRA OF EFFECTIVE ACCELEROGRAM
               SEGMENT DEFINED BY $T_D' = T_m - T_{.05}$

El Centro
No. 12

Artificial
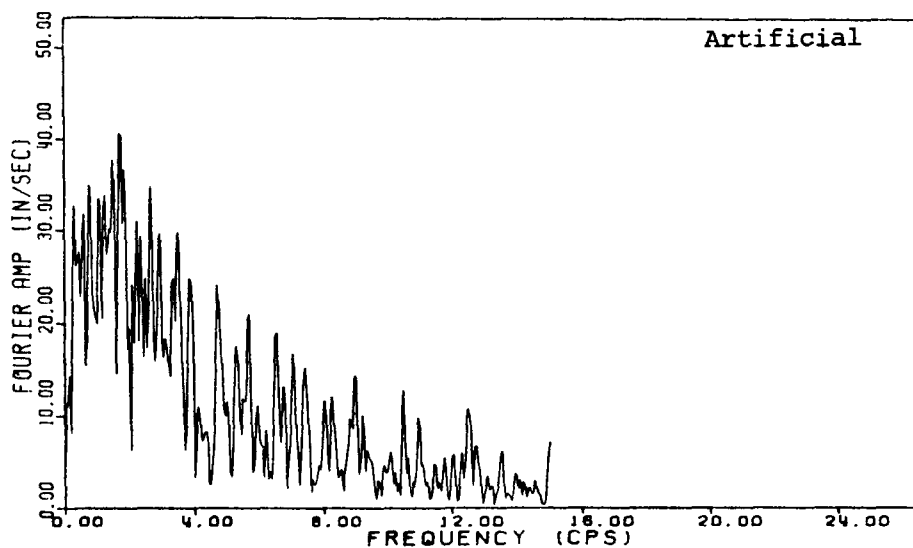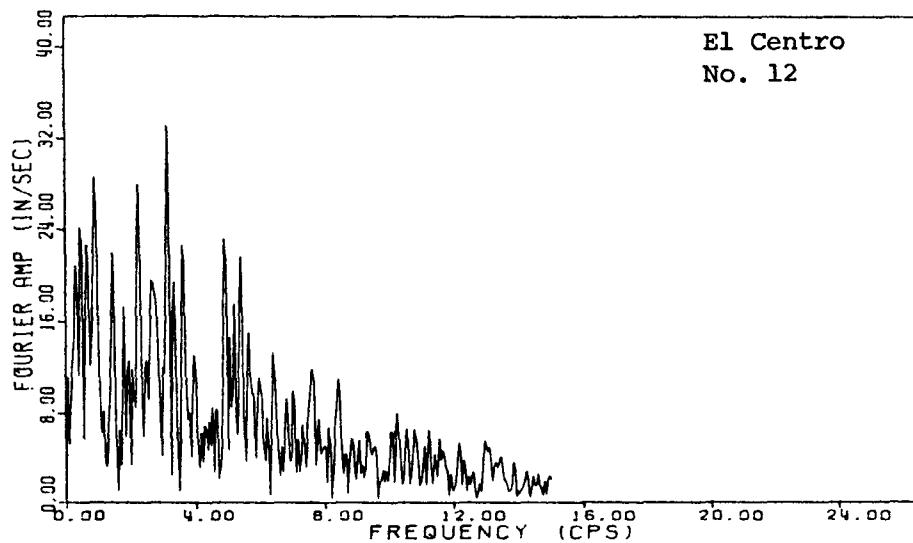
(a) $T_D' > 9$ sec.
(Continued)

FIGURE B-4a.   FOURIER SPECTRA OF EFFECTIVE ACCELEROGRAM
SEGMENT DEFINED BY $T_D' = T_m - T_{.05}$
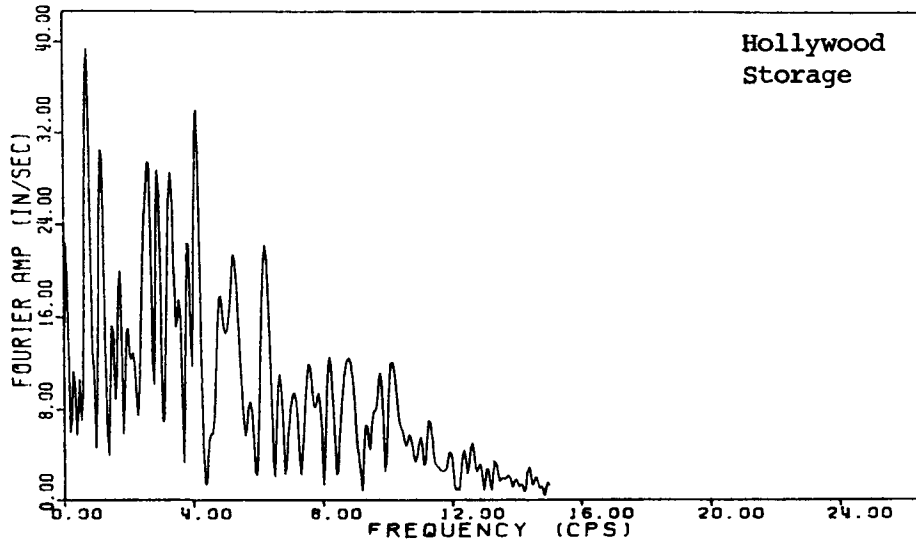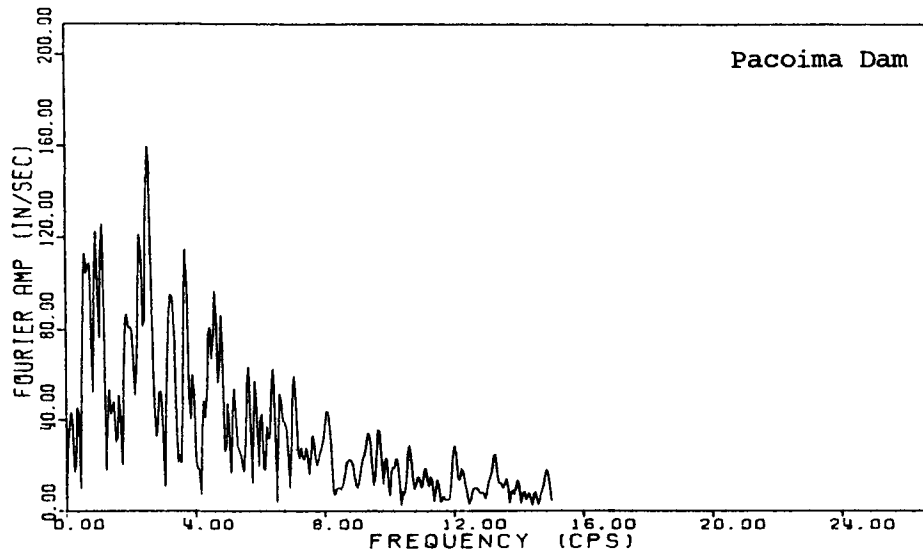
(b) 2.5 sec $\leq T'_D \leq 9$ sec.

FIGURE B-4b.   FOURIER SPECTRA OF EFFECTIVE ACCELEROGRAM
SEGMENT DEFINED BY $T'_D = T_m - T_{.05}$
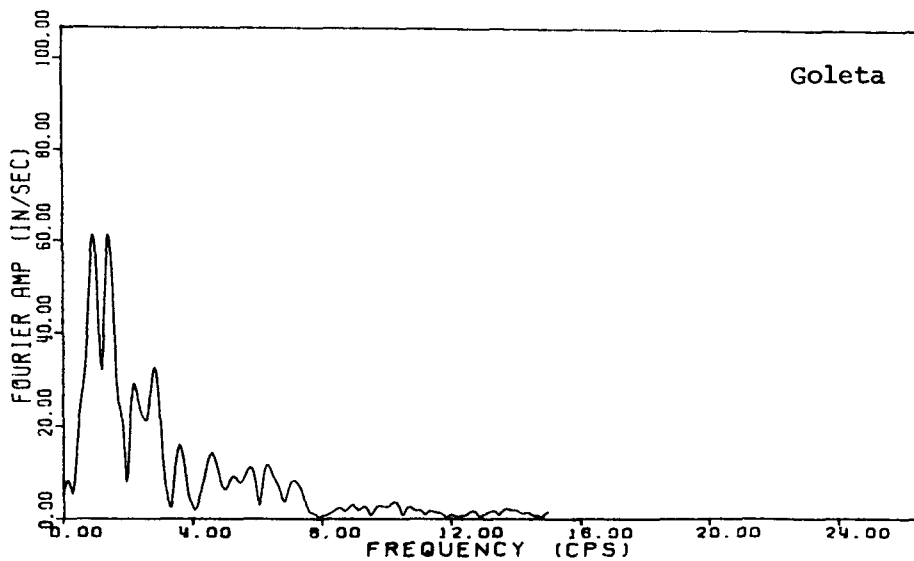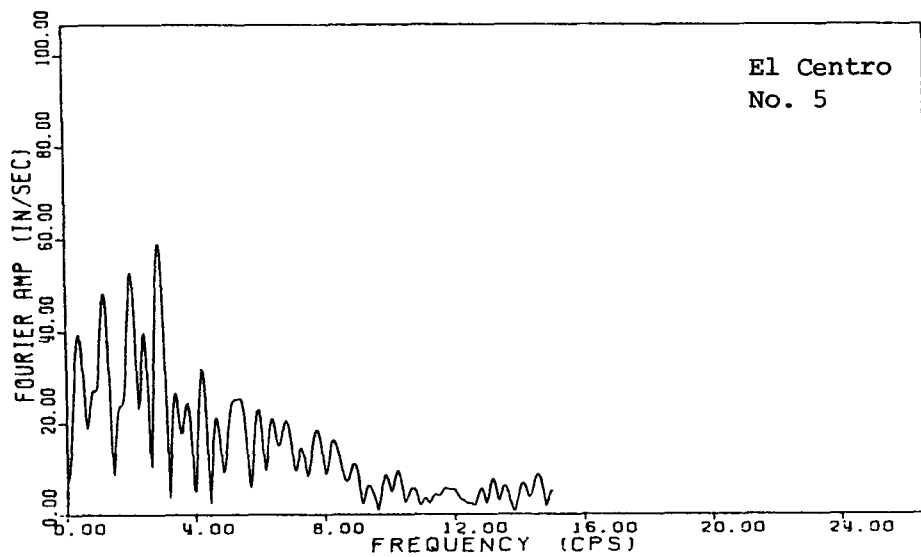
(b) $2.5 \leq T_D' \leq 9$ sec.
(Continued)

FIGURE B-4b.   FOURIER SPECTRA OF EFFECTIVE ACCELEROGRAM
SEGMENT DEFINED BY $T_D' = T_m - T_{.05}$
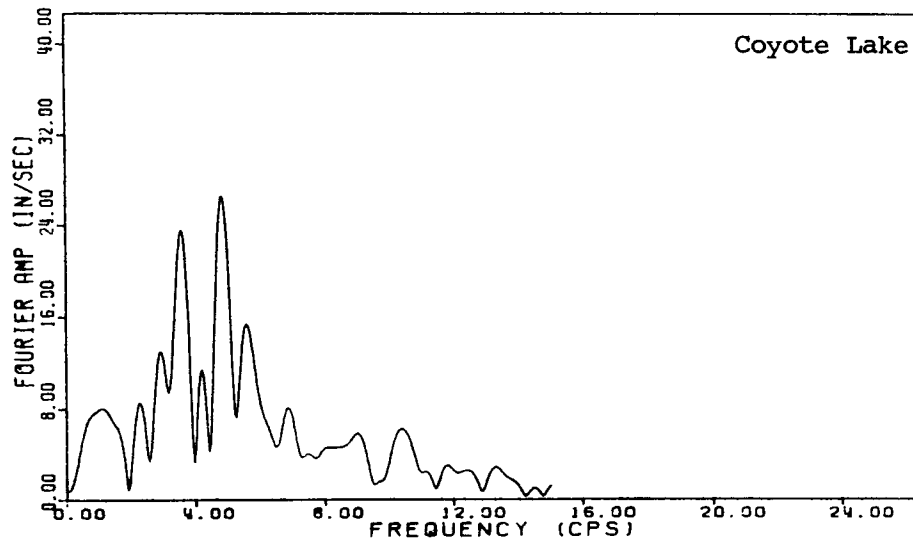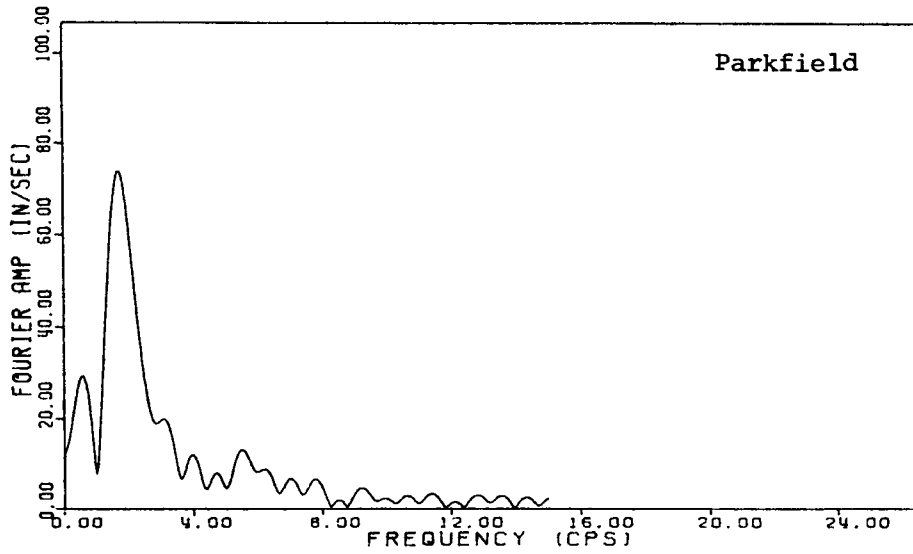
(c) $T_D' < 2.5$ sec.

FIGURE B-4c. FOURIER SPECTRA OF EFFECTIVE ACCELEROGRAM SEGMENT DEFINED BY $T_D' = T_m - T_{.05}$
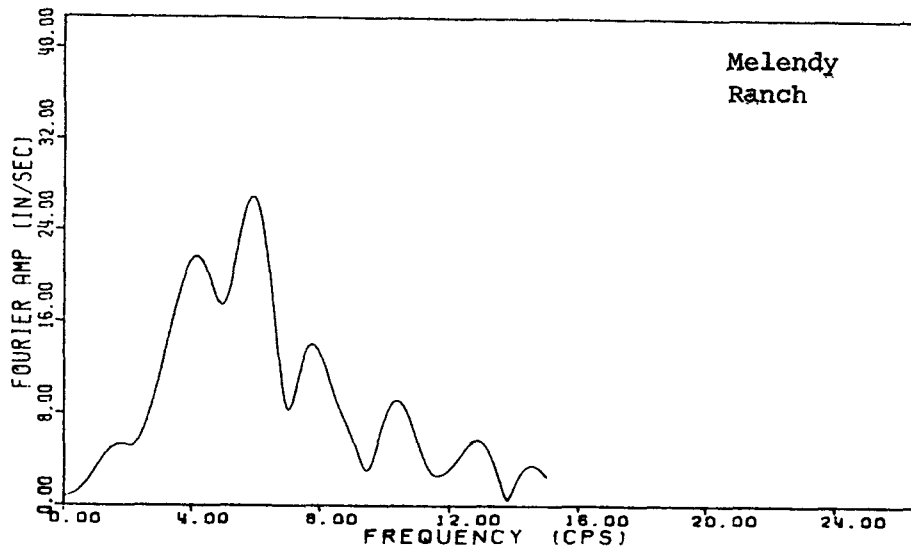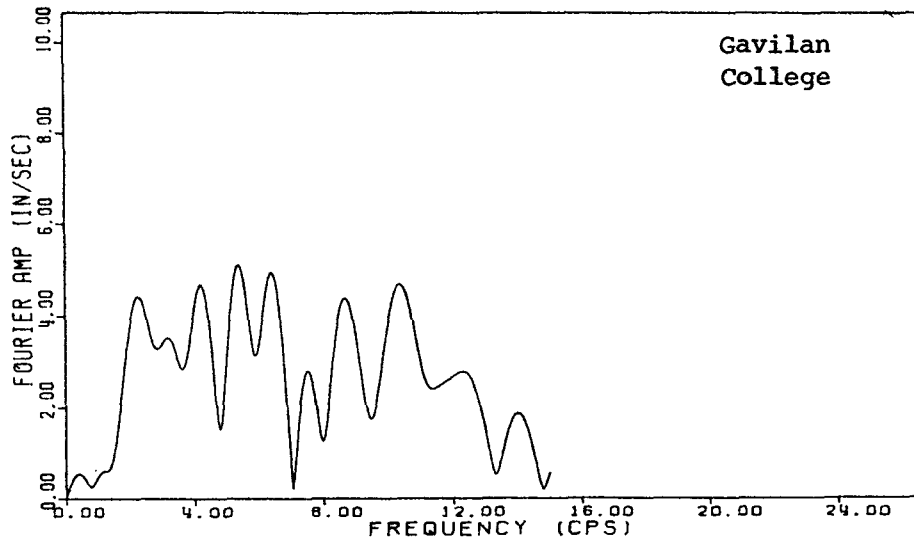
(c) $T_D' < 2.5$ sec.
(Continued)

FIGURE B-4c. FOURIER SPECTRA OF EFFECTIVE ACCELEROGRAM
SEGMENT DEFINED BY $T_D' = T_m - T_{.05}$

FREQUENCY (CPS)

FREQUENCY (CPS)
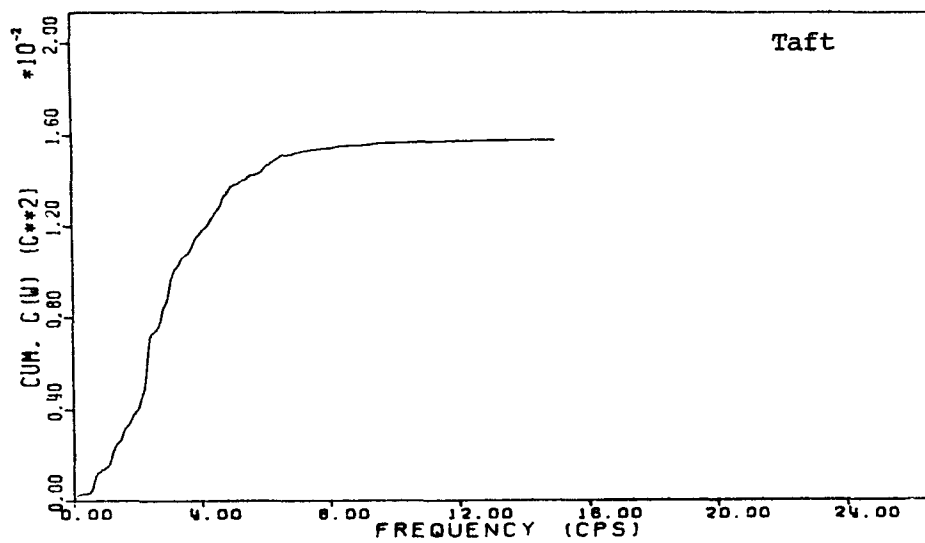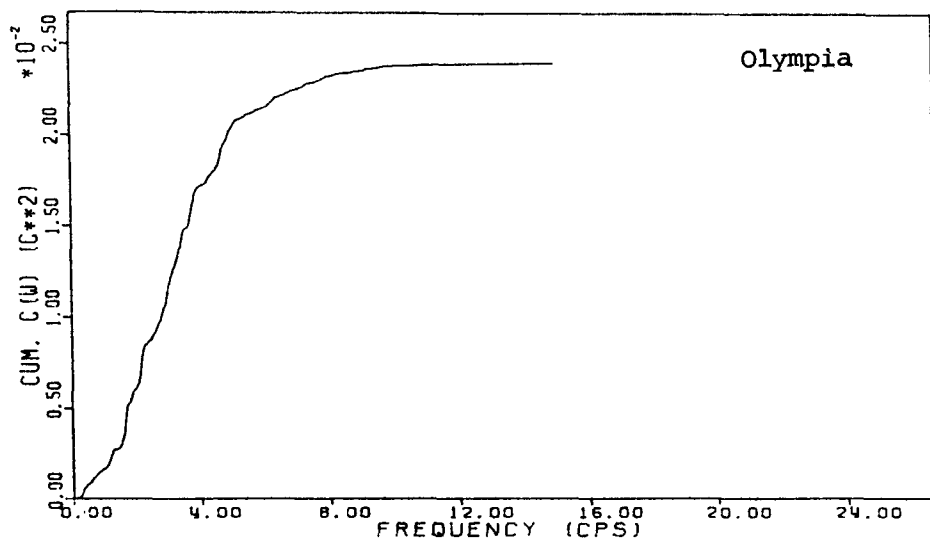
(a) $T_D' > 9$ sec.

FIGURE B-5a.   CUMULATIVE SPECTRAL DENSITY FUNCTIONS OF EFFECTIVE ACCELEROGRAM SEGMENT DEFINED BY $T_D' = T_m - T_{.05}$

El Centro
No. 12

Artificial
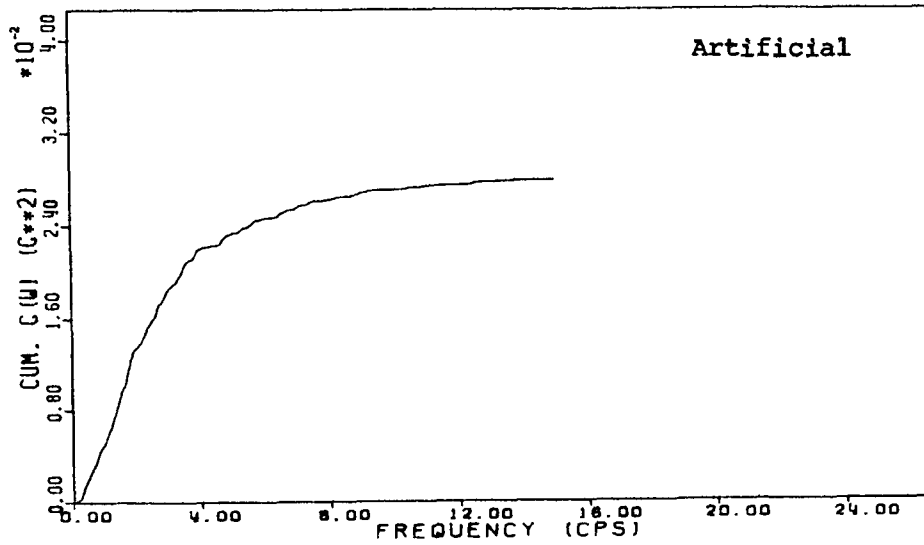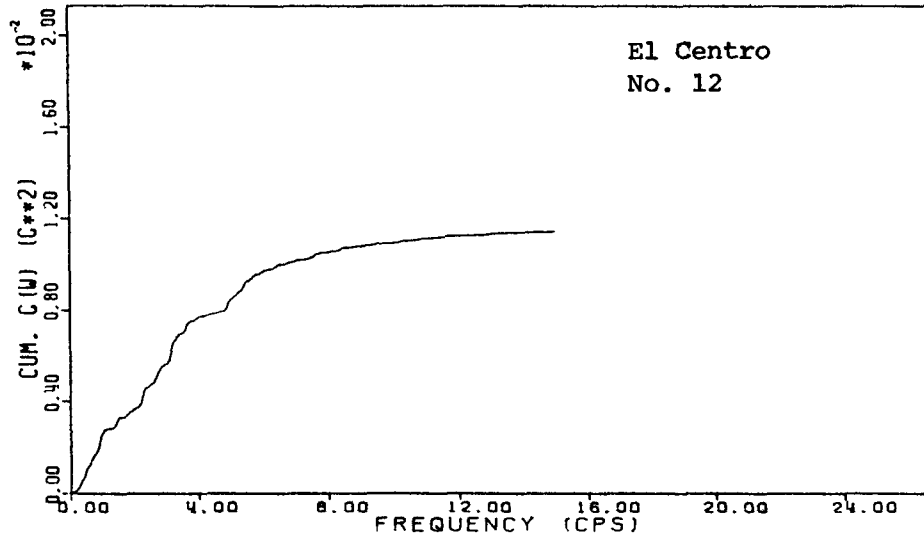
(a) $T_D' > 9$ sec.
(Continued)

FIGURE B-5a.   CUMULATIVE SPECTRAL DENSITY FUNCTIONS OF EFFECTIVE
ACCELEROGRAM SEGMENT DEFINED BY $T_D' = T_m - T_{.05}$
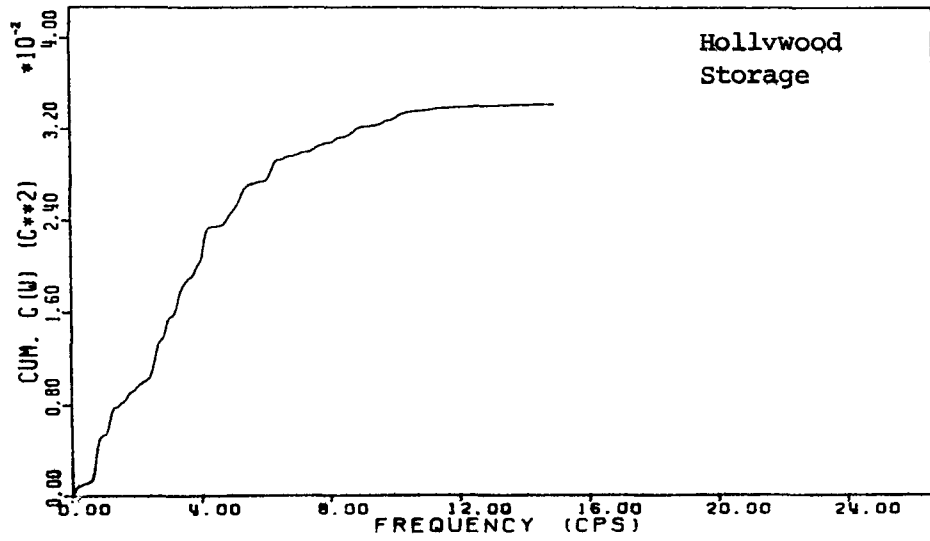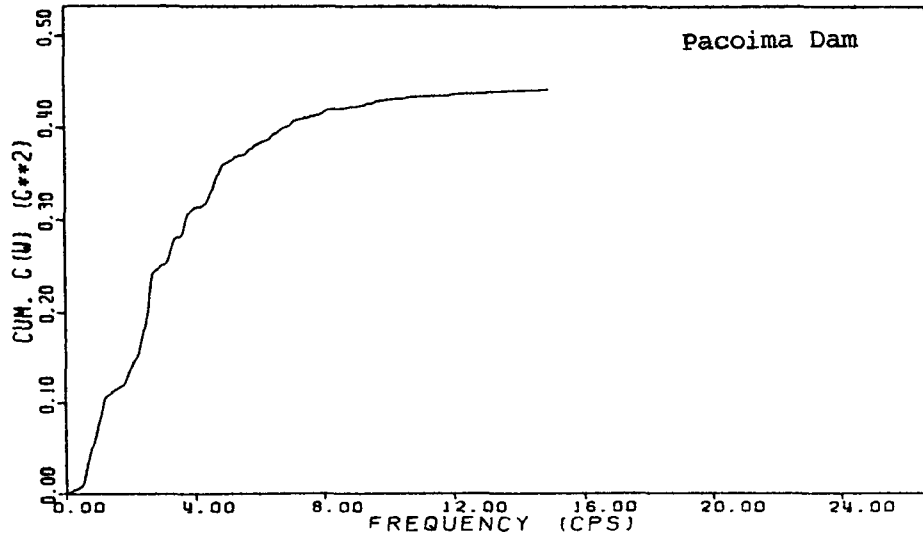
(b) $2.5 \text{ sec} \leq T_D' \leq 9 \text{ sec.}$

FIGURE B-5b. CUMULATIVE SPECTRAL DENSITY FUNCTIONS OF EFFECTIVE
ACCELEROGRAM SEGMENT DEFINED BY $T_D' = T_m - T_{.05}$
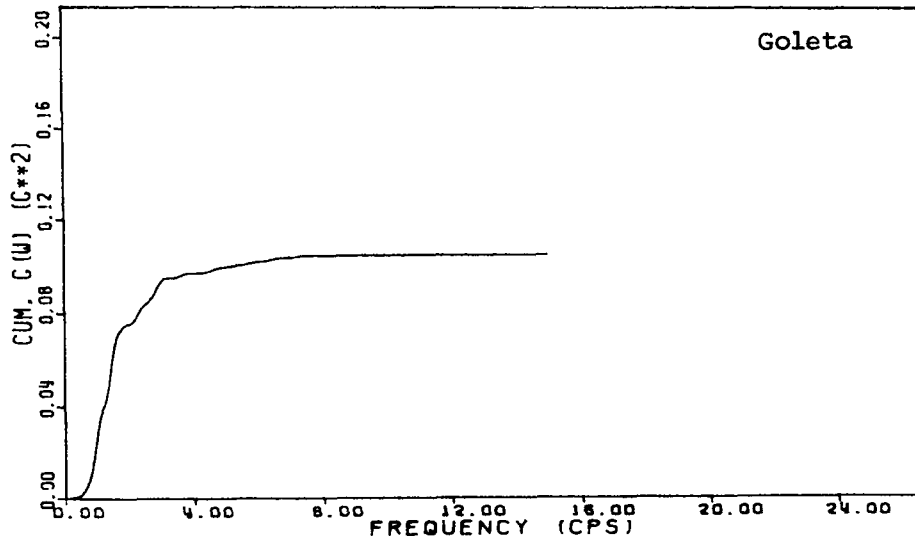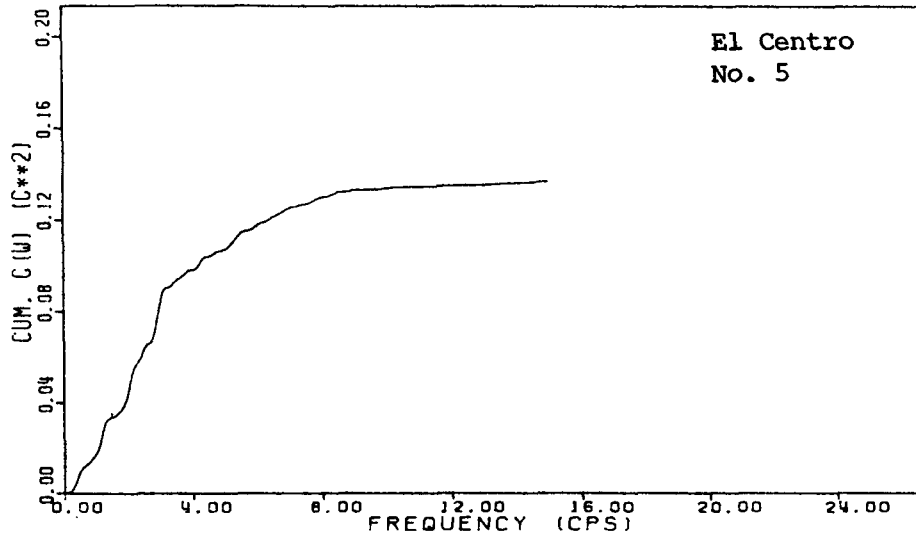
(b) $2.5 \text{ sec} \le T_D' \le 9 \text{ sec.}$
(Continued)

FIGURE B-5b.   CUMULATIVE SPECTRAL DENSITY FUNCTIONS OF EFFECTIVE
ACCELEROGRAM SEGMENT DEFINED BY $T_D' = T_m - T_{.05}$

B-37
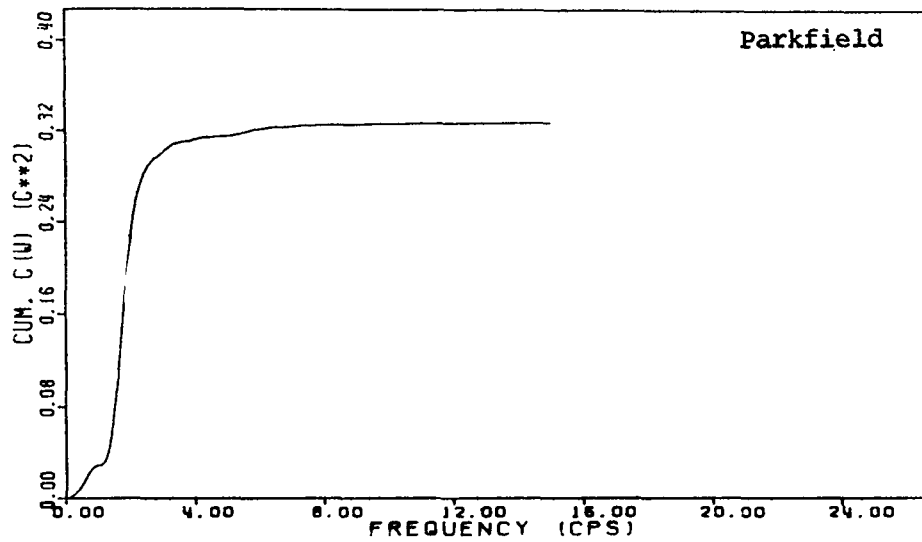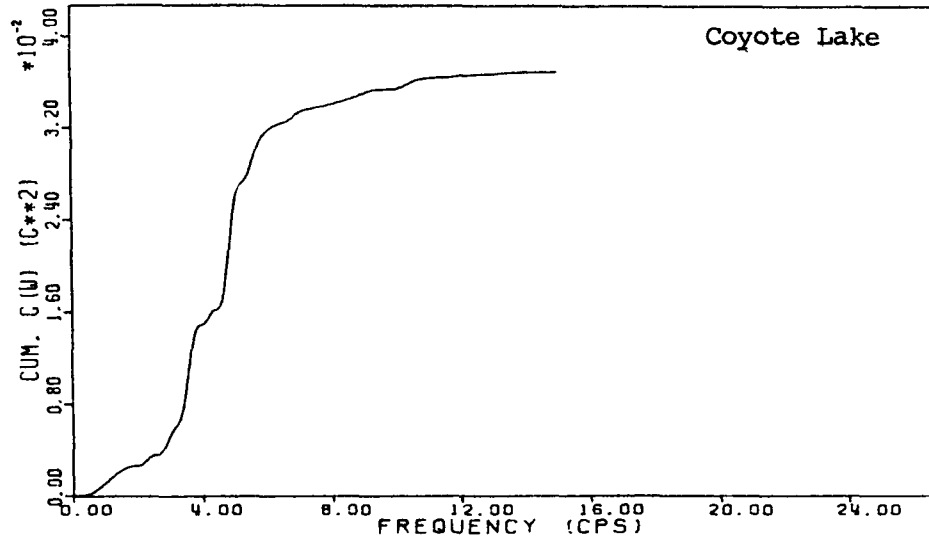
(c) $T_D' < 2.5$ sec.

FIGURE B-5c. CUMULATIVE SPECTRAL DENSITY FUNCTIONS OF EFFECTIVE
ACCELEROGRAM SEGMENT DEFINED BY $T_D' = T_m - T_{.05}$

APPENDIX C

TECHNICAL BACKGROUND ON EQUIVALENT LINEAR RESISTANCE
FUNCTION MODELS

An equivalent linear resistance function model is developed to replace the actual resistance function (Figure 3-1). This equivalent model should be capable of approximating the reduced stiffness and increased hysteretic loop damping associated with a nonlinear response cycle. Figure C-1 shows one such nonlinear cycle from peak negative displacement to peak positive displacement. During this cycle, the equivalent stiffness is K_e given by:

$$\frac{K_e}{K} = \frac{2 + s(\mu_n + \mu_{n*} - 2)}{(\mu_n + \mu_{n*})} \tag{C-1}$$

where $(\mu_n \delta_y)$ is the n-cycle peak nonlinear displacement in one direction and $(\mu_{n*} \delta_y)$ is the preceding peak nonlinear displacement in the opposite direction.

With the equivalent linear resistance function approach, one must also estimate an effective damping ratio. With c defined by Equation 3-5, the total energy dissipation, E_n within a half-cycle oscillation (i.e., from peak response in one direction to peak response in the other direction) as shown in Figure C-1, can be given by:

$$E_n = \frac{\pi K_e \beta (\mu_n + \mu_{n*})^2 \delta_y^2}{4} + \Delta E_n \tag{C-2}$$

where K_e is the effective linear stiffness from peak-to-peak, μ_n is the ductility level in one direction for that response cycle, μ_{n*} is the immediately preceding ductility level in the opposite direction, δ_y is the yield displacement and ΔE_n is the half-cycle hysteretic energy dissipation as defined by Figure C-1. This total energy dissipation in a half-cycle can be rewritten in terms of an effective inelastic damping, β_e:

$$E_n = \frac{\pi K_e \beta_e (\mu_n + \mu_{n*})^2 \delta_y^2}{4} \qquad (C-3)$$

where the effective damping is given by:

$$\beta_e = \beta + \beta_H \qquad (C-4)$$

in which β_H represents an equivalent viscous damping to account for the one-half cycle hysteretic energy dissipation as given by:

$$\beta_H = \frac{4 \Delta E_n}{\pi K_e (\mu_n + \mu_{n*})^2 \delta_y^2} \qquad (C-5)$$

For the shear wall resistance function shown in Figure C-1, the half-cycle hysteretic energy dissipation can be obtained from:

$$\Delta E_n = K \delta_y^2 (1-s) \left\{ (\mu_n + \mu_{n*} - 2X) \right.$$
$$\left. -\tfrac{1}{2} \left[\frac{\mu_n - 1}{\gamma} + \mu_{n*} (Y + 1) - (2X + Y) \right] \left[1 - s(1-\alpha)(\mu_{n*} - 1) \right] \right\} \qquad (C-6)$$

where

$$X = \left\{ \frac{1 + (s + \alpha - s\alpha)(\mu_{n^*} - 1)}{1 + s(\mu_{n^*} - 1)} \right\}$$

$$Y = (1 - \alpha)(1 - s)$$

and α and γ are the unloading stiffness parameter and strength degradation parameter, respectively, as defined in Figure 3-3.

A large number of nonlinear resistance-deformation diagrams were developed for the 4 frequencies and 12 earthquake time histories considered in this study at various maximum ductility ratios, μ, from 1.5 to 5. A limited number of these diagrams are shown in Figures 4-4 through 4-9. Based upon these resistance-deformation diagrams, it was observed that:

$$\mu_n \cong (\mu)^{n/N}$$

$$\mu_{n-1} \cong (\mu)^{(n-1)/N} \tag{C-7}$$

$$\mu_{n^*} \cong (\mu)^{(n-0.5)/N}$$

where N is the number of strong nonlinear cycles through the time of maximum ductility, μ. With these approximations, the effective stiffness and effective damping associated with any individual nonlinear cycle can be estimated by use of Equations C-1 through C-6. The effective frequency, f_e, can be obtained by substituting K_e for K in Equation 3-4.

The cycle with the lowest effective stiffness, K_e, and effective frequency, f_e, and the largest effective damping, β_e corresponds to the last strong nonlinear cycle at which μ is reached (n=N). Table C-1 presents estimates for the secant and effective frequency ratios, and

hysteretic and effective damping percentage for this <u>largest</u> nonlinear cycle as a function of number of strong nonlinear cycles, N, based upon the approximations of Equation C-7. Note that the effective frequency associated with the maximum nonlinear response cycle reduces only slightly as the number of strong nonlinear cycles through the maximum cycle (N) is increased from one to four. Even with only one strong nonlinear cycle, the effective frequency associated with the maximum nonlinear cycle is only 11% greater than the secant frequency for μ = 4.27 and approaches the secant frequency closer as N increases. Thus, for the maximum nonlinear cycle, the secant frequency only slightly underestimates the effective frequency.

The hysteretic damping percentages, β_{H_N} , and total effective damping percentages, β_{e_N} , associated with the maximum nonlinear response cycle increase as N is reduced from 4 to 1. For N=1, the hysteretic damping is considerably greater than for N of 2 and more.

The effective frequency and hysteretic damping in Table C-1 for the largest nonlinear response cycle (n=N) can be approximated by:

$$\left(\frac{f_e}{f}\right)_N \cong \left(\frac{f_s}{f}\right) \tag{C-8}$$

$$\beta_{H_N} \cong C_{NN}(1 - (f_s/f)) \tag{C-9}$$

where

$$C_{NN} \cong 0.55 \qquad (N=1)$$

$$C_{NN} \cong 0.38 \qquad (N=2) \tag{C-10}$$

$$C_{NN} \cong 0.34 \qquad (N=3 \text{ and } 4)$$

Similarly, for elastic response cycles (n=0):

$$(f_e/f)_0 = 1.0 \qquad\qquad \text{(C-11)}$$

$$\beta_{H_0} = 0 \qquad\qquad \text{(C-12)}$$

For any intermediate response cycles (0<n<N), the effective frequency lies between the elastic and the secant frequency and the hysteretic damping β_{H_n} lies between β_{H_N} and zero.

The equivalent linear resistance function model used for computing peak response must represent some average of the effective frequencies for the various linear and nonlinear cycles loading up to peak response. One might define this average effective frequency, f'_e, by:

$$\frac{f'_e}{f} = (1-A) + A(1-f_s/f) \qquad\qquad \text{(C-13)}$$

where A is an empirically determined coefficient which lies between 0 (elastic) and 1.0 (secant). This coefficient would be expected to be about 0.5 for N=1 (midway between the frequency of the elastic cycles and the one strong nonlinear cycle) and should increase with increasing numbers of nonlinear cycles. Furthermore, the coefficient A is expected to increase with increasing ductility ratios.

The equivalent linear resistance function model should retain the same energy dissipation capability as the actual model. Using Equation C-3 to define the energy dissipation capability of each model, the equivalent elastic model must have an effective damping, β'_e, given by:

$$\beta'_e \cong \frac{K_s}{K'_e} \left[\beta + C_{NN}(1 - f_s/f) \right] \tag{C-14}$$

to be equivalent to the __largest__ nonlinear cycle of the actual model when both go from a displacement of $-\mu$ to $+\mu$. Equation C-14 can be rewritten as:

$$\beta'_e \cong \left(\frac{f_s}{f'_e}\right)^2 \left[\beta + C_{NN}(1 - f_s/f) \right] \tag{C-15}$$

by noting that $(K_s/K'_e) = (f_s/f'_e)^2$. Actually, Equation C-15 will over-state β'_e because the last nonlinear cycle has the greatest hysteretic damping while β'_e should express an average damping level during the strong portion of the response time history leading up to the time of peak response. To correct this deficiency, Equation C-15 should be replaced by:

$$\beta'_e \cong \left(\frac{f_s}{f'_e}\right)^2 \left[\beta + C_N(1 - f_s/f) \right] \tag{C-16}$$

where C_N is an empirically determined coefficient which should have a value less than C_{NN} (Equation C-10).

TABLE C-1

SECANT AND EFFECTIVE FREQUENCY RATIO AND HYSTERETIC AND TOTAL EFFECTIVE DAMPING PERCENTAGE
(SHEAR WALL RESISTANCE FUNCTION - LARGEST NONLINEAR CYCLE)

Number of Strong Nonlinear Cycles, N	$\mu = 1.85$				$\mu = 4.27$			
	f_s/f	$(f_e/f)_N$	β_{H_N} (%)	β_{e_N} (%)	f_s/f	$(f_e/f)_N$	β_{H_N} (%)	β_{e_H} (%)
1	0.77	0.81	13	20	0.56	0.62	24	31
2	0.77	0.79	9	16	0.56	0.59	17	24
3	0.77	0.78	8	15	0.56	0.58	15	22
4	0.77	0.78	7	14	0.56	0.57	14	21
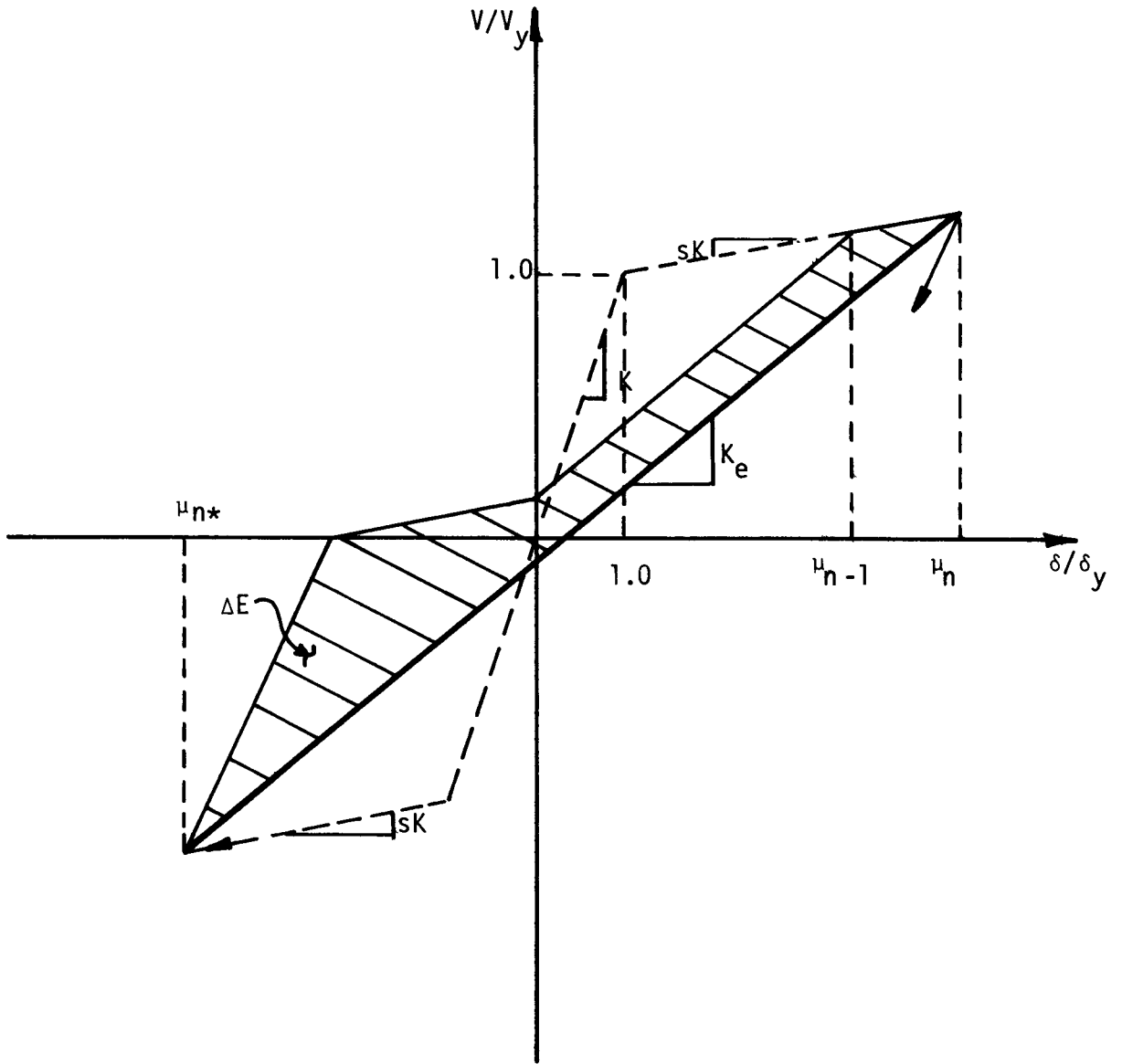
FIGURE C-1. HALF-CYCLE HYSTERETIC ENERGY ABSORPTION

APPENDIX D

PARAMETER STUDIES TO DETERMINE SENSITIVITY OF
NONLINEAR RESPONSE RESULTS TO PROPERTIES OF THE
RESISTANCE FUNCTION MODEL

This appendix presents the results of a few sensitivity studies performed to determine the sensitivity of nonlinear results to properties of the resistance function model. The purpose of these analyses is to demonstrate that the shear wall resistance function properties used in this study tend to conservatively underestimate the input scale factor (inelastic deamplification factor), F. Therefore, the results presented in Chapter 4 tend to be conservative for other model properties. This appendix was written with the assumption that the reader has carefully reviewed Chapters 3 and 4 and does not repeat discussions contained in those chapters.

D.1 INFLUENCE OF NONLINEAR RESISTANCE FUNCTION TYPE

Figure 3-1 compares the bilinear, Takeda, and shear wall resistance functions. It can be seen that for the same ductility level, the Takeda and shear wall model dissipate less hysteretic energy in a given nonlinear cycle than does the bilinear model. Thus, one would expect the Takeda and shear wall models to have similar input scale factors, F, for a given ductility level and for the bilinear model to have a significantly higher input scale factor, F. To demonstrate this expectation, the F factors were determined for the Parkfield record for low and high ductility factors of $\mu = 1.85$, and $\mu = 4.27$, respectively, for a 5.34 Hz structure model with bilinear, Takeda, and shear wall resistance functions. For all three resistance functions, the slope parameter of the post-yield loading curve was $s = 0.1$. For the Takeda and shear wall resistance functions, the unloading stiffness parameter

was α = 0.35, and the strength degradation parameter was γ = 0.95. The only difference between the Takeda and shear wall resistance functions was the pinched behavior of the shear wall model. The resulting F factors were:

Ductility Level	Input Scale Factor, F		
	Bilinear	Takeda	Shear Wall
1.85	1.29	1.24	1.21
4.27	1.51	1.33	1.29

The conclusion is that the shear wall resistance function model conservatively underestimates the input scale factor, F, for the Takeda and bilinear models.

D.2   COMPARISON OF NONLINEAR RESPONSE FOR SHEAR WALL VERSUS BRACED-FRAME MODEL

Diagonal bracing elements are the primary lateral force-carrying elements in braced-steel frames. For nuclear structures, such elements are usually angles, wide flange sections or standard weight or extra-strong steel pipe with diameters ranging from 6-12 inches. The limiting behavior of braced elements with adequate connections is governed by yielding in tension and inelastic buckling in compression. When employed as frame bracing elements for resisting reversing lateral loads, the braces can become subjected to severe axial cyclic loading causing the braces to sequentially buckle and stretch inelastically. Tests indicate that the overall lateral force-displacement behavior of a braced frame is also characterized by pinched hysteresis loops. The degrading, pinched

character of these loops is due primarily to the inelastic behavior of the individual braces under cyclic loading. During a cycle, once the tension diagonal has inelastically lengthened and while the compression brace has buckled upon load reversal, the system is softened until the buckled braced is restraightened and its axial stiffness is recovered. The axial stiffness of a buckled brace is smaller than the stiffness of a straight member. The capacity of a member in compression is also greatly reduced, either due to its bowed shape or previous inelastic strain history. A lateral load-displacement diagram obtained during a structural frame test is shown in Figure 1-9b which illustrates the reverse cycle hysteretic behavior characterized by stiffness degradation and pinching of the resulting hysteresis loops.

The number of investigations involving reversing load tests of braced-frame systems is very limited. Wakabayashi (1973, 1977)* has summarized the laboratory testing conducted on braced frames in Japan. Maison (1980) and Popov (1980) have reported testing on half-scale and one-sixth scale model braced frames. The hysteresis behavior of bracing members under cyclic axial loading has been reported by several investigators (Jain, 1980, 1978b; Gugerli, 1980; Popov, 1979, 1981).

To investigate the effect of the braced-frame resistance function, an example, one-story, single bay, braced-steel-frame was defined, as indicated in Figure D-1. The example structure was modeled directly with DRAIN-2D, utilizing the hysteresis model for steel members developed by Jain (1979) and included in the DRAIN-2D program (Jain and Goel, 1978a). Buckling element, EL9, developed originally by Singh (1977), and modified by Jain (1978a), was utilized to model the yielding and post-buckling behavior of the pin-connected bracing element (8" diameter pipe) defined for the example braced frame. The cyclic loading behavior of the frame model, obtained using DRAIN-2D, is also shown in Figure D-1. As can be noted, the model reflects the pinched, degrading stiffness behavior noted in testing of braced-frame structures.

---

* All references in this appendix are listed in the Reference list for the main body of this report.

Input scale factors, F, were obtained for both the shear wall
and the braced-frame resistance function models with a 5.34 Hz elastic
frequency and 7% elastic damping. The following input scale factors were
obtained for the Taft, Parkfield, and Melendy Ranch records.

Record	Computed Input Scale Factor, F, for 5.34 Hz Structure			
	$\mu = 1.85$		$\mu = 4.27$	
	Shear Wall	Braced Frame	Shear Wall	Braced Frame
Taft	1.25	1.49	1.65	2.17
Parkfield	1.21	1.21	1.29	1.40
Melendy Ranch	1.96	2.04	5.48	5.44

One may note that for the Melendy Ranch record, the input scale
factors are essentially identical for the shear wall and braced-frame
models. However, for the Taft record, the braced-frame model results in
significantly greater input scale factors than does the shear wall model.
Basically, the braced-frame model does not show as much degradation in
stiffness or pinched behavior as does the shear wall model.

In Chapter 4, it was shown for shear walls that the predicted
input scale factor (inelastic deamplification factor), F_μ, was influenced
by the number of strong nonlinear response cycles, N, and thus by the
strong motion duration, T_D'. It was recommended that F_μ could be best
predicted by Equation 4-3 for shear walls. This equation depends upon
the estimate of an effective frequency and an effective damping using

coefficient C_F and C_N from Table 4-2. These coefficients are shown to be a function of N for shear walls. However, for braced-frame and bilinear models, the F_μ does not appear to be as much influenced by N. To investigate this effect, the coefficients $C_F = 1.5$ and $C_N = 0.30$ for N=1 were used for the Taft and Parkfield records. The predicted scale factors, F_μ, for the recommended procedure (Equation 4-3 and Table 4-2) for shear walls is compared with the predicted scale factors obtained for 1) Equation 4-3 and $C_F = 1.50$ and $C_N = 0.30$, 2) the Iwan Method, and 3) the Sozen Method.

Record	Predicted Input Scale Factor, F, for 5.34 Hz Structures $\mu_L = 1.85$			
	Eqn. 4-3 and Table 4-2	Eqn. 4-3 and $C_F = 1.50$; $C_N = 0.30$	Iwan	Sozen
Taft	1.30	1.58	1.78	1.20
Parkfield	1.36	1.38	1.51	0.97
Melendy Ranch	2.08	2.08	2.29	2.20

Record	Predicted Input Scale Factor, F, for 5.34 Hz Structures $\mu_L = 4.27$			
	Eqn. 4-3 and Table 4-2	Eqn. 4-3 and $C_F = 1.50$; $C_N = 0.30$	Iwan	Sozen
Taft	1.68	2.38	2.77	1.62
Parkfield	1.24	1.77	2.08	0.85
Melendy Ranch	5.48	5.48	6.03	7.12

Except for the low ductility (μ_L = 1.85) Parkfield record case, the F_μ predicted by Equation 4-3 and Table 4-2 underestimates the nonlinear time history analysis computed F values for braced frames and bilinear structures for the Taft and Parkfield records. For Melendy Ranch, Equation 4-3 and Table 4-2 accurately predict the time history computed F values for braced frames. On the other hand, the use of Equation 4-3 with the N=1 values of C_F = 1.50 and C_N = 0.30 consistently overpredicts the time history computed F values for braced frames for the Taft and Parkfield records. This brief study suggests the F values for braced frames and bilinear structure models lie approximately midway between the F_μ values predicted using the C_F and C_N values of Table 4-2 and those predicted with C_F = 1.50 and C_N = 0.30

The Iwan method consistently severely overpredicts (unconservative) the time history computed F values for braced frames for the reasons discussed in Chapter 4. The Sozen method is less accurate than Equation 4-3 and Table 4-2 in predicting F values for braced frames for the reasons discussed in Chapter 4.

The conclusion of this brief study is that the C_F and C_N values given in Table 4-2 for shear wall structures overemphasize the importance of strong motion duration, T_D, on F_μ for braced-frame and bilinear structure models. For this reason, the use of C_F and C_N values from Table 4-2 will tend to underpredict (conservative bias) the F_μ values for the longer duration records (N $\geq$ 2). This underprediction occurs because the braced-frame and bilinear models do not have as severe of stiffness degradation and pinched behavior as do the shear wall models used in this study. For braced-frame and bilinear models, a better estimate of F_μ can be obtained by averaging the F_μ values obtained for C_F and C_N values from Table 4-2 with those obtained for C_F = 1.50 and C_N = 0.30.

D.3   INFLUENCE OF RESISTANCE FUNCTION COEFFICIENTS α AND s

The detailed shape of the shear wall resistance function is
significantly influenced by the coefficients α and s where s represents
the ratio of the post-yielding stiffness to the initial stiffness (Figure
3-1) and α represents the degradation in stiffness on unloading (Figure
3-3) with α = 0 indicating no unloading stiffness degradation and
increasing α indicating increased unloading stiffness degradation.

Most real structural systems have an s ratio between about 0.03
and 0.15. Previous studies have indicated variations of s between 0.03
and 0.15 has little effect on the computed ductility level so long as μ is
less than about 5. For this reason, s = 0.10 which is midway within this
normal range was used in this study. For a given ductility, the input
scale factor, F, is not expected to increase significantly for s from 0.03
to 0.15. However, as s increases beyond about 0.15, the F value is
expected to begin to increase significantly for a constant ductility
ratio. This is demonstrated by the following table which tabulates the
time history F values required to develop μ_L = 1.85 for a shear wall
resistance function structural model with an elastic frequency of 5.34 Hz
and various s values subjected to the Parkfield record.

s	F
0	1.16
0.03	1.17
0.10	1.21
0.15	1.26
0.20	1.32
0.50	1.54
1.00	1.85

It is concluded that s = 0.10 gives input scale factors, F, which are accurate for the range 0≤s≤0.15. However, the F values obtained for a resistance function with s = 0.10 will be increasingly conservatively low as s is increased beyond 0.15.

Next, the influence of stiffness degradation on unloading was studied. For this study, α was assigned values of 0.0, 0.35, and 0.50 which covers the range from no unloading stiffness degradation to very severe unloading stiffness degradation. The shear wall resistance function model with an elastic frequency of 5.34 Hz was subjected to the Parkfield record with an input scale factor of 1.21 and the following ductility ratios were obtained:

α	μ
0	1.88
0.35	1.85
0.50	1.84

It was concluded that increases in unloading stiffness degradation actually resulted in a trivial reduction in the ductility factor. The use of an unloading degradation coefficient of α = 0.35 produces results which are representative for the full practical range of 0≤α≤0.50.

D.4   INFLUENCE OF ELASTIC DAMPING

Riddell (1979) has shown increases in elastic damping result in a reduction in the inelastic spectral deamplification factor, F_μ. The methods recommended in this report (Equations 3-14 or 4-3) will also result in a lesser F_μ value with increased elastic damping. This situation results because both elastic damping and inelastic response are energy dissipation mechanisms and absolute addition of the two effects

will overstate the total reduction in response. Therefore, the input scale factors (inelastic deamplification factors) presented in Chapter 4 for 7 percent elastic damped structures are conservatively low for structures with less than 7% damping. This point is illustrated by computing the input scale factors, F, for ductilities of 1.85 and 4.27 for an elastic structural frequency of 5.34 Hz with 3% elastic damping for the Taft, Artificial, and Melendy Ranch records. These 3% damped F values are compared with those shown in Table 4-1 for 7% damping:

| | | Input Scale Factors Deamplification Factors) 5.34 Hz | | | |
| | | 7% Damping | | 3% Damping | |
Ductility	Record	Computed, F	Predicted (Eq. 4-3), F_μ	Computed F	Predicted (Eq. 4-3), F_μ
	Taft	1.25	1.30	1.53	1.54
1.85	Artificial	1.33	1.49	1.48	1.59
	Melendy Ranch	1.96	2.08	2.07	2.21
	Taft	1.65	1.68	2.19	2.20
4.27	Artificial	1.88	1.65	2.38	1.95
	Melendy Ranch	5.48	5.48	6.25	6.14

The above table also shows the inelastic deamplification factors predicted by Equation 4-3 with coefficients from Table 4-2. The effective damping values, β'_{ea}, obtained from Equation 4-6 and Table 4-2 are:

	Effective Damping, β'_{ea} (%)			
	$\mu = 1.85$		$\mu = 4.27$	
Record	$\beta = 7\%$	$\beta = 3\%$	$\beta = 7\%$	$\beta = 3\%$
Taft	7.5	4.5	9.5	6.5
Artificial	7.5	4.5	9.5	6.5
Melendy Ranch	10.5	7.5	12.5	10.0

Note that for these six cases (2 ductilities, 3 records, 1 frequency) which represent a subset of the 96 cases (2 ductilities, 12 records, 4 frequencies) studied in Chapter 4 to develop Equation 4-3 and Table 4-2, the recommended prediction approach does as good a job of predicting the computed F values at 3% elastic damping as it did at 7% elastic damping. At 7% elastic damping, the ratio of predicted to computed F values has a mean of 1.02 and a COV of 0.08 for these six cases. At 3% elastic damping, this ratio has a mean of 0.99 and a COV of 0.09 for these six cases.

Two conclusions are reached from this brief study:

1. The inelastic deamplification factors are larger at 3% elastic damping than at 7% elastic damping. Thus, F factors generated for 7% elastic damped structural models can be conservatively used for structures with damping values less than 7%.

2. The recommended prediction method (Equation 4-3 and Table 4-2) works equally well for structures with 3% elastic damping as it does for 7% elastic damping.
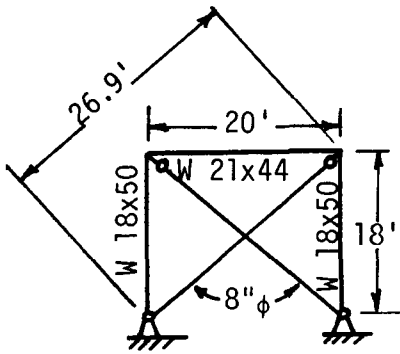
	A	I
W 18 x 50	14.7 in^2	802 in.^{4}
W 21 x 44	13.0	971
8" ϕ	8.4	72.5

$$\left(r = 2.94 \text{in}, \frac{\ell}{r} = \frac{26.9 \times 12}{2.94} \approx 110\right)$$
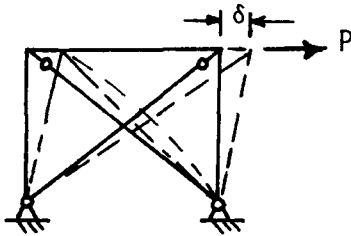
$$K = {}^{P}/_{\delta} = 714 \times \text{kips}$$

(a) Structure Model Definition
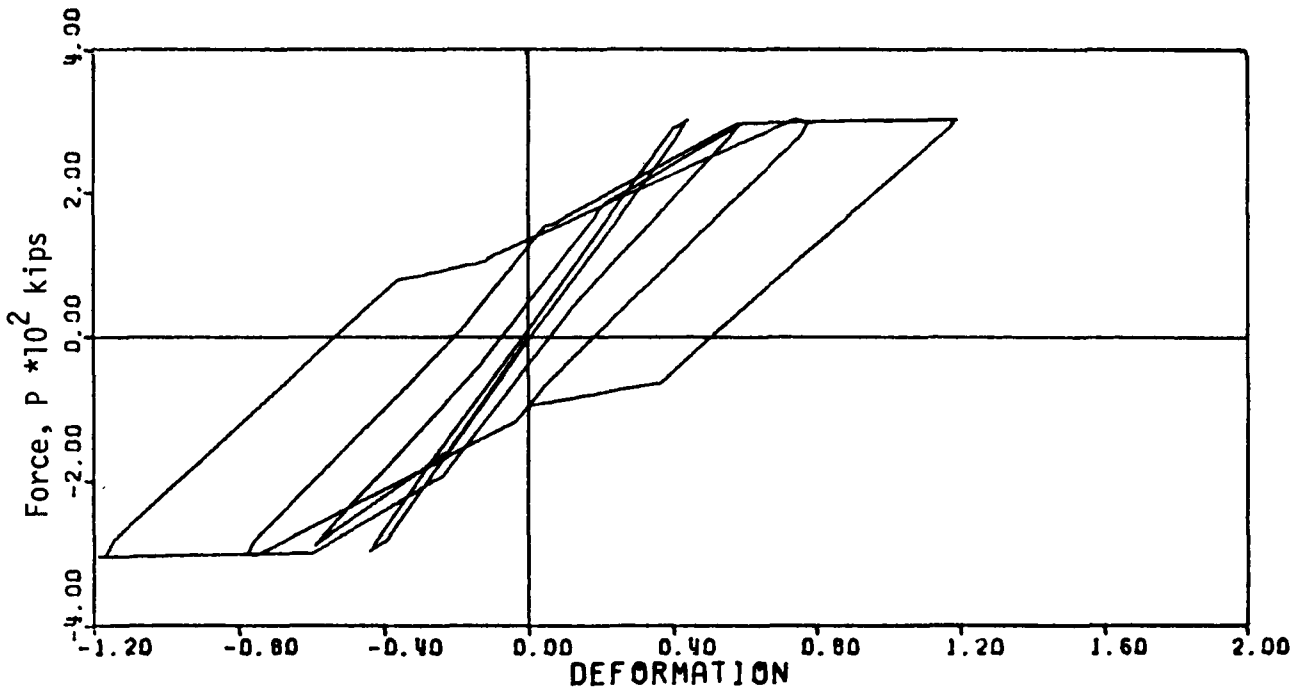
b) Cyclic Loading Behavior Using DRAIN-2D Bracing Element 9 (Jain, 1978a)

FIGURE D-1.   BRACED-FRAME STRUCTURE MODEL
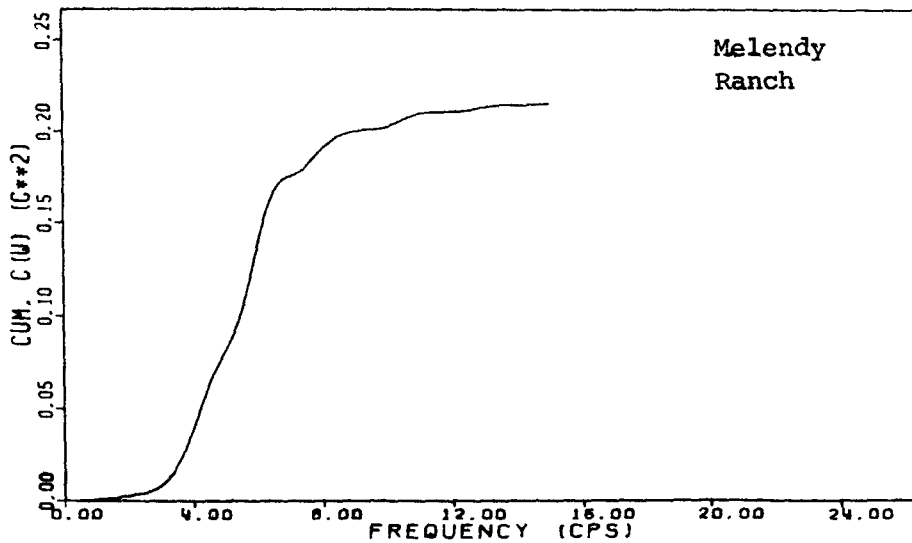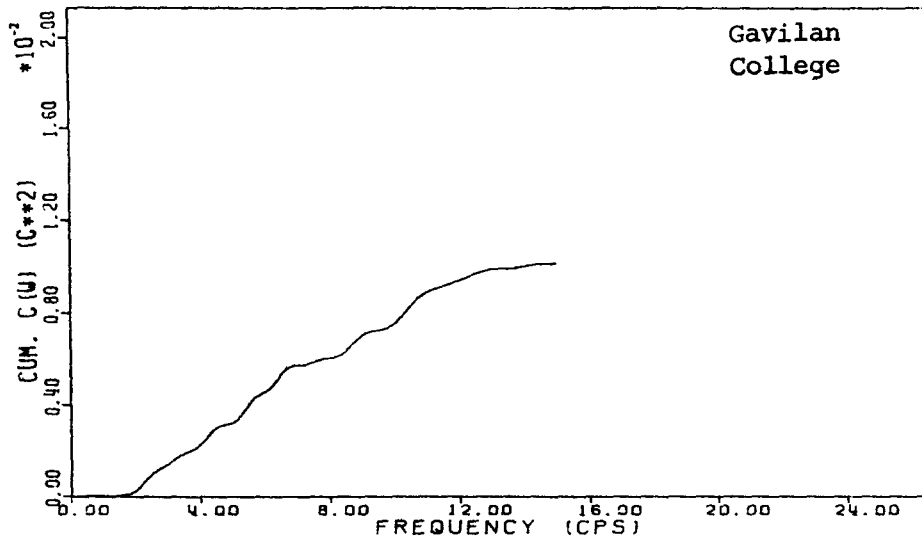
(c) $T'_D < 2.5$ sec.
(Continued)

FIGURE B-5c.   CUMULATIVE SPECTRAL DENSITY FUNCTIONS OF EFFECTIVE
ACCELEROGRAM SEGMENT DEFINED BY $T'_D = T_m - T_{.05}$

APPENDIX E

STRUCTURAL EVALUATION OF EL CENTRO STEAM PLANT UNIT 4
SUBJECTED TO THE 1979 IMPERIAL VALLEY EARTHQUAKE

E.1   INTRODUCTION

The El Centro Steam Plant located in the northeast portion of
El Centro, was subjected to peak horizontal ground accelerations estimated
to be about 0.5g (Reference E-1) as a result of the 1979 Imperial Valley
earthquake. This plant consists of four units. The seismic design basis
for Units 1, 2 and 3 built in 1949, 1952 and 1957, respectively, is
unknown. However, review of the project specifications for Unit 4, which
was built in 1968, indicates that the steel framing was designed for a
lateral static equivalent seismic loading of 0.2g (dead and live loads).
Even though the El Centro Steam Plant was subjected to earthquake ground
motion that was about 2.5 times the design seismic loading, there was
only minor damage observed at the plant following this earthquake. The
purpose of this evaluation is to correlate predicted structural damage
with observed structural damage for the El Centro Steam Plant Unit 4
subjected to the 1979 Imperial Valley earthquake.

Analyses of Unit 4 of the steam plant have been reported in
References E-1 and E-2. However, neither of these evaluations were
conducted for the express purpose of correlating predicted and observed
structural damage. The analysis presented in Reference E-1 was performed
for the purpose of estimating equipment response levels and was based on
a simple structural model. There was no evaluation of structural response
and capacities in this reference. The analysis presented in Reference
E-2 was conducted to demonstrate that a particular set of conservative
design criteria would produce analytical results which would overpredict
observed Unit 4 structural response. This analysis was based on a
detailed three-dimensional model of the Unit 4 structure but which ignored
soil-structure interaction effects. Data from each of these references
have been used in the preparation of this report.

The evaluation of the El Centro Steam Plant as presented herein is based on a relatively detailed structural model which incorporates soil-structure interaction effects. Structural response is calculated with this model by an elastic response spectrum analysis. The seismic excitations are taken from response spectra computed from measured acceleration time histories recorded close to the steam plant site. The calculated structural response is then compared to code-specified ultimate capacities (i.e., from AISC Part 2 and ACI building codes) of structural members and elements to assess predicted structural behavior. The predicted structural behavior is then, in turn, compared with observations of the plant following the earthquake in order to demonstrate how behavior calculated from an elastic structural analysis based on elastic spectra anchored to peak acceleration from recorded motions correlates with actual observed behavior of this structure.

E.2   DESCRIPTION OF THE STRUCTURE

The El Centro Steam Plant consists of four units that generate power by burning oil or natural gas (Figure E-1). Units 1, 2 and 3 were designed by Gibbs and Hill and built in 1949, 1952 and 1957, respectively. Unit 4, the newest and largest with an 80 MW electric output, was designed by Fluor Corporation, Ltd. and built in 1968. Combined output of all four units is 174 MW. Each unit of the plant is structurally independent and contains three structures: a turbine building, a turbine pedestal and a boiler structure. Each of these structures is founded on a single 12.2 foot-thick hollow, honeycomb-like reinforced concrete foundation with plan dimensions of 96 by 207 feet. Soil at the site consists of very deep alluvial deposits composed of stiff to hard clays interlain with laminations of silty clay loam and sandy loam (Reference E-1). Cross sections of Unit 4 are shown in Figures E-2 and E-3 and a plan view of the ground floor is shown in Figure E-4.

The Unit 4 turbine building is a moment-resisting steel frame with reinforced concrete shear walls cast monolithically with the exterior steel frames on the east, west and south sides of the building. The turbine building has plan dimensions of 93 feet by 128 feet and a maximum

height of 55 feet. As shown in Figures E-3 and E-4, the turbine building has four bays: auxiliary, heater, turbine and service. An operating floor 20 feet above the ground floor extends through all four bays. This floor contains a large opening for the turbine pedestal structure. There is also a floor in the heater bay 14 feet above the operating floor. Both the operating and heater bay floors are constructed of metal decking and concrete fill. Covering the auxiliary and heater bays is a roof of metal decking and concrete fill. The roof covering the turbine and service bays is composed of gypsum decking and composition roofing.

The Unit 4 turbine pedestal is a reinforced concrete frame that supports the turbine generator. The pedestal is located within the turbine building but is isolated from the building by a one-inch expansion joint at the operating floor. The pedestal has plan dimensions of 68 feet by 23 feet and is 20 feet high.

The boiler structure for Unit 4 is a braced-steel frame with plan dimensions of 31 by 51 feet and a height of 97 feet. The boiler structure and the turbine building are connected along Column Line G between Column Lines 15 and 16. The boiler is suspended from girders at the top of the steel frame. Lateral support for the boiler is provided by seismic stops at various elevations of the frame. The boiler structure also supports a steel stack.

E.3   EARTHQUAKE GROUND MOTION

On October 15, 1979, a strong earthquake shook the Imperial Valley of California. As reported in Reference E-1, this earthquake had a local magnitude M_L, of 6.6 and a surface wave magnitude, M_S, of 6.9. The earthquake produced 30 km of predominantly strike-slip rupture along the Imperial Fault (Figure E-5). There were many aftershocks, three of which exceeded M_L = 5 within the first 8 hours.

As a result of the 1940 El Centro earthquake and other smaller earthquakes, the Imperial Valley was extensively instrumented by a network of strong motion accelerometers. A 13 station linear array straddling the fault and passing through El Centro is shown in Figure E-5. Included in this array is Station No. 9, the original instrument that recorded the 1940 El Centro ground motion record. Also of interest, is a digital recording differential array installed by the U.S. Geological Survey about two weeks before the 1979 earthquake in a large vacant lot near Unit 4 of the El Centro Steam Plant. Unfortunately, there were several malfunctions in the operation of this system such that useful data was not obtained from most of the instruments in this array. However, a good record was obtained from the instrument labeled No. 5165 El Centro Differential Array installed in a small building at the south end of the array.

The El Centro Steam Plant is located between Stations No. 8, No. 9 and the Differential Array as shown on Figures E-5 and E-6. Stations 8, 9 and 5165 are about 4,000, 3,800 and 2,400 feet from Unit 4 with Station 8 closest to the Imperial Fault and Station 9 furthest from the fault. Station 5165 is located at about the same distance from the fault as the steam plant although this instrument is closer to the earthquake epicenter. Good ground motion records were obtained for this earthquake at Stations 8 and 5165. Because of the age of Station No. 9, there was difficulty in obtaining a complete time history from this instrument. Also, there are questions about the free-field nature of Station No. 9 because it is situated on a large foundation.

For this evaluation, a digitized corrected version of the recorded time history from Station 5165 was used as input excitation for the analysis of the El Centro Steam Plant Unit 4 as reported herein. It is believed that this record is a reasonable estimate of the ground motion at the steam plant site for the following reasons:

a. The steam plant appears to be within a zone along the Imperial Fault where ground motion is relatively constant. Large attenuation of the ground motion is not seen until Station No. 10 located much further away from the fault. Recorded ground motion for the 1979 Imperial Valley Earthquake at Stations 7 through 10 and 5165 are summarized in Table E-1.

b. A Wilmot Seismoscope with a period of 0.75 sec. situated at the bottom floor of the steam plant itself registered a maximum response displacement of 6.57 cm and a maximum response velocity of 55 cm/sec. These are approximately equivalent to the maximum responses at 0.75 sec. period and 10% damping computed from the horizontal time histories at Station 5165. The seismoscope is believed to have a damping of about 10%.

The critical elements of the Unit 4 structure are primarily sensitive to horizontal lateral forces and thus this evaluation considered only the horizontal components of earthquake ground motion. The time histories and response spectra of the north-south and east-west components from Station 5165 are illustrated in Figures E-7, E-8, and E-9. Note that in Figures E-7 and E-8, the 7 percent damped spectra from Station 5165 and Reg. Guide 1.60 (Reference E-6, anchored to the peak acceleration from Station 5165) are compared. The spectra from the recorded earthquake motion generally fall below the Reg. Guide 1.60 spectra with the exception of the region between about 5 and 9 Hz where the east-west motion spectrum from Station 5165 is greater than the Reg. Guide spectrum. The strong motion duration, T'_D, defined in the manner described in Chapter 2 (i.e., T'_D = maximum of T_{pa} or $T_{0.75}$ minus $T_{0.05}$ where $T_{0.05}$ and $T_{0.75}$ are the times associated with 5 and 75 percent of the total cumulative energy for the record and T_{pa} is the time associated with the first zero crossing of the accelerogram following the maximum positive or negative acceleration, whichever occurs later in time) are 2.8 seconds for the north-south motion and 3.7 seconds for the east-west motion. Qualitatively, the Station 5165 motions are moderate duration records.

E.4   EARTHQUAKE DAMAGE

An NRC reconnaissance team visited the steam plant shortly after the earthquake struck. Lawrence Livermore National Laboratory (LLNL) personnel visited the site on March 18, 1980. At the request of LLNL, a representative of Structural Mechanics Associates, Inc. (SMA) inspected the plant and examined the plant log book for the day of the earthquake and for the following day in August, 1980. Based upon the data gathered from these site visits, a record of the damage incurred at the steam plant during the earthquake was presented in Reference E-1. A brief summary of the observed damage extracted from this reference is presented in this section.

When the earthquake occurred, Units 3 and 4 of the El Centro Steam Plant were operating and Units 1 and 2 were shut down for maintenance. The operating units tripped off line when station power was lost because of a short circuit resulting from a broken insulator in a lightning rod in Unit 1. Unit 3 was restored to service within 15 minutes following the main shock and Unit 4 was restored to service within 2 hours. Much of the time was spent by plant personnel inspecting for damage. Later in the day and during the following day, both Units 3 and 4 were removed from service to repair piping.

No significant structural damage was observed. Minor concrete cracking was generally apparent throughout the plant. More significant cracking, on the order of 1 in., was observed at a junction of a floor diaphragm high in the structure and the turbine building shear wall. In addition, concrete cracks were observed at upper elevations between the various units, where larger deflections would be expected. However, in all cases, this cracking was local in nature and overall structural integrity was maintained. Structural steel, for the most part, was not permanently deformed as a result of the earthquake. Significant stressing was apparent on some members through observations of cracked paint on structural sections and the gouging of metal near connections.

One of the few areas where structural damage was observed was the Unit 4 boiler, which is hung in a pendulum fashion using rods supported by a braced frame. Lateral seismic restraints are mounted on the braced frame to minimize excessive motion of the freely supported boiler. Travel through the restraint gap was evidenced by paint chipping in the area and permanent deformation of the restraint. In addition, four diagonal bracing members on the boiler frame buckled (Figure E-10), apparently due to excessive compressive loads. These diagonals were later replaced.

E.5   ANALYTICAL APPROACH

The structural evaluation of El Centro Steam Plant Unit 4 has been conducted using an analytical approach which is consistent with that used for the design of many critical facilities. The structural model consists of beam elements and lumped masses representing the stiffness and inertial characteristics of the structure. Soil springs and radiation damping have been used to account for soil-structure interaction. Seismic response has been computed by a response spectra dynamic analysis employing modal superposition using the SMA version of computer program MODSAP. The computed response is compared with code specified ultimate capacities (i.e., ACI or AISC Part 2) to evaluate predicted behavior. Details of the analytical method are briefly described below.

The structural model consisting of 44 nodes, 67 beam elements and 5 spring elements is illustrated in Figure E-11. This model is capable of considering both north-south and east-west input motions simultaneously. As mentioned previously, because the critical elements of this structure are primarily sensitive to horizontal loads, neither vertical dynamic loads nor dead and live loads were considered. In the model shown in Figure E-11, Beam Elements 1 through 19 represent the boiler structure, Beam Element 44 represents the turbine pedestal and the remaining beam elements represent the turbine building with Beam Elements 17, 18 and 19 at the structural connection of the turbine building and the boiler structure. Spring Elements 1 through 5 represent translational and rotational soil stiffnesses. Nodal coordinates and beam

section properties and connectivities are given on Tables E-2, E-3 and E-4. Lumped masses and rotational inertias are presented in Table E-5. These include weights of structural members and equipment tributary to each node. Units are kips and inches for these tables. Note that the coordinate system used is shown in Figure E-11, X = east-west, Y = north-south and Z = vertical.

For north-south seismic excitation, the reinforced concrete shear walls at Column Lines A and G and the steel frame along Column Lines B, E, F and H^9 are represented by vertical beam elements and diaphragms provided by floors, roofs and horizontal braced frames are represented by horizontal beam elements at the appropriate elevations connecting north-south column lines together structurally. In this manner, the distribution of seismic-induced forces along each column line accounting for relative rigidities and torsion is included in the model.

For east-west seismic excitation, the Unit 4 turbine building and boiler structure are a symmetrical moment-resisting steel frame and a braced steel frame, respectively, with the exception of the shear wall along Column Line 17 on the south side of the turbine building. As a result, the vertical beam elements at Column Lines A through H^9 have lumped properties for east-west direction excitation corresponding to the cumulative stiffness of the structural steel members in the turbine building (columns) and boiler structure (braced frame) of Column Lines 14, 15, 16 and 17. In addition, vertical beam elements representing the south shear wall are included in the model at a southward offset from the elements representing the steel members equal to one-half the building width. For east-west motion, horizontal members represent diaphragms structurally connecting the shear wall to the steel frame and girders running in the east-west direction. Note that torsional stiffness of the boiler structure is included in this model. For east-west shaking, the structural model properly accounts for the relative rigidity and torsion of the steel frame and south shear wall.

The boiler is suspended from the top of the boiler structure and will act as a pendulum under lateral seismic motion with little effect on structural response prior to impact with seismic restraints. When the combined displacements of the boiler and supporting structure are sufficient to overcome the seismic gaps provided, the lateral response of the boiler will influence the response of the structure. The boiler did impact and damage the seismic restraints and the mass of the boiler has been lumped to various nodes of the boiler structure for this evaluation.

Energy dissipation within the structures due to material and structural damping has been represented by specifying equivalent viscous damping in accordance with the U.S. NRC Regulatory Guide 1.61 (Reference E-7) used for design of nuclear power plants. For the evaluation of seismic-induced loads throughout the structure, 7 percent of critical damping has been utilized. From the Regulatory Guide, this damping is appropriate for reinforced concrete (predominant behavior of turbine building and turbine pedestal) and bolted steel structures (boiler structure) subjected to Safe Shutdown Earthquake (SSE) motion. Soil damping is predominantly the loss of energy through propagation of elastic waves from the immediate vicinity of the foundation (i.e., radiation of energy from the structure to the surrounding soil). Radiation damping has been evaluated in the manner described below.

In this evaluation of the El Centro Steam Plant, soil-structure interaction is accounted for in an identical manner to that used in Reference E-1. By this approach, the soil was treated as an elastic half-space and soil springs and dashpots were developed using the relations in Reference E-3. The complex-shaped foundation was transformed to an equivalent rectangle with equal area for calculational purposes. Soil stiffnesses and dampings are based on soil shear wave velocity of 650 fps and shear modulus of 1600 ksf as average strain-compatible values over a depth equal to the foundation width as reported in Reference E-1. The resulting soil stiffnesses evaluated by this approach are represented in the analytical model by soil spring elements attached to the rigid ground

floor-foundation elements as shown on Figure E-11. Values for soil stiff-
nesses are presented in Table E-6 for soil spring element 1 through 5.
The resulting soil dashpot constants representing soil radiation damping
are incorporated into this evaluation by calculating the fraction of
critical damping for each soil response mode (i.e., sliding, rocking and
torsion) and utilizing these soil damping values along with structural
damping to determine modal damping values such that a response spectrum
dynamic analysis may be performed. Soil damping ratios are evaluated
from the assumption of a rigid structure resting on an elastic half-space
such that the soil stiffness and structural mass are used to convert soil
dashpot constants to fractions of critical damping. Fractions of critical
damping in each soil response mode (i.e., associated with soil spring
elements 1 through 5) are presented in Table E-6.

The soil-structure interaction approach employed for this evalua-
tion of the El Centro Steam plant is an approximate method including
several simplifying assumptions. The treatment of the soil as an elastic
half-space ignores layering in the underlying soil which could poten-
tially reduce the radiation damping from that corresponding to an elastic
half-space. The foundation for the El Centro steam plant is embedded
about 12 feet. Embedment effects on soil-structure interaction have been
ignored herein. Also, frequency-independent relations for soil stiffness
and damping are provided in Reference E-1 which are approximations within
a certain frequency band since these soil impedance functions vary with
frequency. Furthermore, the conversion from soil dashpot value to frac-
tion of critical damping depends upon an assumed frequency. As mentioned
above, this conversion was accomplished at frequencies corresponding to
single-degree-of-freedom oscillators in which the rigid structural mass
or rotational inertia is supported by the various soil spring stiffnesses.
In spite of the simplifications employed for soil-structure interaction
in this evaluation, it is judged that adequate estimates of soil stiffness
and damping at the frequencies of the soil-structure system (i.e., at
frequencies between 3.5 and 5 Hz) have been obtained for this evaluation
of the steam plant.

For response spectrum dynamic analyses, it is necessary to evaluate modal damping. To determine equivalent modal damping, beam elements were assigned 7 percent of critical damping and soil spring elements were assigned the radiation damping values listed in Table E-6. Composite modal damping values were then computed by an approach assuming that element damping is proportional to the element stiffness for each element. However, modal damping values were not permitted to exceed 20 percent of critical damping. Use of an upper limit modal damping is commonly used for the design of critical facilities to obtain conservative calculated seismic response. Composite modal damping values with very high soil radiation damping evaluated by the element stiffness weighting technique can be unconservative without an upper cutoff because structural response of combined soil-structure modes can be over-damped due to smearing of soil and structure damping. It is our judgment that an upper cut-off on damping will lead to more accurate seismic response from calculations based on the approximate soil-structure interaction approach used in this study. The calculated modal damping values and the modal damping values used in the response spectrum analysis are presented in Table E-7 for all modes considered.

The frequencies of structural modes and the percentage of mass participating in each mode are presented in Table E-7. About 94 percent of the total structural mass is accounted for by the first 10 modes ranging in frequency from 1.40 to 5.14 Hz. The first 10 modes are qualitatively described in Table E-8. By the 17th mode at 7.70 Hz, over 99 percent of the total structural mass has been included. Thirty-six modes including frequencies up to 18.63 Hz have been used for evaluating structural response in order to include all local seismic vibration modes. This number of modes enabled at least 98 percent of the mass for each horizontal degree of freedom to participate in the seismic response. Individual modal responses are combined to give a total response for each direction of excitation. Responses for each direction are then combined to give total seismic response. Modes are combined in accordance with Reg. Guide 1.92 Section 1.2.2 (Ten Percent Method) which takes the absolute sum of closely-spaced modes and then square-root-of-the-sum-of-the-

squares (SRSS) combination of other modes and summed closely-spaced modes. Total seismic response was evaluated by SRSS combination of combined responses for each excitation direction.

E.6   ANALYTICAL RESULTS

Maximum seismic response displacements and accelerations are presented in Figures E-12 and E-13. From Figure E-12, it may be seen that maximum displacements are at the top of the boiler structure with maximum values of 3.6 inches in the east-west direction and 5.5 inches in the north-south direction. Displacement of the turbine building steel frame at the top of the building is 1.6 inches in the east-west direction and from 1 to 2 inches between Column Lines B and F in the north-south direction. North-south displacements of the concrete shear walls at Column Lines A and G and east-west displacements of the concrete shear wall along Column Line 17 are less than 0.5 inches. The large differences in displacements and in accelerations as shown in Figure E-13, are due to the large differences in rigidities of the various structural components making up this steam plant. The boiler structure is very flexible such that large response displacements occur while the turbine building shear walls are very stiff and have relatively low seismic response displacements. The flexibility of the turbine building steel frame lies between that of the boiler structure and the concrete shear walls. Based on the computed displacements, it is concluded that Unit 4 would not impact Unit 3 and the turbine pedestal would not impact the operating floor during this earthquake.

Peak accelerations, as shown in Figure E-13, are about 3 to 4g in the north-south direction at the wall along Column Line B in the upper portion of the turbine building and at the heater bay floor. Maximum acceleration of the boiler structure is about 2.4g. It is interesting to note that the maximum acceleration of the foundation is about 0.56g and 0.47g in the east-west and north-south directions, respectively, while the maximum earthquake ground accelerations (i.e., ZPA values) are 0.35 and 0.49g in the east-west and north-south directions, respectively.

Thus, there has been a significant amplification from the ground accelera-
tion for east-west earthquake shaking. This amplification is due to soil-
structure interaction effects as treated by this analytical model and may
be an indication of some overconservatism in this treatment. As stated
previously, the approach employed is that typically used for design
analyses of many critical facilities.

In Figure E-13, it is also interesting to note that the north-
south accelerations of the upper portion of the boiler structure along
Column Line G are greater than those along Column Line H^9. At first
inspection, it would be expected that H^9 response accelerations would
be greater since torsional response should be greatest at this column line
which is near the edge of the building and because the boiler structure
is supported by the turbine building shear wall in this direction along
Column Line G. Closer inspection reveals that the north-south response
of Column Line H^9 occurs at a frequency of 1.4 Hz and the north-south
response of Column Line G occurs at about 2.7 Hz (See Table E-8). At
frequencies of 1.4 and 2.7 Hz, the north-south spectral accelerations are
about 0.7 and 1.0g, respectively as shown in Figure E-7. This difference
in spectral acceleration is the reason that the seismic response accelera-
tions at the upper portion of the boiler structure along Column Line G
are larger than at the corresponding elevations along Column Line H^9.

The calculated seismic response moments and shears have been
used to evaluate the predicted performance of El Centro Steam Plant Unit
4. In the following discussion, the calculated seismic response and the
estimated ultimate capacity for the structural elements of the boiler
structure, turbine building and turbine pedestal are compared.

E.6.1   Boiler Structure Response
         For the boiler structure, seismic response shears are obtained
from the beam element model shown in Figure E-11. The critical elements
are the diagonal braces along Column Lines 15, 16, G and H^9 which carry
lateral seismic loads from upper elevations to lower elevations of the

boiler structure and horizontal bracing members which enable transfer of seismic loads in the north-south direction from Column Line H^9 to G at each elevation of the boiler structure. Shears in Elements 1 through 6 and 14 through 19 must be carried by diagonal braces which transfer lateral seismic loads between various elevations of the boiler structure. Shears in Elements 7 through 12 must be carried by horizontal bracing members which transfer north-south seismic loads between Column Lines H^9 and G. For single diagonal braces, two shear capacities are provided depending on whether the diagonal member is in tension or compression. The shear capacity of an element in which lateral seismic resistance consists of a single diagonal brace is the horizontal component of the diagonal member force corresponding to yield level for tension and ultimate buckling capacity (AISC Part 2 criterion as given in Reference E-4) for compression. For k-bracing or x-bracing, only a single shear capacity has been evaluated. This shear capacity is the sum of the horizontal components of the diagonal member forces corresponding to the ultimate buckling capacity for compression members and the ultimate tensile capacity for tension members. For k-braces, the ultimate tensile capacity is the lesser of the yield level or the maximum tensile force which can be supported by the horizontal beam member which must resist the unbalanced load occurring if the forces in each of the k-brace members are unequal.

The elastically computed seismic-induced shears and ultimate shear capacities for diagonal members along Column Lines 15 and 16 in the boiler structure are summarized in Figure E-14. For the diagonal members between Elevations 1011 and 1031, the elastically calculated seismic-induced shear is about 4.8 times the code specified ultimate shear capacity and as shown in Figure E-10, these members did buckle as a result of the 1979 Imperial Valley earthquake. For most of the other diagonal members along Column Lines 15 and 16, the calculated load also exceeded the capacity but by a lesser amount. There was no evidence of buckling for these members as a result of this earthquake including the members between Elevations 998 and 1011 for which the elastically

computed seismic exceeded the ultimate shear capacity by a factor of about 3.5. Buckling of diagonal members subjected to oscillatory loading such as earthquake excitation may not be apparent from post-earthquake observations. For the boiler structure members, the capacities are governed by elastic buckling and during several cycles of seismic response, the diagonal member might buckle and then straingten out under tensile load. Only members which undergo significant deformation into the inelastic range would remain permanently displaced such that their buckling could be detected following the earthquake. Furthermore, for k-braces or x-braces in which one member is always in tension, the deformations of a buckled member would be limited by the tensile member. As a result, it is possible that some of the diagonal members whose calculated seismic response exceeded the code specified ultimate capacity may have actually buckled during this earthquake even though there was no evidence of buckling following the earthquake.

The elastically computed seismic-induced shears and ultimate capacities for diagonal members along column Line H^9 are summarized in Figure E-15. Between Elevations 1031 and 1046, the computed load/ capacity ratio was 3.9 with no observed buckling and between Elevations 1011 and 1031, the computed load/capacity ratio was 4.0 and one of these members was observed to have buckled following the 1979 earthquake. All other diagonal members along Column Line H^9 had computed load/capacity ratios ranging from 1.4 to 2.6 with no buckling of these members observed following the earthquake.

The calculated seismic shears and ultimate capacities for diagonal members along Column Line G are shown in Figure E-16. There was no buckling of these members observed following the 1979 earthquake even though the elastically computed seismic-induced shears exceeded the code specified ultimate shear capacity by as much as a factor of 4.9.

At several elevations of the boiler structure, there are horizontal braced frames acting as horizontal diaphragms as shown in Figure E-17. At Elevation 998, which is at the top of the reinforced concrete shear wall along Column Line G, the seismic-induced diaphragm loads are the greatest. The computed shears in this horizontal braced frame and the ultimate shear capacities for the boiler structure diaphragm at this elevation are summarized in Figure E-17. The elastically calculated seismic-induced loads are as much as a factor of 3.9 greater than the ultimate capacity although no buckling of these members was observed at any elevation of the boiler structure.

The columns throughout the boiler structure are all below their yield or buckling capacities based on their calculated seismic response for the 1979 Imperial Valley earthquake. No damage to these columns was observed following the earthquake.

E.6.2   TURBINE BUILDING RESPONSE

For the turbine building reinforced concrete shear walls cast monolithically with the exterior steel frame on the south, east and west sides of the turbine building, the ultimate shear capacity has been evaluated in accordance with the ACI code (Reference E-5). For these walls, the seismic-induced shear load is carried by both the reinforced concrete wall and the steel frame. Based on the relative rigidities of the wall and frame, 80 to 90 percent of the shear load is carried by the wall and 10 to 20 percent of the shear load is carried by the frame.

On Figure E-18, the elements in the structural model are graphically represented on elevation views of the turbine building walls. Also shown on this figure, are the seismic-induced shear loads and the ultimate shear capacities from the ACI code for each of these elements. All but one of the elements is below the ultimate capacity although the seismic-induced loads are significant such that some cracking might be expected. For Element 19, at the lower region of the west wall, the elastically computed seismic-induced load exceeds the code specified

ultimate capacity by 11 percent. However, it is recognized that the ultimate capacity for shear walls as specified in the ACI code is conservative relative to laboratory tests on shear walls. Furthermore, the ultimate capacity reported in Figure E-18 is based on minimum specified material strengths and the actual strength of the concrete and reinforcing steel for the turbine building walls is likely to be more than the minimum values. As a result, for the small amount of calculated seismic overload in Element 19, no significant damage would be expected. It should be noted that shear stress in these walls are calculated to be generally greater than 110 psi (i.e., about $2\sqrt{f'_c}$) such that some concrete cracking would be expected. The highest calculated shear stress for the turbine building walls is 255 psi for element 19. All other wall elements have calculated shear stresses less than about 200 psi.

The turbine building steel frame is designed predominantly for lateral forces in the east-west direction as the columns are loaded about their strong axis for this direction motion. In addition, the shear wall along the south side of the turbine building carries a significant portion of the east-west lateral forces. As a result, the turbine building moment-resisting steel frame responds to the east-west component of the 1979 Imperial Valley earthquake below the yield stress level.

For lateral forces in the north-south direction, the turbine building steel columns are loaded about their weak axis but lateral forces in this direction are carried by the reinforced concrete shear walls along the east and west sides of the turbine building. There is a problem in this direction in that the only effective diaphragms for transferring seismic-induced loads from the interior steel frame to the exterior concrete walls is the operating floor which is 20 feet above the ground floor and the concrete roof over the heater and auxiliary bays. The roofs over the turbine and service bays are composed of gypsum decking and composition roofing and are not as effective in diaphragm action as the concrete floors and roofs (see Figure E-19).

As a result of the lack of effective diaphragms for transferring loads from the interior steel frame to the exterior concrete walls, some of the frame elements above the operating floor are computed to be strained into the plastic range when subjected to the north-south component of the 1979 Imperial Valley earthquake. Along Column Line B, there is a shear wall as shown in Figure E-19 for which seismic response accelerations of about 4 g's in the north-south direction (see Figure E-13) are computed. The inertial loads from this shear wall must pass down through the portion of the steel frame represented by Element 49 in the structural model to the operating floor and then out to the east shear wall. The resulting seismic response moments in the steel columns at this location are about a factor of 1.9 greater than the plastic moment capacity for these column sections. At Column Lines E and F, the heater bay floor is computed to have seismic response accelerations of about 3 g's in the north-south direction (see Figure E-13). The corresponding inertial loads for the heater bay floor must be transferred through the portion of the steel frame represented by Elements 27, 28 and 38 to the roof or operating floor and out to the west shear wall. The resulting seismic response moments in the steel columns at these locations are from a factor of 1.2 to a factor of 1.8 greater than these column sections as indicated in Figure E-19. As mentioned previously, there was no significant damage in the turbine building as a result of the 1979 Imperial Valley earthquake even though the calculated seismic moments exceeded the plastic moment capacity for some of the steel columns by nearly a factor of 2.

The operating floor, heater bay floor and the roof over the auxiliary and heater bays are effective diaphragms made of metal decking and concrete fill. The shear stresses calculated in the elements of the structural model representing these diaphragm elements are summarized in Table E-9. The maximum shear stress of 253 psi is in Element 23, which transfers the roof loading from east-west shaking between the turbine building steel frame and the south concrete shear wall. No significant damage would be expected for any of the computed shear stresses shown in Table E-9 although some concrete cracking might be expected for shear stresses in excess of about 110 psi (i.e., about $2 \sqrt{f_c'}$).

Other less effective diaphragm action occurs at the roof of the turbine bay and service bays (Elements 41 and 52 for north-south motion and Elements 46 and 47 for east-west motion as shown in Figure E-11). The primary load carrying elements of these diaphragm elements are single angle x-bracing in the horizontal plane. The calculated seismic-induced loads in these diagonal members are as much as 4 times the yield capacity of the member. However, there was no damage in the roof observed following the 1979 earthquake. It should be noted that some of the diaphragm loading could have been transferred by the roof decking. The more complex load pattern of part of the load through roof decking and part of the load through horizontal bracing has not been considered herein.

E.6.3   Turbine Pedestal Response

The turbine pedestal is calculated to respond to the 1979 Imperial Valley earthquake at a relatively low stress level. Calculated stresses correspond to the elastic behavior range. There was no damage observed at the turbine pedestal following this earthquake.

E.7   SUMMARY AND CONCLUSIONS

The El Centro Steam Plant was subjected to the Imperial Valley earthquake which occurred on October 15, 1979. It is estimated that the maximum horizontal earthquake ground acceleration at the plant site was about 0.5g. The steel framing throughout Unit 4 of the plant was designed for an equivalent lateral seismic loading of 0.2g although the plant had additional capacity due to turbine building reinforced concrete shear walls which are capable of resisting lateral seismic loadings. Because of the lack of significant damage at the plant as a result of this earthquake even though earthquake motion spectral acceleration exceeded design levels by a factor of as much as 5 to 6 as shown in Figures E-7 and E-8, a detailed structural evaluation of the El Centro Steam Plant subjected to the 1979 Imperial Valley earthquake was performed and is reported herein as part of the NRC research project on Engineering Characterization of Ground Motion. The purpose of this work was to demonstrate, for this case, whether or not an elastic analysis based on recorded

earthquake ground motion would predict damage in excess of observed damage following the earthquake. In addition, it is of interest to evaluate the factor by which elastically calculated seismic response levels exceed ultimate capacities. For example, studies of several structures subjected to the 1971 San Fernando earthquake indicated that the onset of significant structural damage should not occur at elastically calculated force levels less than 2.5 times the ultimate capacity for San Fernando earthquake ground motion. It was expected that this evaluation of the El Centro Steam Plant would provide further evidence for the need to develop a reasonable design and analysis basis for critical facilities which accounts for the "effective" repeatable ground motion acceleration, the duration of the strong ground motion and the inelastic energy absorption capability of ductile structures.

Unit 4 of the El Centro Steam Plant consists of a steel braced frame boiler structure attached to the turbine building which is a steel moment-resistant frame with three exterior reinforced concrete shear walls and a structurally independent reinforced concrete frame turbine pedestal all on a common foundation mat. The underlying soil consists of deep alluvium.

The October 15, 1979 Imperial Valley earthquake had a local magnitude of 6.6. Ground motion measurements in the vicinity of the El Centro Steam Plant included Stations 8 and 9 of the Imperial Valley linear array and Station 5165 of the USGS differential array. It is judged that Station 5165 located about 2,400 feet from Unit 4 provides a reasonable estimate of the ground motion at the plant site and a digitized version of this recorded time history has been used for this structural evaluation of the steam plant. For the north-south component of motion, the maximum acceleration is 0.49g and the duration of strong motion, T_D', is 2.8 seconds. For the east-west component of motion, the maximum acceleration is 0.35g and the duration of strong motion, T_D', is 3.7 seconds. Thus, the El Centro Steam Plant was subjected to high acceleration earthquake ground shaking of moderate duration.

There was no significant structural damage of the plant as a result of the 1979 earthquake. Most notable damage was at upper elevations of the boiler structure where four diagonal bracing members buckled and there was permanent deformation of boiler seismic restraints. Other damage noted was minor concrete cracking. These structures were in no danger of collapse as a result of the earthquake and, in fact, were returned to operation on the same day of the earthquake. The buckled diagonals were replaced.

A beam element, lumped mass structural model of Unit 4 was developed for this evaluation. Soil-structure interaction was accounted for by soil springs attached to the foundation. Reg. Guide 1.61 damping values for structural elements and calculated radiation damping for soil elements were used to evaluate composite modal damping values. An upper limit of 20 percent of critical damping was imposed in a manner consistent with many design analyses of critical facilities. Seismic response was evaluated by an elastic response spectrum analysis using spectra from Station 5165 horizontal recorded ground motion. Calculated seismic response was then compared to code specified ultimate capacities to assess analytically predicted structure behavior based on elastic analysis and instrumental ground motion.

Based upon this evaluation of the El Centro Steam Plant, there are two general conclusions which can be made:

1. The seismic capacity or resistance of a structure cannot, in general, be directly inferred from the design level earthquake motion.

2. Elastic structural calculations based upon instrumental ground motion which are typically used for design analyses of many critical facilities do not lead to good correlation between calculated and observed structure behavior.

The seismic design basis for the El Centro Steam Plant was an equivalent lateral seismic coefficient corresponding to 0.2g. This horizontal force coefficient was applied to live and dead loads and was

used to design the building steel framing. Details of the design approach are unknown but because the design was performed around 1968, it is likely that the design criterion correspond to working stress values plus one-third increase for dynamic loading as allowable stress limits. In addition, exterior reinforced concrete shear walls on three sides of the turbine building were added to the turbine building steel frame which had already been designed for the horizontal force coefficient of 0.2. As a result of the above factors, it may be seen that seismic resistance cannot be directly inferred from the design level earthquake motion. Although the steam plant Unit 4 structure was designed for a horizontal force coefficient of 0.2, that does not mean that structural failures or damage would be expected for earthquake ground motion greater than 0.2g. The lateral force coefficient ignores dynamic amplification during seismic response of the structure such that inertial loads at higher elevations in the structure for a 0.2g earthquake can be much greater than that corresponding to 0.2g. On the other hand, application of the lateral coefficient to live loads as well as the usage of very conservative allowable stress criteria enable the structure to resist seismic loads significantly greater than that corresponding to a 0.2g earthquake. However, a primary reason that the steam plant can resist motion exceeding 0.2g is the exterior concrete shear walls around the turbine building. These walls are significantly stronger than the steel frame such that they actually dominate the seismic resistance capacity of the turbine building even though they are additional to the basic lateral resistance accounted for by the Unit 4 designer.

From the combination of factors described above, it may be seen that it is impossible to infer the seismic capacity of the El Centro Steam Plant Unit 4 from the design earthquake level. In this case, the structure has considerably greater capacity than that corresponding to an earthquake with peak acceleration of 0.2g due primarily to the presence of additional concrete shear walls. It is our judgment that this situation is not abnormal. Most structures have additional capacity above that accounted for by the designer due to the existence of alternate load paths

not explicitly accounted for in the design, due to strength provided by non-structural elements such as partitions, wall cladding, equipment or piping, etc., and due to the usage of conservative design criteria. These factors may be one of the reasons that the conclusions of Appendix A (i.e., that structures behave much better during actual earthquakes than would be expected based on their design criteria) are seen.

Based upon the evaluation of El Centro Steam Plant Unit 4 reported herein, it is also demonstrated that even if the above factors are accounted for by considering all structural resistance mechanisms available, using code specified ultimate strength limits and using recorded earthquake motion at the site of the structure considered, analytical approaches which are typically used for the design of many critical facilities such as nuclear power plants still underestimate the seismic resistance capacity of the structure and predict more damage than was seen during an actual earthquake.

The analytically predicted structural performance of the various components of the El Centro Steam Plant Unit 4 structure is summarized in Table E-10 in terms of the ratio of seismic response to ultimate capacity or by qualitative description. The only damage occurring to the steam plant as a result of the 1979 earthquake was buckling of diagonal members at upper elevations of the boiler structure. This represents localized minor damage which was easily repairable. Based upon post-earthquake examination of the structure, the steam plant was not in danger of collapse. Yet, based upon the elastically calculated seismic response as summarized in Table E-10, much more substantial damage than was observed would be expected. For the members damaged during the earthquake, the ratio of calculated seismic response to ultimate capacity is 4.0 or greater. For the members undamaged during the earthquake, the ratio of calculated seismic response to ultimate capacity is 4.9 or less. Hence, it may be concluded that for the Imperial Valley earthquake and the steam plant structure, the onset of significant structure damage should not occur at elastically calculated force levels less than about 4.0 times the ultimate capacity.

A primary reason for the lack of damage at the steam plant as a result of the 1979 earthquake was that the structure had substantially greater capacity than the 0.2g design level for the steel frame because of the exterior concrete shear walls on three sides of the turbine building. However, the calculated seismic response based on recorded motions from the 1979 earthquake of individual structural members exceeds their code specified ultimate capacities by as much as a factor of 4.0 or more without any significant structural damage. Based upon elastically calculated seismic response, buckling of more members of the boiler structure and some turbine building damage would have been predicted for the 1979 earthquake. There are a number of reasons for the lack of damage seen in the boiler structure and turbine building steel framing including:

1. Inelastic energy absorption capability is not accounted for by elastic analysis.

2. Foundation level motion may be less than is calculated by the analysis performed due to:

   a. spatial variation of ground motion over the foundation area.

   b. wave scattering or kinematic interaction phenomena.

   c. more complex soil-structure interaction effects than assumed for this analysis including some embedment effects.

3. The analytical technique of employing an upper limit cutoff to composite modal damping may not fully account for soil radiation damping and thus give overly conservative seismic response.

It is not known which of the above factors are the most important reasons for differences between calculated and observed behavior of the El Centro Steam Plant. In our judgment, all of these factors are probably significant.

It is shown by this evaluation of the El Centro Steam Plant that the seismic resistance capacity cannot be directly inferred from the design earthquake level. Factors such as conservatism in the allowable stress criterion and strength of the structure which, for some reason, is not accounted for in the structural design, cause the structure to be capable of withstanding higher ground motion than the design level. It is believed that the steam plant is not abnormal in this regard and that this conclusion is generally true. Another important conclusion to note is that the analytical approach employed for this evaluation, which is generally typical of that used for design analyses of many nuclear power facilities utilizing elastic analysis and instrumental ground motion, does not lead to good correlation between calculated and observed seismic behavior. This method of evaluation underpredicts the seismic capacity of the El Centro Steam Plant by more than a factor of 4. Hence, it is concluded that some or all of the factors such as inelastic energy absorption capability wave scattering phenomena, more complex soil-structure interaction, etc. should be incorporated into the approach used for design analyses of nuclear power plants or other critical facilities such that realistic designs may be achieved.

Table E-1

PEAK ACCELERATIONS RECORDED DURING THE
1979 IMPERIAL VALLEY EARTHQUAKE

Station	Azimuth*	Uncorrected	Corrected
7	230 140 Vertical	.47g .34g .63g	.46g .33g .51g
8	230 140 Vertical	.48g .62g .48g	.47g .61g .41g
5165	360 270 Vertical	.49g .35g .75g	.49g .35g .66g
9	360 090 Vertical	.40g** .27g** .38g**	— — —
10	050 320 Vertical	.18g .23g .11g	.17g .23g .11g

* Numbers are horizontal angle from north measured clockwise

** Estimated Values

Table E-2

NODE COORDINATES

GENERATED NODAL DATA

NODE NUMBER	* BOUNDARY CONDITION CODES X	Y	Z	XX	YY	ZZ	NODAL POINT COORDINATES X	Y	Z
1	0	0	0	0	C	0	.21480E+04	0.	.11640E+04
2	0	0	C	0	C	C	.15360E+04	0.	.11640E+04
3	0	0	0	0	C	G	.21480E+04	0.	.98400E+03
4	0	0	C	0	C	C	.19360E+04	0.	.98400E+03
5	C	0	C	0	C	0	.21480E+04	0.	.74400E+03
6	0	0	0	0	0	C	.15360E+04	0.	.74400E+03
7	0	0	0	0	C	0	.21480E+04	0.	.59640E+03
8	0	0	C	0	C	C	.21480E+04	0.	.45600E+03
9	C	0	0	0	0	0	.21480E+04	0.	.24000E+03
10	0	0	0	0	C	C	.21480E+04	0.	0.
11	0	0	C	0	C	0	.15360E+04	0.	.59640E+03
12	0	0	0	0	C	0	.15360E+04	0.	.45600E+03
13	C	0	0	0	0	0	.15360E+04	0.	.24000E+03
14	0	0	0	0	C	0	.15360E+04	0.	C.
15	0	0	0	0	0	C	.13200E+04	0.	.59640E+03
16	0	0	0	0	C	0	.13200E+04	0.	.40800E+03
17	0	0	0	0	C	0	.1C200E+04	0.	.40800E+03
18	0	0	0	0	C	0	.13200E+04	0.	C.
19	0	0	0	0	0	0	.10200E+04	0.	.59640E+03
20	0	0	0	0	C	0	.13200E+04	.55800E+03	.59640E+03
21	C	C	C	0	C	0	.13200E+04	0.	.24000E+03
22	0	0	0	0	C	0	.13200E+04	.55800E+03	.40800E+03
23	C	0	C	0	C	0	.1C200E+04	0.	.24000E+03
24	0	C	0	0	C	0	.13200E+04	.55800E+03	.24000E+03
25	0	0	0	0	C	0	.10200E+04	0.	0.
26	0	0	0	0	C	0	.13200E+04	.55800E+03	C.
27	C	0	C	0	0	0	.36000E+03	0.	.59640E+03
28	0	0	0	0	C	0	.36000E+03	.55800E+03	.59640E+03
29	0	0	0	0	C	0	.13200E+04	-.5580CE+03	.24000E+03
30	0	0	0	0	C	0	.18000E+03	.55800E+03	.24000E+03
31	0	0	0	0	C	0	.18000E+03	.55800E+03	0.
32	0	0	0	0	C	0	.36C00E+03	0.	C.
33	C	0	1	0	C	C	.78CCE+03	0.	C.
34	0	0	0	0	C	0	.36000E+03	0.	.38040E+03
35	0	0	C	0	C	0	.36CCE+03	.55800E+03	.38040E+03
36	0	0	0	0	C	0	.18CCE+03	.55800E+03	.38040E+03
37	0	0	0	0	C	0	.1800CE+03	-.55800E+03	.24000E+03
38	0	0	C	0	0	0	.180C0E+03	0.	.240C0E+03
39	C	C	0	0	C	C	.18000E+03	0.	C.
40	C	0	0	0	C	C	.36C00E+03	0.	.240C0E+03
41	C	0	1	0	C	0	.78C00E+03	0.	.27000E+03
42	C	0	0	0	C	C	0.	0.	.38040E+03
43	0	0	0	0	C	C	C.	0.	.24000E+03
44	0	0	0	0	C	0	C.	0.	C.
45	1	1	1	1	1	1	.78000E+03	.10000E+03	C.

* 0 — free

   1 — fixed

Note: Units are inches

BEAM PROPERTIES

3 / D   B E A M   E L E M E N T S

```
NUMBER OF BEAMS                      =   67
NUMBER OF GEOMETRIC PROPERTY SETS=   52
NUMBER OF FIXED END FORCE SETS    =    C
NUMBER OF MATERIALS                  =    2
```

MATERIAL PROPERTIES

MATERIAL NUMBER	YOUNG'S MODULUS	POISSON'S RATIO	MASS DENSITY	WEIGHT DENSITY
1	.3000E+05	.3000	0.	0.
2	.31CCE+C4	.2500	0.	C.

BEAM GEOMETRIC PROPERTIES

SECTION NUMBER	AXIAL AREA A(1)	SHEAR AREA A(2)	SHEAR AREA A(3)	TORSION J(1)	INERTIA I(2)	INERTIA I(3)
1	.100CE+05	C.	0.	.1000E+10	.1000E+10	.1000E+10
2	.100CE+05	.1CCCE+02	.1380E+02	.346CE+C6	.1700E+07	.35C0E+07
3	.100CE+05	.7700E+01	.1C00E+02	.2660E+06	.1700E+07	.41C0E+07
4	.100CE+05	.990CE+01	.1110E+02	.3430E+06	.2400E+07	.41C0E+C7
5	.1CCCE+05	.1CCCE+02	.2210E+02	.346CE+C6	.2400E+07	.54C0E+C7
6	.100CE+05	.194CE+02	.2C40E+02	.671CE+06	.5000E+07	.77C0E+07
7	.1C0CE+05	.1970E+02	.1340E+02	.6820E+06	.5000E+07	.1270E+08
8	.100CE+05	.1CCCE+02	.7700E+01	.346CE+06	.9000E+06	.35C0E+C7
9	.100CE+05	.770CE+01	.7400E+01	.266CE+06	.1400E+07	.41C0E+C7
1C	.10CCE+05	.5900E+C1	.9100E+01	.3430E+06	.1400E+07	.41C0E+C7
11	.10CCE+05	.9CCCE+C2	.8930E+04	.311CE+C7	.1C00E+10	.486CE+C8
12	.100CE+05	.173CE+03	.6400E+04	.6C4CE+C7	.1000E+10	.6930E+C8
13	.1CCCE+C5	.176CE+03	.8930E+04	.614CE+C7	.1000E+10	.1143E+09
14	.1CCCE+C5	C.	.2C80E+03	.1000E+00	.1000E+10	.83C0E+04
15	.1CCCE+C5	C.	.2C30E+03	.1000E+CO	.1000E+10	.1450E+05
16	.1000E+C5	C.	.8810E+03	.100CE+00	.1000E+10	.10C0E+02
17	.1C0CE+05	C.	.4800E+03	.1000E+CO	.1000E+10	.1000E+02
18	.100CE+05	C.	.8260E+03	.1C00E+00	.1C00E+10	.1000E+02
19	.1CCCE+05	C.	.1460E+01	.1C00E+CO	.1C00E+10	.97C0E+04
2C	.1CCCE+05	C.	.1880E+01	.1000E+00	.1000E+10	.9700E+04
21	.1CCCE+05	0.	.1660E+01	.1C00E+CO	.1000E+10	.9700E+04
22	.100CE+05	C.	.2C80E+03	.1000E+00	.1C00E+10	.1020E+05
23	.1CCCE+C5	C.	.2030E+03	.100CE+CO	.1000E+10	.2340E+C5
24	.1CCCE+C5	C.	.2C30E+03	.1C00E+00	.1000E+10	.4030E+C5
25	.1CCCE+C5	.3140E+04	0.	.1C00E+CC	.1C00E+02	.1000E+10
26	.1000E+05	.314CE+04	0.	.1000E+0C	.1000E+02	.1000E+10
27	.100CE+05	.4870E+04	0.	.100CE+00	.1000E+02	.10C0E+10
28	.1C0CE+05	C.	.1700E+01	.1000E+00	.1C00E+10	.16C0E+04
29	.1000E+C5	0.	.2140E+01	.1C0CE+00	.1CG0E+10	.2350E+C5
3C	.100CE+05	C.	.3560E+01	.1C00E+CO	.1C00E+10	.3640E+05
31	.1CCCE+C5	C.	.4700E+01	.100CE+CO	.1CC0E+10	.1610E+C5
32	.1C0CE+05	C.	0.	.1C00E+00	.1000E+02	.3750E+05
33	.1CCCE+C5	.134CE+05	.2C00E+05	.100CE+10	.1000E+10	.10C0E+10
34	.1C0CE+C5	C.	.1930E+03	.1C00E+CO	.1C00E+10	.16C0E+04
35	.1CCCE+C5	C.	.3730E+00	.1C0CE+00	.1000E+10	.2350E+05
36	.1C0CE+C5	0.	.2500E+01	.1C0CE+CO	.1C00E+10	.364CE+05
37	.1CCCE+C5	.115CE+04	.1710E+04	.100CE+CC	.1000E+10	.10C0E+1C
38	.100CE+05	C.	.4600E+01	.1000E+00	.1000E+10	.58C0E+04
39	.1CCCE+C5	C.	.2C30E+03	.1C0CE+CC	.1C00E+10	.4510E+05
4C	.100CE+05	C.	.2C30E+03	.1000E+00	.1000E+10	.4510E+05
41	.10CCE+05	.276CE+04	0.	.100CE+CO	.1000E+02	.10C0E+10
42	.100CE+C5	.161CE+04	0.	.1000E+00	.1000E+02	.10C0E+10
43	.1C0CE+05	0.	.5760E+03	.1000E+00	.1000E+10	.1000E+02
44	.1C0CE+05	C.	.6700E+04	.100CE+CC	.1C00E+10	.4700E+C5
45	.1CCCE+C5	C.	.6700E+04	.1000E+00	.1000E+10	.4700E+05
46	.1C0CE+05	.626CE+03	0.	.1000E+1C	.1000E+02	.10C0E+10
47	.100CE+C5	.576CE+03	0.	.1000E+10	.1000E+02	.10C0E+10
48	.10CCE+C5	C.	.7800E+01	.1000E+00	.1000E+10	.10C0E+02
49	.1000E+C5	0.	.4600E+01	.1000E+00	.1000E+10	.1000E+02
5C	.100CE+05	C.	0.	.1C00E+CC	.3750E+05	.1000E+02
51	.100CE+05	C.	.2750E+01	.100CE+CO	.2C00E+06	.10C0E+02
52	.1C0CE+05	C.	.5000E+01	.1000E+CO	.4000E+06	.10C0E+02

Note: Units are kips and inches

Table E-4

BEAM CONNECTIVITY

3/D BEAM ELEMENT DATA

BEAM NUMBER	NODE -I	NODE -J	NODE -K	MATERIAL NUMBER	SECTION NUMBER	A	B	C	D	-I	-J	BAND
1	1	3	2	1	2	0	0	0	0	0	0	18
2	3	5	2	1	3	0	0	C	0	0	0	18
3	5	7	2	1	4	0	0	C	0	0	0	18
4	7	8	2	1	5	0	0	C	0	0	0	12
5	8	9	2	1	6	0	0	C	0	0	0	12
6	9	10	2	1	7	0	0	C	0	0	0	12
7	1	2	3	1	51	0	0	C	0	0	0	12
8	3	4	2	1	52	0	0	C	0	0	0	12
9	5	6	2	1	52	0	0	C	0	0	0	12
10	7	11	2	1	52	0	0	C	0	0	0	30
11	8	12	2	1	52	0	0	0	0	0	0	30
12	9	13	2	1	52	0	0	C	0	0	0	30
13	10	14	2	1	1	0	0	C	0	0	0	30
14	2	4	1	1	8	0	0	C	0	0	0	18
15	4	6	1	1	9	0	0	C	0	0	0	18
16	6	11	1	1	10	0	0	0	0	0	0	36
17	11	12	1	2	11	0	0	0	0	0	0	12
18	12	13	1	2	12	0	0	C	0	0	0	12
19	13	14	1	2	13	0	0	C	0	0	0	12
20	11	15	1	1	14	0	0	C	0	1	0	30
21	13	21	1	1	15	0	0	0	0	1	0	54
22	14	18	1	1	1	0	0	C	0	0	0	30
23	15	20	16	2	16	0	0	C	0	0	0	36
24	16	22	15	2	17	0	0	0	0	0	0	42
25	21	24	15	2	18	0	0	C	0	0	0	24
26	18	26	15	1	1	0	0	C	0	0	0	54
27	15	16	1	1	19	0	0	C	0	0	0	12
28	16	21	1	1	20	0	0	C	0	0	0	36
29	21	18	1	1	21	0	0	C	0	0	0	24
30	15	19	1	1	22	0	0	C	0	0	0	30
31	16	17	1	1	23	0	0	C	0	0	0	12
32	21	23	1	1	24	0	0	C	0	0	0	18
33	18	25	1	1	1	0	0	C	0	0	0	48
34	20	22	28	2	25	0	0	C	0	0	0	18
35	22	24	28	2	26	0	0	C	0	0	0	18
36	24	26	28	2	27	0	0	0	0	0	0	18
37	19	17	1	1	28	0	0	C	0	0	0	18
38	17	23	1	1	29	0	0	C	0	0	0	42
39	23	25	1	1	30	0	0	C	0	0	0	18
40	20	28	35	1	1	0	0	C	0	111	11	54
41	19	27	1	1	31	0	0	0	0	0	0	54
42	24	30	20	1	32	0	0	C	0	0	0	42
43	25	33	1	1	1	0	0	C	0	0	0	53
44	41	33	1	2	33	0	0	C	0	0	0	52
45	33	32	1	1	1	0	0	C	0	0	0	11
46	27	28	35	1	48	0	0	0	0	0	0	12
47	34	35	28	1	49	0	0	0	0	0	0	12
48	27	34	1	1	34	0	0	C	0	0	0	47
49	34	40	1	1	35	0	0	0	0	0	0	42
50	40	32	1	1	36	0	0	C	0	0	0	53
51	28	35	20	2	37	0	0	0	0	0	0	47
52	34	42	1	1	38	0	0	C	0	0	0	53
53	40	38	1	1	39	0	0	C	0	0	0	18
54	38	43	1	1	40	0	0	0	0	0	0	35
55	32	39	1	1	1	0	0	C	0	0	0	47
56	39	44	1	1	1	0	0	C	0	0	0	35
57	35	36	20	1	1	0	0	0	0	0	0	12
58	36	30	20	2	41	0	0	C	0	0	0	41
59	30	31	20	2	42	0	0	C	0	0	0	12
60	38	30	31	2	43	0	0	C	0	0	0	53
61	39	31	30	1	1	0	0	0	0	0	0	53
62	42	43	1	2	44	0	0	C	0	0	0	12
63	43	44	1	2	45	0	0	C	0	0	0	12
64	26	31	20	1	1	0	0	0	0	0	0	36
65	21	29	37	2	46	0	0	C	0	0	0	54
66	29	37	21	1	50	0	0	C	0	0	0	53
67	37	38	21	2	47	0	0	C	0	0	0	12

Table E-5

LUMPED MASSES AND ROTATIONAL INERTIA

N O D A L   L O A D S   (S T A T I C)   O R   M A S S E S   (D Y N A M I C)

NODE NUMBER	LOAD CASE	X-AXIS FORCE	Y-AXIS FORCE	Z-AXIS FORCE	X-AXIS MOMENT	Y-AXIS MOMENT	Z-AXIS MOMENT
1	C	.29300E+0C	.6130CE+C0	.4530CE+00	C.	0.	0.
2	0	0.	.2560CE+00	.12800E+00	C.	0.	0.
3	C	.13570E+01	.4C00CE+C0	.87900E+C0	C.	0.	0.
4	C	.1C9C0E+0C	.3890CE+00	.25300E+C0	C.	0.	0.
5	C	.13600E+01	.8700CE+C0	.11150E+01	C.	0.	0.
6	C	.114C0E+0C	.6C00CE+C0	.3570CE+00	C.	0.	0.
7	C	.966C0E+0C	.8950CE+C0	.931C0E+00	C.	0.	0.
8	C	.12430E+C1	.8870CE+C0	.1C65CE+01	C.	0.	0.
9	C	.15150E+01	.5910CE+C0	.1C530E+01	C.	0.	0.
11	0	.143C0E+01	.1773CE+01	.158C0E+01	.10300E+05	0.	0.
12	C	.39600E+CC	.9440CE+00	.63500E+00	.16300E+05	0.	0.
13	C	.24260E+C1	.3192CE+01	.2772CE+01	.17600E+05	0.	0.
14	C	.15C90E+0C	.1986CE+C0	.15C90E+C0	.116C0E+05	0.	0.
15	0	.33440E+CC	.3344CE+00	.3344CE+00	0.	0.	0.
16	C	.39540E+CC	.3954CE+C0	.39540E+C0	C.	0.	.1180CF+05
17	C	.1493CE+CC	.24C3CE+00	.1493CE+00	C.	0.	0.
19	C	.267C0E+0C	.3814CE+00	.267C0E+C0	C.	.50000E+04	0.
20	C	.28350E+0C	.1365CE+C0	.28350E+C0	C.	.1430CE+05	.35000F+04
21	C	.56950E+CC	.6722CE+00	.62C8CE+00	C.	0.	.1030CF+05
22	C	.28360E+0C	.1218CE+00	.2836CE+C0	C.	.14900E+05	.11000F+04
23	0	.1C270E+0C	.4201CE+00	.2C60CE+00	C.	0.	0.
24	C	.43250E+0C	.5970CE+00	.43250E+C0	C.	.2210CE+05	.35000F+04
25	C	0.	.9460CE-01	0.	C.	0.	0.
26	C	.18420E+CC	.4190CE-01	.18420E+00	C.	.1910CE+05	0.
27	C	.19850E+0C	.1985CE+00	.1985CE+00	.17200E+05	0.	0.
28	C	.899C0E-01	.8990CE-01	.8990CE-01	C.	.8600CE+03	0.
29	C	.18C40E+0C	0.	C.	C.	0.	0.
30	C	.36390E+CC	.7940CE-01	.36390E+00	C.	.42900E+04	0.
31	C	.1CC30E+0C	.4C90CE-C1	.1C030E+00	C.	.2840CE+04	0.
33	C	.45300E+02	.4530CE+02	0.	.48000E+07	.2200CE+08	.26000F+08
34	C	.17320E+0C	.1732CE+00	.17320E+C0	.16300E+05	0.	0.
35	C	.682C0E-C1	.7290CE-01	.68200E-01	C.	.4700CE+03	0.
36	0	.52300E-01	0.	.52300E-01	C.	.17500E+04	0.
37	C	.22200E+0C	0.	0.	C.	0.	0.
38	C	.16920E+CC	.24C4CE+00	.2C50CE+00	C.	0.	0.
40	0	.71600E-01	.3833CE+00	.23990E+00	C.	0.	0.
41	0	.49870E+01	.4987CE+01	0.	.32700E+06	.36900E+05	.36400F+06
42	0	.11840E+0C	.1591CE+00	.11840E+00	.87000E+04	0.	0.
43	C	.31C60E+CC	.4404CE+00	.3285CE+C0	.17500E+05	0.	0.
44	0	.21880E+0C	.2782CE+00	.21880E+00	.16800E+05	0.	0.

T O T A L   M A S S

X-DIRECTION	Y-DIRECTION	Z-DIRECTION
.66907E+02	.67487E+C2	.16686E+02

Note: Units are kips, inches and seconds

Table E-6

SOIL ELEMENT PROPERTIES

Element Number (See Figure E-11	Node (See Figure E-11	Direction*	Spring Stiffness (k/in)	Radiation Damping (Fraction of Critical)
1	33	x-Translation	4.74×10^4	0.89
2	33	y-Translation	5.32×10^4	0.95
3	33	Rotation About x	2.32×10^{10}	0.78
4	33	Rotation About z	3.47×10^{10}	0.49
5	33	Rotation About y	5.46×10^{10}	0.69

*x = East-West

y = North-South

z = Vertical

Table E-7

SUMMARY OF MODES, MASS PARTICIPATION AND MODAL DAMPING

Mode	Freq.(Hz)	Percent of Structure Mass Participating		Modal Damping Fraction of Critical	
		N-S(Y)	E-W(X)	Calculated Value	Value Used in Response Analysis
1	1.40	6.26	2.20	.083	.07
2	1.65	1.66	16.01	.099	.10
3	2.68	3.59	0	.089	.10
4	3.02	0.09	11.99	.121	.10
5	3.22	7.04	0.34	.105	.10
6	3.65	12.31	5.23	.178	.15
7	3.97	2.48	0.37	.091	.10
8	4.61	35.29	10.30	.489	.20
9	4.82	16.65	36.67	.627	.20
10	5.14	8.65	15.71	.360	.20
11	5.73	0.09	0.59	.563	.20
12	6.00	0.01	0.02	.080	.07
13	6.17	0.15	0.03	.077	.07
14	6.53	3.35	0.02	.152	.15
15	6.62	0.21	0.16	.079	.07
16	7.24	0.29	0.10	.086	.07
17	7.70	1.48	0.07	.192	.20
18	8.18	0.23	0	.099	.10
19	8.70	0.02	0.08	.126	.10
20	8.85	0.03	0	.073	.07
21	9.67	0.01	0	.073	.07
22	9.70	0.01	0.02	.072	.07
23	10.26	0.02	0.03	.322	.20
24	10.60	0	0	.070	.07
25	11.10	0.06	0.02	.163	.15
26	11.16	0	0	.071	.07
27	12.07	0	0	.081	.07
28	12.24	0	0	.127	.10
29	14.16	0.01	0	.084	.07
30	15.60	0	0.01	.138	.15
31	15.90	0	0	.291	.20
32	17.09	0	0	.091	.10
33	17.57	0	0	.070	.07
34	17.95	0	0.04	.085	.07
35	18.43	0	0	.135	.15
36	18.63	0	0	.073	.07
Summation =		100.00	100.00		

Total Mass - N-S (Y) = 67.487 k-sec^2/in
E-W (X) = 66.987 k-sec^2/in

Table E-8

DESCRIPTION OF SIGNIFICANT MODES

Mode	Frequency(Hz)	Predominant Behavior
1	1.40	N-S response of Boiler Structure along column line H-9
2	1.65	E-W response of Boiler Structure and Turbine Building Steel Frame
3	2.68	N-S response of upper Boiler Structure along column line G
4	3.02	2nd Mode for E-W response of Boiler Structure and Turbine Building Steel Frame
5	3.22	2nd Mode for N-S response of Boiler Structure along column line H-9
6	3.65	N-S response along column lines E and F, some soil response
7	3.97	N-S response along column line B
8	4.61	N-S soil response, N-S response of column lines B, E and F
9	4.82	E-W soil response
10	5.14	N-S response of column line B Higher Mode E-W Turbine Building Boiler Structure response, soil response

Table E-9

SHEAR STRESSES IN
METAL DECK-CONCRETE FILL DIAPHRAGM ELEMENTS

Element (see Figure 11)	Direction	Description	Elastically Calculated Shear Stress (psi)
20	N-S	heater and	83
30	N-S	auxiliary bay	55
23	E-W	roof	253
24	E-W	heater bay	103
31	N-S	floor	45
21	N-S		145
32	N-S	operating	55
53	N-S	floor	122
54	N-S		127
25	E-W		158
60	E-W		81
65	E-W		114
67	E-W		119

Table E-10

SUMMARY OF CALCULATED SEISMIC BEHAVIOR
FOR EL CENTRO STEAM PLANT UNIT 4 SUBJECTED TO
THE 1979 IMPERIAL VALLEY EARTHQUAKE

Structure	Calculated Behavior
1. Boiler Structure a. Diagonal Bracing	For members that actually buckled during the earthquake, the response/capacity ratio ranged from 4.0 to 4.8. For members which did not buckle, response/capacity was as high as 4.9 in one case, but but generally below 4.0
b. Horizontal Bracing Diaphragm	Response/capacity ratios were as large as 3.9 with no observed damage.
c. Boiler Structure Columns	Elastic behavior below ultimate buckling capacity for seismic loading.
2. Turbine Building a. Concrete Shear Walls	Elastic response/capacity ratio was 1.11 at bottom of west wall and below 1.0 for all other walls.
b. Steel Frame	Elastic behavior for east-west excitation. Seismic response nearly double plastic moment capacity for weak axis bending of interior columns subjected to north-south excitation with no observed damage.
c. Diaphragms	Concrete diaphragms have shear stresses ranging from about 50 to 250 psi. Horizontal bracing angles exceed yield by as much as a factor of 4.0 with no observed damage.
3. Turbine Pedestal	Elastic behavior.
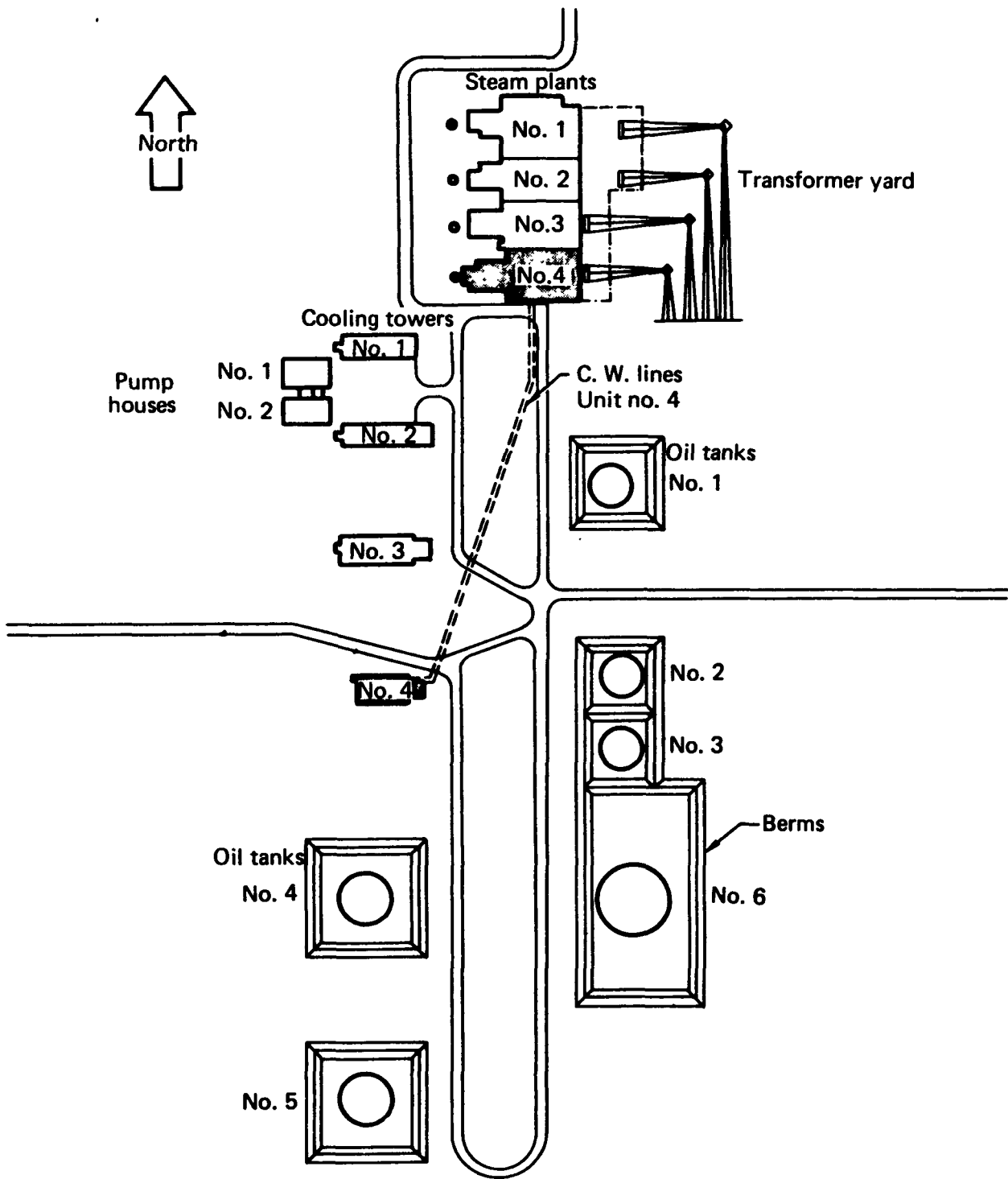
FIGURE E-1. PLOT PLAN OF THE EL CENTRO STEAM PLANT (REFERENCE E-1)
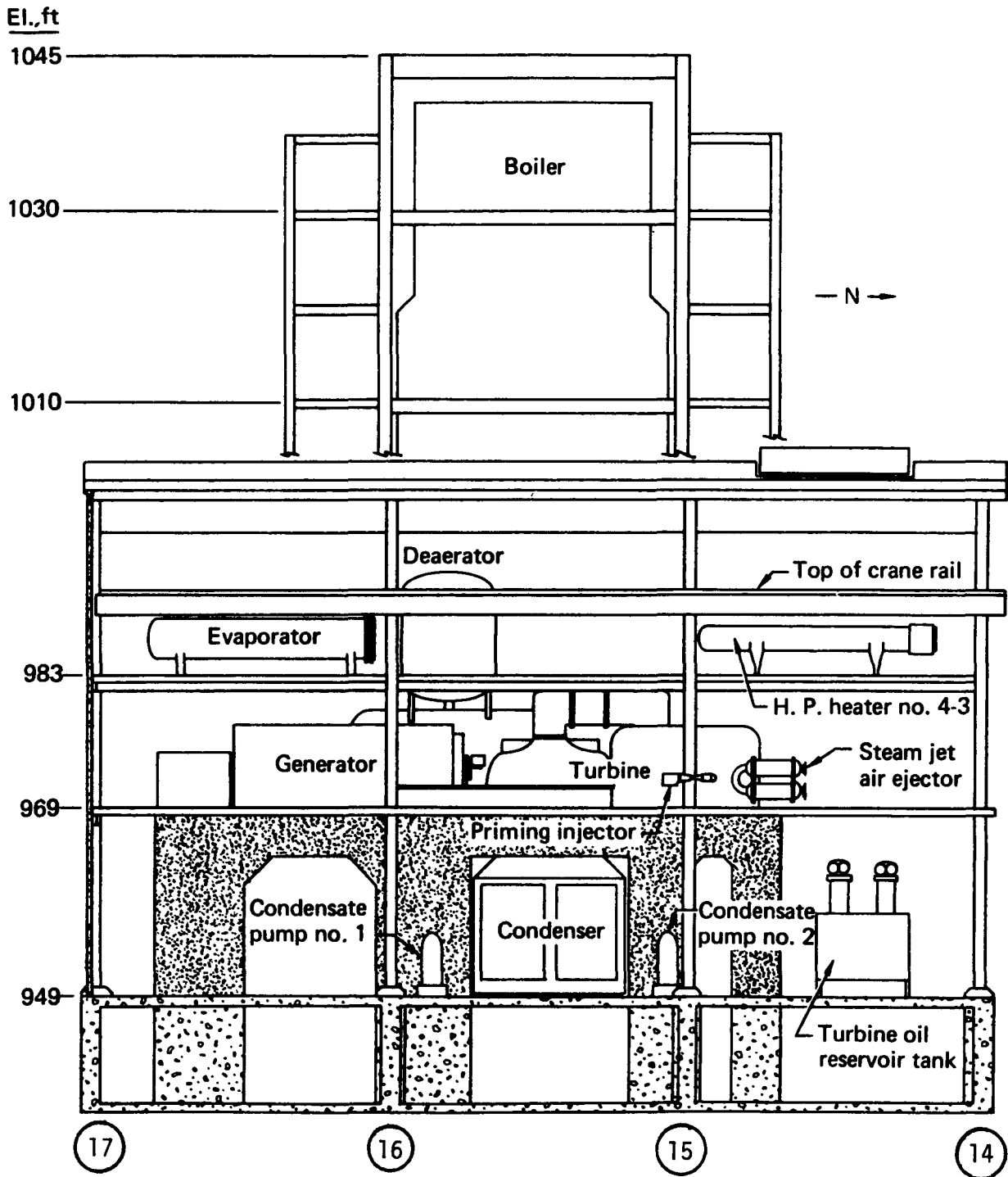
FIGURE E-2. ELEVATION DRAWING, LOOKING WEST AT COLUMN LINE B, OF THE EL CENTRO STEAM PLANT, UNIT 4 (REFERENCE E-1)
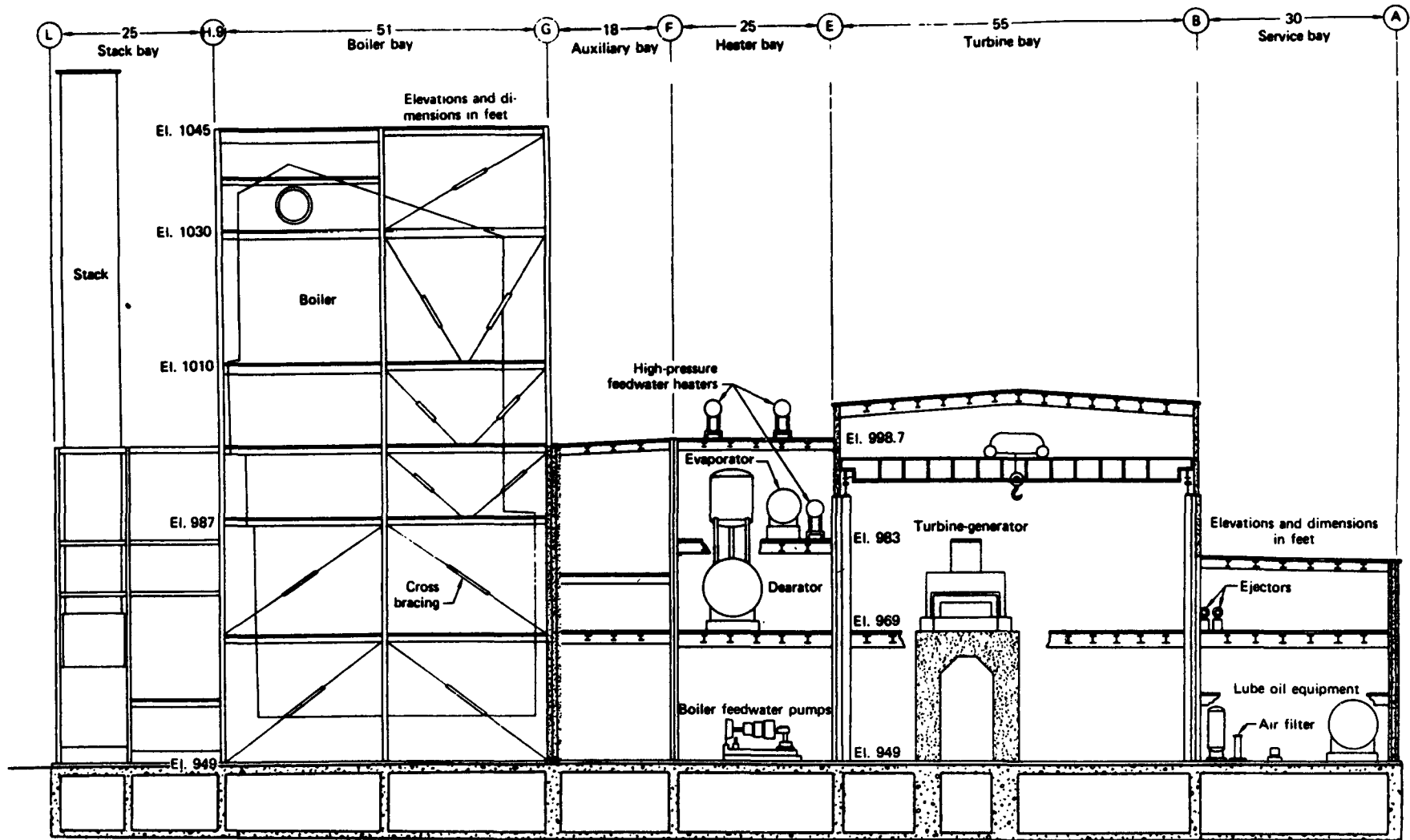
FIGURE E-3. ELEVATION DRAWING, LOOKING NORTH, OF THE EL CENTRO STEAM PLANT, UNIT 4 (REFERENCE E-1)
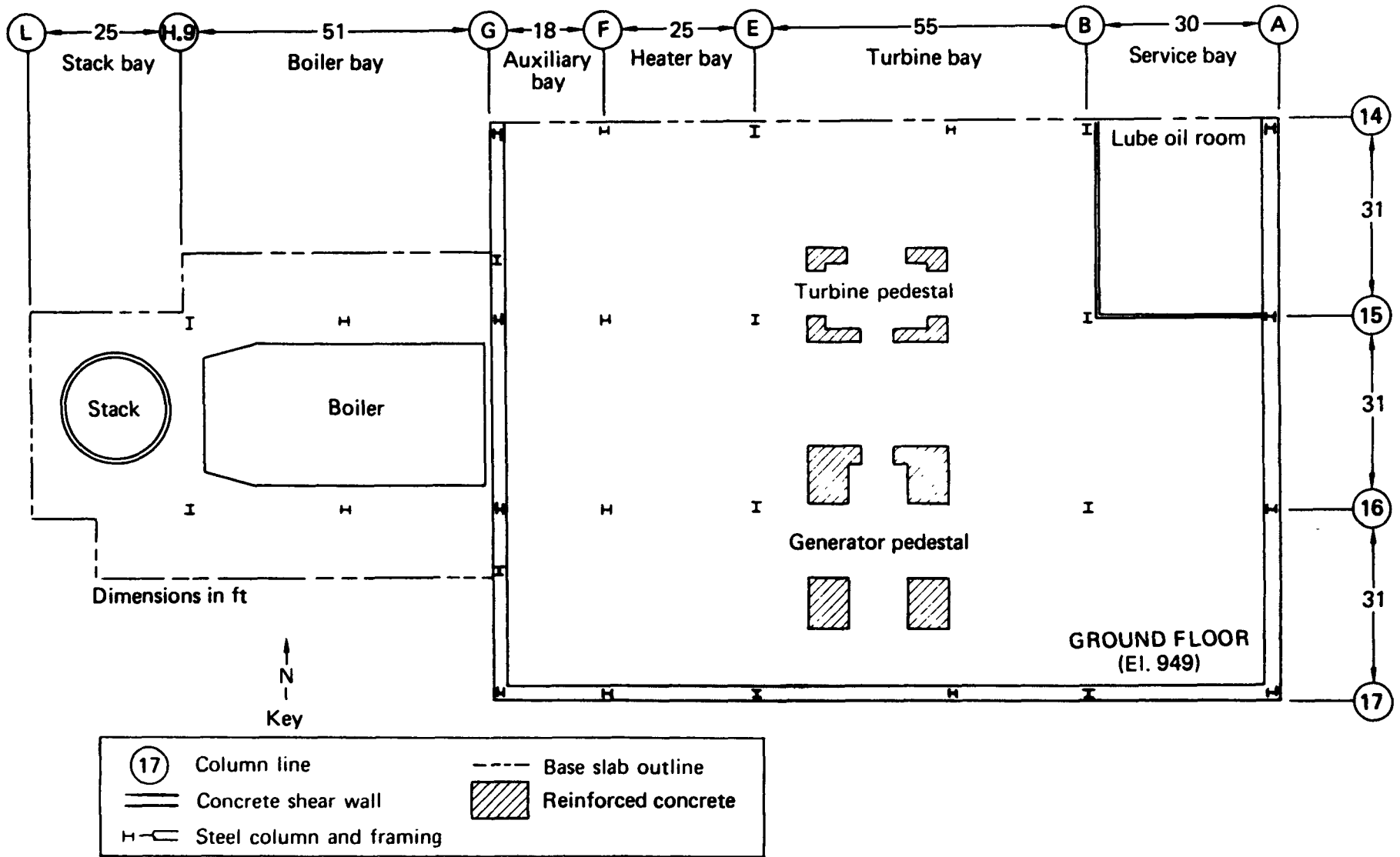
FIGURE E-4. SCHEMATIC PLAN VIEW OF THE UNIT 4 GROUND FLOOR (EL 949 FT) (REFERENCE E-1)
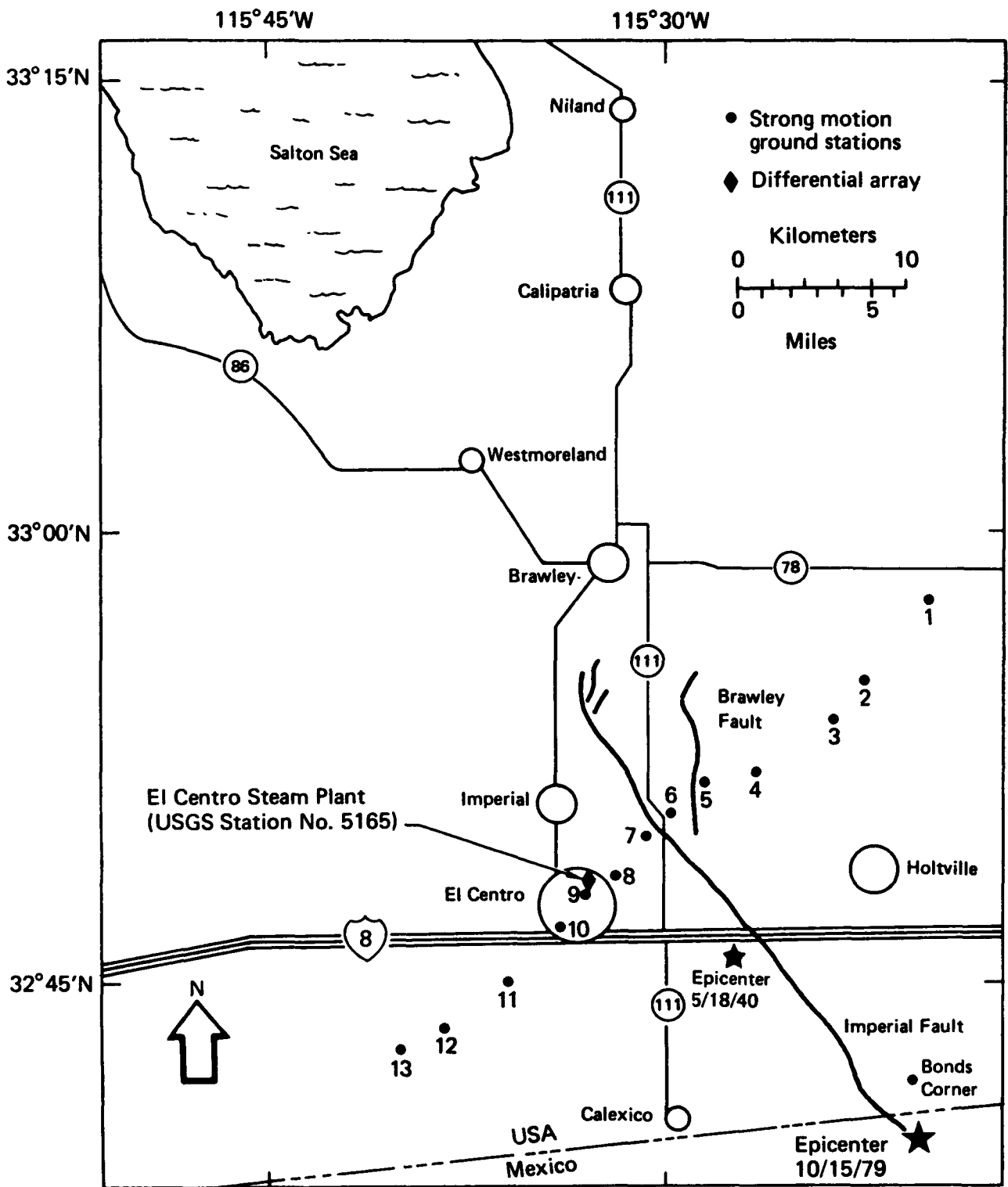
FIGURE E-5. MAP OF THE IMPERIAL VALLEY, CALIFORNIA, SHOWS THE IMPERIAL
FAULT AND THE EL CENTRO STEAM PLANT SITE. ALSO SHOWN IS
THE STRONG MOTION ARRAY THAT STRADDLES THE FAULT. (REFERENCE E-1)

Map labels (as shown):

- Indio 82 mi
- CANAL
- BM-48
- 99
- El Centro Steam Plant Unit 4
- Labor Camp
- Approximate Station 8 Location
- LEVEE
- DATE — 31 — 32 — 33
- Reservoirs
- Station 9 Location
- 3rd Street
- Oil Tanks
- Res
- El Centro 32° 48' Differential Array
- San Diego 116 mi
- BM-48
- BM-46
- 30
- 99
- ADAMS AVE
- T 15 S / T 16 S
- Lincoln Sch
- 4 LANE
- Park
- McKinley Sch
- BM-47
- HOLTON
- Station 516
- Yuma, Ariz 61 mi
- Commercial Avenue
- BM-40
- EL CENTRO
- Imperial Valley College
- Central Union H S
- Park
- MAIN
- Court House
- City Hall
- PO
- Washington School
- Douglas Jr. H S
- 5
- 80
- ORANGE
- 6
- LANDING STRIP
- 4
- Wilson Sch
- Harding Sch
- BM-44
- 32° 47'
- Water Tank
- BM-35
- ROSS
- Hospital
- AVE
- 99
- CENTRAL
- CANAL
- DRAIN
- Radio Sta KXO
- 115° 34'
- Calexico 9.6 mi
- 115° 33'
- 115° 32'
- R 13 E / R 14 E

Legend / details:

El Centro – Terminal Substation

USGS Topographic
Quadrangle: El Centro, California.

Coordinates: 32° 47' 42" N
115° 32' 55" W

Location: N.W. corner of intersection of
Third St. and Commercial Ave.

Structure: Two story, heavy, reinforced concrete
building.

Scale:
0 — 2000 — 4000
Scale in feet

N

STATION LOCATION PLAN
- EL CENTRO -

FIGURE E-6. STEAM PLANT AND ADJACENT GROUND MOTION INSTRUMENT STATIONS
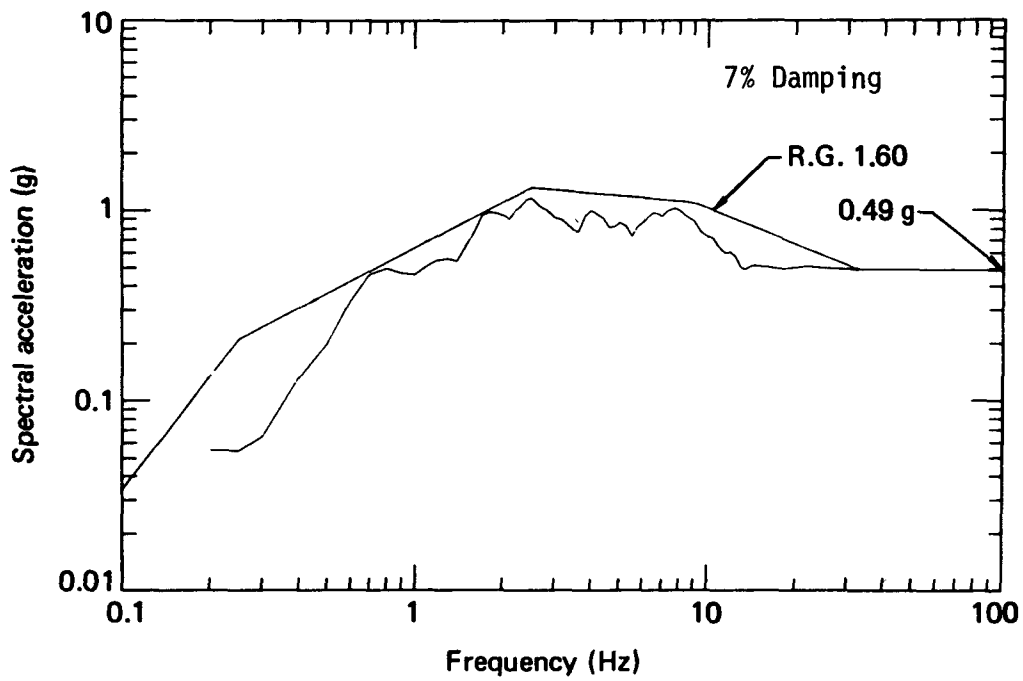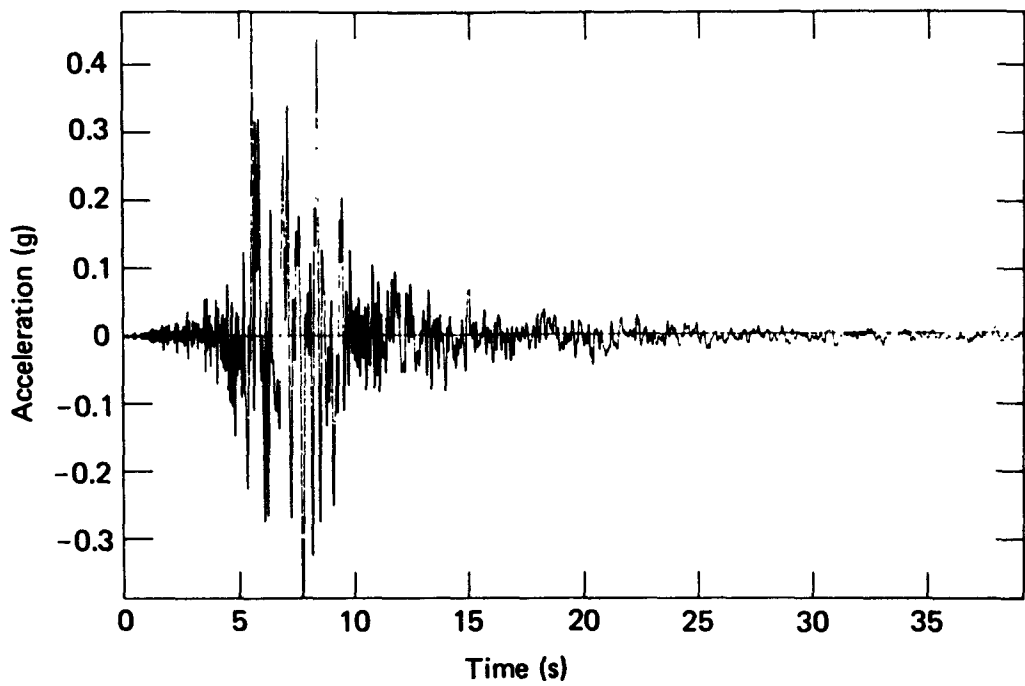
FIGURE E-7. NORTH-SOUTH GROUND MOTION TIME HISTORY AND RESPONSE
SPECTRUM FOR THE OCTOBER 15, 1979 IMPERIAL VALLEY
EARTHQUAKE RECORDED AT U.S. GEOLOGICAL SURVEY STATION
NO. 5165 (REFERENCE E-1)
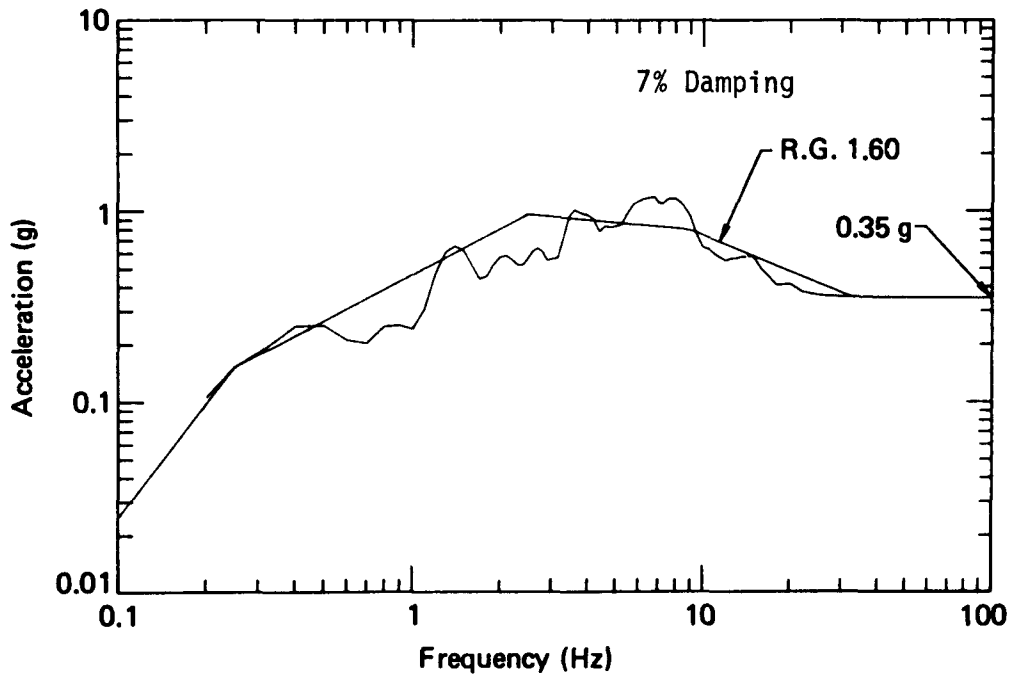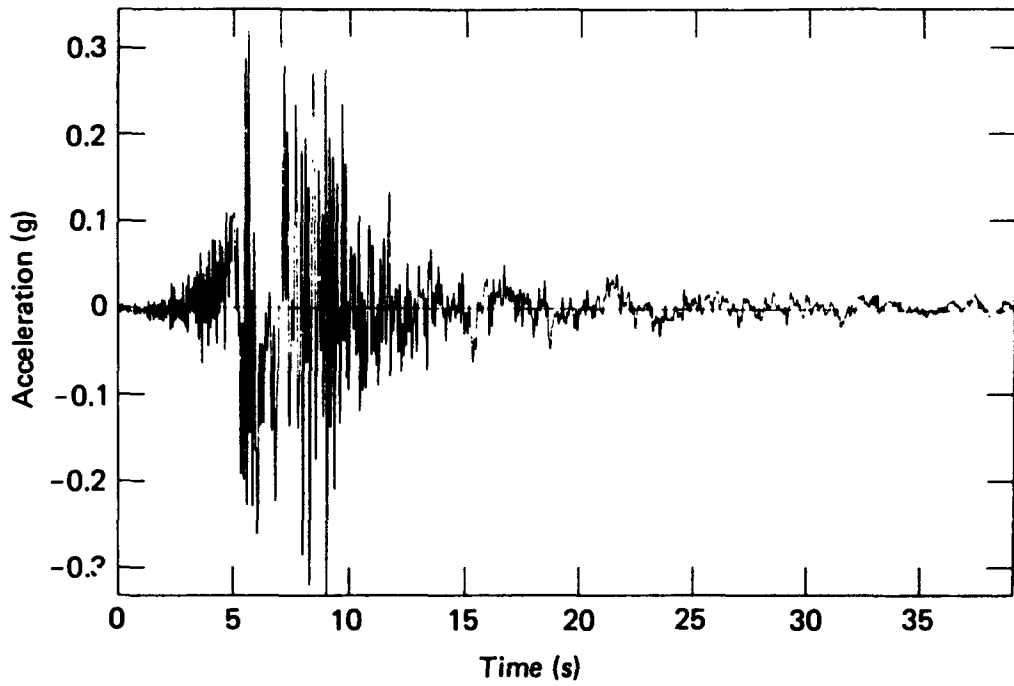
FIGURE E-8. EAST-WEST GROUND MOTION TIME HISTORY AND RESPONSE
SPECTRUM FOR THE OCTOBER 15, 1979 IMPERIAL VALLEY
EARTHQUAKE RECORDED AT U.S. GEOLOGICAL SURVEY STATION
NO. 5165 (REFERENCE E-1)
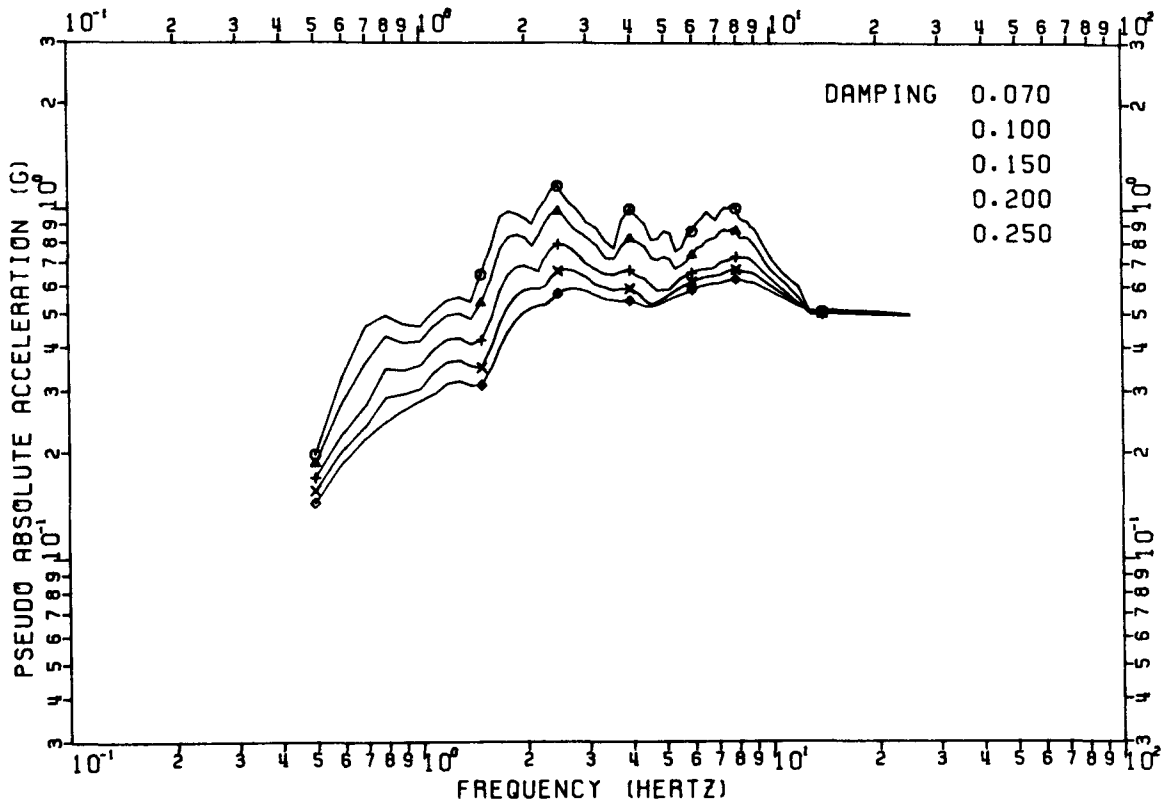
EL CENTRO 1979. N-S
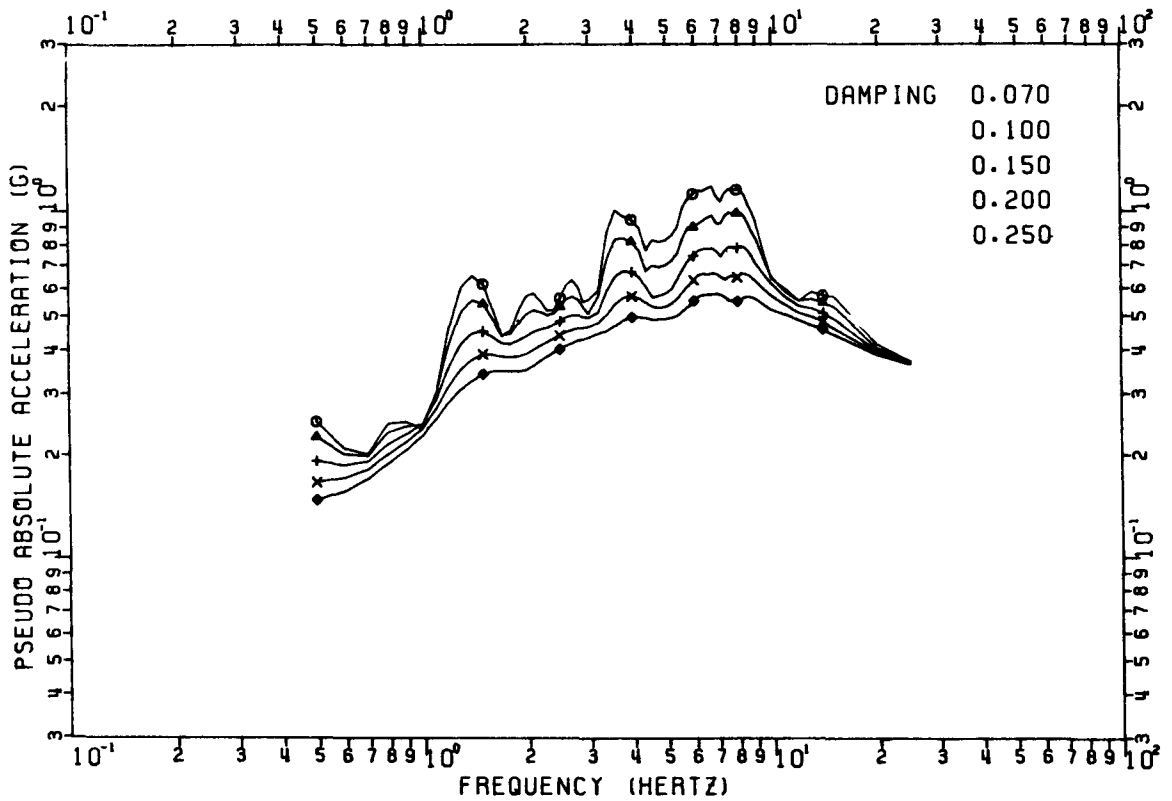
EL CENTRO 1979. E-W

E-44 FIGURE E-9. ELASTIC RESPONSE SPECTRA, DIFFERENTIAL ARRAY (USGS STATION 5165) IMPERIAL VALLEY EARTHQUAKE, OCTOBER 15,1979
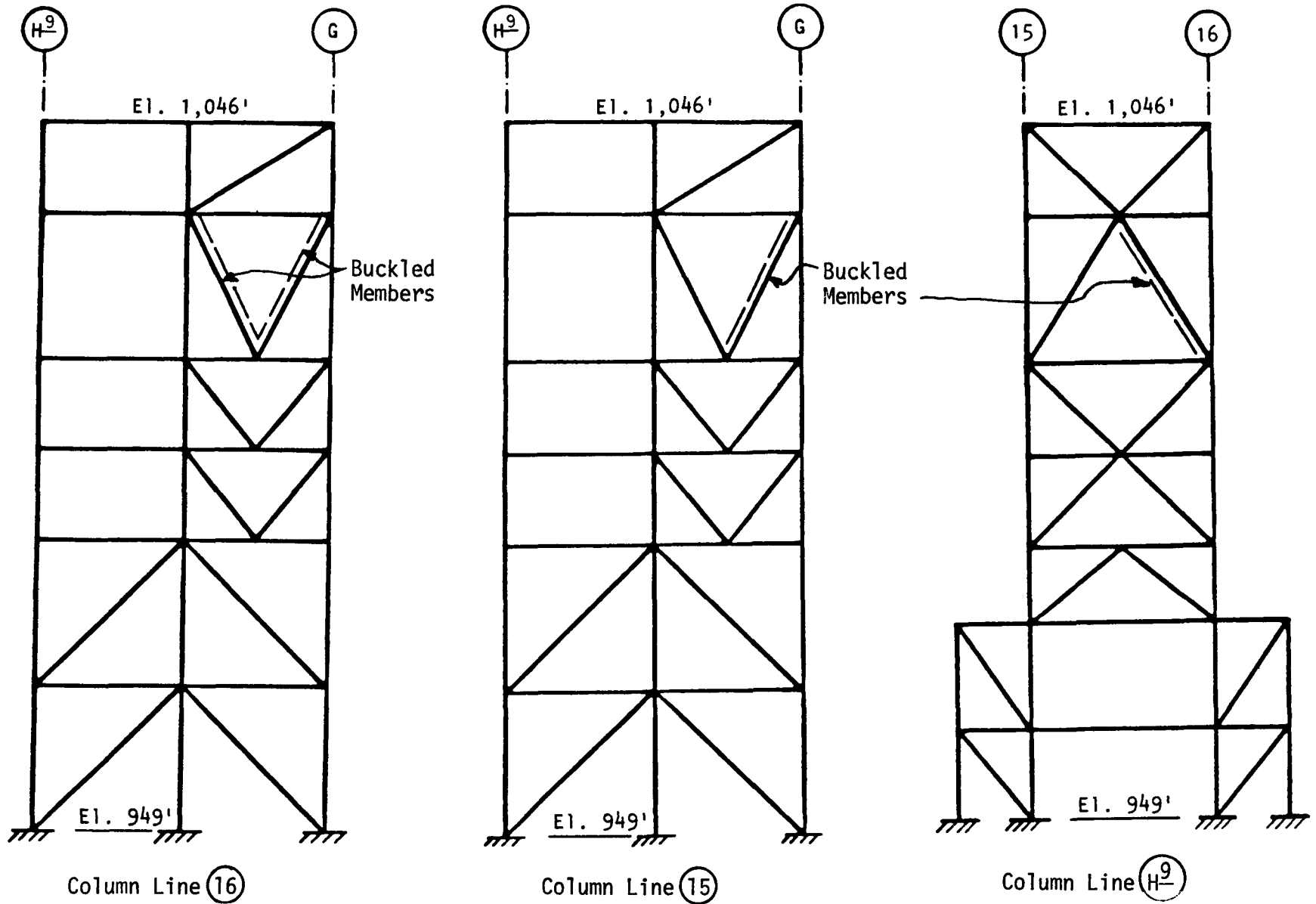
FIGURE E-10. DIAGONAL MEMBERS IN THE UNIT 4 BOILER STRUCTURE WHICH BUCKLED DURING THE 1979 IMPERIAL VALLEY EARTHQUAKE
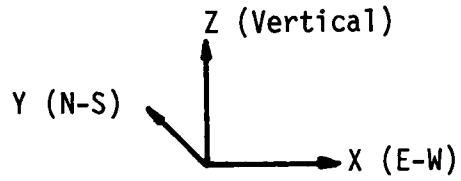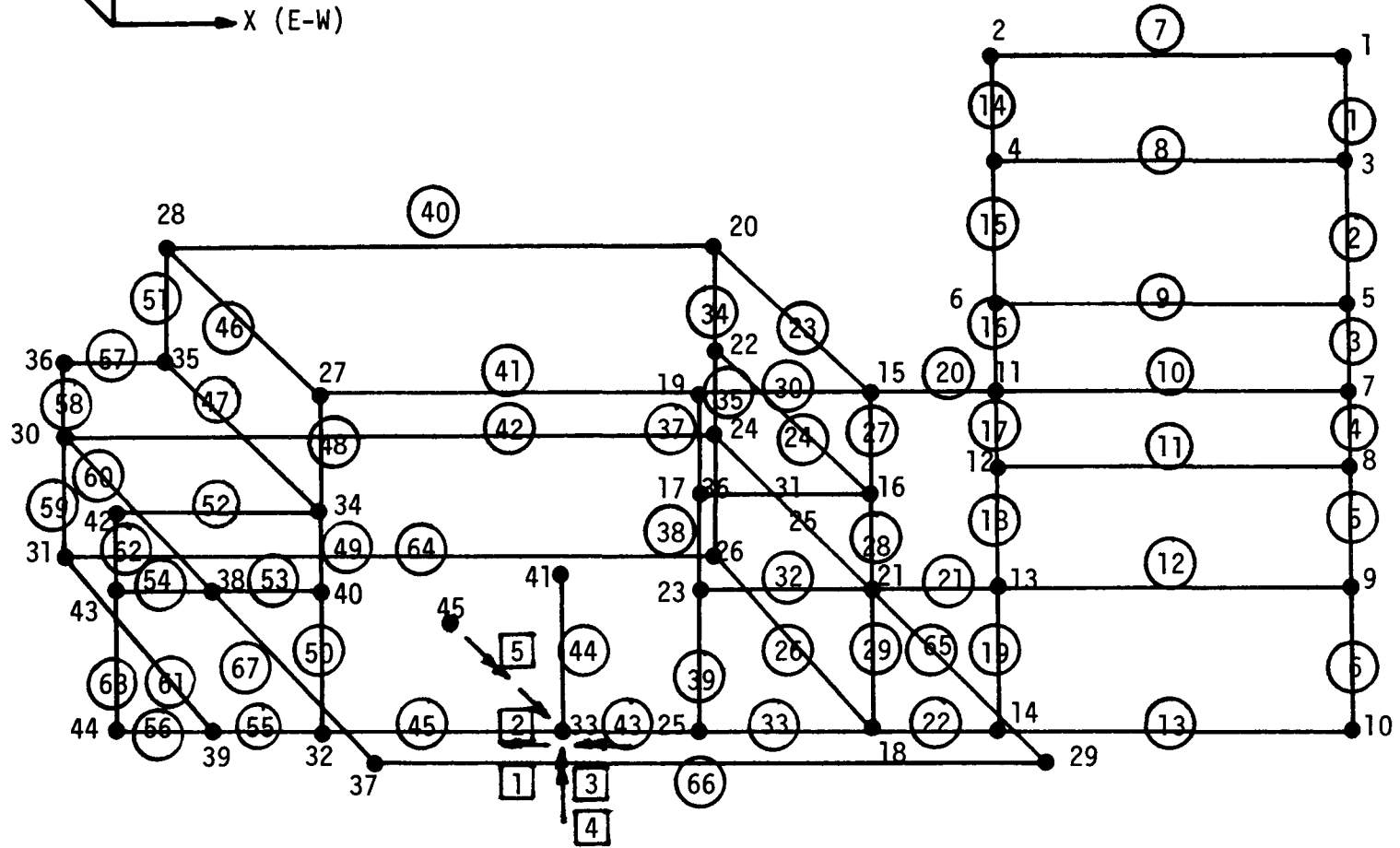
FIGURE E-11. STRUCTURAL MODEL
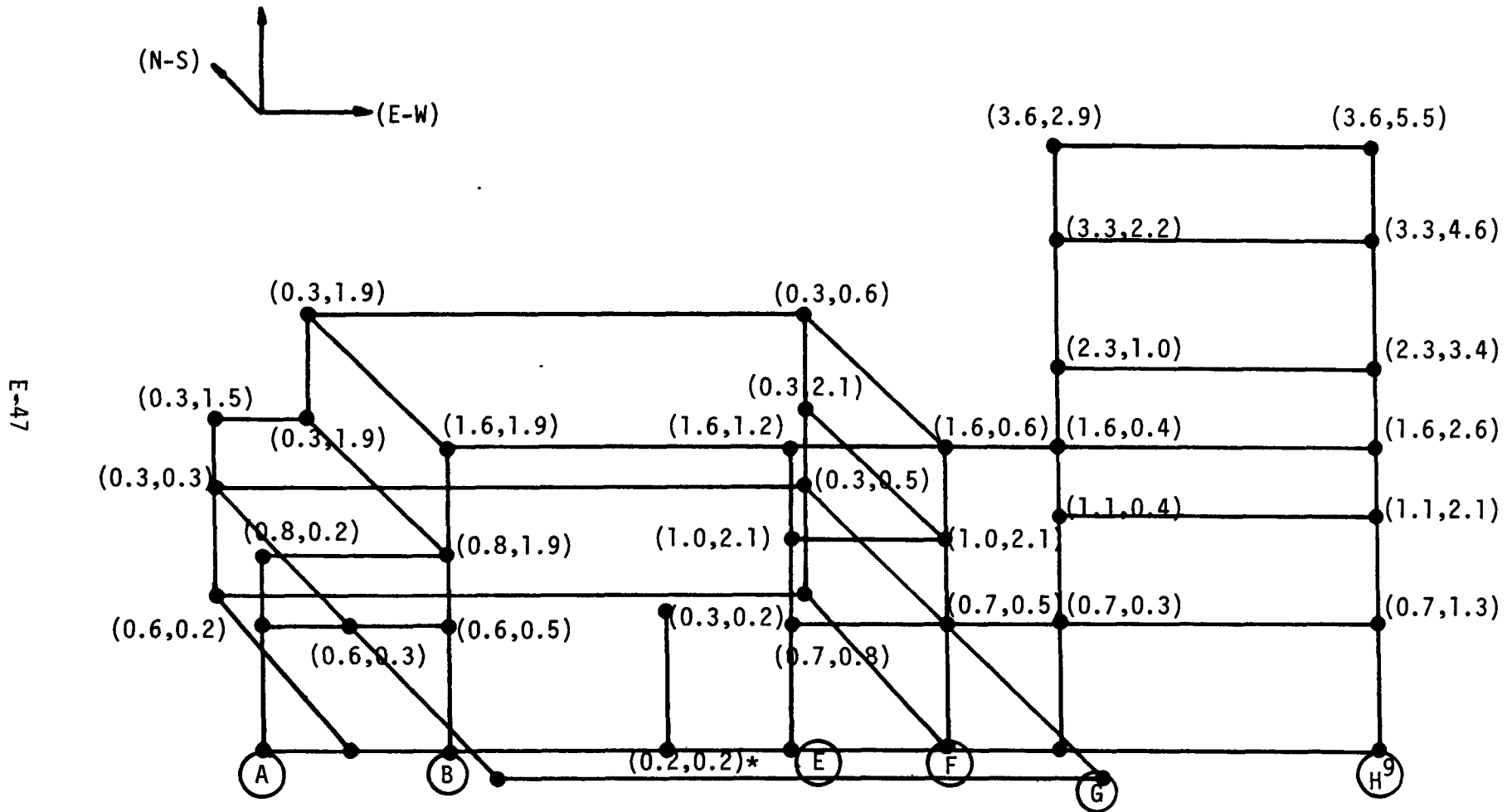
FIGURE E-12. MAXIMUM ELASTICALLY CALCULATED SEISMIC RESPONSE DISPLACEMENTS
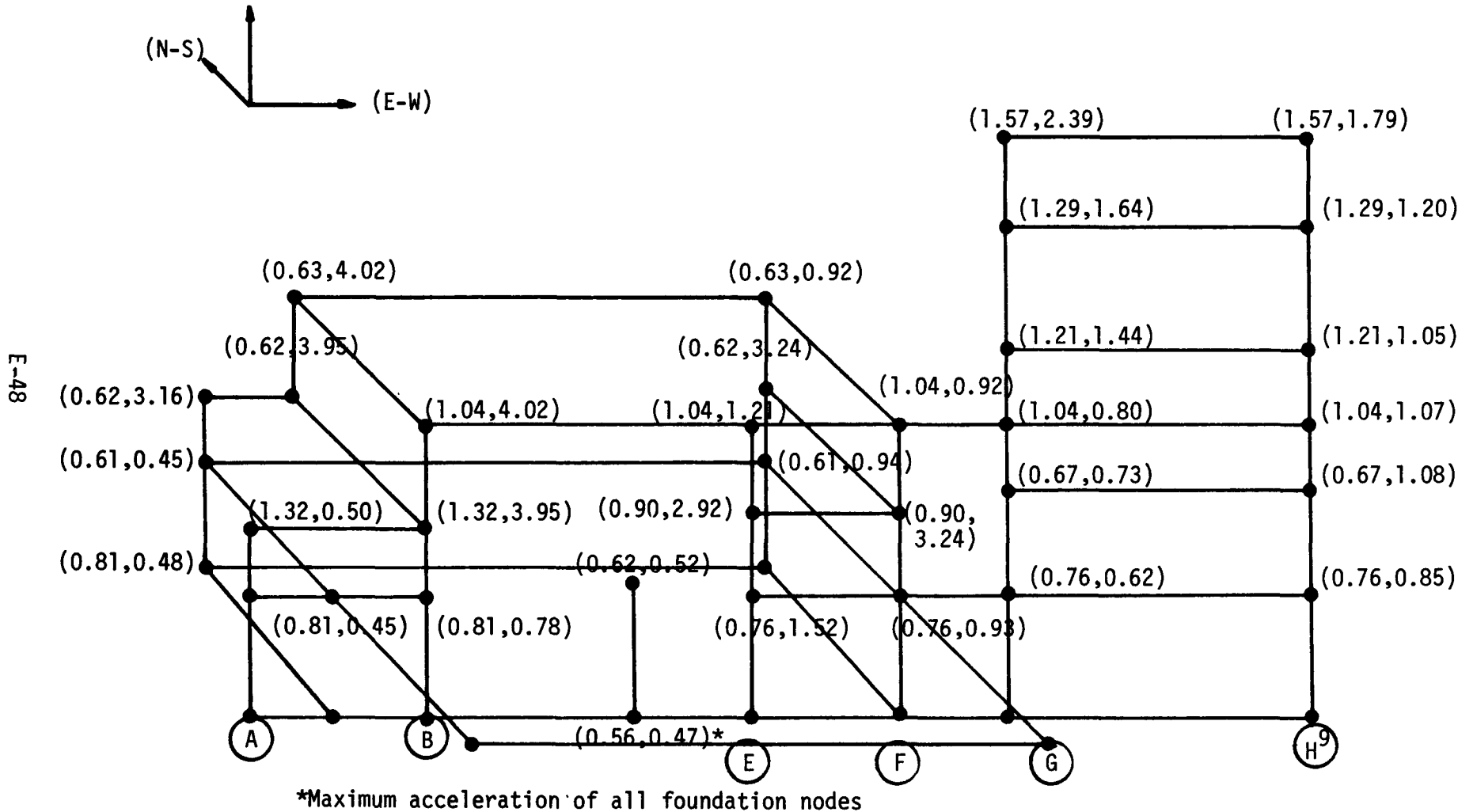
FIGURE E-13. MAXIMUM ELASTICALLY CALCULATED SEISMIC RESPONSE ACCELERATIONS
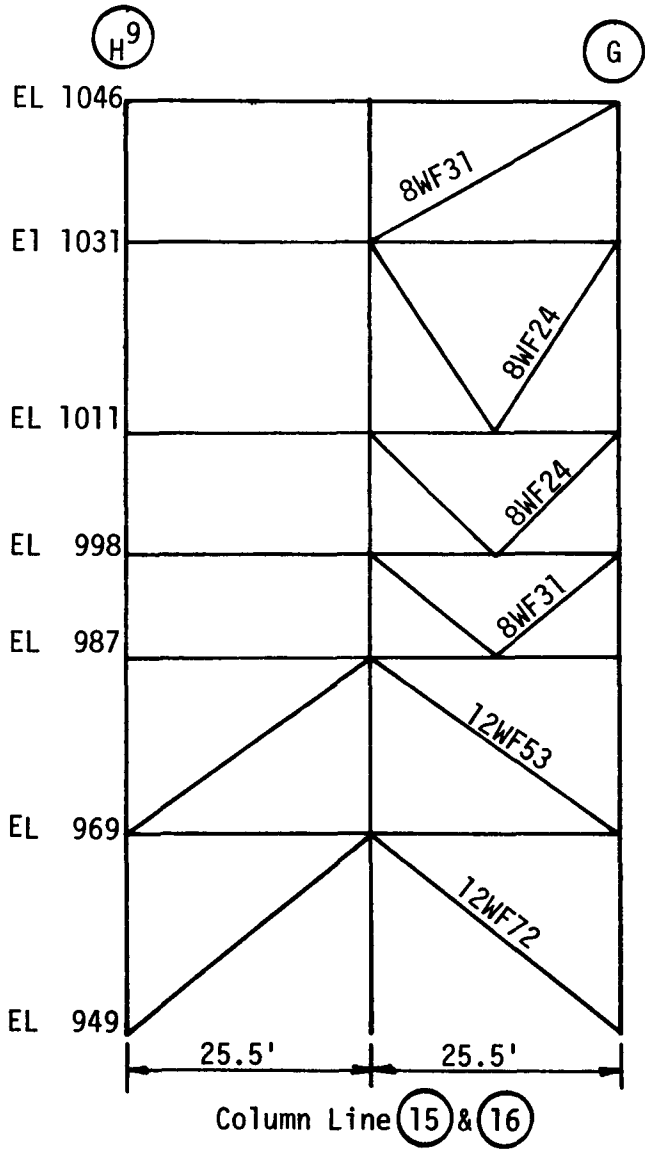
Calculated Seismic Response V(kips)	Ultimate Capacity V_{cr} (kips)	V/V_{cr}
131.8	92.7(C)** 283.0(T)	1.4(C)** 0.5(T)
548.1	113.2	4.8*
723.9	206.5	3.5
545.4	393.8	1.4
630.6	634.8	1.0
676.6	865.6	0.8

*Buckled Members
**(C) = Compression
(T) = Tension

FIGURE E-14. SEISMIC RESPONSE SHEARS & SHEAR CAPACITIES FOR COLUMN LINES (15) and (16) IN BOILER STRUCTURE
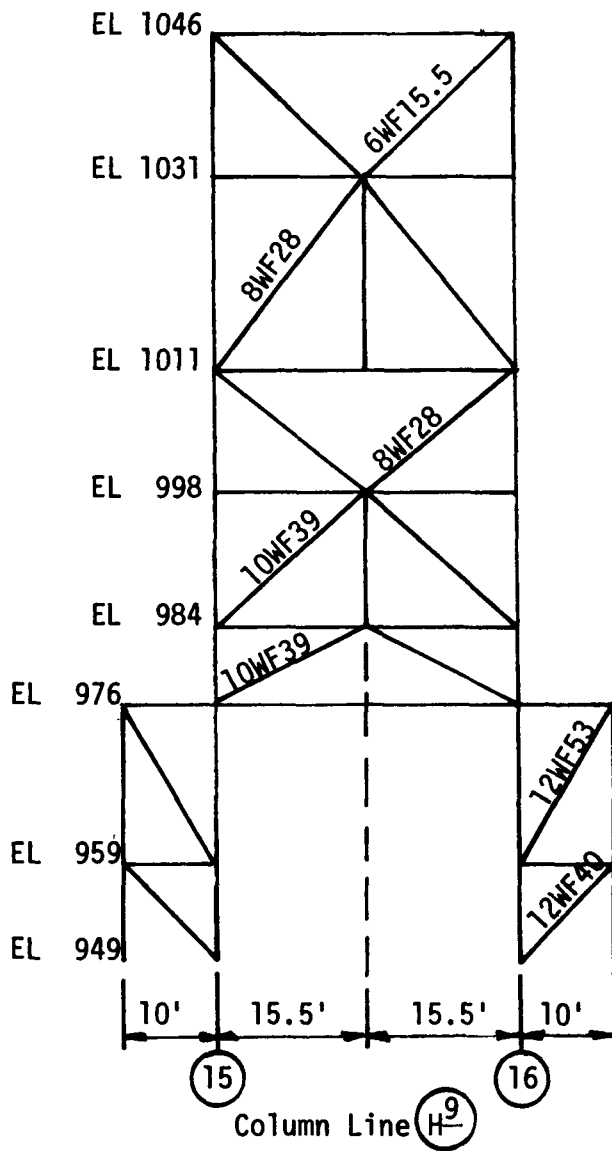
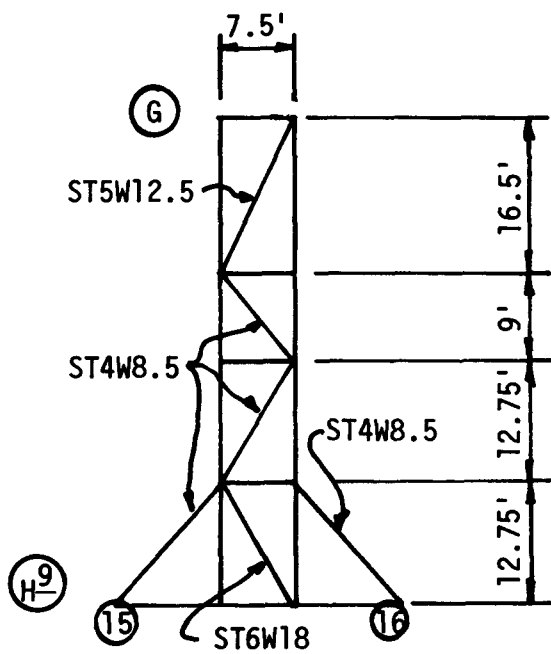| Calculated Seismic Response V(kips)	Ultimate Capacity V_{cr}	V/V_{cr}
378.2	97.1	3.9
510.9	126.6	4.0*
564.6	216.4	2.6
578.2	330.7	1.7
699.6	511.1	1.4
726.5	477.8	1.5
753.4	520.0	1.4

*Buckled Member

FIGURE E-15.   SEISMIC RESPONSE SHEARS & SHEAR CAPACITIES FOR COLUMN
LINE (H9) IN BOILER STRUCTURE
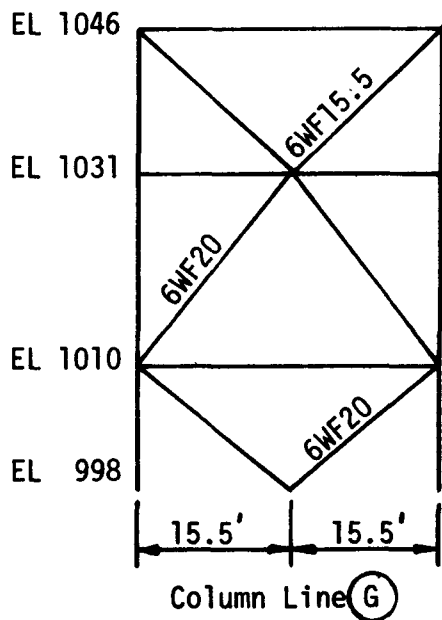
Calculated Seismic Response V(kips)	Ultimate Capacity V_{cr}(kips)	V/V_{cr}
210.7	78.5	2.7
419.5	85.0	4.9
563.5	224.1	2.5

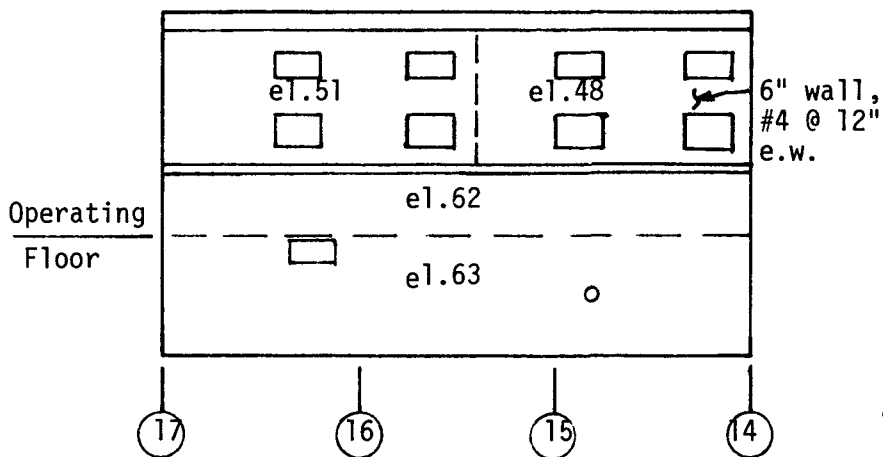FIGURE E-16. SEISMIC RESPONSE SHEARS & SHEAR CAPACITIES FOR COLUMN LINE Ⓖ IN BOILER STRUCTURE

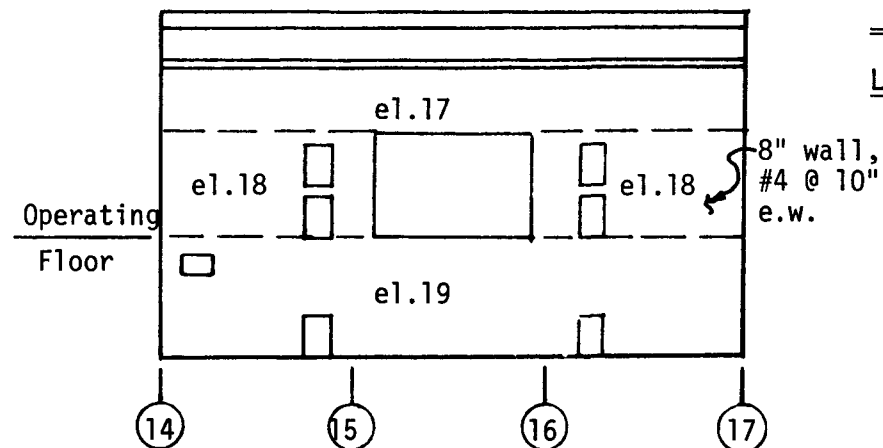| Calculated Seismic Response V(kips)	Ultimate Capacity V_{cr}(kips)	V/V_{cr}
70.3	19.7(C)* 54.9(T)	3.6(C)* 1.3(T)
70.3	31.8(C) 57.7(T)	2.2(C) 1.2(T)
70.3	17.8(C) 45.6(T)	3.9(C) 1:5(T)

*(C) = Compression
 (T) = Tension

FIGURE E-17.   SEISMIC RESPONSE SHEARS & SHEAR CAPACITIES FOR BOILER
                DIAPHRAGM BRACING AT EL 998
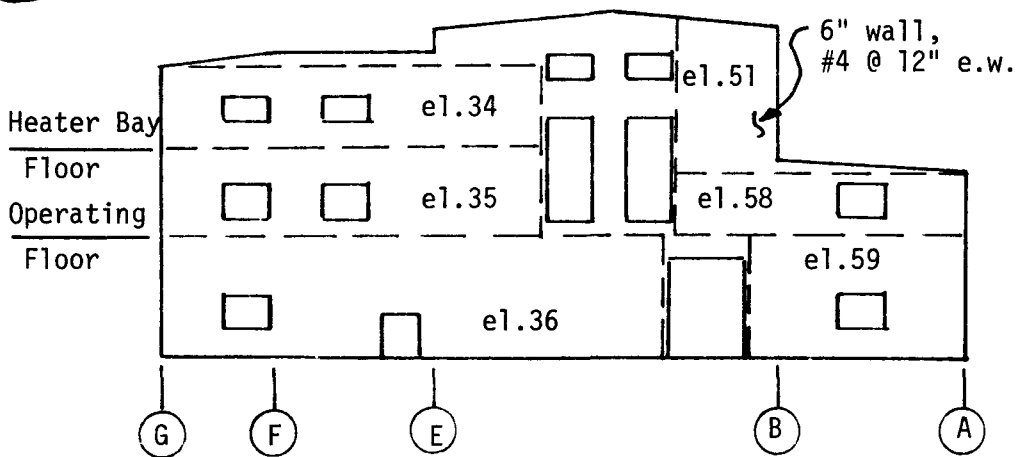
a. South Elevation

b. East Elevation

c. West Elevation

Seismic Loads and Ultimate Capacities (kips)

el.	V	V_{frame}	V_{wall}	V_u	$\dfrac{V_{wall}}{V_u}$
34	457	53	404	623	0.65
35	430	58	372	623	0.60
36	795	93	702	967	0.73
51	244	52	192	228	0.84
58	246	34	212	548	0.39
59	287	64	223	320	0.70
48/51	338	24	314	870	0.36
62	162	18	144	823	0.18
63	734	81	653	823	0.79
17	989	64	925	1706	0.54
18	1201	107	1094	1222	0.90
19	2205	305	1900	1706	1.11

LEGEND

el. 34	− Element number of structural model (see Figure 11)
V	− Total calculated seismic shear
V_{frame}	− Shear carried by steel frame
V_{wall}	− Shear carried by concrete wall
V_u	− Ultimate shear capacity (ACI Code)

FIGURE E-18. TURBINE BUILDING CONCRETE WALL LOADS AND CAPACITIES

FIGURE E-19. TURBINE BUILDING STEEL FRAME NORTH-SOUTH SEISMIC RESPONSE
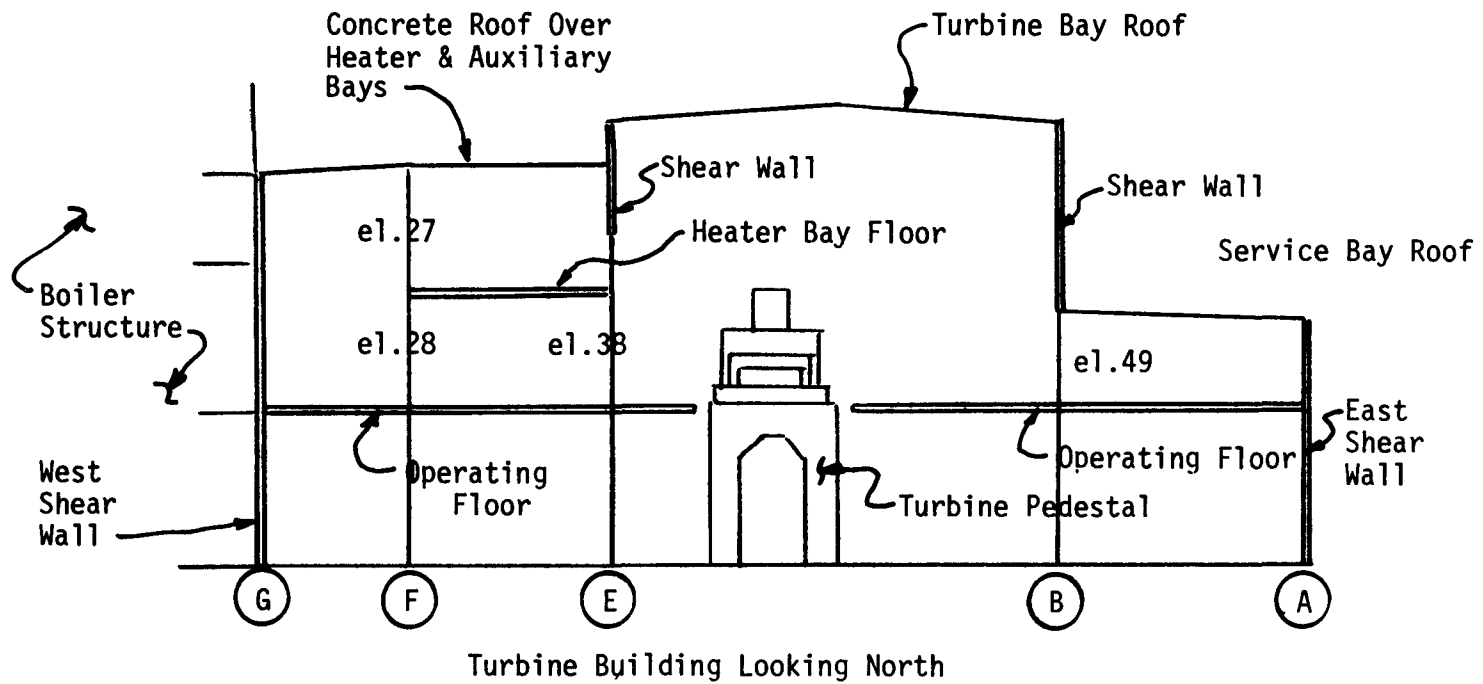
element	$\dfrac{\text{Seismic Induced Moment}}{\text{Plastic Moment Capacity}}$
49	1.9
38	1.2
27	1.4
28	1.8

REFERENCES

E-1   T. A. Nelson, R. C. Murray, et al, "Response of El Centro Steam
       Plant Equipment During the October 15, 1979, Imperial Valley
       Earthquake", Lawrence Livermore Laboratory, NUREG/CR-1665,
       UCRL-53005, September, 1980.

E-2   "Analysis of the El Centro Steam Plant", (draft report) submitted
       to PG&E by URS/John A. Blume, May, 1981.

E-3   Richart, F. E., J. R. Hall and R. D. Woods, Vibrations of Soils and
       Foundations Prentice-Hall, Inc., Englewood Cliffs, New Jersey, 1970.

E-4   American Institute of Steel Construction, Manual of Steel Construc-
       tion, Eighth Edition, 1980.

E-5   Building Code Requirements for Reinforced Concrete (ACI 318-77),
       American Concrete Institute, 1977.

E-6   USNRC Regulatory Guide 1.60, "Design Response Spectra for Seismic
       Design of Nuclear Power Plants", Revision 1, December, 1973.

E-7   USNRC Regulatory Guide 1.61, "Damping Values for Seismic Design of
       Nuclear Power Plant", October, 1973.

Availability of Reference Materials Cited in NRC Publications

Most documents cited in NRC publications will be available from one of the following sources:

1. The NRC Public Document Room, 1717 H Street, N.W.
   Washington, DC 20555

2. The NRC/GPO Sales Program, U.S. Nuclear Regulatory Commission,
   Washington, DC 20555

3. The National Technical Information Service, Springfield, VA 22161

Although the listing that follows represents the majority of documents cited in NRC publications, it is not intended to be exhaustive.

Referenced documents available for inspection and copying for a fee from the NRC Public Document Room include NRC correspondence and internal NRC memoranda; NRC Office of Inspection and Enforcement bulletins, circulars, information notices, inspection and investigation notices; Licensee Event Reports; vendor reports and correspondence; Commission papers; and applicant and licensee documents and correspondence.

The following documents in the NUREG series are available for purchase from the NRC/GPO Sales Program: formal NRC staff and contractor reports, NRC-sponsored conference proceedings, and NRC booklets and brochures. Also available are Regulatory Guides, NRC regulations in the Code of Federal Regulations, and Nuclear Regulatory Commission Issuances.

Documents available from the National Technical Information Service include NUREG series reports and technical reports prepared by other federal agencies and reports prepared by the Atomic Energy Commission, forerunner agency to the Nuclear Regulatory Commission.

Documents available from public and special technical libraries include all open literature items, such as books, journal and periodical articles, and transactions. Federal Register notices, federal and state legislation, and congressional reports can usually be obtained from these libraries.

Documents such as theses, dissertations, foreign reports and translations, and non-NRC conference proceedings are available for purchase from the organization sponsoring the publication cited.

Single copies of NRC draft reports are available free upon written request to the Division of Technical Information and Document Control, U.S. Nuclear Regulatory Commission, Washington, DC 20555.

Copies of industry codes and standards used in a substantive manner in the NRC regulatory process are maintained at the NRC Library, 7920 Norfolk Avenue, Bethesda, Maryland, and are available there for reference use by the public. Codes and standards are usually copyrighted and may be purchased from the originating organization or, if they are American National Standards, from the American National Standards Institute, 1430 Broadway, New York, NY 10018.

GPO Printed copy price $ 8.50